Lectures in
Isotope Geology

Edited by
E. Jäger and J. C. Hunziker

With 149 Figures

Springer-Verlag
Berlin Heidelberg New York 1979

Prof. Dr. EMILIE JÄGER
Priv. Doz. Dr. JOHANNES C. HUNZIKER
Universität Bern, Abteilung für Isotopengeologie
Erlachstrasse 9a, CH-3012 Bern

The cover motive shows the cooling history of the Central Alps derived by different dating methods. (Redrawn after Wagner, Reimer, and Jäger, 1977).

ISBN-13:978-3-540-09158-5 e-ISBN-13:978-3-642-67161-6
DOI: 10.1007/978-3-642-67161-6

Library of Congress Cataloging in Publication Data. Main entry under title: Lectures in isotope geology. Bibliography: p. Includes index. 1. Isotope geology--Addresses, essays, lectures. 2. Geology--Alps--Addresses, essays, lectures. I. Jäger, Emilie, 1926-. II. Hunziker, Johannes Christoph, 1937-. QE501.4.N9L42.551.9 78-26213

2131/3130-543210

Preface

Our colleagues from the French-speaking parts of Switzerland – the Suisses romands – and above all the committee of the 3rd Cycle, Earth Sciences (3^e Cycle, Sciences de la Terre) honored us by asking us to give a course on Isotope Geology for the year 1977. The course, entitled *Evaluation et Interprétation des Données Isotopiques* (evaluation and Interpretation of Isotopic Data), was intended to inform earth scientists, graduate and postgraduate, from the western Swiss Universities on the subject of Isotope Geology.

Such courses usually consist of two parts: lectures and excursions. Thus, in March 1977, we gave such a two-week course at the Mineralogical Institute of the University of Berne.

The first week was devoted essentially to the methods of dating, the second week to the behavior of stable isotopes. In July 1977, on the occasion of an excursion to the Central and Western Alps, we were able to demonstrate our results.

Guest professors were invited to make contributions to the course. Although we were not entirely successful in working our way through the entire field of isotope geology, our documentation was nevertheless felt to give a satisfactory survey, thanks to the careful preparation by the guest professors. Although this survey should also interest a wider public, we must point out that some of the contributions, especially the results from the Alps, the Schwarzwald, and the European Continent, are more of local importance. However, we feel that they, too, may be of greater interest as model examples.

We wish to cordially thank our French-speaking colleagues for their confidence in having such complex material demonstrated in a course of the 3rd Cycle.

Above all, our thanks are due to our guest teachers. They not only gave very good lectures and provided clear documentation (a total of more than 400 pages), but they have also prepared these contributions for publication, bringing them up to date. The authors alone are responsible for the contents of the various contributions.

Like the course, the book is divided into a first part dealing with age determination, and a second part on stable isotopes.

The book will appeal less to specialists than to geologists who desire information on the possibilities of isotope geology.

January, 1979

E. Jäger

J.C. Hunziker

Contents

Contributors

Clark, S.P., Jr., Department of Geology and Geophysics, Yale University, New Haven, CT 06520/USA
Clauer, N., Centre de Sédimentologie et Géochimie de la Surface, Institut de Geologie, 1, Rue Blessig, 67084 Strasbourg-Cedex/France
Dallmeyer, R.D., Department of Geology, K-Ar Laboratory, University of Georgia, Athens, GA 30602/USA
Delaloye, M., Université de Genève, Département de Minéralogie, 13, Rue des Maraîchers, 1211 Genève 4/Switzerland
Dodson, M.H., Department of Earth Sciences, University of Leeds, Leeds LS 2 9JT/England
Gebauer, D., Institut für Kristallographie und Petrographie der ETH, Sonneggstr. 5, 8092 Zürich/Switzerland
Grünenfelder, M., Institut für Kristallographie und Petrographie der ETH, Sonneggstr. 5, 8092 Zürich/Switzerland
Hofmann, A.W., Carnegie Institution of Washington, Department of Terrestrial Magnetism, 5241 Broad Branch Road, NW, Washington, DC 20015/USA
Hunziker, J.C., Universität Bern, Abteilung für Isotopengeologie, Erlachstr. 9a, 3012 Bern/Switzerland
Jäger, E., Universität Bern, Abteilung für Isotopengeologie, Erlachstr. 9a, 3012 Bern/Switzerland
Köppel, V., Institut für Kristallographie und Petrographie der ETH, Sonneggstr. 5, 8092 Zürich/Switzerland
Naeser, C.W., Branch of Isotope Geology, U.S. Geological Survey M.S. 424, Federal Center, Lakewood, CO 80225/USA
Nielsen, H., Geochemisches Institut, Isotopenlabor, Universität Göttingen, Goldschmidtstraße 1, 3400 Göttingen/FRG
O'Neil, J.R., Branch of Isotope Geology, U.S. Geological Survey, 345 Middlefield Road, Menlo Park, CA 94025/USA
Siegenthaler, U., Universität Bern, Physikalisches Institut, Sidlerstraße 5, 3012 Bern/Switzerland
Stahl, W.J., Bundesanstalt für Geowissenschaften und Rohstoffe, Stilleweg 2, 3000 Hannover 51/FRG
Wagner, G.A., Max-Planck-Institut für Kernphysik, Saupfercheckweg, 6900 Heidelberg/FRG

Introduction to Geochronology

E. JÄGER

Geochronology means dating of geological events. Although this expression was first used for geological time estimates, based on sedimentation rates, this term is now commonly applied to geological dating, based on radioactive decay and spontaneous fission.

Geochronology is a discipline that lies between the earth sciences, physics, and chemistry. The problems of geochronology are twofold: technical problems dealing with the highly sophisticated methods of age determination on one hand and the more intuitive approach of the earth sciences on the other hand. Geochronology is therefore the ideal discipline for teamwork. The experimental part of geochronology covers the wide field from trace element chemistry to mass spectrometry with electronics and computer application–and last but not least, mineral separation and all the techniques of mineralogy. Within the last few years the precision of age determination has been improved considerably, to some extent owing to the challenge of working on moon material.

In a well-established laboratory, age determinations are to some extent routine work, but keeping the laboratory functioning well and still improving the precision, is far beyond routine. With the finished age result, a new problem arises for the geochronologist: geochronological data must be interpreted – and the correct interpretation of ages is often just as difficult as the dating itself. In the last few years, models for the interpretation of age results have been established, based on the evaluation of age data in well-studied areas (see the following chapter). Although such models of interpretation can to some extent be applied to other areas with similar geological conditions, a separate interpretation model must be developed for each area to be dated. This is not really a disadvantage for geochronology. We know that different minerals or rocks dated by the different methods furnish specific information. By compiling all the data available, much more can be learned about the geological history of an area than just the time of mineral and rock formation.

The primary answer to geochronological work is time, the date of the geological event. However, the question of whether a mineral or rock reacted to a later event, and to what extent, can also be answered by geochronology. The most important parameters that control the age results are temperature and the presence of fluid phases. Therefore, these parameters can be evaluated by geochronological work, and geochronological data can be used for the construction of metamorphic isograde.

This shows the wide application and the importance of geochronology to geology. This is not only true for Precambrian terranes for which geochronology is the only key to their evolutionary history. Also in geologically well-studied young areas, such as the Japanese islands or the Alpine chain, geochronology has contributed much to the fun-

damental understanding of the crustal evolution. Geochronology and isotope geology are, or should be, an integrated part of the earth sciences.

1. Fundamentals of the Dating Methods

The most commonly used methods of isotope dating, the K-Ar, Rb-Sr, and the U,Th-Pb methods, are based on the radioactive decay of the isotopes: ^{40}K, ^{87}Rb, ^{235}U, ^{238}U, and ^{232}Th. Less frequently applied dating methods are those based on the decay of ^{147}Sm, ^{187}Re, further radioactive isotopes of the U and Th decay series, which are used mainly for dating ocean sediments. The later methods are not discussed in this book. Fission track dating, which makes use of the spontaneous fission of ^{238}U, is gaining importance not only in geochronology, but also in archeometry (see Chap. by Wagner and Naeser).

The speed of radioactive decay, and thus the speed of the geochronological clock, depends only on the stability of the radioactive nucleus; it cannot be changed by outside parameters such as pressure and temperature. Actually, the nature of chemical bond has been found to exert a slight influence on the decay constants of several radioactive isotopes, but this influence is much smaller than the precision of age measurements. Thus we can state that the radiometric clock has a constant speed, independent of the different geological conditions.

The number of isotopes (ΔN) that decay during a certain time interval (Δt) is therefore proportional only to the total number of radioactive isotopes (N):

$$\frac{\Delta N}{\Delta t} = -\lambda N \qquad \text{or} \qquad (1)$$

$$\frac{\Delta N}{N} = -\lambda t \qquad (2)$$

λ, the decay constant

the time integral of Eq. (2) gives:

$$\ln N = -\lambda t + C \qquad (3)$$

the constant C has to be evaluated. With t equeal to zero, i.e., at the beginning of the radioactive decay, the number of radioactive isotopes is supposed to be N_0, and the constant C therefore has to be $\ln N_0$.

$$\ln N = -\lambda t + \ln N_0 \qquad (4)$$

$$\ln \frac{N}{N_0} = -\lambda t \qquad (5)$$

$$\frac{N}{N_0} = e^{-\lambda t} \tag{6}$$

$$N = N_0\, e^{-\lambda t} \tag{7}$$

Equation (7) is the well-known formula for radioactive decay. Equation (5) leads to the age formula:

$$t = \frac{1}{\lambda} \ln \frac{N_0}{N}$$

At time t = 0, only radioactive isotopes, mother isotopes, are in the system, the number being N_0; after time t, a certain number of mother isotopes, M, are left, and daughter isotopes, D, have been formed. Thus we can substitute:

$$M + D = N_0,\ N = M$$

$$t = \frac{1}{\lambda} \ln \left(1 + \frac{D}{M}\right), \tag{8}$$

the Eq. (8).

The speed of the radioactive decay of a particular isotope is described either by the decay constant λ, or by the half-life, $t_{1/2}$. After one half-life, the number of radioactive isotopes left is assumed to be equal to the number of daughter isotopes, M = D, thus Eq. (8) gives the relation between half-life and decay constant:

$$t_{1/2} = \frac{\ln 2}{\lambda} \tag{9}$$

If the half-life is much longer than the measured age, which is true for Alpine ages (10×10^6 years) determined by the Rb-Sr method (half-life 48.8×10^9 years), the expression

$$\frac{D}{M}$$

is much smaller than 1. Therefore,

$$\ln \left(1 + \frac{D}{M}\right) \cong \frac{D}{M} \quad \text{and}$$

$$t \cong \frac{D}{\lambda M} \tag{10}$$

is a good approximation for the age calculation.

In the ideal case, a crystallizing mineral should incorporate only the element with the radioactive isotope, the mother element, and no daughter element. We also have to assume that, immediately after mineral formation, the content of these two elements has been changed only by the radioactive decay: The mineral or rock system has to be closed from the formation until the present for both mother and daughter elements.

The first assumption, i.e., incorporation of only mother and no daughter element, is never realized. Since the mass spectrometer cannot distinguish between the isotope produced by the radioactive decay, the radiogenic isotope, and the same isotope present in the common element, we have to measure the total amount of this isotope. From this total amount the common contribution must be subtracted to find the content of radiogenic isotope. For this subtraction, the content of the particular isotope in the common element should be well known, but this is not always the case. Thus for isotope dating the ratio of mother to daughter element in the mineral or rock sample should be as high as possible; the younger the age result, the higher it must be.

In all the dating methods, but especially in Rb-Sr and U-Pb dating, the ratio of mother to daughter isotope, not being high enough, is the limiting factor in the application of different minerals for dating. For example, Tertiary Rb-Sr ages can usually be measured only on biotites and phengites. Paleozoic ages allow a ratio of Rb/Sr that is ten times smaller; often total rocks (granitic rocks) and muscovites can also be dated.

The second assumption, i.e., a closed system for mother and daughter isotope during the entire period of time, is also rarely realized. The daughter elements – Ar, Sr, and Pb – are trace elements in the host crystal. Furthermore, the radiogenic isotope replaces the mother isotope in the crystal structure. This replacement by another element means different size, charge and polarizing property, giving rise to a preferred loss of the daughter product without significant change of the host crystal. Complete loss of the daughter isotope would mean complete resetting of the geochronological clock – complete rejuvenation. This is not at all a rare case in geochronology. It may occur, especially in crystalline rocks, under conditions of elevated temperatures or low-grade metamorphism that cannot be recognized by other methods. Geochronology takes advantage of this fact (see the following chapter).

The decay constants of the radioactive isotopes used for dating are well known, the uncertainties being of the order of 1 or 2 percent. For the last few years, different decay constants have been used by different authors. For example, the two decay constants used for the ^{87}Rb decay differed by 5%. In 1976, an agreement was reached to recommend the use of uniform decay constants (see Steiger and Jäger, 1977: Subcommission on Geochronology: Convention on the use of uniform decay constants in geo- and cosmochronology; EPSL, 36, 359-362).

The recommended constants are:

Uranium: $\lambda(^{238}U) = 1.55125 \times 10^{-10}/y$
$\lambda(^{235}U) = 9.8485 \times 10^{-10}/y$
atomic ratio $^{238}U/^{235}U = 137.88$

Thorium: $\lambda(^{232}Th) = 4.9475 \times 10^{-11}/y$

Rubidium: $\lambda(^{87}Rb) = 1.42 \times 10^{-11}/y$
atomic ratio $^{85}Rb/^{87}Rb = 2.59265$

strontium atomic ratios: $^{86}Sr/^{88}Sr = 0.1194$
$^{84}Sr/^{86}Sr = 0.056584$

Potassium: $\lambda\,(^{40}K_{\beta-}) = 4.962 \times 10^{-10}/y$
$\lambda\,(^{40}K_e) + \lambda'\,(^{40}K_e) = 0.581 \times 10^{-10}/y$
isotopic abundances: $^{39}K = 93.2581$ at %
$^{40}K = 0.01167$ at %
$^{41}K = 6.7302$ at %
atmospheric argon atomic ratio: $^{40}Ar/^{36}Ar = 295.5$

For fission track dating, decay constants that differ by more than 15% are in use (see Chapter by Naeser).

2. Experimental Work

"Would you please determine one or two ages for me?" – this sentence is well known to every geochronologist. Usually, it is much better to refuse. In most cases it needs ten times more data to explain the first two results; and quite often geologists underestimate the effort and the amount of work involved in dating.

But if the geologist offers cooperation to solve a geologic problem by isotopic dating, the geochronologist working in the area will – or should – be willing to accept it. Even if the geochronologist himself is a geologist by training, he needs cooperation with the geologist. The geologist usually knows the area and the geologic problem much better, he should also be willing to do the fundamental geologic and mineralogic work which might be necessary for the interpretation of the data.

The cooperation should usually start in the field, with appropriate sample collection, made by the geologist together with the geochronologist. Both together can best evaluate which sample is suitable for the method to be applied and for the geologic problem to be solved.

It is usually only after the first set of data is available that the more specific samples can be selected. The interpretation of age results must take into consideration all the geologic facts, but age interpretation is only possible if it is based on a clear age pattern. The geologic situation determines the amount of work necessary for such a clear age pattern to evolve. Generally, more than one method should be applied – a few data or just one age mean nothing. This is not quite the same for U-Pb dating. U-Pb data on a suite of zircons isolated from one rock can date two geologic events (see the chapter by Gebauer and Grünenfelder). However, dating a zircon suite is just as time-consuming as several K-Ar or Rb-Sr measurements. Although U-Pb dating allows a certain self control on the open system behavior, it should not be the only method applied in any particular area.

The mineral separation is usually time-consuming and the help of the geologist is often appreciated for this work; but the mineral separation should be done in the geochronological laboratory. Here, the procedures, such as crushing, grinding, sieving, and the different mineral separation techniques, such as heavy mineral separation on shaking tables and with heavy liquids, are done in routine. Further, magnetic separation

and vibration which separates isometric from flaky grains, are used. Crushing, sieving, and especially the grinding needs strong ventilation. Special care has to be taken to avoid cross contamination, cleaning between different samples has to be done very carefully. The geochronologist is usually aware of the memory problem, which is especially critical for zircon dating. Quite often, a small amount of zircon in the order of tens of milligrams has to be hand-picked, isolated from a large amount of rock. If the cleaning of the whole mineral separation equipment is not done very carefully, milligrams of zircon might be recovered from the previous more zircon-rich sample. Especially for Rb-Sr and U-Pb dating, very clean mineral concentrates are required.

If the cooperating geologist is willing to do other experimental work as well as the mineral separation, he will be welcome in many laboratories. He is not required to have experience in the dating methods, but some general experimental experience is recommended.

At least in Europe, universities, national science foundations, and geologic surveys, where dating is done, prefer to provide equipment, laboratories, and expensive machines rather than new posts. Therefore many geochronological laboratories are well equipped, with an over-capacity of laboratory space and machinery. In these institutions, manpower is the bottle neck. Post-doctoral fellows and guest scientists who come with their own problem, own rock samples – and if possible their own money for their stay – are welcome. The K-Ar method is the easiest and quickest method to learn. If mineral separation does not cost too much time, even a person who has first to learn the techniques can produce a considerable amount of data within a few months. For the Rb-Sr and U-Pb methods at least a year is required, if both the chemical preparation and the mass spectrometric measurement have first to be learned.

Since the content of the radioactive isotope is well known, for example ^{40}K in potassium, it is sufficient to analyze the mother element by a conventional technique. Potassium is determined by flame photometry, atomic absorption, X-ray fluorescence and by chemical precipitation. For very low K-contents, in the order of 0.1% or less, mass spectrometry is more precise.

In connection with mass spectrometry, the "isotope dilution technique", described by G.R. Tilton et al., 1957, is commonly applied. With the mass spectrometer, isotope ratios are measured. The isotopic composition of the element to be determined is changed by adding a known amount of highly enriched isotope, which is the less abundant isotope of the element. The enriched stable isotope, usually called "spike", has a function similar to the radioactive "tracer". By measuring the isotope composition of the spike-sample mixture, the concentration of this element in the sample can be evaluated. Thus the isotopic composition of the spike-sample mixture stands for the concentration of the element. Therefore it is sufficient to make an incomplete and impure extraction of the spike-element mixture for the mass spectrometric measurement.

The radiogenic argon is also determined by isotope dilution, by mixing the argon extracted from the sample with highly enriched ^{38}Ar. The fusion of the mineral or rock sample, the mixing of spike and sample argon, and the cleaning of the argon gas has to be done in a high vacuum line, which is directly connected to the mass spectrometer. With the exception of the metal valves, many argon extraction lines are made of pyrex glass, self-constructed. After the assembling of the whole set-up, the method

has to be evaluated, and the characteristics, such as blank and precision, have to be determined. Further, a regular spike and mass spectrometer check is necessary. Relying on the machine, the procedure and the basic data, the argon extraction and the mass spectrometric measurement is to a great extent routine. The argon mass spectrometry is less difficult than the solid source mass spectrometry of Rb, Sr, U, Th, and Pb. These elements with the radiogenic daughter isotopes are usually determined by isotope dilution and mass spectrometry. Only a small number of laboratories determine the Rb/Sr ratio by X-ray fluorescence, certainly a less precise method.

The mineral or rock samples are dissolved, spike solution is added, and simple chemical procedures (ion exchange) are used to isolate the elements for mass spectrometry. Since the amount of radiogenic strontium and lead is small, especially in young samples, the common contribution introduced by chemistry and mass spectrometry has to be kept as small as possible. This demands a very clean chemistry, and many geochronological laboratories are equipped with clean hoods which operate with filtered air. Again, besides spike checks, blank determination, and evaluation of the method, the chemical sample preparation is to a great extent routine.

Solid source mass spectrometers can be bought. In recent time, nearly all mass spectrometers have been attached to computers; the programming is usually done by the geochronologist. Solid source mass spectrometry is never quite routine. It is of great advantage if members of the geochronology team know enough of electronics and computer science for the construction, refinement, and repair of the equipment.

3. Application of the Different Dating Methods: Interpretation of Data

In this chapter some general statements on the interpretation of age data are given. This is a dangerous attempt, and oversimplification cannot be avoided. Although mother-daughter systems of the different dating methods react most sensitively to temperature and fluid phases, they react to all the geological parameters that are generally hidden in the term "grade of metamorphism." Keeping in mind this restriction, we can still say that a crude model of interpretation has evolved from the many data measured in different areas with different geological conditions. Although such an interpretation model cannot be directly applied to a new area, it may help to understand the problems involved in radiometric dating. It may also demonstrate what geochronology can do and which rocks and minerals should be dated to solve a specific problem.

The most resistant clock for measuring geologic time is the U-Pb dating of zircon and also the Rb-Sr method applied to total rock samples. Under dry conditions both methods seem to have similar stability against even high-grade metamorphism. Mobile phases, fluids and anatectic melts, seem to reset Rb-Sr total rock isochrons. For the explanation of Rb-Sr isochron dating, see the chapter The Rb-Sr Method. In acid volcanic rocks, *U-Pb on zircons* may still give the original age, while Rb-Sr total-rock isochrons give younger ages. Zircons are very stable minerals, the most stable ones for radiometric dating. Zircon as a mineral survives weathering, erosion, sedimentation, and often even high-grade metamorphism. In these zircons the U-Pb memory goes back to the primary formation of the crystal. This is due to the fact that two uranium isotopes

are available for dating. The two clocks allow self-control of the open system behavior of U-Pb. In a suite of zircon with variable, even drastic, lead loss, the original age can still be concluded from such data; for detailed information on U-Pb dating, see the chapter by Gebauer and Grünenfelder.

U-Pb zircon dating is successfully applied to the dating of early high-grade metamorphic phases as well as magmatic rock formation. Early high-grade metamorphic events can heal the radiation damage accumulated in zircon, the metamict state, leaving a more resistant zircon population that can better survive a later metamorphism (see the experiments made by Pidgeon et al., 1966). Zircons seem to give the time of crystallization, not a cooling age. The U-Pb system in monazite is also very stable: It can survive high-grade metamorphism. However, if the U-Pb system in monazite is reset by a metamorphic phase that is followed by slow cooling, U-Pb on monazite will date a cooling time with a blocking temperature similar to that of Rb-Sr on white mica (see Purdy and Jäger, 1976).

Following the discussion of Gebauer and Grünenfelder, it does not seem necessary to collect very fresh samples for zircon dating, the requirement being rather a big enough sample, so that zircon and perhaps also monazite can be separated for U-Pb dating. However, this is a dangerous statement, because often more information is wanted and other methods will be applied to other minerals from the same rock – and in this case, weathered samples must be avoided.

On gneisses from the Alps, generally pre-Alpine *Rb-Sr total rock ages* are found. Pre-Alpine Rb-Sr total rock isochrons are found even in the zones of Alpine staurolite, kyanite, and sillimanite. Only in shear zones, especially in gneiss samples from the vicinity of Mesozoic sediments, were Alpine total rock isochrons measured; the grade of Alpine metamorphism in these rejuvenated rocks is much less than in gneisses with pre-Alpine total rock isochrons. Several factors favor the resetting and the rejuvenation of Rb-Sr total rock ages: mobile phases, especially fluid phases at rather low temperatures, further movements, and shearing and crushing, accompanied by recrystallization. Raheim and Berg (1977) report a total rock Rb-Sr isochron that must date a late deformation and crushing event. Rb-Sr resetting of volcanic tuffs, especially water-laid systems, seems to be quite common, even when no metamorphic event can be recognized (Priem et al., 1977).

The Rb-Sr method on total rock samples is often applied to granites. Generally, during magmatic formation, complete Sr-mixing seems to reset the pregranitic age memory. Only a few cases are known for which partial anatexis does not completely extinguish the premagmatic age (Roddich and Compston, 1977; Pankhurst and Pidgeon, 1976). Except for such rare cases with too old ages, the total rock isochron age must be considered as the time at which Rb-Sr migration within the granite body ends. This time might immediately follow the intrusion, when cooling and crystallization stops the material transport within the melt. However, some late magmatic fluid migration might influence the Rb-Sr system.

On rather solid, mica-poor orthogneisses, the premetamorphic granite formation is generally dated by the Rb-Sr total rock method. On homogeneous paragneisses, which are not layered and rather poor in micas (fluid phases) premetamorphic ages can also be found, dating early diagenetic or metamorphic phases of the sediment. For measuring premetamorphic Rb-Sr ages on paragneisses, very big samples, of the order of 100 kg,

should be analyzed. On mica-rich paragneisses with a well-developed schistosity, the data points in the Sr-evolution diagram in many cases scatter around a straight line, with an age similar to that of the mica age.

Chemical inhomogeneities, such as dykes or layers, can enhance Rb, Sr exchange. During metamorphism, complete exchange may occur between individual layers. For the use of such layered rocks to date metamorphic events, see the Chapter by Hofmann. Weathering also has a strong influence on Rb-Sr systems, especially in micas (see Goldich and Gast, 1966). For Rb-Sr dating only fresh samples should be collected, and samples in the vicinity of dykes, fissures, and veins should be avoided. For total rock and mineral dating our experience with a sample size of 30 kg has been good.

In the Central Alps, many *micas* have been dated by the *K-Ar* and *Rb-Sr methods*, further apatites by the fission track method. A very detailed thermal evolution of this area has been established (see Wagner et al., 1977, and front cover of this book). The Rb-Sr system is less stable in micas than in total rocks. Radiogenic strontium expelled from micas is incorporated in Ca-rich minerals such as plagioclase and apatite; it remains in the rock. Thus total rock Rb-Sr ages survive the Alpine metamorphism, but in the same samples young mica ages are found. In the Central Alps, the stability of Rb-Sr and K-Ar systems in micas has been compared to metamorphic isograds or mineral zones (see Purdy and Jäger, 1976). The assumption is that, above a certain temperature, the clock in the mica is reset, the radiogenic daughter being expelled from the host crystal. Only after cooling to the same temperature, is the daughter isotope accumulated. The clock starts to work when the rock cools through a certain temperature, actually a temperature interval. For the theoretical evaluation of cooling ages, see the chapter by Dodson.

For micas from the Central Alps, the following blocking temperatures have been evaluated:

Rb-Sr in muscovite and phengite	500 ± 50°C
K-Ar in muscovite and phengite	350 ± 50° C
Rb-Sr and K-Ar in biotite	300 ± 50°C

The age relations for micas from the Alps are outlined in Figure 1.

As Figure 1 shows, in areas of amphibolite fazies metamorphism, the metamorphic temperature exceeding 500°C, only cooling ages can be measured on micas, with both the Rb-Sr and K-Ar methods. Only in very resistant rocks, Rb-Sr ages on coarse-grained muscovites can survive this grade of metamorphism. During greenschist fazies metamorphism, muscovite and phengite forms below 500°C, probably on the progressive side of the temperature curve, when fluids are still liberated. Thus muscovite and phengite formed by the greenschist metamorphism will directly date the mica formation when dated with the Rb-Sr method. Since biotite is formed above 300°C, it always dates a cooling stage. However, it must be mentioned that the interpretation of mica ages from the greenschist fazies metamorphism is difficult: Argon overpressure and incomplete Sr exchange within the rock sample make the interpretation uncertain. Particularly in low-grade metamorphic rocks, special care is necessary in mineral separation: Premetamorphic muscovite, which preserved its premetamorphic Rb-Sr age, might be intergrown with young phengite. Since the phengite often has a higher iron content, the intergrown mica mixtures show a wide spectrum of magnetic properties. Only after grinding to extremely thin flakes can a good mica separation with meaning-

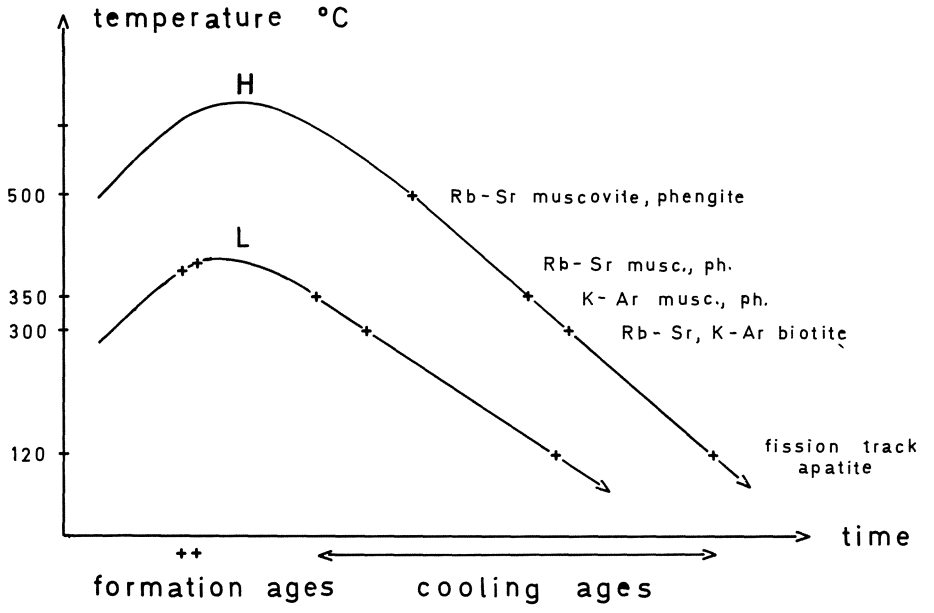

Fig. 1. Interpretation of mineral ages from rocks with low grade and higher grade of metamorphism: formation ages and cooling ages

ful ages be achieved. Generally, in connexion with dating, the white micas should always be analyzed with X-ray techniques for the phengite component and the polymorphs.

The Rb-Sr method has been successfully applied to date sedimentary or diagenetic processes; again, careful mineralogical examination and mineral separation is necessary (see the chapter by Clauer).

The *K-Ar method* can be applied to total rock samples and to isolated minerals to date magmatic, metamorphic, and sedimentation processes. As mentioned above, biotite has about the same blocking temperature, 300°C, for both the Rb-Sr and K-Ar methods. In K-feldspar, argon retention depends on the crystallographic state of this mineral: Sanidin from tuffs seems to preserve the K-Ar age very well, favored by quick cooling. In slowly cooling rocks, argon tends to be lost during microclinization. Therefore the K-Ar method should not be applied to total rock samples of granitic rocks. For basaltic rocks, the K-Ar method has been successfully applied to total rock samples. Gabbroic rocks that crystallize at greater depths often incorporate excess radiogenic argon that has not been degassed during the magmatic stage; they, too, should no be dated by the K-Ar method. Even deep-sea basalts might not be completely degassed: Some glass-rich basalts from the East Pacific Rise with an age of less than 1 m.y. (see Funkhouser et al., 1968) have furnished total rock K-Ar ages of up to 700 m.y. Another process affects the K-Ar ages of submarine basalts, namely, sea water alteration, as described by Ozima et al., 1977.

K-Ar mica ages date cooling stages following the magmatic or metamorphic events. Since phengite forms at temperatures as low as 360°-370°C (Althaus, 1966), even when the K-Ar method is applied to phengitic mica, formation ages might be measured. Amphiboles have a higher retention of argon than micas. Attempts have been made to date the metamorphic phase by dating amphibole (Steiger, 1964). Although technically glaucophane can be dated well by the K-Ar method, excess argon is a serious problem in dating high-pressure metamorphism. Especially under conditions of high-pressure metamorphism, quartz incorporates argon. Two different methods have been proposed for constructing K-Ar isochrons, but none of them seems to be realized. If excess argon is present in the rock, it can be identified by measuring the argon in quartz, but there is no good method to correct for excess argon. For a detailed discussion of the K-Ar method see the Chapter by Hunziker.

The K-Ar method is the most versatile method for dating sediments; the minerals glauconite and illite, especially, are used for K-Ar dating. Both minerals give reliable age results, but only if they are carefully selected by X-ray and chemical analyses (see Odin et al., 1975). Generally, sediment dating should only be done in connection with sediment petrology.

The $^{40}Ar/^{39}Ar$ technique is described in detail by Dallmeyer. The same minerals or total rock samples are dated by the conventional and the $^{40}Ar/^{39}Ar$ techniques. The latter technique seems to have a greater potential for distinguishing between the ideal closed system case, argon loss, and excess argon.

Two contributions, one by Wagner and one by Naeser, deal with *fission track dating.* This method makes use of the crystal damage caused by the spontaneous fission of ^{238}U. For fission track dating the minerals to be used should have enough uranium, as well as a homogeneous uranium distribution. The last requirement is not fulfilled in feldspars and micas. In these minerals, high uranium concentrations are found in single spots and along fissures and cleavage planes. Fission track dating has been successfully applied to apatite, zircon, sphene, and epidote, as well as to volcanic and impact glass. Especially in terranes with rather slow cooling, cooling ages are measrued. The lowest blocking temperature is found for apatite. For Alpine cooling rates of about 50°C per 1 m.y., a blocking temperature of 120°C has been proposed by Wagner and Reimer (1972). Thus, fission track ages on apatite from slowly cooling areas are often much lower than mica ages. From gneisses and granitic rocks, enough apatite can usually be concentrated from a sample size of only several kilograms. Zircon, sphene, and epidote would have higher blocking temperatures, but these minerals present special technical problems in fission track dating. For further information we refer the reader to the chapters by Wagner and Naeser.

Although the Sm-Nd method is not discussed in detail, some remarks on the application of this method are necessary. The Sm-Nd method is based on the α-decay of ^{147}Sm, ($\lambda^{147}Sm = 6.54 \times 10^{-12}/y$). The small fractionation of Sm and Nd, both elements are rare earths, and the long half life limit this method to dating early events. The Sm-Nd method has first been successfully applied to lunar material and meteorites. In a recent work, Hamilton et al., 1977, were able to show that the Sm-Nd method yielded primary total rock ages on volcanics from the Rhodesian greenstone belt. These rocks show alteration and low-grade metamorphism, no reliable Rb-Sr total rock age could be obtained on these samples. The Sm-Nd system seems more stable, less affected by later events.

The Sm-Nd method seems to be a very useful method for dating the early phases in the earth's history.

References

Althaus, E.: Naturwiss. *53*, 105-106 (1966)
Funkhouser, J.G., Fisher, D.E., Bonatti, E.: Excess argon in deep-sea rocks. EPSL *5*, 95-100 (1968)
Goldich, S.S., Gast, P.W.: Effects of weathering on the Rb-Sr and K-Ar ages of biotite from the Morton Gneiss, Minnesota. EPSL *1*, 372-375 (1966)
Hamilton, P.J., O'Nions, R.K., Evensen, N.M.: Sm-Nd dating of Archaean basic and ultrabasic volcanics; EPSL *36*, 263-268 (1977)
Odin, G.S., Hunziker, J.C., Lorenz, C.R.: L'age radiometrique du Miocene inferieur en Europe Occidentale et Centrale. Geol. Rdschau *64*, 570-592 (1975)
Ozima, M., Saito, K., Honda , M., Aramaki, S.: Sea water weathering effect on K-Ar age of submarine basalts. Geochim. Cosmochim. Acta *41*, 453-461 (1977)
Pankhurst, R.J., Pidgeon, R.T.: Inherited isotope systems and the source region pre-history of early Caledonian granites in the Dalradian series of Scotland. EPSL *31*, 55-68 (1976)
Pidgeon, R.T., O'Neil, J.R., Silver, L.T.: Uranium and lead isotopic stability in a metamict zircon under experimental hydrothermal conditions. Science *154*, 1538-1540 (1966)
Priem, H.N.A., Boelrijk, N.A.I.M., Hebeda, E.H., Schermerhorn, L.J.G., Verdurmen, E.A.Th., Verschure, R.H.: Sr isotopic homogenization through whole-rock systems under low-greenschist facies metamorphism in Carboniferous pyroclastics at Aljustrel, Southern Portugal. Lecture ECOG V, Pisa, Italy 1977
Purdy, J.W., Jäger, E.: K-Ar ages on rock-forming minerals from the Central Alps. Mem. Ist. Geol. Min. Univ. Padova. *XXX*, Italy (1976)
Raheim, A., Berg, O., 1977: Open Rb,Sr system behaviour of total-rock samples. Examples from Norway and Tasmania. Lecture ECOG V, Pisa, Italy (1977)
Roddick, J.C., Compston, W.: Strontium isotopic equilibration a solution to a paradox. EPSL *34*, 238-246 (1977)
Steiger, R.: Dating of orogenic phases in the central Alps by K-Ar ages of Hornblende. J. Geophys. Res. *69/24*, 5407-5421 (1964)
Tilton, G.R., Davis, G.L., Wetherill, G.W., Aldrich, L.T.: Isotopic ages of zircon from granites and pegmatites. Trans. Am. Geophys. Union *38*, 360 (1957)
Wagner, G.A., Reimer, G.M.: Fission track tectonics: The tectonic interpretation of apatite fission track ages. EPSL *14*, 263-268 (1972)
Wagner, G.A., Reimer, G.M., Jäger, E.: Cooling ages derived by apatite fission track, mica Rb-Sr and K-Ar dating: The uplift and cooling history of the Central Alps. Mem. Ist. Geol. Min. Univ. Padova *XXX*, Italy (1977)

The Rb–Sr Method

E. JÄGER

1. Introduction

The Rb-Sr method is based on the β-decay of ^{87}Rb which decays to ^{87}Sr with a half life of 48.8×10^9 years. This half-life corresponds to the recommended decay constant (Steiger and Jäger, 1977) of 1.42×10^{-11}/y. In the last years two different decay constants have been used.:

$\lambda (^{87}Rb) = 1.39 \times 10^{-11}$/y and

$\lambda (^{87}Rb) = 1.47 \times 10^{-11}$/y.

Rb-Sr age data which are based on the earlier used decay constants can easily be recalculated according to the age formula:

$$\text{age} = \frac{1}{\lambda} \ln \left(1 + \frac{^{87}\text{Sr rad}}{^{87}\text{Rb}}\right).$$

Recommended isotope ratios:

Rb: 85/87 = 2.59265 Sr: 86/88 = 0.1194

84/86 = 0.056584

In the last years the majority of the laboratories has already used the 86/88 ratio of 0.1194. Although new measurements of the absolute abundance ratios, see Moore et al., 1977, yield a slightly different ratio 86/88, it has been agreed upon further use of 0.1194. The Sr-calculation is not very sensitive to the ratio 84/86 for common Sr. Several laboratories have used a value of 2.591 for $^{85}Rb/^{87}Rb$ instead of the recommended new value of 2.59265, see Catanzaro et al., 1969. Because the recommended isotope ratios are similar to the earlier used values, it is not necessary to recalculate the older data with the new isotope ratios, but recalculation with the new decay constants is necessary.

2. Geochemical Background

Of all dating methods, the Rb-Sr method has the strongest connection with petrology and geochemistry. Rubidium and strontium are rare elements, Rb never forms minerals of its own. The elements Rb and Sr react similarly to K and Ca, therefore the reactions of Rb and Sr trace to some extent the reactions of K and Ca. Especially in granitic

rocks, which are most commonly used for Rb-Sr dating, the elements K and Ca are important constituents which characterize the rock or rock family.

Many more experimental data on the Rb and Sr partition coefficients (see Fung and Shaw, 1978; and Long, 1978) would be necessary for the fundamental understanding of Rb-Sr distribution and redistribution processes. Besides the experimental data, also the many Rb and Sr analyses on isolated minerals may furnish valuable information. In metamorphic terranes, assuming a constant rock chemistry, the phengite component in the white mica is higher under conditions of high pressure metamorphism. Phengite and biotite seem to have similar partition coefficients for Rb and Sr versus the total rock. Thus, in the phengite zone, only a very small fractionation of Rb/Sr in biotite versus white mica (phengite) is found. The fractionation $(Rb/Sr)_{biot.}/(Rb/Sr)_{pheng.}$ ranges from about 0.5 to values of lower than 10. Outside the area of the high pressure metamorphism, in biotite/muscovite pairs a Rb/Sr fractionation of more than 100 has been found.

Of special importance to petrology are the Rb-Sr redistribution processes during metamorphic events. The radiogenic strontium expelled from biotite usually does not leave the rock, it is preferentially incorporated in Ca-rich minerals as apatite or plagioclase. Of all the rock-forming minerals, biotite and phengite have the highest Rb/Sr ratio. Therefore, during rejuvenation, the biotite loses strontium with a high contribution of rad ^{87}Sr, depending on the Rb/Sr ratio in biotite and the pre-metamorphic age. The reactions of this "labeled strontium" within the rock can be traced by mass spectrometric strontium measurements.

The Rb-Sr method is the most versatile method, it can be applied to total rock samples and to isolated minerals, to date magmatic rock formation, metamorphism, and sedimentation, as well as mineral crystallization and different cooling stages, see chapter: Application of the Different Dating Methods, Interpretation of Data. Compared to the U-Pb method, Rb-Sr has the advantage of being applied to the main rock-forming minerals, such as micas and feldspars, to minerals which determine the history of a rock. A zircon suite from a rock might be well dated by the U-Pb method, but the question arises whether this date is connected to the rock formation itself, or whether the age results on the detrital or inherited zircon pre-date the rock formation. As compared to the K-Ar method, the Rb-Sr method has the advantage that the Rb-Sr geochemistry is related to the rock geochemistry. If radiogenic argon is expelled from a mica, accidental facts, such as nearby fissures and fracture zones, determine whether the argon remains in the rock system.

Two facts limit the application of the Rb-Sr method: first the long half life of 48.8×10^9 y, and second the fact that common strontium contains about 7% of ^{87}Sr. Due to the long half life especially in young samples, only a very small portion of the ^{87}Rb has decayed to ^{87}Sr. The small contribution of radiogenic ^{87}Sr is difficult to identify if the sample has a considerable amount of common strontium. Thus, only mineral and rock samples with high Rb/Sr ratios can be dated. The younger the age, the higher this ratio must be. In young, Tertiary rocks, usually only minerals which have the highest Rb/Sr ratios, only biotite and phengite can be dated. According to a decreasing Rb/Sr ratio, the minerals used for Rb-Sr dating can be listed in the following order: biotite, phengite, muscovite, chlorite (when formed from biotite), K-feldspar, which is often similar in its Rb/Sr ratio to the total rock sample – and minerals which

concentrate preferentially Sr against Rb, such as plagioclase, apatite, fluorite, epidote, and garnet.

3. Presentation and Interpretation of Rb-Sr Data

As mentioned above, no mineral or rock incorporates only rubidium and no strontium. Besides the radiogenic ^{87}Sr, there is always a common component of ^{87}Sr. To find the radiogenic ^{87}Sr, the common contribution has to be subtracted from the measured total amount of radiogenic and common ^{87}Sr. For the subtraction of common ^{87}Sr it is necessary to know – or to assume – the $^{87}Sr/^{86}Sr$ ratio of common strontium in the particular sample. Depending on the rock type, the $^{87}Sr/^{86}Sr$ ratio of ocean water strontium or of mantle strontium can be used. There is generally good agreement about these ratios and their growth rate, see the contributions by Hofmann on the *Isotope and Trace Element Geochemistry of the Earth's Mantle* and *Rb-Sr Dating of Sedimentary Rocks* by Clauer.

The assumption of the isotope ratio 87/86 of common strontium in a particular sample introduces an uncertainty. It is much safer to measure the isotopic composition of common strontium. This can be done if several samples incorporate strontium with the same 87/86 ratio. If several total rock samples from one granite body are dated, both the age and the isotopic composition of the incorporated common strontium, the "initial strontium", can be determined. This is best demonstrated by plotting the Rb-Sr data on a Sr-evolution diagram as has been developed by the Bernard Price Institute, see Nicolaysen, 1961.

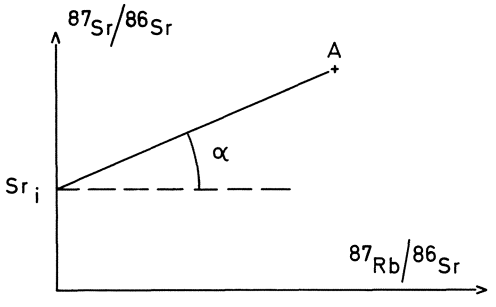

Fig. 1. Sr-evolution diagram with mineral or rock analysis A and initial strontium Sr_i

In this Sr-evolution diagram the $^{87}Sr/^{86}Sr$ ratio is plotted versus $^{87}Rb/^{86}Sr$, see Figure 1. The $^{87}Rb/^{86}Sr$ ratio stands for the geochemical Rb/Sr ratio. Each single age determination represents a point in the Sr-evolution diagram, sample point A in Figure 1. The initial strontium which is the strontium without radiogenic contribution or without rubidium, is located on the ordinate, Sr_i in Figure 1. In this diagram, the age value is proportional to the slope of the straight line which connects sample point A with the position of the initial strontium:

$$\tan \alpha = \frac{^{87}Sr/^{86}Sr \text{ total} - {}^{87}Sr/^{86}Sr_i}{^{87}Rb/^{86}Sr}$$

eliminating ^{86}Sr leaves: $\tan \alpha = \frac{^{87}Sr \text{ total} - {}^{87}Sr_i}{^{87}Rb}$

$$\text{total } ^{87}Sr - {}^{87}Sr_i = \text{rad } ^{87}Sr$$

$$\tan \alpha = \frac{\text{rad } ^{87}Sr}{^{87}Rb}$$

The age equation $t = \frac{1}{\lambda} \ln (1 + \frac{\text{rad } ^{87}Sr}{^{87}Rb})$ can therefore be expressed in relation to the presentation in the Sr-evolution diagram: $t = \frac{1}{\lambda} \ln (1 + \tan \alpha)$.

We can assume, that at time zero of a granite formation, the strontium incorporated in the melt has been mixed and homogenized. The following crystallization started to fractionate Rb and Sr again, the Sr being enriched in the more Ca-rich earlier crystallizing granite or granodiorite. In a granodiorite-granite association formed by differentiation, the youngest granite of the whole series has usually the highest Rb/Sr ratio. Even in one granite body, the Rb/Sr ratio can vary from one place to another, especially from the usually more Sr-rich core to the Rb-rich rim. But the isotopic composition of strontium, which has once been homogenized during formation and migration of the melt, cannot be fractionated any more by any chemical process. Thus, if several samples of one granite should be analyzed immediately after crystallization, they all would contain strontium with the same isotopic composition, the "initial strontium." In the Sr-evolution diagram these samples would define a straight line, parallel to the abscissa. With increasing time, this straight line would turn around the point of the initial Sr, Sr_i in Figure 1. If several samples from one granite body are analyzed by the Rb-Sr method, they usually define a straight line in the Sr-evolution diagram. The initial strontium 87/86 ratio is found by the intercept on the ordinate, the age by the slope of the equal age line – the "isochron." We speak of an "isochron" if the data points deviate from the line only within a certain tolerance. An "errorchron" means scattering of the points around the straight line, the deviation being outside the tolerance limit.

It has already been mentioned that Rb-Sr systems in rocks are much more stable than in minerals. Rock systems are much less affected by later metamorphic events. Partial Sr-exchange can occur at rather low temperatures between adjacent minerals. Even complete Sr-exchange and Sr isotopic homogenization between the different minerals of a rock sample do not require a molten state, but certainly some fluids are necessary for the material transport. Under conditions of amphibolite facies metamorphism, usually complete Sr-homogenization between the different minerals takes place. The only mineral which might resist against Sr-exchange and rejuvenation, is often muscovite, especially the coarse-grained pegmatitic muscovite. If complete isotopic homogenization of strontium should occur within a rock sample, all the

mineral points will again define a straight line in the Sr-evolution diagram. This line has a smaller slope, according to the younger age of the metamorphism. It is quite frequent that Rb-Sr systems in total rock samples survived a later metamorphic event, while complete Sr-homogenization has taken place between the different minerals of a rock sample.

To demonstrate these age relations, the Rb-Sr results on the Rotondo granite from the Central Alps are presented in Figures 2 and 3. This granite belongs to the Gotthard massif, with pre-Alpine rocks metamorphosed by the Tertiary Lepontine phase of Alpine metamorphism. It is situated in the zone of Alpine chloritoid. The Rotondo granite has preserved to a great extent its pre-Alpine structures, in more sheared zones this granite looks like a gneiss, with the Alpine crystallization of phengite. The Rotondo granite is the youngest of a granite family, it is highly differentiated and in itself fractionated with an U, Th-poor core and an U, Th-rich rim, see Rybach et al. (1962).

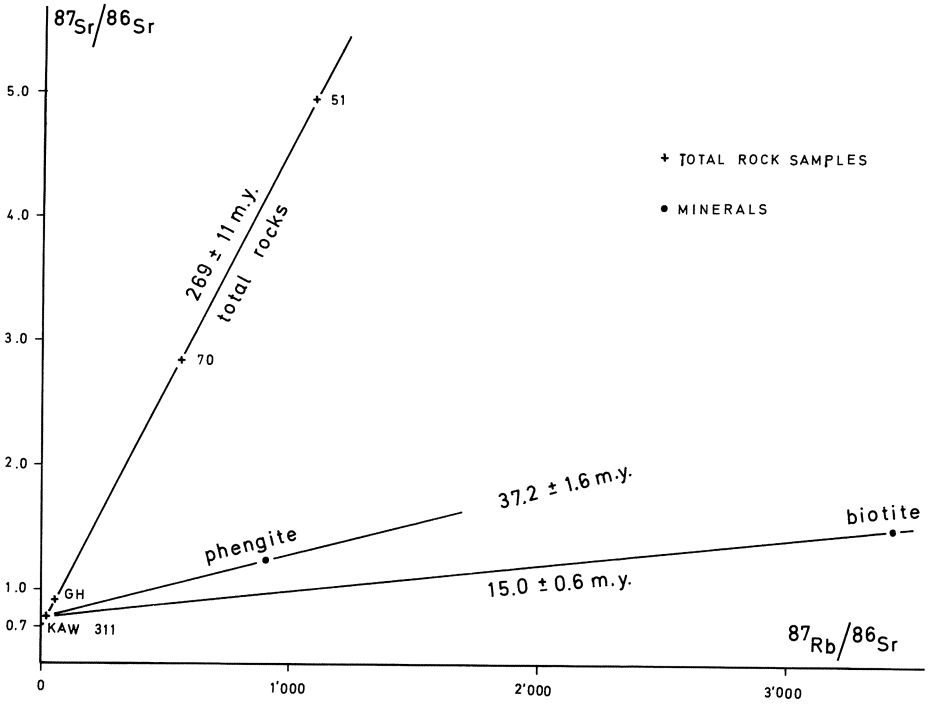

Fig. 2. Sr-evolution diagram for total rock samples and micas from the Rotondo granite, Central Alps

In an earlier paper, Jäger and Niggli (1964) presented Rb-Sr total rock and mineral analyses from the Rotondo granite. They found complete Alpine Sr-homogenization between the minerals K-feldspar, plagioclase and biotite from one rock sample. For the total rock analyses samples in the size of hand specimens have been used. For two reasons this sample size cannot be sufficient for total rock dating: first the Alpine

metamorphism has caused local Rb-Sr re-arrangement, and second the rock is inhomogeneous not only on the large but also on the small scale. The total rock results therefore defined an errorchron, with an impossibly low initial $^{87}Sr/^{86}Sr$ value of 0.685 and an age of 272 m.y. (recalculated with the new constants). The value of the initial $^{87}Sr/^{86}Sr$ is lower than the lowest possible $^{87}Sr/^{86}Sr$ ratio BABI (basaltic achondrite best initial) of 0.69898 ± 3, the primitive $^{87}Sr/^{86}Sr$ ratio on meteorite and lunar material, based on extremely precise Rb-Sr measurements performed at the Lunatic Asylum, California Institute of Technology, see Papanastassiou and Wasserburg (1971). This demonstrates clearly that the earlier published total rock results on the Rotondo granite are based on an errorchron, the Rb-poor samples showing the largest deviation from a straight line.

Therefore, four new total rock samples of 30 kg each have been collected from the U, Th-poor core, where we find the samples with the lowest Rb/Sr ratio. The four samples alone have a rather small spread in their Rb/Sr ratios, they define an isochron of 267 ± 14 m.y., with an initial $^{87}Sr/^{86}Sr$ ratio of 0.7104 ± 0.0017. Together with three earlier published total rock data, the four new samples define an isochron of 269 ± 11 m.y., with an initial 87/86-strontium ratio of 0.7105 ± 0.0012. Within the error limit, the two isochrons are identical. Because of the enormous spread in the $^{87}Rb/^{86}Sr$

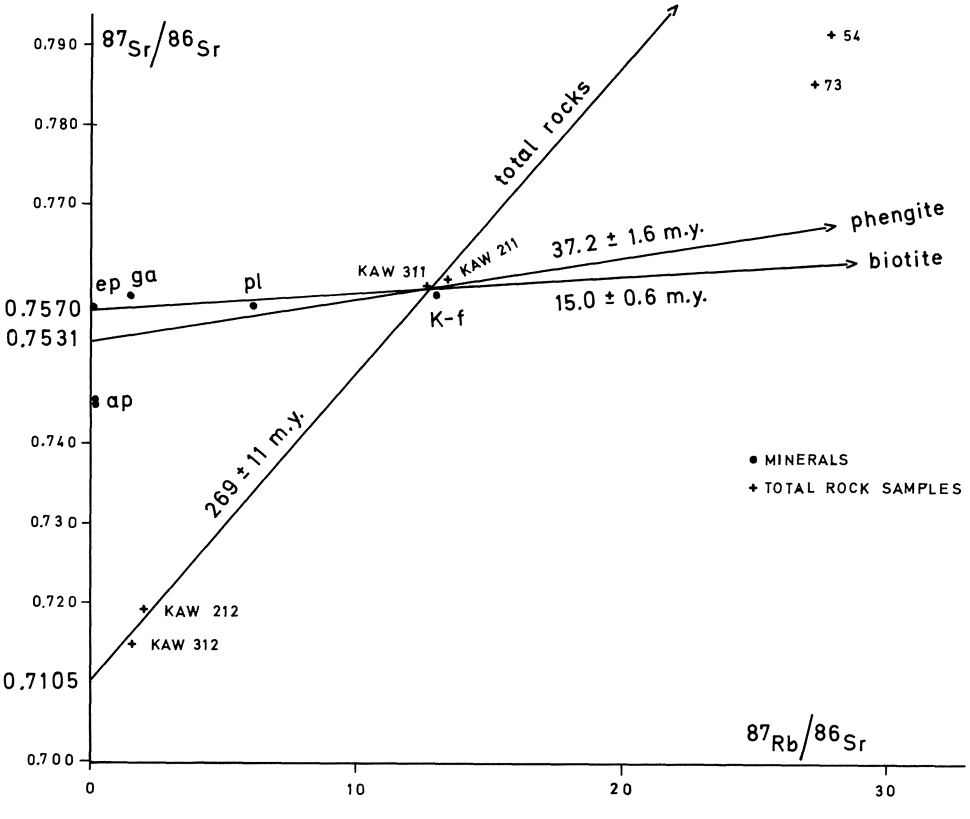

Fig. 3. Sr-evolution diagram, enlarged scale, for minerals and total rock samples from the Rotondo granite; minerals: epidote *(ep)*, garnet *(ga)*, plagioclase *(pl)*, K-feldspar *(K-f)* and apatite *(ap)*

ratios it is impossible to plot all the data on one diagram. Figure 2 shows the results on micas and four total rock samples, Figure 3 the other minerals and total rock samples in a diagram with enlarged scale. The error estimates are max. 2% for $^{87}Rb/^{86}Sr$ and 3‰ for $^{87}Sr/^{86}Sr$. The isochrons have been calculated according to G. Brooks et al., 1972, the errors correspond to 2 σ. The two omitted total rock samples, no. 54 and 73, plot far off the isochron, outside the analytical error. With better rock sampling, a good isochron for the total rock samples has been achieved.

Figure 3 shows clearly that the minerals epidot, garnet, plagioclase, and K-feldspar define an isochron together with biotite, rather than with phengite. The age result of 15.0 m.y. represents a cooling age, this means that all these minerals acted as open systems for Rb-Sr until the closure in biotite, until the time when the regional cooling has reached a temperature of about 300°C. Phengite is an Alpine mineral, formed during the Lepontine phase of Alpine metamorphism. Since phengite is formed below its blocking temperature of 500°C, it dates the time of crystallization. In a detailed study on the meaning of Rb-Sr and K-Ar data on phengite, Steinitz and Jäger (in prep.) were able to show that in a similar grade of metamorphism, the phengite age has to be calculated as phengite–total rock isochron, to yield a meaningful age. This means that during the phengite formation, the strontium within the total rock sample was already homogenized. This is a reasonable assumption, because the phengite must have been formed near the climax of the metamorphism. The result of 37 m.y. fits well to the set of phengite data of 35-40 m.y. found in this zone. This age also corresponds well with the geologic time estimate of the metamorphism, near to the boundary Eocene/ Oligocene.

Interesting are the Rb-Sr results on apatite. Two independent analyses clearly fall off the mineral isochron. Apatite either did not completely exchange the strontium with the other minerals, or it has been disturbed by some later event. The first assumption seems more reasonable. In rocks of similar metamorphic grade, Jäger, Wagner and Miller found by means of fission track dating apatites which still preserve a distinct, U-rich core which is overgrown by an U-poor rim.

The total rock age of 269 m.y. dates the Hercynian granite formation. During the Alpine metamorphism total rock samples of 30 kg behaved as closed systems for Rb-Sr. The enormous spread of $^{87}Rb/^{86}$ ratios from 1.5 to 1100 on total rock samples agrees with the idea of formation form a differentiated melt. The initial $^{87}Sr/^{86}Sr$ of the total rock isochron of 0.7105 ± 0.0012 points to formation from crustal material, or at least some crustal contribution. Of special interest is the comparison with the initial $^{87}Sr/^{86}Sr$-values of the Alpine mineral isochrons. The earlier published mineral isochron of sample GH (Jäger and Niggli, 1964) has yielded an age result of 14 m.y. with an initial $^{87}Sr/^{86}Sr$ of 0.9017. The new mineral isochron with the age result of 15.0 ± 0.6 m.y. on sample KAW 311 gave a lower initial $^{87}Sr/^{86}Sr$ of 0.7570 ± 0.0010, according to the lower Rb/Sr ratio of this rock sample. We can state that in two samples of the Rotondo granite, the $^{87}Sr/^{86}Sr$ ratio has grown from 0.7104 269 m.y. ago to values of 0.7570 and 0,9017 15 m.y. ago. But in the pre-granitic history of the parent material, from the age of the earth to the granite formation, the $^{87}Sr/^{86}Sr$-ratio has grown much less, in the maximum from BABI, from 0.69898 to 0.71, within a time span of more than 4 billion years. This shows that during granite formation, a chemical reaction must have increased the Rb/Sr ratio considerably. Based on this evidence, granite formation by total anatexis of old crustal material can be excluded.

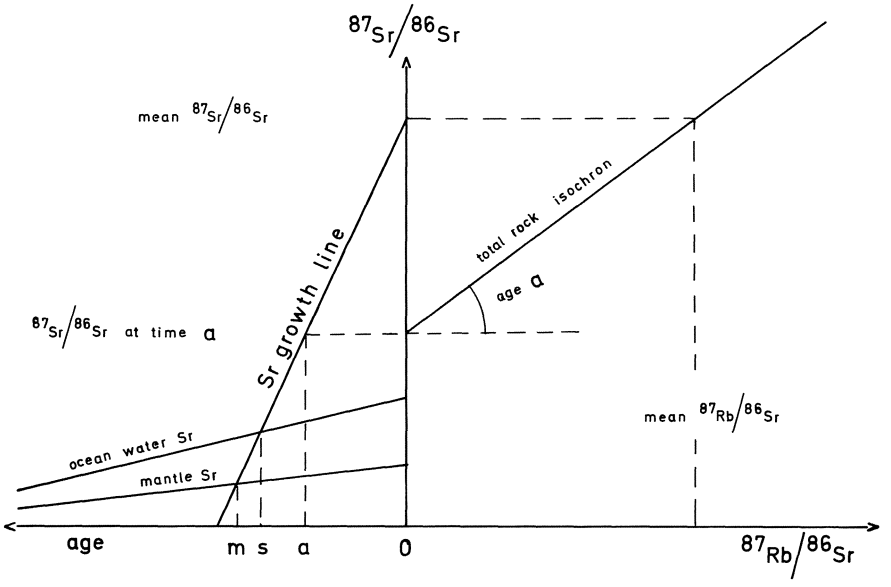

Fig. 4. Sr-evolution diagram combined with a diagram $^{87}Sr/^{86}Sr$ versus time; with growth lines for strontium from the rock body, ocean water and mantle; *m*, age of magmatic rock formation; *s*, sedimentation age; *a*, age of metamorphism or granite intrusion

A more quantitative approach to this problem has been proposed by Hurley et al., 1962, and Faure and Hurley, 1963. Besides Rb-Sr dating of several samples, the mean Rb/Sr ratio for the whole granite body should be analyzed. For this analysis many more samples than the ones used for dating are necessary; further, the sample collection should cover the whole area of the granite. From the mean $^{87}Rb/^{86}Sr$ ratio we can conclude the actual mean $^{87}Sr/^{86}Sr$ ratio of the rock, see Figure 4, as it is situated on the total rock isochron. The initial $^{87}Sr/^{86}Sr$ gives the isotopic composition of strontium at the time when the granite has been formed. The two ratios, the actual mean 87/86 ratio and the initial 87/86 ratio give the growth of $^{87}Sr/^{86}Sr$ of this granite with time. This growth line is plotted in a time versus $^{87}Sr/^{86}Sr$ diagram, see the left diagram of Figure 4. In this diagram also the growth lines for ocean water and mantle strontium are outlined. The mantle $^{87}Sr/^{86}Sr$ ratio is the lowest possible strontium ratio for the source material of the granite. Therefore the intersect of the 87/86 growth line of the granite with the mantle line gives the highest possible age for the granite formation. If the granite has not been differentiated from mantle material, the $^{87}Sr/^{86}Sr$ ratio of the source material must be higher, the maximum possible age of the chemical formation of the granite in this case must be lower. This maximum age of magmatic rock formation, *m* in Figure 4, is meaningful only if the granite body has remained a closed system from time *m* to present. This model of interpretation is still valid, even if internal Rb-Sr redistribution of Sr-homogenization has occurred. Open system behavior from the granite to the country rock makes such an interpretation impossible.

Even orthogneisses can be treated in the same way, with total rock isochrons which represent the age of metamorphism. Again, the interpretation is valid only when the rock has remained a closed system against the outside, even during the metamorphism.

Rb-Sr data on paragneisses can also be treated in the same way. This method is applied to metasedimentary rocks which show Sr-homogenization during a metamorphic phase. In this case the total rock isochron gives the time of metamorphism, the initial $^{87}Sr/^{86}Sr$-value gives the 87/86-strontium ratio at the time of metamorphism. Again, the mean Rb/Sr ratio for the whole paragneiss sequence under consideration has to be measured. The intersect of the $^{87}Sr/^{86}Sr$ growth line of the sediment with the ocean water strontium line will give the time of sedimentation, *s* in Figure 4, if several assumptions are valid:

1) The sediments did exchange the strontium with the ocean water. Detrital material which did not exchange with the ocean water would have a higher $^{87}Sr/^{86}Sr$-value, the measured age would be too old.

2) Sr-homogenization must have occurred during a metamorphic event. This can be checked by Rb-Sr total rock dating.

3) From the time of sedimentation or early diagenesis until the present time, the rock sequence must have remained as a closed system in respect to Rb and Sr against the country rocks. Even during the metamorphism, Rb and Sr should not have been exchanged with other rocks.

The assumption of a closed system behavior of paragneisses seems unrealistic. Grauert (1969) has been able to demonstrate that this interpretation model is very insensitive to changes in the Rb and Sr content, when rocks with relatively high Rb/Sr ratios around 1 are measured, and in cases where the metamorphism is not much older than the sedimentation. In the time – $^{87}Sr/^{86}Sr$ diagram of Figure 4 this would mean, in cases where the slope of the sediment $^{87}Sr/^{86}Sr$-evolution line is very steep and the distance between *s* and *a*, the time difference between sedimentation and metamorphism, very short.

On the European continent the time interval between sedimentation and metamorphism generally seems to be very short. Wherever this method of dating the sedimentation has been applied in Central and Western Europe, maximum sedimentation ages of 600 to 900 m.y. have been found. We can conclude that just one or a few "sedimentation ages" would not mean much; but the concordance of these data from different regions and applied to different rock types must mean that really the early phases in the history of these metasedimentary rocks have been dated.

4. Experimental Procedures, Technical Problems

In this chapter only those techniques and those problems are described which are important and specific for Rb-Sr dating. For Rb-Sr total rock dating the analyzed samples should have a spread in Rb/Sr-ratios. Therefore *rock sampling* is done in two steps: first many small samples in the size of hand specimens are collected and their Rb/Sr ratios determined by any semi-quantitative method such as X-ray fluorescence applied directly to rock powder. The big samples used for dating are collected in a second cam-

paign, selected according to their Rb/Sr ratios. Generally only fresh samples should be used for Rb-Sr dating, the sample size being adopted to the problem to be dated.

Especially for dating young samples, a good *mineral separation* is necessary. As the example of the Rotondo granite shows, the Rb/Sr fractionation between different minerals from one rock can be very high, in the Rotondo granite the Rb/Sr fractionation between the mineral pairs biotite/epidote or biotite/apatite exceeds to 30,000. Thus, a small amount of apatite intergrown with biotite would make the Rb-Sr age determination on biotite impossible.

Quite often different generations of micas show parallel intergrowth. For a good mica separation it is necessary to cleave the micas to very thin flakes. This is achieved by repeated grinding under alcohol, drying, and sieving. Grinding under alcohol keeps the micas cool. Even on extremely thin flakes with grain diameters smaller than 50 μ, no argon loss has been observed. For the separation of feldspars, flaky grains which pass the vibrating tables together with the micas are used. These grains are not intergrown, therefore they yield the better mineral concentrates. Accessory minerals, such as apatite, epidote, and garnet are best recovered from the Wilfley-table concentrates.

On the clean mineral concentrates and final total rock samples, semi-quantitative Rb and Sr measurements are made to find the best mixing ratio between the enriched isotope "spike" (for explanation see the chapter *Introduction to Geochronology: Experimental Work*) and the sample. Highly enriched isotopes ^{87}Rb and ^{84}Sr are commonly used as spike. For the *chemical separation of rubidium and strontium* the samples are dissolved with a mixture of hydrofluoric and perchloric acid or hydrofluoric and nitric acid. Only quartz-glass, teflon, and platinum should be used for the sample treatment. The spike solutions are added to aliquots of the sample solutions. After mixing the spike and sample solutions and evaporation, rubidium can be directly measured at the mass spectrometer. Rb does not need any special enrichment, it shows a high sensitivity for the mass spectrometric measurement which is not disturbed by the presence of other elements. Strontium is usually less abundant in the sample, and much less sensitive in the mass spectrometric measurement. Strontium has to be concentrated before the mass spectrometric measurement, purified especially from rubidium by precipitation of K and Rb-perchlorate, followed by ion exchange separation. Even so, some rubidium is at the beginning always present during the *mass spectrometer measurement.* This small amount of rubidium has first to be evaporated before the stable strontium emission starts. This is necessary because the mass spectrometer does not distinguish between ^{87}Rb and ^{87}Sr. The indicator for Rb is the mass 85, the main isotope of rubidium. One of the most serious problems of mass spectrometry is fractionation due to fractional evaporation. For a difference of two mass units, such as ^{87}Rb and ^{85}Rb, the fractionation of the measured isotope ratios may exceed 1%. Rubidium has only two naturally occurring isotopes, there is no possibility of correcting the measured isotope ratios for fractionation. For precise measurements it is necessary to follow a very strict standard procedure both for standards and samples. Strontium has four isotopes, 84, 86, 87, and 88. The measured 84/86 gives the concentration of strontium in the sample, 87/86 the contribution of radiogenic ^{87}Sr and the ratio 86/88 is used for standardization to the value 0.1194. This standardization allows a correction of the fractionation which occurs during the mass spectrometric measurement. Isotope ratios, standard deviations and the normalizations are calculated during the measurement at the on-line computers.

Several standard minerals have been distributed for *interlaboratory comparison* of Rb-Sr and K-Ar age results. Lanphere and Dalrymple (1965) prepared 1.1 kg of muscovite. This standard, the USGS interlaboratory standard muscovite no. P-207 has been distributed to 55 K-Ar and Rb-Sr dating laboratories. 33 laboratories have reported K-Ar data, 14 institutions also Rb-Sr ages. In 1976, Lanphere and Dalrymple published the final compilation of the K-Ar and Rb-Sr age determinations on muscovite P-207. The reported ages agree quite well, they indicate an average interlaboratory standard deviation of 1.2% for K-Ar ages and 2.8% for Rb-Sr ages. Recalculated with the new constants, the mean K-Ar age for muscovite P-207 is 83.0 m.y. and the mean Rb-Sr age 85.7 m.y. According to the authors this age difference may be due to anomalous composition of common strontium. Although the Rb-Sr ages agree quite well, there are considerable differences in the reported contents of common strontium. Thus, the isotope ratios $^{87}Sr/^{86}Sr$ and $^{87}Rb/^{86}Sr$ show an enormous spread, the reported $^{87}Sr/^{86}Sr$ values range from 0.9940 to 1.103, the $^{87}Rb/^{86}Sr$ data from 198 to 336.

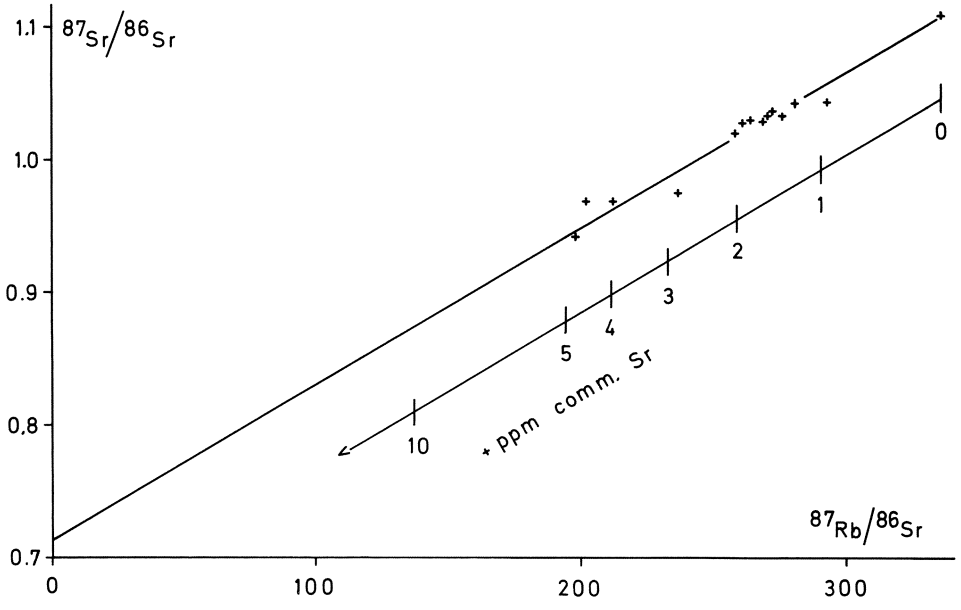

Fig. 5. Rb-Sr data on USGS interlaboratory standard muscovite P-207 presented in the Sr-evolution diagram; each *point* represents the analysis or the mean of the analyses from one laboratory; the *lines* represent the mixture with common Sr

Figure 5 gives the Sr-evolution diagram with the data on the standard muscovite P-207. Each point represents one or the mean value reported from one laboratory. The points scatter around a straight line which represents the mixtures between samples and common strontium. Such a mixing line is indicated in Figure 5, it connects the sample with the smallest content of common strontium to an assumed common strontium with $^{87}Sr/^{86}Sr$ of 0.710, parallel to this line the amount of excess common strontium to produce this spread of data is presented. The amount of excess common

strontium is in the range of 1 to 5 ppm. Based on the data itself, it cannot be decided whether the additional common strontium has a normal or perhaps a somewhat higher ratio $^{87}Sr/^{86}Sr$. This means that the data do not allow to distinguish between excess common strontium due to contamination in the laboratory or inhomogeneous distribution of Sr-rich inclusions in the mica. Wasserburg et al. (1964) were able to show that Sr-contamination in the ppm range occurs with micas if the samples are treated in glassware. Feldspars which are treated the same way do not show this effect. According to Wasserburg et al., some corrosive acid components may remain in the mica residue which is not completely dried after dissolution with hydrofluoric and perchloric acid. These components may leach the glass. Again, the linear array of data points in the Sr-evolution diagram represents a mixing line between the muscovite and common strontium, it should not be mistaken for an isochron.

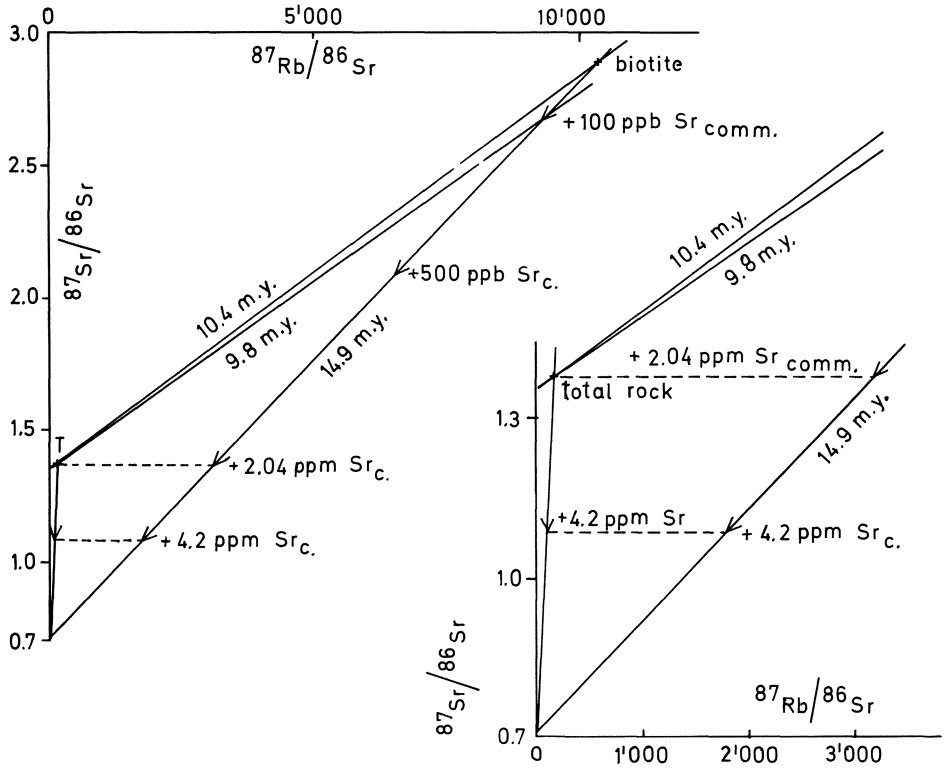

Fig. 6. Sr-Evolution diagram for biotite and total rock from the aplite Chessiturm, Central Alps; reduction of the biotite-total rock age from 10.4 to 9.8 m.y. by contamination with 100 ppb common Sr, contamination with 2.04 ppm comm. Sr reduces the biotite-total rock age to zero m.y. if biotite alone is contaminated, or 4.2 ppm comm. Sr if both the biotite and the total rock samples are contaminated

Contamination with common strontium is a serious *problem in dating young micas.* Only samples which contain much rubidium, being poor in strontium, can be dated.

But these samples are very sensitive to contamination with common strontium. One of the most extreme cases has been published by Wüthrich (1965). For the aplite from the Chessiturm, Central Alps, Wüthrich found a pre-Alpine total rock age and an Alpine biotite-total rock isochron. The experimental data with possible contamination of common strontium are presented in the Sr-evolution diagram, Figure 6. If one assumes Sr-contamination only in the mica and not in the total rock, 100 ppb of common Sr will reduce the age result from 10.4 to 9.8 m.y. If 2.04 ppm of common strontium are added to the biotite, the biotite-total rock age is reduced to zero m.y. If both the total rock and the mica samples are contaminated, it needs 4.2 ppm common strontium to reduce the age to zero. By measuring less sensitive samples from rocks nearby it could be demonstrated, that the 10 m.y. are found on biotite-total rock measurements from the whole area. The last two examples should demonstrate that the dating of extreme samples still offers some technical problems.

References

Brooks, C., Hart, S.R., Wendt, I.: Realistic use of two-error regression treatments as applied to rubidium-strontium data. Rev. Geophys. Space Phys. *10*, 551-577 (1972)

Catanzaro, E.J., Murphy, T.J., Garner, E.L., Shields, W.R.: Absolute isotopic abundance ratio and atomic weight of terrestrial rubidium. J. Res. U.S. Nat. Bur. Stand., Sect. A. *73 A*, 511-516 (1969)

Faure, G., Hurley, P.M.: The isotopic composition of strontium in oceanic and continental basalts; application to the origin of igneous rocks. J. Petrol. *4*, 31 (1963)

Fung, P.C., Shaw, D.M.: Na, Rb and Tl distribution between phlogopite and sanidine by direct synthesis in a common vapor phase. Geochim. Cosmochim. Acta *42*, 703-708 (1978)

Grauert, B.: Die Entwicklungsgeschichte des Silvretta-Kristallins auf Grund radiometrischer Altersbestimmungen. Dissertation Bern, 1969

Hurley, P.M., Hughes, H., Faure, G., Pinson, W.H., Fairbairn, H.W.: Radiogenic Strontium-87 model of continent formation. J. Geophys. Res. *67*, 5315 (1962)

Jäger, E., Niggli, E.: Rubidium-Strontium-Isotopenanalysen an Mineralien und Gesteinen des Rotondogranites und ihre geologische Interpretation. Schweiz. Min. Petr. Mitt. *44*, 61-81 (1964)

Jäger, E., Wagner, G.A., Miller, D.S.: Apatite fission track ages from the Suretta-nappe, Central-Alps (in prep.)

Lanphere, M.A., Dalrymple, G.B.: P-207 – An interlaboratory standard muscovite for argon and potassium analyses. J. Geophys. Res. *70*, 3497-3503 (1965)

Lanphere, M.A., Dalrymple, G.B.: Final compilation of K-Ar and Rb-Sr measurements on P-207, the USGS interlaboratory standard muscovite. US Geol. Survey Prof. Paper *840*, 127-130 (1976)

Long, P.E.: Experimental determination of partition coefficients for Rb, Sr, and Ba between alkali feldspar and silicate liquid. Geochim. Cosmochim. Acta *42*, 833-846 (1978)

Moore, L.J., Barnes, I.L., Murphy, T.J.: The absolute abundance ratios and the atomic weight of a reference sample of strontium. J. Res. U.S. Nat. Bur. Stand., Sect. A (1977)

Nicolaysen, L.O.: Graphic interpretation of discordant age measurements on metamorphic rocks. Ann. New York Acad. Sci. *91*, 198-206 (1961)

Papanastassiou, D.A., Wasserburg, G.J.: Lunar chronology and evolution from Rb-Sr studies of Apollo 11 and 12 samples. Earth Plan. Sci. Lett. *11*, 37-62 (1971)
Rybach, L., Hafner, S., Weibel, M.: Die Verteilung von U-Th, Na, K und Ca im Rotondogranit. Schweiz. Min. Petr. Mitt. *42*, 307-320 (1964)
Steiger, R.H., Jäger, E.: Subcommission on Geochronology: Convention on the use of decay constants in geo- and cosmochronology. Earth Plan. Sci. Lett. *36*, 359-362 (1977)
Steinitz, G., Jäger, E.: K-Ar and Rb-Sr age determinations on phengites from the Suretta-nappe, Central Alps (in prep.)
Wasserburg, G.J., Wen, T., Aronson, J.: Strontium contamination in mineral analysis. Geochim. Cosmochim. Acta *28*, 407-410 (1964)
Wüthrich, H.: Rb-Sr-Altersbestimmungen am alpin metamorph überprägten Aarmassiv. Schweiz. Min. Petr. Mitt. *45*, 875-971 (1965)

Rb–Sr Dating of Thin Slabs: an Imperfect Method to Determine the Age of Metamorphism

A. W. HOFMANN

The isotopic dating of metamorphic events is inherently difficult, because the rise and fall of metamorphic temperature may be very gradual, and the distance over which isotopic equilibrations occurs is not known a priori. One is therefore faced with the following dilemma: if the system chosen for dating is small, e.g., individual mineral grains, isotopic equilibration may continue long after the event of metamorphic crystallization, and the isotopic age reflects some point during uplift and cooling of the terrane. If the system chosen for dating is very large, one cannot be sure that isotopic equilibration ever did occur during the metamorphism. For example, in dating a body of orthogneiss by the Rb-Sr whole-rock method, the geochronologist does not know whether the whole-rock isochron dates the event of the original igneous intrusion, or the event of metamorphism which transformed the granite into a gneiss. If the geochronologist chooses one of these interpretations simply on the basis of the whole-rock isochron, he merely misleads the geologist, who wishes to use geochronological information.

What then is the correct size of the isotopic system for the purpose of dating the metamorphism? In most cases we do not know. The method of whole-rock Rb-Sr dating of thin slabs from a hand specimen of a banded gneiss *may* in many cases be a good compromise between too large and too small. Examples of attempts to date metamorphic events in this manner may be found in papers by Pidgeon and Compston (1965), Krogh et al. (1968), Krogh and Davis (1969, 1971, 1973), Hofmann (1972), Hofmann and Grauert (1973), Grauert (1974), Grauert and Hall (1974). The results of these efforts are promising, but less conclusive than one would wish. For example, in the series of studies of Krogh and Davis, it was discovered that different sequences of thin slabs from the same outcrop yielded significantly different ages. Consequently, this approach does not lend itself to indiscriminate application to any metamorphic rock, as is also true for any other method.

Several theoretical and empirical approaches to the problem appear possible:

1. One may choose petrographic and major chemical criteria to find the *maximum* volume of rocks that reached equilibrium during metamorphism. This may be a reaction zone between a pelitic and a carbonate layer. Major element equilibrium can be checked by microprobe analysis of individual mineral phases (check for uniform composition). If one assumes that the trace elements Rb and Sr had approximately the same kinetic behavior (= range of equilibration), this volume of rock may be chosen for thin-slab dating. This system will then yield a well-defined isochron dating the metamorphism, or it will yield scattered data if the system suffered postmetamorphic disturbance. However, such a disturbance should also be reflected in other chemical data (oxygen isotopes, retrograde reactions).

2. One may choose an outcrop and carry out a large number of Rb-Sr determinations, whereby the size of the system is gradually increased for each series of measurements: if the smallest practical systems, the mineral grains, were affected by postmetamorphic loss of radiogenic daughter isotope, the mineral ages may be concordant or discordant, depending for example on the cooling rate. If one increases the size from the millimeter to the centimeter range of small whole-rock samples, a new concordant age may be found, when concordance is defined as agreement between ages obtained from different parts of the same outcrop. Finally, larger samples (kg size) from the same outcrop or from the entire formation may "look through" the metamorphic event and date some earlier geologic event (intrusion, sedimentation, diagenesis?).

3. Experimental data may be used to estimate a reasonable range of isotopic equilibration. However, convective movement of pore fluids (infiltration) is very difficult to assess quantitatively. Intuitively, one expects an inverse relation between metamorphic temperature and the range of equilibrium due to moving fluids. This is based on the fact that sediments and low-grade metasediments have higher water contents than high-grade metasediments. Many metamorphic reactions involve dehydration of crystalline phases, and large amounts of aqueous solutions are expected to make their way through low-grade rocks. At higher temperatures, the rocks become comparatively dry, and diffusion becomes the effective transport mechanism. Diffusion data are therefore useful for estimating *minimum* transport and equilibration distances in metamorphic rocks. At 700°C, the diffusion coefficient for Sr is probably on the order of $D = 10^5\ cm^2 s^{-1}$ in aqueous solutions (estimated from ionic conductance data, see Fletcher and Hofmann, 1974), $D = 10^{-10}\ cm^2 s^{-1}$ in a granitic melt (measured in obsidian glass; Magaritz and Hofmann, 1978) and $D \cong 10^{-13}\ cm^2 s^{-1}$ in the crystalline phases (estimated from Sr diffusion data in feldspar; Misra and Venkatasubramanian, 1977). These values lead to transport distances of several hundreds of meters, about one meter, and a few centimeters, respectively, if the duration of the metamorphic event is 10 m.y. These distances must be further reduced, especially in the case of diffusion in an aqueous pore fluid, because the effective diffusion coefficient of the rock is smaller than the diffusion coefficient in the fluid alone (melt or aqueous). Assuming local equilibrium between fluid and solid phases, this is given by

$$D_{rock} = \frac{\beta D_{fluid}}{\tau\,[(1-\beta)\,k + \beta]}$$

where β is the volume fraction of the pore fluid, τ is the tortuosity of the diffusion path, and k is the bulk partition coefficient between solid and liquid phases, $k = C_S/C_L$ (for more details, see Hofmann and Magaritz, 1977). Transport distances derived in this manner should only be used as approximate guides to estimate the order of magnitude of equilibration distances for different metamorphic environments. It appears from this that the slab method is most promising in migmatites where the presence of a partial melt has equilibrated the rock over distances of up to one meter.

References

Fletcher, R.C., Hofmann, A.W.: Simple models of diffusion and combined diffusion-infiltration metasomatism. In: Geochemical Transport and Kinetics. Hofmann, A.W., Giletti, B.J., Yoder, Jr., H.S., Yund, R.A. (eds.). Carnegie Inst. Wash. Publ. 634, 1974, pp. 243-259

Grauert, B.: Rb-Sr isotopic study on whole rocks and minerals from the Baltimore Gneiss of the Phoenix Dome, Baltimore County, Maryland. Carnegie Inst. Washington Yearb. *73*, 1003-1007 (1974)

Grauert, B., Hall, L.M.: Rb-Sr isotopic study on small whole-rock slabs and their minerals from the Manhattan Schist, Manhattan Prong, New York. Carnegie Inst. Washington Yearb. *73*, 1007-1010 (1974)

Hofmann, A.W.: Effect of regional metamorphism on the behavior of Rb and Sr in micas and whole-rock systems of the Belt Series, northern Idaho. Carnegie Inst. Washington Yearb. *71*, 559-563 (1972)

Hofmann, A.W., Grauert, B.: Effect of regional metamorphism on whole-rock Rb-Sr systems in sediments. Carnegie Inst. Washington Yearb. *72*, 299-302 (1973)

Hofmann, A.W., Magaritz, M.: Equilibrium and mixing in a partially molten mantle. pp. 37-41; in: Magma Genesis. Proceedings of the Chapman Conference on Partial Melting in the Earth's Upper Mantle. H.J.B. Dick (ed.). Oregon Dept. Geology and Mineral Industries, Bulletin 96 (1977)

Krogh, T.E., Davis, G.L.: Geochronology of the Grenville Province. Carnegie Inst. Washington Yearb. *67*, 224-233 (1969)

Krogh, T.E., Davis, G.L.: Paragneiss studies in the Georgain Bay area 90 km southeast of the Grenville Front. Carnegie Inst. Washington Yearb. *69*, 339-341 (1971)

Krogh, T.E., Davis, G.L.: The effect of regional metamorphism on U-Pb systems in zircons and a comparison with Rb-Sr systems in the same whole rock and its constituent minerals. Carnegie Inst. Washington Yearb. *72*, 601-610 (1973)

Krogh, T.E., Davis, G.L., Aldrich, L.T., Hart, S.R., Stueber, A.: Geological history of the Grenville Province. Carnegie Inst. Washington Yearb. *66*, 528-536 (1968)

Magaritz, M., Hofmann, A.W.: Diffusion of Sr, Ba, and Na in obsidian. Geochim. Cosmochim. Acta *42*, 595-605 (1978)

Misra, N.K., Venkatasubramanian, V.S.: Strontium diffusion in feldspars – a laboratory study. Geochim. Cosmochim. Acta *41*, 837-838 (1977)

Pidgeon, R.T., Compston, W.: The age and origin of the Cooma Granite and its associated metamorphic zones, New South Wales. J. Petrol. *6*, 193-222 (1965)

A New Approach to Rb–Sr Dating of Sedimentary Rocks

N. CLAUER

The Rb-Sr dating method is a classical isotopic method used successfully for many years to date the intrusion of plutonic rocks, the effusion of volcanic rocks, or the recrystallization of metamorphic rocks. The recent application of this method to sedimentary rocks and minerals, since Cormier's first study of glauconites (1956), has been relatively misleading, probably for three reasons:

1) because most of the studies, with the exception of some attempts made on glauconites or separated clay minerals, were carried out on whole rocks;

2) because these studies were made almost without mineralogical control;

3) because the metamorphic history of the sediments was often unknown or disregarded.

In 1966, Bonhomme et al. considered a new approach for dating sedimentary rocks using only the clay minerals. These minerals represent only one silicate fraction of a sedimentary rock which is able to take form, to equilibrate, and to remain stable in the thermodynamic conditions of the earth's surface (Millot, 1964, 1970). This approach requires the understanding of the genesis of the clay minerals, because only those which are "newformed" during the sedimentation, or "transformed" during a period closely following the deposition, could equilibrate their isotopical composition with the environment, and can be used for sedimentary geochronology.

This new approach in using the Rb-Sr method to date sedimentary formations is presented here. The contribution is divided into three parts, the first being a brief review of sedimentary petrography, because this method requires an important preliminary mineralogical study. This review is followed by the demonstration of the method with some examples chosen from well-known stratigraphic sedimentary levels which represent different genesis types of the clays. Finally, the third part is an application of the method to Precambrian sediments.

1. A Brief Review of Sedimentary Petrography

The clay minerals of a sedimentary rock are concentrated in the size fraction smaller than 2 μ, which can be easily extracted (see for example Thiry, 1974). Generally, this size fraction contains only clayey minerals, but others like quartz, calcite, or feldspars can occur in it. Mineralogical control by X-ray diffraction is necessary for the fine fraction smaller than 2 μ to determine the types of the clays and the presence of other minerals.

1.1 The Different Groups of Clays

The clay minerals can be grouped into different families which can be characterized more or less easily by X-ray diffraction (Thorez, 1975). For this, the separated clays are treated with ethylene-glycol, then hydrazine-monohydrate vapors for over 12 h each, and then heated at 490°C for 4 h. After each treatment, the extracted fractions are analyzed by X-rays and the records are compared. The reaction of the clays to these treatments permits their characterization, and allows an estimation of their abundance.

The Mica Group. Illite is the major clay mineral of the mica group. It is a very common clay which has the particular characteristic of being insensitive to the three treatments presented above. Glauconite, which represents an iron variety of illite, is also classified in this group.

The Chlorite Group. Chlorites are also frequent clay minerals. Insensitive to ethylene-glycol and hydrazine-monohydrate treatments, they react variably on heating according to their iron content.

The Kaolin Group. The most frequent mineral of the kaolin group is kaolinite with a first X-ray reflection corresponding to the form [001] near 7Å, where it is sometimes difficult to distinguish from chlorite. Insensitive to ethylene-glycol, kaolinites are unstable on heating. Moreover, kaolinite is modified into dickite or pyrophyllite as soon as diagenesis and slight metamorphism occur (Dunoyer, 1969). Kaolinite is also sensitive to hydrazine-monohydrate vapors: the basic X-ray reflection at 7Å moves toward 10Å, which allows it to be distinguished easily from chlorite.

Kaolinite is a mineral which is generated almost exclusively in weathering profiles on continents (Paquet, 1970). Its presence in a clay fraction is useful for geochronologists because either (1) the kaolinite is authigenic and subsequently the rock is weathered or (2) the kaolinite is detrital and cannot be dated, as it is useless to try to date weathered rocks (see Clauer, 1976).

The Smectite Group. Smectites, also called montmorillonites, represent the family of the "expandable clay minerals". The bonds between the layers of these minerals are weak, which allows water molecules to slip into the structure. The result of this addition of water is a variable periodicity of the layering. The usual treatments will act on these minerals:

- untreated smectites have a periodicity around 14Å;
- ethylene-glycol, which takes the place of the water between the layers, causes expansion and produces a basal [001] reflection at 17Å;
- after hydrazine-monohydrate, this reflection moves from 14Å to 12Å;
- and after removal of the water by heating, the [001] reflection stays at 10Å.

The smectite group is divided into numerous types according to the importance of tetrahedral silicon substitutions by aluminum, the valence and the chemical nature of the octahedral cations, and the nature of the compensating cations in the interlayers. Particulars can be obtained in Millot's book (1964, 1970).

The "Mixed-Layers" Group. The term "mixed-layers" includes a large family of often poorly known clay minerals. A nomenclature review can be found in Lucas (1962, 1968), and Thorez (1975) devoted a large part of this book to these minerals. One can say roughly that these clays have layers of different nature which can alternate regularly or irregularly. The combinations can evidently be multiplied infinitely, but in fact, it seems that the most common types consist in associations of illite and smectite layers or of chlorite and smectite layers.

The Palygorskite Group. The palygorskites, especially attapulgite which will be studied here, represent a group of peculiar clay minerals because they are fibrous and not flat. Their structure, made with jointed laths, generates channels where cations can lodge.

Conclusion. This review is purposely concise. It must, however, be added that these clay minerals are seldom found alone in the size fractions smaller than 2 μ. These fractions are almost always mixtures of two or more components.

1.2 The Different Types of Clay Genesis

Sedimentologists distinguish at present four mechanisms of clay genesis (Millot, 1964, 1970; Lucas, 1962, 1968; Trauth, 1974):

1. The inheritance, which is the mechanical deposit of detrital clay particles removed from continents into sedimentary basins;
2. The newformation, which is the result of a chemical precipitation of ions from sedimentary environment;
3. The transformation, which is the alteration of an original clay mineral into another clay mineral by ion exchange with the environment; this occurs *without* a structure modification (for example a transformation of a flat smectite into a flat illite);
4. The recrystallization, which is also the result of the alteration of an original clay, but *with* a structure modification (for example a recrystallization of a flat smectite into a fibrous attapulgite).

Among these four mechanisms, the first three are used most often to explain the presence of clay minerals in sediments. A recrystallization process has been recently described for the genesis of attapulgite (Trauth, 1974). It must be added here that disagreements between specialists of different "schools" are numerous concerning clay genesis. Thus, most of the American and Soviet specialists think that, with the exception of glauconites, the majority, if not all, of the other clays are detrital, while Millot and his collaborators think that the mechanical deposit remains the common mechanism with the three other possibilities of genesis existing in specific environmental conditions.

The importance of a mineralogical analysis before the geochronological study of a sedimentary formation thus becomes evident. Indeed, it is necessary to know the origin of the clays, since only a portion of them is able to equilibrate in the earth's surface environment.

1.3 Some Useful Laboratory Techniques

With the classical field observations (facies, structures, deformations, schistosities, . . .), mineralogical techniques based on X-ray diffractometry can help to determine the nature and origin of clay minerals. These techniques can be easily used, but can only be applied to illites. Chemical results can also be used to characterize the environment of the clays.

The Illite Crystallinity Index. The width of the diffraction peaks of minerals greater than 100Å depends on the regularity of the net, meaning it depends on the crystallinity of the minerals. Thus a well-crystallized illite has sharp peaks, and a disorderly illite will have, on the contrary, wide and perhaps irregular peaks.

The technique used to determine the illite crystallinity index is the one proposed by Kubler (1966): the width of the [001] peak at half height. Simple, rapid, precise, independent of the height of the peaks, and of the clay slide preparation, this method also has inconveniences. It depends strictly on the experimental conditions, particularly on the chart speed and the time constant of the detector circuits.

According to the values of this index, the illites will characterize the sedimentary or diagenetic zone, the very low-grade metamorphic zone (also called anchizone) or the greenschist facies (or épizone).

The Illite Polymorphs. The illites are essentially represented by two different polymorphs: the types 1M and 2M. The determination method can be seen in Dunoyer (1969).

The 2M polymorph forms only at high temperature. Its occurrence in a sediment can only be interpreted in two ways (1) either the rock is metamorphosed, which must be determined by other criteria, or (2) the rock is unaffected by any recrystallization, which indicates that the illites are detrital. Formed elsewhere, they are liberated on the continent by erosion and weathering, then transported by fluvial processes into a sedimentary basin. The 1M polymorph forms at low temperature and represents an illite variety whose genesis can be the newformation, the transformation or the recrystallization, as previously discussed. Laboratory studies made by Harder (1974) have moreover shown that illite can form at room temperature and pressure from seawater. The two illite polymorphs correspond to two different genesis mechanisms for the same mineral and this double or triple possibility exists for many clays.

Some simple laboratory experiments permit notable differences to be shown in the isotopic behavior of strontium content in 2M and 1M illites. A detrital 2M illite extracted from a Triassic sandstone from the Vosges (France) and a sedimentary 1M illite extracted from a Precambrian shale from Mauritania were identically leached with diluted acid (2.5 N cold HCl for 15 min). The different fractions (untreated illite, silicate residue after leaching, leaching solution) were analyzed at the same time, followed by the analysis of an associated limestone. In the case of the 2M illite, the point of the limestone (carbonate) lies on the line drawn through the three points (untreated illite, residue and solution) of the illite (Fig. 1A). This means, without much detail, that the adsorbed strontium on the illite, which was leached by the diluted acid (solution), is in equilibrium isotopically with the strontium from the interstitial environment

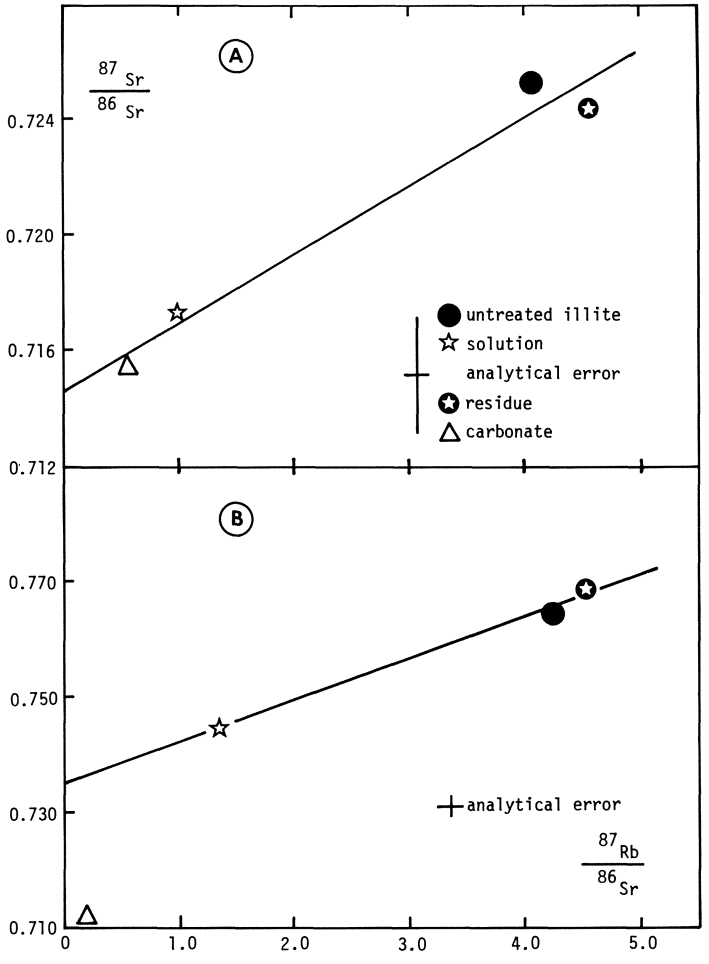

Fig. 1. Effect of leaching by diluted hydrochloric acid (2.5N) on the 87/86 strontium ratio of a 1 M illite and a 2M illite

represented by the strontium from carbonate. This could be shown in several additional examples. In the case of the 1M illite, the point of the carbonate is clearly located below the line drawn through the points of the illite (untreated, residue, solution) (Fig. 1B). The explanation is that here the acid leaching removes not only the adsorbed strontium on the minerals, but also extracts radiogenic strontium 87 from the minerals, which is not evident for the 2M illite. The retention power of the radiogenic strontium 87 is higher for a 2M illite, which has a better crystallinity, thus stronger connections in the interlayer, than for a 1M illite. This difference in the geochemical behavior is an important argument in favor of a sedimentary or diagenetic origin for the 1M illites.

The Amount and Isotopic Composition of Strontium Contained in Carbonates Associated with Clays. All studies and laboratory experiments made on the strontium content

in carbonates show that these minerals behave always, whatever the degree of transformation, as an open-system strontium donor (see references in Clauer, 1974). Therefore, aragonite is very rich in strontium (about 8000 μg/g), primary calcite contains only about 500 μg/g and secondary calcite, dolomite, or marble contain still less (about 100 μg/g). The amount of strontium in carbonates associated with the clays can also be a good control of the state of the chosen sedimentary level.

The strontium in the carbonates is in isotopic equilibrium with the seawater from which it precipitates. During geologic time, the 87/86 ratio of the strontium from carbonates varied systematically and this variation can be followed, especially during the Phanerozoic, by analysis of the $^{87}Sr/^{86}Sr$ ratio of stratigraphically controlled carbonates (see Faure and Powell, 1972). For the Precambrian, the results are fewer. Summarized, the 87/86 ratio of the marine strontium had a value about 0.7055 1000 m.y. ago, a value around 0.7094 580 m.y. ago, then it decreased irregularly to reach 0.7067 during the Oxfordian, only to increase again to 0.7090 in modern seawater. This contribution will show the importance of knowing these values, because on the one hand we know by experience that the strontium contained in metamorphic limestones has almost always 87/86 ratios different than the range 0.7055-0.7090. On the other hand, if clay minerals are formed or modified by ionic exchanges in a sedimentary environment, they contain strontium in which the $^{87}Sr/^{86}Sr$ ratios should theoretically be equal or near the value of the environmental strontium, that is to say the strontium adsorbed on the clays or trapped in the nearby limestones.

1.4 Conclusion

The notions of sedimentary petrography presented here show that clay minerals are divided into families which can be recognized by X-rays, that, except kaolinite which is always detrital, they could have four different origins: inheritance, newformation, transformation or recrystallization, and that finally one type of clay could have several possible origins.

The use of mineralogical criteria like the polymorph type of the illites or their crystallinity index is necessary in a geochronological study of sedimentary rocks, because they allow determination of the origin of the clays. The amount and the isotopical composition of strontium from carbonates are also useful indexes which give information on the state of the chosen sedimentary level: if it is slightly metamorphosed, diagenetic or unaltered by any recrystallization, the values will be different.

It is important to know all this information, with the field observations, before starting any isotopic study, because together they induce the interpretation of the final result.

2. Demonstration of the Method

The reliability of all analytical methods must be demonstrated. The demonstration proposed in this part is based on some examples of sedimentary levels, well defined by

biostratigraphic studies, and chosen on the basis of the origin of the clay minerals they contain.

2.1 Examples of Clays in Recent Sediments

A very complete study made by Dasch (1969) on clays sampled in the Atlantic Ocean has shown that these detrital minerals were not in isotopic equilibrium with the surrounding seawater. Other studies made later gave the same results. However, with sediments from the South Pacific Ocean, it can be shown that smectites and zeolites are now the result of an interaction between basalts and seawater.

A core 20 cm in length was sampled north of the Touamotou Archipelago at 4650 m depth. The surface sediment, 10 cm thick, is a homogeneous brown mud with palagonite, phillipsite, manganese micronodules, and some nontronite (iron smectite). Below this loose sediment occurs an indurated volcano-sedimentary level which evolved at the expense of volcanic material into a rock rich in phillipsite with a small smectitic clay fraction. Between seawater and sediment occur polymetallic nodules whose "hearts" show properties similar to the indurated level: they contain volcano-sedimentary material very rich in phillipsite with smectite. Some samples were leached with diluted acid (HCl, 1N) before isotopic analysis and the three fractions (untreated sample, residue after leaching, leaching solution) were analyzed separately. The results are plotted on Figure 2. The representative points plot along three lines which all have negative slopes. They are obviously mixing lines, since isochrons always have positive slopes in such diagrams. To check if these lines are mixing lines, it is sufficient to plot the points in a [$^{87}Sr/^{86}Sr$; $^{1}/Sr$] diagram (Fig. 3). The points fall again along a line with a negative slope, which means that the strontium 87/86 ratio depends especially on the amount of strontium; the radioactive rubidium 87 has only a negligible effect. The analyzed samples contain a mixture of strontium which is representative of the extreme points of the line shown in Figure 3: modern marine strontium with an 87/86 ratio equal to 0.7090 (intercept of the line) and another strontium with a 87/86 ratio of 0.7045 (residue of the rock 1). If one considers the Eocene age of this material, which was determined by the radiolarian fauna, the last ratio becomes a value of 0.7035, and is characteristic of a basaltic origin.

Figure 4 is a scheme for the interpretation of the results in terms of genesis conditions and geochemical evolution. First of all (Fig. 4.1), newly formed phillipsite traps the strontium directly from weathered basalt ($^{87}Sr/^{86}Sr = 0.7035$) and the rubidium probably from seawater; its representative point moves horizontally as the Rb/Sr ratio increases. At the same time, smectites are generated with a strontium 87/86 ratio intermediate ($^{87}Sr/^{86}Sr = 0.7065$) between the value of the marine strontium and the strontium from the basaltic rocks. The strontium trapped primarily by the smectites is probably a mixture of both. These minerals also trap rubidium and the representative points lie on a second line parallel to the first one. As 87 radiogenic strontium accumulates in the lattices (Fig. 4.2), both lines, which are isochrons, rotate around their intercepts. During the same time, these minerals adsorb more or less marine strontium (Fig. 4.3) and the result is several mixing lines.

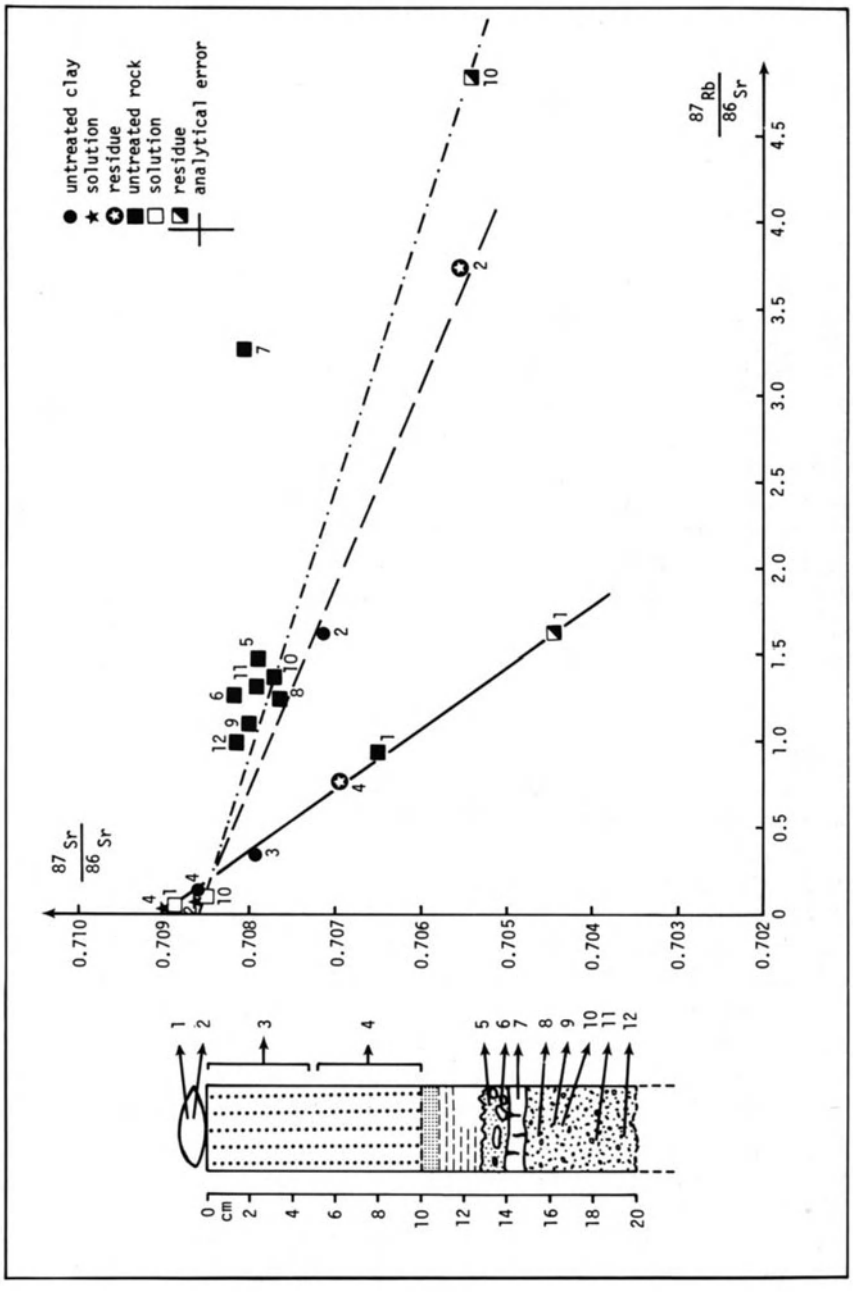

Fig. 2. Bore core of sediments from the southern Pacific Ocean near Touamotou archipelago. [$^{87}Sr/^{86}Sr$; $^{87}Rb/^{86}Sr$] diagram

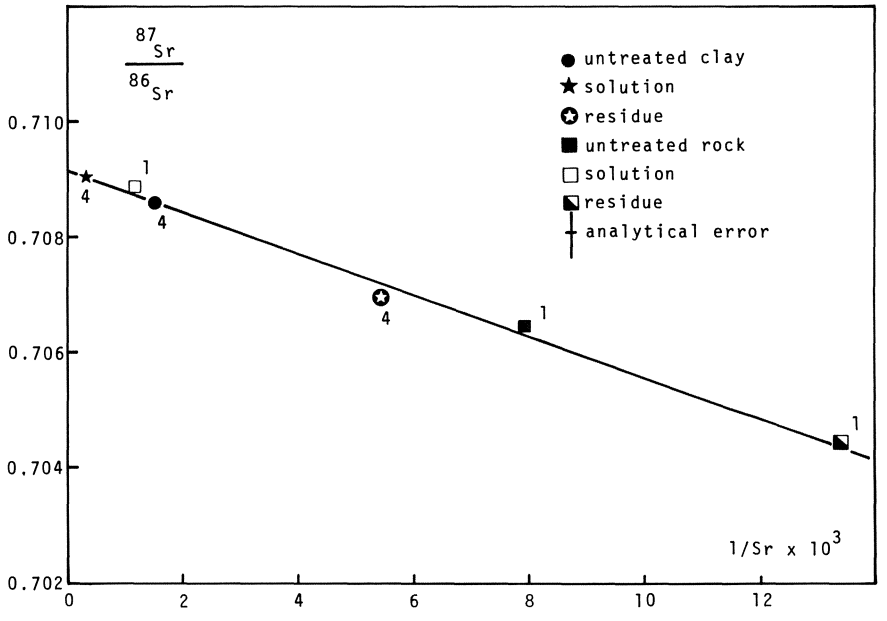

Fig. 3. [$^{87}Sr/^{86}Sr$; $^{1}/Sr$] diagram of the upper sediment from the Southern Pacific Ocean

In conclusion, the different minerals of this sediment from the South Pacific Ocean do not represent residual detrital material, but authigenic material newly formed from basaltic rocks during weathering. It is then possible to find in sediments other clay minerals than glauconites which are authigenic.

It can be added that in the Atlantic Ocean, smectites with the same authigenic origin exist near the Azores Archipelago (Clauer, 1976) and that isotopic analyses of strontium contained interstitial waters of recent sediments show that geochemical exchanges occur between clays and their environment (Clauer et al., 1975). In summary, the study of recent sediments has shown that, even though the majority of the clays now found on the bottom of the oceans and the seas are detrital, authigenic clays can exist, and these minerals can have geochemical exchanges with the interstitial waters.

2.2 Examples of Detrital Clays

The results reported by Dasch (1969) have shown that detrital clays do not equilibrate isotopically with strontium in seawater. A second example to illustrate this isotopic heterogeneity is the study of the clay fraction of Triassic sandstones from the Vosges (France). This clay fraction contains especially 2M illite, most associated with chlorite and sometimes with kaolinite. All these minerals are evidently detrital in sandstones. The analytical points of some of these clays are scattered on an isochron diagram (Fig. 5). This result is the logical conclusion of the preliminary mineralogical study,

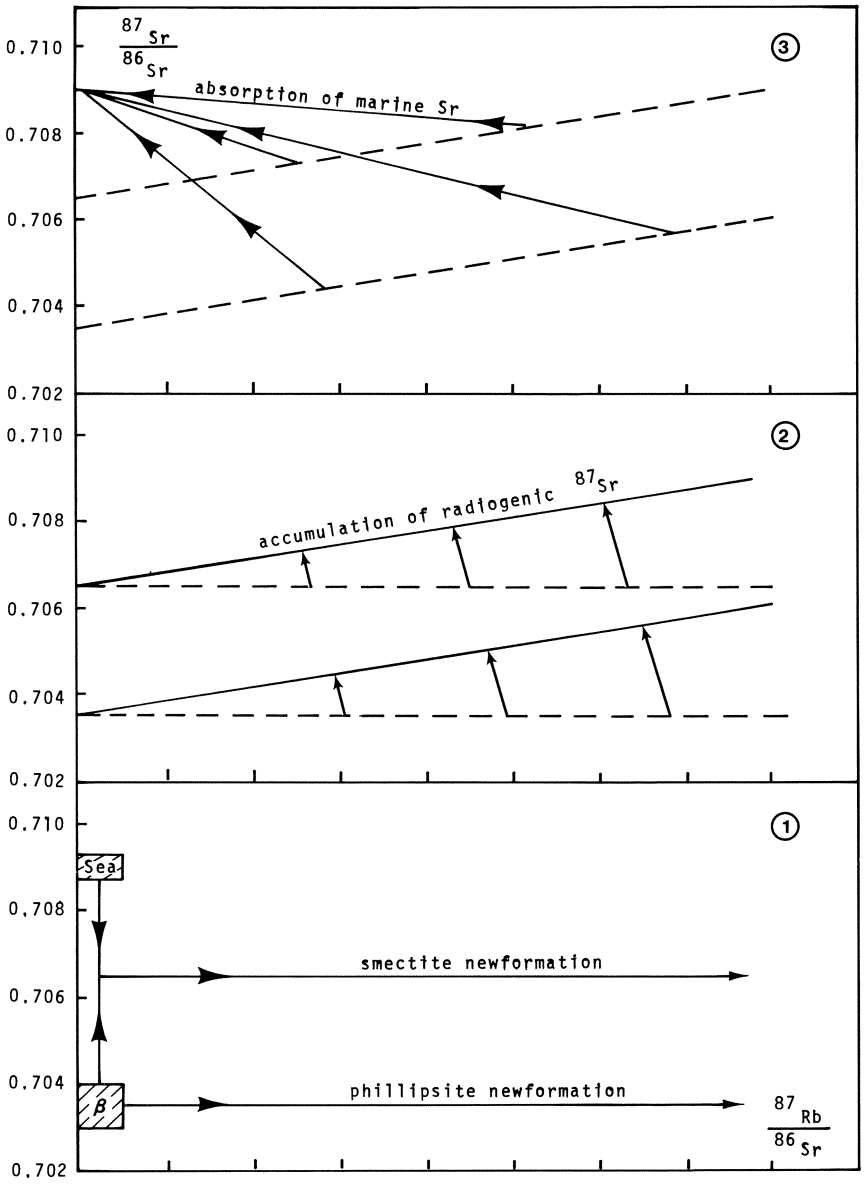

Fig. 4. Interpretative scheme of the results obtained on the sediments from the Southern Pacific Ocean

since the clay fractions contain minerals which are relatively resistant to continental weathering (the illites), minerals which are more sensitive to continental weathering (the chlorites), and finally, minerals which form during weathering (the kaolinites). The isotopic composition of strontium is necessarily erratic.

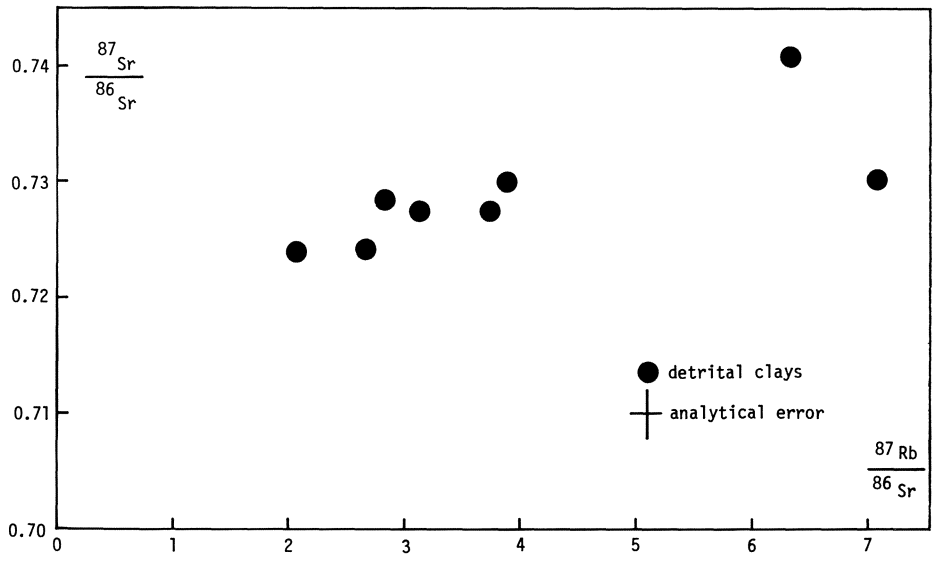

Fig. 5. Fine fractions, smaller than 2 μ, of Triassic sandstones from Vosges (France). [$^{87}Sr/^{86}Sr$; $^{87}Rb/^{86}Sr$] diagram

2.3 Examples of Newly Formed Clays

Glauconites represent the prototype of newly formed clays. Two Turonian glauconites in pellets from Touraine (France) were extracted from clayey chalks, as well as the smectite fraction. Only the line drawn through the points of the whole rock and the two glauconites (Fig. 6) gives an age of 86 million years, which is consistent with the stratigraphy. In this case, the value of the intercept of the line (0.706) is near the value of the 87/86 ratio of the Turonian marine strontium (0.707). The rock is a chalk formed mainly by carbonate with a high common strontium content; and if the glauconite age is in agreement with the stratigraphy, the isotopical composition of the strontium in the glauconites at the time of formation must be identical with the strontium contained in the carbonate fraction of the rock, that is to say with the environmental strontium. The mechanism which causes this identity is the newformation by chemical precipitation. In this case, the point of the smectite does not fit on the isochron: there is no isotopical similarity between the smectite and the glauconites.

In other studies, the age of glauconites is only consistent with the stratigraphy if the 87/86 ratio of their primary strontium is equal to the contemporary marine strontium (Bonhomme et al., 1970; Clauer, 1976). In all these cases there is never an isotopical similarity between the glauconites and the other clays associated with them.

2.4 Examples of Transformed Clays

In the western part of the Basin of Paris, the Lutetian stage begins with a continental level in which a montmorillonite is progressively transformed (modified) into a beidellite;

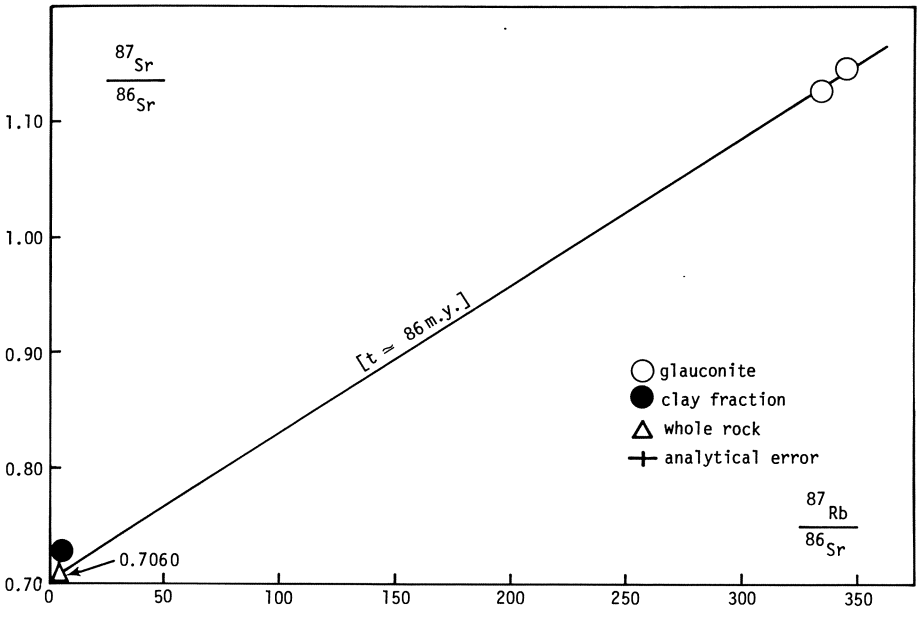

Fig. 6. Turonian chalk from Paris basin (France). [$^{87}Sr/^{86}Sr$; $^{87}Rb/^{86}Sr$] diagram

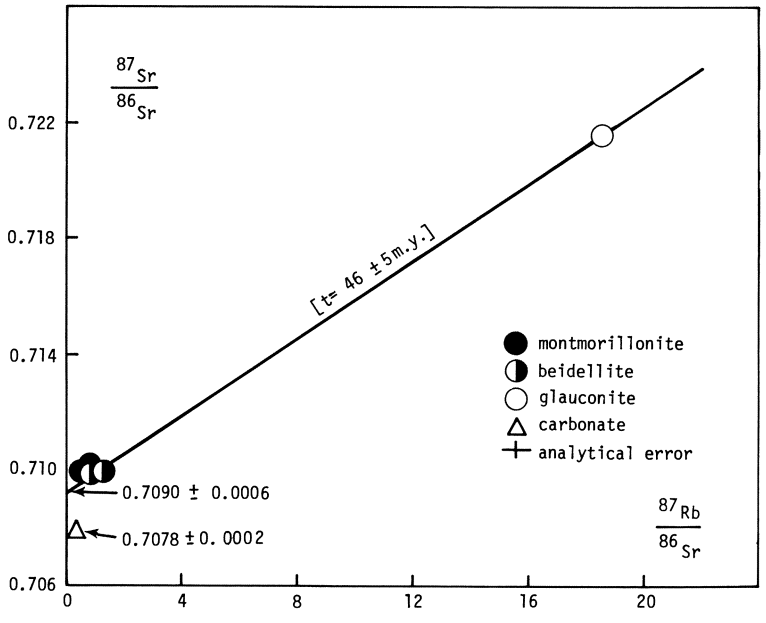

Fig. 7. Lutetian level from Paris basin (France). [$^{87}Sr/^{86}Sr$; $^{87}Rb/^{86}Sr$] diagram

then the sea recovers this continental material and the beidellite, more or less rich in iron, traps potassium to give a glauconite by transformation (Trauth et al., 1969). The representative points of the montmorillonite, the beidellite, and the glauconite fall along a line (Fig. 7). This line, formed by the points of different minerals having the same origin, can be considered as an isochron with an age of 46 ± 5 m.y., which is in agreement with the Lutetian stage (between 39 and 44 m.y.). The intercept of the isochron (0.7090 ± 0.0006) is slightly different than the 87/86 ratio of the Lutetian marine strontium (0.7078 ± 0.0002); this difference is logical since the four analyzed smectites are continental and remain in their environment.

Additional examples of isochrons formed with the points of the rock, the glauconite and the associated clay have been obtained (Clauer, 1976). In all these cases, it can be considered that an isotopical bond exists between the glauconites and the clays, and therefore the intercepts of the isochrons are always slightly different than the value of the 87/86 ratio of the contemporary common strontium. The only mechanism which permits explanation of these observations is the synsedimentary transformation.

Some examples with glauconites have shown that this mineral, like illite or smectite, can have several origins and can generate according to different mechanisms.

2.5 Example of Recrystallized Clays

In the Mormoiron basin (Vaucluse, southeastern France) a continental sequence, without fossils but recovered by Eocene sediments, begins with sands, followed by a heterogeneous level with kaolinite, illite and smectite, a clayey horizon called terre à foulon with smectite and attapulgite, and finally a limestone with attapulgite. Trauth (1974) showed that the smectites from the terre à foulon level were derived from the detrital smectites located below in the heterogeneous level by a transformation mechanism. This author also showed that the attapulgites from the terre à foulon level were derived from the same detrital smectites of the heterogeneous level by a recrystallization mechanism.

Ten different fractions of this sedimentary sequence have been analyzed: two detrital smectites of the heterogeneous level, two transformed smectites, two mixtures of smectite and attapulgite, three attapulgites of the terre à foulon horizon and finally, the carbonate fraction of a representative rock of the lacustrian environment. The points of all these clays fit along a line (Fig. 8) with an age of 59.1 ± 1.4 m.y. and an intercept of 0.7089 ± 0.0004. This age is in good agreement with the stratigraphy, since these azoic sediments are covered by dated Eocene. The line is probably an isochron whose points represent detrital, transformed, and recrystallized material dating the end of the smectite transformation and the end of the attapulgite recrystallization. As in the case of transformed glauconites, the value of the intercept of the isochron is slightly different from the 87/86 ratio of the environmental strontium: 0.7089 ± 0.0004 and 0.7077 ± 0.0002, respectively.

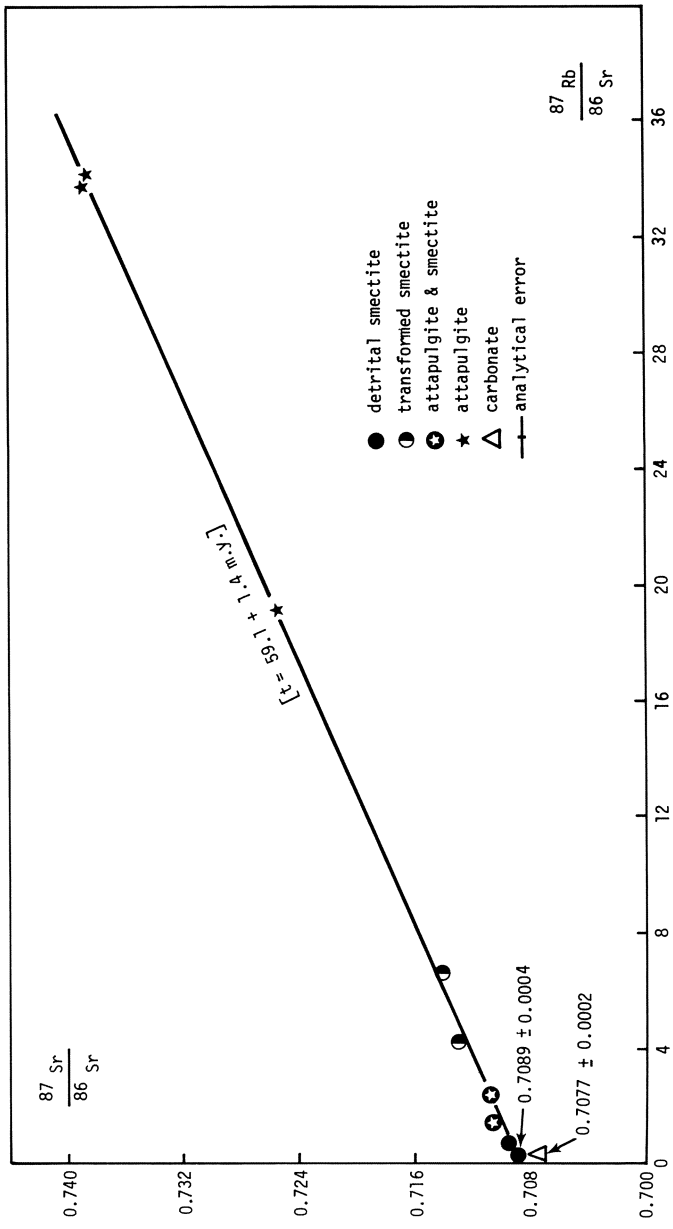

Fig. 8. Tertiary sedimentary sequence from Mormoiron basin (France). [$^{87}Sr/^{86}Sr$; $^{87}Rb/^{86}Sr$] diagram

2.6 Conclusion

The demonstration of the Rb-Sr method for dating clay minerals from sedimentary levels shows clearly that the strontium isotopic homogeneity, or its heterogeneity, depends on the genesis mechanism:

1. If this mechanism is inheritance, the minerals are heterogeneous and useless for dating. In all other cases they are homogeneous, which satisfies one of the necessary conditions for dating.
2. If this mechanism is newformation, the homogeneity of the strontium is acquired between the minerals themselves and between the minerals and the environment, because the strontium, like the other elements, comes directly from the environment.
3. If this mechanism is transformation, the isotopical homogeneity occurs during the modification of the original mineral. The isotopical composition of the primary strontium of the new mineral is then slightly different from the environmental strontium.
4. At last, if this mechanism is recrystallization, the new mineral seems to use the strontium obtained directly from the parent-mineral. This strontium also has an isotopic composition slightly different from the environmental strontium.

It must be remembered that a clay mineral does not correspond to one genesis mechanism. This is the case not only for illites and smectites, but also for glauconites and probably for attapulgites.

3. Application of the Method

In the previous chapter the mineralogical and geochemical criteria presented in the first chapter have only been used a few times, because the examples were chosen as a function of the *known* clay genesis. These criteria became necessary in the routine application to determine this genesis mechanism. Obradovich and Peterman's study (1968) on glauconites from the Precambrian Sun River Formation in the USA is moreover an interesting example to introduce this chapter. Indeed, Figure 9 shows that the carbonate plots on the isochron drawn through the glauconites: an isotopical homogeneity exists between the environment, the carbonate and the glauconites at the time the system became closed. However, the error of the isochron intercept does not allow recognition of the distinct genesis mechanism. What is then important is the comparison between the value of the isochron intercept and the 87/86 ratio of the environmental strontium, which can be found in the literature, and the use of other criteria like those proposed above.

3.1 Dating of Sedimentary Levels

In Mauritania (Western Africa), the Precambrian sedimentary sequence rests on an old basement and contains many shaly horizons. Some of these levels have been selected for geochronologic study. The results obtained on three of them: I_2, I_5 and I_6 (nomen-

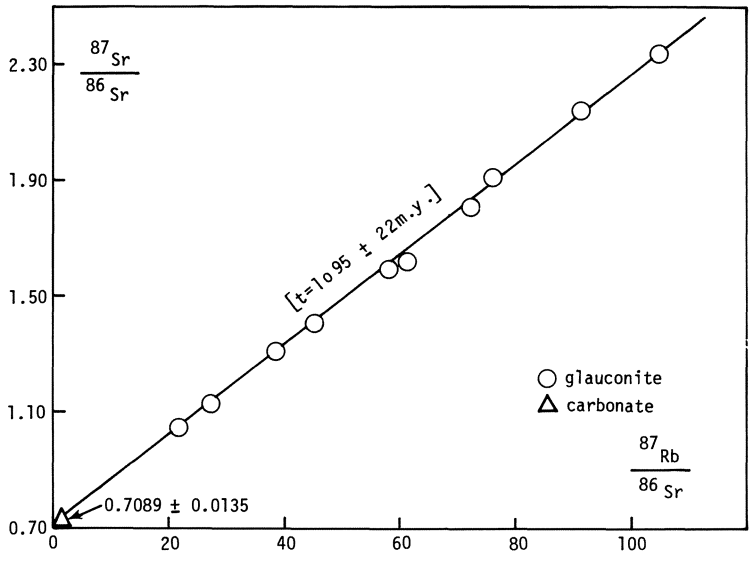

Fig. 9. Precambrian Sun River sequence from Montana (USA) after Obradovich and Peterman (1968). [$^{87}Sr/^{86}Sr$; $^{87}Rb/^{86}Sr$] diagram

clature and description in Trompette, 1973), located respectively about 250, 500 and 600 m above the base of the sequence, are presented here. Most of the clay fractions contain a mixture of illite and smectite. The illite, sometimes pure, is always present as the 1M polymorph and its crystallinity index is always characteristic of the sedimentary domain. With the X-ray diffraction equipment available, the limit between the sedimentary zone and the very low-grade metamorphism is located at an index of 5.75, while the values for the illites of the I_2, I_5, and I_6 levels range between 6.0 and 9.7. In the two lowest levels, the associated dolomites contain respectively 60 μg/g and 153 μg/g strontium, which are consistent with the nature of the carbonate. The calcite of level I_5 contains 337 μg/g strontium, which allows consideration of a primary origin of this mineral.

For the three levels, the isochrons drawn through the points of the clay minerals contain the associated carbonates (Fig. 10). Furthermore, the intercept of the isochrons agree with the values of the 87/86 ratios of the common strontium for the Upper Precambrian: the intercepts lie between 0.7071 and 0.7088, while the limits of the $^{86}Sr/^{87}Sr$ are at 0.7055 1000 m.y. ago and at 0.7094 580 m.y. ago. The ages obtained for each isochron decrease logically from the bottom to the top of the sequence; one can thus consider that these isochrons represent the result of early isotopic homogenizations and that the ages can be related to the sedimentary epochs.

Some points of clay minerals are, however, below the isochrons: one clay for the I_2 level and three for the I_6 level (Fig. 10). These clays have been extracted from the rocks with diluted hydrochloric acid, which is always necessary for carbonate rocks. In a previous chapter, a lab experiment has shown that diluted acid carries radiogenic 87 strontium out of 1M illites. These points below the isochrons are supplementary proofs in favor of a sedimentary origin for these illites.

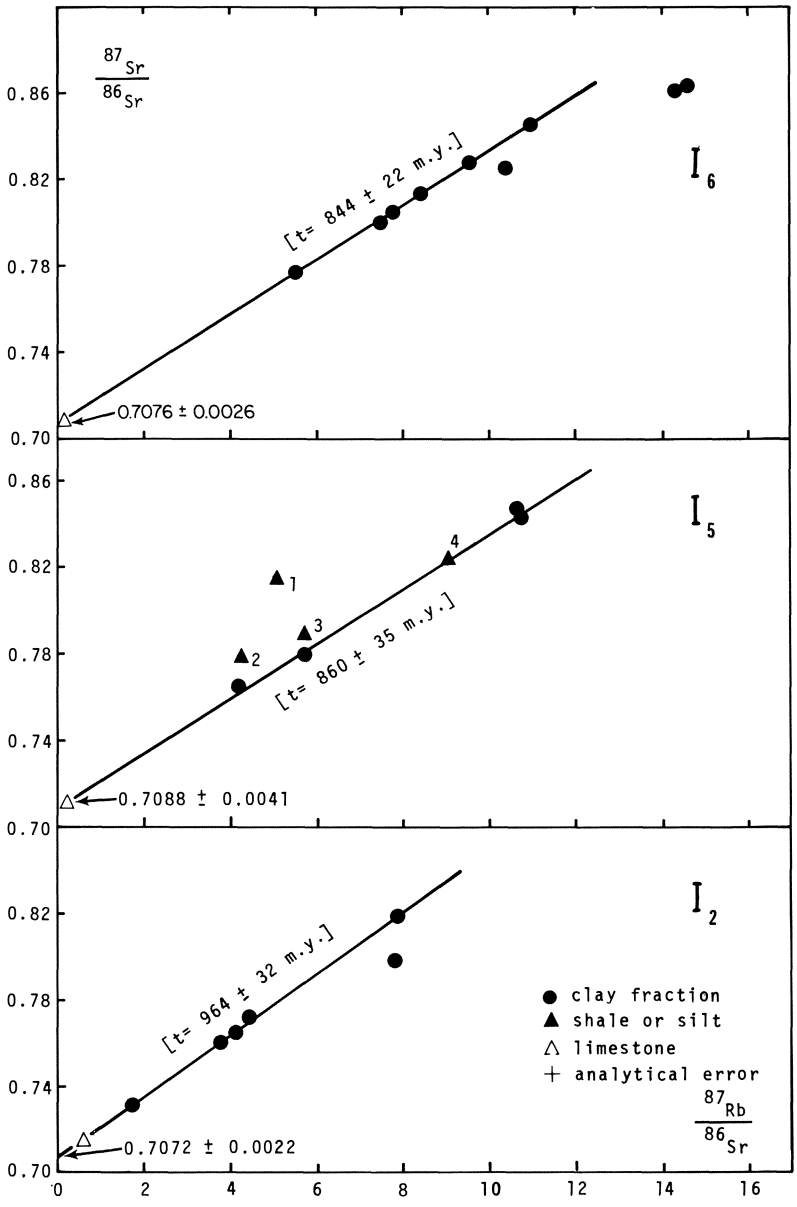

Fig. 10. I_2, I_5, and I_6 levels of the Upper Precambrian sequence from Mauritania. [$^{87}Sr/^{86}Sr$; $^{87}Rb/^{86}Sr$] diagrams

The whole rocks have seldom been mentioned in this contribution up to now. The study of four more or less silty rocks from I_5 level seems significant enough. X-ray studies have shown that the rock 1 contains around 15% detrital microcline; in the two rocks 2 and 3, the microcline is also present, but only in trace amounts, while the

last one, 4, does not contain any microcline. The three rocks with microcline, 1, 2, and 3, lie above the isochron (Fig. 10); the one without, 4, plots on the isochron. The presence of detrital material in a sample induces analytical scattering (see the paragraph devoted to this subject) and abnormally high $^{87}Sr/^{86}Sr$ values owing to the presence of inherited radiogenic strontium 87. In summary, the study of whole rocks is advised against, because they often contain detrital minerals which can mask the isotopic homogeneity of other minerals.

In conclusion, dating of sedimentary formations is possible if one studies shaly levels. The ages obtained from the clays and the associated carbonates, if they are checked by mineralogical and chemical criteria, correspond to early isotopical homogeneities related to the times of deposition.

3.2 Dating of Diagenetic Levels

Buried sediments can undergo diagenetic modifications having a thermal or chemical origin. To illustrate this case, another horizon from the Upper Precambrian sequence of Mauritania has been studied: the CO_3 level located about 1700 m above the sequence base. The lowest part of this level is formed by a siliceous shale, which is covered by a soft turquoise-green shale (Trompette, 1973). The clay fraction of the samples from the lowest part contains a mixture of illite and chlorite. The crystallinity index, between 6.5 and 7.8, characterizes a level unaffected by any metamorphic recrystallization; the limit between the sedimentary and the anchimetamorphic domain lies at 5.75 with the equipment available here. In the uppermost soft shale, the clays are mixed-layers with crystallinity indexes ranging between 9.8 and 14.3, values higher than those found for the illites of the lowest siliceous part. These mixed-layers are less evolved than the clays found in the lowest part.

The representative points of these clays fit into two lines according to their mineralogical composition (Fig. 11). The clays from the lower siliceous level fit a first line, with two calcites, which has an intercept of 0.7136 ± 0.0021. Eight of the ten mixed-layers from the upper soft part fall around a second line, with a baryte, with an intercept of 0.7102 ± 0.0052. Finally, two points are scattered between the two lines. The upper line can be considered as an isochron resulting from the early homogenization of the mixed-layers. Additional support is provided by the intercept of the isochron which remains close to the 87/86 ratio of the common contemporaneous strontium. This ratio was 0.7094 ± 0.0005 580 m.y. ago. The lower line is probably the result of a late geochemical diagenesis of the clays extracted from the siliceous shale. This diagenesis, probably related to the devitrification of volcanic glass found by microscopical study in this part of the sequence, modified the mineralogy, the chemistry and the isotopical equilibria of the original sedimentary clay minerals. It also induced the recrystallization of the calcite which contains only 208 μg/g of strontium with a 87/86 ratio of 0.7135 ± 0.0020, higher than the value given above for the common strontium. The clays register distinctly the late influence by their mineralogical and isotopical composition, thus it is probable that the remobilization was complete, and that the calculated age corresponds to the end of the late diagenesis.

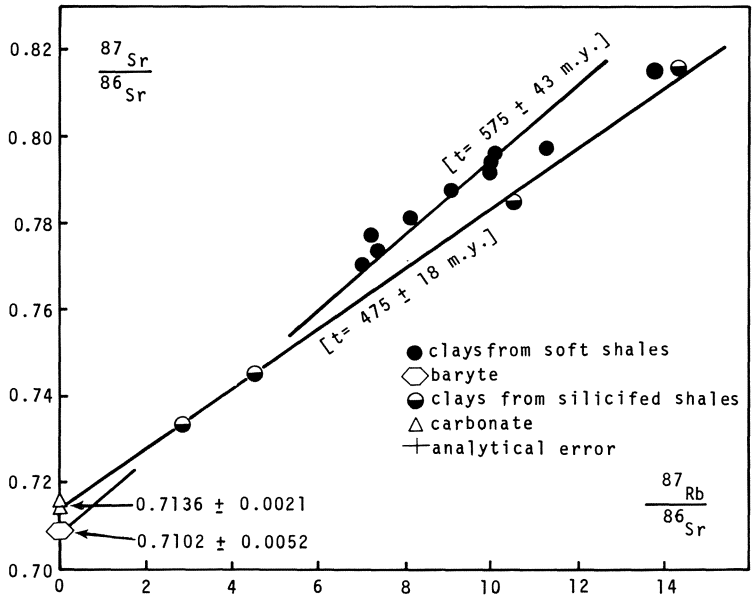

Fig. 11. CO_3 level of the Upper Precambrian sequence from Mauritania. [$^{87}Sr/^{86}Sr$; $^{87}Rb/^{86}Sr$] diagram

It must be pointed out in this example of a late diagenetic modification of clays, that the normally used mineralogical criteria have not permitted differentiation of the sedimentary minerals from those of diagenetic origin. Sedimentary associations of illite and chlorite, here of diagenetic origin, have been found elsewhere in the Mauritanian sequence. The distinction between sedimentary and diagenetic clays was only possible with the value of the isochron intercept, which clearly becomes higher than that of the 87/86 ratio of the common strontium. This difference has been confirmed by other examples of diagenetic material (Clauer, 1976).

3.3 Dating of Slightly Metamorphosed Levels

Numerous studies made on slightly metamorphosed sediments have shown that from the anchizone (or very low-grade metamorphism or zeolite facies) the clay minerals record the effects of the metamorphism and lose their previous memory. This can be illustrated by an example chosen in the Precambrian II which crops out in the Moroccan Anti-Atlas. The fine fraction of these rocks, which are sericitic schists and hematitic schists, contains a mixture of illite, chlorite, and mixed-layers. The values of the illite crystallinity index range between 4.0 and 2.7, the values are around the limit between the anchizone and the épizone (or limit between the prehnite-pumpelleyite facies and the greenschist facies), which is situated at a value of 3.6 with the equipment available here. In this domain, the illite polymorph is normally of 2M type. The formation studied

here does not contain limestones, but in a neighboring level of the same sequence, calcite contains 72 μg/g strontium. This amount is consistent with a metamorphic recrystallization.

The fine fractions, except one, and some whole rocks give an isochron with an age corresponding to the tectono-metamorphic event which affected the sequence (Fig. 12). In this case, the value of the isochron intercept is abnormally high: 0.7134 ± 0.0026.

The geochronological study of whole rocks is not suitable even in slightly metamorphosed sedimentary formations. Indeed, the scattered representative points of the whole rocks above the isochron (Fig. 12) indicate that incompletely homogenized detrital material remains in these rocks.

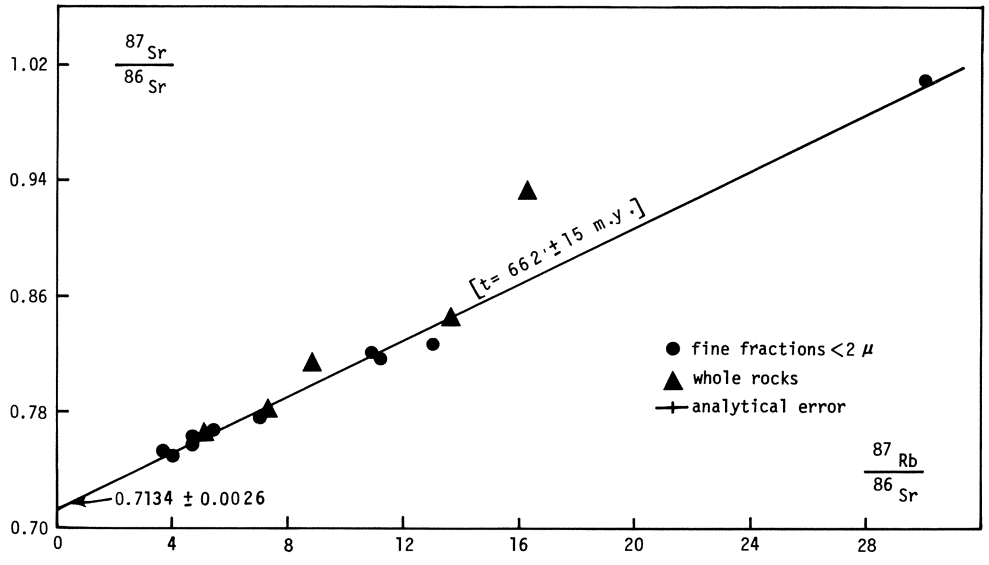

Fig. 12. Precambrian II from the Bou Azzer window, Moroccan Anti-Atlas. [$^{87}Sr/^{86}Sr$; $^{87}Rb/^{86}Sr$] diagram

Conclusion

Rb-Sr dating of sedimentary rocks could be possible from the following propositions:

1. to avoid the study of whole rocks which contain too often detrital minerals other than clays, especially feldspars;

2. to separate the clay minerals of shaly levels, studying their mineralogy to determine their origin: with detrital clays no dating is possible, but it becomes possible with newly formed or transformed (modified) or recrystallized clay minerals in the sedimentary basin;

3. to interpret the final result by combining the clay mineralogical (illite polymorphs and crystallinity index), the carbonate chemical (strontium amount) and the isotopical (value of the isochron intercept) studies.

If the mineralogical study indicates that the clay minerals are of sedimentary origin and that the value of the isochron intercept is near the 87/86 ratio of the contemporary strontium, then the homogenization was early and can be assumed as the age of the sedimentary epoch. If the minerals are always of sedimentary origin, but if their primary strontium has an 87/86 ratio very different from the common strontium contemporary with the sedimentation, then the homogenization was diagenetic and late with regard to the time of deposition. Finally, if the mineralogical study points out the existence of a metamorphism, even of a very low grade, the 87/86 ratio of the primary strontium in the carbonates and the micaceous minerals must be different from the 87/86 ratio of the common strontium. In this case, the obtained age is characteristic of the time of metamorphism.

Acknowledgments. I thank Professor E. Jäger and Dr. J. Hunziker for their invitation to collaborate at a seminar in Isotope Geology which they organized at Bern University during March, 1977. My sincere thanks also to C.D. Nardone, who kindly polished the English translation, to K.S. Tyler, who drew the figures, and to E.H. Baird, who typed the text, all at The Ohio State University, Columbus, Ohio.

Note. No analytical results and only a few references are purposely given in this contribution. The analytical results and broader discussion of most of the examples presented here, as well as a more complete bibliography, can be found in Clauer's book (1976). The English translation of some references are available and given below.

References

Bonhomme, M., Lucas, J., Millot, G.: Signification des déterminations isotopiques dans la géochronologie des sédiments. Actes du 151^{e} Coll. Int. C.N.R.S., Nancy 1965, 1966, p . 541-565

Bonhomme, M., Clauer, N., Odin, S.: Résultats préliminaires de datation rubidium-strontium sur des sédiments glauconieux dans le Paléogène d'Angleterre. Bull. Serv. Carte Géol. Alsace Lorraine, Strasbourg, *23*, 209-214 (1970)

Clauer, N.: Utilisation de la méthode rubidium-strontium pour la datation d'une schistosité de sédiments peu métamorphisés: application au Précambrien II de la boutonnière de Bou Azzer – El Graara (Anti-Atlas, Maroc). Earth Plan. Sci. Lett. *22*, 404-412 (1974)

Clauer, N.: Géochimie isotopique du strontium des milieux sédimentaires. Application à la géochronologie de la couverture du craton ouest-africain. Mém. Sci. Géol., Strasbourg, *45*, 256 p. (1976)

Clauer, N., Hoffert, M., Grimaud, D., Millot, G.: Composition isotopique du strontium d'eaux interstitielles extraites de sédiments récents: un argument en faveur de l'homogéneisation isotopique des minéraux argileux. Geochim. Cosmochim. Acta *39*, 1579-1582 (1975)

Cormier, R.F.: Rubidium-strontium ages of glauconite and their application to the construction of a post-Precambrian Time-Scale. Ph.D. Thesis, Massachusetts Institute of Technology, Cambridge, Mass., 1956

Dasch, E.J.: Strontium isotopes in weathering profiles, deep-sea sediments and sedimentary rocks. Geochim. Cosmochim. Acta *33*, 1521-1552 (1969)
Dunoyer de Segonzac, G.: Les minéraux argileux dans la diagenèse. Passage au métamorphisme. Mém. Serv. Carte Géol. Alsace Lorraine *29*, 320 p. (1969)
Faure, G., Powell, J.L.: Strontium Isotope Geology. Berlin-Heidelberg-New York: Springer, 1972, 188 p.
Harder, H.: Illite mineral synthesis at surface temperatures. Chem. Geol. *14*, 241-254 (1974)
Kubler, B.: La cristallinité de d'illite et les zones tout à fait supérieures du métamorphisme. Colloque sur les étages tectoniques. Univ. Neuchatel. A la Baconnière, Neuchatel, Suisse, 1966, p. 105-122
Lucas, J.: La transformation des minéraux argileux dans la sédimentation. Etude sur les argiles du Trias. Mém. Serv. Carte Géol. Alsace Lorraine, Strasbourg, *23*, 202 p. (1962)
Lucas, J.: The transformation of clay minerals during sedimentation. A study on triassic clays. Translation of the previous reference. Published for the U.S. Department of Agriculture and the Natural Science Foundation, Washington D.C., by the Israel Program for scientific translations, 1968, 203 p.
Millot, G.: Géologie des argiles. Paris: Masson, 1964, 499 p.
Millot, G.: Geology of clays. Weathering, Sedimentology, Geochemistry. Translation of the previous reference by W.R. Farrand and H. Paquet. Berlin-Heidelberg-New York: Springer. Paris: Masson; London: Chapman and Hall 1970, 429 p.
Obradovich, J.D., Peterman, Z.E.: Geochronology of the Belt series, Montana. Can. J. Earth Sci. *5*, 737-747 (1968)
Paquet, H.: Evolution géochimique des minéraux argileux dans les altérations et les sols des climats méditerranéens et tropicaux à saisons contrastées. Mém. Serv. Carte Géol. Alsace Lorraine, Strasbourg, *30*, 212 p. (1970)
Thiry, M.: Technique de préparation des minéraux en vue de l'analyse aux rayons X. Rapport interne du Centre de Sédimentologie et Géochimie de la Surface, Strasbourg, 1974, 25 p.
Thorez, J.: Phyllosilicates and Clay Minerals. A laboratory handbook for their X-ray diffraction analysis. Lelotte, G. (ed.), B 4820. Dison, Belgique: 1975, 579 p.
Trauth, N.: Argiles évaporitiques dans la sédimentation carbonatée continentale tertiaire. Bassins de Paris, de Mormoiron et de Salinelles (France), Jbel Ghassoul (Maroc). Thèse Sci., Strasbourg, 1974, 309 p.
Trauth, N., Sommer, F., Lucas, J.: Evolution géochimique d'une série sédimentaire paléogène dans le Bassin de Paris. Bull. Serv. Carte Géol. Alsace Lorraine, Strasbourg, *22*, 279-310 (1969)
Trompette, R.: Le Précambrien supérieur et le Paléozoique inférieur de l'Adrar de Mauritanie (bordure occidentale du Bassin de Taoudeni, Afrique de l'Ouest). Un exemple de sédimentation de craton. Etude stratigraphique et sédimentologique. Trav. Lab. Sci. Terre, St. Jérôme, Marseille, *13*, 702 p. (1973)

Potassium Argon Dating

J.C. HUNZIKER

1. Overview of Technique and Systematics

The main principle of the conventional K-Ar method is very simple. ^{40}K decays to ^{40}Ar, and assuming we know the decay constants and are capable of measuring parent and daughter isotopes rather precisely, we should succeed in calculating an age.

The history of the K-Ar method best illustrates that there are still some minor complications worth discussion. Although the β-activity of K was discovered as early as 1905 by J.J. Thomson, it was only in 1928 that the γ-activity of K was discovered by Kohlhörster. Nier (in 1935) actually discovered the ^{40}K isotope and found its abundance to be 1.19×10^{-4} of the total K in mol.

Von Weizsäcker (1937) concluded from the argon abundance evidence that the total activity of K is due to ^{40}K and postulated the existence of the electron capture process.

On this basis von Weizsäcker suggested:

1. the measurement of ^{40}Ar in rocks and minerals as a dating method, and
2. the entire excess of ^{40}Ar in the atmosphere is due to the ^{40}K decay by electron capture.

From this beginning it still took very long until the first good results were obtained in the early 1950's. This fact is partly due to the complicated decay scheme (see Fig. 1), to complications with the vacuum extraction system, and last but not least also to the difficulties in attaining a good estimate for the decay constants.

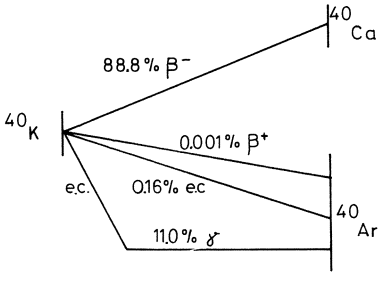

Fig. 1. Decay scheme with the double decay of ^{40}K to ^{40}Ar and to ^{40}Ca by combined electron capture, β^-, β^+, and γ-decays

In Sydney in 1976, the Subcommission on Geochronology of the International Union of Geological Sciences proposed the following decay constants and isotope

ratios compiled by Steiger and Jäger (1977). In addition the current most used constants proposed by Wetherill (1966) are also listed (old constants).

	New constants	Old constants
$\lambda^{40}K$	5.543×10^{-10}/y	5.305×10^{-10}/y
$\lambda^{40}K^{e} + \lambda^{40}K^{e'}$	0.581×10^{-10}/y	0.585×10^{-10}/y
$\lambda^{40}K^{\beta-}$	4.962×10^{-10}/y	4.72×10^{-10}/y

Isotopic abundance in atomic percent

^{39}K	93.2581	93.08
^{40}K	0.01167	0.0119
^{41}K	6.7302	6.91
^{40}Ar	99.600)	
^{38}Ar	0.063)	Atmospheric argon
^{36}Ar	0.337)	

40/36 Argon atmospheric = 295.5.

Now we have all we need for the age calculation. The formula is somewhat more complicated than the Rb-Sr age equation, due to the double decay of ^{40}K.

The principal age Eq. (1)

$$\frac{dN}{dt} = -\lambda N \tag{1}$$

can be changed into Eq. (2) by integrating

$$\ln \frac{N_t}{N_0} = -\lambda t \qquad \text{or into Eq. (3)} \tag{2}$$

$$N_t = N_0 \; e^{-\lambda t} \tag{3}$$

where λ = decay constant
t = time
T = atoms of daughter isotope
N_0 = atoms of mother isotope at time zero
N_t = atoms of mother isotope at time t

as $T + N_t = N_0$. Eq. (3) can be written as follows

$$T = N_0 \, (1 - e^{-\lambda t}) \tag{4}$$

The two decays of ^{40}K give us two equations

$$T_1 = \frac{\lambda\beta-}{\lambda} N_0 \; (1 - e^{-\lambda t}) \text{ for the } ^{40}Ca \text{ branch and} \tag{5}$$

$$T_2 = \frac{\lambda e}{\lambda} N_0 \ (1 - e^{-\lambda t}) \text{ for the } {}^{40}\text{Ar branch} \tag{6}$$

dividing Eq. (5) by Eq. (6) we obtain

$$\frac{T_1}{T_2} = \frac{\lambda\beta^-}{\lambda_e} \qquad \text{or } T_1 = \frac{T_2 \ \lambda\beta^-}{\lambda_e} \tag{7}$$

and can rewrite as the final equation

$$t = \frac{1}{\lambda} \ln\left(\frac{N_0 \lambda_e}{N_0 \lambda_e - T_2 \lambda}\right) \qquad \text{or}$$

$$t = \frac{1}{\lambda} \ln\left(1 + \frac{\lambda \ T_2}{\lambda_e \ N_t}\right) = \frac{1}{5.543} \ln\left(\frac{1 + 5.543}{0.581} \ \frac{{}^{40}\text{Ar rad}}{{}^{40}\text{K}}\right). \tag{8}$$

With this we have reduced the problem to the measurement of ^{40}K and ^{40}Ar rad.

Let us start with ^{40}K. The abundance of ^{40}K in K is 1.167×10^{-4} mol of ^{40}K per mol of K so that for most purposes we can deduce the ^{40}K content from the K content. K-contents are analyzed very precisely by flame photometry, atomic absorption, X-ray fluorescence, wet chemical techniques or isotope dilution.

As interelement effects are strongly disturbing in all the classical methods, it is advisable to dilute the potassium down to the ppm range and to use many standards for calibration.

The errors commonly accepted for the range of 3%-12% K are in the order of ± 1% but easily reach the ± 10% down at the 0.1% K level and below; for such low K contents it is wiser to use the mass spectrometric isotope dilution method. Problems encountered by the isotope dilution technique are mainly the high sensitivity of the method for K which for instance makes it a terrible task to clean the filaments of the MS properly, because of blank problems. With the isotope dilution technique ± 2% error can be reached down to the ppm level of K.

Now to the determination of the radiogenic argon. Most laboratories today measure argon by the isotope dilution technique, although in the literature a lot of data are still found that have been measured by the volumetric method.

The sample is introduced into a high vacuum extraction line, which consists either of steel or glass (Fig. 2).

The furnace, (Fig. 3) shows a very fancy device, which consists of a glass-quartz tube mostly water-cooled with a molybdenum crucible inside, with or without a lid. Nobody actually knows what a lid is for except to increase the blank! If a sample explodes, and some samples have a strong tendency to do so, no lid will prevent such a sample from sputtering around the whole furnace.

Some people work with a so-called Christmas tree, a device to store samples, that allows the possibility of extracting one sample after the other without breaking the

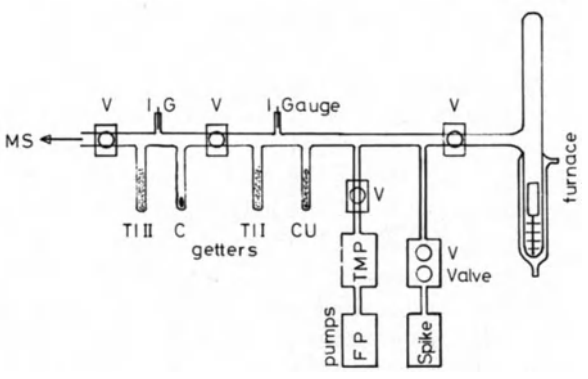

Fig. 2. Ar extraction system

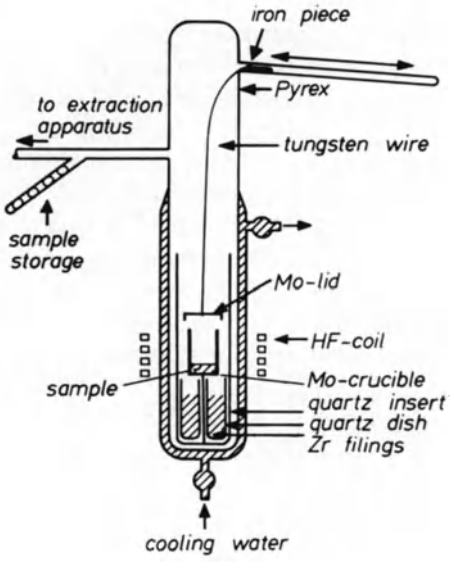

Fig. 3. Argon extraction furnace

vacuum. Normally the furnace is loaded before weekends and the following week samples are measured. The danger of cross contamination is very great. In addition, according to Murphy's law the furnace is never loaded before weekends, so that we see no disadvantage in using a clean furnace for every sample. Cross contamination occurs in the following way: each extraction will build up a mirror, mainly of alkalies, on the cool furnace walls, this mirror will trap some of the released argon from the first sample. The water of the second sample will partly destroy this mirror, thus releasing the trapped argon of the first sample and allowing it to mix with the second sample's argon. Especially with young samples, where the line and furnace volumes are small, such a mirror from a dirty furnace causes trouble, that can be avoided by changing the furnace with every sample – a good pumping system will help to overcome the disadvantages.

For the evaluation of the argon content of a sample, a known amount of ^{38}Ar spike is added to the sample. The purity of the spike available today is 99.9997% ^{38}Ar so that the sample's ratio of 38/40 gives us the content of ^{40}Ar in the sample. Up to this point we have found absolutely no problems, but they start here.

The ^{40}Ar content of a sample is composed of ^{40}Ar rad, hopefully the greater part. If a somewhat inferior spike is used, the spike will also contribute some ^{40}Ar. Then the residual gas of the line will contribute additional ^{40}Ar, and last but not least the sample itself contains both incorporated and adsorbed ^{40}Ar of nonradiogenic origin.

The residual ^{40}Ar content of a clean line should be about three orders of magnitude smaller than the measured ^{40}Ar contents, in other words practically negligible. The ^{40}Ar added with the spike can be measured and if need substracted. The small amounts found in a good spike pose heavy problems for measurements due to blank and memory, but on the other hand are practically negligible with regard to the age value, for an isochron treatment of the data nevertheless a precise knowledge of the amount of ^{40}Ar and of ^{36}Ar in the spike is indispensable.

The ^{40}Ar incorporated in the crystal lattice during crystallization is of the order of 10^{-3} to 10^{-7} cm^3 ^{40}Ar/gSTP, strongly dependent on crystal lattice and argon pressure during crystallization. Here we run into problems, specially with young ages. Model ages normally are calculated assuming that this argon has atmospheric 40/36 ratios of 295.5. Often this is true and we are lucky; sometimes this is not the case and we should note it.

Assuming that most of the ^{40}Ar in the atmosphere comes from the ^{40}K decay, the 40/36 ratio must have grown to its present value of 295.5 at some stage of the earth's history. Do we then have to use different air argon corrections for different ages? We can either assume that this 40/36 ratio has a linear growth (I) or some sort of a curved growth (II, III), or else that already early in the earth's history equilibrium was reached (IV), as shown in Figure 4 by Lippolt (1970).

Data on this problem are very scarce; only one good point is known, Carelian graphite of 1.8 by giving todays 40/36 ratio within the error margins, so that we can assume

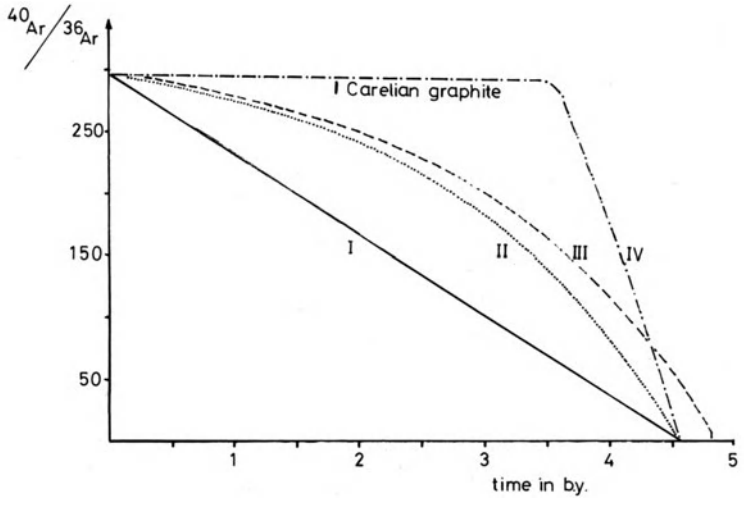

Fig. 4. Atmospheric argon evolution models after Lippolt (1970)

that at least for the last 2 b.y. this ratio has remained constant. Fortunately, most ages over 300 m.y. are already over 90% radiogenic, so that the uncertainty of the remaining 10% non-radiogenic argon is negligible.

Far more critical is the fact that both young and old samples often show inherited argon with ratios quite different from 295.5. This problem is very severe in polymetamorphic and or polyphasic terrains. In polymetamorphic terrains radiogenic argon from a former phase can partially or completely be released by a subsequent metamorphism. This radiogenic argon then either finds its way to the atmosphere, or becomes trapped in minerals and rocks. To be sure if a paragenesis is free of inherited radiogenic argon, cogenetic K-free or K-poor minerals, such as quartz, epidote, chloritoid, garnet, staurolite, kyanite, and chlorite can be measured. If the argon extracted from these minerals has a 40/36 ratio of around 300, we can be quite confident that the other minerals of the rock will yield ages. If the 40/36 ratio is higher, we can plot all the minerals on a $^{40}Ar/^{36}Ar$ versus $^{40}K/^{36}Ar$ isochron diagram and hope for a linear array. Only in very few cases will this be true. For instance in high pressure low temperature terrains, mostly a terrible scatter will be found (see Fig. 5.).

The other possibility to treat K-Ar data graphically was given by Harper (1970). ^{40}Ar radiogenic is plotted versus ^{40}K. Argon gain or loss and less likely K gain or loss can be detected by isochrons not passing through the origin (Fig. 6).

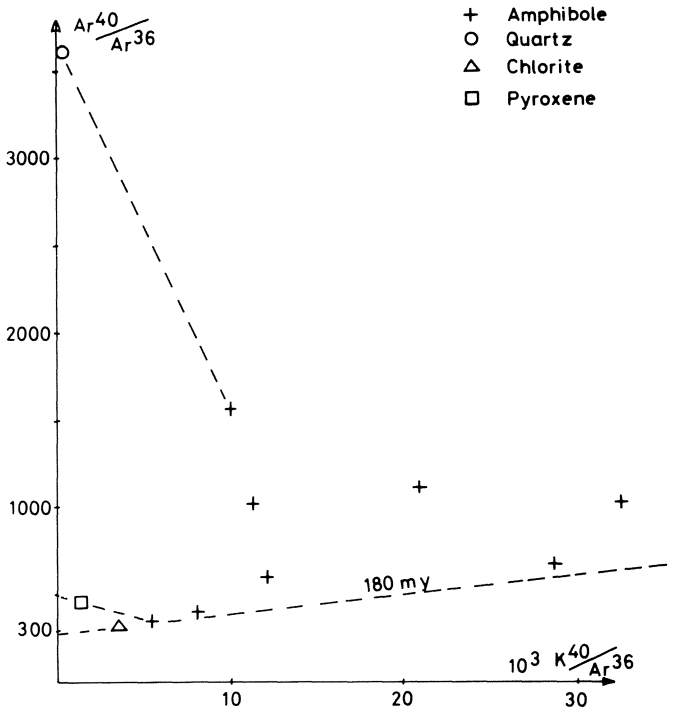

Fig. 5. Blue amphiboles and quartz, chlorite, pyroxene from the pre-Alpine Vannoise basement show great amounts of inherited argon. Blue-shist metamorphism in the Mesozoic ophiolites of the cover occurred between 120 and 60 m.y. and clearly postdates the magmatic age of the ophiolites (180 m.y. reference line). Bocquet et al.(1974)

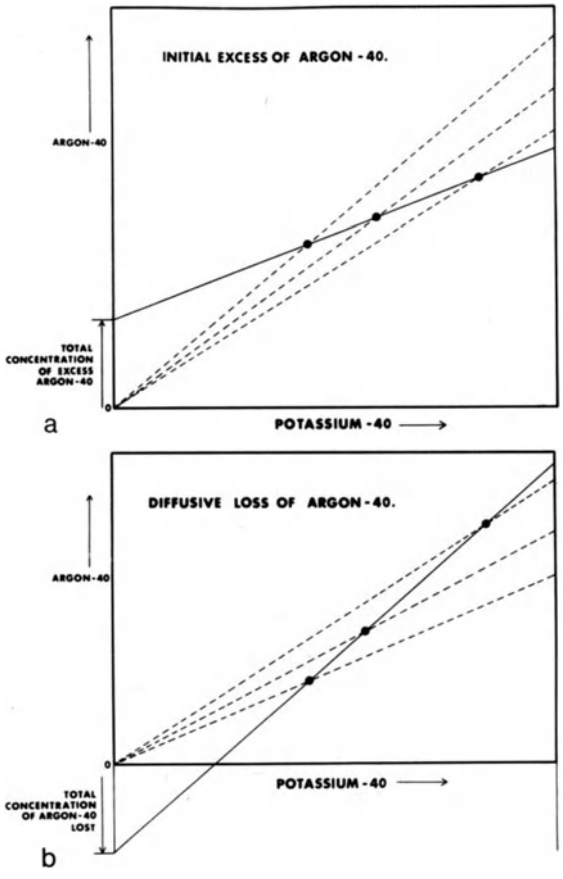

Fig. 6. a and b. Graphical solution to the problem of radiogenic ^{40}Ar loss

Unfortunately, Harper's data were not too convincing, and so the method has not achieved the attention it deserved, nevertheless K-Ar data should always be drawn on such plots to ensure consistency.

2. Selected Case Histories, Predominantly from the Alpine Domane

2.1 K-Ar Dating of Sedimentation and or Diagenesis

In dating a sediment by isotopic methods we find two extremes: a conglomerate will tell us something about the source region, but the answer will not be very representative, as hard rocks are prevailing and the brittle rocks have mostly disappeared. The same thing can be said about sands, where detrital minerals will give us the age of the rock-forming events in the source region. With this method the paleogeography of the Torridonian sandstones was elucidated, and also the nordic provenance of the Gansinger Keuper, showing detrital muscovites of Caledonian age could be ascertained.

The other extreme, clay-rich and marly sediments seem more suitable to furnish sedimentation ages. Assuming a complete exchange of the clay minerals with ocean water, we could expect to date sedimentation or early diagenesis. Unfortunately, this exchange for potassium must be quite complete to reset the K-Ar age. Kulp and Engels (1963) have shown that nearly 90% of the K must be removed out of a mica before a noticeable lowering of the age was found (see Fig. 7).

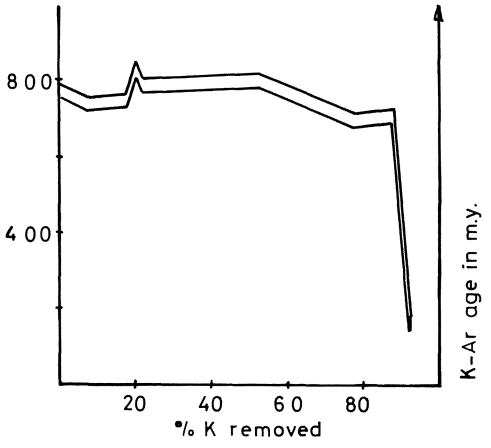

Fig. 7. Effect of removing potassium from biotite by base exchange. Data from Kulp and Engels (1963)

Hurley et al. (1961) showed that recent illite and illite/montmorillonite clay fractions from the Mississippi Delta had not exchanged with the water, they still showed ages between 100 and 200 m.y. Hurley, as well as Frey and coworkers, found that the detrital high-temperature 2 Ml-type micas showed higher ages than the low-temperature autigenic or recrystallized 1 Md-type micas. Unfortunately, in clays and shales we mostly find a mixture of the two polymorphs. Often 2 M 1-type micas still reflect their pre-sedimentary origin, while the 1 Md polymorph crystallizes or recrystallizes under diagenetic conditions. The coincidence of K Ar whole-rock ages on slates with the age of sedimentation can be explained as a result of a mixture of 2 Ml older ages and 1 Md younger ages in the right proportions, in other words as a chance result. The only promising result can be expected from pure 1 Md micas – most likely this would provide a possibility to date the diagenesis. A further way of dating the sedimentation process is given by the *glauconite-montmorillonite* family. Since the work of Obradovich (1964) and Hurley (1966) these green pellets have been considered suspicious. Only the school of Bruxelles, the school of Strasbourg and Odin's work have demonstrated the value of glauconites as a tool for sediment dating. Hurley's as well as Obradovich's work was undertaken on glauconites, that were not chosen according to the very severe criteria used today. In the 1960's green pellet in the sediment was already considered as glauconite, but as we have seen, glauconite is only the 10 Å end member of the glauconite (10 Å) montmorillonite (14 Å) family.

Montmorillonite has expandable interlayers, and thus is not an ideal mineral for K-Ar dating, as alkalies, as well as argon, are exchanged too easily from these expandable interlayers.

By means of X-ray diffractrometric methods Odin (1975) established criteria for the choice of reliable glauconites. The choice of the sample leads over three stages (1) Geologic selection, (2) Sedimentology, (3) Separation and purification.

1. Field Criteria. As for every other dating problem, absolute freshness of the sample is indispensable. Water horizons should definitely be avoided, as well as any trace of tectonic overprint. If possible the glauconite should have had less than 300 m of overload, although glauconites from 1500-m-deep holes have also given good results.

2. Sedimentologic Criteria. These help to choose the proper sample. Glauconite from clays is preferred to samples from carbonates, clay-rich sands are better than sands and pure clays. Considerable amounts of kaolinite in the clay fraction are incompatible with a ripe and evolved glauconite. Sediments with abundant glauconite are preferred to sediments with scarce glauconite. The coarsest glauconite is usually the best.

In conclusion: the ideal sediment contains more than 10% green pellets mainly in the fraction greater than 200 μ. The sediment shows less than 10% carbonates and the clay fraction should contain less than 10% kaolinite.

3. Preparation and Purification. After being seived and washed, the grains are classified according to different magnetic susceptibility and different density. Each of these concentrates is then checked by X-ray diffractometry, to choose the sample nearest to a

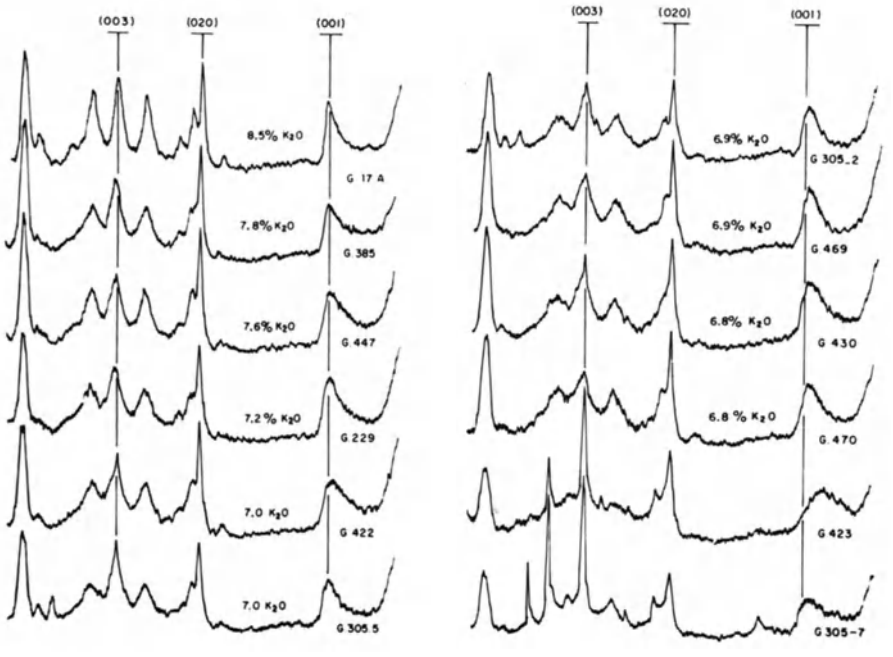

Fig. 8. Estimation of crystallinity and K-content by means of X-ray diffraction patterns of glauconite

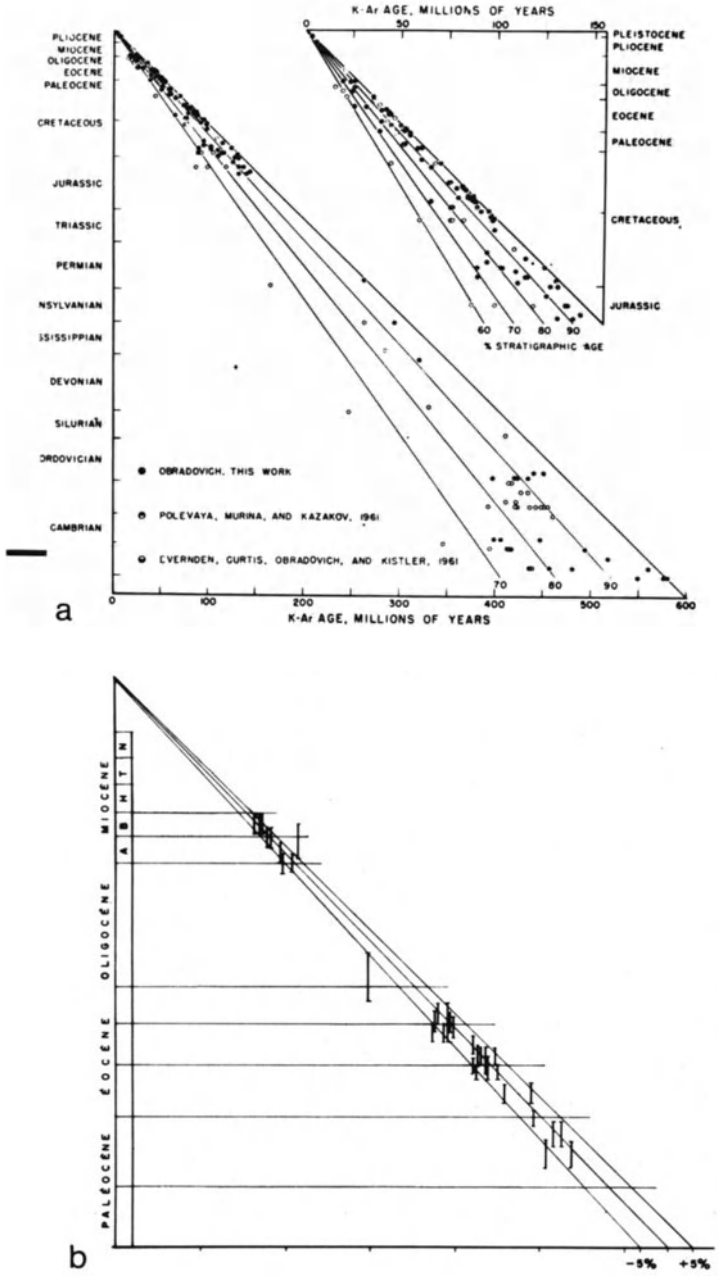

Fig. 9 a and b. Dispersion of glauconite ages. The severe application of Odin's criteria have led to minimizing the dispersion of glauconite ages from the ± 20% of Obradovich (1964) to ± 5% today

1 Md mica [(112) and ($11\bar{2}$) present] with less than 10% expandable layers. A very good glauconite contains between 8% and 8.5% K_2O, a good glauconite 7.5% and 8% K_2O. Below 7% K_2O a glauconite should only be used with great caution.

For preevaluation the potassium content of glauconite can be estimated from the X-ray diffraction pattern using the shape of the (001) 10 Å peak and the shape of the (003) 3.3 Å reflex (Fig. 8).

The end of the purification is an ultrasonic treatment in distilled water to clean all the small cracks of the pellets from clay particles and to break off the usually less well crystallized surface. Then the glauconites are dried at about 80°C. For more details see Odin (1975). Using Odin's criteria eight or nine out of every ten samples are eliminated, so that for the solution of a dating problem with glauconites we have to start with a large number of big samples. The severe application of Odin's criteria have led to minimize the dispersion of glauconite ages from the ± 20% found in the 1960's to ± 5% today, in other words to the analytical error (see Fig. 9).

The control of K-Ar glauconite ages with Rb-Sr glauconite ages is not yet established in a satisfactory way. In part this is due to the scarce Rb-Sr data. Nevertheless the data of the Cenomanian/Albian boundary of Odin and Hunziker (1976) are very promising (see Fig. 10).

The close control of glauconite ages with other isotopic ages on high-temperature minerals and rocks is still unsatisfactory. Partly this is due to the scarcity of stratigraphically datable high-temperature rocks in the European Mesozoic and Tertiary stratotypes, where most of Odin's glauconite work has been performed. These facts still leave open the question of whether glauconites give us the correct age, or if the whole iternally consistent glauconite time scale shows a slight shift towards younger ages.

Synsedimentary Volcanic Rocks. These are by far the most widespread method of dating sedimentation. Two possibilities are found in the literature: whole-rock dating of volcanics and dating of discrete mineral phases of these rocks. Coarse-grained volcanics, as well as inhomogeneous rocks should not be dated by the whole rock method, because we have two different aliquots for K and Ar in the conventional K-Ar method. Whole-rock analysis of fine-grained rocks should never be performed on one single sample; multiple samples of the same rock unit provide cross control and are much better than duplicate analysis of only one sample. Alteration and specially devitrification pose strong problems for the K-Ar dating of volcanic rocks, during these processes potassium is mobile and the measured age can be affected. This was demonstrated by Bernoulli and Peters (1974). A tuff from the Ammonitico Rosso, i.e., from the boundary Oxfordian–Titonian, in other words around 140 m.y. contains sanidine. A detailed study of this sanidine shows a rim of autigenic K-feldspar around the sanidine. Most probably this rim is a product of the later devitrification of the acid tuffs (see Fig. 11). The ages found on the composite K-feldspar/sanidine sample scatter between 136 and 100 m.y. depending on the relative amounts of rim and core analyzed. This devitrification event thus must have occurred less than 100 m.y. ago. As a high-temperature fixed point for the stratigraphic column this sample is of limited value, but it shows nevertheless how careful one must be.

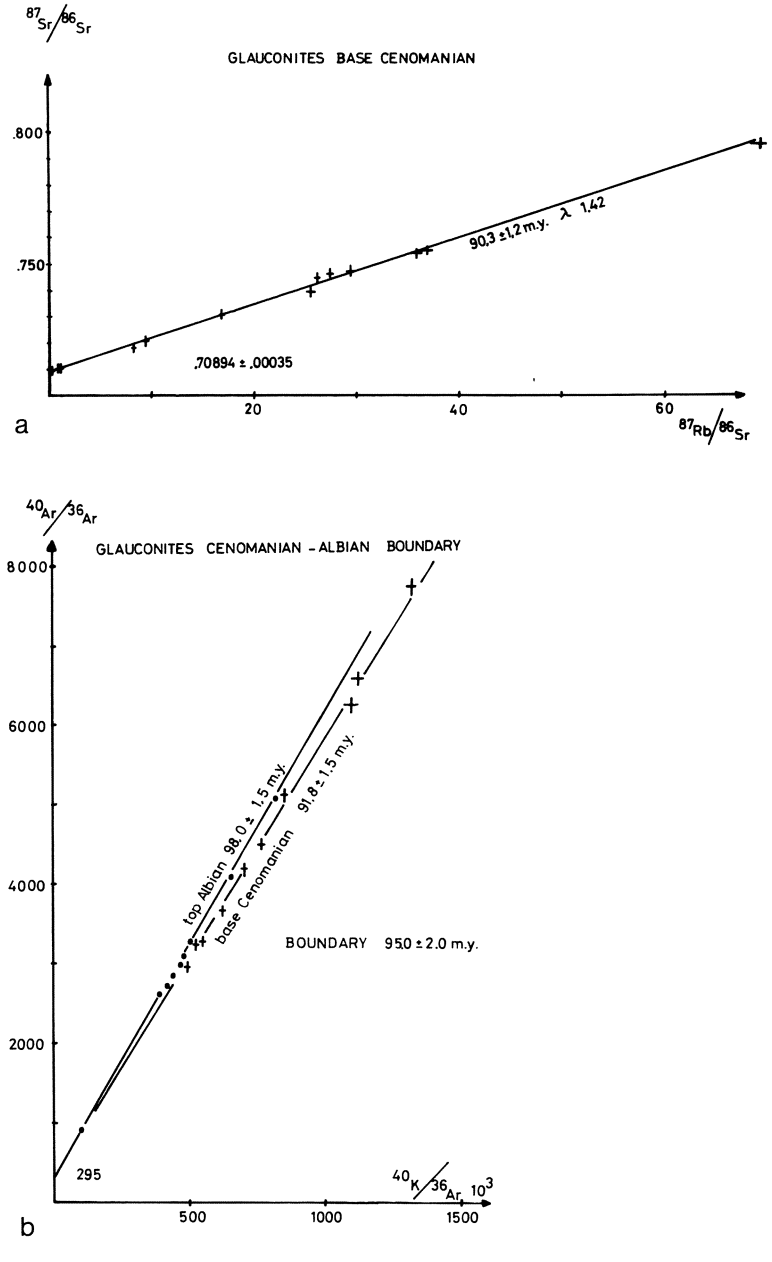

Fig. 10 a and b. Rb-Sr isochron of glauconites of the Cenomanian base compared with KAr isochrons of glauconites from the Cenomanian base and from the top Albanian

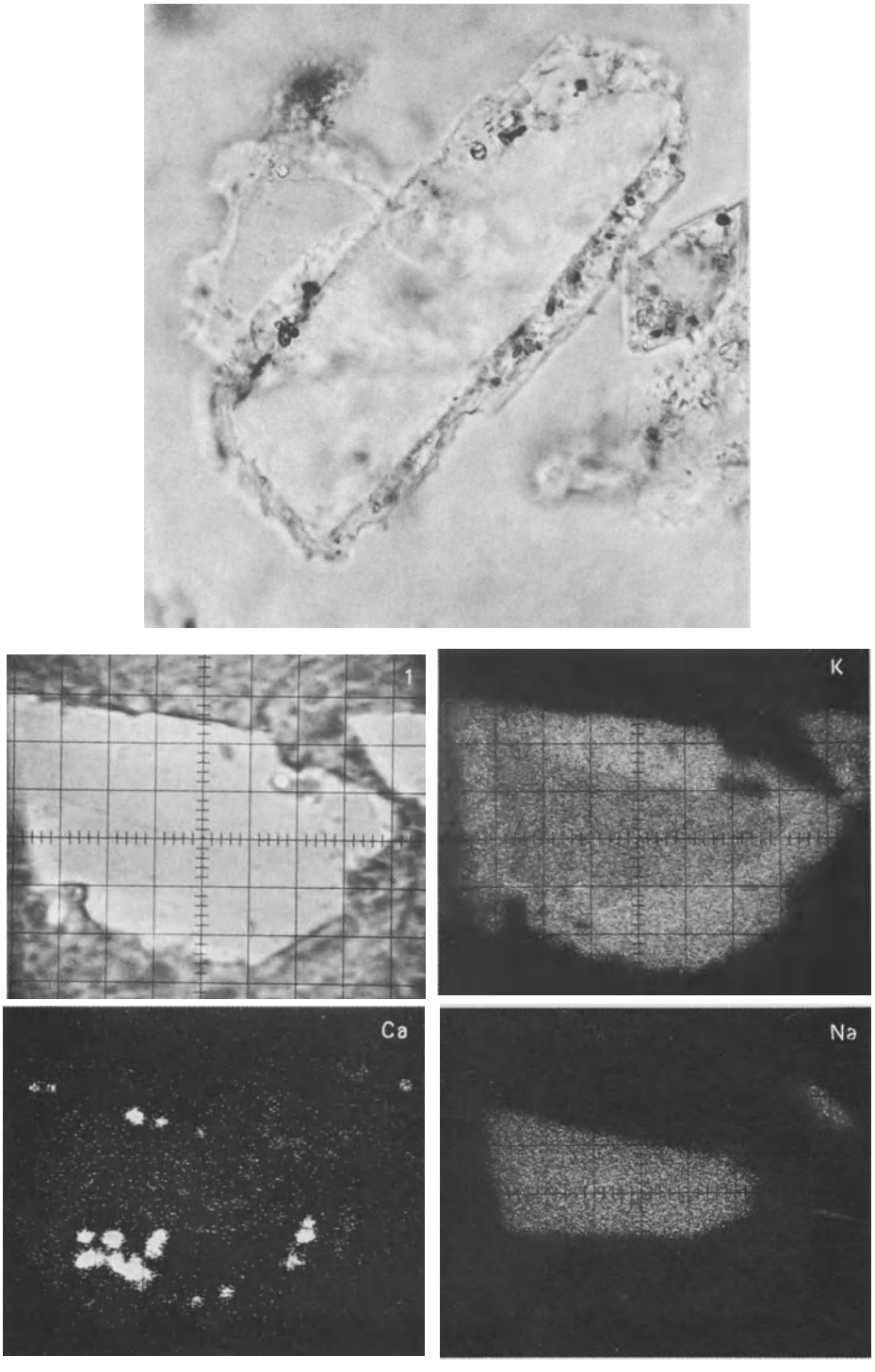

Fig. 11. Photomicrograph (above) and electron micrographs (below) of a feldspar grain showing a sanidine core and an authigenic K-feldspar rim, with calcite inclusions. Bernouilli and Peters (1974)

2.2 K-Ar Dating in Low-Grade Metamorphic Terranes

The use of *whole rock samples of slates and phyllites* for dating in metamorphic terranes is widespread. Harper (1970) proposed plotting the whole rock data on a ^{40}K versus ^{40}Ar radiogenic isochron diagram. The data of Harper on the Scottish Caleonides with 470-500 m.y.-old rocks show concordance between the whole rock sample and the mica fraction. This is not always the case, as can best be shown with the samples of Alpine age. In polymetamorphic and or polyphasic terranes radiogenic argon from an earlier phase can be liberated from the K-bearing phases during a later event and subsequently become trapped in fluid inclusions of quartz and or be incorporated in other potassium-bearing minerals. Kligfield et al. (1977) could demonstrate this mechanism in the Alpi Apuane. In other words, whole rock data on slates and phyllites are not reliable. The *mica fraction* of such fine-grained rocks can easily be enriched by means of sedimentation, and also by a paramagnetic separation and flotation. This enrichment hand in hand with the choice of the proper grain size eliminates fluid inclusions in quartz and also facilitates the interpretation of the data as discrete mineral concentrates are measured. The higher K-content of the samples tends to decrease the error on the potassium determination. Grain sizes below 2 μ, 2-6 μ tend to show no difference in age if the same minerals of the same tectonic or metamorphic phase are enriched in these fractions. In an age comparison of these small mica grains with mica of millimetric and decimetric diameter, no argon diffusion out of the 2 μ grains could be noticed (Frey et al., in prep.).

Illite tends to recrystallize to 2 Ml K-white mica at anchizonal conditions, as can be seen by electron microscopy. This recrystallized K-white mica can be used safely to determine the age of metamorphism from the transition anchizone-epizone up to higher degrees of metamorphism. A good means to determine whether an illite mica is suitable for dating or not is the measurement of the illite crystallinity according to Kübler (1966). On the fraction smaller than 2 μ of illite, the wideness at half height of the (001) 10 Å peak is measured in millimeters under standardized conditions by X-ray diffractometry. With increasing metamorphic grade, the wideness at half height of the peak decreases as the crystallinity of the illite increases. Values of 7.5 mm mark the transition from diagenesis (greater than 7.5) to anchizonal metamorphism (7.5-4.0 mm) and values of less than 4.0 represent a greenschist facies overprint. Hunziker and Frey (1973) and Frey et al. (in prep.) have shown that at the border of the Alpine chain illitic fractions extracted from the Keuper already show the beginning of this recrystallization (Fig. 12).

Metamorphic grade in the Helvetic nappes increases from north toward the south. Toward the Aare and Gotthard-Massif we reach the zone of epimetamorphism with temperatures of 300°-400°C. How do illite K-Ar ages reflect these changes in metamorphic conditions? In the unmetamorphic section of the Jura mountains we have two sets of illites with different provenance reflected in the ages (nordic and Vindelician-Keuper) giving 185 and 115 m.y. respectively. Both ages can be explained as mixtures of 1 Md and 2 Ml detrital micas of different provenance, as we have already seen in the discussion of the sedimentation ages nordic Keuper with Caledonian detritus and Vindelician-Keuper with Herzynian detritus. The overload of at least 3.5 km at present temperatures of around 100°C in the drill holes of the Molasse plane did not

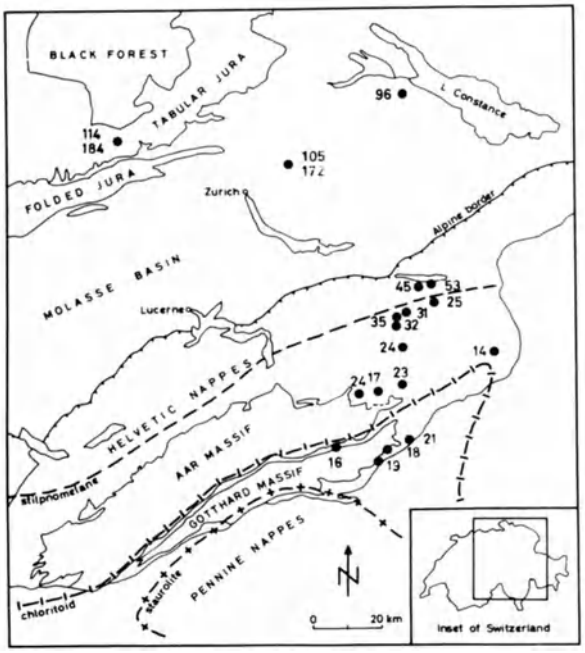

Fig. 12. Distribution of K-Ar ages on illitic-phengitic micas $< 2\ \mu$ along a profile from the tabular Jura to the Gotthard Massif. Frey et al. (in prep.)

affect the ages very much, and it is only at the Alpine border that we begin to see a stronger effect at metamorphic temperatures of around 200°C. The phengite ages in the Helvetic nappes decrease from N to S from 56 m.y. to around 18 m.y. in the Gotthard-Lukmanier area. These later ages are in good agreement with Rb-Sr and K-Ar cooling ages on millimetric rockforming micas from the adjacent basement and also with decimetric fissure micas of the region. The problem remaining is the interpretation of the data. The first information that can be deduced from this age pattern is that it is a posttectonic product. In other words, that the metamorphism in question took place close to the present position of the nappes and no longer in the depositional environment. Since the Glarus Alps are a very complex part of the Helvetic nappes, the age pattern of a transported metamorphism would be much more disrupted. The distribution of the K-Ar ages on white K-micas from the Glarus Alps shows four distinct groups. The samples showing illite crystallinities of the lower anchizone, show mixed ages of 40-56 m.y. From the higher anchizone and transition anchizone-epizone we have three groups of ages. The older group comprises ages from 29 to 37 m.y., and a younger group of 18 to 27 m.y. with a maximum around 24 m.y. As the illite crystallinity pattern is slightly displaced across the Glarus thrust, and phengite out of the mylonites of the Glarus thrust plane gave age values of 19-25 m.y., most likely the age of the metamorphism linked to the main tectonic phase could be around 35 m.y. and a later tectonic phase led to recrystallization at the Oligocene/Miocene boundary. Very late movements are recorded in tectonically more complex rocks, where the illites yielded ages around 15 m.y., in good agreement with the ages from stilpnomelane grown on the thrust plane of the Mürtschen-Kammlistock wedge giving an age of 14 m.y.,

and also with alcaliamphiboles grown on thrust planes giving an age of 17 m.y. This shows that illite ages are very susceptible to last motions along faults, a fact already discussed by Lyons and Snellenburg (1971)

For the 24 and the 14-17 m.y. event, the interpretation is unambiguous, as the dated illites are completely recrystallized under greenschist facies conditions. For the 29-37 m.y. illites partial recrystallization and therefore also partial adjustment to metamorphic conditions cannot yet be ruled out completely. If this is the case, not only the 40-56 m.y. but also the 29-37 m.y. group would represent mixed ages. To clarify this problem more work has to be done.

Another problem in low-grade metamorphism is encountered with *detrital micas.* Schamel (1973) has shown in the Monte Antola nappe of the Apennines where Alpine biotite already growns, that detrital muscovite with intergrowth of new-formed chlorite still holds its old age. Specially in the regions with metamorphic temperatures around 350°C only a careful diffractometric analysis will show if the white mica is still detrital or newly formed. In the presence of detrital white K-mica the illite crystallinity of coarser fractions tends to be much higher than for the finer fractions. Mostly detrital mica can already be seen by the eye on a clean rock surface. Such samples then have to be avoided for age determinations. Recently Zingg et al. (1976) have dated illites out of the meta sediments of the Canavese (Fig. 13).

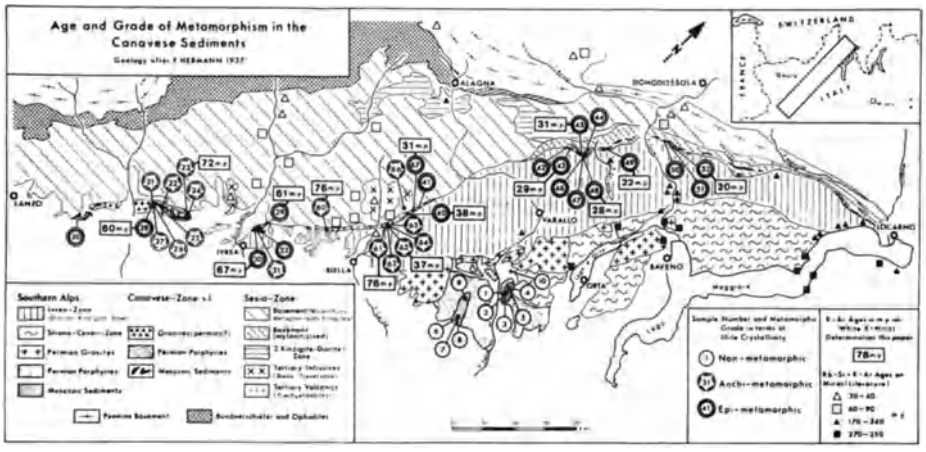

Fig. 13. Distribution of K-Ar phengite ages of the fraction $< 2\ \mu$ of the Canavese sediments. Zingg et al. (1976)

From the lithological point of view, the sediments of the Canavese s.str. are very similar to the South Alpine sediments, but in contrast to the latter, the Canavese sediments have been affected by Alpine deformation and metamorphism of anchi- to epizonal grade. K-Ar age determinations yield an eo-Alpine age for this metamorphism. Across the Insubric Line, opposite the Canavese s.str., eo-Alpine high pressure/low temperature metamorphism occurred contemporaneously. Thus the Insubric Line in

this region separates two eo-Alpine metamorphic facies domains of different pressure regimes.

The Canavese NE of Biella has been affected by the Lepontine phase of metamorphism in greenschist facies. The ages determined range between 38 and 19 m.y., dropping off towards the Lepontine area. The age of 38 m.y. comes from the westernmost border of the Lepontine influence area, and could well date the climax of the Lepontime phase.The neighboring basement of the Sesia-zone shows the same Lepontine overprint in greenschist facies and the same age pattern as the Canavese sediments.

In the northern Apennines, the Alpi Apuane Kliegfield et al. (1977) have described three major phases of deformation Dm, Dl, Dll, having affected the Paleozoic/Mesozoic and Tertiary rocks of the Apuane window. Illite crystallinity, phengite content of K-white mica and mineral paragenesis indicate that temperatures reached during all three deformation phases must have been between 300° and 400° C. Choosing adequate lithologies, according to microscopic and megascopic criteria, minerals growing during the early, main, and the latest deformation phases could be isolated and the time span between Dm and Dll could be determined at 26 and 11 m.y., respectively, in good agreement with the geologic restrictions.

Ahrendt et al. (1978a) could also distinguish two phases of low-grade metamorphism in the Naukluft nappes of the Damara orogeny of SW Africa (Fig. 14).

The metamorphic grade of the Naukluft nappes, as well as the underlying Nama beds, corresponds to the higher part of the anchi-zone and to the lower epi-zone. Determinations on K-white micas, both of the millimetric and of the $< 2\,\mu$ fraction, define two isochrons with ages of 495 and 530 m.y. (Fig. 15).

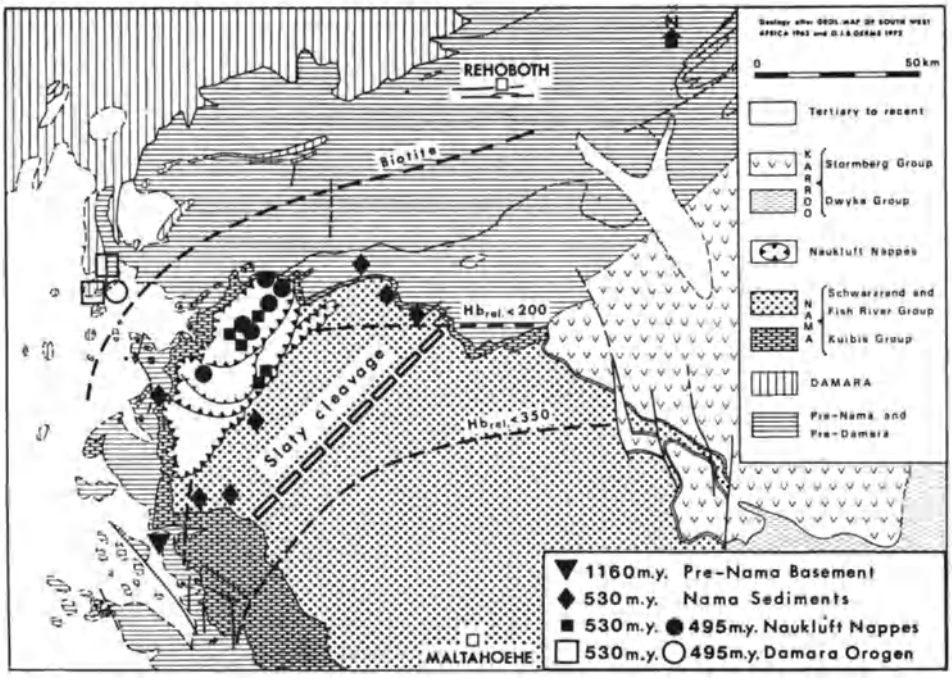

Fig. 14. Sample localities, K-Ar ages, isolines of illite crystallinity and biotite isograd in the Naukluft nappes, Damara orogeny, SW Africa. After Ahrendt et al. (1978)

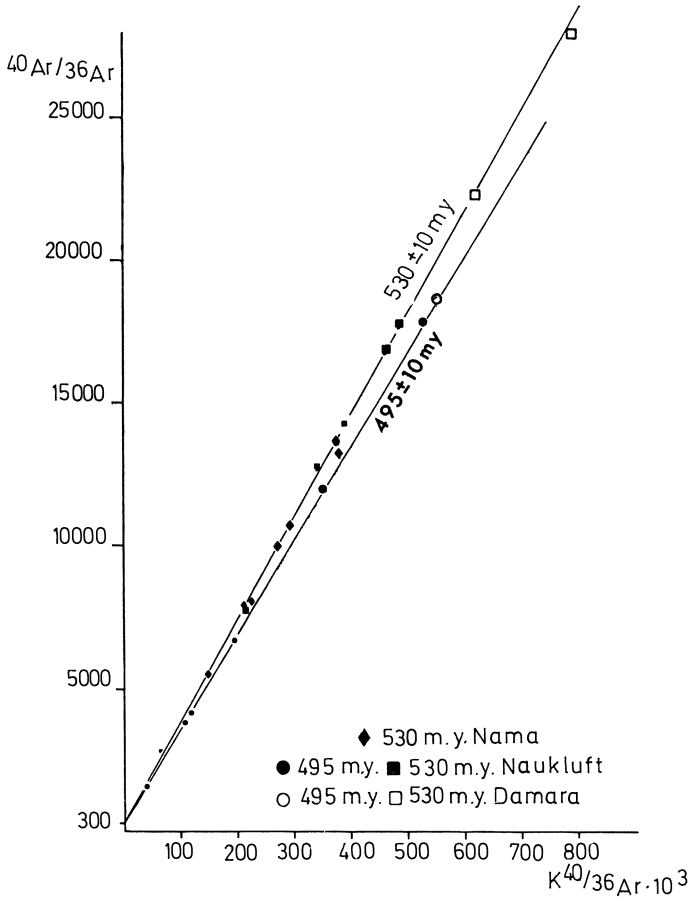

Fig. 15. $^{40}Ar/^{36}Ar$ versus $^{40}K/^{36}Ar$ isochron plot of white micas of the Nama sediments, the Nankluft nappes and the Damara orogen, SW Africa

No grain size effect could be detected. The age of 530 m.y. was interpreted as the peak of metamorphism and the age of syn-crystalline deformation. The age of 495 m.y. can be interpreted as a cooling age of the higher metamorphic rocks or as dating of a rejuvenation caused by a second post-crystalline deformation in parts of the Naukluft and Damara rocks. The age of 495 m.y. was also found in the fraction $< 2\ \mu$ of the main thrust plane mylonite, and most likely represents the time of emplacement of the Naukluft nappes.

Ahrendt et al. (1978b) could show in the anchi-metamorphic Devonian to Carboniferous slates of the Rheinisches Schiefergebirge, that even in such low-grade rocks the K-white mica fractions $< 2\ \mu$ can yield reliable K-Ar ages, provided only micas of neoformation are analyzed.

The grade of metamorphism of metavolcanic rocks there reaches the prehnite pumpellyite quartz subfacies and according to the illite crystallinity only anchimetamorphic conditions were reached. An upper Carboniferous (Westphalian) age of metamorphism

can be deduced on geologic cryteria. Over 20 K-white mica fractions $< 2\ \mu$ of devitrified tuffs were analyzed along a NS profile through the Rheinisches Schiefergebirge.

The K-Ar ages increase from 300 m.y. in the NE to 330 m.y. in the S. As metamorphic conditions in these rocks never reached the blocking temperature of K-white mica of around 350°C, these ages are interpreted as formation ages. From the fact that with respect to folding and first schistosity the metamorphism is synkinematic, the authors deduced that they not only dated the metamorphic event, but also the time of deformation.

Work in progress by Baud and Masson (1976) on the thrustfault of the Gummfluh in the Préalpes médianes rigides has shown that while the surrounding area only shows anchizonal overprint, the thrust plane of 10 to 50 m thickness has been affected by greenschist metamorphism. This greenschist overprint is obviously caused by the thrusting movement – a splendid occasion to date this tectonic phase.

Glauconite is a mineral with a very fast response to a metamorphic overprint, specially with respect to K-Ar dating. Frey et al. (1973) could show in the Glarus Alps (see Fig. 16), that glauconites from the Teriary and from the Cretaceous had already lost 20%-30% of their argon at the border of the Alpine chain at estimated temperatures of 100°-200°C. It is not until we reach anchimetamorphic conditions with temperatures between 200° and 300°C that these changes of glauconite can be seen optically. The first reaction to be seen is

glauconite + chlorite + quartz = stilpnomelane + K-feldspar + H_2O + O_2.

A further reaction at temperatures between 300° and 400°C toward the beginning of the greenschist facies leads to the formation of biotite by the reaction

chlorite + K-feldspar = biotite + stilpnomelane + quartz + H_2O.

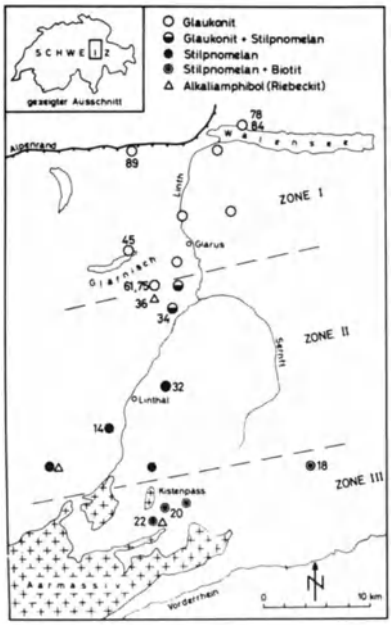

Fig. 16. Distribution of K-Ar ages in m.y. and index-minerals in glauconite bearing horizons between Walensee and Vorderrheintal

Glauconite, stilpnomelane, biotite, and mixtures of these minerals were analyzed with the K-Ar method.

First glauconite loses argon, the mixture stilpnomelane/glauconite shows an age of 34 m.y. in good agreement with the older age group of the illites and also with a riebeckite giving 36 m.y. The biotite ages of around 20 m.y. are in good agreement with the cooling ages on rock-forming biotites from the adjacent basement.

The same arguments already used for the illites hold for glauconite, stilpnomelane, and biotite. Although the ages around 34 and 36 m.y., specially the age of the riebeckite, are a strong hint for a Lepontic, Eocene/Oligocene phase in the Helvetic domaine, only more data can help here to clarify the picture.

Volcanic Rocks in Metamorphic Terranes. These not only change their mineralogy very fast, but also tend to show a great scatter in their K-Ar ages. As it is only in the past few years that work in low-grade metamorphic terranes has been in progress, and on the other hand most of the fixed points of the time scale are measured on volcanic rocks, the question arises how many metavolcanics have been used for the timescale.

The 30 available isotopic age data on ophiolites from the Alps Bertrand and Delaloye (1976) best illustrate this fact. The data seem to point to two groups, 165-180 m.y. and 135-150 m.y. However, it must be held in mind that the range of 210-38 m.y. was covered by these data and that all the analyzed ophiolites came from an Alpine prehnite-pumpellyite to greenschist facies environment, so that the question arises as to how much of the primary age and how much of the metamorphic overprint is reflected by the scattering ages; and we are not at all sure that completely unmetamorphosed ophiolites could not even be older than 180 m.y.

Delaloye and Sawatzki (1975) presented data of andesitic pebbles from the Eocene/Oligocene Taveyanne sandstone, defining an ^{40}Ar rad/K isochron of 24 ± 1 m.y., which does not pass through the origin. These pebbles come from a laumontite facies terrane

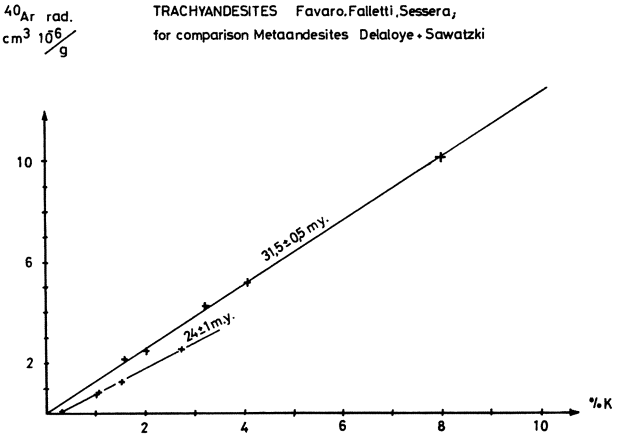

Fig. 17. ^{40}Ar rad versus K isochron plot of andesites from the volcano sedimentary cover of the Sesia-zone. For comparison the data of Delaloye and Sawatzki (1975). The latter have been affected by a metamorphism under laumontite facies conditions around 24 m.y., the resulting rejuvenation of the K-Ar system is clearly shown by the isochron, not passing through the origin

and demonstrate that already at such low temperatures volcanic rocks seem to equilibrate (Fig. 17).

For comparison the trachy-andesites from the Tertiary sedimantary cover of the Sesia-zone are on the same isochron plot. A connection between both andesitic volcanisms is quite plausible, but must be ruled out because the detrital mica in the Sesia tuffites is a 3 T phengite of eo-Alpine age, while the detrital 2Ml muscovite from the Taveyanne sandstone shows a Hercynian age and therefore paleogeographically could better be connected with the Apennines.

A classical example for the tricky business of dating volcanic rocks is found on Iceland. The oldest rocks on Iceland are dated by K-Ar with 17 m.y. On the other hand a paleobotanical work of Manum (1962) describes an Eocene flora on Iceland. There are three ways of interpretation for these discordant data:

1. The Eocene-flora is not Eocene but younger.
2. The rocks in the neighborhood of the Eocene plants have not been dated.
3. The Eocene volcanic rocks stayed hot and did not retain their argon until 17 m.y. ago.

Although the ocean floor spreading rates of the Atlantic strongly depend on the age of the magmatism on Iceland, nobody seems to care about these little details.

2.3 K-Ar Dating in High-Pressure Low-Temperature Terranes

Problems encountered in high-pressure low-temperature terranes have been described by Hunziker (1974). Therefore only a short review is given here.

In (1) overview of technique we have seen that in high-pressure terranes inherited argon 40 radiogenic is widespread. In high-pressure low-temperature terranes *monometamorphic and monophasic* rocks tend to give the best results, as no ^{40}Ar rad from older minerals is in the system at the moment of crystallization. The Pennine eclogites of the Piedmont region represent already a more complex situation, as they are *monometamorphic, but polyphasic.* In these rocks potassium-free minerals will show if inherited ^{40}Ar rad is present or not – only paragenesis devoid of inherited argon will yield ages. In the Piedmont region three different glauconphane generations were found, yielding ages of 80-100 m.y., 40-50 m.y. and 15-30 m.y. Most likely the lower limit of these age groups i.e., 80, 40 and 15 m.y. are the closest "guess" of the true age of the glaucophane generations, the higher ages being caused by small amounts of inherited argon, due to the polyphase character of the Alpine metamorphism.

The question arises whether or not in the Western Alps we have to account for three subsequent high-pressure phases with new formation of glaucophane. More likely glaucophane only shows a tendency to recrystallize under metastable conditions in response to subsequent tectonic and greenschist metamorphic overprint after the formation under high pressure conditions. This recrystallization seems to go hand in hand with a nearly complete resetting of the age. The 80-100 m.y. glaucophane shows a tendency to be randomly oriented, while on the other hand the 15-30 m.y. glaucophane shows a preferred orientation parallel to the lineation of the late backfolding. In the Pennine area of the Western Alps, phengites yielded K-Ar ages of 40-50 m.y. in close agreement with the second group of amphiboles. Rb-Sr ages on the same white

K-micas revealed ages of 36-40 m.y., showing that also for phengites the ages over 40 m.y. are due to considerable amounts of inherited argon – the true age of this metamorphic phase being 36-40 m.y., as in the Central Ticino area, the Lepontine phase. In the *polymetamorphic and polyphasic* Austro-Alpine basement of the Sesia-Zone, where the eo-Alpine high-pressure, low-temperature metamorphism overprints a Hercynian metamorphism of intermediate conditions, K-Ar ages on glaucophanes scatter terribly. $^{40}Ar/^{36}Ar$ on K-free minerals revealed great amounts of inherited argon, depending predominantly on the schistosity of the rock, shists showed lower apparent argon ages than massive rocks. Cogenetic phengites yielded ages of 60-90 m.y. showing that also phengites can incorporate considerable amounts of inherited radiogenic argon, accumulated since the Hercynian metamorphism and not completely lost during the eo-Alpine event.

At present the main problem is found in the pre-Triassic Briançonnais-Bernhard basement, where jadeite, quartz, and glaucophane are found, while the post-Triassic cover sediments reach up to the Paleocene, with many depositional and erosional gaps. How old is this high-pressure metamorphism in the Briançonnais basement? 80-100 m.y. or 35-40 m.y. K-Ar ages on 3 T phengites from the Bernhard basement are as high as 300 m.y., glaucophanes gave 240 m.y. and biotite ages from the same basement show 140 m.y. Here Rb-Sr determinations on selected Sr-poor phengites will give the answer, but also K-Ar determinations on the only monometamorphic Mesozoic cover-rocks. The same problems were also found in the Gruppo di Voltri eclogites and in the blue-schist terranes of Corsica.

Conclusion. In high-pressure metamorphism, great care must be taken to avoid systems with inherited radiogenic argon that could not leave the system during the high pressure event. Control with K-free cogenetic phases and with other methods alone will give reliable age data. Glaucophanes should only be analyzed after a careful microscopic study, otherwise the data are difficult to interpret. Due to the complexity of the mineral systems, whole rock data cannot be interpreted.

2.4 K-Ar Dating of High-Grade Metamorphic Rocks

In the Central Alps, the Lepontine region with its well-studied metamorphic zonation, (see the special volume of SMPM, 1974) offers a unique possibility to test the response of the different isotope systems to regional metamorphic conditions.

The work of Jäger et al. (1967), of Jäger and Hunziker (1969) and of Purdy and Jäger (1976) shows, that as a consequence of the Alpine amphibolite facies metamorphism in the Central Lepontine only Tertiary Alpine mica ages are found.

Wenk (1943) could show that in this region all the micas have recrystallized during the Alpine metamorphism. Jäger (1973) and Jäger et al. (1967), from the approximate coincidence of the northern boundary of the staurolite zone with the limits of the field of young muscovites in the Lepontine, postulated a blocking temperature of 500 ± 50°C for the Rb-Sr system of K-white mica.

All the K-Ar mica ages in this zone are younger than the Rb-Sr K-white mica ages and therefore represent cooling ages.

Purdy and Jäger (1976) have established the following age sequence in the Lepontine.

Rb-Sr K-white mica > K-Ar K-white mica > Rb-Sr biotite = K-Ar biotite, and derived a blocking temperature of 350° ± 50°C for the K-Ar system of K-white mica and of 300° ± 50°C for the K-Ar system of biotite.

A similar behavior has been described by Hart (1964) and by Hanson and Gast (1967) for contact metamorphic aureoles. Although the two effects, regional metamorphism and contact metamorphism, seem to give the same age pattern, the differences between the two regimes should be kept in mind. During a regional metamorphism temperatures have been high for some 10 to 50 m.y. whereas during a contant metamorphic event the thermal peak was only at very short duration and disequilibrium assemblages are more probable. The behavior of the K-Ar system of minerals in polyphasic and or polymetamorphic rocks under greenschist facies conditions shows strong similarity to that under blueschist conditions. Disequilibrium is very common in this regime and therefore different rock types and different minerals should be analyzed as a check for concordance. Viability of metamorphic fluids, and/or tectonic movements, often also linked together, strongly affect the response of the K-Ar system. For more details see Purdy and Jäger (1976) and Frey et al. (1976).

Under amphibolite facies conditions equilibrium not only from the mineralogical, but also from the chemical and isotope point of view, is more easily reached; here ages tend to be more concordant. As the blocking temperatures for the K-Ar system of most minerals is lower than the temperature reached under amphibolite facies conditions, the measured ages here are cooling ages. Under normal cooling rates of 20°-50°C per m.y. the difference between cooling age and formation age can only be made for the Alpidic cycle. For pre-Alpine ages this difference mostly disappears in the error limits of the age determination.

In favorable cases, where due to a very slow uplift and erosion, the cooling rate is especially low (5° to 10°C/m.y.) the distinction between cooling and formation age may also be made for older than Alpine events.

2.5 K-Ar Dating of Igneous Rocks

K-Ar dating of igneous rocks gives the most clear-cut answers. For plutonic rocks discrete mineral separates should be analyzed, as a whole rock treatment mostly is not possible, because of grain size problems. (In a coarse-grained rock it is mostly impossible to obtain two identical aliquot samples small enough for an extraction line.)

Volcanic rocks are generally treated as whole-rock samples, if the grain size is small enough, or the minerals are extracted and measured separately. The most common minerals analyzed here are sanidine, amphibole, and biotite. The measurement of dykes poses special problems as the chilled margins generally seem to show disequilibrium conditions. As a general rule the cores of thick dykes seem to give quite reliable data.

References

Ahrendt, H., Hunziker, J.C., Weber, K.: Age and degree of metamorphism and time of nappe emplacement along the southern margin of the Damara Orogen/Namibia (SW-Africa). Geol. Rdsch. *67* (1978a)

Ahrendt, H., Hunziker, J.C., Weber, K.: K/Ar Altersbestimmungen an Gesteinen des Rheinischen Schiefergebirges. Z. Dtsch. Geol. Ges. (1978b)

Baud, A., Masson, H.: Deformation ductile et bréchification le long du plan de chevauchement de l'écaille de la Gummfluh (Préalpes médianes rigides, Suisse). Eclogae *69/2* (1976)

Bernoulli, D., Peters, Tj.: Traces of Rhyolitic-Trachytic volcanism in the Upper Jurassic of the Southern Alps. Reply Eclogae *67/1* (1974)

Bertrand, J., Delaloye, M.: Datation par la méthode K-Ar de diverses ophiolites du Flysch des Gêts (Haute-Savoie, France) Eclogae *69* (1976)

Bocquet, J., Delaloye, M., Hunziker, J.C., Krummenacher, D.: K-Ar and Rb-Sr dating of blue amphiboles, micas, and associated minerals from the Western Alps. Contrib. Mineral. Petrol. *47*, 7-26 (1974)

Delaloye, M., Sawatzki, G.: Géochronométrie des élements volcaniques du flysch helvétique du synclinal de Thônes (Haute-Savoie, France). Arch. Sci. Geneve *28* (1975)

Frey, M., Hunziker, J.C., Clauer, N., Flemig, W., Hochstrasser, K., Roggwiller, P.: The illite-muscovite transition: mineraological and isotope data. (In prep.)

Frey, M., Hunziker, J.C., O'Neil, J.R., Schwander, H.W.: Equilibrium-disequilibrium relation in the Monte Rosa Granite, Western Alps: petrological, Rb-Sr and stable isotope data. Contr. Mineral. Petrol. *55* (1976)

Frey, M., Hunziker, J.C., Roggwiller, P., Schindler, C.: Progressive niedriggradige Metamorphose glaukonitführender Horizonte in den helvetischen Alpen der Ostschweiz. Contr. Mineral. Petrol. *39*, 185-218 (1973)

Hanson, G.N., Gast, P.W.: Kinetic studies in Contact Metamorphic Zones. Geochim. Cosmochim. Acta *31* (1967)

Harper, C.T.: Graphical solutions to the problem of radiogeneic argon-40 loss from metamorphic minerals. Eclogae *63*, 1 (1970)

Hart, S.R.: The petrology and isotopic mineral age relation of a contact zone in the front range, Colorado. J. Geol. *72* (1964)

Hunziker, J.C.: Rb-Sr and K-Ar age determination and the alpine tectonic history of the western Alps. Memorie di Padova *XXXI* (1974)

Hunziker, J.C., Frey, M.: K-Ar and Rb-Sr age determinations and progressive low grade metamorphism in the sediments of the Helvetic nappes of Eastern Switzerland. Abstract Fortschritte der Mineralogie *50*, 3 (1973)

Hurley, P.M.: K-Ar Dating of Sediments in Potassium Argon Dating by Schaeffer, D.A., Zähringer, J. (eds.). Berlin-Heidelberg-New York: Springer 1966

Hurley, P.M., Brookins, D.G., Pinson, W.H., Hart, S.R., Fairbairn, H.W.: K-Ar age studies of Mississippi and other river sediments. Bull. Geol. Am. *72*, 1807 (1961)

Jäger, E., Hunziker, J.C.: In: Colloquium on the Geochronology of Phanerozoic Orogenic belts. Field Trip, Guide Book, Switzerland (1969)

Jäger, E., Niggli, E., Wenk, E.: Rb-Sr Altersbestimmungen an Glimmern der Zentralalpen. Beitr. Geol. Karte d. Schweiz, N.F. *134* (1967)

Kligfield, R., Hunziker, J.C., Schamel, S.: K-Ar Ages of multiply deformed metasedimentary rocks from the Alpi Apuane, Northern Apennines and their tectonic implications, Abstract ECOG Pisa 1977.

Kohlhörster, W.: Gammastrahlen an Kaliumsalzen. Naturwissenschaften *16*, 28 (1928)

Kübler, B.: La cristallinité de l'illite et les zones tout a fait supérieures du métamorphisme. Etages téctoniques Neuchâtel, 1966

Kulp, J.L., Engels, J.: Discordances in K-Ar and Rb-Sr Isotopic Ages. In: Radioactive Dating, Vienna: Int. Atomic Energy Agency, 1963, pp. 219-238
Lippolt, H.J.: Argon-Isotopen-Anomalien in Gesteinen. Habilitationsschrift Universität Heidelberg (1970)
Lyons, J.B., Snellenburg, J.: Dating faults. Geol. Soc. Am. Bull. *82*, 1749-1752 (1971)
Manum, S.: Studies in the Tertiary flora of Spitzbergen with notes on Tertiary floras on Ellesmere Island, Greeland, and Iceland. Norsk Polarinst. Skr. 125 Oslo (1962)
Nier, A.O.: Evidence for the existence of an isotope of potassium of mass 40. Phys. Rev. *48*, 283 (1935)
Obradovich, J.D.: Problems in the use of glauconite and related minerals for radioactivity dating. Dissertation, Univ. of California, Berkeley (1964)
Odin, G.S.: Les glauconies, constitution, formation, âge. Thèse d'Etat Univ. P. et M. Curie, Paris 1975
Odin, G.S., Hunziker, J.C.: Glauconite dating of the Cenomanian/Albanian Boundary. Abstract ECOG (1976) Amsterdam
Purdy, J.W., Jäger, E.: K-Ar ages on rock-forming minerals from the Central Alps. Memorie di Padova *XXX* (1976)
Schamel, S.: Eocene subduction in Central Liguria, Italy. Thesis Yale Univ. (1973)
Steiger, R.H., Jäger, E.: Subcommission on geochronology: Convention on the use of decay constants in geo- and cosmochronology. E.P.S.L. *36*, 359-362 (1977)
Thomson, J.J.: On the emission of negative corpuscles by the alkali metals. Phil. Mag. *10*, 584 (1905)
Weizsäcker, C.F. von: Über die Möglichkeit eines dualen Beta-Zerfalls von Kalium. Phys. Z. *38*, 623 (1937)
Wenk, E.: Ergebnisse und Probleme von Gefügeuntersuchungen im Verzascatal (Tessin). SMPM *23* (1943)
Wetherill, G.W.: Radioactive decay constants and energies. In: Clark, S.P., Jr. (ed.) Handbook of Physical Constants, Geol. Soc. Am. Memoir *97*, 587 (1966)
Zingg, A., Hunziker, J.C., Frey, M., Ahrendt, H.: Age and degree of metamorphism of the Canavese zone and of the sedimentary cover of the Sesia zone. SMPM *56*, 361-375 (1976)

Text Books:

Dalrymple, G.B., Lanphere, M.A.: Potassium-Argon-Dating. San Francisco: Freeman, 1966
Schaeffer, O.A., Zähringer, J. (eds.): Potassium Argon Dating. Berlin-Heidelberg-New York: Springer, 1966

$^{40}Ar/^{39}Ar$ Dating: Principles, Techniques, and Applications in Orogenic Terranes

R. D. DALLMEYER

1. Introduction

The $^{40}Ar/^{39}Ar$ dating technique is a recently developed analytical variation of the conventional K-Ar method. It has greatly enhanced the general applicability of K-Ar geochronology because it has the ability to distinguish between: (1) samples which have lost a component of radiogenic argon since their initial crystallization, (2) samples which have remained closed systems with respect to potassium and argon since their initial crystallization, and, (3) samples which contain a component of extraneous argon of non-atmospheric $^{40}Ar/^{36}Ar$ ratio. In principle this potential has not yet been fully realized. However, basic systematics of the technique are still in the developmental stages and initial results are encouraging.

2. Basic Principles

The $^{40}Ar/^{39}Ar$ technique was first described by Sigurgeirsson (1962). It was more fully discussed in subsequent reports by Merrihue (1965), Merrihue and Turner (1966), and Mitchell (1968). The theory and analytical techniques used in the method are generally similar to those for conventional K-Ar dating. The primary difference is that in $^{40}Ar/^{39}Ar$ geochronology no direct chemical analysis of potassium is required. It is measured as a function of ^{39}Ar which is produced from ^{39}K by neutron-activation. Hence, only determination of the ratio of radiogenic ^{40}Ar to neutron-produced ^{39}Ar is required for age determinations.

In the $^{40}Ar/^{39}Ar$ method, whole-rock or mineral samples are encapsulated in small quartz vials and arranged in a fixed geometry with several encapsulated standards (often termed "monitors") of known K-Ar age (Fig. 1). This package is then placed in the core of a nuclear reactor and irradiated with a flux of approximately 10^{18} fast neutrons/cm^2. Several thousand nuclear reactions occur as a result of the irradiation, but the reaction $^{39}K(n,p)^{39}Ar$ is the most important for dating as it produces ^{39}Ar (with a 265 year half-life) from ^{39}K. After a measurable quantity of ^{39}Ar has been produced, the irradiation is stopped and short-lived radionuclides allowed to decay (2-3 weeks). Following this "cooling-off" period, the irradiation package is returned to the laboratory, disassembled, and samples are loaded in an ultra-high vacuum extraction system (identical to that used in K-Ar dating). They are then fused with a radiofrequency induction heater. Gases liberated from the sample are scrubbed and analyzed with a mass spectrometer.

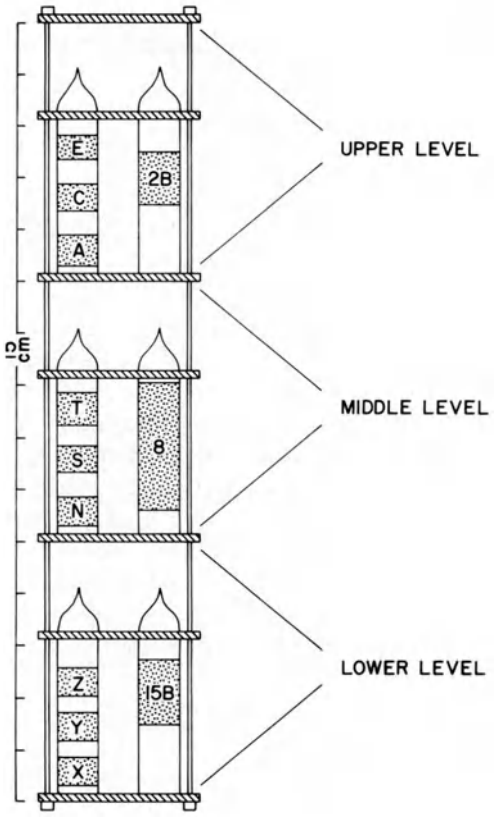

Fig. 1. Typical geometry of samples and monitors for irradiation in the United States Geological Survey TRIGA reactor (Denver). Each "level" consists of seven positions. Three monitors are loaded in one position within each "level". The other positions are loaded with samples of unknown age. In this illustration only one sample position is shown along with the monitors

The amount of ^{39}Ar produced within a sample during irradiation may be calculated from the following equation:

$$^{39}Ar_K = {}^{39}K\,\Delta T \int \Phi(\epsilon)\sigma(\epsilon)d\epsilon \qquad (1)$$

^{39}K = number of atoms of ^{39}K in the sample
$^{39}Ar_K$ = number of atoms of ^{39}Ar produced from ^{39}K in the irradiation
$\Phi(\epsilon)$ = fast neutron flux at energy ϵ
$\sigma(\epsilon)$ = neutron capture cross-section of $^{39}K(n,p)^{39}Ar$ at energy ϵ
ΔT = duration of the irradiation
(the integration is performed over all incident neutron energies).

^{40}Ar is also present in the sample as a result of the spontaneous decay of ^{40}K. For a sample with an apparent K-Ar age of t, the amount of radiogenic argon is given by the standard K-Ar dating equation:

$$^{40}Ar^* = {}^{40}K \frac{\lambda_e}{\lambda_e + \lambda_\beta} (e^{t/\tau} - 1) \qquad (2)$$

^{40}K = number of atoms of ^{40}K present in the sample
$^{40}Ar^*$ = number of atoms of radiogenic ^{40}Ar present in the sample
λ_e = decay constant of ^{40}K by k-electron capture
λ_β = decay constant of ^{40}K by β-emission
τ = mean half-life of $^{40}K = 1.885 \times 10^9$ yr.

Combining Eq. (1) and (2), the $^{40}Ar^*/^{39}Ar$ ratio measured for an irradiated sample of age t may be expressed as:

$$\frac{^{40}Ar^*}{^{39}Ar_K} = \frac{^{40}K}{^{39}K} \frac{\lambda}{\lambda_e + \lambda_\beta} \frac{1}{\Delta T} \frac{(e^{t/\tau} - 1)}{\int \Phi(\epsilon)\sigma(\epsilon)d\epsilon}. \quad (3)$$

Obviously, this is a cumbersome equation, with irradiation parameters difficult to compute. However, as a standard of known K-Ar age was included in the irradiation package, Eq. (3) may be greatly simplified. First, a quantity J is defined as:

$$J = \frac{^{39}K}{^{40}K} \frac{\lambda_e + \lambda_\beta}{\lambda_e} \Delta T \int \Phi(\epsilon)\sigma(\epsilon)d\epsilon.$$

From Eq. (3),

$$J = \frac{(e^{t/\tau} - 1)}{^{40}Ar^*/^{39}Ar_K}.$$

This expression may be rewritten as

$$t = \tau \ln\{1 + J(^{40}Ar^*/^{39}Ar_K)\}. \quad (4)$$

Substituting the known K-Ar age of the standard for t in Eq. (4), the value of J may be calculated directly from measurement of the $^{40}Ar^*/^{39}Ar_K$ ratio of the irradiated standard. Once a value of J has been determined for a particular portion of the irradiation package, ages of unknown samples may be calculated by measurement of their $^{40}Ar^*/^{39}Ar_K$ ratios and using the appropriate value for J. Because the fast neutron flux is inhomogeneous over short distances within most reactor cores, it is necessary to include several standards and calculate the value of J for specific intervals within the irradiation package (Fig. 2).

Example

A biotite standard with a K-Ar age of 800 m.y. was included in the irradiation package illustrated in Figure 1. Monitor "N" was analyzed and yielded a $^{40}Ar^*/^{39}Ar_K$ ratio of 84.56 (corrected for atmospheric contamination and mass-discrimination). A J-value of 0.006252 may be calculated for this interval within the irradiation package:

$$J = \frac{e^{t/\tau} - 1}{^{40}Ar^*/^{39}Ar_K} = \frac{\frac{0.800 \times 10^9 yr}{e^{1.885 \times 10^9 yr} - 1}}{84.56} = 0.006252.$$

The $^{40}Ar^*/^{39}Ar_K$ ratios for the other monitors in this package are listed in Table 1. A graph of J-value vs. position in the reactor package for this irradiation is shown in Figure 2.

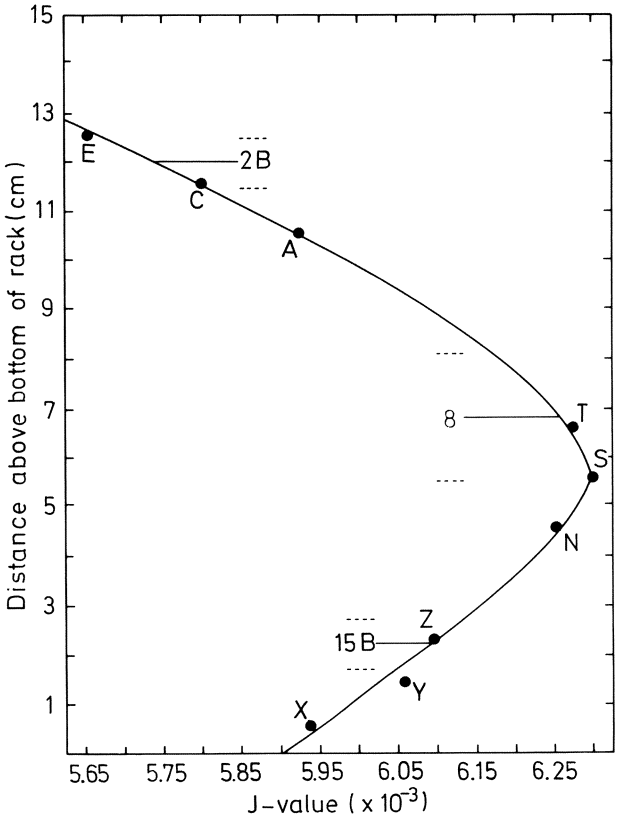

Fig. 2. Variation of J-value with monitor position in the irradiation package illustrated in Figure 1 (see Table 1 for listing of the monitor data). Also shown are relative positions of samples used in following examples and their respective J-values

A biotite sample (289 mg) was irradiated in position 15B in this package (Fig. 1). After applying mass-discrimination corrections, the following signal levels were measured (listed in millivolts):

$^{40}Ar_m$ = 12,003.05 mV
$^{36}Ar_m$ = 2.125 mV
$^{39}Ar_m$ = 464.17 mV

Table 1. Analytical data for monitors in the reactor package illustrated in Figure 1

Monitor	$^{40}Ar^*/^{39}Ar_K$	J-value
E	93.49	0.005655
C	91.15	0.005800
A	89.23	0.005925
T	84.25	0.006275
S	83.92	0.006300
N	84.56	0.006252
Z	86.74	0.006095
Y	87.25	0.006059
X	89.15	0.005930

The $^{40}Ar^*/^{39}Ar_K$ ratio of the sample may be calculated as

$$^{40}Ar^*/^{39}Ar_K = (^{40}Ar_m - 295.5\ ^{36}Ar_m)/^{39}Ar_m = 24.51.$$

An average J-value of 0.006099 characterizes the length of position 15B (see Fig. 2), and an age of 263 m.y. may be calculated for the biotite:

$$t = 1.885 \times 10^9 \text{ yr } \ln\{1 + (0.006099)(24.51)\} = 263 \text{ m.y.}$$

3. Correction for Interfering Isotopes

For rock and mineral samples with large K/Ca ratios, $^{40}Ar/^{39}Ar$ ages may be directly calculated according to Eq. (4) (as in the above example). However, such a simple type of calculation is not possible for samples with large Ca/K ratios because of the production of argon isotopes by nuclear reactions other than $^{39}K(n,p)^{39}Ar$. These reactions have been described by Turner (1971) and Brereton (1970). There are three sources of interference:

1. ^{40}Ar produced by a $^{40}K(n,p)$ reaction
2. ^{36}Ar produced by a $^{40}Ca(n,n\alpha)$ reaction
3. ^{39}Ar produced by a $^{43}Ca(n,\alpha)$ reaction.

Production of $^{40}Ar_K$ and $^{39}Ar_{Ca}$ directly complicates measurement of the $^{40}Ar^*/^{39}Ar_K$ ratio. Production of $^{36}Ar_{Ca}$ is undesirable when it is necessary to apply a correction for atmospheric ^{40}Ar on the basis of the atmospheric ^{36}Ar content of a sample. Fortunately, ^{37}Ar is also produced during neutron irradiation. Two reactions have been described:

1. ^{37}Ar produced by a $^{40}Ca(n,\alpha)$ reaction
2. ^{37}Ar produced by a $^{39}K(n,nd)$ reaction.

Because $^{37}Ar_K$ generally accounts for less than 0.05% of the total neutron-produced ^{37}Ar, measurement of the relative volume of ^{37}Ar liberated from a sample may be used

to estimate the extent of interference of $^{36}Ar_{Ca}$ and $^{39}Ar_{Ca}$ (such small quantities of $^{40}Ar_K$ are produced during irradiation that they may be ignored in most age calculations). Empirical production ratios of $(^{36}Ar/^{37}Ar)_{Ca}$ and $(^{39}Ar/^{37}Ar)_{Ca}$ are determined by analysis of irradiated Ca-salts. Production ratios for $(^{40}Ar/^{39}Ar)_K$ may be determined by analysis of irradiated K-salts. Production ratios measured for three commonly used reactors are listed in Table 2.

Table 2. Production ratios for interfering argon isotopes

Reactor	Reference	$(^{36}Ar/^{37}Ar)_{Ca}$ ($\times 10^{-4}$)	$(^{39}Ar/^{37}Ar)_{Ca}$ ($\times 10^{-4}$)	$(^{40}Ar/^{39}Ar)_K$
U.S.G.S. TRIGA	1	2.72	6.33	0.0059
Herald	2	2.47	7.19	0.0123
McMaster	3	2.7	8.5	0.031

1 = Dalrymple and Lanphere (1971)
2 = Brereton (1970)
3 = Berger and York (1970)

For rock or mineral samples with large Ca/K ratios, the $^{40}Ar^*/^{39}Ar_K$ ratio used in Eq. (4) must be determined as:

$$\frac{^{40}Ar^*}{^{39}Ar_K} = \frac{^{40}Ar_m - (^{36}Ar_m - ^{36}Ar_{Ca})\ 295.5 - ^{40}Ar_K}{^{39}Ar_m - ^{39}Ar_{Ca}}. \quad (5)$$

Using the production ratios of Ca-derived ^{36}Ar and ^{39}Ar and the production ratio of K-derived ^{40}Ar, the $^{40}Ar^*/^{39}Ar_K$ ratio may be calculated directly by using measured ratios of $^{40}Ar/^{39}Ar$ and $^{36}Ar/^{39}Ar$ and the corrected $^{37}Ar/^{39}Ar$ ratio (corrected for the decay of ^{37}Ar in the interval between irradiation and analysis; 35.1 day half-life). For packages irradiated in the United States Geological Survey TRIGA reactor, an equation of the following form may be used (see Table 2):

$$\frac{^{40}Ar^*}{^{39}Ar_K} = \frac{(^{40}Ar/^{39}Ar)_m - 295.5(^{36}Ar/^{39}Ar)_m + 295.5(^{37}Ar/^{39}Ar)_c(0.000272)}{1 - ^{37}Ar/^{39}Ar)_c(0.000633)}. \quad (6)$$

Example

A hornblende sample (1054 mg) was irradiated in position 8 in the package illustrated in Figure 1. Forty-one days following the irradiation, the following signal levels were measured (after applying mass-discrimination corrections):

$$^{40}Ar_m = 6{,}642.75 \text{ mV} \quad (^{40}Ar/^{39}Ar)_m = 36.85$$
$$^{36}Ar_m = 2.866 \text{ mV} \quad (^{36}Ar/^{39}Ar)_m = 0.016$$
$$^{39}Ar_m = 180.25 \text{ mV} \quad (^{37}Ar/^{39}Ar)_m = 2.625.$$
$$^{37}Ar_m = 473.16 \text{ mV}$$

Correcting for the decay of ^{37}Ar in the forty-one days between irradiation and analysis, an initial $^{37}Ar/^{39}Ar$ ratio of 5.888 may be calculated. The $^{40}Ar^*/^{39}Ar_K$ ratio may be determined as:

$$\frac{^{40}Ar^*}{^{39}Ar_K} = \frac{36.85 - 295.5(0.016) + 295.5(5.888)\,(0.000272)}{1 - (5.888)\,(0.000633)} = 32.74.$$

A radiogenic yield of 88.36% was obtained from the sample and the amount of Ca-derived ^{36}Ar was 10.07% of the total measured ^{36}Ar. An average J-value of 0.006250 characterizes the length of position 8 (see Fig. 2). Using Eq. (4), a $^{40}Ar/^{39}Ar$ age for the hornblende may be calculated as shown below:

$$t = 1.885 \times 10^9 \text{ yr} \ln\{1 + (0.006250)\,(32.74)\} = 351 \text{ m.y.}$$

4. Age Spectra

Following irradiation, a sample may be totally fused and all liberated argon analyzed in a single experiment. The $^{40}Ar/^{39}Ar$ age calculated by Eq. (4) is termed a total-fusion age and it is roughly analogous to a conventional K-Ar date. However, the greatest potential of the $^{40}Ar/^{39}Ar$ technique is through an incremental (step-wise) heating of irradiated samples. In this method, instead of fusing a sample and analyzing all liberated argon, the sample is heated in steps for fixed periods of time (typically for 1 h). Argon released in each temperature increment is scrubbed and treated as an unknown sample for which an apparent age may be calculated from its $^{40}Ar^*/^{39}Ar_K$ ratio [using Eq. (4)]. Thus, a series of apparent ages (each corresponding to a specific temperature) is generated for an individual sample. These incremental ages are plotted as a function of experimental temperature (commonly expressed as an accumulative percentage of $^{39}Ar_K$ released), giving an "age spectrum" for the sample (Fig. 3). Characteristics of the age spectrum permit evaluation of the behavior of potassium and argon within rock and mineral samples, and thus provide a more thorough understanding of the geologic significance of geochronological results than can be obtained from conventional K-Ar studies.

The theoretical basis and advantages of the $^{40}Ar/^{39}Ar$ incremental heating technique were first described by Merrihue and Turner (1966). They were more fully defined in subsequent papers by Turner (1968, 1969, 1970a, b), Fitch et al. (1969), Lanphere and Dalrymple (1971), Brereton (1972), Dalrymple and Lanphere (1974), Dallmeyer (1974, 1975a, b, c), and Dallmeyer and Sutter (1976). If a sample contains no extraneous argon and if it has behaved as a closed system with respect to addition

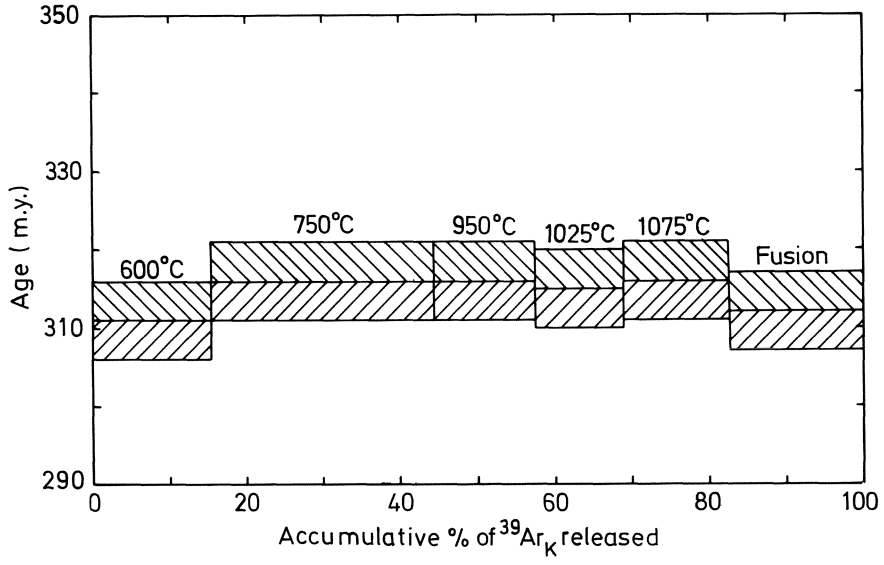

Fig. 3. $^{40}Ar/^{39}Ar$ age spectrum for biotite sample loaded in position 2B in the reacto package illustrated in Figure 1 (see Table 3 for analytical data). Analytical uncertainty (2 σ, rounded to 5 m.y.) is indicated by width of bar. Release temperatures shown above each gas increment

or loss of potassium and argon (except for the internal accumulation of radiogenic argon), the ratio of $^{40}Ar^*$ to neutron-produced $^{39}Ar_K$ should be the same for each incremental gas fraction. Ages calculated for each increment should be mutually similar and approximate the total-gas age defined by the $^{40}Ar^*/^{39}Ar_K$ ratio of the sum quantity of all the gas released throughout the incremental heating experiment. The resultant age spectrum will be essentially concordant (Fig. 3). However, if a sample contains a component of extraneous argon, or if as a result of physical or chemical disturbance it has not behaved as closed isotopic system, apparent ages of the various gas increments will be different and the resultant age spectrum of a more complex, discordant form. Obviously, total-gas $^{40}Ar/^{39}Ar$ and K-Ar ages of samples with discordant age spectra have little geologic significance. However, inferences of geologic history and estimates of original age may often be possible through examination of discordant age spectra. The most promising potential is the ability to recognize thermally overprinted samples which have been partially degassed as a result of geologic reheating.

Turner (1968) assumed that thermally induced argon loss was largely controlled by volume diffusion, and he calculated a series of theoretical gas-loss curves for isotropic material of various grain geometries (Fig. 4). These predicted that incremental gas fractions from thermally undisturbed samples should record similar $^{40}Ar^*/^{39}Ar_K$ ratios and thereby define concordant age spectra. Samples experiencing diffusive argon loss were predicted to display more complex age spectra in which ages of incremental gas fractions systematically increase from low to high release temperatures (the particular form of discordant spectra being a function of the extent of diffusive argon loss

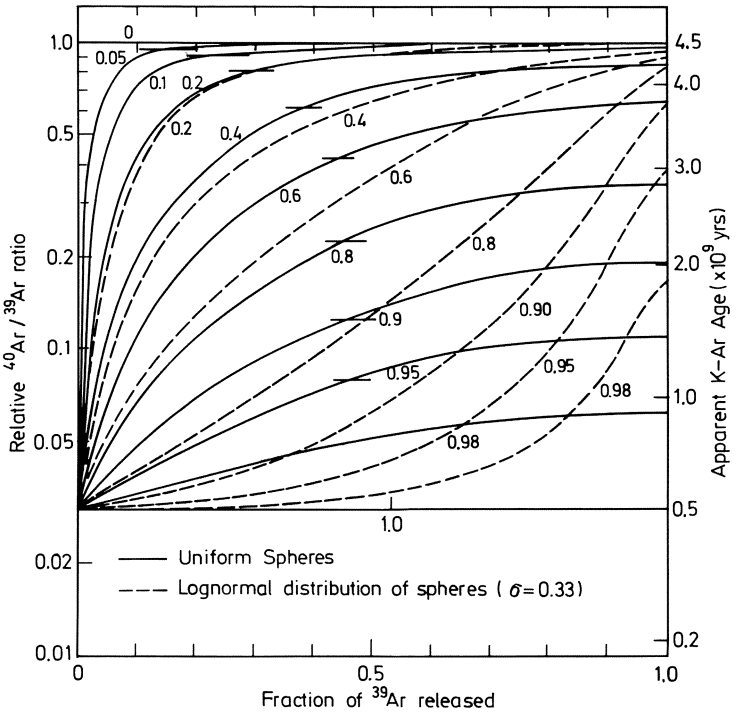

Fig. 4. Theoretical $^{40}Ar/^{39}Ar$ age spectra for thermally disturbed samples of various grain shapes (from Turner, 1968). Spectra apply to 4.5 b.y. samples which were thermally overprinted at 500 m.y. Numbers on each spectrum indicate the fraction of radiogenic ^{40}Ar lost during geologic reheating

and the average grain geometry). Turner predicted that age spectra of thermally overprinted samples should reveal both the time of geologic reheating (ages recorded by low-temperature intercept, Fig. 4) and the initial argon retention age (dates recorded by highest temperature fractions). Subsequent investigation of meteorite samples revealed numerous "plateau-type" concordant age spectra (Turner, 1969, 1970a, b). As ages defined by the concordant spectra were similar to those determined by Rb-Sr and U-Pb methods, it appeared that well-defined $^{40}Ar/^{39}Ar$ plateau dates were geologically meaningful. Many of the more complex release spectra generally followed Turner's theoretical predictions (Fig. 5), and a model of volume diffusive argon loss was also supported.

Considering that most potassium in meteorite samples is located within interstitial glass, it is understandable that Turner's theoretical gas-loss curves (which were modeled on diffusive loss from isotropic material) can be successfully applied. It should be anticipated that their application to thermally disturbed terrestrial rock and mineral samples would be less successful, because potassium is most often located in specific crystallographic sites, each with a particular activation energy threshold for diffusive mobility. Indeed, although subsequent studies of terrestrial samples have verified the ability of $^{40}Ar/^{39}Ar$ incremental heating experiments to discriminate between undisturbed

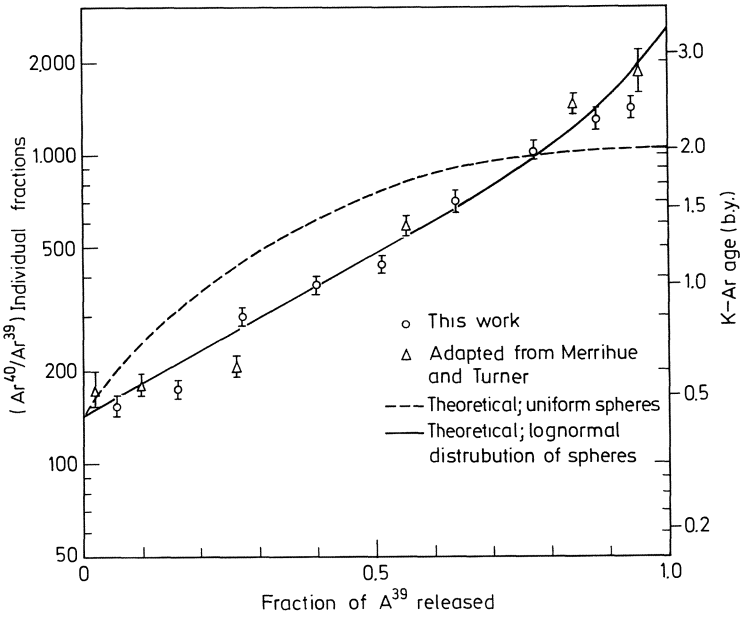

Fig. 5. $^{40}Ar/^{39}Ar$ incremental gas release pattern of the Bruderheim meteorite compared with theoretical release spectra of thermally overprinted samples (from Turner, 1968). Note that the Bruderheim data appears to fit a 90% gas-loss curve for volume diffusive loss of radiogenic ^{40}Ar from a lognormal distribution of spheres

samples (with concordant age spectra) and disturbed samples (which record discordant age spectra), a wide variation in the form of discordant spectra has been reported (see, for example, Fitch et al., 1969; Lanphere and Dalrymple, 1971; Dallmeyer, 1974, 1975a, b, c).

Example

A biotite concentrate (297 mg) was loaded in position 2B in the irradiation package illustrated in Figure 1. A six-step $^{40}Ar/^{39}Ar$ incremental heating experiment was carried out (the sample was maintained for 1 h at each temperature increment). The signal levels and age calculations for this sample are tabulated below (a J-value of 0.005741 characterizes the length of position 2B, see Fig. 2). These data are plotted as a $^{40}Ar/^{39}Ar$ age spectrum in Figure 3. Note that the spectrum is concordant, suggesting that the biotite is undisturbed (i.e., it has not been physically or chemically affected since its last cooling through argon retention temperatures).

Table 3. $^{40}Ar/^{39}Ar$ analytical data for biotite loaded in position 2B in the irradiation package illustrated in Figure 1

Release Temp.	$^{40}Ar_m$ (mV of signal)	$^{39}Ar_m$ (mV of signal)	$^{36}Ar_m$ (mV of signal)
600°C	2757.39	78.55	1.016 ± 0.061
750°C	4681.77	141.43	0.649 ± 0.032
950°C	2128.01	64.01	0.318 ± 0.009
1025°C	1853.85	56.72	0.182 ± 0.011
1075°C	2227.02	68.69	0.143 ± 0.010
Fusion	2780.78	87.04	0.161 ± 0.009
Total	16428.82	496.44	2.469

Release Temp.	% radiogenic	$^{40}Ar^*/^{39}Ar_K$	% of total ^{39}Ar released	Age (m.y.)
600°C	89.11	31.28	15.82	311 ± 5
750°C	95.90	31.75	28.49	316 ± 5
950°C	95.58	31.78	12.89	316 ± 5
1025°C	97.09	31.73	11.43	315 ± 5
1075°C	98.10	31.81	13.84	316 ± 5
Fusion	98.29	31.40	17.53	312 ± 5
Total	95.96	31.63	100.00	315 ± 5

5. $^{40}Ar/^{39}Ar$ Isochron Diagrams

During analysis of argon released from a rock or mineral sample, it is commonly assumed that, except for neutron-induced isotopes, all of the ^{36}Ar present is of atmospheric origin. It is typically necessary to make this assumption so that the atmospheric ^{40}Ar component may be subtracted from the total ^{40}Ar measured. If extraneous argon is present within a sample, then the standard procedure for calculating atmospheric ^{40}Ar will be incorrect.

Argon isotopic correlation diagrams may be used to calculate $^{40}Ar/^{39}Ar$ ages without determination of atmospheric components (Merrihue and Turner, 1966; Berger and York, 1970; Brereton, 1970; Dalrymple and Lanphere, 1974). The $^{40}Ar/^{39}Ar$ correlation diagram (or isochron plot) is generally equivalent to the isochron plot used for conventional K-Ar data. However, the diagram is obtained from the incremental gas fractions liberated from an individual sample. This is a marked advantage over the K-Ar isochron plot where it is necessary to use several different samples with similar geologic settings and with sufficient variations in their K and Ar concentrations so as to provide a reasonable spread of data.

The total measured ^{40}Ar within an irradiated rock or mineral sample is a sum of ^{40}Ar derived from various sources. It may be expressed as:

$$^{40}Ar_m = {}^{40}Ar_A + {}^{40}Ar_E + {}^{40}Ar_R + {}^{40}Ar_K + {}^{40}Ar_{Ca} - {}^{40}Ar_{RM} \quad (7)$$

$^{40}Ar_m$ = total measured ^{40}Ar
$^{40}Ar_A$ = atmospheric ^{40}Ar
$^{40}Ar_R$ = radiogenic ^{40}Ar
$^{40}Ar_K$ = ^{40}Ar neutron-produced from K
$^{40}Ar_{Ca}$ = ^{40}Ar neutron-produced from Ca
$^{40}Ar_E$ = extraneous ^{40}Ar
$^{40}Ar_{RM}$ = ^{40}Ar removed by neutron-induced reactions.

Similarly, the total amount of ^{36}Ar measured in an irradiated sample may be expressed as [subscripts as Eq. (7)]:

$$^{36}Ar_m = {}^{36}Ar_A + {}^{36}Ar_E + {}^{36}Ar_{Ca} - {}^{36}Ar_{RM}. \quad (8)$$

Negligible quantities of ^{36}Ar and ^{40}Ar are actually removed by neutron-induced reactions and the $^{36}Ar_{RM}$ and $^{40}Ar_{RM}$ terms may be ignored. Also, the measured quantities of ^{36}Ar and ^{40}Ar may be easily corrected for neutron-produced interference isotopes following the methods outlined earlier. Thus, the corrected quantities of measured ^{36}Ar and ^{40}Ar may be expressed as:

$$^{40}Ar_c = {}^{40}Ar_A + {}^{40}Ar_E + {}^{40}Ar_R \quad (9)$$

$$^{36}Ar_c = {}^{36}Ar_A + {}^{36}Ar_E. \quad (10)$$

Defining a term F,

$$F = {}^{40}Ar_R/{}^{39}Ar_K,$$

Eq. (9) may be expressed as:

$$^{40}Ar_c = {}^{40}Ar_A + {}^{40}Ar_E + F({}^{39}Ar_K). \quad (11)$$

Dividing Eq. (11) by $^{36}Ar_c$

$$\frac{^{40}Ar_c}{^{36}Ar_C} = \frac{^{40}Ar_A + {}^{40}Ar_E}{^{36}Ar_A + {}^{36}Ar_E} = \left(\frac{^{39}Ar_K}{^{36}Ar_c}\right) F \quad (12)$$

yields an equation of a straight line with slope F and an intercept of $^{40}Ar_A + {}^{40}Ar_E/{}^{36}Ar_A + {}^{36}Ar_E$. As the slope of the line is equal to the $^{40}Ar^*/{}^{39}Ar_K$ ratio, it may be used to calculate an age t according to Eq. (4):

$$t = 1.885 \times 10^9 \text{ yr } \ln(1 + J \times F). \quad (13)$$

To calculate an age by the isochron method, the ratios $^{40}Ar_{R+AE}/^{36}Ar_{AE}$ and $^{39}Ar_K/^{36}Ar_{AE}$ are determined for each gas increment in a stepwise heating experiment (R = radiogenic, AE = atmospheric and extraneous, K = potassium-derived by irradiation: the extraneous component includes all argon other than radiogenic, atmospheric, and neutron-produced; in an ideal system it will be equal to zero). These ratios are then plotted on an isochron diagram with $^{40}Ar_{R+AE}/^{36}Ar_{AE}$ on the ordinate and $^{39}Ar_K/^{36}Ar_{AE}$ on the abscissa (Fig. 6).

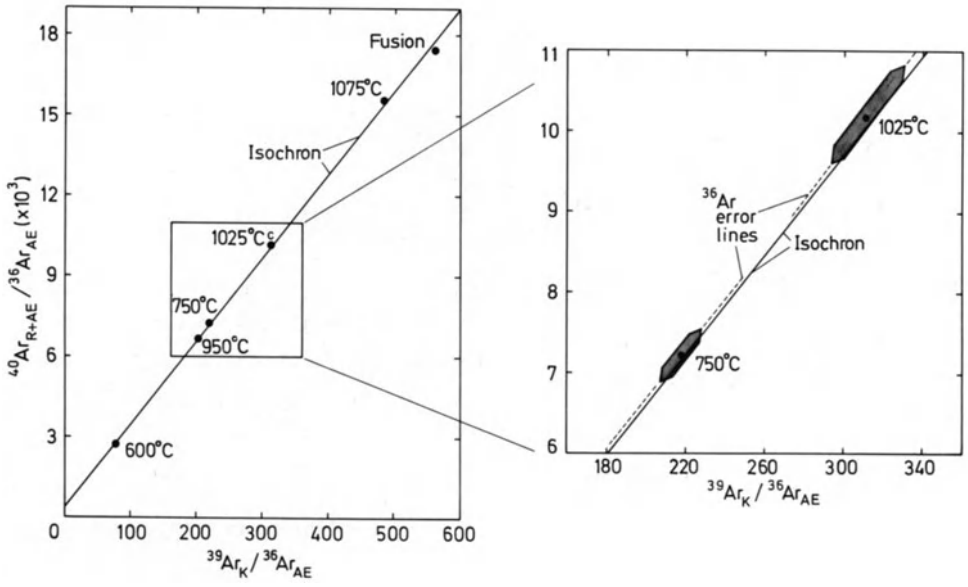

Fig. 6. $^{40}Ar/^{39}Ar$ isochron diagram for biotite loaded in position 2B in the irradiation package illustrated in Figure 1 (see Tables 3 and 4). Data define an isochron with an intercept of 325 ± 65 and a slope of 31.54 (corresponding to an age of 314 m.y.). Note in the enlarged portion of the diagram that large error correlations in the plotted ratios (largely a result of uncertainty in measurement of ^{36}Ar) causes points to move along ^{36}Ar error lines whose slopes are similar to that of the isochron

Slopes of isochrons are generally determined by least-squares regression and several equations which include two-error parameters have been developed for use in Rb-Sr dating. However, the method of York (1969) is most suitable for $^{40}Ar/^{39}Ar$ isochrons as it accomodates correlation of errors. This is required because the measured quantity of ^{36}Ar is typically much smaller than either ^{40}Ar or ^{39}Ar, and its analysis is commonly subject to rather large errors. This produces errors in the plotted ratios of typically between 10% and 15%, although ^{40}Ar and ^{39}Ar may be measured with a precision of at least 0.5%. Thus, errors in the plotted ratios are strongly correlated in a positive sense, and tend to shift points along an ^{36}Ar error line which passes through the origin (Fig. 6). Because the isochron intercept is also close to zero (relative to the typical magnitude of plotted ratio values), the ^{36}Ar error lines are commonly subparallel to the isochron. As a result, large uncertainty in measurement of ^{36}Ar moves points along the isochron and has a minimal effect on its slope (Fig. 6).

Example

$^{40}Ar/^{39}Ar$ analytical data for the biotite loaded in position 2B (Fig. 1) was previously listed in Table 3 and an age spectra presented in Figure 3. These data are now considered in construction of a $^{40}Ar/^{39}Ar$ isochron (shown in Fig. 6). Ratios determined from the analytical data are listed below (uncertainties in the ratios are a result of the uncertainty in ^{36}Ar measurement shown in Table 3). The isochron defined by these data has a slope of 31.54 and an intercept of 325 ±65. This corresponds to an isochron age of 314 m.y.:

$$t = 1.885 \times 10^9 \text{ yr } \ln\{1 + (0.005741)(31.54)\} = 314 \text{ m.y.}$$

Table 4. $^{40}Ar/^{39}Ar$ analytical data for biotite loaded in position 2B in the irradiation package illustrated in Figure 1

Release Temp.	$^{40}Ar_{R+AE}/^{36}Ar_{AE}$	$^{39}Ar_K/^{36}Ar_{AE}$
600°C	2714 ± 174	77 ± 5
750°C	7213 ± 374	218 ± 11
950°C	6692 ± 195	201 ± 6
1025°C	10185 ± 655	312 ± 20
1075°C	15574 ± 1171	480 ± 36
Fusion	17272 ± 1023	541 ± 32

6. Examples of the Application of $^{40}Ar/^{39}Ar$ Dating in Orogenic Terranes

Perhaps the most significant potential of $^{40}Ar/^{39}Ar$ dating is its ability to discriminate between samples which record cooling, gas-retention ages (with concordant age spectra), and samples which have lost a component of argon as a result of geologic reheating (with discordant age spectra). Because of this potential, the technique has particular application in orogenic terranes with locally complex metamorphic histories. It has been utilized in several areas within the Appalachian orogen to establish the local chronology of thermal events (Dallmeyer, 1975a, b, c, 1978; Dallmeyer et al., 1975; Dallmeyer and Sutter, 1976). Several of these studies are outlined below as examples of the applications of the $^{40}Ar/^{39}Ar$ technique.

6.1 $^{40}Ar/^{39}Ar$ Ages from a Remetamorphosed Basement Terrane

Dallmeyer (1975a) carried out a $^{40}Ar/^{39}Ar$ investigation of a portion of the west-central Blue Ridge tectonic province (Fig. 7) where a segment of the Appalachian Precambrian basement (Grenville-age gneisses) was progressively retrograded by a regional Ordovician (Taconic) metamorphic event (Fig. 8). The study was undertaken to evaluate the particular form of discordant age spectra which characterizes thermally overprinted biotite and hornblende.

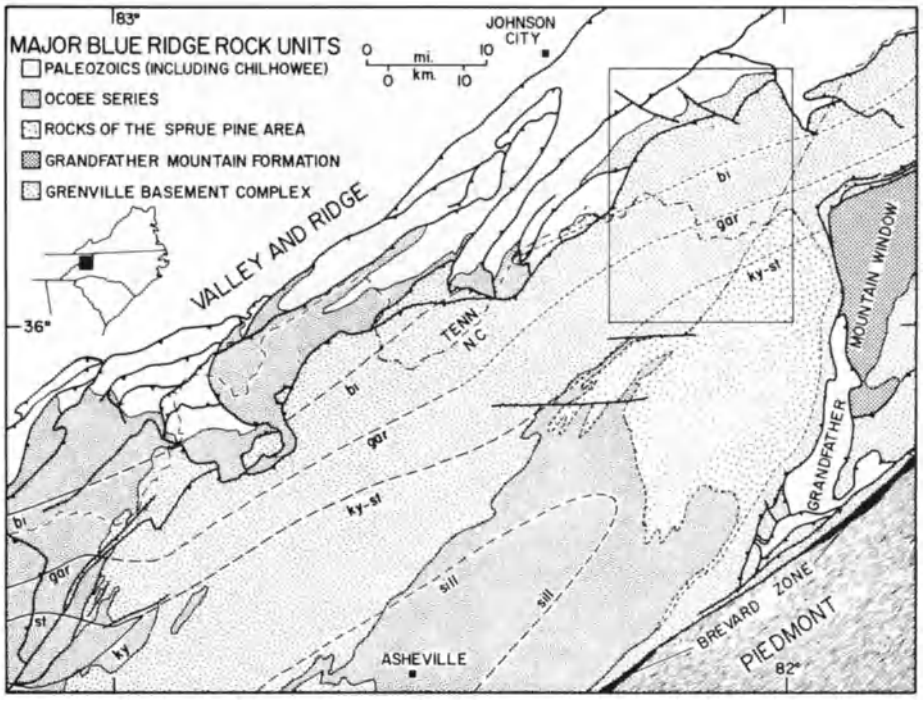

Fig. 7. Generalized geologic map of the central Blue Ridge tectonic province in eastern Tennessee and western North Carolina (from Dallmeyer, 1975a). Paleozoic metamorphic isograds are shown

In the northwestern portion of the area the basement terrane shows little petrographic evidence of retrograde alteration. Biotite occurs as fox-red, generally subhedral laths which show only slight chloritization along some grain margins (Fig. 8; samples 1, 3, 4, and 6). In this area hornblende occurs as unaltered, inclusion-free, subhedral grains (samples 2, 5, and 7). Southeastward, biotite becomes progressively paler in color, but extensive retrograde alteration is restricted. Biotites examined from this area (samples 8 and 9) show only peripheral chloritization and selection of fine-grained fractions allowed for clean concentrates to be obtained. Hornblende from this area (samples 9-11) remains unaltered. Retrograde alteration of biotite becomes progressively more extensive to the southeast and fine-grained, micaceous aggregates of chlorite and sericite develop along biotite cleavage. Concentrates from this zone (samples 12-15) show considerable contamination of this type. Hornblende in this area also begins to show marginal chloritization, yet finer-grained fractions show minor contamination (samples 13 and 14).

Retrograde alteration of biotite becomes pervasive to the southeast where pseudomorphic aggregates of chlorite and sericite totally replace biotite laths. Eventually, an extremely fine-grained, greenish-black and chemically distinct generation of biotite is added to this aggregate. This zone of the first appearance of the new biotite is shown in Figure 8. Biotite samples 16, 19, and 20 are the first uncontaminated concentrates

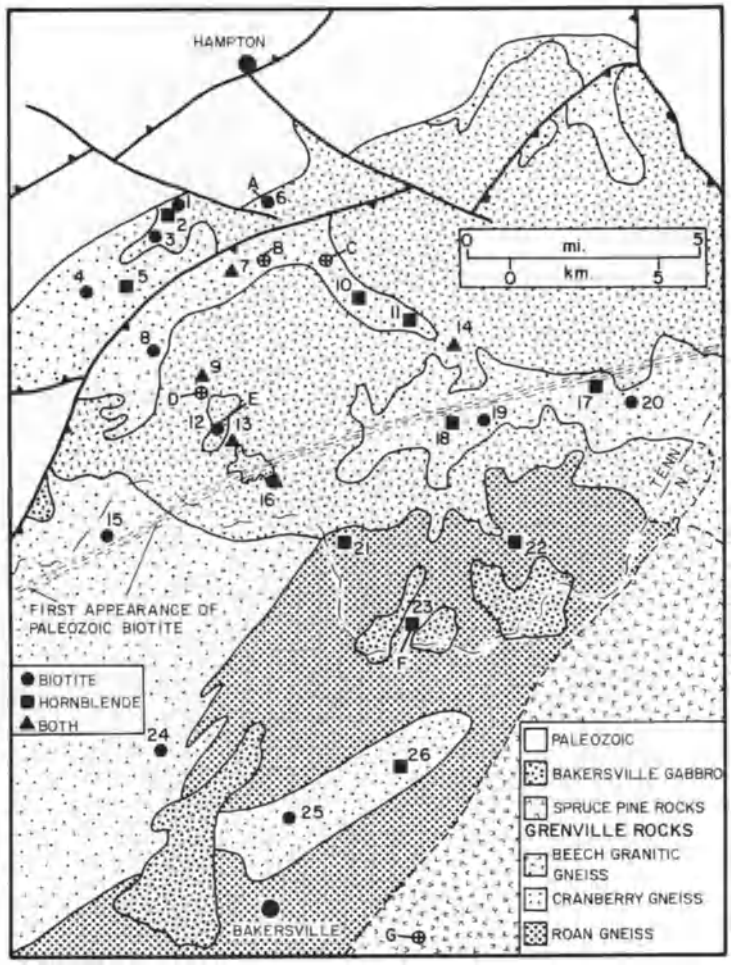

Fig. 8. Generalized geologic map of the Blue Ridge study area (from Dallmeyer, 1975a). Sample localities are shown. Zone of first appearance of Paleozoic biotite in retrograded basement rocks is indicated

of the new biotite which could be obtained. The new generation of biotite becomes coarser-grained southeast of the biotite isograd (samples 24 and 25).

Severe retrograde alteration of hornblende is not found for 2 km southeast of the first appearance of new biotite. Samples in the vicinity of the biotite isograd (17, 18, and 21) show more extensive chloritization along grain margins, yet clean concentrates were obtained. Southeastward from the biotite isograd, this alteration begins to develop along hornblende cleavage, and precludes processing of pure concentrates. This region of extensive hornblende alteration is followed to the southeast by the appearance of a new generation of optically and chemically distinct hornblende. Three samples of this new hornblende phase have been examined (samples 22, 23, and 26).

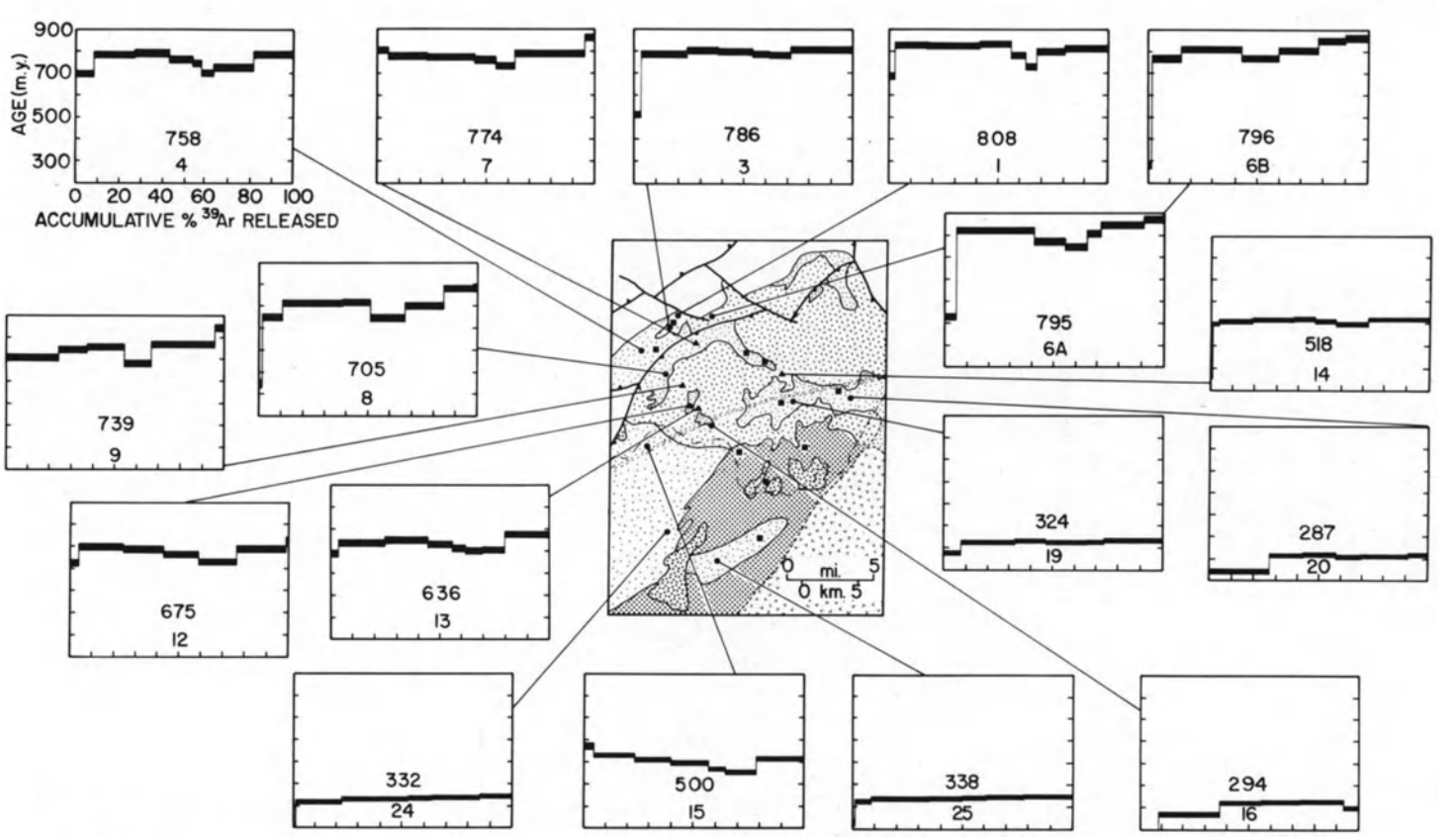

Fig. 9. $^{40}Ar/^{39}Ar$ age spectra of biotite from variably retrograded basement gneisses in the west-central Blue Ridge (from Dallmeyer, 1975a). All spectra have coordinates shown in *upper left*. Estimated uncertainties indicated by *width of bar*. Total-gas ages (in m.y.) shown on each spectrum

All of the biotite $^{40}Ar/^{39}Ar$ analytical data are displayed as age spectra in Figure 9 (samples are numbered consecutively from 1 to 26 to generally correspond with increasingly higher grades of Paleozoic metamorphism). Release spectra of the petrographically unaltered older biotite generation in the northwestern portion of the area are compared in Figure 10. Sample 3 displays the least disturbed spectrum, with a nearly concordant pattern defining a total-gas date of 786 m.y. This age and the plateau nature of the spectrum are remarkably identical to that of biotite described by Dallmeyer et al. (1975) from nonretrograded Grenville gneisses of the northeastern Reading Prong in New York. The remaining Blue Ridge biotite samples show a progressive modification of the plateau-type spectrum with development of low age "saddles" in intermediate temperature fractions. Initially, the "saddle" is restricted (sample 1), but it progressively widens in samples to the southeast (samples 4, 6, and 7). Ages

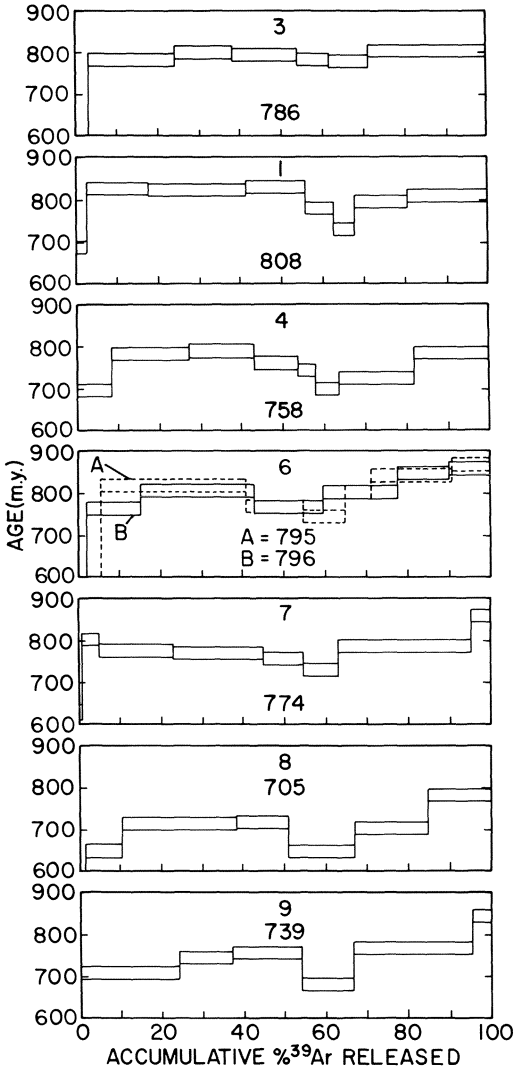

Fig. 10. Comparison of $^{40}Ar/^{39}Ar$ spectra of biotite from the northwestern portion of the Blue Ridge study area. Spectra are listed in order of increasing intensity of Paleozoic metamorphism *(top to bottom)*. Data plotted as in Figure 9. Total-gas ages (in m.y.) shown on each spectrum

defined by the low and high temperature sides of the "saddle" are consistently similar to the plateau age of sample 3. Eventually, the saddle widens to encompass most of the intermediate temperature fractions (samples 8 and 9), and ages defined by gas fractions on the low temperature side of the "saddle" are noticeably younger than those of the high temperature gas fractions.

X-ray diffraction scans of these eight biotite concentrates show no significant contamination, and the disturbed release spectra must be a result of the experimental outgassing of thermally altered biotite. The marked similarity in age of the plateau spectra of sample 3 and of the low and high temperature sides of the "saddle" spectra with that of biotite from the Reading Prong suggests a similar post-Grenville cooling history. The progressive southeastward modification of the plateau spectra is correlative with increasing intensity of Paleozoic metamorphism, and it appears that the "saddle" spectra are an expression of the Paleozoic thermal overprinting on the Grenville biotites. However, the disturbed spectra do not compare with those expected if simple volume diffusion loss of radiogenic argon had occurred during the geologic reheating (see Fig. 4).

The chemically distinct biotites from the southeastern portion of the study area record markedly younger ages (total-gas ages of 328-287 m.y., Fig. 9), and generally display undisturbed release spectra. This range of total-gas ages is similar to that of biotite from recrystallized Blue Ridge basement rocks elsewhere in the southern Appalachians, and they are interpreted as dating times of argon retention following a 480 m.y. metamorphic event. Total-gas ages of samples from the transitional zone in Figure 8 (samples 12-15) are intermediate between those of the Paleozoic biotites and those of the disturbed Grenville biotites (675-500 m.y.). The spectra of these samples are variably complex (Fig. 9), but because all concentrates show some degree of contamination, the significance of these spectra is uncertain.

All of the hornblende age spectra are shown in Figure 11. Samples from the northwestern portion of the study area record variably disturbed release spectra. Several record anomalous old ages in low temperature release fractions (samples 2, and 7). A similar pattern has been described in studies of thermally undisturbed metamorphic hornblende in other areas (Dallmeyer, 1975b, c) and appears to reflect the experimental outgassing of a small component of loosely-bound extraneous argon (of nonatmospheric $^{40}Ar/^{36}Ar$ ratio) in low temperature fractions. It is interesting that in the present study, the remaining release spectra of the older hornblende generation do not display evidence of this contamination, and all show evidence of partial argon loss during Paleozoic reheating. This may suggest that if initially present, the extraneous argon was liberated during geologic reheating.

Except for the anomalous age of the low temperature release fraction, sample 2 records an undisturbed release spectrum. The total-gas age is 1003 m.y. Although similar total-gas ages are recorded by samples 5, 7, 9, 10, and 13 (1059-956 m.y.), the release spectra are disturbed to different degrees.

As with biotite from this area, the extent of modification of the hornblende spectra increases southeastward, suggesting Paleozoic thermal overprinting. The progressive modification of the spectra is noticeably different from that of the biotite spectra, and approximately follows a model of diffusive argon loss; incremental ages becoming progressively older from low to high release temperatures (see Fig. 4). Initially, only the

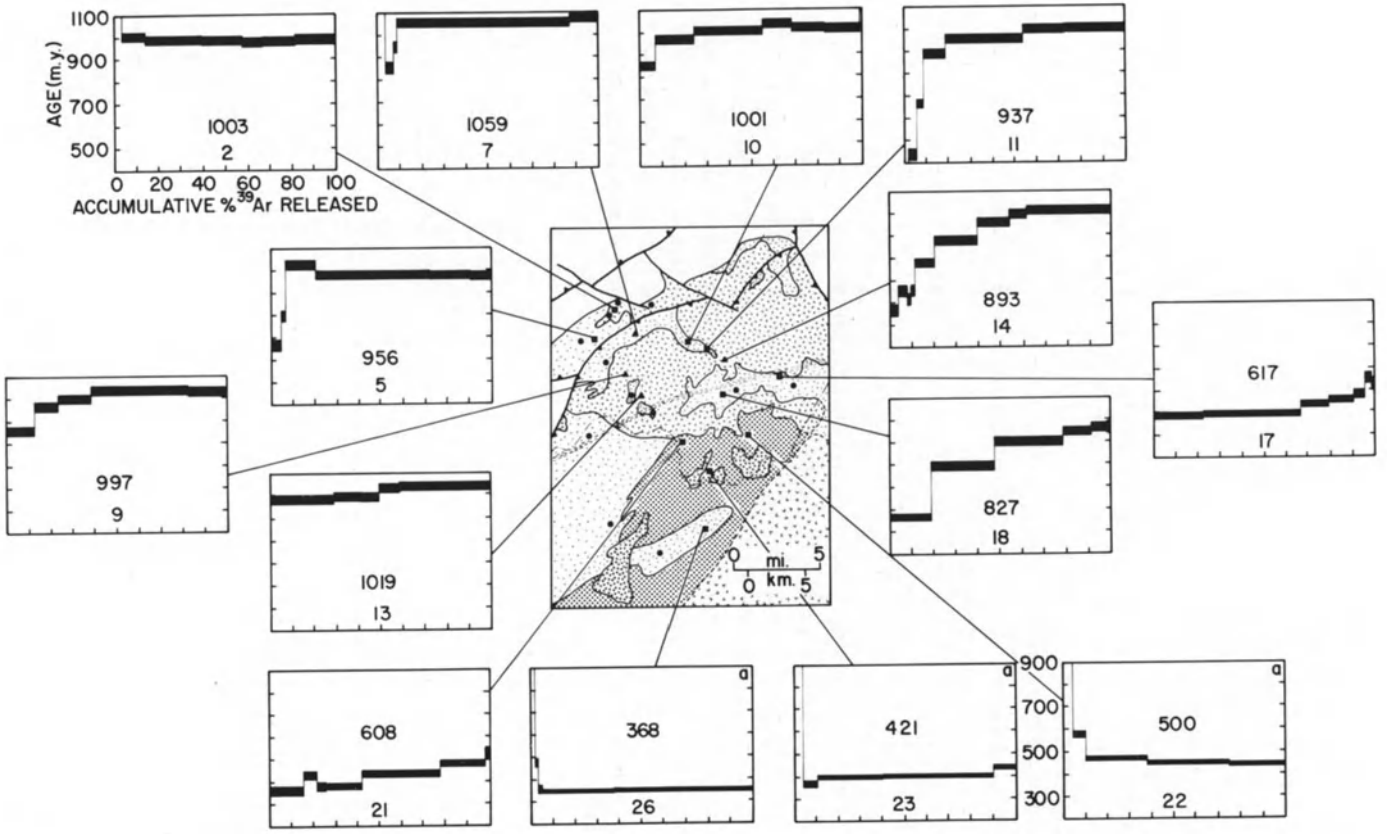

Fig. 11. $^{40}Ar/^{39}Ar$ age spectra of hornblende from variably retrograded basement gneisses in the west-central Blue Ridge (from Dallmeyer, 1975a). Similar coordinates *(upper left)* used for all spectra except three on *lower right (a)* which have different vertical scale. Estimated uncertainties indicated by *width of bar*. Total-gas ages (in m.y.) shown on each spectrum

lowermost temperature increments record younger ages (samples 7, 9-11, and 13), and a substantial portion of the release spectra records ages near 1000 m.y. (similar to that of sample 2). Samples 14 and 18 show more extensive argon loss and only the highest temperature fractions retain approximately 1000 m.y. dates. Eventually, Paleozoic metamorphic temperatures appear to have been high enough to effect diffusive loss of most radiogenic argon within the hornblende, because in samples 17 and 21, the 1000 m.y. age is not recorded in even the highest temperature fractions.

Although a model of diffusive argon loss during Paleozoic reheating is suggested by the disturbed release spectra, it appears that the actual time of Paleozoic reheating cannot be precisely determined. Following Turner's predictions (1968; see Fig. 4) for diffusive loss spectra, ages of low temperature gas fractions of the most disturbed samples should approximate the time of partial argon loss. In the present case, this age would be 600-550 m.y. (see samples 14, 17, 18, and 21). This is older than previous estimates of the actual time of Blue Ridge metamorphism and is incompatible with geologic constraints because Lower Ordovician rocks are affected by the event. Turner's theoretical gas loss spectra were calculated using models of argon loss from isotropic material. Considering the possible variations in activation energies of potential argon sites within hornblende, it is not surprising that total resetting of all sites was not accomplished by Paleozoic reheating in this area. It is likely that actual recrystallization may be necessary to reset hornblende ages totally.

The new hornblende generation developed in the southeastern portion of the study area (samples 22, 23, and 26) records generally undisturbed spectra. Although their total-gas ages are different (460, 400, and 355 m.y.), all are older than biotite plateau dates within the area. Many workers have demonstrated that hornblende retains argon at higher temperatures than biotite, and it appears that following the 480 m.y. Blue Ridge metamorphic event, hornblende closed with respect to continuous argon loss prior to biotite and, therefore, records older ages. Plateau ages defined by the three hornblende samples decrease in age to the southeast, in the same direction as Paleozoic metamorphic grade increases. Thus, the difference in hornblende total-gas dates may reflect diachronous post-metamorphic cooling as a result of variations in initial Paleozoic metamorphic conditions.

6.2 $^{40}Ar/^{39}Ar$ Mineral Ages Across the Georgia Inner Piedmont

The southern portion of the Appalachian orogen has been divided into several tectono-metamorphic belts, each generally differing in predominant lithologies, metamorphic grade, structural history, and physiography (Fig. 12). The metamorphic history of the crystalline terrane within the southern Appalachian Piedmont has long been uncertain. Kulp and Eckelmann (1960) made the first regional geochronological attempts to delineate the extent and timing of Paleozoic thermal events within the area by reconnaissance determination of K-Ar and Rb-Sr mica ages. Although these ages showed considerable variation, ranging from 350 to 250 m.y., they followed a generally consistent geographic distribution with younger ages confined to a narrow, northeast-trending belt extending through Georgia and the Carolinas (Fig. 13). Mica ages consistently increased away from this belt into areas characterized by 350 m.y. dates. Kulp and

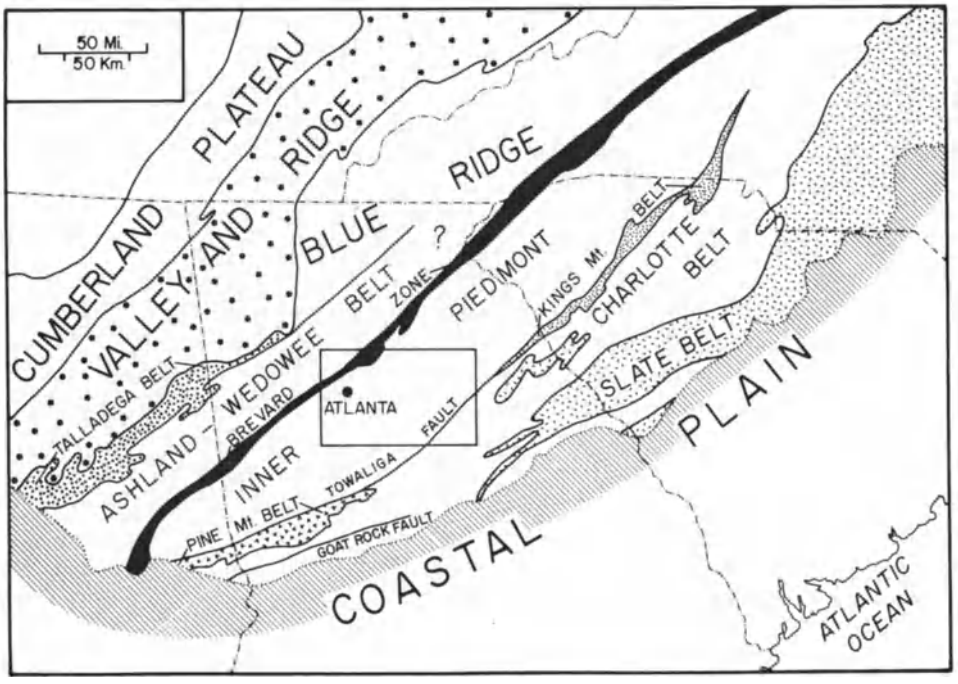

Fig. 12. Regional tectonometamorphic belts within the southern Appalachians (from Dallmeyer, 1978). Area of $^{40}Ar/^{39}Ar$ traverse is outlined (area of Fig. 14)

Eckelmann considered the geographic distribution of mica ages to be a result of the effects of several superimposed Paleozoic metamorphic events. They proposed that most of the southern Appalachian Piedmont underwent widespread metamorphic recrystallization at 350 m.y., but that within the 250 m.y. geochronological province, a Late Paleozoic regional metamorphism totally reset mica ages. Outward from this zone, they suggested that mica ages were variably reset by the Late Paleozoic thermal event, thereby producing the observed systematic increase in mica dates from 250 m.y. to 350 m.y.

Since these initial efforts, considerable field work has been carried out in the southern Appalachian Piedmont, and little evidence of Late Paleozoic orogenic activity has been described. In addition, it has now been established that systematic regional variations in K-Ar and Rb-Sr mineral ages can develop as a result of differential cooling (with resultant diachronous retention of mobile radiogenic products) following an individual metamorphic event. As a result, the geologic significance of the 250 m.y. age belt within the southern Appalachian Piedmont has been questioned.

Because $^{40}Ar/^{39}Ar$ incremental-release dating has the potential of distinguishing gas-retention (cooling) K-Ar ages from disturbed K-Ar ages (which are likely to characterize a terrane affected by partially superimposed thermal events), it provides a means of evaluating the significance of the southern Appalachian 250 m.y. age belt. For this reason, Dallmeyer (1978) utilized the technique to study variations in the ages of biotite and hornblende in a traverse across the 250 m.y. age province within the Inner

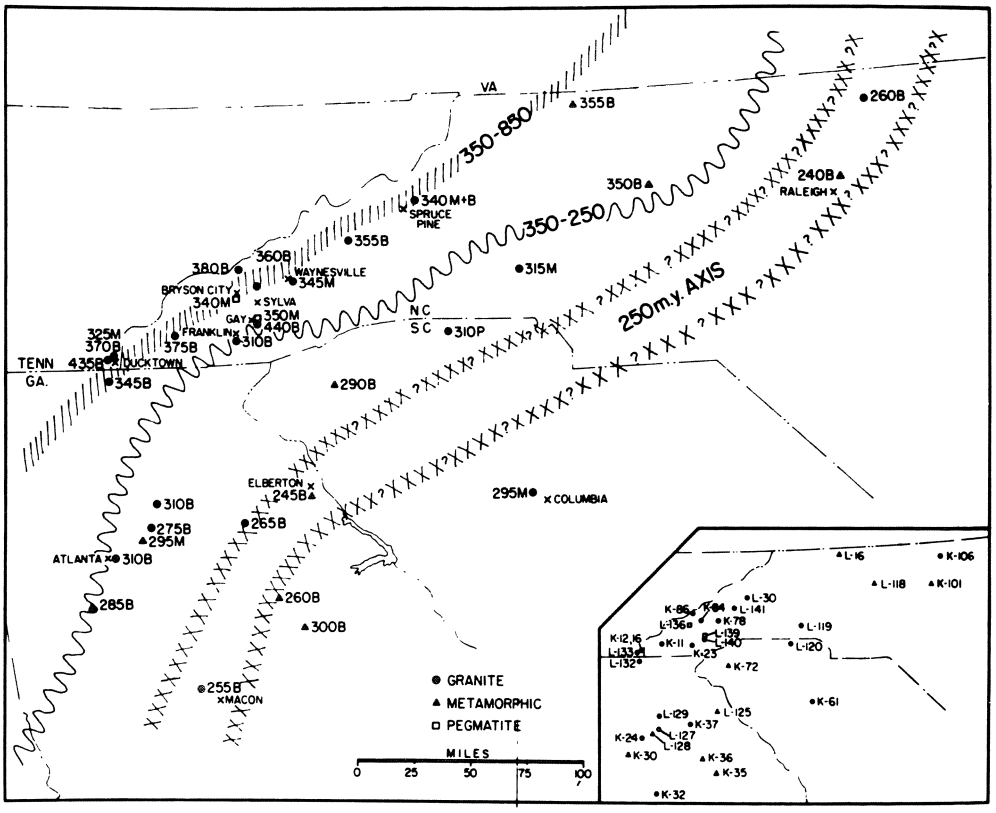

Fig. 13. Geochronological provinces within the southern Appalachians (from Kulp and Eckelmann, 1960). The 250 m.y. axis was interpreted by Kulp and Eckelmann as a zone of Late Paleozoic regional metamorphism superimposed on a terrane previously metamorphosed at 350 m.y.

Piedmont of Georgia (Fig. 14). Most of the traverse area is characterized by migmatitic muscovite-biotite quartzofeldspathic gneisses and granitic gneisses. Amphibolite is locally common. An overall southeasterly increase in degree of migmatite development is apparent, and it appears to be related to a general increase in metamorphic grade (kyanite developed in appropriate bulk compositions in the northwest, sillimanite developed in the southeast, Fig. 14).

$^{40}Ar/^{39}Ar$ age spectra of biotite and hornblende from the traverse are shown in Figures 15 and 16. All of the spectra are undisturbed (concordant), and thus are inconsistent with previous interpretations of the 250 m.y. age belt as a distinct zone of Late Paleozoic regional metamorphism. Instead, the undisturbed spectra together with the consistent geographic distribution of total-gas ages (older dates recorded in the northwest for each mineral phase) combine to suggest that all of the ages may be considered cooling, gas-retention dates. This interpretation is supported by the total absence of any retrogressive mineral assemblages in the samples examined in conjunction with this study. Because older ages are recorded by both biotite and hornblende in the north-

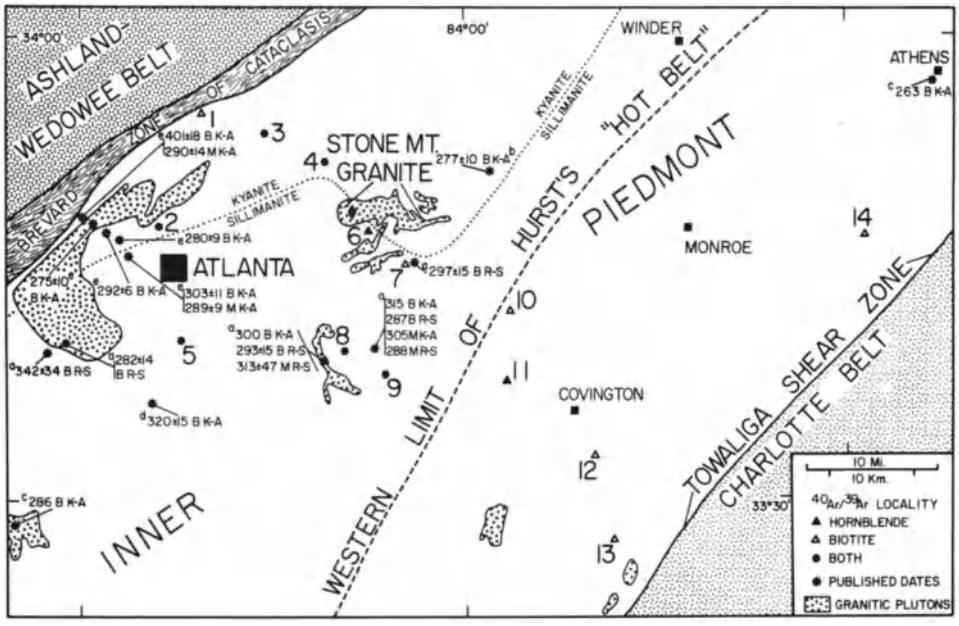

Fig. 14. Generalized geologic map of the Georgia Inner Piedmont in the vicinity of the $^{40}Ar/^{39}Ar$ traverse (from Dallmeyer, 1978). Western limit of the 250 m.y. Piedmont mica age belt is defined by Hurst's "hot belt"

western portion of the Georgia Inner Piedmont, it is implied that following metamorphism, this region must have cooled below argon retention temperatures prior to the southeastern terrane. Lower-grade metamorphic conditions do appear to have characterized the northwestern flank of the Inner Piedmont, and it is likely that the diachronous post-metamorphic cooling is, in part, a result of original differences in maximum metamorphic conditions. However, it does not appear that maximum metamorphic conditions were drastically different along the sample traverse, and it is unlikely that the large variation in $^{40}Ar/^{39}Ar$ total-gas dates (317-236 m.y.) could, in total, be only a result of a northwest-southeast temperature gradient in metamorphic temperatures. Thus, it is likely that there were northwest-southeast variations in post-metamorphic cooling rates and/or uplift rates. Through consideration of available Rb-Sr dating of metamorphic plutonic events, it has been possible to document the Late Paleozoic-Early Mesozoic tectonothermal history of the Inner Piedmont and show that its rapid uplift as a mobile orogenic core was a major source of tectonic force during the late Paleozoic history of the Appalachian orogen.

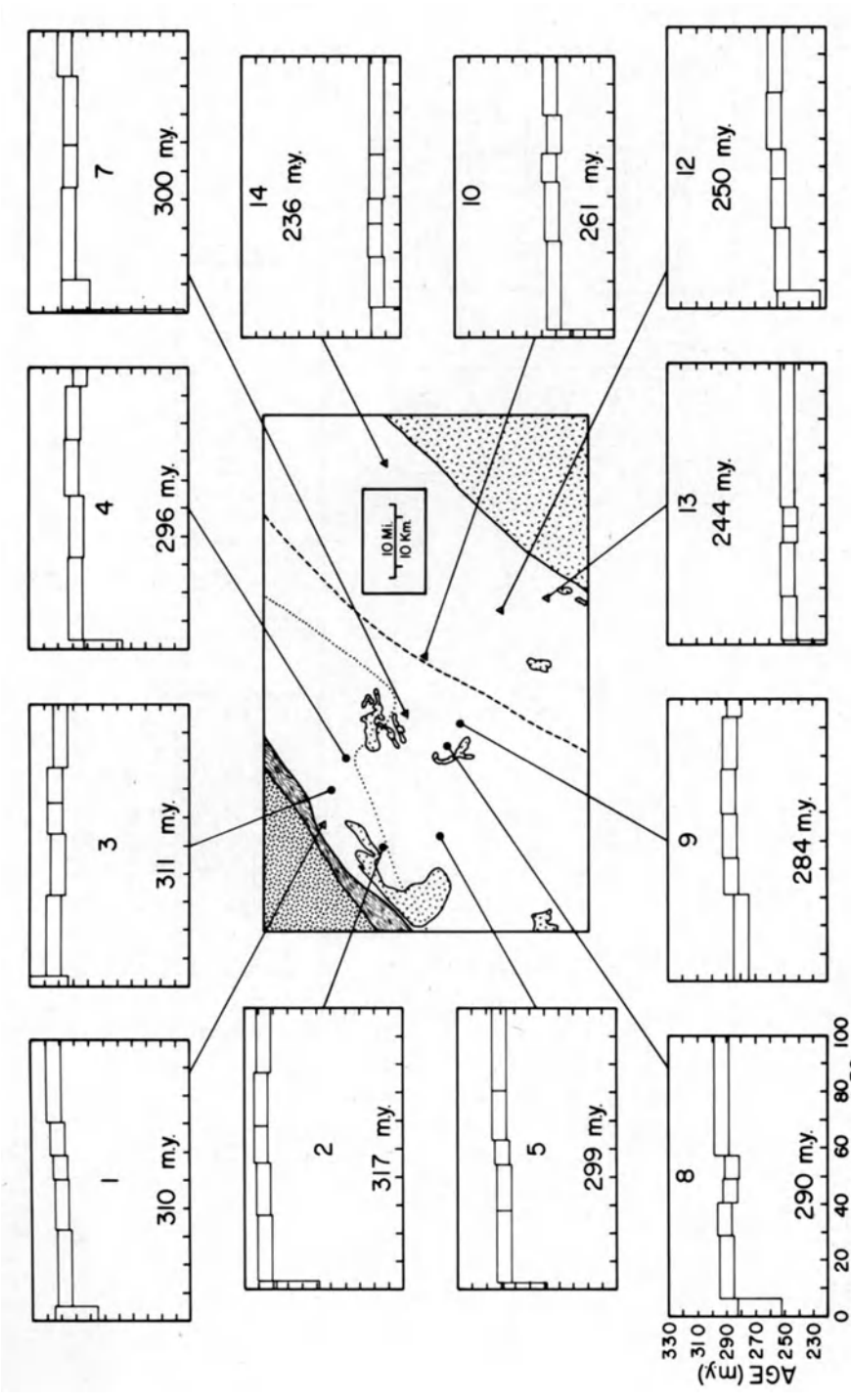

Fig. 15. $^{40}Ar/^{39}Ar$ age spectra of biotite from the Georgia Inner Piedmont (from Dallmeyer, 1978). Estimated uncertainties indicated by *width of bar*. All spectra have coordinates show in *lower left* (total-gas ages shown on each spectrum)

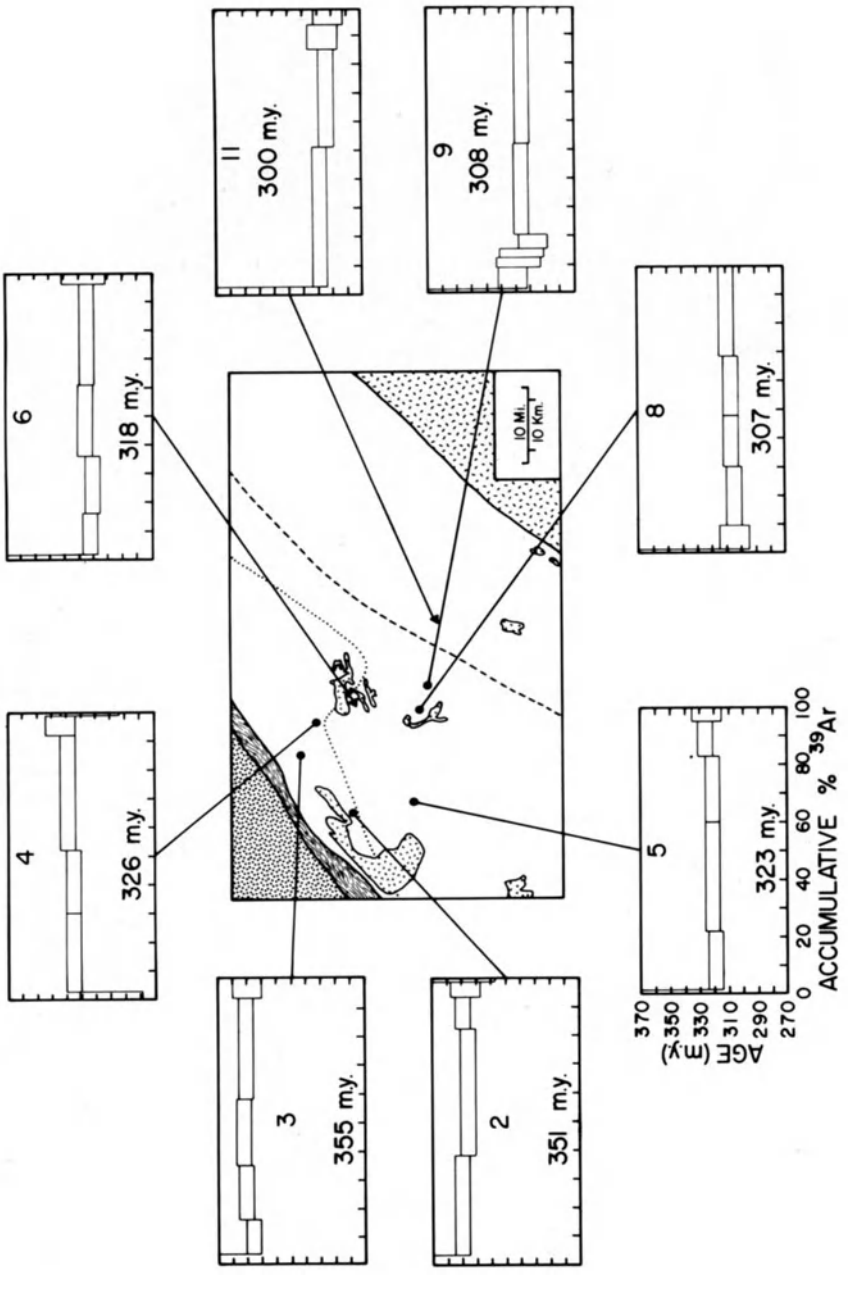

Fig. 16. $^{40}Ar/^{39}Ar$ age spectra of hornblende from the Georgia Inner Piedmont (from Dallmeyer, 1978). Estimated uncertainties indicated by *width of bar*. All spectra have coordinates shown in *lower left* (total-gas ages shown on each spectrum)

References

Berger, G.W., York, D.: Precision of the $^{40}Ar/^{39}Ar$ dating technique. Earth and Planet. Sci. Lett. *9*, 39-44 (1970)

Brereton, N.R.: Corrections for interfering isotopes in the $^{40}Ar/^{39}Ar$ method. Earth and Planet. Sci. Lett. *8*, 427-433 (1970)

Brereton, N.R.: A reappraisal of the $^{40}Ar/^{39}Ar$ stepwise degassing technique. R. Astr. Soc. Geophys. J. *27*, 449-478 (1972)

Dallmeyer, R.D.: $^{40}Ar/^{39}Ar$ incremental release ages of biotite and hornblende from pre-Kenoran gneisses between the Matagami-Chibougamau and Frotet-Troilus greenstone belts, Quebec. Can. J. Earth Sci. *11*, 1586-1593 (1974)

Dallmeyer, R.D.: $^{40}Ar/^{39}Ar$ ages of biotite and hornblende from a progressively re-metamorphosed basement terrane: Their bearing on interpretation of release spectra. Geochim. Cosmochim. Acta *39*, 1655-1669 (1975a)

Dallmeyer, R.D.: Incremental $^{40}Ar/^{39}Ar$ ages of biotite and hornblende from retrograded basement gneisses of the southern Blue Ridge: Their bearing on the age of Paleozoic metamorphism. Am. J. Sci. *275*, 444-460 (1975b)

Dallmeyer, R.D.: $^{40}Ar/^{39}Ar$ release spectra of biotite and hornblende from the Cortlandt and Rosetown plutons, New York, and their regional implications. J. Geol. *83*, 629-643 (1975c)

Dallmeyer, R.D.: $^{40}Ar/^{39}Ar$ incremental-release ages of hornblende and biotite across the Georgia Inner Piedmont: Their bearing on Late Paleozoic-Early Mesozoic tectonothermal history. Am. J. Sci. *278*, 214-238 (1978)

Dallmeyer, R.D., Sutter, J.F.: $^{40}Ar/^{39}Ar$ incremental-release ages of biotite and hornblende from variably retrograded basement gneisses of the northeasternmost Reading Prong, New York: Their bearing on Early Paleozoic metamorphic history. Am. J. Sci. *276*, 731-747 (1976)

Dallmeyer, R.D., Sutter, J.F., Baker, D.J.: Incremental $^{40}Ar/^{39}Ar$ ages of biotite and hornblende from the northeastern Reading Prong. Their bearing on Late Proterozoic thermal and tectonic history. Geol. Soc. Am. Bull. *86*, 1435-1443 (1975)

Dalrymple, G.B., Lanphere, M.A.: $^{40}Ar/^{39}Ar$ age spectra of some undisturbed terrestrial samples. Geochim. Cosmochim. Acta *38*, 715-738 (1974)

Fitch, J.G., Miller, J.A., Mitchell, J.G.: A new approach to radio-isotopic dating in orogenic belts. In: Time and Place in Orogeny. Kent, P.E., Sattherthwaite, G.E., Spencer, A.M. (eds.). Geol. Soc. London Spec. Publ. *3*, 1969, pp. 157-195.

Kulp, J.L., Eckelmann, F.D.: Potassium-Argon Isotopic Ages on Micas from the southern Appalachians. Ann. N.Y. Acad. Sci. *91*, 408-419 (1960)

Lanphere, M.A., Dalrymple, G.B.: A test of the $^{40}Ar/^{39}Ar$ age spectrum technique on some terrestrial materials. Earth and Planet. Sci. Lett. *12*, 359-372 (1971)

Merrihue, C.: Trace element determinations and potassium-argon dating by mass spectroscopy of neutron-irradiated samples (abst.). Trans. Am. Geophys. Univ. *46*, 125 (1965)

Merrihue, C., Turner, G.: Potassium-argon dating by activation with fast neutrons. J. Geophys. Res. *71*, 2852-2857 (1966)

Mitchell, J.G.: The argon-40/argon-39 method for potassium-argon age determination. Geochim. Cosmochim. Acta *32*, 781-790 (1968)

Sigurgeirsson, T.: Dating recent basalt by the potasssium-argon method. Rep. Phys. Lab. Univ. Iceland, 9 p. (1962)

Turner, G.: The Distribution of Potassium and Argon in Chondrites. In: Origin and Distribution of the Elements. Ahrens, L.H. (ed.). London: Pergamon Press, 1968, pp. 387-398

Turner, G.: Thermal histories of meteorites by the ^{39}Ar-^{40}Ar method. In: Meteorite Research. Millman, P.M. (ed.). Reidel, 1969, pp. 407-417
Turner, G.: Argon-40/argon-39 dating of lunar rock samples. Proc. Apollo 11 Lunar Sci. Conf. Geochim. Cosmochim. Acta, Suppl. 1, Vol. 2, 1665-1684 (1970a)
Turner, G.: Thermal histories of meteorites. In: Paleogeophysics, Runcorn, S.K. (ed.). New York: Academic Press, 1970b, pp. 491-502
Turner, G.: ^{40}Ar-^{39}Ar age determination of lunar rock 12013. Earth and Planet. Sci. Lett. *9*, 177-180 (1970c)
Turner, G.: $^{40}Ar/^{39}Ar$ ages from the lunar maria. Earth and Planet. Sci. Lett. *11*, 169-191 (1971)

U–Th–Pb Dating of Minerals

D. GEBAUER and M. GRÜNENFELDER

1. The U-Th-Pb Decay Schemes

Natural U consists of two radioactive parent-isotopes, ^{238}U and ^{235}U, the half-lives of which fall into the range of geologic time. Outside this range is the half-life of ^{232}Th, which represents the only natural isotope of Th.

$$^{238}U \xrightarrow{\substack{8 \text{ alphas} \\ 6 \text{ betas}}} {}^{206}Pb; \text{ half-life } T = 4468 \text{ m.y.}$$

$$^{235}U \xrightarrow{\substack{7 \text{ alphas} \\ 4 \text{ betas}}} {}^{207}Pb; \text{ half-life } T = 704 \text{ m.y.}$$

$$^{232}Th \xrightarrow{\substack{6 \text{ alphas} \\ 4 \text{ betas}}} {}^{208}Pb; \text{ half-life } T = 14010 \text{ m.y.}$$

The spontaneous decay of these three parent isotopes enables us to perform three independent age determinations. The number of atoms of ^{206}Pb, ^{207}Pb, and ^{208}Pb which accumulate in a time t are given in terms of the present amounts of ^{238}U, ^{235}U, and ^{232}Th:

$$^{206}Pb = {}^{238}U\,(e^{\lambda_8 t} - 1) \tag{1}$$

$$^{207}Pb = {}^{235}U\,(e^{\lambda_5 t} - 1) \tag{2}$$

$$^{208}Pb = {}^{232}Th\,(e^{\lambda_2 t} - 1) \tag{3}$$

where λ_8, λ_5, and λ_2 are the decay constants for ^{238}U, ^{235}U, and ^{232}Th, respectively (Le Roux and Glendenin, 1963; Jaffey et al., 1971).

An additional age, the so-called lead/lead age, can be obtained from the isotopic analysis of lead alone, i.e., from the $^{207}Pb/^{206}Pb$ ratio. Usually, this ratio, as well as the total concentration of radiogenic lead, has to be corrected for common, i.e., non-radiogenic, lead consisting of the masses 204, 206, 207, and 208. This nonradiogenic lead might be incorporated into the analyzed mineral during crystallization and/or recrystallization. To some extent it is always present due to contamination during the analytical procedure.

The $^{207}Pb/^{206}Pb$ ratio is itself time-dependent, because of the different half-lives of ^{235}U and ^{238}U. Thus, the lead/lead age can be calculated by dividing Eq. (2) by Eq. (1):

$$^{207}Pb/^{206}Pb = \frac{1\,(e^{\lambda_5 t} - 1)}{137{,}88\,(e^{\lambda_8 t} - 1)}$$

where 1/137.88 is the present-day atomic ratio $^{235}U/^{238}U$ (Shields, 1960).

2. Minerals Most Frequently Used for U-Th-Pb Chronology

In principle, any U-Th bearing mineral, such as apatite, xenotime, allanite, uraninite, or thorite can be used for dating. U-Th-Pb whole-rock analyses have also been used for age determinations (e.g., Rosholt and Bartel, 1970; Farquharson and Richards, 1970; Sinha, 1972; Nunes and Steiger, 1974; Moorbath et al., 1975; Oversby, 1975). However, as zircon is by far the most frequent mineral dated by the U-Pb method, the following chapters concern mainly this material.

Table 1. Minerals most frequently used for U-Th-Pb chronology

Mineral	Zircon	Monazite	Sphene
Chemical formula	$ZrSiO_4$	$CePO_4$	$CaTiSiO_5$
Primary occurrence	Gabbros to granites	Granitic rocks and high-grade metasediments	Gabbros to granites
U-concentrations (ppm)	10-4000	2000-10000	20-200
Th-concentrations (ppm)	3-1000	10000-100000	70-600

3. Sampling, Mineral Separation and Chemical Extraction of U and Pb

The most critical step in U-Pb dating of minerals is the mass-spectrometric analysis of Pb. Generally, on the order of 100 ng (= 10^{-9} g) are necessary for a good routine measurement. Therefore, the quantity of rock collected in the filed has to account for this. Mainly three factors have to be considered: the concentration of zircon in the rock, the U-content, and the age of the zircon to be analyzed.

In the case of the most frequently dated rock types – unmetamorphosed granitic rocks, felsic para- and orthogneisses – a rough estimate of the zircon concentration

can be made by the amount of zircon found in thin sections and/or the amount of Zr in a rock powder (e.g., X-ray fluorescence analysis). In the case of mafic and especially ultramafic rocks, zircons are – if they are present at all – much more difficult to recognize in thin sections. The Zr-content in the corresponding rock powder may not be a reliable indicator of the zircon amount, however, as hornblendes, pyroxenes, olivines, and garnets might trap large amounts of Zr. Thus, the safest method to check the amount of zircon from these rock types is to crush a hand specimen of rock and concentrate zircons by using heavy liquids.

The age and U-content of zircons are the other two important factors for sampling in the field. Of course, a U-rich zircon population extracted from a 3.7 b.y. old rock, e.g., from West Greenland, might have a radiogenic lead content which is higher by abouth three orders of magnitude than the lead content of a U-poor zircon population extracted from an alpine peridotite. In most cases estimates of minimum and maximum ages can be made from geologic arguments and/or already existing age data. The U-content can be roughly estimated from the rock type, although large variations might be possible. After mineral separation it can be determined with sufficient accuracy using an alpha-counter.

In case of Phanerozoic samples, typical quantities of rock are on the order of 50 kg, as the zircon population should be split up into several size- and magnetic fractions.

Naturally, it is safest to take fresh, completely unaltered rocks. However, tests on zircons and monazites extracted from completely disintegrated orthogneisses from two areas of the French Central Massif (Gebauer and Grünenfelder, unpubl.), containing roots and other biogenic matter, proved that the corresponding U-Pb systems remained unaffected by weathering. These results conform with the obviously closed-system behavior of detrital zircons from unmetamorphosed sediments during weathering, transport, and diagenesis (Ledent et al., 1964; Tatsumoto and Patterson, 1964; Grauert et al., 1973; Abdel-Monem, 1977; Gaudette et al., 1977; Gebauer and Grünenfelder, 1977b). Closed U-Pb zircon systems during weathering were also reported by Grünenfelder and Silver (1958).

However, there is also another observation contrasting the closed-system behavior during weathering. Stern et al. (1966) found evidence for recent lead loss during weathering in the residual clay of the Archean Morton gneiss in Minnesota. Possibly the strong metamictization of the zircons from the residual clay of the Morton gneiss is the cause for loss of radiogenic lead due to groundwater interaction. In contrast, the relatively weak radiation damage produced in the relatively young zircons from the French Central Massif might have prevented a recent opening of the corresponding U-Pb systems. Also, the degree of weathering seems to be much stronger for the residual clay of the Morton gneiss than for the disintegrated, sandy orthogneiss of the French Central Massif still showing a nebulous gneissic structure. In a paper by Naylor et al. (1970) the authors explain the results of Stern et al. (1966) as being possibly due to recent lead loss during acid washing treatment. Whatever might be true, it goes without saying that no one should feel encouraged to take samples for U-Pb dating of minerals with a spade. Nevertheless, the understanding of the behavior of U-Pb systems in zircons and monazites during weathering of the host rock is very important for the interpretation of the U-Pb ages of detrital zircons in unmetamorphosed and metamorphosed sediments.

In order to separate zircon from its host rock it is necessary to crush, mill, and sieve the rock. The sieve fraction below the maximum grain size of the zircons, e.g., about 200-300 μ, is put on a Wilfley shaking table to separate the heavy mineral fraction. Depending on the rock type, magnetic minerals like biotite, garnet, hornblende, or pyroxene can be removed using a magnetic drum separator. If these minerals are not very abundant one might directly continue by using heavy liquids. For the first step this will be in general methyleniodide (density 3.3 g/cc). Mainly feldspars and quartz, as well as micas, are removed by this procedure. The remaining fraction with a density above 3.3 g/cc might be split up with an isodynamic magnetic separator into fractions of higher and lower magnetic susceptibilities. The zircons will concentrate in the relatively nonmagnetic fractions which then are generally passed through Clerici solution with a density of about 4.1 g/cc. The final purification might be done magnetically or, if this does not help, by tedious handpicking under a binocular.

Typically, fractions on the order of 10 mg are necessary for a good routine analysis if we are dealing with about 300-m.y.-old zircons containing around 500 ppm of U. However, in future it will become feasible to use even smaller quantities of zircon. This will require a reduction of the contamination of common lead introduced during the chemical procedure and mass spectrometric improvements which allow accurate ratios to be determined from even smaller ion currents of Pb and U, i.e., ion currents on the order of 10^{-14}-10^{-13} amps.

To separate lead and uranium from zircon it is necessary to decompose the sample. Since about 1973 this has generally been done with HF in teflon capsules confined by stainless steel jackets at temperatures of 220°C (Krogh, 1973). After separation of U and Pb using anion exchange columns, both elements are ready for mass spectrometric analysis. For routine measurements of 10-mg samples, the common lead introduced during the chemical procedure is on the order of 1 ng (= 10^{-9} g).

4. The Concordia Diagram

U/Pb age results are generally presented graphically in the concordia diagram introduced by Wetherill (1956a). The atomic ratios of $^{206}Pb/^{238}U$ are plotted against those of $^{207}Pb/^{235}U$ (Fig. 1) The concordia curve is then the locus of all points for which the $^{206}Pb/^{238}U$ ages equal the $^{207}Pb/^{235}U$ ages. In a similar diagram one can also plot the $^{208}Pb/^{232}Th$ ratio against that of $^{207}Pb/^{235}U$. However, it should be noted that the Th-Pb method is of much less practical value than the U-Pb method, as it often yields ages which can be difficult or impossible to interpret.

The great advantage of the U-Pb systems is that there are two coupled systems with differing decay constants which therefore offer a simple method for testing the assumption of a closed U-Pb system with a single analysis. A closed-system behavior is fulfilled if during the lifetime of the mineral neither lead, uranium, nor thorium, nor the respective intermediate daughter products have left or entered the mineral. In such a case the two U-Pb ages will agree, i.e., will be concordant if also no radiogenic daughter product was incorporated into the mineral at the time of formation. However, this conditon is not always fulfilled.

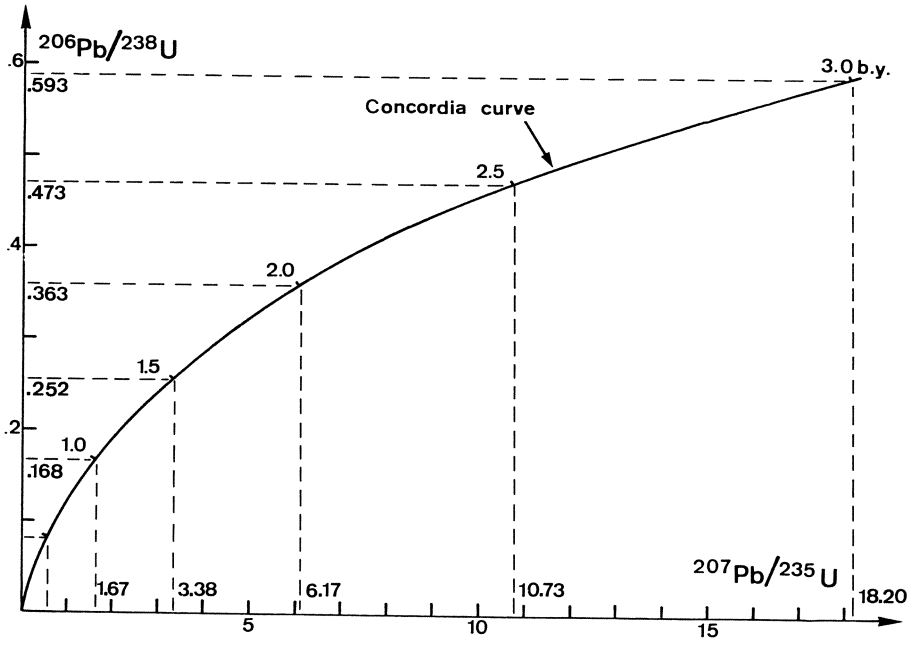

Fig. 1. Conventional concordia diagram (Wetherill, 1956a). The Concordia curve is the locus of points for which the $^{206}Pb/^{238}U$ age equals the $^{207}Pb/^{238}U$ age. It is curved due to the different half-lives of ^{238}U and ^{235}U

5. Discordant Age Patterns

In contrast to many monazite ages (see Chapter 10) and sphene ages (e.g., Tilton and Grünenfelder, 1968), zircon ages are generally discordant (Fig. 2). Taking the data from Central Europe, only about seven rocks are known containing a concordant zircon population (Gebauer and Grünenfelder, 1973b; Grauert et al., 1974a; Gebauer and Grünenfelder, 1977a). It is interesting to note that they were almost all obtained on unmetamorphosed intermediate to mafic magmatic rocks. Only in one case were concordant zircons found in highest-grade rocks, such as garnet-peridotites and associated metapyroxenites (Gebauer and Grünenfelder, 1977a). In the majority of the cases, however, the three ages are grossly discordant outside the limits of analytical error. The commonly observed pattern is (Fig. 2):

$$^{207}Pb/^{206}Pb > ^{207}Pb/^{235}U > ^{206}Pb/^{238}U.$$

Experience has shown that if a suite of uranium-bearing minerals – in most cases zircons – is analyzed, one often observes a linear array of data points on the concordia diagram. It was first found by Silver and Deutsch (1963) that the finer and/or more magnetic a zircon fraction within a given, cogenetic zircon population is, the younger the apparent Pb/U ages are (Fig. 3). Also, there generally is a strong correlation between U-content on one hand and grain size and magnetic susceptibility on the other: the smaller grain size and the higher the magnetic susceptibility, the higher is the U-content (Fig. 3).

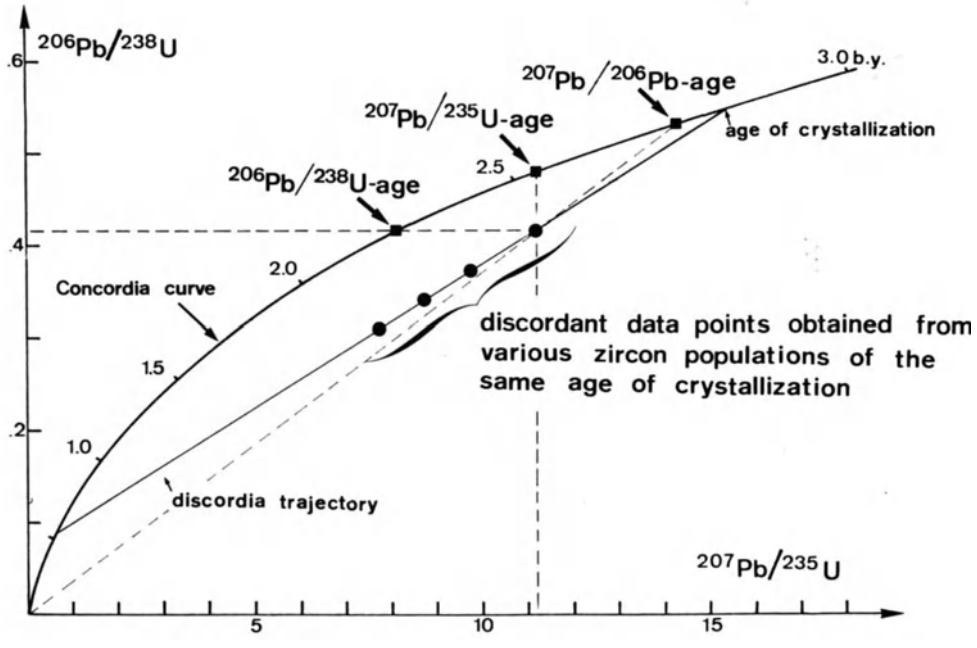

Fig. 2. Concordia diagram showing data points of four zircon populations, e.g., from various rock samples taken within the same granite pluton. For the uppermost data point the apparent U/Pb-ages, as well as the Pb/Pb-age, are given by the *intersections of the dashed lines* with the concordia curve. Normally, the lead/lead age is the highest age, and the $^{206}Pb/^{238}U$-age the lowest age

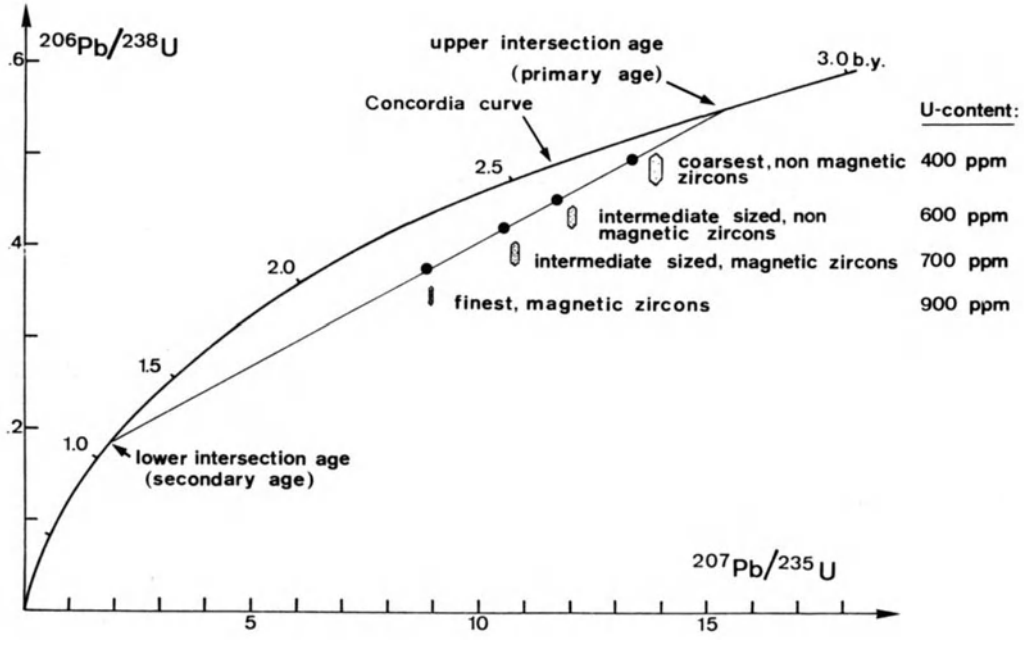

Fig. 3. Concordia diagram showing the influence of U-content, grain size and magnetic susceptibility on the degree of discordance. Such a data pattern is typical for numerous zircon populations of granitic, igneous rocks in Precambrian terranes. For the interpretation of the secondary age a number of models are applied

6. Interpretation of Discordant Age Patterns

As the interpretation of discordant age patterns will always be subjected to the prejudices of scientists, this is the most crucial point in U-Pb dating. This uncertainty is based on the existence of a series of models developed over the last 20 years. We will discuss these in the sequence in which they were published.

6.1 Episodic Model (Wetherill, 1965a, b)

In this classical and most frequently applied model, U-Pb mineral systems are thought to have been opened during a secondary event, in the course of which radiogenic lead was lost (Fig. 4). Alternatively, there might have been a U-gain, although there are

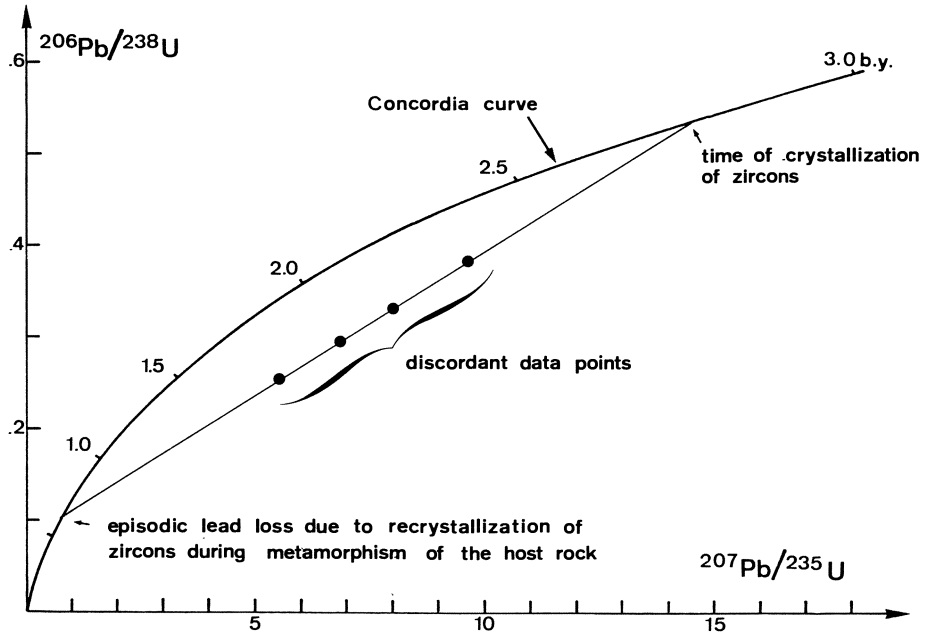

Fig. 4. Concordia diagram showing the effect of episodic lead loss on a cogenetic zircon suite. The lower intercept age corresponds to the time of metamorphism of the host rock in the course of which its radiation-damaged zircon population recrystallized. As lead does not fit well into the crystallographic structure of zircon, it will be partly expelled at this time. Lead loss due to recrystallization is often thought to be the most important mechanism to produce discordant age results

generally few indications for this process. Two ages will be obtained in such a case: the age of crystallization and the age of episodic lead loss of the analyzed mineral (Fig. 4). Based on the data of Ahrens (1955a, b), Wetherill (1956a) suggested "chemical leaching or alteration at a single episode" to be the cause of discordant age patterns for the Witwatersrand uraninites and Rhodesian monazites.

6.2 Diffusion Model (Nicolaysen, 1957; Tilton, 1960; Wasserburg, 1963)

The data points lie on a curve the upper part of which resembles a straight line (Fig. 5). Only when 70% or more of the radiogenic lead is lost by continuous (Tilton, 1960) or by time-dependent (Wasserburg, 1963) diffusion will the data points lie in the curved part of the discordia (Fig. 5). The lower intercept of the extrapolated straight part of the discordia with the concordia has no geologic significance, the upper intersection age closely approaches the age of formation or complete resetting of the analyzed mineral. So far data points in the curved part of a diffusion trajectory were not observed. This model is frequently used in Precambrian terranes if there is no further independent evidence for the "event" found by linear down-ward extrapolation of the data points. In a number of cases, especially for data from Phanerozoic terranes, diffusion trajectories cannot be forced through the data points.

Diffusion coefficients of lead in zircon, monazite, sphene and apatite have been determined by Shestakov (1972). His experimental results demonstrate that diffusion

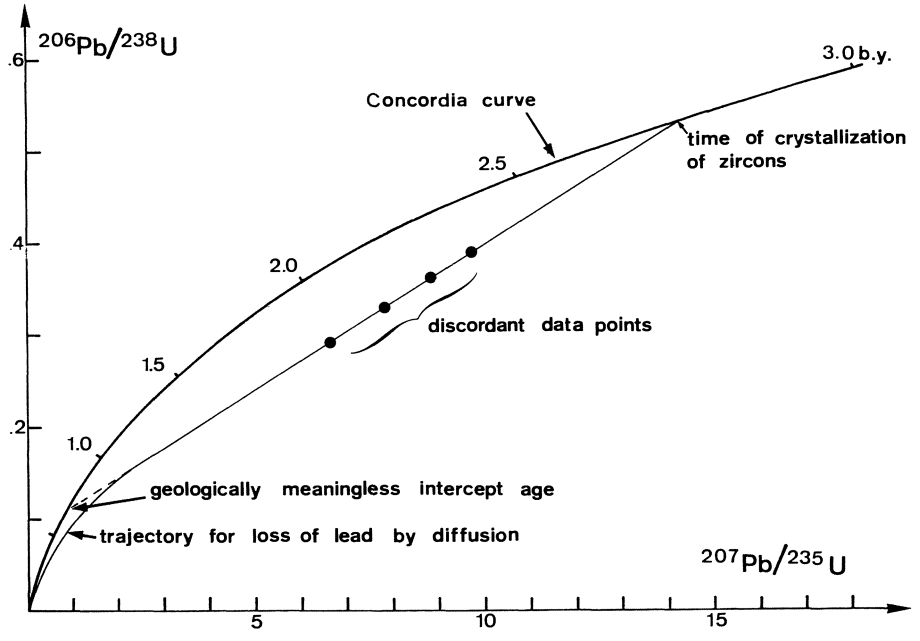

Fig. 5. Concordia diagram showing a diffusion trajectory through the experimental data points. As diffusion curves, based either on continuous (Tilton, 1960) or time-dependent (Wasserburg, 1963) diffusion, are very similar, their application will result in practically the same primary ages.

Taking data from Northern America, Africa, Europe, Australia and Asia Tilton (1960) showed that they all scattered closely around a discordia line intersecting the concordia curve at 2.8 b.y and 600 m.y., respectively. As there was in neither of the cases independent evidence for an event at 600 m.y., Tilton concluded that all the data points might fall on a trajectory caused by continuous diffusion of lead out of zircon at low temperatures. As such a diffusion trajectory is curved in its lower part, the linearly extrapolated lower intersection age is geologically meaningless

coefficients of lead at room temperature are too small by many orders of magnitude to explain low-temperature diffusion of lead within minerals.

6.3 Complex Models (Wetherill, 1963; Allègre et al., 1974)

These models apply for complex histories with more than one episodic lead loss or episodic lead loss superimposed upon lead loss by diffusion. Such a behavior of the U-Pb system can also lead to regular or quasi-linear arrays of data points (Fig. 6). The upper intercept of such discordia lines with the concordia curve yields a minimum primary age, whereas the lower extrapolated intercept has no geologic significance. Generally, it will be too old for the last and too young for the next-to last metamorphism. Such data patterns are likely to occur in polymetamorphic rocks, for instance in those of the Alps.

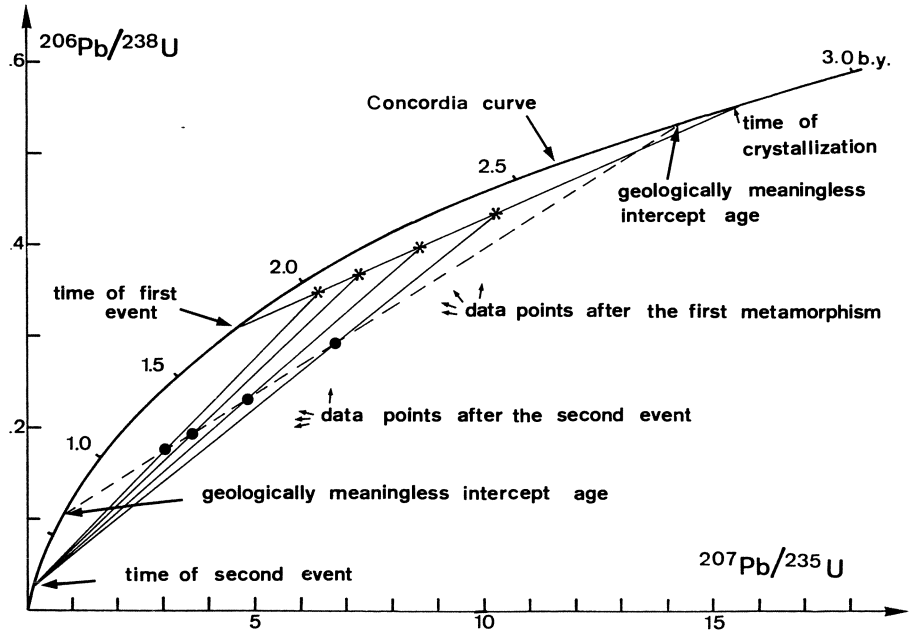

Fig. 6. Concordia diagram showing data points (•) the position of which is the result of a two-stage opening of U-Pb zircon systems. *Crosses* (*) mark the positions the data points would have today if the second event would not have reopened the U-Pb systems. If a linear array results at all after the second event both intersection ages are geologically meaningless, although in certain cases they might be close to one or even two events. However, this has to be established independently by other dating techniques

6.4 Dilatancy Model (Goldich and Mudrey, 1972)

In this model (Fig. 7) it is suggested that radiogenic lead is lost from zircons during crustal uplift as water held in the microchannels of the metamict zircon lattice

(Grünenfelder, 1963; Shukolyukov, 1964) could escape during pressure release together with dissolved radiogenic lead (Fig. 7). Applying this model to date from Nothern America, Goldich and Mudrey found agreement between various secondary ages and the probable time of uplift of the corresponding basement as derived by paleogeographic evidence.

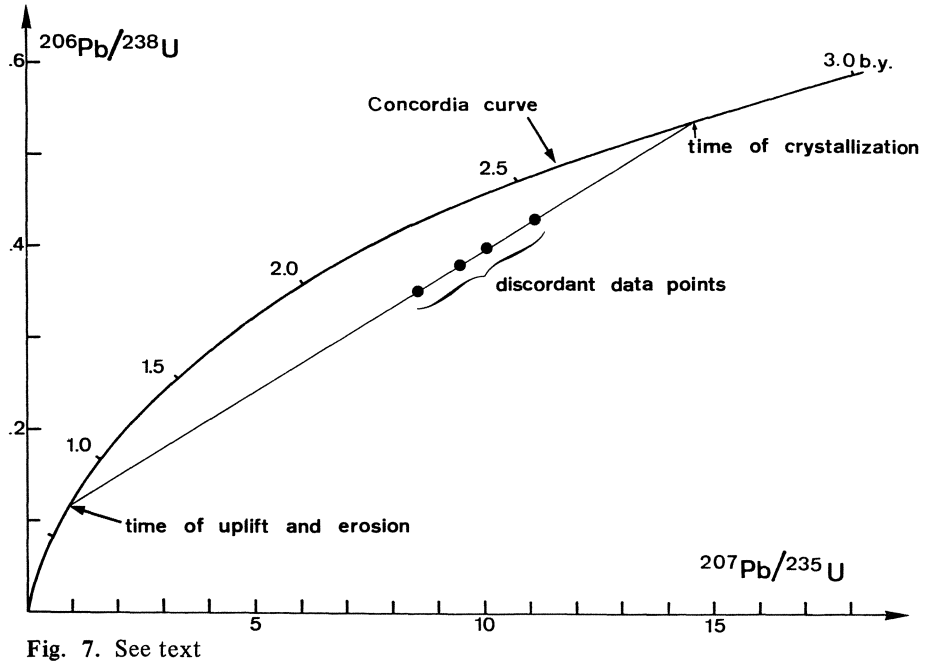

Fig. 7. See text

6.5 Alteration Model (Krogh and Davis, 1975)

Recently Krogh and Davis were able to demonstrate a "contributing factor if not the major cause of the discordance of zircons". The authors found that alteration zones within metamict zircons yield younger U-Pb ages than the remaining non-altered zones, which could be analyzed separately after leaching away the altered regions (Fig. 8). The time of lead loss in the altered zones was found in a few cases to be correlated with the well-known Grenville event in Northern America, in another with an event at 500 m.y. which, however, is not supported by any other evidence.

6.6 Low-Temperature Annealing Model (Gebauer and Grünenfelder, 1976)

This model is based on the observation that highly radiation-damaged zircons will recrystallize and consequently lose lead episodically at temperatures as low as 300°C or even less (Fig. 9). Such a process for temperatures above 350°C was predicted by Pidgeon et al. (1973) based on laboratory experiments, and is now confirmed by U-Pb and cell-dimension data obtained on zircons recrystallized in a natural environ-

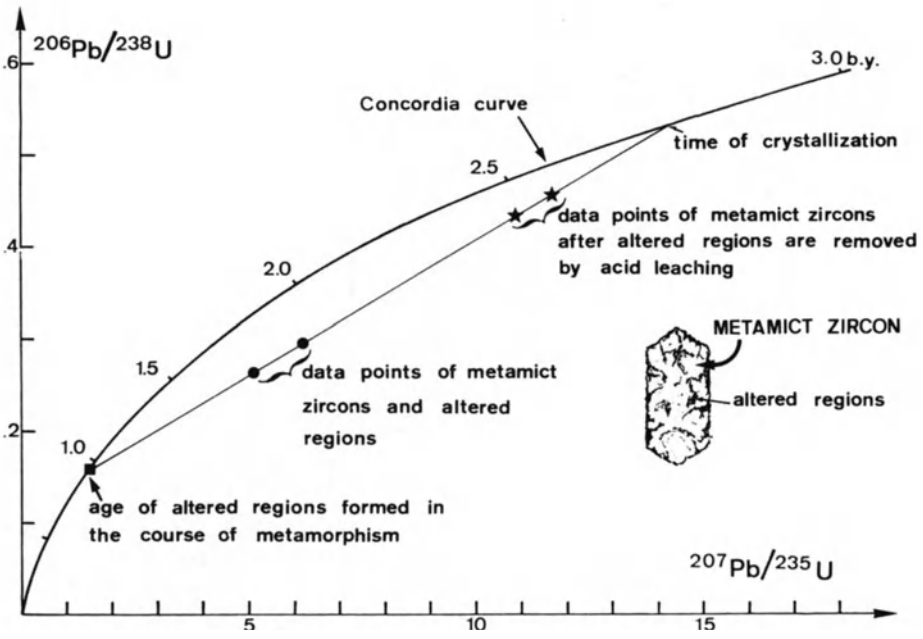

Fig. 8. Concordia diagram with data points of zircon fractions containing variable amounts of altered regions (●). The age of these altered regions might be obtained by analyzing an acid leach of such a zircon fraction (■). The nonaltered part is more or less metamict, depending on the radiation dosage. In contrast to the age of the relatively unstable altered regions, which might be 100% discordant (i.e., concordant at the secondary age), this part is much less discordant (★) and might be even concordant at the primary age

ment. Low-temperature annealing of old metamict zircons can readily help to explain the fact that the numerous zircon suites from ancient shield areas are strongly discordant and yield "lower intercept ages", which are not correlated to any independently dated geologic event. Thus, either a weak thermal pulse, not necessarily registered by the mineral assemblage of the host rock, and/or elevated temperatures during burial in the crust might supply enough energy for a structural reordering and simultaneous lead loss of at least the most disordered domains in zircons.

6.7 Mixing Models

A linear data array can also be produced by mixing of old zircons with those which crystallized much later in the course of high-grade metamorphism (Fig. 10). Sometimes it might be possible to distinguish the two types of zircon optically, and consequently it might become possible to analyze them separately for U-Pb. In a similar way a discordia trajectory can be produced by a mixed zircon population formed in an igneous rock by the assimilation of country rocks.

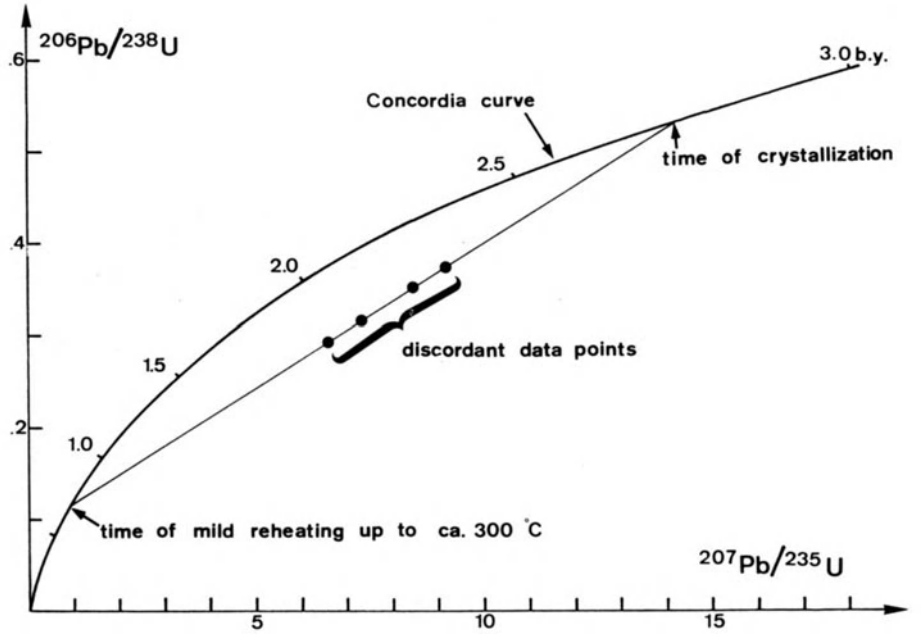

Fig. 9. Concordia diagram with data points of a zircon suite which lost lead due to low-temperature recrystallization at or below ca. 300°C. The condition to anneal zircon at these low temperatures is the existence of a strongly radiation-damaged crystal structure. Thus, U-Pb systems in strongly metamict zircons will respond to events which are not detected by other dating systems. In contrast, annealed zircons are very stable with respect to lead loss, i.e., they can survive temperatures above 600°C

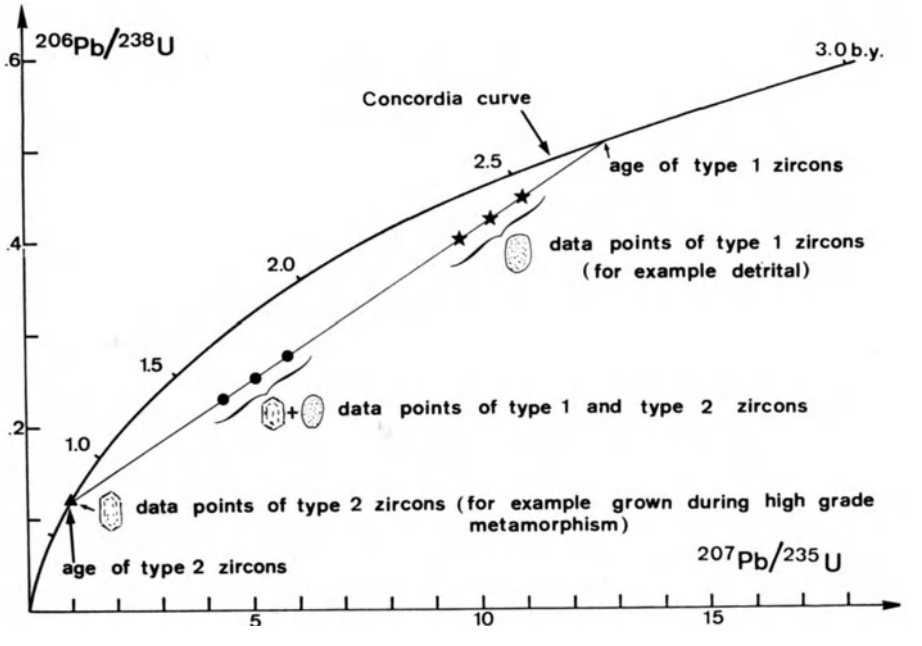

However, even within a single zircon crystal more than one age might occur. This is due to unmixing of phases and/or the formation of domanes rich in water and heavy elements. The proof for such a cause of discordant age patterns has been found by Grünenfelder (1963) and Grünenfelder et al. (1964, 1968). Similarly, Steiger and Wasserburg (1969) concluded that discordant age data might be explained by a mixing of highly discordant and almost concordant phases. More recently Sommerauer (1974, 1976) showed that zircon rich in minor elements, above ca. 2 mol% substitution for $ZrSiO_4$, might consist of two phases. One with a thermally stable structure and low trace-element concentrations, and another relatively unstable phase with high concentrations of trace elements including U, Th, and H_2O. The latter is considered to form a micro-heterogeneous mixture of two amorphous subsystems dominated by ZrO_2 and SiO_2. As this phase is likely to lose lead more readily than the other crystallographically well-ordered phase, it will dominate the degree of discordance. Also, this phase will tend to recrystallize already at low temperatures enlarging the degree of discordance even more.

7. Dating of Igneous Rocks

7.1 Felsic Rocks

A great number of zircon data has been obtained on these rocks, especially on granites and granodiorites. In ancient shield areas, i.e., mainly in Northern America but also in Australia, Scandinavia, USSR etc. data patterns as shown in Figure 5 are commonly observed. The primary ages are always interpreted as reflecting the intrusion ages. Generally, no geologic meaning is attributed to the secondary ages frequently ranging between 600 m.y. and 0 m.y. The discordant data patterns are mainly explained by diffusion models, the episodic model or the dilatancy model (e.g., Zhirova et al., 1961; Silver and Deutsch, 1963; Silver et al., 1963; Kuovo and Tilton, 1966; Steiger and Wasserburg, 1966, 1969; Tilton and Steiger, 1969; Naylor et al., 1970; Nunes and Tilton, 1971; Gulson and Krogh, 1975; Krogh and Davis, 1975; Krogh et al., 1975a; Van Schmus, 1976; Anderson and Silver, 1977; Hurst and Farhat, 1977).

Especially in the Western United States, i.e., in areas influenced by the Laramide event (ca. 100 m.y.) the low-temperature recrystallization model might explain the observed data patterns. Nevertheless, the interpretation of these so-called geologically meaningless secondary ages remains one of the major problems of zircon dating.

In younger terranes, e.g., of Phanerozoic ages, zircon dating of felsic igneous rocks becomes more complicated. This is due to the observation that zircons from granitic rocks might contain considerable amounts (up to 30%) of inherited radiogenic lead (e.g., Grauert and Hofmann, 1973; Gulson and Krogh, 1973; Gebauer and Grünenfelder,

◀ **Fig. 10.** Concordia diagram with the data points of a zircon suite consisting of a mixed population (●). One part might be concordant at the secondary age (▲) and the other discordant lying in between the primary and secondary age (★). Such a data pattern might occur in high-grade metamorphic terranes in which zircon is newly formed during metamorphism

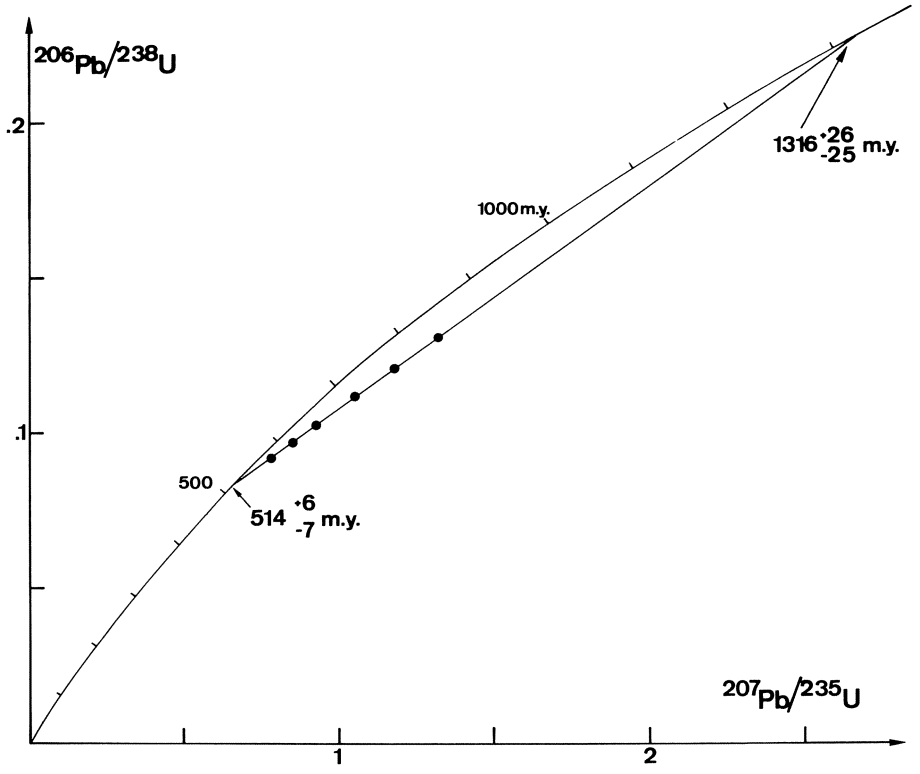

Fig. 11. Concordia diagram showing the data points of 6 size- and magnetic fractions of the Ben Vuirich granite in Scotland (Pankhurst and Pidgeon, 1976). For geologic constraints, the lower intercept age of 514 m.y. represents the age of emplacement of the granite. The upper intercept of 1315 m.y. is interpreted to reflect the age of xenocrysts incorporated into the granite magma during partial fusion of the source rocks. The coarsest zircon fraction (uppermost data point) contains about 30% of 1316 m.y. old lead. Rb-Sr whole-rock data scatter around an "errorchron" of 564 m.y. indicating, together with the high initial $^{87}Sr/^{86}Sr$ ratio of about 0.716, crustal source rocks and incomplete homogeneization of Sr-isotopes

1974; Pidgeon and Johnson, 1974; Pankhurst and Pidgeon, 1976; Higgins et al., 1977). Therefore, the lower intersection age generally reflects the time of emplacement, while the upper intersection age gives us information on the average age of the crustal rocks from which these melts were formed and/or which they assimilated (Fig. 11). The presence of such inherited radiogenic lead might be predicted from the presence of older cores within the magmatic zircons differing in shape and/or color. However, it could be shown (Gebauer and Grünenfelder, 1974, and unpublished data) that euhedral, clear zircons either completely recrystallized or more probably newly formed in an anatectic melt are just as discordant as cloudy, detrital zircons. Both types of zircon – similar to those drawn in Figure 10 – were extracted from a diatexite formed by in situ melting of a paragneiss. Thus, besides the rare possibility of high common lead contents in zircon, there also exists the possibility of finding high contents of radiogenic lead in freshly (re)crystallized zircons.

In contrast to zircons from ancient shield areas, there is in many cases no indication for open-system behavior after intrusion of Phanerozoic, igneous rocks. However, it must be stressed that this cannot be taken for granted (e.g., Williams, 1977). Therefore, additional data, e.g., on monazite and/or Rb-Sr mineral and/or whole-rock data are always desirable.

The detection of inherited radiogenic lead is of petrogenetic importance as it is in favor of a crustal origin for at least part of the analyzed rock. It is interesting to note that inherited radiogenic lead seems to be absent in felsic igneous rocks of Precambrian shield areas. Together with the low initial Sr-isotopic values of these rocks this argues for a genesis caused by crystallization differentiation of melts formed in the lower crust or the mantle. In contrast, Phanerozoic granitic rocks, e.g., from Central Europe, are often believed to have formed by anatexis of curstal material. High initial Sr-isotopic ratios and inherited radiogenic lead contents in their zircon populations support this assumption.

7.2 Intermediate and Mafic Rocks

Zircon dating of intermediate and mafic igneous rocks is only rarely applied. This is due to the fact that zircons are generally believed to be scarce or absent in these rock types. From our own experiences, however, we must conclude that this opinion is fortunately too negative. Taking the few data (Nunes and Tilton, 1971; Gebauer and Grünenfelder, 1973b; Grauert et al., 1974a; Gulson and Krogh, 1975; Krogh and Davis, 1975; Higgins et al., 1977; Gebauer et al., in prep.) it can be shown that zircons from dioritic and gabbroic rocks are closer to the concordia than zircons from unmetamorphosed granitic rocks. In some cases they are even concordant or quasi-concordant. Generally, no indications for the presence of inherited radiogenic lead are found. This is in accordance with the probable origin of these rocks in the lower crust or in the mantle. As must be expected, the average U-concentrations of these zircons are below those of zircons from granitic rocks, although U-concentrations of up to 1000 ppm were found in zircons extracted from a potassium-rich gabbro (Gebauer and Grünenfelder, 1973b). In two cases (Gebauer et al., in prep.) zircons from quartz-diorites of the French Central Massif were found to have lost lead recently.

8. Dating of Sedimentary Rocks

Zircons found in clastic sediments are of detrital origin. The possibility of authigenic formation of zircon, however, has been postulated (Saxena, 1966). The main application of dating these zircons is to shed light on the provenance of the detritus (Fig. 12). Naturally, it must be expected that we deal here with a mixture of zircon derived from rock types of different ages and from different geologic units. Thus, the data pattern might vary considerably, depending on the number of age groups and their quantitative contribution to the analyzed zircon population. Additionally, recent lead loss might play a role, making an interpretation of the data points more difficult or even impossible. Nevertheless, the available data (e.g., Ledent et al., 1964; Tatsumoto and

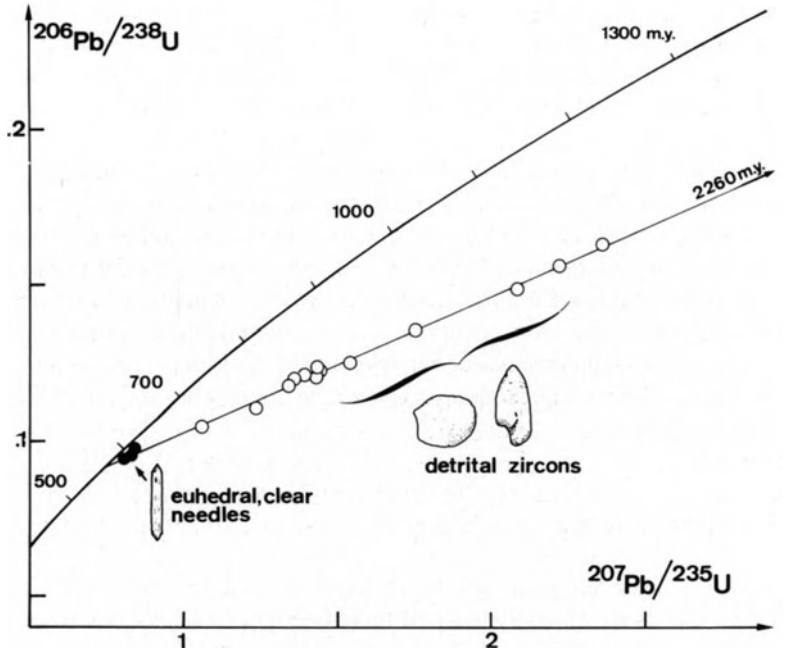

Fig. 12. Concordia diagram with the data points of zircons from sandstones and quartzites (Bohemian Massif) separated into fractions of different size, magnetic susceptibility, color and shape (Grauert et al., 1973). The intercept ages are interpreted to reflect ages mainly of about 2.3 b.y and 550 to 600 m.y. for the source rocks of the Cambro-Ordovician detritus

Patterson, 1964; Grauert et al., 1973; Abdel-Monem, 1977; Gaudette et al., 1977; Gebauer and Grünenfelder, 1977b) generally can still be used for a good estimate of the age of the corresponding provenance(s). Dating of single, detrital zircon crystals, or at least of zircons of the same type, e.g., of the same color and crystal habitus, will give more detailed information. So far open-system behavior of detrital zircons during sedimentation and/or diagenesis could not be proven, although it cannot be generally excluded. The same seems to be true for detrital monazites (Gebauer and Grünenfelder, in prep.)

9. Dating of Metamorphic Rocks

9.1 Metasedimentary Rocks

Most data on this rock type have been obtained on amphibolite facies paragneisses. Similarly to igneous rocks, the data patterns from ancient shield areas are different from those obtained on Phanerozoic rocks. In ancient shield areas the upper intercept ages are sometimes interpreted as reflecting the time of new formation or complete

resetting of the zircons during high-grade metamorphism. The secondary ages might be caused either by a later metamorphic overprint and/or by diffusion, dilatancy or another unknown mechanism (Catanzaro and Kulp, 1964; Kouvo and Tilton, 1966; Davis et al., 1968; Hart and Davis, 1969; Nunes and Tilton, 1971; O'Nions and Baadsgaard, 1971; Peterman et al., 1972; Gulson and Krogh, 1975; Krogh and Davis, 1975; Baadsgaard et al., 1976; Bowes et al., 1976; Lancelot et al., 1976; Steiger et al., 1976). In contrast, it can be shown for Phanerozoic rocks that the secondary ages are correlated with events of metamorphism which formed the corresponding metasediment (e.g., Grauert and Arnold, 1968; Pidgeon, 1969; Pidgeon et al., 1970; Köppel and Grünenfelder, 1971; Gebauer and Grünenfelder, 1974, 1976; Grauert et al., 1974a, b; Köppel, 1974; Nunes and Steiger, 1974; Gulson and Rutishauser, 1976). Generally, no post-metamorphic opening of U-Pb systems is observed here. The upper intercept age, however, is interpreted as reflecting the average age of the provenance. There is no plausible reason why metasedimentary zircons from ancient shield areas should have been in a number of cases completely reset and/or newly formed at the time of metamorphism while zircons in Phanerozoic rocks, e.g., of Central Europe, retained between 5% and 20% of an older lead component. Interestingly, first analyses of single zircon

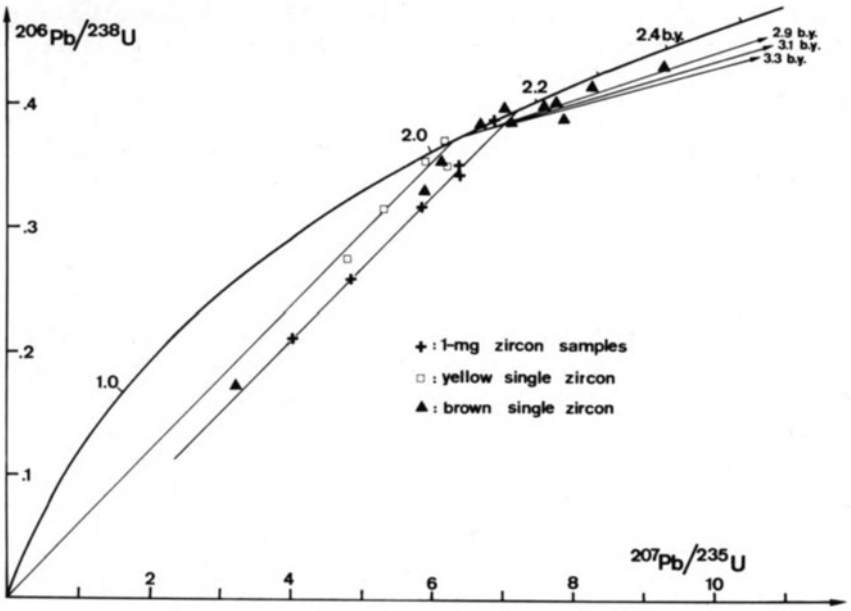

Fig. 13. Concordia diagram with data points of mg-sized zircon fractions and single zircon crystals from a charnockitic paragneiss from the In'Ouzzal (Ahaggar, Algeria; Lancelot et al., 1976). The mg-sized fractions consist of a mixture of yellow and brown zircons. The upper intersection age of the corresponding discordia trajectory is at 2.17 b.y. However, from the analyses of the yellow euhedral crystals, it can be shown that the metamorphism was at 2.06 b.y. and not at 2.17 b.y., as is derived from the upper intercept age of the mixed zircon population. The brown crystals which seem to be detrital clearly contain an older inherited radiogenic lead component which is the cause of the erroneously high age derived from the data of the mixed, multigrain fractions

crystals differing in color and morphology but occurring in the same charnockitic paragneiss (Lancelot et al., 1976) revealed two age groups (Fig. 13). One reflects the time of high-grade metamorphism and the other one, containing an older radiogenic lead component, the premetamorphic history of the rock. Applying the conventional technique using mg-size samples, the extrapolated upper intersection age is in excess of the time of metamorphism and therefore has no geologic meaning. Thus, ages obtained on metasediments from ancient shield areas should be treated with caution, although they often might give a sufficient approximation of the true age of metamorphism of the host rock. The same holds true for the lower intercept ages obtained, for example, in Central European metasediments that were metamorphosed during the Phanerozoic. As most of these rocks are polymetamorphic, a multistage history of the detrital zircons may produce intercepts lying between the ages of the metamorphic overprints. Unfortunately, a linear array of the experimental data points is not indicative for a simple history of the corresponding U-Pb zircon systems.

From the data on Phanerozoic, low-grade metasediments, i.e., phyllites and micaschists, it could be shown that old (ca. 2 b.y.) strongly radiation-damaged zircons can recrystallize at temperatures as low as about 350°C (Gebauer and Grünenfelder, 1976). As recrystallization is generally paralleled by lead loss, it is possible to date the time of metamorphism of these rocks (Fig. 14). On the other hand, temperatures of up to 600°C or more might not be sufficient to open the U-Pb systems in zircons with annealed crystal lattices or with a structure only weakly damaged by radiation. Consequently, dating of the first metamorphic event of polymetamorphic, low-grade metasediments might often be more successful than dating of the same event in the high-grade metamorphic equivalents because temperatures during the younger low-grade metamorphic overprint(s) were most probably not high enough to reopen U-Pb systems. In contrast, in high-grade polymetamorphic rocks the younger metamorphism(s) might reach temperatures high enough to reopen the U-Pb zircon systems invalidating the geologic meaning of the lower intercept age.

In contrast to the results obtained by Grauert and Hofmann (1973) on the Lower Beltian metasediments (Idaho, USA), no correlation between degree of discordance and degree of metamorphism has been found in Central European low-grade to high-grade metasediments (e.g., Michot and Deutsch, 1970; Gebauer and Grünenfelder, 1976). They are all around 80%-95% discordant. Only in rocks transformed under the conditions of the granulite fracies is a pronounced increase of discordance generally observed both in Phanerozoic and Precambrian terranes (e.g., Pidgeon and Bowes, 1972; Pidgeon and Aftalion, 1972; Köppel, 1974; Grauert and Wagner, 1975).

9.2 Metaigneous Rocks

The majority of ages of this rock type have been obtained on felsic, plutonic rocks. Again, a distinction between data from ancient shield rocks and Phanerozoic rocks is observed. For the first group the time of crystallization is generally given by the upper intercept ages (e.g., Steiger and Wasserburg, 1969; Goldich et al., 1970; Naylor et al., 1970; Nunes and Tilton, 1971; O'Nions and Baadsgaard, 1971; Peterman et al., 1972; Pidgeon and Raheim, 1972; Grauert, 1974; Krogh et al., 1975a; Pasteels and

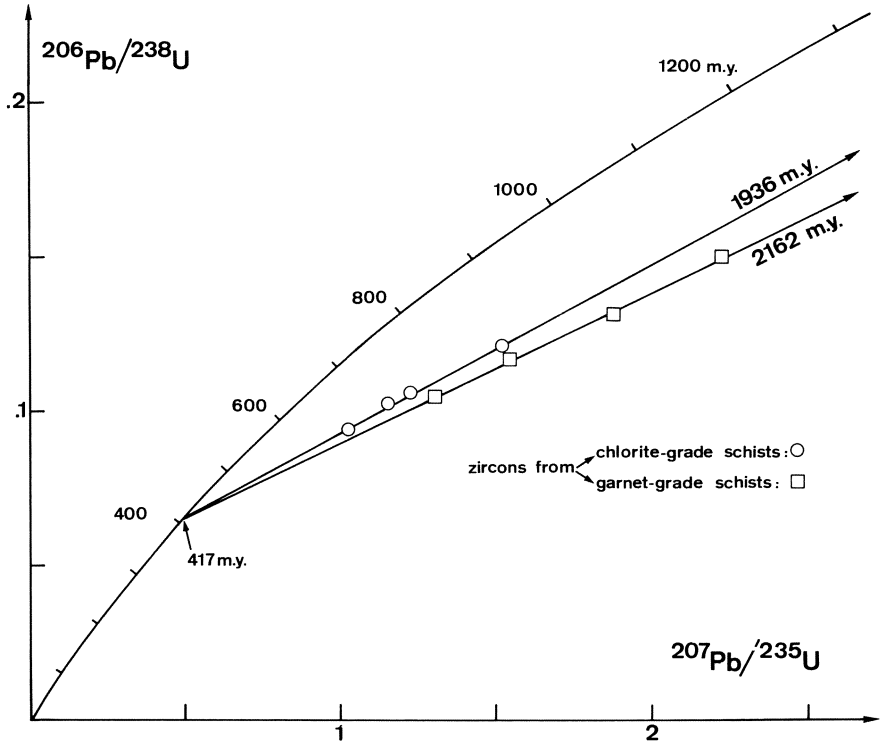

Fig. 14. Concordia diagram showing the data points of size and magnetic fractions from two detrital zircon populations (Montagne Noire, Southern France; Gebauer and Grünenfelder, 1976). ○ represent fractions from a chlorite-grade quartz-phyllite; □ represent fractions from a garnet-grade quartz-mica schist. Zircons from staurolite-grade paragneisses taken within the same metamorphic profile are similarly discordant and yield within limits of analytical error identical intercept ages. Such a data pattern is typical for many zircon suites extracted from Central European paragneisses. It indicates drastic lead loss of about 2-b.y.-old detrital zircons during metamorphism of the host rock. In cases where the zircons are strongly radiation-damaged, temperatures of up to around 300°C are sufficient for annealing of the zircon structure in the course of which around 80%-95% of radiogenic lead can be lost.

Michot, 1975; Pidgeon and Hopgood, 1975; Michard-Vitrac et al., 1977). If such zircons were opened and/or newly crystallized during only one metamorphism, the secondary age will reflect this time. Data patterns as given in Figure 4 will be the result. However, recent lead loss and/or polymetamorphism might obscure the geologic meaning of the lower intercept.

In the case of Phanerozoic rocks, postmetamorphic lead loss unrelated to a geologic event is rare. However, as many of the premetamorphic source rocks were formed by anatexis of crustal rocks, they may contain a portion of inherited zircons and thus variable amounts of inherited radiogenic lead (e.g., Grauert and Arnold, 1968; Pidgeon et al., 1970; Köppel and Grünenfelder, 1971; Gebauer and Grünenfelder, 1973a;

Gebauer, 1975; Hänny et al., 1975; Vitrac-Michard and Allègre, 1975). Open-system behavior during already one metamorphic overprint would consequently produce wrong intercept ages, i.e., too old intrusion ages and too old metamorphic ages if a linear array of data points results at all. Based on zircon data, the nonmetamorphic equivalents of most Central European felsic orthogneisses might have been formed by anatexis of the paragneisses in which they occur. However, it must be noted that due to a very poor data spread, and due to the probably presence of inherited radiogenic lead, no precise intercept ages can be derived.

In contrast to felsic metaigneous rocks, metamorphosed mafic and ultramafic rocks have so far only rarely been dated (Pidgeon, 1969; Krogh et al., 1975b; Steiger et al., 1976; Gebauer and Grünenfelder, 1977a; Gebauer and Grünenfelder, 1978; Gebauer et al., in prep.). In contrast to the Phanerozoic felsic orthogneisses, zircons from these rock types – amphibolites, eclogites, meta-gabbros, meta-pyroxenites, meta-peridotites etc. – seem to have been cogenetic at the time of magmatic crystallization, i.e., they did not contain inherited radiogenic lead (Fig. 15). This conforms with the fact that the unmetamorphosed equivalents are derived from the lower crust or the mantle. However, even if there was assimilation of crustal rocks during the uprising of the mafic melts, the U-Pb systems of crustal zircons would very probably be reset completely if such zircons could physically survive at all. This must be expected from the considerably higher temperatures of mafic versus anatectic granitic melts. Thus, the main condition to date metaigneous rocks successfully, i.e., a pre-metamorphic cogenetic zircon population, can here be expected to exist also for Phanerozoic rocks. The lower intercept ages of such zircon suites reflects the age of metamorphism during which the primary zircons recrystallized. Additionally, overgrowth and/or complete new growth of zircon might occur in the course of metamorphism, and thus enlarge the degree of discordance (Fig. 15). Even for the case of a poly-metamorphic history for such rocks, the probability that the zircons stayed closed systems during the metamorphic cycles is higher than for zircons extracted from felsic rocks. This will be partly due to the relatively low U-content of these zircons, i.e., due to a relatively weaker radiation damage when compared to U-richer zircons of felsic rocks having the same geologic history. Also, a generally low concentration of fluid phases and a relatively high resistance of most of these rocks to mechanical deformation increase the chances for U-Pb zircon systems to survive further metamorphism of the host rocks. The first analyses of zircons from alpine-type garnet-peridotites including various types of meta-pyroxenites gave concordant age result for one case and discordant ages in two other cases (Gebauer and Grünenfelder, 1977a; Gebauer et al., in prep.). Multiple euhedral zoning of heavy elements, as detected by microprobe cathode luminiscence patterns, is indicative that zircons can be of primary magmatic origin also in ultramafic rocks.

The morphologic characteristics of zircon, as well as their U-Pb age patterns, will be a helpful tool to distinguish between amphibolites formed from a sediment and those derived from mafic igneous rocks. At least, this is probable for amphibolites and possibly also eclogites from the Central European basement as in this area detrital zircons from metasediments plot within a characteristic field of the concordia diagram (Fig. 14). Thus, detrital zircons from para-amphibolites are likely to fall into such a data filed as has been found for rocks of the Gotthard massif in the Central Alps (Gebauer and Grünenfelder, unpubl.).

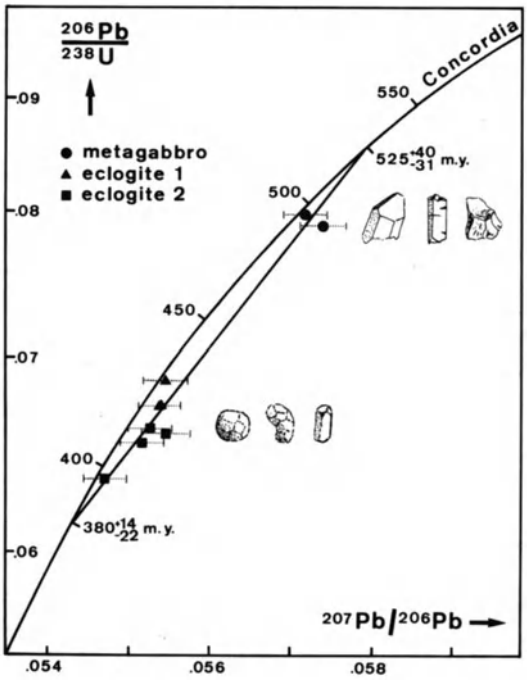

Fig. 15. Concordia diagram with the data points of zircon fractions from a meta-gabbro and two eclogites from the Münchberg Gneiss Massif, NE-Bavaria (Gebauer and Grünenfelder, 1978). As the conventional concordia curve is only very slightly curved in the range of Phanerozoic ages a $^{206}Pb/^{238}U$-$^{207}Pb/^{206}Pb$ plot was chosen. In this plot a non-linear scale is used on the ordinate by calibrating it with the reciprocal of the $^{206}Pb/^{238}U$-ratio. Thus, the concordia is curved more in the range of Phanerozoic ages. Plotting the lead/lead age on the abscissa allows one to draw rectangular error bars. Note that recent lead loss would shift the data points downwards parallel to the Y-axis.
Samples are taken from an eclogite body and a metagabbro about 1 km apart. Zircons in the metagabbro show a typical magmatic morphology, while zircons in the eclogites seem to have lost the euhedral habitus to a large extent during metamorphism. The degree of discordance of all zircons from these cogenetic rocks seems to follow the degree of metamorphic recrystallization and/or new formation during eclogite facies metamorphism at 380 m.y. "Retrograde" formation of hornblende and phengite took place immediately after the eclogite facies conditions, as shown by Rb-Sr mineral ages (ca. 379 m.y.) from eclogite 2 and the metasedimentary country rocks

10. Monazite Dating

Besides zircon, monazite is a most useful accessory mineral for U-Pb dating. In contrast to sphene, the content of common lead in monazite generally does not influence the quality of the age data obtained on young, e.g., Phanerozoic rocks. As the U-content of monazite (Table 1) is much higher than in zircon or sphene (Table 1) it can be effectively used for the dating of young rocks, for example of alpine age.

In the case of magmatic rocks, the occurrence of monazite is largely tied to the felsic members, i.e., to granodiorites, granites, aplites, and pegmatites. In one case monazite was found in a gabbroic rock, and it gave the same concordant age as zircon extracted from the same sample (Gebauer and Grünenfelder, 1973b). In metasediments, monazite appears to be absent in low- and medium-grade rocks (Overstreet, 1967). It seems to be formed first in the course of high-grade metamorphism.

The first age data on monazite have been obtained mainly on unmetamorphosed granitic rocks (e.g., Vinogradov, 1956; Burger et al., 1965). Only since the early 70's has monazite been used systematically for the dating of metamorphic rocks, mainly for those of Central Europe (Köppel and Grünenfelder, 1971; Gulson and Krogh, 1973; Gebauer and Grünenfelder, 1974; Grauert et al., 1974a; Köppel, 1974; Hänny et al., 1975; Köppel and Grünenfelder, 1975). The majority of monazite data obtained in this area is concordant, providing a powerful tool for dating metamorphic events. For a number of cases (Köppel and Grünenfelder, 1975; Gebauer et al., in prep.) it could be demonstrated that monazite, once formed, can survive high-grade metamorphism(s) reaching temperatures of around 600°C or more.

Closed-system behavior of monazite is not only found under high-grade metamorphic conditions but also during weathering (Gebauer et al., in prep.).

In contrast to detrital zircon, detrital monazite seems to be not very abundant in clastic sediments. First age results (Gebauer and Grünenfelder, in prep.) suggest that detrital monazites can remain closed for U and Pb during diagenesis and very low-grade metamorphism. Thus, similarly to zircons, they might be of great value to determine the age of the provenance of a sediment.

Acknowledgments. We wish to thank Drs. G.R. Tilton and V. Köppel for critically reading the manuscript and F. Corfu for drafting the figures.

References

Abdel-Monem, A.A.: U-Pb dating of detrital zircon from Egypt. Twenty-first progress report, for 1974-1976. M.I.T. Geochronology Laboratory, 1977, pp. 79-87

Ahrens, L.H.: The convergent lead ages of the oldest monazites and uraninites (Rhodesia, Manitoba, Madagascar, Transvaal). Geochim. Cosmochim. Acta *7*, 294-300 (1955a)

Ahrens, L.H.: Implications of the Rhodesian age patterns. Geochim. Cosmochim. Acta *8*, 1-15 (1955b)

Allègre, C.J., Albarède, F., Grünenfelder, M., Köppel, V.: $^{238}U/^{206}Pb$-$^{235}U/^{207}Pb$-$^{232}Th/^{208}Pb$ zircon geochronology in Alpine and non-Alpine environment. Contrib. Mineral. Petrol. *43*, 163-194 (1974)

Anderson, T.H., Silver, L.T.: U-Pb isotope ages of granitic plutons near Cananea, Sonora. Econ. Geol. *72*, 827-836 (1977)

Baadsgaard, H., Lambert, R.St.J., Krupicka, J.: Mineral isotopic age relationships in the polymetamorphic Amitsoq gneisses, Godthaab District, West Greenland. Geochim. Cosmochim. Acta *40*, 513-527 (1976)

Bowes, D.R., Hopgood, A.M., Pidgeon, R.T.: Source ages of zircons in an Archean quartzite, Rona, Inner Hebrides, Scotland. Geol. Mag. *111*, 545-552 (1976)

Burger, A.J., Von Knorring, O., Clifford, T.N.: Mineralogical and radiometric studies of monazite and sphene occurrences in the Namib Desert, South West Africa. Mineral. Mag. *35*, 519-528 (1965)

Catanzaro, E.J., Kulp, J.L.: Discordant zircons from the Little Belt (Montana), Beartooth (Montana) and Santa Catalina (Arizona) Mountains. Geochim. Cosmochim. Acta *28*, 87-124 (1964)

Davis, G.L., Hart, S.R., Tilton, G.R.: Some effects of contact metamorphism on zircon ages. Earth Planet. Sci. Lett. *5*, 27-34 (1968)

Farquharson, R.B., Richards, J.R.: Whole-rock U-Th-Pb and Rb-Sr ages of the Sybella microgranite and pegmatite, Mount Isa, Queensland. J. Geol. Soc. Aust. *17*, 53-62 (1970)

Gaudette, H.E., Hurley, P.M., Fairbairn, H.W., Lajmi, T.: Source area for the Numidian flysch of Tunisia determined by U-Pb zircon ages. 21st progress report for 1974-1976, M.I.T. Geochronology Laboratory, 1977, pp. 35-41

Gebauer, D.: Rb-Sr Gesamtgesteins- und Mineralsysteme sowie U-Pb Systeme in Zirkonen während der progressiven Gesteinsmetamorphose. Ph.D. thesis, ETH Zürich, 1975, unpublished

Gebauer, D., Bernard-Griffiths, J., Krebs, O., Grünenfelder, M.: U-Pb zircon and monazite dating of metagabbros, eclogites and garnet-peridotites as well as their country rocks. Example: The mafic to ultramafic massive of Sauviat-sur-Vige (French Central Massif). In Preparation for Earth Planet. Sci. Lett. (1979)

Gebauer, D., Grünenfelder, M.: U-Pb zircon and Rb-Sr systems during progressive metamorphism. Fortschr. Mineral. *50*, 76-78 (1973a)

Gebauer, D., Grünenfelder, M.: Vergleichende U/Pb- und Rb/Sr-Altersbestimmungen im bayerischen Teil des Moldanubikums. Fortschr. Mineral. *50*, Beih. 34, 4 (1973b)

Gebauer, D., Grünenfelder, M.: Comparative studies of U-Pb systems in zircons and monazites as well as Rb-Sr systematics in minerals and whole-rocks during the anatexis of a polymetamorphic paragneiss (crystalline basement of NE-Bavaria). Internat. meeting for geochronology, cosmochronology and isotope geology, Paris abstracts, 1974

Gebauer, D., Grünenfelder, M.: U-Pb zircon and Rb-Sr whole-rock dating of low-grade metasediments. Example: Montagne Noire (Southern France). Contrib. Mineral. Petrol. *59*, 13-32 (1976)

Gebauer, D., Grünenfelder, M.: U-Pb Zirkondatierungen mafischer und ultramafischer Gesteine. Arbeitstagung der OeMG gemeinsam mit der SMPG. (Abstract), Salzburg 1977a

Gebauer, D., Grünenfelder, M.: U-Pb systematics of detrital zircons from some unmetamorphosed to slightly metamorphosed sediments of Central Europe. Contrib. Mineral. Petrol. *65*, 29-37 (1977b)

Gebauer, D., Grünenfelder, M.: U-Pb zircon and Rb-Sr mineral dating of eclogites and their country rocks. Example: Münchberg Gneiss Massive, NE-Bavaria. To be published in Earth Planet. Sci. Lett. (1978)

Goldich, S.S., Hedge, C.E., Stern, T.W.: Age of the Morton and Montevideo Gneisses and related rocks, Southern Minnesota. Bull. Geol. Soc. Am. *81*, 3671-3696 (1970)

Goldich, S.S., Mudrey, Jr.: Dilatancy model for discordant U-Pb zircon ages. In Contrib. to recent geochemistry and analytical chemistry (Vinogradov volume). Moscow: Nauka Publ. Office, 1972, pp. 415-418

Grauert, B.: U-Pb systematics in heterogeneous zircon populations from the Precambrian basement of the Maryland Piedmont. Earth Planet. Sci. Lett. *23*, 238-248 (1974)

Grauert, B., Arnold, A.: Deutung diskordanter Zirkonalter der Silvretta Decke und des Gotthardmassivs (Schweizer Alpen). Contrib. Mineral. Petrol. *20*, 34-56 (1968)

Grauert, B., Hänny, R., Soptrajanova, G.: Age and origin of detrital zircons from the Pre-Permian basements of the Bohemian Massif and the Alps. Contrib. Mineral. Petrol. *40*, 105-130 (1973)

Grauert, B., Hänny, R., Soptrajanova, G.: Geochronology of a polymetamorphic and anatectic gneiss region: the Moldanubicum of the area Lam-Deggendorf, Eastern Bavaria, Germany. Contrib. Mineral. Petrol. *45*, 37-63 (1974a)

Grauert, B., Hofmann, A.: Effects of progressive regional metamorphism and magma formation on U-Pb systems in zircon. Third European Colloquium of Geochronology, Cosmochronology and Isotope Geology (abstract) Oxford, 1973

Grauert, B., Seitz, M.G., Soptrajanova, G.: Uranium and lead gain of detrital zircon studied by isotopic analyses and fission track mapping. Earth Planet. Sci. Lett. *21*, 389-399 (1974b)

Grauert, B., Wagner, M.E.: Age of the granulite-facies metamorphism of the Wilmington Complex, Delaware-Pennsylvania Piedmont. Am. J. Sci. *275*, 683-691 (1975)

Grünenfelder, M.: Heterogenität akzessorischer Zirkone und die petrogenetische Deutung ihrer Uran/Blei-Zerfallsalter. I. Der Zirkon des Granodioritgneisses von Acquacalda (Lukmanierpass). Schweiz. Mineral. Petrogr. Mitt. *43*, 235-257 (1963)

Grünenfelder, M., Hanson, G.N., Brunner, G.O., Eberhard, E.: U-Pb discordance and phase unmixing in zircons. In: Abstracts for 1966 Geol. Soc. Am. Spec. Paper *101*, 80 (1968)

Grünenfelder, M., Hofmänner, F., Grögler, N.: Heterogenität akzessorischer Zirkone und die petrogenetische Deutung ihrer Uran/Blei-Zerfallsalter. II. Präkambrische Zirkonbildung im Gotthardmassiv. Schweiz. Mineral. Petrogr. Mitt. *44*, 543-558 (1964)

Grünenfelder, M., Silver, T.: Radioactive age dating and its petrologic implications for some Georgia granites (abstract). Bull. Geol. Soc. Am. *69*, 1574 (1958)

Gulson, B., Krogh, T.E.: Old lead component in the young Bergell Massif, South-east Swiss Alps. Contrib. Mineral. Petrol. *40*, 239-252 (1973)

Gulson, B.L., Krogh, T.E.: Evidence of multiple intrusion, possible resetting of U-Pb ages, and new crystallization of zircons in the post-tectonic intrusions ('Rapakivi granites') and gneisses from South Greenland. Geochim. Cosmochim. Acta *39*, 65-82 (1975)

Gulson, B.L., Rutishauser, H.: Granitization and U-Pb studies of zircons in the Lauterbrunnen Crystalline Complex. Geochem. J. *10*, 13-23 (1976)

Hänny, R., Grauert, B., Soptrajanova, G.: Palaeozoic migmatites affected by high-grade Tertiary metamorphism in the Central Alps (Valle Bodengo, Italy). Contrib. Mineral. Petrol. *51*, 173-196 (1975)

Hart, S.R., Davis, G.L.: Zircon U-Pb and whole-rock Rb-Sr ages and early crustal development near Rainy Lake, Ontario. Bull. Geol. Soc. Am. *80*, 595-616 (1969)

Higgins, M.W., Sinha, A.K., Zartman, R.E., Kirk, W.S.: U-Pb zircon dates from the central Appalachian Piedmont: A possible case of inherited radiogenic lead. Bull. Geol. Soc. Am. *88*, 125-132 (1977)

Hurst, R.W., Farhat, J.: Geochronologic investigations of the Sudbury Nickel Irruptive and the Superior Province granites north of Sudbury. Geochim. Cosmochim. Acta *41*, 1803-1815 (1977)

Jaffey, A.H., Flynn, K.F., Glendenin, L.E., Bentley, W.C., Essling, A.M.: Precision measurements of half-lives and specific acitivities of ^{235}U and ^{238}U. Phys. Rev. C. *4*, 1889-1906 (1971)

Köppel, V.: Isotopic U-Pb ages of monazites and zircons from the crust-mantle transition and adjacent units of the Ivrea and Ceneri zones (Southern Alps, Italy). Contrib. Mineral. Petrol. *43*, 55-70 (1974)

Köppel, V., Grünenfelder, M.: A study of inherited and newly formed zircon from paragneisses and granitised sediments of the Strona-Ceneri-Zone (Southern Alps). Schweiz. Mineral. Petrogr. Mitt. *51*, 385-409 (1971)

Köppel, V., Grünenfelder, M.: Concordant U-Pb ages of monazites from the Central Alps and the timing of the high temperature Alpine metamorphism, a preliminary report. Schweiz. Mineral. Petrogr. Mitt. *55* (1975)
Kouvo, O., Tilton, G.R.: Mineral ages from the Finnish Precambrian J. Geol. *74*, 421-442 (1966)
Krogh, T.E.: A low-contamination method for decomposition of zircon and extraction of U and Pb for isotopic age determinations. Geochim. Cosmochim. Acta *37*, 485-494
Krogh, T.E., Davis, G.L., Harris, N.B.W., Ermanovics, I.F.: Isotopic ages in the Eastern Lac Seul region of the English River gneiss belt. Carnegie Inst. Washington Yearb. *74*, 623-625 (1975a)
Krogh, T.E., Davis, G.L.: Alteration in zircons and differential dissolution of altered and metamict zircon. Carnegie Inst. Washington Yearb. *74*, 619-623 (1975)
Krogh, T.E., Mysen, B.O., Davis, G.L.: A Palaeozoic age for the primary minerals of a Norwegian eclogite. Carnegie Inst. Washington Yearb. *73*, 575 (1975b)
Lancelot, J., Vitrac, A., Allègre, C.J.: Uranium and lead isotopic dating with grain by grain zircon analysis: a study of complex geological history with a single rock. Earth Planet. Sci. Lett. *29*, 357-366 (1976)
Ledent, D., Patterson, C., Tilton, G.R.: Ages of zircon and feldspar concentrates from Northern American beach and river sands. J. Geol. *72*, 112-122 (1964)
Le Roux, L.J., Glendenin, L.E.: Half-life of ^{232}Th. Proc. Nat. Meet. Nucl. Energy, Pretoria, South Africa 83-94 (1963)
Michard-Vitrac, A., Lancelot, J., Allègre, C.J.: U-Pb ages on single zircons from the Early Precambrian rocks of West Greenland and the Minnesota River Valley. Earth Planet. Sci. Lett. *35*, 449-453 (1977)
Michot, J., Deutsch, S.: U/Pb zircon ages and polycyclism of the gneiss de Brest and the adjacent formations (Brittany). Eclogae geol. Helv. *63*, 215-227 (1970)
Michot, J., Pasteels, P.: The prospects of the Rb-Sr and the U-Pb methods for an advanced geochronological investigation of the Precambrian of Southern Norway. Nor. Geol. Unders. *258*, 17-26 (1969)
Moorbath, S., O'Nions, R.K., Pankhurst, R.J.: The evolution of Early Precambrian crustal rocks at Isua, West Greenland – geochemical and isotopic evidence. Earth Planet. Sci. Lett. *27*, 229-239 (1975)
Naylor, R.S., Steiger, R.H., Wasserburg, G.J.: U-Th-Pb and Rb-Sr systematics in 2.700 x 10^6 year old plutons from the southern Wind River Range, Wyoming: Geochim. Cosmochim. Acta *34*, 1133-1159 (1970)
Nicolayson, L.O.: Solid diffusion in radioactive minerals and the measurement of the absolute age. Geochim. Cosmochim. Acta *11*, 41-59 (1957)
Nunes, P.D., Steiger, R.H.: A U-Pb zircon, and Rb-Sr and U-Th-Pb whole-rock study of a polymetamorphic terrane in the Central Alps, Switzerland. Contrib. Mineral. Petrol. *47*, 255-280 (1974)
Nunes, P.D., Tilton, G.R.: Uranium-lead ages of minerals from the Stillwater Complex and associated rocks, Montana. Bull. Geol. Soc. Am. *82*, 2231-2250 (1971)
O'Nions, R.K., Baadsgaard, H.: A radiometric study of polymetamorphism in the Bamble Region, Norway. Contrib. Mineral. Petrol. *34*, 1-21 (1971)
Oversby, V.M.: Lead isotopic systematics and ages of Archean acid intrusions in the Kalgoorlie-Norseman area, Western Australia. Geochim. Cosmochim. Acta *39*, 1107-1125 (1975)
Overstreet, W.C.: The geologic occurrence of monazite. Prof. Pap. U.S. Geol. Surv. *530* (1967)
Pankhurst, R.J., Pidgeon, R.T.: Inherited isotope systems and the source region pre-history of early Caledonian granites in the Dalradian series of Scotland. Earth Planet. Sci. Lett. *31*, 55-68 (1976)
Pasteels, P., Michot, J.: Geochronologic investigation of the metamorphic terrain of Southwestern Norway. Nor. Geol. Tidsskr. *55*, 111-134 (1975)

Peterman, Z.E., Goldich, S.S., Hedge, C.E., Yardley, D.H.: Geochronology of the Rainy Lake Region, Minnesota-Ontario. Mem. Geol. Soc. Am. *135*, 193-215 (1972)
Pidgeon, R.T.: Zircon U-Pb ages from the Galway granite and the Dalradian, Connemara, Ireland. Scott. J. Geol. *5*, 375-392 (1969)
Pidgeon, R.T., Aftalion, M.: The geochronological significance of discordant U-Pb ages of oval-shaped zircons from a Lewisian gneiss from Harris, Outer Hebrides. Earth Planet. Sci. Lett. *17*, 269-274 (1972)
Pidgeon, R.T., Bowes, D.R.: Zircon U-Pb ages of granulites from the Central Region of the Lewisian, northwestern Scotland. Geol. Mag. *109*, 247-258 (1972)
Pidgeon, R.T., Köppel, V., Grünenfelder, M.: U-Pb isotopic relationship in zircon suites from a para- and orthogneiss from the Ceneri zone, Southern Switzerland. Contrib. Mineral. Petrol. *26*, 1-11 (1970)
Pidgeon, R.T., Hopgood, A.M.: Geochronology of Archean gneisses and tonalites from north of the Frederikshabs isblink, Southwest Greenland. Geochim. Cosmochim. Acta *39*, 1333-1346 (1975)
Pidgeon, R.T., Johnson, M.R.W.: A comparison of zircon U-Pb and whole-rock Rb-Sr systems in three phases of the Carn Chuinneag granite, Northern Scotland. Earth Planet. Sci. Lett. *24*, 105 (1974)
Pidgeon, R.T., O'Neil, R.J., Silver, L.T.: Observations on the crystallinity and the U-Pb system of a metamict Ceylon zircon under experimental hydrothermal conditions. Fortschr. Mineral. *50*, 118 (1973)
Pidgeon, R.T., Raheim, A.: Geochronological investigation of the gneisses and minor intrusive rocks from Kristiansund, West Norway. Nor. Geol. Tidsskr. *52*, 241-256 (1972)
Rosholt, J.N., Bartel, A.J.: U-Th-Pb and Rb-Sr ages in granite reference from southwestern Saskatchewan. Can. J. Earth Sci. *7*, 184-187 (1970)
Saxena, S.K.: Evolution of zircons in sedimentary and metamorphic rocks. Sedimentology *6*, 1-13 (1966)
Shestakov, G.I.: Diffusion of lead in monazite, zircon, sphene and apatite. Trans. Geokhimiya *10*, 1197-1202 (1972)
Shields, W.R.: Comparison of Belgian Congo and Synthetic "Normal" Samples. Table 6 in Appendix A, Report No. 8, National Bureau of Standards Meeting of the Advisory Committee for Standard Materials and Methods of Measurement, May 17 and 18, 1960, 37 pp, unpublished, 1960
Shukolyukov, Y.A.: Interpretation of discordant ages calculated from the isotopic ratios: $^{206}Pb/^{238}U$ and $^{207}Pb/^{235}U$. Geochem. Int. *5*, 843-852 (1964)
Silver, L.T., Deutsch, S.: Uranium lead variations in zircon: a case study. J. Geol. *71*, 747-758 (1963)
Silver, L.T., McKinney, C.R., Deutsch, S., Bolinger, J.: Precambrian age determinations in the western San Gabriel mountains, Calif. J. Geol. *71*, 196-214 (1963)
Sinha, A.K.: U-Th-Pb systematics and the age of the Onverwacht Series, South Africa. Earth Planet. Sci. Lett. *16*, 219-227 (1972)
Sommerauer, J.: Trace element distribution patterns and the mineralogical stability of zircon – an application for combined electron microprobe techniques. Proc. Vol. 4. Electron Microscopy Soc. of Southern Afria (1974)
Sommerauer, J.: Die chemisch-physikalische Stabilität natürlicher Zirkone und ihr U-(Th)-Pb System. Ph.D. thesis ETH Zürich, 1976, unpublished
Steiger, R.H., Harnik-Soptrajanova, G., Zimmermann, E., Henriksen, N.: Isotopic age and metamorphic history of the banded gneiss at Danmarkshavn, East Greenland. Contrib. Mineral. Petrol. *57*, 1-24 (1976)
Steiger, R.H., Wasserburg, G.J.: Systematics in the Pb^{208}-Th^{232}, Pb^{207}-U^{235}, and Pb^{206}-U^{238} systems. J. Geophys. Res. *71*, 6065-6090 (1966)
Steiger, R.H., Wasserburg, G.J.: Comparative U-Th-Pb systematics in 2.7 x 10^9 year plutons of different geologic histories. Geochim. Cosmochim. Acta *33*, 1213-1232 (1969)

Stern, T.W., Goldich, S.S., Newell, M.F.: Effects of weathering on the U-Pb ages of zircon from the Morton gneiss, Minnesota. Earth Planet. Sci. Lett. *1*, 369-371 (1966)
Tatsumoto, M., Patterson, C.: Age studies of zircon and feldspar concentrates from the Franconia sandstone. J. Geol. *72*, 232-242 (1964)
Tilton, G.R.: Volume diffusion as a mechanism for discordant lead ages. J. Geophys. Res. *65*, 2933-2945 (1960)
Tilton, G.R., Grünenfelder, M.: Sphene, uranium-lead ages. Science *159*, 1458-1461 (1968)
Tilton, G.R., Steiger, R.H.: Mineral ages and isotopic composition of primary lead at Manitouwadge, Ontario. J. Geophys. Res. *74*, 2118-2132 (1969)
Van Schmus, W.R.: Geochronologic comparison of Early Proterozoic events in Southern Finland and in the Lake Superior Area, North America. Fourth European Colloquium of Geochronology, Cosmochronology and Isotope Geology, Amsterdam 1976, volume of abstracts, 1976
Vinogradov, A.P.: Comparison of data on the age of rocks obtained by different methods and geological conclusions. Geokhimiya *5*, 3-17 (1956)
Vitrac-Michard, A., Allègre, C.J.: ^{238}U-^{206}Pb, ^{235}U-^{207}Pb, systematics on Pyrenean basement. Contrib. Mineral. Petrol. *51*, 205-212 (1975)
Wasserburg, G.J.: Diffusion processes in lead-uranium systems. J. Geophys. Res. *68*, 4823-4846 (1963)
Wetherill, G.S.: An interpretation of the Rhodesia and Witwatersrand age patterns. Geochim. Cosmochim. Acta *9*, 290-292 (1956a)
Wetherill, G.S.: Discordant uranium-lead ages, I. Trans. Am. Geophys. Union *37*, 320-326 (1956b)
Wetherill, G.S.: Discordant uranium-lead ages, II. Discordant ages resulting from diffusion of lead and uranium. J. Geophys. Res. *68*, 2957-2965 (1963)
Williams, I.S.: The Berridale batholith: a lead and strontium isotopic study. Ph.D. thesis, Australian National University, 1977, unpublished
Zhirova, V.V., Zykov, S.I., Tugarinov, A.I.: Ages of zircons from ancient formations in the Kola Peninsula. Geokhimiya *4* (1961)

The Total Lead Method

M. DELALOYE

1. Principle

The method relies on the determination of the total amount of U, Th, and Pb in a mineral without isotopic analysis.

This method is very old, and is also known under other names such as the *chemical lead method,* the *alpha lead method,* and the *Larsen method.* This author has shown in 1952 that, unlike minerals rich in U and Th, those in which they occur as trace elements (zircon, monazite, sphene, xenotime) are able to give good geochronological results. In effect, they do not incorporate any common lead at the time of crystallization, and make good closed systems in their resistance to alteration.

To obtain good results, two basic conditions have to be satisfied:

1) all lead in the mineral must be radiogenic.

2) the mineral must be a closed system for U, Th, and Pb, since crystallization.

In actual fact, isotopic studies have shown that the above conditions are only rarely satisfied.

2. Determination of U, Th, and Pb

U and Th are radioactive and can be determined by several methods:
Optical spectrography
X-ray fluorescence
Alpha activity
Fluorimetry
Autoradiography

Pb can be determined by:
Optical spectrography
X-ray fluorescence
Atomic absorbtion

For all these methods, sensitivity and precision are highly variable. The choice of method depends on a number of criteria; not the least of which is the availability of the apparatus.

3. Formula Used to Calculate the Age

Two different equations can be used, depending on the age of the sample. Between 0 and 200 m.y. the equation used is:

$$t = C \times Pb\ (ppm) \times \alpha\ (mg^{-1} h^{-1})$$

where C is a factor related to the ratio U/Th. If there is only uranium, then C = 2600; while if there is only thorium in the mineral, C = 1990.

Above 200 m.y. a correction must be introduced, to account for the decay of U and Th. Thus

$$t_0 = t - 1/2\ Kt^2 \qquad \text{and}$$

$$t = C \times Pb\ (ppm) \times \alpha\ (mg^{-1} h^{-1})$$

$$K = 1.9 \times 10^{-4} \text{ for } U/Th = \infty \qquad \text{or}$$
$$0.5 \times 10^{-4} \text{ for } U/Th = 0$$

The exact value of K is calculated in each case when the ratio U/Th is determined.

4. Validity of the Method

The total lead method is of exploratory value only; it is also rapid and relatively cheap. It is used, almost exclusively, to date zircons which occur as accessory minerals. These are common in acidic and intermediate rocks, and usually contain 300 to 3000 ppm U, 100 to 2500 ppm Th and 10 to 200 ppm Pb.

The method is, however, inexact for two reasons which arise from the fact that the required conditions, mentioned above, are in general no strictly fulfilled:

1) the zircons contain quantities of common lead which are often not negligible; this lead is lodged in the crystal at the time of its formation. It results in apparent ages which are *too high.*

2) The possible *loss* (or post-crystallization variations arising from the fact that the mineral does not constitute a closed system strictly) of U and Th cannot be revealed by this method, as is the case with isotopic methods. This loss results in apparent ages that are *too low*, and the total lead age reflects chiefly the $^{206}Pb/^{238}U$ isotopic age.

In practice, the errors due to these two factors tend to offset each other; unfortunately they cannot be detected during analysis. It seems that for zircons, of a certain age at least, the second cause of error outweighs the first, so that the apparent ages tend to be too low.

Isotope Geochemistry of Lead

V. KÖPPEL and M. GRÜNENFELDER

The variations of lead isotopic ratios are a powerful tool in helping to solve problems of petrogenesis and metallogenesis, in that they provide answers to questions of the origin and time of magma generation and metal concentrations. As the isotopic ratios conserve a time-integrated record of the U/Pb and Th/Pb ratios of the sources in which the lead developed, they also shed light upon the time-dependent geochemical behavior of these elements within the lithosphere.

In contrast to the ages determined by the U-Th-Pb method utilizing the disintegration of the radioactive parent from the time t up to the present, the common lead method is based upon the evolution of the lead since the time T, when the earth started to act as a closed system for U, Th, and Pb to the time t when the lead was isolated from its radioactive parents.

Considering the earth as a closed system for U, Th, and Pb we can describe the growth of the lead isotope ratios by the following equations:

$$(^{206}Pb/^{204}Pb)_t = (^{206}Pb/^{204}Pb)_0 + \mu\,(e^{\lambda_8 T} - e^{\lambda_8 t}) \quad (1)$$

$$(^{207}Pb/^{204}Pb)_t = (^{207}Pb/^{204}Pb)_0 + \frac{\mu}{137.88}\,(e^{\lambda_5 T} - e^{\lambda_5 t}) \quad (2)$$

$$(^{208}Pb/^{204}Pb)_t = (^{208}Pb/^{204}Pb)_0 + W\,(e^{\lambda_2 T} - e^{\lambda_2 t}) \quad (3)$$

$(^{206}Pb/^{204}Pb)_0 = a_0 = 9.307$
$(^{207}Pb/^{204}Pb)_0 = b_0 = 10.294$
$(^{208}Pb/^{204}Pb)_0 = c_0 = 29.479$

primordial lead (= Pb isotopic composition at time T) (Tatsumoto et al., 1973)

T = age of the Earth (calculated with the new decay constants) = 4.57 b.y. (Tilton, 1973).

Other calculations using the new decay constants yielded: 4.49 b.y. (Patterson, 1956), 4.55 b.y. (Tilton and Steiger, 1965, recalculated with the new values for a_0 and b_0), 4.57 b.y. (Tatsumoto et al., 1973).

$\mu = {}^{238}U/{}^{204}Pb$
$W = {}^{232}Th/{}^{204}Pb$
$137.88 = {}^{238}U/{}^{235}U$

λ_8, λ_5, λ_2: decay constants of ^{238}U, ^{235}U, and ^{232}Th respectively.

If we consider, however, only a part of the Earth, i.e., the mantle, the crust, or even smaller units such as a granite body, the Eqs. (1) to (3) no longer apply because the assumption that the lead of such a subsystem developed since T in a closed U-Th-Pb system with μ and W values that changed only due to the radioactive decay is no longer valid. U, Th, and Pb fractionate during geochemical processes whereby U is preferentially enriched in acidic rocks. Consequently, if we look at a specific unit of the earth we have to consider it as a system that was open during all events that lead eventually to its present-day appearance; it possibly was also open during prolonged time intervals prior to its final formation. The lead of most ore deposits will have a complicated history involving, for example, a period of mantle residence (μ_1), a period of crustal residence (μ_2) accompanied possibly by metamorphism (μ_3), erosion and sedimentation (μ_4), until the lead was finally extracted during a volcanic cycle or by the action of hot brines, and concentrated in an ore deposit.

The change of ^{206}Pb and ^{238}U, for example, can then be generally described by expressions such as:

$$\frac{d^{206}Pb}{dt} = {}^{238}U - L(t)\,(^{206}Pb) + G(t) \qquad (4)$$

L(t) : loss of ^{206}Pb
G(t) : gain of ^{206}Pb from outside sources

$$\frac{d^{238}U}{dt} = {}^{238}U - L'(t)\,(^{238}U) + G'(t) \qquad (5)$$

L'(t) : loss of ^{238}U other than by radioactive decay
G'(t) : gain of ^{238}U
(Allègre and Michard, 1973)

In spite of these complications Eqs. (1) to (3) have in the past been widely used to describe in a first approximation the evolution of common lead. The term common lead refers to a lead that developed in environments with U/Pb and Th/Pb ratios that never greatly exceeded the range observed in average crustal rocks (U/Pb: 0.05-1, Th/Pb: 1-10). Such leads are commonly found in whole rock samples, in feldspars, and in sulfides.

Besides the decay constants they require the knowledge of the primordial lead isotope ratios and of T. Geologic processes have obliterated all traces of the Earth's primordial lead and thus the chances of finding the primordial lead on Earth are extremely small. Assuming, however, a common origin of the solar system and its meteorites, one may expect to find the primordial lead in U- and Th-free phases of meteorites. Patterson (1953), indeed, first observed in troilite from the Canyon Diablo meteorite with extremely low U and Th concentrations the lowest lead isotopic ratios, i.e., $^{206}Pb/^{204}Pb$, $^{207}Pb/^{204}Pb$ and $^{208}Pb/^{204}Pb$. The age of the Earth, T, was determined from the lead isotopic ratios of meteorites with differing U/Pb ratios (Patterson et al., 1955; Patterson, 1955, 1956). T thus denotes the time when the

solar system with uniform U/Pb and Th/Pb ratios and an isotopically homogeneous lead differentiated into bodies with distinctly different U/Pb and Th/Pb ratios.

Although these assumptions have recently been questioned (for further references see Cumming and Richards, 1975) they still appear valid for satisfying first approximations.

Equations (1)–(3) and (6) can be used to calculate an age of the Earth, provided the age of a single-stage lead is precisely known. The difficulties of knowing the age of the lead can theoretically be avoided by using a lead of 0 m.y. of age, such as for instance the lead from manganese nodules or from volcanic rocks. The problem of finding a single-stage lead, however, remains. Averaging a hypothetical modern lead would also have to take into account the distribution of lead within the various geochemical units of the Earth (Chow and Patterson, 1959; Stacey and Kramers, 1975; Cumming and Richards, 1975).

Using Eqs. (1)–(3) we can plot the growth of the lead isotope ratios with time for given values of μ and W (Fig. 1). Figure 1 cannot be used for deriving model ages from the measured isotopic ratios of, for instance, a galena, because we do not know the μ nor the W values in which the lead developed from time T until its separation from U and Th at time t.

Equations (1) and (2), however, contain as unknowns μ and t, and by dividing Eq. (2) by Eq. (1), it is possible to eliminate μ:

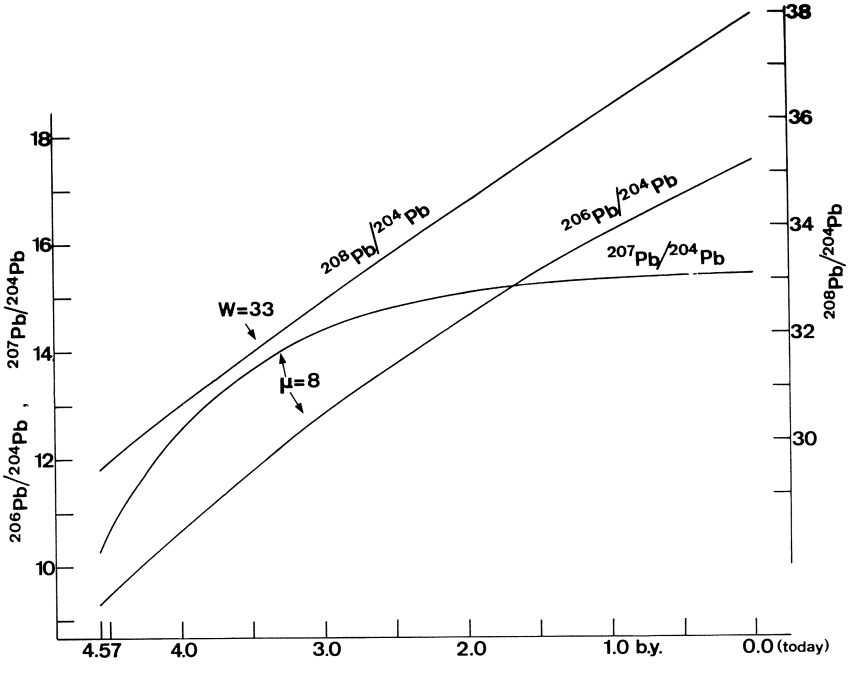

Fig. 1. Growth of lead isotope ratios with time. W and μ are parameters ($\mu = {}^{238}U/{}^{204}Pb$, $W = {}^{232}Th/{}^{204}Pb$)

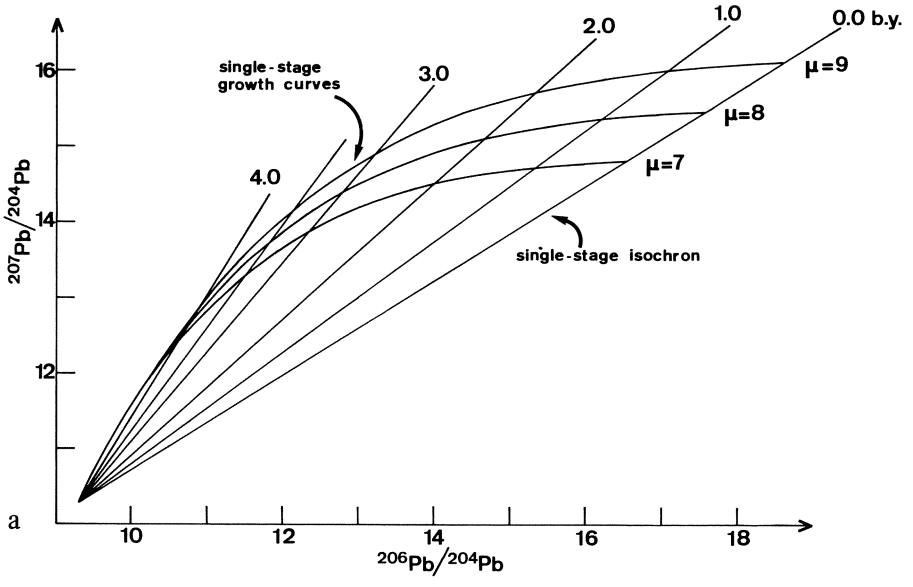

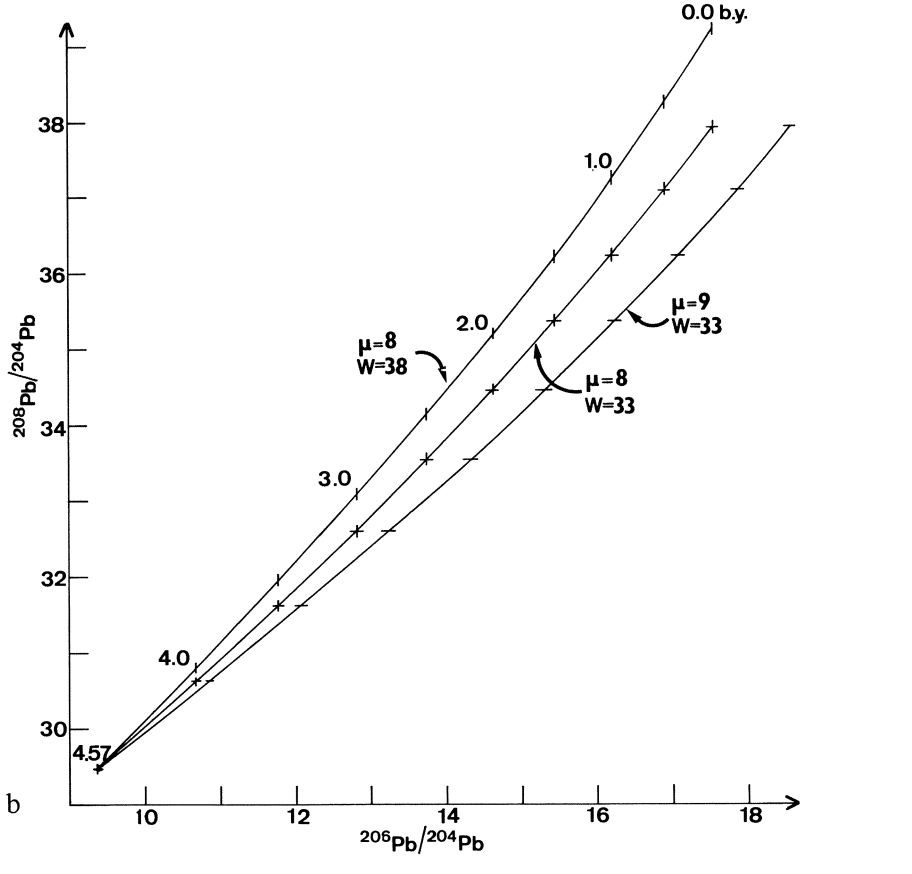

Fig. 2. a Diagram of $^{207}Pb/^{204}Pb$ versus $^{206}Pb/^{204}Pb$ showing single-stage growth curves with μ as a parameter and single-stage isochrons [Eq. (6)]. **b** Diagram of $^{208}Pb/^{204}Pb$ versus $^{206}Pb/^{204}Pb$ showing single-stage growth curves [Eqs. (1) and (3)] for different pairs of μ and W

$$\frac{(^{207}Pb/^{204}Pb)_t - b_0}{(^{206}Pb/^{204}Pb)_t - a_0} = \frac{1}{137.88} \times \frac{(e^{\lambda_5 T} - e^{\lambda_5 t})}{(e^{\lambda_8 T} - e^{\lambda_8 t})} \quad (6)$$

This is the equation of a straight line, the so-called isochron.

$$\frac{^{207}Pb}{^{204}Pb_t} = b_0 + \frac{1}{137.88} \times \frac{(e^{\lambda_5 T} - e^{\lambda_5 t})}{(e^{\lambda_8 T} - e^{\lambda_8 t})} \times \left[\frac{^{206}Pb}{^{204}Pb_t} - a_0\right] \quad (7)$$

All the leads that evolved between T and t in reservoirs with different μ values will lie on a $^{207}Pb/^{204}Pb$ versus $^{206}Pb/^{204}Pb$ plot on a straight line passing through a_0 and b_0 (Fig. 2).

1. Lead Evolution Models

The Pb evolution model proposed by Houtermans (1946) and Holmes (1946, 1947, 1949), known as the Holmes-Houtermans model, assumed that lead evolved since T in chemically closed environments with differing U/Pb ratios. The model therefore assumes a family of growth curves originating at time T from the starting point defined by lead of the troilite phase of the Canyon Diable meteorite. The model ages were then calculated using Eq. (6).

Stanton and Russell (1959) observed that a number of strata-bound (conformable) lead-bearing sulfide deposits, which were thought to have originated from island arc, as well as from submarine volcanism, exhibited each a uniform lead isotopic composition that plotted in both lead-lead diagrams on a curve that closely followed a single-stage growth curve. The model ages calculated from Eqs. (1)–(3) for such ore deposits agreed reasonably well with the ages determined by other methods. Such leads were therefore called single-stage leads, and it was thought that they originated from the mantle. Because of their geologic setting, only the mantle could possibly be conceived as a homogeneous reservoir with respect to U, Th, and Pb, the crust being too heterogeneous to produce a regular array of the data points without extensive mixing processes prior to the time of ore formation.

Leads from vein-type deposits normally yield data points which scatter on the lead-lead diagrams, and the model ages do not agree with the known ages. This behavior is attributed to the crustal origin of the lead, which obviously developed in several stages and often was only incompletely mixed prior to deposition as is often shown by variable isotope ratios from lead of a single deposit (for example see Doe, 1970).

The concepts of a single-stage lead evolution upon which the models of Holmes and Houtermans as well as of Russell et al. rested were already questioned early (see Russell and Farquhar, 1960) and today they have been abondoned. Analyses of volcanic rocks from oceanic regions showed that the mantle could not be regarded as a uniform reservoir for U, Th, and Pb. In view of the concepts of plate tectonics, a

number of more complex models were proposed involving differentiation and mixing processes (Kanasewich, 1968; Armstrong, 1968; Russell, 1972; Armstrong and Hein, 1973; Sinha and Tilton, 1973; Robertson, 1973; Russell and Birnie, 1974; Church and Tatsumoto, 1975; Sun et al., 1975).

A major break-through was brought about by the availability of absolute Pb isotopic standards, improvements in the techniques of measuring lead isotope ratios which reduced the uncertainty of uncontrolled fractionation, and finally by the redetermination of the primordial lead in the Canyon Diablo meteorite (Tatsumoto et al., 1973). The new values for the lead in the troilite phase of this meteorite shifted the growth curve for single-stage leads in such a way that it was no longer possible to fit the ore lead of strata-bound deposits on a curve such that the model ages, especially of the Phanerozoic deposits, agreed with the stratigraphic ages (Fig. 3a, b).

Two models have been proposed to accomodate the data of strata-bound ore leads on revised growth curves: Stacey and Kramers (1975) introduced a model with a two-stage growth curve. Approximately 3.7 b.y. ago a major first differentiation of the Earth into a crust and mantle occurred, whereby the crust was enriched in U and Th with respect to the mantle. The effects of later differentiation within the crust or the mantle were largely obliterated by mixing processes. Mixing of mantle and crustal lead is considered to be of minor but not negligible importance (Fig. 3a, b). The nature of the fundamental event required by the model is not clear. The authors state that the 3.7 b.y. event may just represent an approximation for a prolonged period of crustal formation which ended approximately 2.5 b.y ago.

Cumming and Richards (1975) proposed another model similar to Sinha and Tilton (1973) in which μ and W increase linearily with time:

$$\mu(t) = u(1 - \epsilon t)$$
$$W(t) = W(1 - \epsilon' t)$$
$$\epsilon = 0.050 \times 10^{-9}/y, \quad T = 4.509 \text{ b.y.}$$
$$\epsilon' = 0.037 \times 10^{-9}/y$$

They force the growth curves through the data points of the Canyon Diablo lead and of the lead from Captains Flat (Australia), a stratiform Pb-Zn-Cu deposit of Silurian age, assigning an age of 430 m.y. to this deposit. They choose the present-day μ value to make a best fit for different pairs of T and ϵ. The continuous linear increase of the μ and W values can be related to continuous differentiation processes; however, a continuous linear increase of U and Th concentrations in the crust cannot occur forever.

Both models yield ages for strata-bound sulfide deposits that agree well with the ages obtained by other geochronological methods (Fig. 3a, b). It should again be noted that both models are based on the lead isotope ratios of a selected number of strata-bound ore deposits (Cobalt, Ont. and SW Finland are epigenetic deposits, a summary of these deposits is given in Köppel and Saager, 1976) that were formerly believed on the basis of their geologic setting, as well as of their lead isotopic pattern to contain mantle-derived lead. According to the model proposed by Stacey and Kramers (1975), the lead of these deposits represents an average crustal lead and according to the model of Cumming and Richard (1975), the lead would be a mixture of crustal and mantle lead dominated by the former. Doe and Zartman (in press, 1978) proposed a model

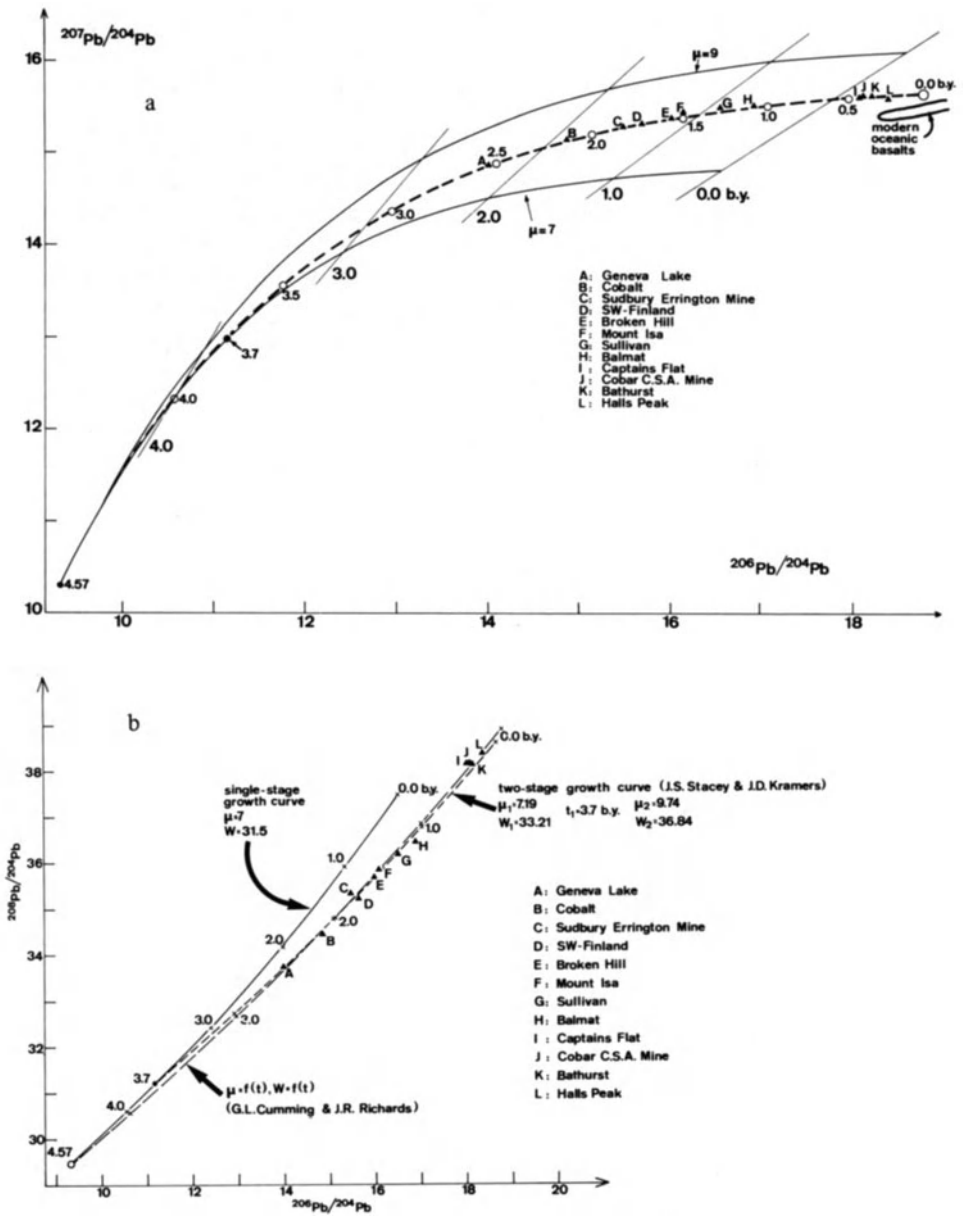

Fig. 3a and b. Data points of galenas from ores that were used to define the single-stage growth curve. With the new values of the lead from troilite of the Canyon Diablo meteorite the model ages of all Phanerozoic deposits become negative. *Broken curve* comprises the two-stage growth curve proposed by Stacey and Kramers (1975) and the growth proposed by Cumming and Richards (1975) with continuously increasing μ and W values (the scale of the drawings permits a separation of the two curves only in the $^{208}Pb/^{206}Pb$ versus $^{206}Pb/^{204}Pb$ diagram)

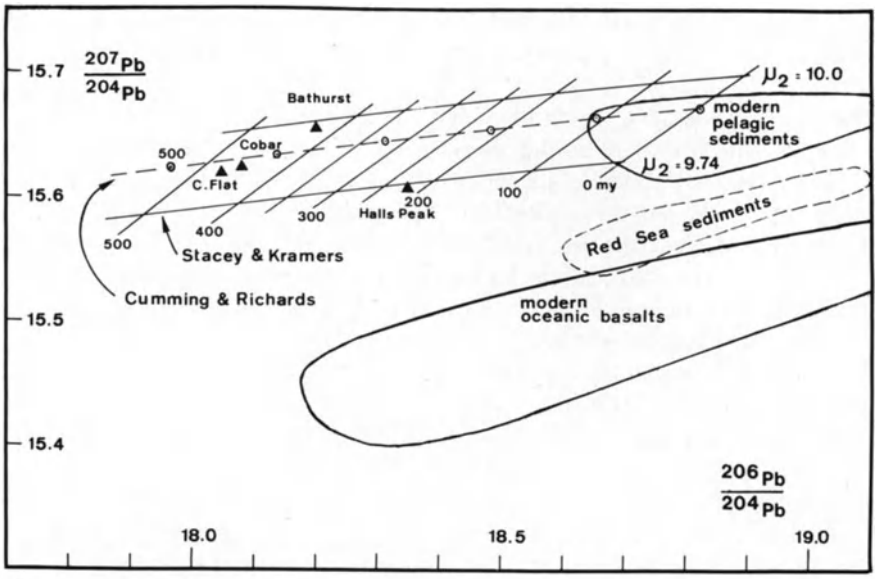

a

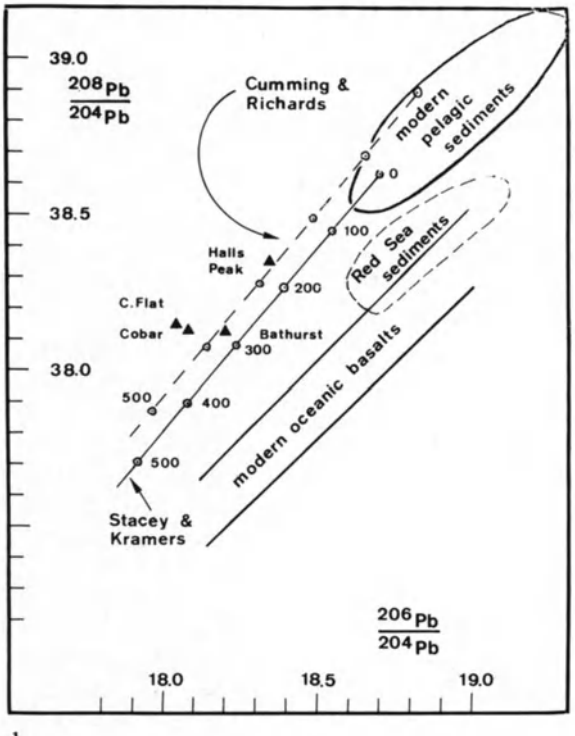

b

Fig. 4a and b. The data points of some Phanerozoic strata-bound ores, modern oceanic basalts (e.g., Church and Tatsumoto, 1975; Sun et al., 1975), pelagic sediments (e.g., Reynolds and Dasch, 1971), and Red Sea sediments, ores and basalts (Delevaux and Doe, 1974)

which describes the evolution of the lead growth curve defined by the lead from strata-bound and stratiform deposits as a consequence of repeated mixing processes during orogenies.

It must be borne in mind that both models may be biased insofar as the number of strata-bound and stratiform ore deposits from which reliable lead isotope data existed at the time these models were conceived is restricted to North-American and Australian deposits. Recent investigations (Köppel, 1978) of deposits in Southern Africa indicate that large-scale areal variations of the μ values may exist.

In contrast to the crustal lead, the lead from oceanic basaltic rocks developed in an environment, i.e., the mantle, with a low μ value. However, large variations of the apparent μ and W values do exist in the mantle, as can be seen especially in the lead isotopic data from oceanic islands and rises which indicate μ and W values often higher than the crustal average (Gast et al., 1964; Tatsumoto, 1966; Sun et al., 1975; Church and Tatsumoto, 1975). These variations of the μ and W values occurred relatively late in the Earth's history, so that the distinction between mantle and crustal lead is possible. It is noteworthy that the lead of some strata-bound sulfide deposits in island arc environments, Japan (Sato and Sasaki, 1973) or oceanic rift systems, Red Sea (Delevaux and Doe, 1974) do contain a pronounced or even dominant mantle component (Fig. 4a, b).

2. "Anomalous" Multistage Lead, Secondary Isochrons, Mixing Lines

The term anomalous lead was used to refer to any lead that was not a single-stage lead. It is probably safe to say that a single-stage lead will never be found in a geologic sample. Therefore all lead samples are anomalous, and this term might as well be abandoned. On the other hand, it may retain some of its usefulness in distinguishing lead that may be explained by simple models such as proposed by Stacey and Kramers (1975) or by Cumming and Richards (1975) from those which evolved in a more complex fashion.

Many lead isotope studies, especially from vein-type ore deposits, have revealed the presence of linear arrays of data points in either one or both lead-lead diagrams. They may be mixing lines or have the significance of isochrons. In both types of diagram straight lines will be produced by incomplete mixing of two different common leads. The slope of the line has then no age meaning. Isochrons, on the other hand, may be produced in two ways:

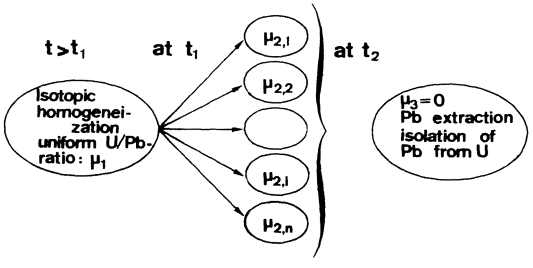

Fig. 5. Diagram illustrating the development at t_1 of U-Pb subsystems with $\mu_{2,1}$ to $\mu_{2,n}$ by fractionation of an isotopically homogeneous source

1. At some time t, prior to t_1, isotopic homogeneization occurred, for instance by magmatic processes. At time t_1 differentiation processes led to the formation of various subsystems, each having its own μ value ($\mu_{2,1}$ to $\mu_{2,n}$) (Figs. 5, 6). At time t_2 lead was extracted from these subsystems and isolated from uranium and thorium. Equations (1) and (2) may then be rewritten:

$$(^{206}Pb/^{204}Pb)_{t_2 i} = (^{206}Pb/^{204}Pb)_{t_1} + \mu_{2,i}\,(e^{\lambda_8 t_1} - e^{\lambda_8 t_2}) \tag{8}$$

$$(^{207}Pb/^{204}Pb)_{t_2 i} = (^{207}Pb/^{204}Pb)_{t_1} + \frac{\mu_{2,i}}{137.88}\,(e^{\lambda_5 t_1} - e^{\lambda_5 t_2}) \tag{9}$$

Combining the two equations yields the equation of a straight line:

$$\left(\frac{^{207}Pb}{^{204}Pb}\right)_{t_2 i} = \left(\frac{^{207}Pb}{^{204}Pb}\right)_{t_1} + \frac{1}{137.88}\left(\frac{e^{\lambda_5 t_1} - e^{\lambda_5 t_2}}{e^{\lambda_8 t_1} - e^{\lambda_8 t_2}}\right)\left[\left(\frac{^{206}Pb}{^{204}Pb}\right)_{t_2 i} - \left(\frac{^{206}Pb}{^{204}Pb}\right)_{t_1}\right] \tag{10}$$

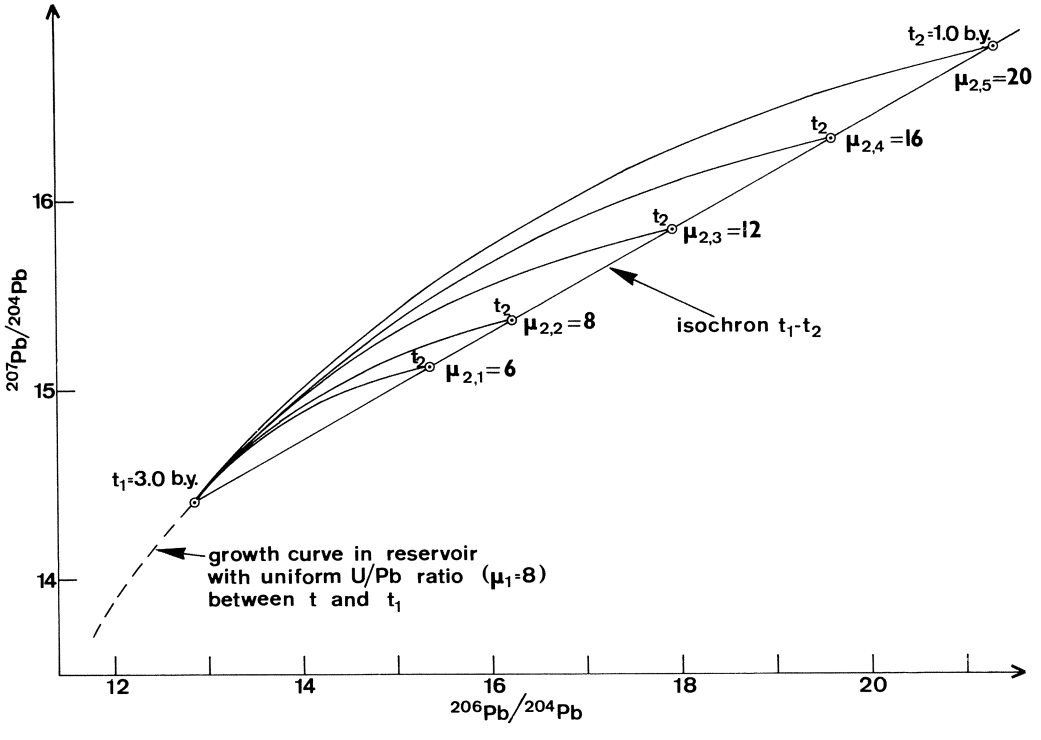

Fig. 6. The growth curve of different subsystems $\mu_{2,i}$ is shown for the time interval t_1-t_2. At time t_2 the data points will lie on the isochron t_1-t_2

2. Radiogenic lead developed between t_1 and t_2 in a system with a value of $\mu = \infty$, i.e., free of ^{204}Pb, for instance in uranium ores or minerals such as zircons or monazites. At time t_2 the radiogenic lead, or part of it, is extracted and added to a homogeneous common lead with which it is, however, only incompletely mixed (Fig. 7). The mixing line will also have a time meaning, the slopes of the line being the $^{207}Pb/^{206}Pb$ ratio of the radiogenic lead:

$$s = \frac{\Delta\,(^{207}Pb/^{204}Pb)}{\Delta\,(^{206}Pb/^{204}Pb)} = \left(\frac{^{207}Pb}{^{206}Pb}\right)_{rad} = \frac{1}{137.88}\left(\frac{e^{\lambda_5 t_1} - e^{\lambda_5 t_2}}{e^{\lambda_8 t_1} - e^{\lambda_8 t_2}}\right) \qquad (11)$$

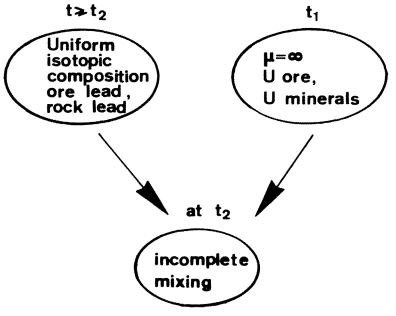

Fig. 7. Diagram illustrating how a lead-lead isochron can be obtained by incomplete mixing of a homogeneous common lead with a radiogenic lead free of ^{204}Pb

It should be noted that in the $^{208}Pb/^{204}Pb$ versus $^{206}Pb/^{204}Pb$ diagram, a linear array is in both cases not necessarily observed. In the first case the fractionation of uranium and lead is independent of the uranium and thorium fractionation, and in the second case the U/Th ratios of the system with $\mu = \infty$ may not be the same in all parts of the system.

From Eq. (11) one may either calculate t_1 or t_2. In case 1 (Fig. 5), t_1 is the age of the source rock from which lead was extracted at time t_2 to form a mineralization. In case 2 (Fig. 7), t_1 is the age of the source of the radiogenic component. In both cases t_2 corresponds to the time of mineralization if deposition occurred shortly after extraction.

If neither t_1 nor t_2 are known, then one my let $t_1 \Rightarrow t_2$ $(= t_i)$, and the formula for the slope s is:

$$s = \frac{1}{137.88}\;\frac{\lambda_5 e^{\lambda_5 t_i}}{\lambda_8 e^{\lambda_8 t_i}} \qquad (12)$$

t_i is then the maximum age of the mineralization and the minimum age for the source out of which the lead developed. For a rigorous treatment of multistage leads see Gale and Mussett (1973).

Two examples will serve to illustrate the use of lead isotopes and U-Pb systematics in solving problems related to metallogenesis and petrogenesis.

3. Uranium Mineralization in the Beaverlodge Area, Saskatchewan, Canada

This example demonstrates the usefulness of a combination of U-Pb analyses of uranium minerals and of Pb isotopic analyses of associated Pb minerals (Köppel, 1968).

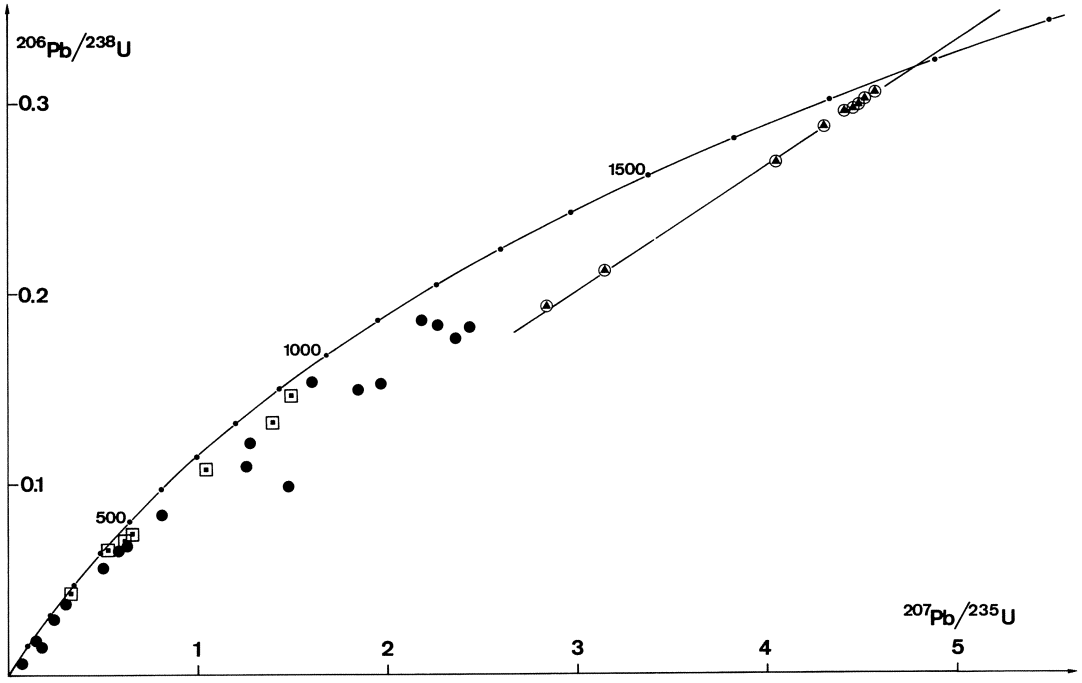

Fig. 8. Concordia diagram showing the data points of U minerals from epigenetic vein type deposits of the Beaverlodge area, Saskatchewan, Canada (Köppel, 1968). ◓ Denotes massive pitchblende accompanied by very little sulfides; the pitchblende is not oxidized and is free of hematite. ▣ denotes pitchblende intergrown with hematite. ● Denotes pitchblende often fine-grained, and/or intergrown with sulfides. Samples with apparent ages of less than 500 m.y. were often highly oxydized

Figure 8 shows the data points of the pitchblende analyses. From their scatter it is obvious that the history of the uranium mineralization is a complex one. However, for one group of samples, a relatively simple history may be deduced from their age pattern. These samples have the following characteristics not shown by the others: 1) The pitchblendes are massive on the scale of a centimeter or more, 2) they do not show any signs of oxydation, and 3) they are accompanied by minor amounts of sulfides and hematite is absent. The array of data points indicates a time of deposition of 1780 ± 20 m.y. and an episodic lead loss in the recent past.

However, fine-grained pitchblende associated with sulfides and/or oxides, and often in a state of higher oxydation, yielded apparent ages indicating a more complicated history. Adhering to episodic lead loss models the data require an event between 900 and 1200 m.y., one around 700 m.y. and a more recent one. The lead isotopic ratios of galena and clausthalite provided independent evidence for the 900 to 1200 m.y. event.

Figure 9 shows the lead isotopic ratios of galena and clausthalite samples associated with the uranium mineralization. Most of the samples show a considerable excess of radiogenic ^{206}Pb and ^{207}Pb. One may reasonably assume that this excess lead derived from the pitchblende which shows ample evidence of lead loss. The situation prevailing in this case is therefore similar to the one shown in Figure 7. The slope of the linear array is equal to the $^{207}Pb/^{206}Pb$ ratio attained in the pitchblende at the time of lead loss. Equation (11) therefore applies and thus allows the calculation of t_2, the time of lead loss, because we know from the concordia diagram t_1 to be 1780 m.y., t_2 is then 1140 ± 50 m.y.

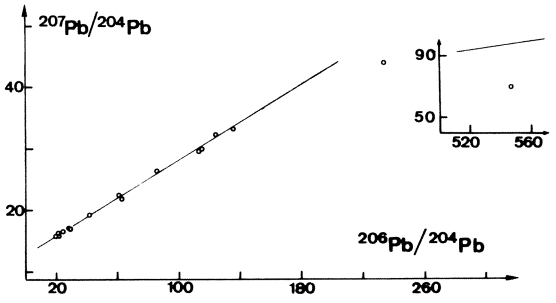

Fig. 9. Lead isotopic ratios of galena and clausthalite samples associated with the uranium mineralization in the Beaverlodge area Saskatchewan, Canada (Köppel, 1968)

The $^{208}Pb/^{204}Pb$ ratios are comparatively low, ranging from about 35 to 44, with only two samples between 40 and 44. The low content of thorogenic lead, as seen from the isotopic analyses of the pitchblende lead, also argues for a derivation of the excess uranogenic lead from pitchblende.

Interestingly, the data points of all pitchblende samples intergrown with hematite plot further to the left in the concordia diagram (Fig. 8) and thus suggest either a major lead loss around 1100 m.y. from the 1780 m.y. old pitchblende or a new crystallization of the uraniumoxide 1100 m.y. ago.

The pitchblende data with $^{207}Pb/^{206}Pb$ ages of less than 1100 m.y. suggest one or more events later than 1100 m.y. ago. One of the samples yielded within the analytical uncertainties a concordant age around 270 m.y. The only event that occurred in the area at about this time is an upwelling of the crust West of the Hudson Bay to Illinois. The sensitivity of the U-Pb systems in pitchblende to events not recorded in other isotopic systems appears to be related to the occurrence of the mineral in faults which may easily be reworked by events otherwise not registered in the country rocks. During such periods of reworking, the U-Pb system of pitchblende may easily be re-opened by circulating water and changing redox conditions.

Figure 9 reveals that not all galena data plot on the linear array. Two samples fall below the best fit line. The $^{207}Pb/^{206}Pb$ of this radiogenic lead component is obvious-

ly lower than in the majority of the samples, indicating thereby an additional lead loss later than 1140 m.y. ago.

This type of study demonstrates how U-Pb and Pb isotopic studies complement each other. A similar example has been reported by Hills and Richards (1976).

4. Lead Isotopic Provinces in the Western United States

Zartman (1974) convincingly demonstrated a correlation between the lead isotopic pattern of Mesozoic to Tertiary magmatic rocks and related ore leads of hydrothermal ore deposits on the one hand and the geotectonic setting on the other hand.

By restricting the comparison to young rocks one avoids much of the uncertainties introduced by the lead correction due to the in situ decay of uranium and thorium in the rock samples since the time of their crystallization. The lead correction is based on the assumption of closed U-Pb and Th-Pb systems. This assumption can, of course, be checked by analyzing a number of cogenetic rock samples and treating the data in the same way as Rb-Sr isochron data. The uncertainty whether the closed system condition is fullfilled or not, does, however, not introduce a large uncertainty in the case of young rocks. Therefore, ore lead and rock lead can be compared with a high degree of confidence.

Furthermore, the comparatively short time span of about 200 m.y. allows for only small purely time-dependent variations of the isotopic ratios.

As can be seen from Figure 10 the isotopic variations by far exceed any variations which would result solely from the age differences of the samples. The variations therefore reflect long time variations of the U/Pb and Th/Pb ratios of the source materials from which the magma derived.

Figure 10 shows how the three isotopic fields correlate with three distinct areas of the Western United States.

Zartman's interpretation is based upon the distribution pattern of U and Pb within the Earth's lithosphere. In the lower crust, i.e., in granulite facies rocks uranium is depleted with respect to lead and thorium, whereas in upper crustal rocks uranium is enriched with respect to lead. The behavior of thorium is less well understood at the present. All three elements are depleted in the mantle with respect to the crust.

Area I (Fig. 10) is underlain by thick Precambrian crust which consolidated 2.7 and 1.8 b.y. ago. If magma generation occurs involving the lower crust, then the lead isotopes should reflect the old uranium depletion by a retarded development of the uranogenic lead isotopes. This is indeed the pattern that one observes in the Mesozoic and Tertiary magmatic rocks.

The majority of the associated hydrothermal ore deposits contain lead with similar isotopic patterns. A minority of the lead samples do contain, however, a more radiogenic lead. Such samples come from minor ore deposits and within a restricted area they often form linear arrays on the $^{207}Pb/^{204}Pb$ versus $^{206}Pb/^{204}Pb$ diagram. The slope of the arrays does reflect the age of consolidation of basement.

Area II is characterized by the presence of a more than 15-km-thick sequence of miogeosynclinical sediments of late Precambrian to Phanerozoic in age. Precambrian

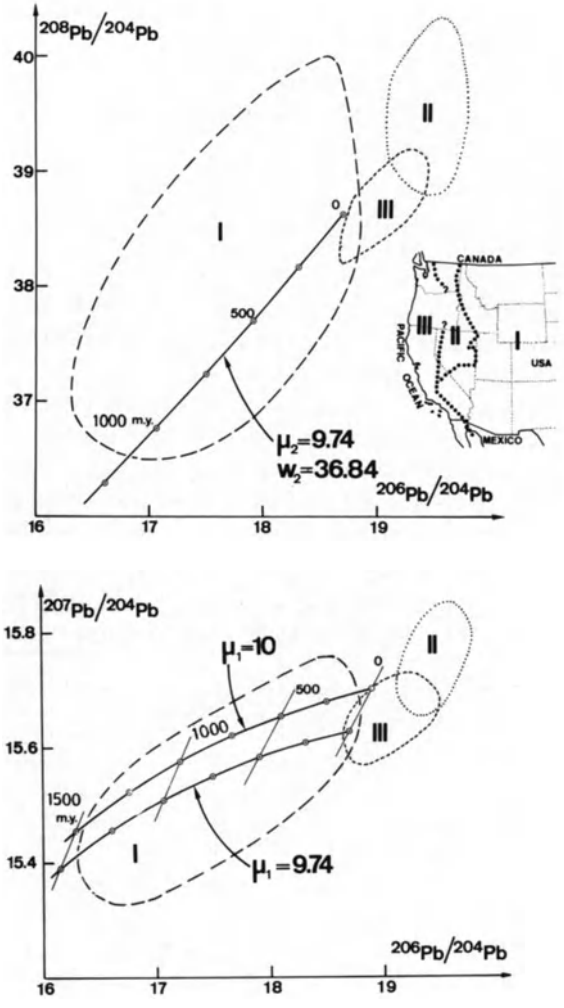

Fig. 10. Lead isotopic ratios of Mesozoic to Tertiary igneous rocks from the Western United States (areas *I, II,* and *III*) plot in the two lead-lead diagrams in the respective fields. The three fields comprise together more than 240 analyses. The three areas correspond to distinct geotectonic settings (Zartman, 1974)

crystalline basement rocks are virtually unknown in this area. It is plausible to assume that the material of the miogeosynclinical sediments represents eroded upper crustal material of the basement. Upper crustal rocks are enriched in U compared to lower crustal or mantle rocks (Doe, 1970). They will therefore in time develop excess radiogenic lead. The comparatively radiogenic nature of the lead from area II suggests an upper crustal origin of the sedimentary pile. As magmas are generally generated at much greater depths than 15 km, one may assume that also a mantle component is present, but compared to the upper crustal component it is negligible. The samll spread of the isotopic data is probably due to a mixing effect of U, Th, and Pb during sedimentation. Within area II ore and rock leads are indistinguishable, and thus must originate from the same source.

Good agreement between ore and rock leads is also observed in area III. Within this area a thick sequence of eugeosynclinical rocks of Mesozoic to Tertiary age

occurs. The lead resembles oceanic lead from recent sediments, which is thought to represent a fair average of crustal and mantle lead.

The idea of correlating lead isotope data with the geotectonic setting has been further pursued by Doe and Zartman (in press, 1978). Such studies provide important information on questions of magma generation and the provenance of metals in ore deposits.

Acknowledgements. We thank Drs. George Tilton and Dieter Gebauer for carefully reading the manuscript and for their helpful contributions to improve its content.

Suggested Further Reading. For literature prior to 1970 compare Doe (1970).

The following list of selected references is far from complete.

Problems related to ore formation:

Doe, B.R., Deleveaux, M.H.: Source of lead in southeast Missouri galena ores. Econ. Geol. *67*, 409-425 (1972)

Doe, B.R., Stacey, J.S.: The application of lead isotopes to the problem of ore genesis and ore prospect evaluation: a review. Econ. Geol. *69*, 757-776 (1974)

Dymond, J., Corliss, J.B., Heath, G.R., Field, C.W., Dasch, E.J., Veeh, H.H.: Origin of metalliferous sediments from the Pacific Ocean. Bull. Geol. Soc. Am. *84*, 3355-3372 (1973)

Farquharson, R.B., Richards, J.R.: U-Th-Pb systematics related to igneous rocks and ore Pb, Mount Isa, Queensland. Miner. Deposita *9*, 339-356 (1974)

Gulson, B.L.: Differences in lead isotope composition in the stratiform McArthur zinc-lead-silver deposits. Miner. Deposita *10*, 277-286 (1975)

Gulson, B.L.: Exploration and mapping around a base metal sulfide deposit using trace lead isotopes. Miner. Deposita *11*, 1-5 (1976)

Hills, J.H., Richards, J.R.: Pitchblende and galena ages in the Alligator Rivers region, Northern Territories, Australia. Miner. Deposita *11*, 133-154 (1976)

Houtermans, F.G.: Die Bleimethoden der geologischen Altersbestimmung. Geol. Rundsch. *49*/1, 168-196 (1960)

Köppel, V., Saager, R.: Lead istope evidence on the detrital origin of Witwatersrand pyrites and its bearing on the prevenance of the Witwatersrand gold. Econ. Geol. *69*, 318-331 (1974)

Kuo, S.-L., Folinsbee, R.E.: Lead isotope geology of mineral deposits spatially related to the Tintina Trench, Yukon Territory. Econ. Geol. *69*, 806-813 (1974)

Lancelot, J., Sarazin, G., Allègre, C.J.: Composition isotopique du plomb et du soufre des galènes liées aux formations sédimentaires. Interprétations géologiques et géophysiques. Contrib. Mineral. Petrol. *32*, 315-333 (1971)

Lougnon, J., Duthou, J.-L., Lasserre, M.: Les gisements plombozincifères du seuil du Poiton et de sa bordure limousine. Bull. Bur. Rech. Geol. Minières, Sect. II, *5*, 453-476 (1974)

Mitchell, R.H., Krouse, H.R.: Isotopic composition of sulfur and lead in galena from the Greenhow-Skyreholme arc, Yorkshire, England. Econ. Geol. *66*, 243-251 (1971)

Ozarel, J.M., Glawson, W.F., Russell, R.D.: An integrated model for lead isotopic evolution for samples from the Canadian shield. Can. J. Earth Sci. *10*, 529-537 (1973)

Reynolds, P.H.: A U-Th-Pb lead isotope study of rocks and ores from Broken Hill, Australia. Earth Planet. Sci. Lett. *12*, 215-223 (1971)

Reynolds, P.H., Sinclair, A.J.: Rock and ore-lead isotopes from the Nelson batholith and the Kootenay Arc, British Columbia, Canada. Econ. Geol. *66*, 259-266 (1971)
Richards, J.R.: Major lead ore bodies – Mantle origin? Econ. Geol. *66*, 425-434 (1971)
Richards, J.R.: Lead isotope data on three North Australian galena localities. Miner. Deposita *10*, 287-301 (1975)
Rye, D.M., Doe, B.R., Deleveaux, M.H.: Homestake Gold Mine, South Dakota: II Lead isotopes, mineralization ages and source of lead in ores of the Northern Black Hills. Econ. Geol. *69*, 814-822 (1974)
Saager, R., Köppel, V.: Lead isotopes and trace elements from sulfides or Archean Greenstone belts in South Africa – a contribution to the knowledge of the oldest known mineralizations. Econ. Geol. *71*, 44-57 (1976)
Sangster, D.F.: Isotopic studies of ore leads in the Hanson Lake – Flin Flon – Snow Lake mineral belt, Saskatchewan and Manitoba. Can. J. Earth Sci. *9*, 500-513 (1972)
Sato, K.: Unilateral isotopic variation of Miocene ore leads from Japan. Econ. Geol. *70*, 800-805 (1975)
Small, W.D.: Isotopic composition of selected ore leads from northeastern Washington. Can. J. Earth Sci. *10*, 670-678 (1973)
Thorpe, R.: Lead isotope evidence on the genesis of the silverarsenide vein deposits of the Cobalt and Great Bear Lake areas, Canada. Econ. Geol. *69*, 777-791 (1974)
Zartman, R.E., Stacey, J.S.: Lead isotopes and mineralization ages in the Belt supergroup rocks, northwestern Montana and northern Idaho. Econ. Geol. *66*, 849-860 (1971)

Lead isotopes in crustal rocks and in igneous rocks in continental and island arc surroundings:

Armstrong, R.L., Cooper, J.A.: Lead isotopes in island arcs. Bull. Volcanol. *35*/1, 27-63 (1971)
Church, S.E.: Limits of sediment involvement in the genesis of orogenic volcanic rocks. Contrib. Mineral. Petrol. *39*, 17-32 (1973)
Church, S.E., Tilton, G.R.: Lead and strontium isotopic studies in the Cascade Mountains: bearing on andesite genesis. Bull. Geol. Soc. Am. *84*, 431-454 (1973)
Cumming, G.L., Tsong, F.: Variation of the isotopic composition of volatilized lead and the age of the western granodiorite, Yellowknife, Northwest Territories. Can. J. Earth Sci. *12*, 558-573 (1975)
Doe, B.R., Deleveaux, M.H.: Variations in lead isotopic compositions in Mesozoic granitic rocks of California: A preliminary investigation. Bull. Geol. Soc. Am. *84*, 3513-3526
Kramers, J.D.: Lead and strontium isotopes in Cretaceous kimberlites and mantle-derived Xenoliths from Southern Africa. Earth Planet. Sci. Lett. *34*, 419-432 (1977)
Lancelot, J.R., Allegre, C.J.: Origin of carbonatite magma in the light of the U-Th-Pb isotope system. Earth Planet. Sci. Lett. *22*, 233-238 (1974)
Lipman, P.W., Doe, B.R., Hedge, C.E., Steven, T.A.: Petrologic evolution of the San Juan volcanic field, southwestern Colorado: Pb and Sr isotope evidence. Bull. Geol. Soc. Am. *89*, 59-82 (1978)
Manton, W.I., Tatsumoto, M.: Some Pb and Sr isotopic measurements on eclogites from the Roberts Victor mine, South Africa. Earth Planet. Sci. Lett. *10*, 217-226 (1971)
Moorbath, S., Park, R.G.: The Lewisian of the southern region of the Scottish mainland. Scott. J. Geol. *8*, 51-74 (1971)
Oversby, V.M.: Genetic relations among the volcanic rocks of Reunion: Chemical and lead isotopic evidence. Geochim. Cosmochim. Acta *36*, 1167-1179 (1972)

Robertson, D.K., Folinsbee, R.E.: Lead isotope ratios and crustal evolution of the Slave Craton at Ghost Lake, Northwest Territories. Can. J. Earth Sci. *11*, 819-827 (1974)
Vollmer, R.: Rb-Sr and U-Th-Pb systematics of alkaline rocks: the alkaline rocks from Italy. Geochim. Cosmochim. Acta *40*, 283-295 (1976)
Vollmer, R.: Isotopic evidence for genetic relations between acid and alkaline rocks in Italy. Contrib. Mineral. Petrol. *60*, 109-118 (1977)
Zartman, R.E., Tera, F.: Lead concentration and isotopic composition in five peridotite inclusions of probable mantle origin. Earth Planet. Sci. Lett. *20*, 54-66 (1973)

For lead isotopes in oceanic rocks compare:

Tatsumoto, M.: Lead isotopes in volcanic rocks and possible oceanfloor thrusting beneath island arcs. Earth Planet. Sci. Lett. *6*, 369-376 (1969)
Tatsumoto, M.: Isotopic composition of lead in oceanic basalts and its implication to mantle evolution. Earth Planet. Sci. Lett. *38*, 63-87 (1978)

Lead isotopes in lunar rocks:

Tera, F., Wasserburg, G.J.: U-Th-Pb systematics of lunar rocks and inferences about lunar evolution and the age of the Moon. Proc. 5th Lunar Sci. Conf., 1974, pp. 1571-1599
Unruh, D.M., Tatsumoto, M.: Evolution of mare basalts: the complexity of the U-Th-Pb system. Proc. 8th Lunar Sci. Conf., 1977, pp. 1673-1696

Further references, also to the Russian literature and lead isotopes in meteorites may be found in:

Gmelin: Handbuch der anorganischen Chemie, Blei, Teil A2a, Vorkommen, 8. Aufl. Berlin, 1976

References

Allègre, C.J., Michard, G.: Introduction à la Géochimie. Paris: Presses Universitaires de France, 1973, 220 pp.
Antweiler, J.C., Doe, B.R., Delevaux, M.H.: Lead isotope and other evidence on the bedrock source of placer gold at Hahns Peak, Colorado. Econ. Geol. *67*, 302-314 (1972)
Armstrong, R.L.: A model for the evolution of Sr and Pb isotopes in a dynamic Earth. Rev. Geophysics *6*/2, 175-200 (1968)
Armstrong, R.L., Hein, S.M.: Computer simulation of Pb and Sr isotope evolution of the Earth's crust and upper mantle. Geochim. Cosmochim. Acta *37*, 1-18 (1973)
Burger, A.J., Nicolaysen, L.O., de Villiers, J.W.L.: Lead isotopic compositions of Galenas from the Witwatersrand and Orange Free State, and their relation to the Witwatersrand and Dominion Reef uraninites. Geochim. Cosmochim. Acta *26*, 25-59 (1962)
Chow, T., Patterson, C.C.: Lead isotopes in manganese nodules. Geochim. Cosmochim. Acta *17*, 21-31 (1959)
Church, S.E., Tatsumoto, M.: Lead isotope relations in Oceanic Ridge basalts from the Juan de Fuca – Gorda ridge area, N.E. Pacific Ocean. Contrib. Mineral. Petrol. *53*, 253-279 (1975)

Cumming, G.L., Gudjurgis, P.J.: Alteration of trace lead isotopic ratios by positive metamorphic and hydrothermal activity. Can. J. Earth Sci. *10*, 1782-1789 (1973)
Cumming, G.L., Richards, J.R.: Ore lead isotope ratios in a continuously changing earth. Earth Planet. Sci. Lett. *28*, 155-171 (1975)
Delevaux, M.H., Doe, B.R.: Preliminary report on U, Th, and Pb contents and lead isotopic composition in sediment samples from the Red Sea. In: Whitmarsh, R.B., et al.: Initial Reports of the deep Sea Drilling project V. XXIII, 1974, pp. 943-946
Doe, B.R.: Lead Isotopes. Berlin, Heidelberg, New York: Springer, 1970, 137 pp.
Doe, B.R., Zartman, R.E.: Plumbotectonics I, The Phanerozoic. In: Geochemistry of Hydrothermal Ore Deposits, 2nd ed. Barnes, H. (ed.), in press, 1978
Gale, N.H., Mussett, A.E.: Episodic uranium-lead models and the interpretation of variations in the isotopic composition of lead in rocks. Rev. Geophys. Space Phys. *11*, 37-86 (1973)
Gast, P.W., Tilton, G.R., Hedge, C.E.: Isotopic composition of lead and strontium from Ascension and Gough islands. Science *145*, 1181-1185 (1964)
Holmes, A.: An estimate of the age of the Earth. Nature (London) *157*, 680 pp. (1946)
Holmes, A.: A revised estimate of the age of the Earth. Nature (London) *159*, 127pp. (1947)
Homes, A.: Lead isotopes and the age of the Earth. Nature (London) *163*, 453 pp. (1949)
Houtermans, F.G.: The isotope ratios in natural lead and the age of uranium. Naturwissenschaften *33*, 185-186 (1946)
Kanasewich, E.R.: The interpretation of lead isotopes and their geological significance. In: Radiometric Dating for Geologists. Hamilton, E.I., Farquhar, R.M. (eds.). New York: Interscience Publ. 1968
Köppel, V.: Age and history of the uranium mineralization of the Beaverlodge Area, Sask. Geological Survey of Canada, Dept. of Energy, Mines and Resources, paper 67-31, 1968
Köppel, V.: Lead isotope studies of stratiform ore deposits of Namaqualand, Northwest Cape Province, South Africa, and their implications on the age of the Bushmanland Sequence. US Geol. Survey, Open-File Report 78-701, pp. 223-226
Köppel, V., Saager, R.: Uranium, Thorium and Lead isotope studies of strata-bound ores. In: Handbook of Strata-Bound and Strati-Form ore Deposits. Wolf, K.H. (ed.). Amsterdam: Elsevier Sci. Publ. Co., 1976, pp. 267-316
Moorbath, S., Welke, H., Gale, N.H.: The significance of lead isotope studies in ancient high-grade metamorphic basement complexes as exemplified by the Lewisian rocks of northwest Scotland. Earth Planet. Sci. Lett. *6*, 245-256 (1969)
Patterson, C.C.: The isotopic composition of meteoritic, basaltic and oceanic leads and the age of the earth. Proc. 1st Conf. on Nuclear Processes in Geological Settings, 1953, pp. 36-40
Patterson, C.C.: The $^{207}Pb/^{206}Pb$ ages of some stone meteorites. Geochim. Cosmochim. Acta *7*, 151 (1955)
Patterson, C.C.: Age of meteorites and the earth. Geochim. Cosmochim. Acta *10*, 230 (1956)
Patterson, C.C., Tilton, G.R., Inghram, M.G.: Age of the earth. Science *121*, 69 (1955)
Reynolds, P.H., Dasch, E.: Lead isotopes in marine manganese nodules and the ore lead growth curve. J. Geophys. Res. *76*, 5124-5129 (1971)
Robertson, D.K.: A model discussing the early history of the Earth based on a study of lead isotope ratios from veins in some Archean cratons of Africa. Geochim. Cosmochim. Acta *37*, 2099-2124 (1973)
Russell, R.D.: Evolutionary model for lead isotopes in conformable ores and in oceanic volcanics. Rev. Geophys. Space Phys. *10*, 529-549 (1972)
Russell, R.D., Birnie, D.J.: A bi-directional mixing model for lead isotope evolution. Phys. Earth Planet. Interiors *8*, 158-166 (1974)
Russell, R.D., Farquhar, R.M.: Lead isotopes in Geology. New York, London: Interscience Publishers, 1960, 243 pp.

Sato, K., Sasaki, A.: Lead isotopes of the Black Ore ("Kuroko") deposits from Japan. Econ. Geol. *68*, 547-552 (1973)
Sinha, A.K., Tilton, G.R.: Isotopic evolution of common lead. Geochim. Cosmochim. Acta *37*, 1823-1849 (1973)
Stacey, J.S., Kramers, J.D.: Approximation of terrestrial lead isotope evolution by a two-stage model. Earth Planet. Sci. Lett. *26*, 207-221 (1975)
Stanton, R.L., Russell, R.D.: Anomalous leads and the emplacement of lead sulfide ores. Econ. Geol. *54*, 588-607 (1959)
Sun, S.-S., Tatsumoto, M., Schilling, J.-G.: Mantle plume mixing along the Reykjanes ridge axis: Lead isotopic evidence. Science *190*, 143-147 (1975)
Tatsumoto, M.: Isotopic composition of lead in volcanic rocks from Hawaii, Iwo Jima and Japan. J. Geophys. Res. *71*, 1721-1733 (1966)
Tatsumoto, M., Knight, R.J., Allegre, C.J.: Time difference in the formation of meteorites as determined from the ratio of lead-207 to lead-206. Science *180*, 1279-1283 (1973)
Tilton, G.R.: Isotopic lead ages of chondritic meteorites. Earth Planet. Sci. Lett. *19*, 321-329 (1973)
Tilton, G.R., Steiger, R.H.: Lead isotopes and the age of the Earth. Science *150*, 1805-1808 (1965)
Zartman, R.E.: Lead isotopic provinces in the Cordillera of the Western United States and their geological significance. Econ. Geol. *69*, 792-805 (1974)

Fission-Track Dating and Geologic Annealing of Fission Tracks

C. W. NAESER

1. Introduction

Fission-track dating is one of the newest methods that geologists have to help them determine the ages of minerals and natural glasses. Fission tracks are stable over different temperature intervals in different minerals and glasses, and by dating several different minerals present in a rock it is possible to obtain a better understanding of its thermal history. This dating method, used in conjunction with other dating methods, is a powerful tool for the geologist as he tries to reconstruct the geologic history of a region.

The purpose of this paper is to present the theory of fission-track dating and to show how it is possible to gain valuable information about the thermal history of a rock through the concordance or discordance of the fission-track ages of the accessory minerals present in the rocks and the relationship of these ages to the ages obtained from other age techniques used to date rocks and their minerals.

2. History and Theory

Techniques used for dating geologic and archeologic materials using fission-fragment tracks have evolved over the last decade. Fission-track dating is just one facet of the rapidly expanding field of Solid State Track Recorders (SSTR; Fleischer et al., 1975). The early developmental work on SSTR was done by three physicists, Robert L. Fleischer, P. Buford Price, and Robert M. Walker, working at the General Electric Companies Research Laboratory in Schenectady, New York. Although they did not discover that charged particles leave a damage zone in a solid, they are the ones largely responsible for SSTR's current state of development.

The first charged-particle tracks observed were those produced by fission fragments. Initial discoveries of tracks were reported by Young (1958) and Silk and Barnes (1959). Young observed shallow pits in lithium fluoride crystals which had been etched after being irradiated with fission fragments. Silk and Barnes, using an electron microscope, observed fission fragment tracks in a piece of mica; but the tracks they observed faded quickly in the electron beam. Price and Walker (1962) discovered that the damage zone created by the passage of a fission fragment could be made visible in an optical microscope by chemical etching. This enlarged the tracks and made them visible with the aid of an optical microscope. Early studies dealt with the dating

of micas (Price and Walker, 1962) and natural glasses (Fleischer and Price, 1963). Their early studies have led to the use of SSTR in many diverse fields: geology, biology, archeology, high-energy physics, nuclear physics, and the study of extraterrestrial materials such as meteorites and returned lunar samples.

A charged-particle track is the damage zone formed as a charged particle passes through a solid. A number of different types of track exists (Fleischer et al., 1975). The length and shape of the different tracks are dependent on the type of particle that formed the track. In terrestrial samples there is only one common, naturally occurring track: the fission track. Most of the other types of natural tracks are found in meteorites and in lunar minerals and glasses. These tracks are caused by cosmic-ray interactions within the extraterrestrial materials. Because the earth's atmosphere absorbs most of the cosmic rays capable of forming a track, these tracks are not seen in terrestrial materials. The remainder of this paper will be devoted to the fission track, the track formed by the two nuclei of a fissioning heavy element such as uranium; the original nucleus breaks up into two lighter nuclei of approximately equal mass and liberates about 200 MeV of energy. The two nuclei recoil from each other in opposite directions. Figure 1 shows what is generally thought to be the track-forming mechanism (Fleischer et al., 1965a). The fragments formed at the time of fission are highly charged nuclei that disrupt the electron balance of the atoms in the mineral lattice along their path. As the fission fragment passes, it leaves a zone of positive charge in its wake. This causes the positively charged ions in the lattice to repulse each other and force themselves into the crystal structure, forming the track or damage zone. The new track is only angstroms wide and about 10-20 μm long. The track is stable in all insulating solids, but conducting and semi-conducting solids do not retain tracks as movement of electrons rapidly neutralizes the ions produced.

Three naturally occurring isotopes spontaneously fission: ^{232}Th, ^{235}U, and ^{238}U. Of these, only ^{238}U produces a significant number of fission events. The other two have such long half-lives for spontaneous fission that, for all practical purposes, all

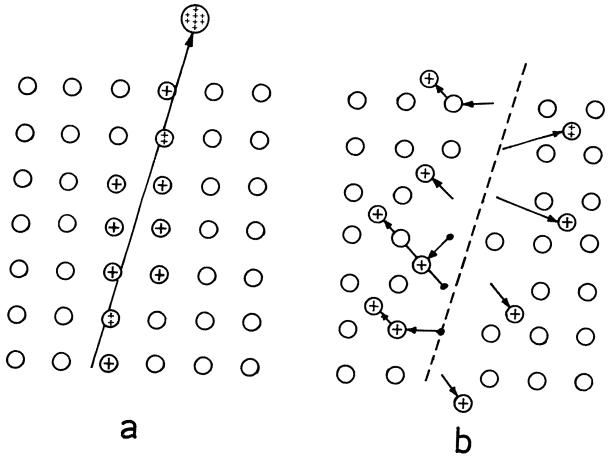

Fig. 1. Track formation in a simple crystalline solid: **a** The atoms have been ionized by the massive charged particle which has just passed; **b** the mutual repulsion of the ions has separated them and forced them into the lattice. (Courtesy of R.L. Fleischer)

fission tracks can be assumed to have come from ^{238}U. ^{238}U decays by alpha emission as well as by spontaneous fission. Millions of uranium atoms decay by alpha emission for each atom that decays by spontaneous fission.

Once a track is formed it is stable in most insulating materials at temperatures less than 100°C (Fleischer et al., 1975). With increasing temperature, the atomic movement in a solid increases, and the displaced ions along this damage zone will diffuse back into the track and cause the damage zone to fade until it can no longer be seen by etching. Track fading, annealing, and its usefulness will be covered in a later section of this paper. Assuming a track formed at a time when the temperature of a solid was below the temperature at which fading begins, it will be stable over a long period of time.

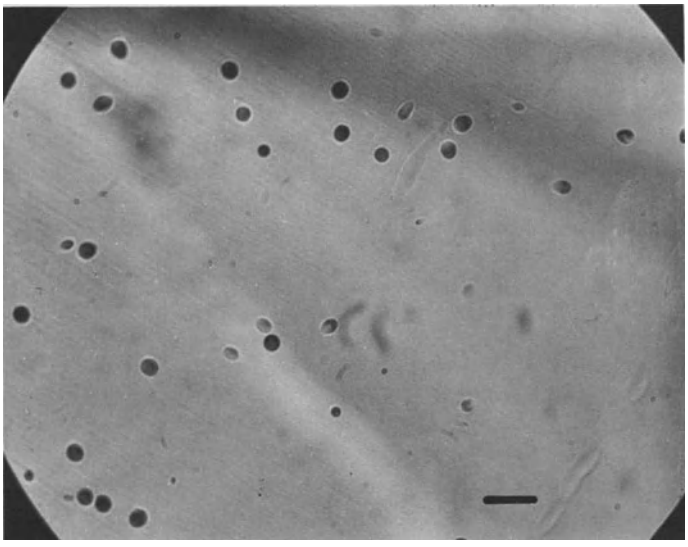

Fig. 2. Fission tracks in glass, the length of the *bar* is 10 μm in this and the following figures

Tracks in their natural state are too small to be seen except with an electron microscope. By choosing the proper chemical etchant, it is possible to dissolve out the damage zone and not dissolve its crystal (Price and Walker, 1962). Once the track is etched, it can be observed in an optical microscope at moderate magnifications (x 200-500). Common etchants used include nitric acid (apatite), hydrofluoric acid (micas, glass), and concentrated basic solutions and fluxes (sphene, zircon; Fleischer et al.,1975). Figures 2 through 4 show tracks in two minerals (apatite and zircon) and in a piece of synthetic glass (microscope slide). Other common minerals in which fission tracks have been seen include sphene, garnet, epidote, muscovite, and biotite. Natural glasses such as tektite, obsidian, and glass shards also contain fission tracks. Fleischer et al. (1975) present an extensive list of minerals which may contain fission-tracks, along with the proper etchants and etching conditions to develop the tracks.

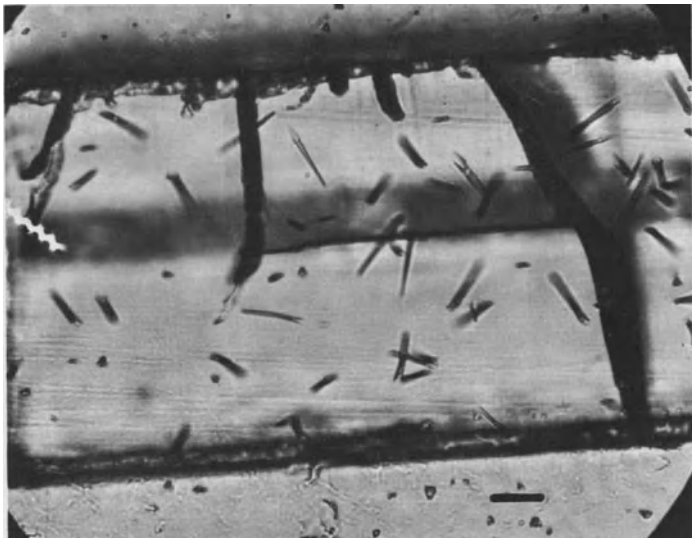

Fig. 3. Fission tracks in an apatite crystal

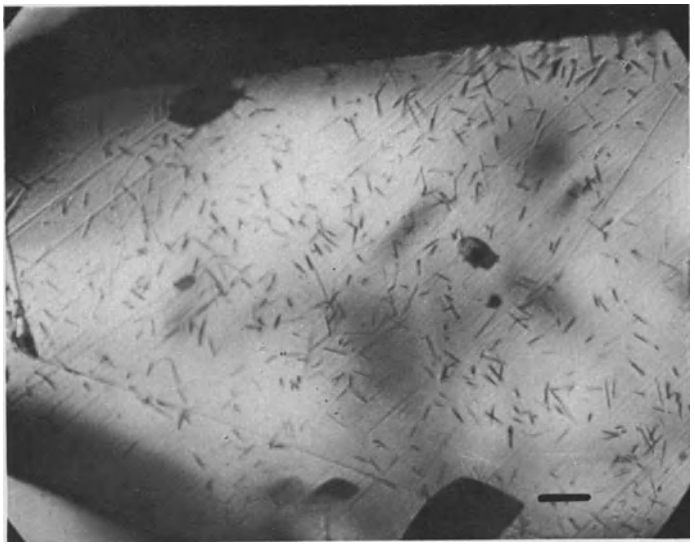

Fig. 4. Fission tracks in a zircon crystal

A given mineral can be dated if enough time has elapsed since its formation to accumulate a significant number of tracks. The track density or number of tracks per unit of surface area is a function of the age of the material and its uranium concentration. In very young rocks, minerals having a high concnetration of uranium must be

found; in old Precambrian rocks, the problem is to find minerals that have a low concentration of uranium. Zircons are generally very good minerals for dating Cenozoic rocks, but they usually have too high a track density to be useful in dating Precambrian rocks. In order to calculate the age of a mineral or glass, we need the spontaneous track density and the uranium concentration.

The fission-track-age equation is as follows (Price and Walker, 1963):

$$A = \ln\left[1 + \frac{\rho_s}{\rho_i} \cdot \frac{\lambda_D \phi \sigma I}{\lambda_F}\right] \frac{1}{\lambda_D}$$

Describing the various terms in this equation will show how a fission track age is determined. The fossil track density "ρ_s" is dependent on the age and uranium concentration of mineral. The Cenozoic zircon could have the same track density as a Precambrian epidote. So if the uranium concentration can be determined, we can calculate the age. The best way to determine the uranium concentration is to induce a new set of fission tracks. To do this we utilize the neutron fission reaction of ^{235}U. If a sample is sent to a nuclear reactor and exposed to thermal neutrons, a new set of tracks is made. The terms ρ_i, ϕ, σ, and I are related to the irradiation process: ρ_i is the density of neutron induced tracks, ϕ is the number of neutrons per square centimeter that pass through the sample, σ is the cross-section for neutron fission reaction of ^{235}U; I is the atomic ratio $^{235}U/^{238}U$. λ_D is the total decay constant for ^{238}U decay and λ_F is the decay constant for spontaneous fission. The values for the constants are listet below:

$I = 7.252 \times 10^{-3}$
$\lambda_D = 1.551 \times 10^{-10}\,yr^{-1}$
$\lambda_F = 6.85 \times 10^{-17}\,yr^{-1}$ (Fleischer and Price, 1964a)
$7.03 \times 10^{-17}\,yr^{-1}$ (Roberts et al., 1968)
or $8.42 \times 10^{-17}\,yr^{-1}$ (Spadavecchia and Hahn, 1967; Wagner et al., 1975)
$\sigma = 580 \times 10^{-24}\,cm^2$

Three methods are commonly used to determine ρ_i independent of ρ_s.

The first is to divide the mineral grains into two groups (Naeser, 1967). The first group is mounted in epoxy and polished. These grains will be used to determine the fossil-track density. The second group is heated in a furnace to a temperature high enough to cause complete annealing of the fossil tracks. These grains are then irradiated. Following the irradiation they are mounted, polished, and etched along with the first mount. The induced track density is then determined from the grains in this group. This method can be used only if the uranium concentration of all the grains is uniform. Apatite usually can be dated this way. This method requires a minimum of several hundred grains.

A second method is to use an external detector arrangement (Fleischer et al., 1964; Naeser and Dodge, 1969). For this, a mineral is mounted in epoxy, polished, and etched in order to reveal the fossil tracks. The grain mount is then covered with a piece of clean, low-uranium muscovite or lexan (a polycarbonate plastic), and irradiated with a neutron

dose monitor. The uranium that fissions near the surface of the grain will send fission fragments into the adjacent muscovite detector. After irradiation, the muscovite is etched and the induced tracks are counted. The advantage of this method is that the fossil tracks are counted on the grain and the induced tracks are counted on the image of the grain in the detector; therefore, variations in uranium concentrations can be

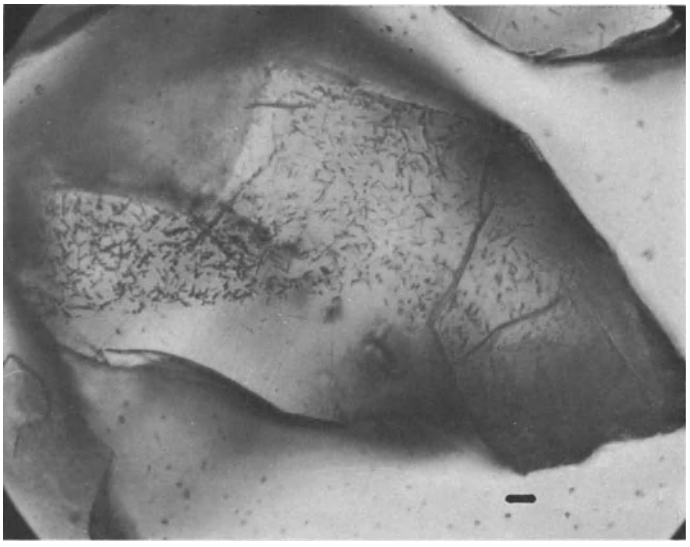

Fig. 5. Sphene grain etched for fossil fission tracks, note the zoning of the uranium within the crystal

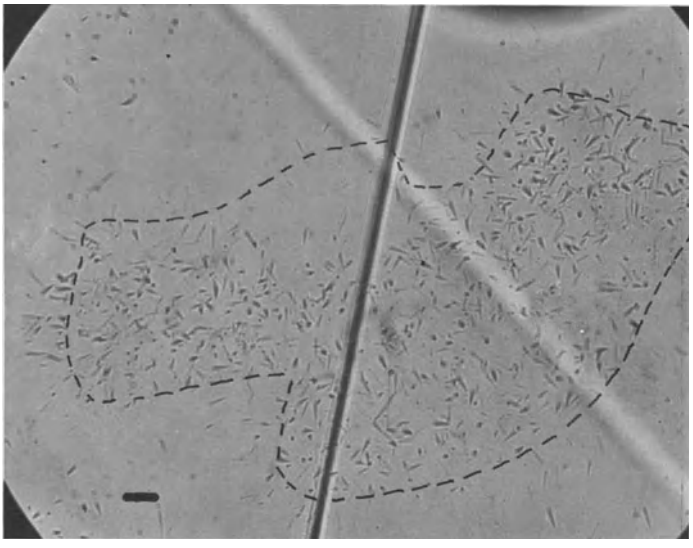

Fig. 6. Induced tracks from sphene grain in Figure 5 recorded in a muscovite detector. Edge of sphene grain has been outlined

dealt with. It is possible, but not recommended, to date only one grain using this method; normally five or more grains would be dated. This method is used for most minerals other than apatite. An assumption made is that the etching efficiencies for the mineral and the muscovite are similar, or that if they are not, the proper correction has been made. Figures 5, 6, 7, and 8 show a sphene grain and induced tracks from it in a muscovite detector.

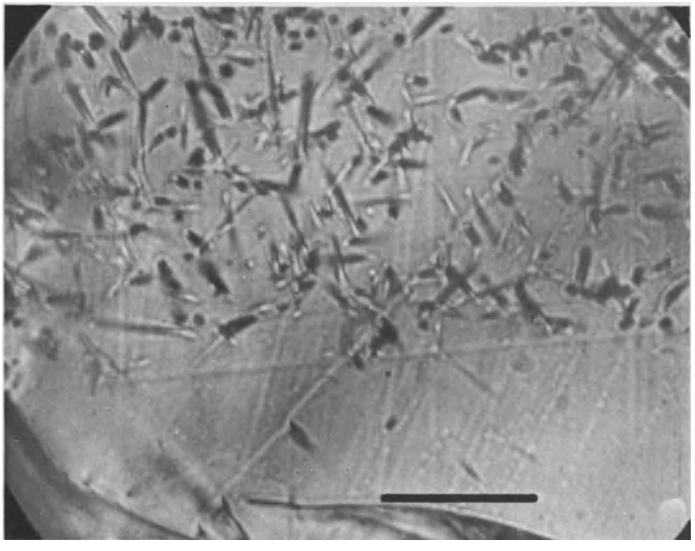

Fig. 7. Higher magnification of sphene grain in Figure 5, showing fossil fission tracks

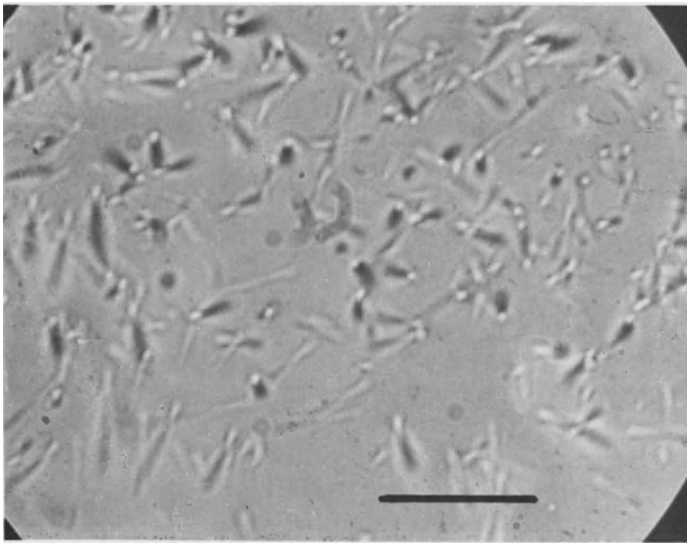

Fig. 8. Higher magnification of muscovite shown in Figure 6

A third method, which is primarily used for dating glass (Fleischer and Price, 1963), involves mounting, polishing, and etching a sample prior to irradiation. The sample is irradiated, and after irradiation the fossil track density is determined. The sample is then repolished (to remove about 20-30 μm), etched, and counted again. The second count contains both the fossil and induced tracks. The induced-track density is obtained by subtracting the fossil-track density from the combined track density. A variation of this method is to split the sample and do a population type of procedure (see preceding discussion for apatite), except to omit the annealing prior to irradiation. Annealing of glass can alter its properties, which could change the etching characteristic of the glass. This probably would cause a spurious age. This procedure is used for glass because it has a very much lower etching efficiency than muscovite, which prevents the use of an external detector.

Terrestrial samples as young as 8000 yr (Storzer et al., 1971) and as old as 2.7 x 10^9 yr (Naeser, unpubl. data, 1971), have been dated using fission-track procedures. Generally, fission-track ages of minerals such as apatite, zircon, and sphene from young, Cenozoic, volcanic deposits are concordant with each other and with the K-Ar ages of those deposits (Naeser and McKee, 1970; Naeser, 1971; Izett and Naeser, 1976). Natural glasses are both concordant and discordant (Fleischer and Price, 1964b; Storzer and Wagner, 1969; Storzer, 1970). Tests for annealing should be made before accepting a fission-track age on glass (Storzer and Poupeau, 1973; Storzer and Wagner, 1969). Minerals such as apatite, zircon, and/or sphene dated by fission tracks from plutonic and metamorphic rocks can show discordant ages (Naeser and Dodge, 1969; Wagner, 1968; Wagner and Storzer, 1970, 1975; Naeser and Ross, 1976). These discordant ages are caused by track fading under geologic conditions. Track fading is one of the most useful aspects of fission-track dating.

3. Annealing

In fission-track dating, the term annealing is used for the partial to complete erasure of tracks (Fleischer et al., 1965b). The fading occurs when some of the ions that were displaced during formation of the track diffuse back into the track and heal some of the broken bonds. This diffusion is temperature-dependent. As annealing progresses, the average etchable length of the track becomes progressively shorter until it can no longer be etched and observed in an optical microscope. The annealing process appears to slow the etching rate, and so the etchant takes longer and longer to etch out the track. After a certain amount of annealing, the track has been broken by diffusion so many times that it etches at the same rate as the crystal and therefore cannot be seen.

Annealing (Fleischer et al., 1965b) results largely from heating a sample rather than from pressure. The effect of an elevated temperature is very dependent on time. The same degree of annealing can be obtained by heating a sample to a high temperature for a short time or to a low temperature for a long time. For example, apatite will lose all of its tracks in 1 h at 350°C, whereas it will take over a million years to achieve the same effect if the sample is held at 100°C (Naeser and Faul, 1969). Annealing can prevent the dating of the primary age of a mineral, but it can be helpful in understanding

the thermal history of an area. In some cases, such as that of glass, a sample showing reduced track diameters can be corrected for partial annealing (Storzer and Wagner, 1969; Storzer and Poupeau, 1973) to give the primary cooling age. Fortunately, each mineral species has a characteristic temperature at which annealing takes place. For example, it takes 1 h at 750°C to remove all the tracks in epidote (Naeser et al., 1970), whereas 1 h at 350°C is sufficient to remove the tracks in apatite (Naeser and Faul, 1969). Fleischer et al. (1975) have summarized the available annealing data for a number of minerals and glasses. In order to determine the annealing characteristics of a mineral, it is necessary to heat it in the laboratory at known temperatures and times and then determine the reduction of the track density. This laboratory data must then be extrapolated to geologically meaningful times and temperatures. Figure 9 is such an extrapolation. Apatite is one of the few minerals that has been studied to determine its annealing characteristics in more than one laboratory. The results presented by Wagner (1968) and Naeser and Faul (1969) are in good agreement for apatite.

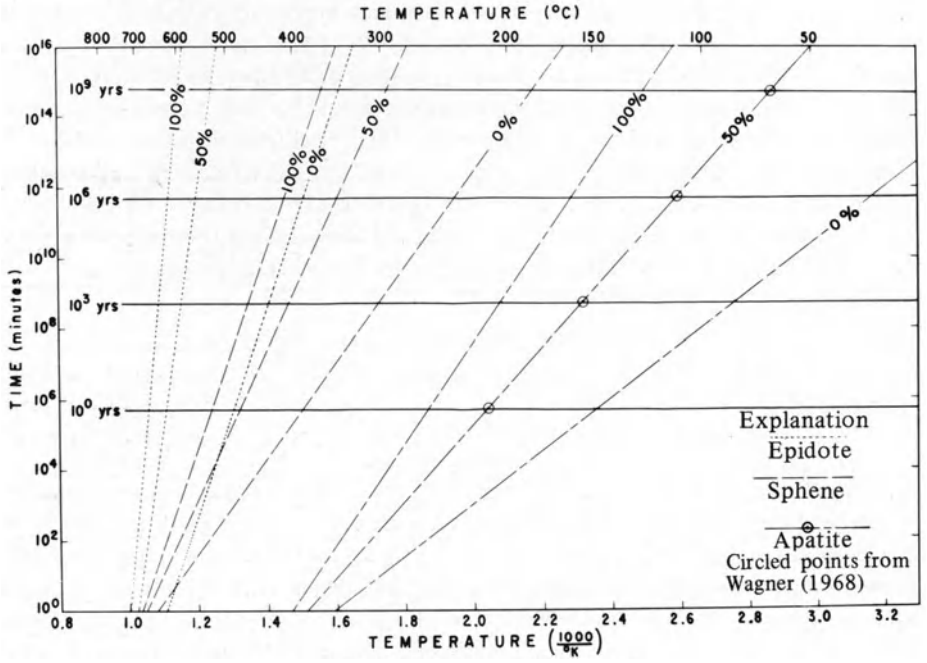

Fig. 9. Extrapolated annealing data for fission tracks in epidote, sphene, and apatite

Using extrapolated annealing data such as shown in Figure 9, it is possible to reconstruct the thermal history of a rock by dating various minerals present in the rock. For example, consider the mineral pair apatite and sphene. If they have the same age, it indicates that the rock has cooled very rapidly from temperatures in excess of 500°C to temperatures less than 100°C within a short period of time. If the apatite is younger than the sphene, there was either: (1) a very slow cooling of the rock, as in cooling

following a regional metamorphic event, or (2) a younger thermal event that caused the apatite to lose some or all of its tracks.

Figure 10 illustrates how a younger thermal event can cause a resetting of one or both minerals. Apatite and sphene present a granitic pluton in California, intruded by a younger basalt, were dated by the fission-track technique (Calk and Naeser, 1973). Within a few meters of the contact, both the apatite and sphene in this granite were reset to the age of the intrusive basalt; at distances of a kilometer or more, the two minerals are concordant with the age of the primary intrusion; but, in between, the ages are discordant.

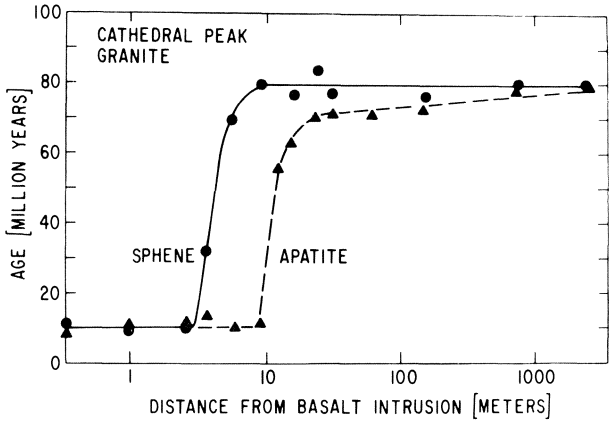

Fig. 10. Fission-track ages of sphene and apatite in a quartz monzonite as a function of distance from a basalt intrusion (Calk and Naeser, 1973)

Until recently, annealing data for track fading in minerals were acquired under laboratory conditions. The laboratory data were extrapolated to geologically reasonable times and temperatures. Samples from two holes in the crust have recently been used to study the effect of increased temperature with depth on the K-Ar and fission-track age systems in minerals recovered from cores (Turner and Forbes, 1976; Naeser and Forbes, 1976). One hole penetrated almost 3000 m of a Mesozoic metamorphic complex near Eielson Air Force Base, Alaska. The bottom-hole temperature in the Eielson, Alaska, deep test hole was 96°C. The second deep drill hole is in New Mexico, where a geothermal test hole was drilled on the western flank of the Valles caldera, a Pleistocene volcanic center. The hole is about 2900 m deep and the bottom-hole temperature is 197°C. The lower 2200 m of this hole was drilled in a Precambrian igneous and metamorphic complex. By dating the various minerals present in core recovered from these holes, it is possible to get a better understanding of how fission-track age systems behave under long-term geologic heating and how these ages compare to ages determined by other dating methods.

Twenty apatite concentrates and one zircon concentrate have been dated from the Eielson deep hole and its related exploratory holes. The fission-track ages of these minerals are shown in Figure 11, along with the K-Ar trends for biotite and hornblende. The fission-track ages for the apatite range from about 100 m.y. near the surface to about 14 m.y. at the bottom of the hole. Only one zircon concentrate was obtained,

and it had an age that is older than the coexisting apatite and younger than the K-Ar age of the biotite from the same depth. The apatite data show a large scatter, because these apatites contain less than 0.5 ppm U; fossil-track counts are therefore very low, resulting in a high analytical uncertainty for the apatite ages. If the apatite data are extrapolated to a depth at which apatite would give a zero age, the temperature at that depth would be about 105°C. This is a region where Mesozoic metamorphism has been followed by a period of slow uplift. This apatite at the bottom of the hole has therefore been at a temperature of greater than 100°C for at least 100 m.y.

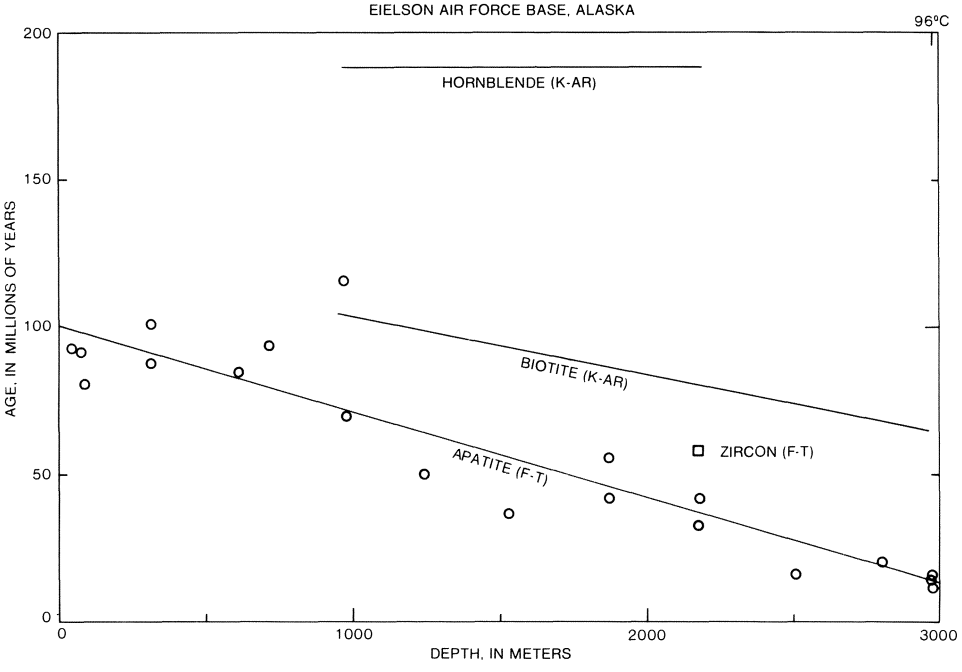

Fig. 11. Fission-track ages of apatite and zircon in the Eielson Air Force Base, Alaska, deep drill hole

A second example of long-term natural annealing is shown in Figures 12 and 13. Figure 12 shows the ages of apatite in the Precambrian rocks intersected in the Los Alamos Scientific Laboratories geothermal test wells 1 and 2. The apatite has a zero apparent age at a temperature of about 135°C. Figure 13 shows both the sphene and apatite fission-track age data. The sphene does not show any age reduction until temperatures are in excess of 177°C. The rocks in this hole have been heated only very recently (within a few million years). From the above two studies, geologic evidence that supports the laboratory data is available of the time-temperature dependency for annealing. A slow-cooling regional metamorphic complex gives a zero age at about 105°C, whereas a recent thermal pulse, on the order of 1 m.y. ago, requires the higher temperature of 135°C for complete annealing of the apatite.

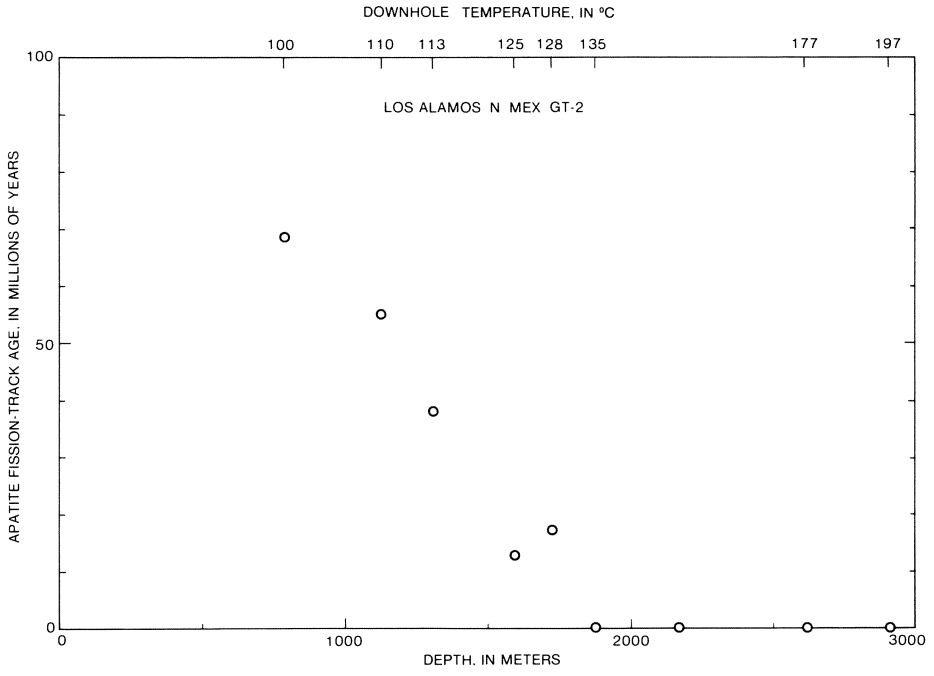

Fig. 12. Fission-track ages of apatite in the Los Alamos, New Mexico deep drill holes GT-1, GT-2

The extrapolated laboratory annealing data, shown in Figure 9 for apatite, are within about 30°C of the values determined in the deep holes. Although the apatite data are in good agreement with the laboratory results, the sphene data are not. The laboratory data suggest that a temperature of about 250°C for a million years would be necessary to begin annealing in sphene. This is over 50°C higher than the temperature observed in the Los Alamos geothermal hole.

This natural data for the apparent zero age of apatite can be used to help understand the tectonic history of a region. Figure 14 shows the age of apatite on Mt. Evans (4346 m), just west of Denver, Colorado, as a function of elevation. Mt. Evans is made up of Precambrian igneous and metamorphic rocks. Apatite below 3000 m reflects the rapid uplift of the Rocky Mountains during the Laramide orogeny starting about 65 m.y. ago. The apatite above 3000 m was only partially annealed during the Cretaceous burial prior to the uplift.

Prior to the Laramide uplift in latest Cretaceous time there was about 3000 m of upper Paleozoic and Mesozoic sedimentary rocks over the Front Range of Colorado (Tweto, 1975). The following quote from Tweto (1975, p. 1) is based on the geologic record of the basins surrounding the Front Range, and is instructive as to the timing of the Laramide uplift.

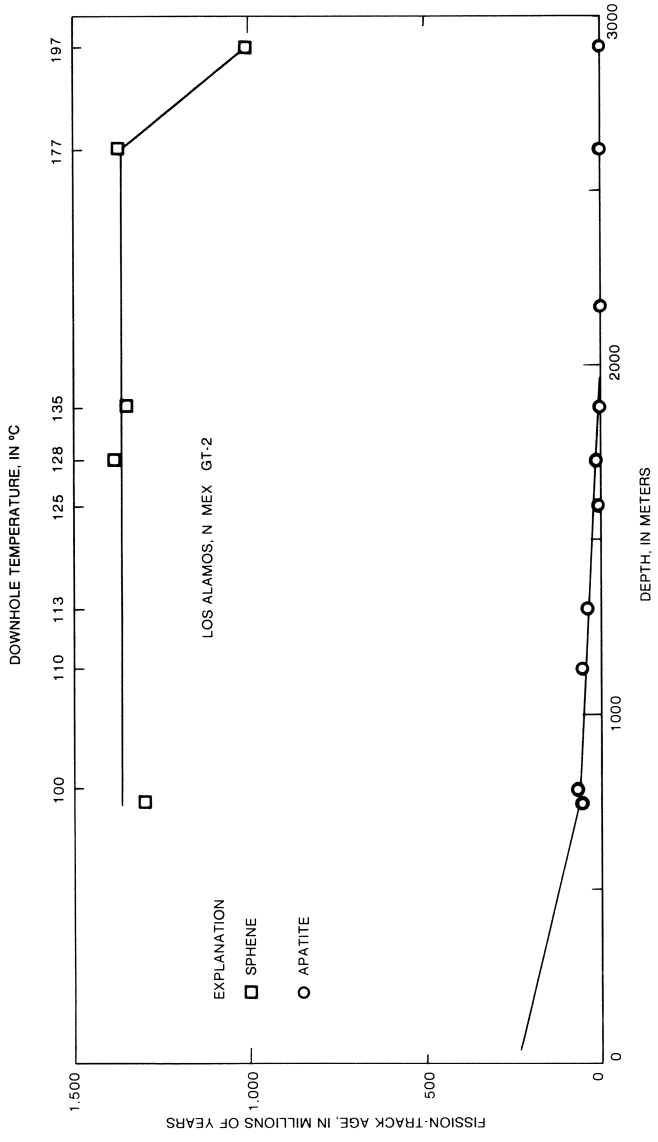

Fig. 13. Fission track ages of apatite and sphene in the Los Alamos, New Mexico, deep drill holes GT-1, GT-2

"The Front, Park-Sierra Madre, and Medicine Bow Ranges on this site of the late Paleozoic Front Range Highland, rose after the marine Fox Hill Sandstone was deposited over their sites 67.5 m.y. ago. Uplift and erosion were rapid. By 66 to 65 m.y., and before the close of Cretaceous time, 3,000 meters of sedimentary rocks had been eroded from at least parts of these ranges, and streams were carrying detritus from Precambrian rock to bordering basins".

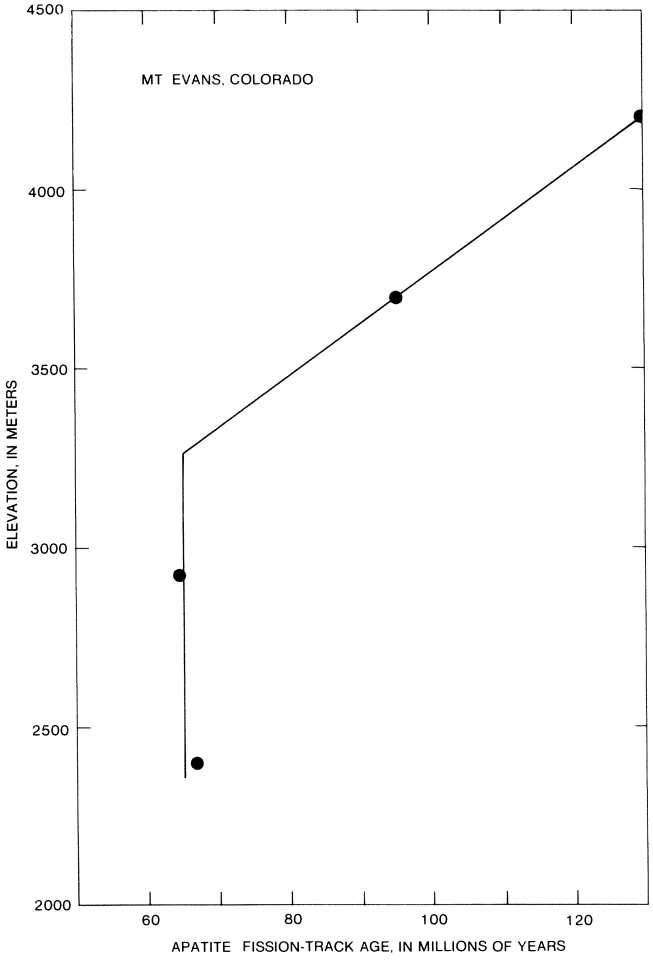

Fig. 14. Fission track ages of apatite in the Precambrian rocks exposed on Mt. Evans, Colorado

The inflection point at about 3000 m represents the position of the 105°C isotherm (based on the Eielson data) prior to the Laramide uplift. The present geotherm in the Front Range is 29°C/km (Roy et al., 1968). If the gradient was the same in Cretaceous time, the point which is now 3.3 km above sea level was about 3 km below sea level 66 m.y. ago. Thus the total uplift since latest Cretaceous time has been about 6 km. Wagner and Reimer (1972) have presented similar data for apatites in the Swiss Alps.

4. Conclusions

Fission-track dating has a wide variety of uses for the geologist. For volcanic and shallow-level plutonic rocks, it can identify the time of extrusion or emplacement. In areas having a more complex hisotry, it can help to work out the post-emplacement history. Apatite

can be very useful in studying the tectonic patterns and history of an area, because it records the last time the rock cooled below about 100°C.

Acknowledgments. I wish to thank Glen Izett and John Obradovich (U.S. Geological Survey, Denver) for their constructive comments of an earlier version of this paper.

The data on the deep drill holes are part of a larger study being done in conjunction with Robert Forbes and Donald Turner of the University of Alaska. This research was funded in part by a grant from ERDA to the University of Alaska. William Laughlin of the Los Alamos Scientific Laboratory kindly provided samples of the Los Alamos deep drill core. The Mt. Evans data are part of a larger study being done with Bruce Bryant (U.S. Geological Survey, Denver) on apatite ages in the Front Range of Colorado.

References

Calk, L.C., Naeser, C.W.: The thermal effect of a basalt intrusion on fission tracks in quartz monzonite. J. Geol. *81*, 189-198 (1973)

Fleischer, R.L., Price, P.B.: Charged particle tracks in glass. J. Appl. Phys. *34*, 2903-2904 (1963)

Fleischer, R.L., Price, P.B.: Decay constant for spontaneous fission of ^{238}U. Phys. Rev. *133*, 1363-1364 (1964a)

Fleischer, R.L., Price, P.B.: Glass dating by fission fragment tracks. J. Geophys. Res. *69*, 331-339 (1964b)

Fleischer, R.L., Price, P.B., Walker, R.M.: Fission track ages of zircons. J. Geophys. Res. *69*, 4885-4888 (1964)

Fleischer, R.L., Price, P.B., Walker, R.M.: The ion explosion spike mechanism for formation of charged particle tracks in solids. J. Appl. Phys. *36*, 3645-3652 (1965a)

Fleischer, R.L., Price, R.B., Walker, R.M.: Effects of temperature, pressure, and ionization of the formation and stability of fission tracks in minerals and glasses. J. Geophys. Res. *70*, 1497-1502 (1965b)

Fleischer, R.L., Price, P.B., Walker, R.M.: Nuclear Tracks in Solids. Principles and applications. Berkeley: Univ. of Calif. Press 1975, 605 pp.

Izett, G.A., Naeser, C.W.: Age of the Bishop Tuff of eastern California as determined by the fission-track method. Geology *4*, 587-590 (1976)

Naeser, C.W.: The use of apatite and sphene for fission track age determinations. Bull. Geol. Soc. Am. *78*, 1523-1526 (1967)

Naeser, C.W.: Geochronology of the Navajo-Hopi Diatremes, Four Corners area. J. Geophys. Res. *76*, 4978-4985 (1971)

Naeser, C.W., Dodge, F.C.W.: Fission-track ages of accessory minerals from granitic rocks of the central Sierra Nevada Batholith, California. Bull. Geol. Soc. Am. *80*, 2201-2212 (1969)

Naeser, C.W., Engles, J.G., Dodge, F.C.W.: Fission-track annealing and age determination of epidote minerals. J. Geophys. Res. *75*, 1579-1584 (1970)

Naeser, C.W., Faul, H.: Fission track annealing in apatite and sphene: J. Geophys. Res. *74*, 705-710 (1969)

Naeser, C.W., Forbes, R.B.: Variation of fission-track ages with depth in two deep drill holes. EΦS, Trans. Am. Geophys. Union *57*, 353 (1976)

Naeser, C.W., McKee, E.H.: Fission-track and K-Ar ages of Tertiary ash-flow tuffs, north-central Nevada. Bull. Geol. Soc. Am. *81*, 3375-3384 (1970)

Naeser, C.W., Ross, D.C.: Fission-track ages of sphene and apatite of granitic rocks of the Salinion Block, Coast Ranges, California. J. Res. U.S. Geol. Surv. *4*, 415-420 (1976)
Price, P.B., Walker, R.M.: Chemical etching of charged particle tracks. J. Appl. Phys. *33*, 3407-3412 (1962)
Price, P.B., Walker, R.M.: Fossil tracks of charged particles in gneiss and the age of minerals. J. Geophys. Res. *68*, 4847-4862 (1963)
Roberts, J.H., Gold, R., Armani, R.J.: Spontaneous fission decay constant of ^{238}U. Phys. Rev. *174*, 1482-1484 (1968)
Roy, R.F., Decker, E.R., Blackwell, D.D., Birch, Francis: Heat flow in the United States. J. Geophys. Res. *73*, 5207-5222 (1968)
Silk, E.C.H., Barnes, R.S.: Examination of fission fragment tracks with an electron microscope. Philos. Mag. *4*, 970-971 (1959)
Spadavecchia, A., Hahn, B.: Die Rotationskammer und einige Anwendungen. Heav. Phys. Acta *40*, 1063-1079 (1967)
Storzer, D.: Fission track dating of volcanic glasses and the thermal history of rocks. Earth Planet. Sci. Lett. *8*, 55-60 (1970)
Storzer, D., Horn, P., Kleinmann, B.: The age and the origin of Köfels structure, Austria. Earth Planet. Sci. Lett. *12*, 238-244 (1971)
Storzer, D., Poupeau, G.: Ages-plateaus de mineralix et verres par la methode des traces de fission. C.R. Acad. Sc. Paris *276*, Series D, 137-139 (1973)
Storzer, D., Wagner, G.A.: Correction of thermally lowered fission-track ages of tektites. Earth Planet. Sci. Lett. *5*, 463-468 (1969)
Turner, D.L., Forbes, R.B.: K-Ar studies in two deep basement drill holes: a new geologic estimate of argon blocking temperature for biotite. EΦS, Trans. Am. Geophys. Union *57*, 353 (1976)
Tweto, Odgen: Laramide (Late Cretaceous-Early Tertiary) Orogeny in the southern Rocky Mountains. Geol. Soc. Am. Mem. *144*, 1-44 (1975)
Wagner, G.A.: Fission-track dating of apatites. Earth Planet. Sci. Lett. *4*, 411-415 (1968)
Wagner, G.A., Reimer, G.M.: Fission-track tectonics: the tectonic interpretation of fission track apatite ages. Earth Planet. Sci. Lett. *14*, 263-268 (1972)
Wagner, G.A., Reimer, G.M., Carpenter, D.S., Faul, H., Van der Linden, R., Gijbels, R.: The spontaneous fission rate of V-238 and fission track dating. Geochim. Cosmochim. Acta *39*, 1279-1286 (1975)
Wagner, G.A., Storzer, D.: Die Interpretation von Spaltspurenaltern (Fission track ages) am Beispiel von natürlichen Glasen, Apatiten und Zirkonen. Eclogae Geol. Helv. *63*, 335-344 (1970)
Wagner, G.A., Storzer, D.: Spaltspuren und ihre Bedeutung für die thermische Geschichte des Odenwaldes. Aufschluß *27*, 79-85 (1975)
Young, D.A.: Etching of radiation damage in lithium fluoride. Nature (London) *182*, 375-377 (1958)

Correction and Interpretation of Fission Track Ages

G. A. WAGNER

In its early stages, fission track dating was often underrated and regarded as an unreliable age determination method since its data frequently turned out as younger than independently determined ages on the same samples. Obviously, the prerequisite that all fission tracks must be retained since the formation of the sample was not met. It is now known that track retention is a very temperature-sensitive and characteristic property of minerals and natural glasses. The understanding of track retention is the key for the proper interpretation of fission track ages.

Various parameters, such as heat, pressure, hydrous solutions, and ionizing radiation, acting for sufficiently long time on a sample, can erase the latent fission tracks (Fleischer et al., 1965a; Lakatos and Miller, 1972; Burchardt and Reimer, 1972). It seems that heat has the most important influence on the instability of tracks.

Thermal track fading of various materials which are of interest in fission track dating were investigated in laboratory experiments (for compilation of data see articles by Fleischer and Hart, 1972; Wagner, 1972, 1978; Fleischer et al., 1975). In a typical track fading experiment, the sample is first heated sufficiently to remove all fossil tracks. Then, the sample is irradiated with thermal neutrons in order to induce fresh fission tracks. The sample is then divided into many pieces which are annealed at various temperatures for various durations. After that, the pieces are etched (using precisely the same etching conditions) and the fission tracks are studied.

The results of numerous track fading experiments can be summarized as follows: firstly, with increasing annealing duration and annealing temperature the track density decreases in a characteristic way. This is shown in Figure 1, with a logarithmic scale for annealing duration and a reciprocal scale for annealing temperature ("Arrhenius plot"). All points with identical track density reduction lie on a straight line in such a diagram, resulting in typical "track retention fans". Secondly, the fission tracks do not disappear abruptly when the temperature is increased. The fading process is gradual. As becomes clear from Figure 1, there exists a transitional zone of partial track fading before complete track loss sets in. Thirdly, different materials have different retention properties. For instance, fission tracks are more stable in zircon than in apatite, and are more stable in acidic natural glasses than in basic ones. Fourthly, running parallel with the track density reduction during the fading process there is also a track size reduction, i.e., partially annealed tracks are smaller than unannealed tracks (after etching under the same conditions). There exists a relationship between track density and track size (Fig. 2) for the various materials. Therefore, by track size studies it is possible to determine from curves such as in Figure 2 ("correction curves") the degree of track fading and calculate the pre-annealing track density.

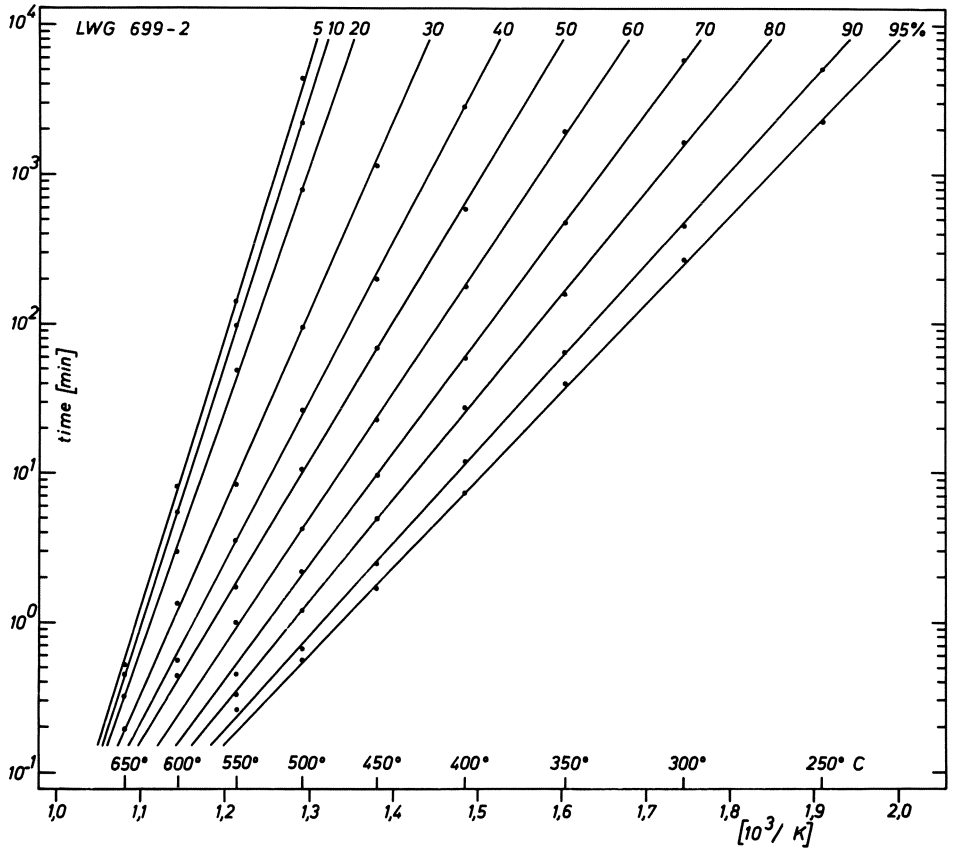

Fig. 1. Arrhenius plot of fission track annealing experiments with Libyan Desert Glass. The *straight lines* of the "track retention fan" represent the different percentages of fission track density left over after various degrees of annealing (etching time: 120 s in 48% hydroflouric acid at 23°C)

For this discussion of age interpretation let us consider a mineral (or rock) which forms at a given time and at a temperature above that of fission track retention. Subsequently the mineral cools through the different temperature zones of fission track instability, partial stability and full stability (Fig. 3). The fission track accumulation in this mineral and the resulting fission track age would be cruicially dependent upon the particular thermal history. Three basic models of thermal history are discussed: fast-cooling model (A), slow-cooling model (B), and complex-cooling model (C).

1. Fast-Cooling Model (A)

In this model low temperatures are reached soon after mineral (or rock) formation causing track stability to occur early. The fission track age its practically that of the

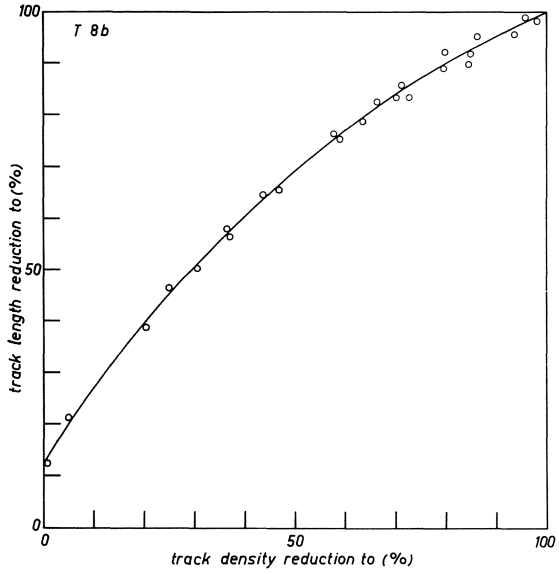

Fig. 2. The mean length reduction of etched (15 s in 65% nitric acid at room temperature) fission track channels in apatite depends in a characteristic manner on the reduction of track density after various degrees of partial track fading. The track lengths were measured as they appear projected on the (0001) face (oil immersion)

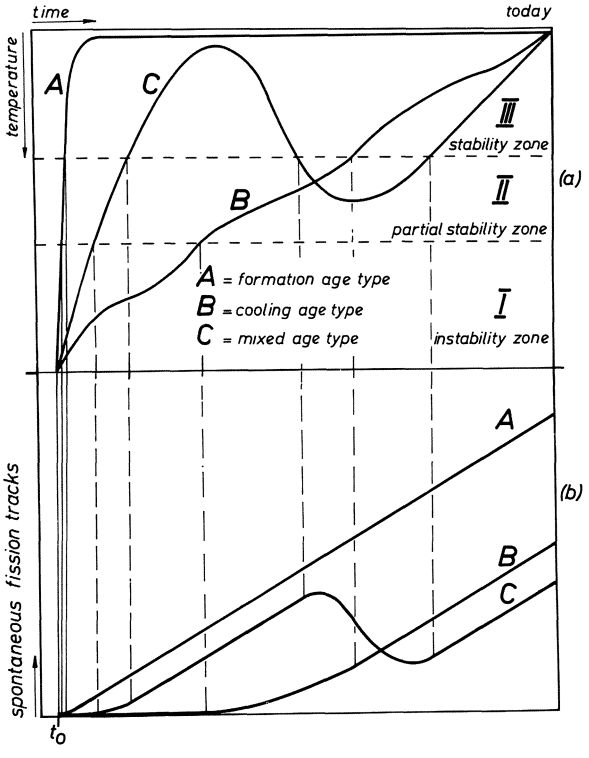

sample formation. When co-existing minerals are dated, concordant ages are found. The fast-cooling model is characteristic of volcanic rocks. There are many examples of dating the formation of volcanic glasses and minerals with fission tracks, for instance pumice from the Olduvai Gorge (Fleischer et al., 1965b), obsidian from Italy (Bigazzi et al., 1971), sphene, zircon, and apatite from tertiary ash-flow tuffs (Naeser and McKee, 1970), glass shards from submarine tephra horizons (Seward, 1974), and basaltic glasses dredged from the Mid-Atlantic ridge (Storzer and Selo, 1976). Similar to volcanic rocks, tektites (Fleischer and Price, 1964; Gentner et al., 1969), and impact craters (Storzer and Wagner, 1977) are successfully dated with the fission track method. Actually, the fission track dating of volcanic rocks and impactites is not as straight-forward as it might seem, since nearly all glasses and many apatites show some fossil track fading. Both materials have relatively low fission track retentivities, thus, the ambient temperatures may be high enough to cause partial track fading. This necessitates a correction for track fading (see below). So far no fossil track fading has been observed in volcanic zircons and sphenes.

2. Slow-Cooling Model (B)

In this model, the fission tracks become stable long after mineral formation. The fission track age dates a moment of cooling to a temperature somewhere within the zone of partial track stability. It is a "cooling age". When co-existing minerals are dated, discordant ages are found. Due to different fission track retentivity of each mineral the time since cooling to different temperatures is measured. The explicit temperatures ("blocking" temperatures) to which the rocks have cooled at the time given by the fission track age can be inferred from annealing experiments (Wagner, 1968) or directly from age data on deep drill cores (Naeser, this vol.). Reasonable assumptions on the cooling rate have to be made for the estimation of the "blocking" temperatures. The values of the "blocking" temperatures depend also somewhat on the etching conditions (for instance, fission tracks in sphene have apparently a higher retentivity when revealed with NaOH-etch instead of HCl-etch; Calk and Naeser, 1973). The slow-cooling model is typical for plutonic and metamorphic (post-metamorphic cooling) rocks. For the co-existing mineral pair sphene and apatite, commonly, higher fission track ages are found for sphene (Naeser and Dodge, 1969; Wagner, 1976). For the pair epidote and apatite from the Central Alps, consistently higher fission track ages were reported for epidote (Reimer and Wagner, 1971). Such data provide the ability to deduce the cooling history of rocks, especially when combined with other radiometric age results. The use of apatite is of special interest in studying the thermal history of rocks. Due to its sensitive fission track retentivity it dates the cooling to low temperatures (around 110°C). When cooling is caused by uplift and erosion, uplift rates can

◀ **Fig. 3.** Three hypothetical cooling models (fast-cooling *A*, slow-cooling *B*, complex-cooling *C*) and their consequence for fission track age interpretation (**a**). In the temperature *zone I* there is no track record, in the *zone II* there is partial track fading and record, and in the *Zone III* there is complete track record (**b**)

be determined from fission track ages. In the Central Alps an increase of apatite fission track ages with increasing topographic elevation was observed (Wagner and Reimer, 1972; Wagner et al., 1977) from which uplift rates between 0.2 and 1.1 mm/year were calculated.

3. Complex-Cooling Model (C)

The mineral or rock cools down first to temperatures within the track stability zone as in models (A) or (B). Later it suffers thermal overprinting with temperatures reaching the partial track stability zone. Due to this partial track fading the measured fission track age would be a "mixed age" which does not date a significant geologic event. However, by track size studies (see below) it is possible to determine the age of the overprinting event, as was first demonstrated by Storzer (1970) for Permian pitchstone from the Bozner Quarzporphyr. If the temperature during thermal overheating reaches the zone III of complete track loss with subsequent slow cooling, the fission track age would date the post-metamorphic cooling [see model (B)].

Complex cooling histories may be caused by igneous intrusive heating, metamorphism and tectonic subsidence. Calk and Naeser (1973) studied the effect of a later basaltic intrusion on track fading in sphene and apatite from the granitic country rock. Since partial track fading can occur at temperatures far below those of metamorphic reactions, low temperature phases can be detected by fission track dating, especially by using apatite (Kelly and Wagner, 1977). Occasionally different cooling models are obtained for co-existing minerals with different track retentivity. This is the case for sphene and apatite from the crystalline Odenwald basement. Hercynian fission track ages were found for sphene, whereas the apatite fission track clock was completely reset during the Mesozoic subsidence of the basement (Wagner and Storzer, 1975).

For the interpretation of fission track ages, it is very important to recognize which of the cooling models occurred. One way of achieving this is to take into account all independent geologic information. Also additional radiometric age data are very helpful. Fortunately, fission track studies themselves contribute to this problem, namely by analyzing the track sizes. In this way it is possible to establish for a given fission track population which fraction of it suffered partial fading and which fraction accumulated after the last fading event. Geologically meaningful ages can be calculated from each sub-population of fission tracks (Storzer, 1970). For model (A), the fossil fission tracks have virtually the same size distribution as induced fission tracks. For model (B), the fossil fission track population contains comparatively more small tracks than the induced tracks (Fig. 4). For model (C) there is a characteristic bimodal size distribution of fossil tracks.

In all cases where partially faded fission tracks are recognized, a correction for the fading process can be applied. In this way, fission track ages lowered by thermal fading can be corrected. Currently, there are two age correction techniques: the "track size" and the "plateau" techniques.

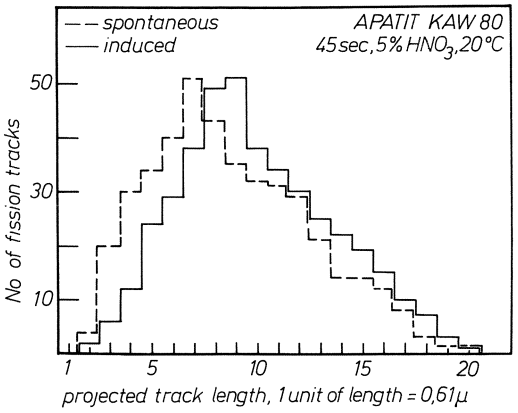

Fig. 4. Distribution histogram of fission track lengths in an apatite from the Alps. Clearly, the spontaneous fission track population contains more smaller tracks than the induced ones. This is due to partial track fading as the apatite cooled slowly through the zone of partial track stability

Track Size Correction Technique. This technique uses the smaller size of partially faded tracks compared to freshly induced tracks (Storzer and Wagner, 1969). From the degree of track size reduction, the original, pre-fading track density can be recalculated by using the experimentally established correlation between track density and track size reduction due to partial fading ("correction curves," Fig. 2). This technique is very time-consuming because it necessitates tedious size measurements and correction curves should be established for each sample. This correction technique has been applied to tektites (Storzer and Wagner, 1969; Durrani and Khan, 1970), volcanic glasses (Storzer, 1970; Suzuki, 1973) and apatite (Wagner and Storzer, 1969).

Plateau Correction Technique. This technique uses the higher thermal stability of partially faded tracks compared to fresh, induced tracks (Storzer and Poupeau, 1973). In the laboratory fossil and induced tracks are annealed together in several steps under controlled conditions. The ratio of fossil to induced track density is plotted as a function of the temperature of continued annealing. For a sample with partial loss of fossil tracks, the ratio increases and reaches finally a plateau value. The age calculated from this value is corrected for the original, partial track loss. With this technique, fission track ages of tektites, obsidians, and apatites were corrected.

When both correction techniques are carefully applied to the same objects, concordant age results are found. This has been demonstrated for obsidian (Wagner et al., 1976), tektites and crater glasses (Storzer and Wagner, 1977), and apatite from the Katzenbuckel volcano (70 m.y.). For the interpretation of the corrected fission track ages it must be kept in mind that only the partial track fading is corrected. Therefore the corrected fission track age dates the time when the sample crossed last from the temperature zone of track instability to partial track stability. This may be, again, either a formation age or a cooling age. For example, a corrected age in

model (B) is still a cooling age, but it is related to higher temperatures than the uncorrected age.

In conclusion, although fission track dating may seem rather easy at first glance, its instrumental simplicity should not be allowed to cause a superficial age interpretation. When applied thoughtfully, fission track dating reveals the age of mineral and rock formations and it can decipher the thermal history of rocks. This is probably its greatest potential.

References

Bigazzi, S.G., Bonadonna, F.P., Belluomini, G., Malpieri, L.: Studi sulle ossidiane italiane. IV. Datazione con il metode delle trace difissione. Boll. Soc. Geol. It. *90*, 469-480 (1971)

Burchart, J., Reimer, G.M.: Effect of ionic solutions on fission track stability in apatite. Trans. Am. Nucl. Soc. *15*, 129-130 (1972)

Calk, L.C., Naeser, C.W.: The thermal effect of a basalt intrusion on fission tracks in quartz monzonite. J. Geol. *81*, 189-198 (1973)

Durrani, S.A., Khan, H.A.: Annealing of fission tracks in tektites: corrected ages of bediasites. Earth Planet. Sci. Lett. *9*, 431-445 (1970)

Fleischer, R.L., Hart, H.R., jr.: Fission track dating: techniques and problems. Proceedings Burg Wartenstein Conference on Calibration of Hominoid Evolution. Bishop, W.W., Miller, D.A., Cole, S. (eds.). Edinburgh: Scottish Acadmic Press, 1972, pp. 135-170

Fleischer, R.L., Price, P.B.: Fission track evidence for the simultaneous origin of tektites and other natural glasses. Geochim. Cosmochim. Acta *28*, 755-760 (1964)

Fleischer, R.L., Price, P.B., Walker, R.M.: Effects of temperature, pressure and ionization on the formation and stability of fission tracks in minerals and glasses. J. Geophys. Res. *70*, 1497-1502 (1965a)

Fleischer, R.L., Price, P.B., Walker, R.M., Leakey, L.S.B.: Fission track dating of Bed I, Olduvai Gorge. Science *148*, 72-74 (1965b)

Fleischer, R.L., Price, P.B., Walker, R.M.: Nuclear Tracks in Solids. Berkeley: Univ. of Calif. Press, 1975c

Gentner, W., Storzer, D., Wagner, G.A.: New fission track ages of tektites and related glasses. Geochim. Cosmochim. Acta *33*, 1075-1081 (1969)

Kelly, W.C., Wagner, G.A.: Paleothermometry by combined application of fluid inclusion and fission track methods. N.Jb. Min. Mh., Jg. 1977, 1-15 (1977)

Lakatos, S., Miller, D.S.: Evidence for the effect of water content on fission track annealing in volcanic glass. Earth Planet. Sci. Lett. *14*, 128-130 (1972)

Naeser, C.W., Dodge, F.C.W.: Fission track ages of accessory minerals from granitic rocks of the Central Sierra Nevada batholith, California. Bull. Geol. Soc. Am. *80*, 2201-2212 (1969)

Naeser, C.W., McKee, E.H.: Fission track and K-Ar-ages of Tertiary ash-flow tuffs, North-Central Nevada. Bull. Geol. Soc. Am. *81*, 3375-3384 (1970)

Reimer, M., Wagner, G.A.: Fission track studies of Alpine epidots and garnets. Ann. Soc. Geol. Belg. *94*, 127 (1972)

Seward, D.: Age of New Zealand Pleistocene substages by fission track dating of glass shards from tephra horizons. Earth Planet. Sci. Lett. *24*, 242-248 (1974)

Storzer, D.: Fission track dating of volcanic glasses and the thermal history of rocks. Earth Planet. Sci. Lett. *8*, 55-60 (1970)

Storzer, D., Poupeau, G.: Ages-plateaux de minereaux et verres par la methode des traces de fission. C.R. Acad. Sci. Paris *276*, Serie D, 137-139 (1973)
Storzer, D., Selo, M.: Uranium content and fission track ages of some basalts from the FAMOUS area. Bull. Soc. Geol. France *18*, 807-810 (1976)
Storzer, D., Wagner, G.A.: Correction of thermally lowered fission track ages of tektites. Earth Planet. Sci. Lett. *5*, 463-468 (1969)
Storzer, D., Wagner, G.A.: Fission track dating of meteorite impacts. Meteoritics *12/3* (1977)
Suzuki, M.: Chronology of prehistoric human activity in Kanto, Japan. Part I – Frame for reconstructing human activity in obsidian. J. Fac. Sci. Univ. of Tokyo, Sec. V, *IV*, 241-318 (1973)
Wagner, G.A.: Fission track dating of apatites. Earth Planet. Sci. Lett. *4*, 411-415 (1968)
Wagner, G.A.: Spaltspurenalter von Mineralen und Gesteinen: eine Übersicht. Fortschr. Min. *49*, 114-145 (1972)
Wagner, G.A.: Spaltspurendatierung an Apatit und Titanit aus den Subvulkaniten des Kaiserstuhls. N.Jb. Min. Mh., Jg. 1976, 389-393 (1976)
Wagner, G.A.: Archaeological Applications of fission track dating. Nuclear Track Detection *2*, 51-64 (1978)
Wagner, G.A., Reimer, G.M.: Fission track tectonics: The tectonic interpretation of fission track apatite ages. Earth Planet. Sci. Lett. *14*, 263-268 (1972)
Wagner, G.A., Reimer, G.M., Jäger, E.: Cooling ages derived by apatite fission track, mica Rb-Sr and K-Ar dating: The uplift and cooling history of the Central Alps. Memoir. Istit. Geol. Min. Univ. Padova *30*, 1-27 (1977)
Wagner, G.A., Storzer, D.: Interpretation von Spaltspurenaltern am Beispiel von natürlichen Gläsern, Apatiten und Zirkonen. Eclogae Geol. Helv. *63/1*, 335-344 (1970)
Wagner, G.A., Storzer, D.: Spaltspuren und ihre Bedeutung für die thermische Geschichte des Odenwaldes. Aufschluß, Sonderband *27*, 79-85 (1975)
Wagner, G.A., Storzer, D., Keller, J.: Spaltspurendatierung quartärer Gesteinsgläser aus dem Mittelmeerraum. N. Jb. Min. Mh., Jg. 1976, 84-94 (1976)

Archaeometric Dating

G. A. WAGNER

Archaeology has been much affected by the application and development of new techniques adapted from the physical, chemical, biological, and earth sciences during the past two decades. The new techniques include chemical and isotopic analyses, age determination, prospecting, and others. The term "archaeometry" has been coined for this new discipline.

1. Summary of Physical and Chemical Dating Methods

The aim of this lecture is to give a brief introduction to the physical and chemical dating techniques currently employed in archaeology. Table 1 gives a summary of these techniques. Although other geologic and biologic dating methods, such as stratigraphy, varve chronology, pollen analysis, and dendrochronology in a wider sense belong also to archaeometry, they are not included here.

Among the archaeometric clocks, the most important are those which are based on *radioactivity*. These clocks are independent and, in principle, do not need calibration, since the rates of radioactive decay are known and constant. Strictly, the latter statement must be somewhat qualified, at least for the radiocarbon method. The original assumption that the radiocarbon content in the atmosphere and the biosphere has not changed during the past, has turned out to be wrong due to variations in cosmic ray intensity. Therefore, extensive tree ring calibrations on radiocarbon dates have been carried out lately. Currently, the radiocarbon method is routinely employed in numerous archaeological laboratories all over the world.

The K-Ar method is rarely used in archaeometry, since it cannot be applied to samples in the age range much below 10^5 years, which is commonly of archaeological interest. A well-known example of its use is the dating of basalt from the Olduvai Gorge by Curtis and Evernden with the early hominid remains.

The less well-known methods of thermoluminescence and fission track dating, both based on radiation damage effects by nuclear radiation, are discussed in more detail in the following chapters.

The uranium-series dating methods are based on the disturbance of radioactive equilibrium among the daughter products of uranium. The Th-230/U-234 and Pa-231/U-235 ratios are mainly used for the dating of paleolithic calcareous cave deposits. The Pb-210/Ra-226 ratio is applied to assess the authenticity of paintings which contain lead pigments.

Table 1. Physical and chemical methods of archaeometric dating

Method	Age range	Dated event	Important materials
Potassium-Argon (K-Ar)	$\geqslant 10^5$ a	Rock and mineral formation or last heating	Volcanic ash falls and lava flows, feldspar, biotite
Fission-Track (FT)	$\geqslant 10^3$ a	Rock and mineral formation or last heating	Natural glass (obsidian, pumice), artificial glass, zircon, sphene, apatite
Thermoluminescence (TL)	$\geqslant 10^2$ a	Last heating	Ceramics (pottery, bricks) heated rocks (flint, sandstone) slags
Uranium series			
Th-230	$\leqslant 3 \times 10^5$ a	Calc. carbonate formation	Corals, bones, travertine, stalagmites
Pb-210	$\leqslant 200$ a	Lead smelting	Lead white pigment
Radiocarbon (C-14)	$\leqslant 5 \times 10^4$ a	Death of organism	Wood, charcoal grains, seeds, nuts, peat, ivory, bones, shells
Archaeomagnetism	in principle unlimited	Last heating	Ceramics (bricks, tiles, pottery), baked soils (kilns, fire pits), slags
Hydration	$\leqslant 10^5$ a	Fracturing (artifact fabrication)	Obsidian
Iridescence (weathered glass layer counting)	$\leqslant 2 \times 10^3$ a	Burial in soil	Artificial glass
Fluor-Uranium-Nitrogen-Test (FUN)	for large age differences	Death and subsequent burial	Bones, antler, teeth
Racemization	$\leqslant 10^6$ a	Death and subsequent burial	Bones, teeth, ivory

Archaeomagnetic dating uses the *thermoremanent magnetization* of ceramics, kilns, and burnt soils which accumulates during the cooling process after firing. In this way the intensity and direction of the earth's magnetic field – which varies over the years – is recorded. This method necessitates regional calibration curves of the temporal variations of the magnetic field parameters.

The remaining methods in Table 1 are all based on *chemical reactions:* the diffusion and reaction of soil moisture on the surface of obsidian artifacts (hydration); the layered weathering crust of iridescent artificial glasses (iridescence); the uranium and fluorine increase and organic matter decrease in bones by exchange with the ground-

water (FUN-test); and the racemization of amino acids in bones. The major limitation of these methods is local and temporal variations of the reaction rates. These methods provide the possibility of establishing the age succession of samples from the same physicochemical environment. For explicit age measurements the reaction rates have to be determined by independent dating methods. For details the reader is referred to the literature at the end of this article.

2. Thermoluminescence (TL) Dating

Many attempts have been made to apply TL-dating to geologic materials (McDougall, 1968). However, because of the complexities of the TL phenomenon itself and of difficulties in determining the dose rate the results are problematic. Nevertheless, great progress has been made in the TL dating of ceramics (Aitken, 1974).

Due to its complexities TL dating is far from being a routine method of archaeological dating. However, it has already been successfully used to solve many archaeological dating problems. One of its great advantages is that it can be applied to an archaeological material, namely pottery, on which many prehistoric chronologies are based. Speaking in geologic terms, this is the fortunate situation of dating the "index fossils" directly. Archaeological materials other than ceramics to which TL dating can be applied are glass, bones, shells, burnt soils, and fired rocks. Although in its early stages, the TL dating of heated rocks seems very promising, especially for fired flint and sandstone.

TL is the emission of light which occurs, in addition to the normal incandescent glow, when a material is heated. It does not reappear when the heating is repeated. Although the TL phenomenon is not yet fully understood, in simple terms, it is believed to be radiation emitted as metastable electrons return to their stable position within dielectric solids. The metastable electrons are released from traps through thermal activation. The graph of the TL light output vs. heating temperature is called the glow-curve (Fig. 1). The higher the glow-curve temperature, the deeper are the electron traps which are emptied. Consequently, the TL emitted at high glow-curve temperatures is more resistant to thermal fading.

As an example of TL dating, consider a potsherd buried in soil. To some degree, pottery and soil contain the radioactive elements uranium, thorium (normally a few ppm), and potassium (normally a few percent). Throughout the time of burial the ionizing radiation from the radioactive decay of these elements steadily bombards the potsherd. Due to their limited range, the α- (about 25 μm) and β- (few mm) radiations have their origin in the potsherd itself. The surrounding soil is the primary contributor of the γ-radiation (ca. 30 cm range). The effect of the ionizing radiation on the potsherd is to remove electrons from their parent atoms. Part of these electrons are trapped as metastable electrons, most of them return immediately to their stable position. Thus, the potsherd acts as natural radiation dosimeter and one can read the dosimeter by measuring the TL emitted by the potsherd. The area beneath the NTL-curve in Figure 1 represents the radiation dose the potsherd has received in its past. If, the annual rate of radiation dose is known, the duration of the samples exposure

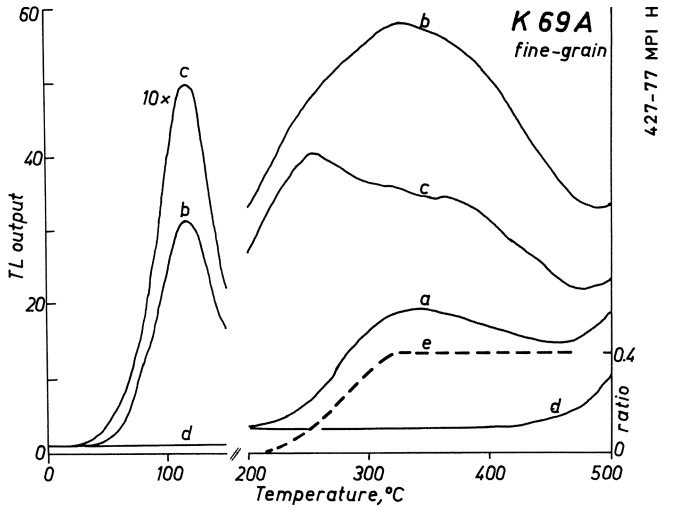

Fig. 1. Thermoluminescence glow-curves of a brick from a Roman villa in Bad Kreuznach: *a*, natural thermoluminescence *(NTL)*. *b*, NTL + TL induced by an artificial β-irradiation with a dose of 1500 rad; *c*, TL induced by artificial β-irradiation (1100 rad) after draining the NTL by heating; *d*, back-ground incandescence. The "plateau test" *(e)* represents the ratio a/(b-a) and indicates the absence of natural fading for the NTL appearing at glow-curve temperatures above 330°C

to the radiation can be determined. The dose rate is calculated from the uranium, thorium, and potassium contents in the potsherd and in the surrounding soil. The TL age is expressed by the general equation

$$\text{Age} = \frac{\text{Archaeological dose}}{\text{Annual dose rate}}$$

Because TL is removed by heating, the TL age represents the time since the last heating above 450°C (the temperature required to remove the TL). For most ceramic materials this is the date of firing.

Although in principle TL dating seems simple, frequently, there are major complications. There may be other causes than radiation for trapped electrons, such as pressure, friction, and light. Also, during the heating of the sample, chemical reactions and phase transitions may emit light. If not avoided, such "spurious" sources of TL would result in ages too high.

Furthermore, the TL may become saturated at low radiation doses. Also, there may occur nonthermal, anomalous fading of TL; the latter two effects would cause too low TL ages. Other sources of erroneous ages are, first the disruptions of the radioactive equilibrium of the uranium and thorium decay series by radon escape, and second, the radiation-shielding effect by varying moisture contents in the pore space of potsherd and soil.

Usually, ceramics consist, mineralogically, of a mixture of fine-grained clay matrix with coarse grains, such as quartz and feldspar. Occasionally, also heavy minerals, such as zircon and apatite, are embedded. In the early stages of TL dating, the pottery was used unseparated. However, in this approach systematic errors appeared because the various mineral phases differ by several orders of magnitude in their TL sensitivity and their radioactive content. For example, consider a quartz grain of 100 μm diameter embedded in the fine-grained matrix. Quartz has a much higher TL sensitivity and a much lower radioactivity content than the clay matrix. Due to the limited range of α-particles (only ca. 25 μm), the interior of the quartz grains is shielded from α-radiation. Consequently, the α-dose rate for the quartz grains, which give a large TL signal, would be overestimated, and the resulting TL age would be too low. Because of such consideration of micro-dosimetry, TL dating is carried out on different size and mineral fractions. There are currently two major dating techniques, the fine-grain and the quartz-inclusion techniques. In the fine-grain technique (Zimmerman, 1971), the size fraction between 1 and 8 μm is separated. The dose rate is composed of the α- and β-contributions of the sherd itself and γ-contribution from the surrounding soil. In the quartz-inclusion technique (Fleming, 1970), the quartz grains of ca. 100 μm are separated. Before measuring the TL, their surface layer, which received the α-radiation is etched away with hydrofluoric acid. The dose rate of the remaining quartz cores is composed only of the β- and γ-contributions. Ideally, both techniques should give concordant ages when applied on the same object. There are many examples in which the reliability of both techniques has been demonstrated. One of them is the TL dating of drain pipes and a stove from a Roman villa in Bad Kreuznach (Fig. 1). Both, the fine-grain and the quartz-inclusion ages ranging between 1690 and 1910 years agree well with the known construction and dwelling periods of this villa in the 2nd and 3rd century A.D.

A further application, in which TL dating is routinely used, is authenticity testing (Fleming, 1975) of art pieces. Usually it is necessary to distinguish between a young age of presumed faking (normally less than 100 years) and an age of presumed authenticity (up to several thousand years). Although here much less age accuracy is necessary than in archaeological dating, one has to work with much less material (normally ca. 30 mg), because of the great value of many art pieces.

Despite the uncertainty about the γ-dose rates from the surroundings, TL authenticity tests nearly always give clear answers. For example, the fragment of a "Corinthian" vase (Fig. 2) with a swan painted on it, belongs in style to the 6th century B.C. Archaeologists, however, became suspicious about its authenticity; and indeed, TL authenticity testing does indicate an age of less than 100 years, proving that the piece is a modern forgery.

3. Fission-Track (FT) Dating

The FT method, which has proved to be very useful in geochronology, has so far found little application in archaeological dating, mainly because of the small number of tracks which accumulate in archaeological materials during man's relatively short

Fig. 2. "Corinthian" vase, apparently dating from the 6th century B.C. Thermoluminescence authenticity dating revealed that it was no more than 100 years old

presence on earth. Several hundred, or even better, a thousand tracks should be counted in order to achieve a reliable age. This requires a sufficiently high uranium content in the archaeological materials as can be seen from Figure 3. A uranium content of 10 ppm produces only a few tracks per cm^2 in 1000 years. Counting such low track densities is very time-consuming. For example, a bluish glass shard from a wall of a Roman bath in Chassenon near Limoges had a uranium content of only 3 ppm. To establish a FT age of 1830 years about 100 h of track counting was required. Thus the FT dating of most artificial glasses is impractical although the method works well. The prerequisite of sufficiently high uranium content restricts the method to few materials found in archaeological contexts.

FT dating is based on the spontaneous fission of uranium-238. Although the rate of this fission is very slow (halflife ca. 10^{16} years), it can be used for age determination because the single fission event can be made visible. Along their path the fission fragments leave atomically highly disordered channels which can be etched until they reach a microscopically visible size (Fig. 4). Fission tracks are found in many electrically nonconducting minerals and glasses. The number of such "spontaneous" or "fossil" fission tracks depends on the age and on the uranium content of a sample. In order to determine its uranium content, the sample is irradiated with thermal neutrons. By

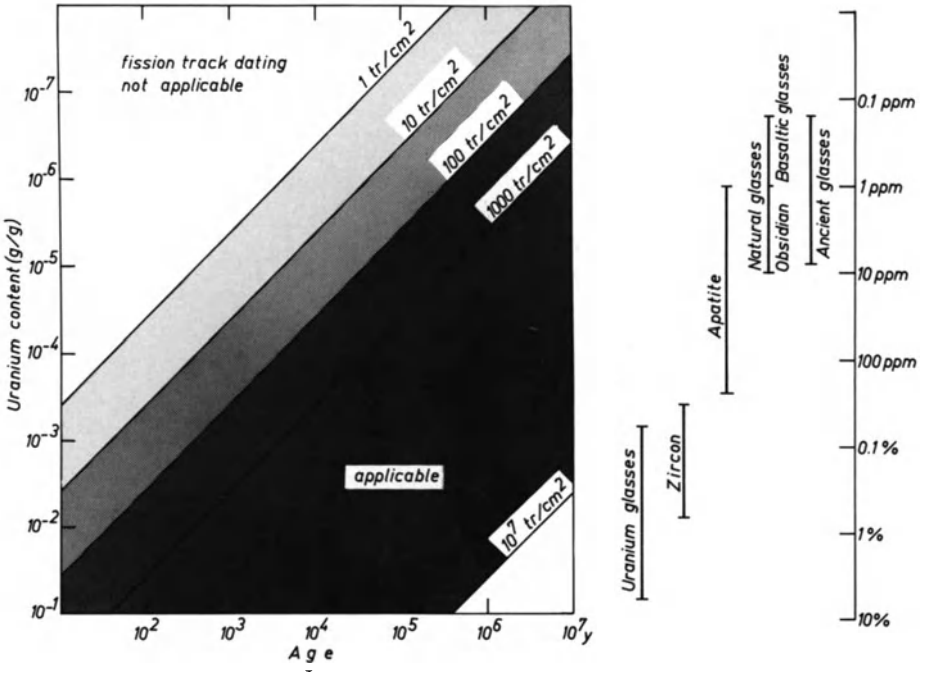

Fig. 3. Usefulness of a sample for fission-track dating in relation to its uranium content and its age. Counting of track densities below 100 tracks/cm^2 is very time-consuming

this irradiation, fission of uranium-235 is induced which also results in etchable tracks – quite analogous to the spontaneous uranium-238 fission. From the number of these "induced" fission tracks, the uranium content is calculated.

In dating practice the sample is first ground, polished, and etched. The fossil tracks are counted using an optical microscope. Next, the sample is sufficiently heated to produce complete fading of the fossil tracks. The sample is irradiated with thermal neutrons. After renewed grinding, polishing and etching, the induced fission tracks are counted. The FT age is calculated according to the equation

$$\text{FT age} = \frac{p_s \cdot n \cdot \sigma_f \cdot I}{p_i \cdot \lambda_f}$$

where p_s = spontaneous fission track density

p_i = induced fission track density

σ_f = fission cross-section of ^{235}U (= 580 x 10^{-24} cm^2)

I = isotopic ratio $^{235}U/^{238}U$ (= 0.007253)

λ_f = decay constant for spontaneous ^{238}U fission (= 8.46 x 10^{-17} a^{-1}; there are also different constants used in FT age calculation; the reader is referred to Dr. Naeser's paper, this volume.)

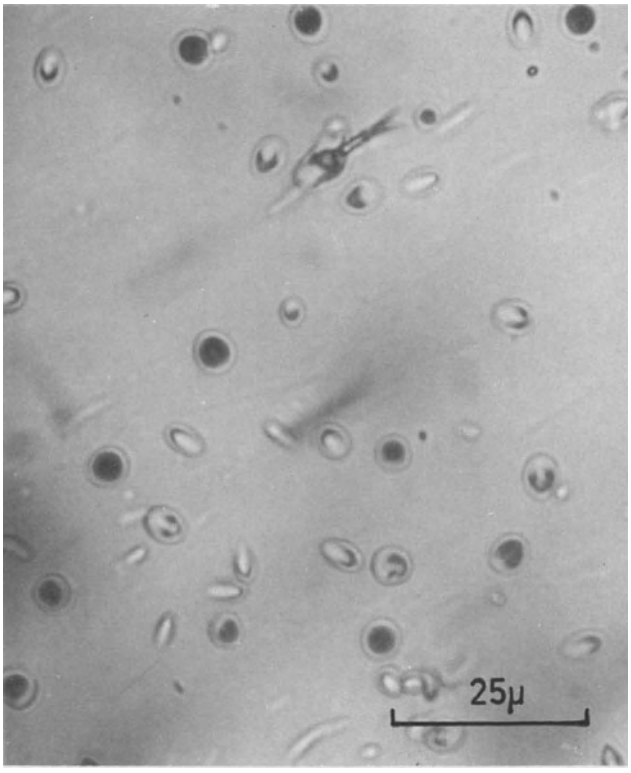

Fig. 4. Numerous induced fission tracks in an obsidian from Gabelotto/Lipari (etched 3 min in 16% hydrofluoric acid at 23°C)

For the interpretation of the fission track age, an understanding of the phenomenon of track fading is essential. This and other problems are discussed in more detail in the chapters on the geologic application of the FT method in this volume. All that needs to be pointed out here is that the latent tracks fade at elevated temperatures. The temperatures critical for track fading differ from material to material. And according to the degree of annealing the tracks may fade partially or completely.

In other words, complete loss of tracks resets the FT clock. This is best explained by using obsidian as an example. Obsidian is a natural glass which forms through rapid cooling of lava. If all tracks are stored after the glass solidified, the FT age gives the time of obsidian formation. If prehistoric man picked up the obsidian rock for the purpose of tool making and at some stage during tool fabrication heated the obsidian to a temperature (above ca. 400°C) that resulted in complete track loss, then the FT age of the obsidian would be the time of tool fabrication. On the other hand, the heating might have only resulted in partial fading of the pre-existing tracks. The FT age of such an artifact would be somewhere between the ages of rock formationand tool fabrication. By track-size studies both ages can still be determined because partially

annealed tracks are smaller than unannealed tracks. Finally, there may have been no heating at all during fabrication of the tools, thus their FT age would be the time of geologic obsidian solidification.

Actually, all these hypothetical cases were encountered when dating obsidian tools and flakes from Ecuador (Fig. 5). Even on the same archaeological site, unannealed flakes occur together with annealed ones. Currently it is not yet clear at which stage

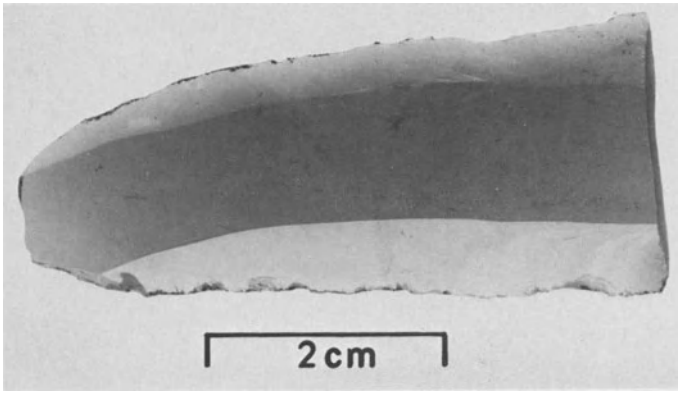

Fig. 5. Obsidian knife from Ecuador. Its fission track age of 1.64 Ma dates the geologic formation. This age helps to identify the geographic source of the obsidian raw-material

of tool making (obsidian quarrying or fabrication) or even of tool use, the heating was applied. Nevertheless, the archaeological information of track studies in obsidian is manyfold. Besides the age of tool making or use, it reveals the degree of heating; and from the geologic age of the obsidian, the source of the raw material can be identified.

In an analogous way, uranium-rich mineral inclusions in rocks can be used for archaeological dating. Here the potential of the FT method has not yet been fully effected. Consider a prehistoric fire-place made up of granitic boulders. Granite contains apatite, zircon, sphene, and other uranium-bearing crystals as accessory minerals. By firing, the FT clocks in some or even all these minerals, depending on the degree of heating, may be reset. Also pottery and ceramics often contain such uranium-rich minerals within the clay matrix. The age of firing and even firing temperatures of rocks and pottery might be determined in this way.

Apart from the direct application to artifacts themselves, FT dating can also be used occasionally for stratigraphic sequences containing artifacts and hominid finds. This is the case when the layers are intercalated with volcanic tuffs and flows which are suitable for FT dating. Either the glassy parts (pumice, obsidian etc.) or minerals, such as apatite, sphene, and zircon, of these rocks can be taken for FT dating. This kind of application was demonstrated for the hominid-bearing sites at Olduvai Gorge by Fleischer et al. and at East Rudolph Lake by Hurford et al. In both cases the FT

method supplemented the K-Ar method. As has been seen in the age controversies over both these sites, the K-Ar age of volcanic rocks is often discrepant due to excess argon contamination or due to argon loss.

4. Concluding Remarks

Since both geology and archaeology are historical sciences, age determination is of great importance to them. Both sciences have been greatly affected by the introduction of physical and – to a lesser degree – chemical dating methods. Whereas in earth science such methods are already well established, the methods are still undergoing rapid development in the archaeological sciences. Each year the existing methods are improved further and extended to wider applications and new methods are developed. Many methods used for the dating of archaeological events were originally developed for the age determination of young rocks. Therefore, there exist close links between the two fields of geochronology and archaeometry. As indicated in this lecture on thermoluminescence and fission-track dating, most methods work only in a limited portion of the archaeological time-scale, are applicable to only a few materials, and have to be carried out in special laboratories.

In solving archaeological dating problems the combined effort of various scientific disciplines, extending from the physical and earth sciences to the archaeological sciences, is essential. This interdisciplinary cooperation is a characteristic which is most stimulating, and which has proved to be very important in the successful development of geochronology.

References and Suggested Readings

Aitken, M.J.: Physics and Archaeology. Oxford: Clarendon Press 1974
Bishop, W.W., Miller, J.A. (eds.): Calibration of Hominid Evolution. Edinburgh, New York: Scott. Academic Press, 1972
Brothwell, D., Higgs, E., Clark, G. (eds.): Sciences in Archaeology, 2nd ed. Bristol: Thames and Hudson, 1969
Fleischer, R.L., Price, P.B., Walker, R.M., Leakey, L.S.B.: Fission track dating of bed I, Olduvai Gorge. Science *148*, 72-74 (1965)
Fleming, S.J.: Thermoluminescent dating: refinement of the quartz inclusion method. Archaeometry *12*, 133-145 (1970)
Fleming, S.J.: Authenticity in art: The Scientific Detection of Forgery. London, Bristol: Inst. of Physics, 1975
Fleming, S.J.: Dating in Archaeology. London: Dent 1976
Hurford, A.J., Gleadow, A.J.W., Naeser, C.W.: Fission track dating of pumice from the KBS tuff, East Rudolf, Kenya. Nature (London) *263*, 738-740 (1976)
Leakey, L.S.B., Evernden, J.F., Curtis, G.H.: Age of bed I, Olduvai Gorge, Tanganyika. Nature (London) *191*, 478-479 (1961)
McDougall, D.J. (ed.): Thermoluminescence of Geological Materials. London, New York: Academic Press 1968

Michael, H.N., Ralph, E. (ed.) Dating Techniques for the Archaeologist. Cambridge/ Mass., London: MIT Press, 1971
Michels, J.W.: Dating Methods in Archaeology. New York, London: Seminar Press, 1973
Newton, R.G.: The enigma of the layered crusts on weathered glasses, a chronological account of the investigations. Archaeometry *13*, 1-9 (1971)
Tite, M.S.: Methods of physical examination in archaeology. London, New York: Seminar Press 1972
Wagner, G.A.: Radiation damage dating of rocks and artifacts. Endeavour *35*, 3-8 (1976)
Wagner, G.A., Storzer, D., Keller,J.: Spaltspurendatierung quartärer Gesteinsgläser aus dem Mittelmeerraum. Neues Jahrb. Mineral. Monatsh. Jg. 1976, 84-94 (1976)
Zimmerman, D.W.: Thermoluminescent dating using fine grains from pottery. Archaeometry *13*, 29-52 (1971)

Diffusion Experiments in Isotope Geology

A. W. HOFMANN

Volume diffusion is one possible mechanism whereby chemical elements and isotopes can migrate through rocks and minerals. Other mechanisms include *recrystallization* acting together with grain boundary or volume diffusion, and *infiltration* of aqueous or silicate fluids. Diffusion is often much slower than other transport processes but it never stops completely (except at absolute zero temperature), and it can therefore equilibrate minerals *isotopically* when the rock is sufficiently close to *chemical* equilibrium so that other reaction mechanism cease to operate.

Diffusion in solid silicates is very difficult to determine experimentally, because it is very slow. For example, most experimental determinations of argon diffusion in minerals show such poor reproducibility that they are essentially useless (see for example Mussett, 1969).

One frequently used experimental technique involves heating the fine-grained minerals in vacuum under isothermal conditions or with stepwise or continuously increasing temperatures. This method has been especially popular in measurements of rare gas diffusion in minerals (see for example the review of Mussett, 1969, on argon diffusion). It has recently been revived in the $^{39}Ar/^{40}Ar$ dating method. The diffusion coefficient is calculated from the fraction of gas lost, the duration of the experiment, and the size of the mineral grains. Solutions of the diffusion equation for different grain shapes that can be approximated by spheres, infinite cylinders, or infinite sheets are given by Crank (1975). Because micas and amphiboles are particularly useful for K-Ar dating, many workers have used the vacuum-extraction method to measure Ar diffusion in these minerals. However, none of these efforts has yielded meaningful volume diffusion data, because hydrous minerals, being unstable in vacuum at elevated temperatures, break down and release much or all of their argon during this breakdown reaction. This is definitely not a volume-diffusion process. It might be argued that argon loss in the natural environment may also be governed by breakdown reactions, but the vacuum experiments can hardly be said to reproduce the conditions at which natural metamorphic reactions occur.

Giletti (1974a) has given a review of diffusion data related to geochronology and pointed out that meaningful and reproducible diffusion experiments are possible. Important experimental requirements are: (1) The mineral phase must be stable during experiment and there should in general be only one mineral phase present. (2) The effective grain geometry must be determined. (3) Either a significant amount of the migrating species must be exchanged with the environment of the mineral grains, or if possible, the actual concentration gradient in the mineral should be determined. (4) Isothermal time studies must be conducted to demonstrate that the time depen-

dence follows the diffusion laws. The range of durations of individual experiments should be varied by at least a factor of 10.

To satisfy the criterion of stability, diffusion experiments on hydrous minerals must be done hydrothermally, and the hydrothermal solution must be adjusted to approximate an equilibrium composition sufficiently closely, so that mineral grains do not react or recrystallize. Some examples of such hydrothermal diffusion experiments are given by Hofmann and Giletti (1970), Giletti (1974b), Foland (1974), and Yund and Anderson (1974, 1978).

Another method, which in principle is superior to the bulk exchange (or bulk loss) methods discussed above, is the determination of actual concentration gradients in the sample. This is done routinely on materials of relatively high diffusivity (metals, salts, glasses), but in many silicate minerals the diffusion coefficients are so small that the experimentally attainable diffusion gradients penetrate less than 1 μm from the surface into the grain. This can be overcome by conducting the experiments at higher temperatures (if mineral stability permits) or by improving the resolution of the gradient measurement. Buening and Buseck (1973) and Misener (1974) studied Fe-Mg interdiffusion in olivine at high temperatures, using the electron microprobe to determine the chemical gradients. Misra and Venkatasubramanian (1977) used a sectioning and counting technique to determine diffusion gradients of ^{90}Sr in feldspars. Perhaps the most promising method is the use of the ion microprobe in order to measure submicron chemical or isotopic gradients (Hofmann et al., 1974; Giletti et al., 1978). In this technique, the primary ion beam removes thin layers (tens of angstroms) of material from the sample surface. The material thus removed is analyzed for isotopic (or element) abundance in the secondary mass spectrometer.

The high resolution of the ion microprobe opens up the potential for measuring diffusivities directly at the metamorphic temperature of interest. For example, if a diffusion gradient of 100 Å can be resolved in this way, a diffusion coefficient as low as $D \approx x^2/t = 10^{-19}$ cm^2 s^{-1} can be determined for an experimental diffusion run of four months. This diffusion coefficient would require $t = x^2/D \approx 30$ m.y. to generate a gradient of 100 μm length, and these length and time scales are of the approximate order of magnitude that are relevant to the loss of a significant fraction of radiogenic strontium or argon from mineral grains.

Recent results of interest to isotope geologists are listed in Table 1, where the diffusion coefficient is given by the Arrhenius equation $D = D_0 \exp[-Q/RT]$, where Q = activation energy (cal mol^{-1}), R = 1.9872 (cal mol^{-1} deg^{-1}), T = absolute temperature (deg. Kelvin).

Attempts to evaluate the effect of pressure on diffusion coefficients in silicates were made first by Misener (1974), who found that Fe-Mg interdiffusion coefficient in olivine decreases by a factor of 10 when the pressure is increased to 35 kbar. Giletti and Tullis (1977) found no significant change in argon diffusivity in phlogopite between 2 and 15 kbar water pressure. Finally, Yund and Anderson (1978) found the oxygen diffusivity *increases* by a factor of ten as the water pressure is increased from 125 to 4000 bars. They attributed this to the increased activity of "water" (H_2O, H^+, or OH^-) in the feldspar.

Many petrologists and isotope geochemists have argued that volume diffusion data are not relevant to the processes that occur in geologic environments. This argument is

Table 1

Element	Material	Run conditions	D_o	$10^{-3}Q$	Temperature °C	Reference
Ar	Phlogopite	1 atm-15 kbar hydrothermal	0.75	57.9	550-1080	Giletti (1974b) Giletti and Tullis (1977)
Ar	Orthoclase	2 kbar hydrothermal and in vacuum	9.82×10^{-3}	43.8	500-800	Foland (1974)
Sr	Orthoclase normal to (001)	In air	6×10^{-4}	42.2	800-870	Misra and Venkatasubramanian (1977)
Sr	Microcline normal to (010)	In air	5×10^{-4}	38.6	800-870	Misra and Venkatasubramanian (1977)
Sr	Obsidian	In air	0.055	42.7	680-950	Magaritz and Hofmann (1978)
Sr	Basalt	In air	0.278	43.5	1260-1440	Hofmann and Magaritz (1977)
O	Basalt	In CO_2 or O_2	$\sim 6.0 \times 10^{4}$ (computed from publ. figure)	$\sim$ 87.5	1250-1525	Muehlenbachs and Kushiro (1974)
O	Phlogopite	2 kbar hydrothermal	1.03×10^{-9}	29	500-800	Giletti and Anderson (1975)
O	Microcline	2 kbar hydrothermal	2.8×10^{-6}	29.6	400-700	Yund and Anderson (1974)
O	Adularia	2 kbar hydrothermal	5.3×10^{-7}	29.6	400-700	Yund and Anderson (1974)
O	Albite	2 kbar	2.3×10^{-5}	37	600-800	Anderson and Kasper (1975)

derived from the fact that metamorphism is normally accompanied by considerable recrystallization. Also it is widely accepted that the rates of metamorphic reaction are greatly enhanced by the presence of a hydrothermal fluid. This point of view is no doubt justified in many instances. Nevertheless, we owe our ability to observe metamorphic assemblages in rocks to the fact that the reactions stop at some point near (what is believed to be) the maximum temperature and that the assemblages are subsequently frozen in. Volume diffusion, however, continues after this time until the system has cooled sufficiently so that the diffusion distances become negligible relative to grain size. Thus it seems that the loss of radiogenic isotopes by *volume diffusion* provides the only consistent explanation why different parent-daughter isotopic systems yield different apparent ages for the same minerals (such as have been documented for Alpine phengites by Purdy and Jäger, 1976, and for biotites reheated by contact metamorphism around the Eldora stock by Hart, 1964). The gradients within single biotite grains shown by Hart (1964) are also consistent with this. On the other hand, Jäger and Hunziger (pers. comm.) have noted that Alpine cooling ages are frequently independent of grain size. This observation is not consistent with volume-diffusion control unless the effective grain size for diffusion is somehow consistently smaller than the total grain size. Perhaps the solution to this problem lies in the presence of inclusions in the mica, which act as local sinks of radiogenic strontium supplied by volume diffusion during the cooling process. The inclusions would then be lost from the system during mineral separation and purification. Perhaps a very detailed study of single grains and their inclusions could resolve the question of loss mechanism.

The rather strong dependence of oxygen diffusivity on water pressure (Yund and Anderson, 1978) might cause the oxygen isotopic equilibration to "freeze in" at the time when the rock becomes "dry" at or after the time of peak metamorphism. However, no detailed applications of these diffusivity data have yet been attempted.

References

Anderson, T.F., Kasper, R.B.: Oxygen self-diffusion in albite under hydrothermal conditions. EOS *56*, 459 (1975)

Buening, D.K., Buseck, P.R.: Fe-Mg lattice diffusion in olivine. J. Geophys. Res. *78*, 6852-6862 (1973)

Crank, J.: The Mathematics of Diffusion, 2nd ed. Oxford University Press, 1975

Foland, K.A.: Ar^{40} diffusion in homogeneous orthoclase and an interpretation of Ar diffusion in K-feldspars. Geochim. Cosmochim. Acta *38*, 151-166 (1974)

Giletti, B.J.: Diffusion related to geochronology. In: Geochemical Transport and Kinetics. Hofmann, A.W., Giletti, B.J., Yoder, Jr., H.S., Yund, R.A. (eds.). Carnegie Inst. Washington Publ. *634*, 61-76 (1974a)

Giletti, B.J.: Studies in diffusion I: argon in phlogopite mica. In: Geochemical Transport and Kinetics. Hofmann, A.W., Giletti, B.J., Yoder, Jr., H.S., Yund, R.A. (eds.). Carnegie Inst. Washington Publ. *634*, 107-115 (1974b)

Giletti, B.J., Anderson, T.F.: Studies in diffusion II: Oxygen in phlogopite mica. Earth Planet. Sci. Lett. *28*, 225-233 (1975)

Giletti, B.J., Semet, M.P., Yund, R.A.: Studies in diffusion III: Oxygen in feldspars, an ion microprobe determination. Geochim. Cosmochim. Acta *42*, in press (1978)

Giletti, B.J., Tullis, J.: Studies in diffusion IV: Pressure dependence of Ar diffusion in phlogopite mica. Earth Planet. Sci. Lett. *35*, 180-183 (1977)
Hart, S.R.: The petrology and isotopic-mineral age relations of a contact zone in the Front Range, Colorado. J. Geol. *72*, 493-525 (1964)
Hofmann, A.W., Giletti, B.J.: Diffusion of geochronologically important nuclides in minerals under hydrothermal conditions. Eclogae Geol. Helv. *63*, 141-150 (1970)
Hofmann, A.W., Giletti, B.J., Hinthorne, J.R., Andersen, C.A., Comaford, D.: Ion microprobe analysis of a potassium self-diffusion experiment in biotite. Earth Planet. Sci. Lett. *24*, 48-52 (1974)
Hofmann, A.W., Magaritz, M.: Diffusion of Ca, Sr, Ba, and Co in a basalt melt: Implications for the geochemistry of the mantle. J. Geophys. Res. *82*, 5432-5440 (1977)
Magaritz, M., Hofmann, A.W.: Diffusion of Sr, Ba, and Na in obsidian. Geochim. Cosmochim. Acta *42*, 595-605 (1978)
Misener, D.J.: Cationic diffusion in olivine to 1400°C and 35 kbar. In: Geochemical Transport and Kinetics. Hofmann, A.W., Giletti, B.J., Yoder, Jr., H.S., Yund, R.A. (eds.). Carnegie Inst. Washington Publ. *634*, 117-129 (1974)
Misra, N.K., Venkatasubramanian, V.S.: Strontium diffusion in feldspars – a laboratory study. Geochim. Cosmochim. Acta *41*, 837-838 (1977)
Muehlenbachs, K., Kushiro, I.: Oxygen isotope exchange and equilibrium of silicates with CO_2 or O_2. Carnegie Inst. Washington Yearb. *73*, 232-236 (1974)
Mussett, A.E.: Diffusion measurements and the potassium argon method of dating. Geophys. J. R. Astron. Soc. *18*, 257-303 (1969)
Purdy, J.W., Jäger, E.: K-Ar ages on rock-forming minerals from the central Alps. Mem. Ist. Geol. Min. Univ. Padova *30*, 1-31 (1976)
Yund, R.A., Anderson, T.F.: Oxygen isotope exchange between potassium feldspar and KCL solution. In: Geochemical Transport and Kinetics. Hofmann, A.W., et al. (eds.). Carnegie Inst. Washington Publ. *634*, 99-105 (1974)
Yund, R.A., Anderson, T.F.: The effect of fluid pressure on oxygen isotope exchange between feldspar and water. Geochim. Cosmochim. Acta *42*, in press (1978)

Theory of Cooling Ages

M. H. DODSON

It is widely accepted that radiometric ages determined on metamorphic minerals from orogenic belts generally reflect their cooling history rather than their primary crystallisation. Armstrong (1966) first developed this concept in detail, while Harper (1967) pioneered its application to the British Caledonides. Its general acceptance, however, stems largely from the investigations of the Central Alps by Professor Jäger and her colleagues at Bern, reviewed elsewhere in this volume. In a young mountain belt the precision of some dating systems, notably Rb-Sr on biotite, K-Ar on biotites and muscovites, and U-fission tracks on apatite, is sufficient to build up a consistent picture of rocks cooling through a succession of different "blocking temperatures", that is, temperatures at which the various systems start to retain their radiogenic daughter products. Above its blocking temperature each system appears to lose its daughter product completely, and below it the daughter product is quantitatively retained.

Estimates of blocking temperatures in the Alps range from about 500°C for Sr in muscovite to $\sim$ 100°C for fission tracks in apatite. Those values have been obtained in three distinct ways. First, the Bern group employed metamorphic mineral assemblages to estimate temperatures in the Alpine "mixed-age" zone, in which Palaeozoic micas partially lost radiogenic Sr during Alpine metamorphism: they assumed that the temperature of opening of these micas to Sr migration is the same as the temperature of closing during slow cooling. Secondly, isotopic age gradients observed in boreholes can sometimes be used to estimate by extrapolation the depths and temperatures at which certain minerals just begin to retain their radiogenic daughter product (Turner and Forbes, 1976; Naeser and Forbes, 1976). The third approach, and the one with which this paper is primarily concerned, is to predict theoretical blocking temperatures from experimental measurements of the rate of loss of daughter product at high temperatures.

Because the theory described here is concerned solely with slow cooling, the term "closure" is preferred to "blocking" temperature. The "opening" of geochronological systems by thermal pulses has been considered elsewhere (Dodson, 1976).

1. Definition of Closure Temperature

The concept of closure temperature is illustrated in Figure 1. It is assumed that, while the system is near to the temperature of crystallisation, the daughter nuclide diffuses out as fast as it is produced by radioactive decay. As the system cools, it enters a tran-

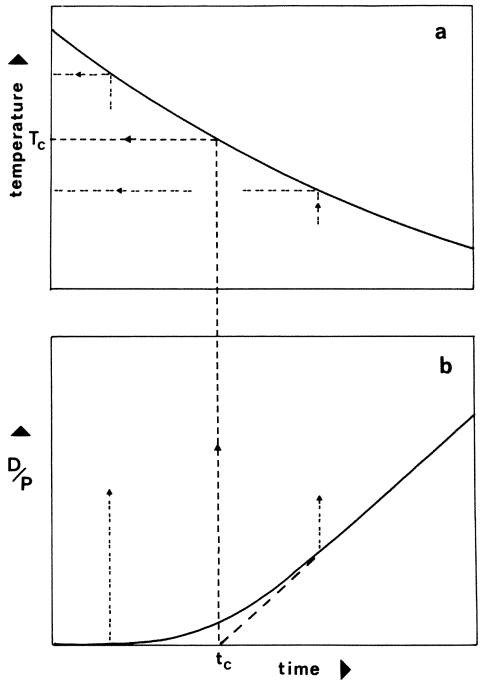

Fig. 1 a and b. Definition of closure temperature. **a** Cooling curve; **b** accumulation curve. *D/P* daughter/parent ratio. *Fine broken lines* show approximate limits of transitional time-temperature range

sitional temperature range within which some of the daughter product accumulates in the mineral, and some is lost. Eventually, at temperatures near ambient, the losses are negligible, and the daughter product accumulates without any loss whatsoever. In calculating an "age" for the system, we in effect extrapolate the last portion of the curve back to the time axis, as shown by the broken line. According to this picture, the closure process is not a sharply defined event. Nevertheless closure temperature T_C can be given the simple and precise definition illustrated in Figure 1, namely *the temperature of the system at the time given by its apparent age*; on this basis it can be directly related to cooling history.

It is easy to imagine that closure temperature may vary with cooling rate; the slower the rate of cooling, the longer will be the time during which total or partial loss of daughter product may occur, and the lower will be both the apparent age and the corresponding closure temperature. Wagner and Reimer (1972) confirmed this supposition in the first theoretical study of closure temperature, which was a numerical analysis of fission-track annealing in slowly cooling apatites. They showed that large changes in cooling rate affected T_C, though not very strongly, in the direction suggested above. Dodson (1973, 1976) presented analytic solutions suitable for closure of slowly cooling K-Ar and Rb-Sr systems, and explained their physical significance. The methods and results of that work will be outlined here, and its extension to fission-track dating will be discussed.

2. The Basic Model

A datable mineral such as biotite is considered to be physically connected (probably through a fluid phase) with a very large reservoir or sink within which radiogenic isotopes can be effectively lost. Radiogenic argon, of course, is likely to leave the rock altogether, while radiogenic strontium probably enters a strontium-rich phase such as apatite or plagioclase, causing little change in the concentration or isotopic composition of Sr in that phase. Two mechanisms of loss may be considered. The simplest is first-order loss, independent of the geometry of the grain. For example, the rate of loss might be controlled entirely by the rate at which radiogenic atoms leave the site in which they were formed. More probable is loss by volume diffusion, in which the rate of loss depends upon the size of either the whole mineral grain or some smaller volume, which may be controlled by the distribution of cleavage fractures, planes of dislocation or other imperfections in the crystal structure.

Approximate expressions for T_c may be derived by a simple physical argument. First one determines the time required for significant loss of daughter product at any fixed temperature, using the appropriate loss coefficient (see below). Sine the loss coefficients are strongly temperature-dependent, so also are the estimated times required for loss to occur. Dodson (1976) showed that, at the closure temperature, the time for isothermal loss of daughter products should be of the same order as a quantity called the *cooling time constant*, which is defined as the time required for the loss coefficient to diminish by a factor e ($\cong 2.7$). An expression in the form of Eq. (6) below follows directly, relating temperature to cooling rate and loss coefficients. An analytical treatment of the problem gives a more precise result.

3. Mathematical Treatment

Differential equations can be set up as follows.
First order loss:

$$dc/dt = -k(t)c + p \tag{1}$$

Volume diffusion

$$\frac{\partial c}{\partial t} = \frac{D(t)}{a^2} \nabla^2 c + p \tag{2}$$

c is the concentration of radiogenic isotope, and p its production rate: k is a first-order rate coefficient, D a diffusion coefficient, a a diffusion size and t is time. Both equations have to be integrated from $c = 0$ at $t = 0$, and in the volume diffusion process the surface concentration is assumed to be zero at all times.

Both k and D are functions of temperature, and therefore of time. To make the equations tractable it is assumed, first, that k and D both obey the Arrhenius law, viz.,

$$(k, D) = (k_0, D_0) \exp(-E/RT) \tag{3}$$

where E, R and T are respectively the activation energy, gas constant, and absolute temperature; k_0 and D_0 are pre-exponential constants, corresponding to the limit of k and D as T becomes very large. We next suppose that, over the transitional temperature range, the cooling history can be approximated by a linear increase in 1/T with time, so that we can immediately replace k and D in Eqs. (1) and (2) by

$$(k, D) = (k_0, D_0)\, e^{-t/\tau} \tag{4}$$

where τ, which is the cooling time constant mentioned above, is given by

$$\tau = -RT_c^2/E\dot{T} \tag{5}$$

Methods of integration of Eqs. (1) and (2) were given by Dodson (1973); they involve transformation of the time variable so that the coefficients of c and $\nabla^2 c$ are constant. With one further assumption, namely that $k\tau$ or $D\tau/a^2$ is very much greater than unity at the temperature of crystallisation (which is a mathematical way of saying that the initial rate of loss is very rapid), simple analytical expressions for closure temperature are obtained. These are

$$E/RT_c = \ln(1.78\tau k_0) \tag{6a}$$

for first order loss and

$$E/RT_c = \ln(A\tau D_0/a^2) \tag{6b}$$

for volume diffusion, where

A = 8.7 (linear diffusion across an infinite plane sheet)
A = 27 (radial diffusion in an infinite cylinder)
A = 55 (radial diffusion in a sphere)

Substituting for τ by Eq. (5), we obtain the following relationship between closure temperature T_c, cooling rate $\dot{T}$, activation energy E and frequency factor D_0/a^2:

$$E/RT + \ln(E/RT_c^2) = \ln(-AD_0/a^2\dot{T}) \tag{7}$$

The relationship between T_c and $\dot{T}/(AD_0/a^2)$ is plotted on Figure 2 for various values of E. It can be seen that closure temperature is much more sensitive to E than to cooling rate. Also the greater the activation energy, the less T_c depends upon cooling rate.

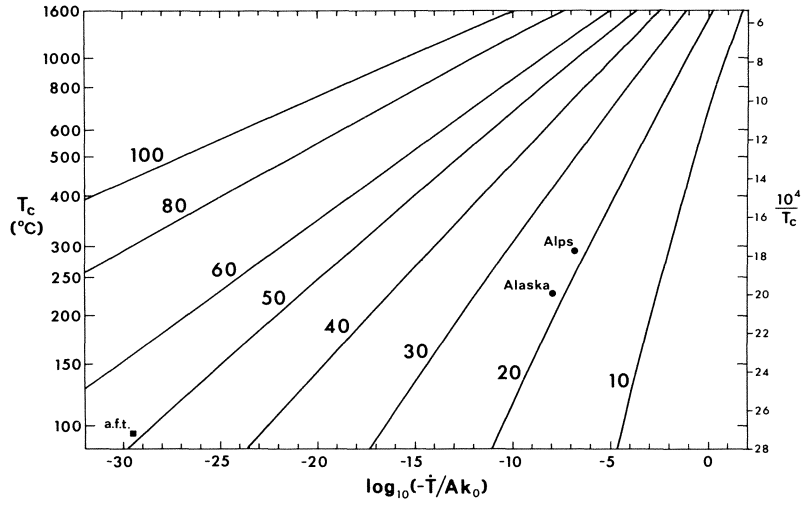

Fig. 2. Closure temperature (T_C) vs. cooling rate ($-\dot{T}$). For volume diffusion k_0 is replaced by D_0/a^2. Figures on curves are activation energy in kcal/mol. Point *a.f.t.* represents closure of apatite fission track system cooling at 10°C per m.y. *Alps* and *Alaska* refer to biotite Rb/Sr systems cooling at different rates (see text)

4. The Calculation of Closure Temperatures

Equation (7) on its own is insufficient to calculate a closure temperature without a knowledge of the cooling rate. However, for a young Alpine mica one can use the present-day temperature (T_p) as an additional constraint, so that both the unknown quantities can be determined. Assuming, for example, a linear rate of cooling we have

$$\dot{T} = (T_c - T_p)/t_m \tag{8}$$

where t_m is the measured age of the mineral. This can be substituted in Eq. (7) to give a single equation which can be solved iteratively for T_C:

$$\frac{E}{RT_c} = \ln\left[\frac{-AD_0\, t_m}{a^2(T_c - T_p)} \quad \frac{RT_c^2}{E}\right] \tag{9}$$

Iteration is performed most simply by guessing at a value of T_C, substituting on the right of Eq. (9), and calculating a new value. The new value is in turn substituted on the right. Successive values of T_C converge rapidly. Calculations of this kind for biotites must use the data of Hofmann and Giletti (1970) on diffusion of Rb in biotite, since no suitable diffusion data for Sr in biotite is available. We use here $D_0 = 2.09 \times 10^{-10}\,cm^2/s$ and E = 21 kcal/mol. A typical grain-size for Alpine biotites in gneissic rocks is 0.7 mm, so we set a = 0.035 cm. Next, it is reasonable to assume cylindrical geometry (A = 27),

since diffusion in micas probably takes place parallel to the cleavage planes rather than across them (Hofmann et al., 1974). Finally we take T_p, the present-day temperature, to be 0°C, and obtain these results:

10 m.y. biotite: $T_c = 288°C$
20 m.y. biotite: $T_c = 268°C$

The cooling time constants for these two cases are about 1 m.y. and 2 m.y., respectively.

The results differ slightly from those of Dodson (1973), because in that paper a linear increase of 1/T from t_m to the present was assumed, rather than a linear decrease in T. The choice is arbitrary: integration of the equations assumes simply that the cooling history can be approximated by a linear increase in 1/T *over the transitional temperature range;* errors due to this approximation are likely to be small compared with those due to uncertainties in the kinetic data.

Theoretical closure temperatures are given in Table 1 for several other minerals with a = 0.5 mm and cooling rates of 30°C and 3°C/m.y. The faster rate corresponds roughly to recent Alpine history, but no geochronological data is yet available to test the theoretical results.

Table 1. Predicted closure temperatures for 1 mm diameter grains

Mineral (method)	D_0 (cm^2/s)	E (kcal/mol)	A	T_c [a] (°C)	T_c [b] (°C)	References
Biotite (Rb/Sr)	2.1×10^{-10}	21	27	311	250	1
Phlogopite (K/Ar)	0.75	57.9	27	464	425	2
Orthoclase (Rb/Sr)	6×10^{-4}	41.2	55	352	314	3
Microcline (Rb/Sr)	5×10^{-4}	38.6	55	317	280	3

[a] 30°C/m.y.; [b] 3°C/m.y.
1, Hofmann and Giletti, 1970; 2, Giletti, 1974; 3, Misra and Venkatasubramanian, 1977.

5. Comparison with Geological Estimates

The agreement between calculated and observed closure temperatures in the Alps is gratifying, but subject to one major criticism: that is, that biotites from Alpine fissures up to 30 cm across give the same age, and so must have the same closure temperature, as adjacent gneissig biotites less than 1 mm in diameter. There seem to be three possible explanation for this anomaly:

1) diffusion geometry is independent of physical grain size for widely different biotites

2) the loss occurs by a first-order mechanism
3) the "closure" temperature is not kinetically-controlled, but depends on some change in the biotite lattice at 300°C.

A kinetic model is favoured by age gradients from the Eielson borehole[1], Alaska (Turner and Forbes, 1976), showing an uplift-cooling rate of 0.05 mm/yr and a closure temperature of 225°C for argon in biotite. This result and the closure temperature for Alpine biotites are plotted on Figure 2, from which it can be seen that the difference in closure temperature is consistent with the difference in cooling rates (a factor of 10), assuming the same diffusion size. A kinetic model is also supported by field observations on relative closure temperatures of biotite and muscovite for both argon and strontium. The results are qualitatively consistent with laboratory experiments on the retentivities of these two minerals for radiogenic argon.

The evidence at present available appears on the whole to support a kinetic model for closure of Rb/Sr and K/Ar systems in slowly cooling micas, but implies either that the diffusion size for newly formed biotites is independent of the physical grain size or that the loss occurs by a first-order mechanism.

6. Closure of Fission-Track Dating System

In contrast to radiogenic strontium in biotites, there can be no doubt that the closure process for fission tracks is directly related to the kinetics of fission-track annealing. If we consider only apatite, numerical investigations by Wagner and Reimer (1972) and Haack (1977) yielded closure temperatures of 125°C and 95°C respectively with a cooling rate of 10°C/m.y.; those figures are in reasonable agreement with the extrapolated observation of 105°C by Naeser and Forbes (1976) for the Eielson borehole (cooling rate ∿3°C/m.y.). Even so it would be useful to have an analytic solution to the fission-track problem, if only to obviate the time-consuming calculations used in the afore-mentioned numerical work.

Direct application of Eq. (6a) does not, unfortunately, provide a rigorous solution to the problem, firstly because that equation refers to first-order processes, which fission-track annealing is not, and secondly because the activation energy varies with the degree of annealing. However, in the absence of a more sophisticated theory, it seems reasonable to apply the general physical argument outlined in Section 2 of this paper by equating the time needed for 50% track loss under isothermal conditions (t_{50}) with the cooling time constant obtained from the appropriate activation energy (E_{50}).

Thus if we write

$$t_{50} = B \exp(E_{50}/RT) \tag{10}$$

---

[1] The age gradient reflects the fact that deep samples have cooled through their blocking temperature more recently than shallow samples: linear gradients, as observed in this instance, imply a steady rate of erosion and cooling over very long periods.

then, from Eq. (5), closure temperature is given by

$$B \exp(E_{50}/RT_c) = -RT_c^2/(E_{50}\dot{T}) \quad (11)$$

From Naeser and Faul (1969) we can estimate, for apatite, $B = 10^{22.3}$ yr, and $E_{50}/R = 24000$K, whence we can solve Eq. (11) to give:

Cooling rate	T_c
30°C/m.y.	105°C
10°C/m.y.	98°C
3°C/m.y.	92°C

These results are not based on a rigorous theoretical analysis, so they should not be given more weight than the published numerical estimates. However, the broad agreement between the various results, calculated and observed, overwhelmingly supports the kinetic interpretation of fission track closure.

7. Closure of Geochemical Systems

The closure of a geochemical system in which the distribution of a component between phases depends on temperature is closely analogous to closure of geochronological systems. At high temperatures the concentration of a mobile component follows closely its equilibrium values, but upon cooling its mobility diminishes until eventually its distribution approaches a static state ("false equilibrium") from which a closure temperature can be inferred. It was shown by Dodson (1973) that for a minor component the closure temperature is related to cooling rate by Eq. (6a) or (6b), provided that the true equilibrium concentration varies approximately linearly with time. Closure temperatures estimated from observations of this kind could be used to calculate cooling rates, given appropriate kinetic data, but the precision is unlikely to be very great because of the logarithmic character of the relationship. Numerical and theoretical work on this subject has been described for oxygen-18 distribution in igneous and metamorphic rocks (Bottinga and Javoy, 1975; Javoy, 1977), for Mg/Fe exchange near the surface of garnet grains (Lasaga et al., 1977) and for nickel concentrations in taenite lamellae in iron meteorites (Goldstein and Short, 1967).

References

Armstrong, R.L.: K-Ar dating of plutonic and volcanic rocks in orogenic belts. In: Potassium-Argon Dating, Schaeffer, O.A., Zähringer, J. (eds.). Berlin, Heidelberg, New York: Springer, 1966, pp. 117-133

Bottinga, Y., Javoy, M.: Oxygen isotope partitioning among the minerals in igneous and metamorphic rocks. Rev. Geophys. Space Phys. *13*, 410-418 (1975)

Dodson, M.H.: Closure temperature in cooling geochronological and petrological systems. Contrib. Mineral. Petrol. *40*, 259-274 (1973)
Dodson, M.H.: Kinetic Processes and Thermal History of Rocks. Carnegie Inst. Yearb. *74*, 210-217 (1975)
Dodson, M.H.: Kinetic processes and thermal history of slowly cooling solids. Nature (London) *259*, 551-553 (1976)
Giletti, B.J.: Studies in diffusion I: Argon in phlogopite mica. In: Geochemical Transport and Kinetics. Hofman et al. (eds.). Carnegie Institution of Washington, 1974, pp. 107-115
Goldstein, J.I., Short, J.U.: Cooling rates of 27 iron and stony-iron meteorites. Geochim. Cosmochim. Acta *31*, 1001-1023 (1967)
Haack, U.: The closing temperature for fission track retention in minerals. Am. J. Sci. *277*, 459-464 (1977)
Harper, C.T.: The geological interpretation of potassium-argon ages of metamorphic rocks from the Scottish Caledonides. Scott. J. Geol. *3*, 46-66 (1967)
Hofmann, A.W., Giletti, B.J.: Diffusion of geochronologically important nuclides under hydrothermal conditions. Eclogae Geol. Helv. *63*, 141-150 (1970)
Hofmann, A.W., Giletti, B.J., Hinthorne, J.R., Anderson, C.A., Comaford, D.: Ion microprobe analysis of a potassium self-diffusion experiment in biotite. Earth Planet. Sci. Lett. *24*, 48-52 (1974)
Javoy, M.: Stable isotopes and geothermometry. J. Geol. Soc. Lond. *133*, 609-636 (1977)
Lasaga, A.C., Richardson, S.U., Holland, H.D.: The mathematics of cation diffusion and exchange between silicate minerals during retrograde metamorphism. In: Energetics of Geological Processes. Saxena and Bhattacharji (eds.). Berlin-Heidelberg-New York: Springer, 1977, pp. 353-388
Misra, N.K., Venkatasubramanian, V.S.: Strontium diffusion in feldspars – a laboratory study. Geochim. Cosmochim. Acta *41*, 837-838 (1977)
Naeser, C.W., Faul, H.: Fission track annealing in apatite and sphene. J. Geophys. Res. *74*, 705-710 (1969)
Naeser, C.W., Forbes, R.B.: Variation of fission-track ages with depth in two deep drill holes. (Abstract) EOS, Trans. Am. Geophys. Union *57*, 353 (1976)
Turner, D.L., Forbes, R.B.: K-Ar studies in two deep basement drill holes: a new geological estimate of argon blocking temperature for biotite. (Abstract) EOS Trans. Am. Geophys. Union *57*, 353 (1976)
Wagner, G.A., Reimer, G.M.: Fission track tectonics: the tectonic interpretation of fission track ages. Earth Planet. Sci. Lett. *14*, 263-268 (1972)

Isotope and Trace Element Geochemistry of the Earth's Mantle

A. W. HOFMANN

Chemical and isotopic information about the Earth's mantle can be obtained from several sources, but all require certain assumptions:

1. Chondritic Meteorites are assumed to represent primitive matter of the solar system. Chemical models for the mantle usually assume loss of volatile elements, possibly including alkalis, during and after accretion, and segregation of Fe and Ni (+ some lighter elements such as O, Si or S) into the core and lithophile elements into the crust.

2. Basalt is known to be derived from the mantle. Experimental petrology can delineate the composition of possible source rocks. Ambiguities include disagreements between experimental results from different laboratories, assumptions about the degree of melting of the source rock, the degree of crystal fractionation and wall rock contamination, and the basic difficulty that the composition of the melt will be largely independent of the proportions of components in the system, if the system contains invariant points.

3. Ultramafic inclusions are solid samples of mantle rock that are brought to the surface by rapidly ascending alkali basalt magmas. However, it is not clear to what extent these nodules represent "normal" mantle and to what extent they have been depleted of their low-melting fraction. In addition some nodules may represent early cumulus aggregates formed from the melt itself.

4. Alpine peridotites appear to be pieces of mantle that are tectonically emplaced in orogenic belts. Again, it is not clear whether these peridotites are representative of normal mantle. More likely, they are pieces of the uppermost mantle, from which the low-melting fraction has been extracted.

5. The Earth's heat budget may be used to make inferences about the *K, U, and Th abundances* in the mantle (e.g., Hanks and Anderson, 1969). This was relatively straightforward as long as one could assume that heat was transported by conduction alone. However, it is now almost universally accepted that there is convective heat transport, which cannot be measured by simple heat flow measurements because much of the heat brought to the surface is concentrated at midocean ridges where most of it appears to be lost by hydrothermal circulation (Williams and Von Herzen, 1974).

6. The ratios of some elements, such as U/Pb, Rb/Sr, and Sm/Nd, in the mantle can be estimated by measuring the relative abundance of the daughter isotopes. For example, Gast (1960) showed by comparing $^{87}Sr/^{86}Sr$ ratios of terrestrial rocks and chondrites that the Earth's upper mantle has a much lower Rb/Sr ratio than chondrites and is therefore probably depleted in alkalis relative to chondrites. These estimates have been reviewed by O'Nions et al. (1977). Despite the uncertainties involved in all these estimates, there is today surprisingly good agreement about the approximate composi-

tion of the mantle. For example, the lherzolite composition used as a model for the mantle composition by many petrologists differs only in detail from the so-called "pyrolite" model advocated by others. This composition also appears to be compatible with geophysical properties. This is not true for an eclogite composition which has also occasionally been advocated.

Current research in geochemistry has focused on the fine structure of the isotopic and trace element abundances in mantle-derived rocks. In oceanic regions the following pattern is emerging: (1) Mid-ocean ridge (MOR) basalts (mostly tholeiites) are almost unique in their relative uniformity of composition. They have especially *low* abundances of LIL (large-ion-lithophile) elements (e.g., K, Rb, Cs, Sr, Ba, light rare earths) and they have low $^{87}Sr/^{86}Sr$ ratios ($\sim$0.7020 to 0.7035) low $^{206}Pb/^{204}Pb$ ratios, high $^{143}Nd/^{144}Nd$ ratios and low La/Sm ratios (Hart, 1971; Sun and Hanson, 1975; Hofmann and Hart, 1978; Schilling, 1975; De Paolo and Wasserburg, 1976). All these features indicate that the source mantle of MOR basalts has been depleted in LIL elements, probably by previous extraction of melt. (2) Isolated oceanic islands and island chains (e.g., the Emperor Seamount-Hawaiian Island chain) consist of tholeiites and alkali basalts and have a much more variable LIL and isotopic chemistry. They have generally a much less depleted character, i.e., higher $^{87}Sr/^{86}Sr$ (0.703 to 0.706) and $^{206}Pb/^{204}Pb$ ratios, lower $^{143}Nd/^{144}Nd$ ratios, and higher La/Sm ratios. (3) Island arc lavas are even more variable in composition and may be tholeiitic, alkaline, or calc-alkaline in character. In their trace element concentrations and isotopic compositions they resemble the oceanic islands, but rare earth patterns of many of the tholeiites resemble those of the MOR basalts (Jakes and White, 1972; Meijer, 1976). (4) Continental basalts are also quite variable in composition without showing any of the depleted characteristics of MOR basalts. Some continental flood basalts are so radiogenic as to fall outside the range of Sr isotopic compositions traditionally thought to represent "mantle" compositions. It is not clear at present whether these rocks contain a significant crustal component or whether the subcontinental mantle is in some places more radiogenic than was previously believed (Brooks et al., 1976b).

1. Apparent Isochrons

One surprising feature of the isotopic data of mantle-derived rocks is that they appear to form isochrons, that is the data fall on roughly linear arrays when plotted on $^{207}Pb/^{204}Pb$ versus $^{206}Pb/^{204}Pb$ or $^{87}Sr/^{86}Sr$ versus $^{87}Rb/^{86}Sr$ diagrams (Sun and Hanson, 1975; Church and Tatsumoto, 1975; Brooks et al., 1976a). Model ages calculated from the best fit lines of Pb data for young oceanic basalts are approximately 1.5 to 2.0 x 10^9 years. An apparent Rb-Sr isochron for oceanic tholeiites yields a model age of about 1.6 x 10^9 years. It is presently not clear whether this age represents some mantle-wide "event", or whether it is the result of a continuous evolution of the mantle. The simplest interpretation is that of an event (Brooks et al., 1976a; Hart and Brooks, 1977), but there is so far no independent confirmation.

2. Scale of Mantle Heterogeneity

Several geochemists have recently argued that the isotopic differences between the different types of basalt can be explained by disequilibrium melting of a source in which the individual mineral grains are not in isotopic equilibrium with each other and with the melt. O'Nions and Pankhurst (1974) were among those to propose this, but rejected their own hypothesis in a later paper (O'Nions et al., 1976). In a general review of this problem, Hofmann and Hart (1978) argued on the basis of incomplete diffusion data that, in a completely solid mantle, disequilibrium will probably persist for geologically long times on a scale of a few centimeters. However, once a partial melt is present, local equilibration on a meter-scale will be relatively rapid. These conclusions are in agreement with the fact that mantle xenoliths (presumably derived from the completely solid lithosphere) frequently show internal disequilibrium. The melts, on the other hand, tend to be quite uniform in composition, and were probably formed under conditions of chemical equilibrium.

If the above conclusion is correct, the isotopic data indicate that the mantle is chemically and isotopically stratified with only limited exchange between the upper and lower reservoirs. Furthermore, assuming that the mid-ocean ridge basalts are derived from the upper mantle (asthenosphere), the oceanic islands must come from the deeper reservoir, perhaps in the form of chemical plumes (Morgan, 1972; Schilling, 1973).

Unfortunately, the isotopic data for Sr and Pb from island arcs appear to contradict this interpretation, because these rocks are undoubtedly derived from the *upper* mantle, yet show some of the isotopic abundance patterns of the supposedly plume-derived ocean islands. Perhaps the answer to this dilemma lies in the alteration and metamorphism of the oceanic crust. This altered material will contain more radiogenic isotopes than the fresh oceanic crust, and it will then be remelted to produce the compositions typical of island arc volcanism. This question may be resolved in the near future by Nd isotopic data, which appear to be less affected by alteration than are Sr and Pb isotopes. Hawkesworth et al. (1977) have shown Nd isotopic data from the South Sandwich Islands, which are identical to isotope ratios from the nearby Scotia Rise.

There is no agreement in the current literature on the above model of mantle stratification. Alternative views are that the inhomogeneities are relatively small in size and irregularly distributed (e.g., Sleep, 1974), or that the mantle is chemically stratified but in the opposite sense, namely with an enriched asthenosphere and a depleted deeper mantle (e.g., Green and Lieberman, 1976). The solution to this controversy can probably be found only when the geochemical data are combined with other information, such as seismic evidence for deep or shallow "roots" of oceanic islands.

References

Brooks, C., Hart, S.R., Hofmann, A.W., James, D.E.: Rb-Sr mantle isochrons from oceanic regions. Earth Planet. Sci. Lett. *32*, 51-61 (1976a)

Brooks, C., James, D.E., Hart, S.R.: Ancient lithosphere: its role in young continental volcanism. Science *193*, 1086-1094 (1976b)

Church, S.E., Tatsumoto, M.: Lead isotope relations, in oceanic ridge basalts from the Juan de Fuca-Gorda ridge area, N.E. Pacific ocean. Contrib. Mineral. Petrol. *53*, 253-279 (1975)

DePaolo, D.J., Wasserburg, G.J.: Inferences about magma sources and mantle structure from variations of $^{143}Nd/^{144}Nd$. Geophys. Res. Lett. *3*, 743-746 (1976)

Gast, P.W.: Limitations on the composition of the Upper mantle. J. Geophys. Res. *65*, 1287-1297 (1960)

Green, D.H., Liebermann, R.C.: Phase equilibria and elastic properties of a pyrolite model for the oceanic upper mantle. Tectonophysics *32*, 61-92 (1976)

Hanks, T.C., Anderson, D.L.: The early thermal history of the earth. Phys. Earth Planet. Interiors *2*, 19-29 (1969)

Hart, S.R.: K, Rb, Cs, Sr and Ba contents and Sr isotope ratios of ocean floor basalts. Philos. Trans. R. Soc. Lond. A *268*, 573-587 (1971)

Hart, S.R., Brooks, C.: The geochemistry and evolution of Early Precambrian mantle. Contrib. Mineral. Petrol. *61*, 109-128 (1977)

Hawkesworth, C.J., O'Nions, R.K., Pankhurst, R.J., Hamilton, P.J., Evensen, N.M.: A geochemical study of island-arc and back-arc tholeiites from the Scotia Sea. Earth Planet. Sci. Lett. *36*, 253-262 (1977)

Hofmann, A.W., Hart, S.R.: An assessment of local and regional isotopic equilibrium in the mantle. Earth Planet. Sci. Lett. *38*, in press (1978)

Jakes, P., White, A.J.R.: Major and trace element abundances in volcanic rocks of orogenic areas. Geol. Soc. Am. Bull. *83*, 29-40 (1972)

Kay, R., Hubbard, N.J., Gast, P.W.: Chemical characteristics and origin of oceanic ridge volcanic rocks. J. Geophys. Res. *75*, 1585 (1970)

Meijer, A.: Pb and Sr isotopic data bearing on the origin of volcanic rocks from the Mariana island-arc system. Geol. Soc. Am. Bull. *87*, 1358-1369 (1976)

Morgan, W.J.: Deep mantle convection plumes and plate motions. Am. Assoc. Petrol. Geol. Bull. *56*, 203-213 (1972)

O'Nions, R.K., Evensen, N.M., Hamilton, P.J., Carter, S.R.: Melting of the mantle past and present: isotope and trace element evidence. Paper presented at Royal Society Meeting on "Terrestrial Heat and the Generation of Magmas". Jan. 1977 (1977)

O'Nions, R.K., Pankhurst, R.J.: Petrogenetic significance of isotope and trace element variations in volcanic rocks from the Mid-Atlantic. J. Petrol. *15*, 603-634 (1974)

O'Nions, R.K., Pankhurst, R.J., Grönvold, K.: Nature and development of basalt magma sources beneath Iceland and the Reykjanes Ridge. J. Petrol. *17*, 315-338 (1976)

Schilling, J.-G.: Iceland Mantle Plume: geochemical evidence along Reykjanes Ridge. Nature (London) *242*, 565-571 (1973)

Schilling, J.-G.: Rare-earth variations across "normal segments" of the Reykjanes Ridge, 60°-53°N, Mid-Atlantic Ridge, 29°S and East Pacific Rise, 2°-19°S, and evidence on the composition of the underlying low-velocity layer. J. Geophys. Res. *80*, 1459-1473 (1975)

Sleep, N.H.: Segregation of magma from a mostly crystalline mush. Geol. Soc. Am. Bull. *85*, 1225-1232 (1974)

Sun, S.S., Hanson, G.N.: Evolution of the mantle: Geochemical evidence from alakali basalt. Geology *3*, 297-302 (1975)

Williams, D.L., Von Herzen, R.P.: Heat loss from the Earth: new estimate. Geology *2*, 327-328 (1974)

Archaean Geochronology

M. H. DODSON

1. Archaean Geology

The Archaean era, sometimes known as the Archaeozoic, is the earliest part of geological history. It extends from about 2500 million years ago (m.y.a.) to at least 3700 m.y.a. Its younger limit is marked by a change in tectonic style: the characteristic greenstone belts of Archaean time, described below, give way to the sedimentary basins and linear orogenic belts of later geological history. Its older limit predates the oldest isotpic events recorded in terrestrial rocks. These events, 3700 to 3800 m.y.a., reflect the metamorphism of high-grade gneisses which carry evidence of earlier plutonic and supracrustal history. However, a coherent record of geological history may not extent much beyond 4000 m.y.a.; at about that time many of the major surface features of the moon were produced by cataclysmic impacts of asteroidal-sized bodies, and it seems likely that the earth's surface then suffered an even more violent bombardment.

Archaean rocks have been the subject of intensive study in recent years, including many important geochronological investigations. Much attention has been devoted to Archaean cratons in West Greenland, North America, Southern Africa, and Western Australia, but Archaean terrain in India, Equatorial Africa, South America, Siberia, northwest Scotland, and northern Norway, has also contributed valuable data. Recent research on Archaean rocks has been summarised by Windley (1977), and compendia of papers, partly or wholly concerned with Archaean studies, have been edited by Windley (1976), Sutton and Windley (1973), Glover (1971), and the Geological Society of South Africa (1969).

Two types of Archaean rock associations are recognised, namely *high-grade* and *granite-greenstone* terrain. Until recently the latter was the more thoroughly studied, because of its distinctive geological character compared with post-Archaean terrain. The two types will be reviewed before considering, very briefly, some problems of methodology and some important geochronological results.

1.1 Granite-Greenstone Terrain

Large areas of granitoid rocks, predominantly of tonalitic, monzonitic, or granodioritic composition, are interspersed with the characteristic Archaean supracrustal rocks of the so-called greenstone belts. The latter are distinguished from post-Archaean orogenic belts by their small size (typically of the order of 100 km), arcuate or irregular shape, low metamorphic grade (predominantly greenschist to lower amphibolite facies) in

conjunction with strong polyphase deformation, and wide-spread gold mineralisation. Most important of all, their stratigraphy, which is dominated by volcanic rocks, usually approximates to the following model:

	Principal rock types	*Subsidiary rock types*
Sedimentary Group	Mudstones, siltstones	Volcanic rocks rare or absent
	Coarse conglomerates and grits	Banded ironstones, cherts
Mafic-felsic Volcanic Group	Basic, intermediate, and some acid lavas	Cherts, banded ironstones, occasional limestones, rare clastic sediments.
Ultramafic-mafic Volcanic Group	Basaltic lavas Ultrabasic lavas	
? Basement	Gneisses	

The extrusive nature of the ultrabasic lavas is shown by pillow structures in many localities and widespread quench textures (skeletal and spinifex olivines). They contain up to 30% MgO, having liquidus temperatures of 1600°-1700°C, and they must represent very high degrees of partial melting of mantle. The basaltic lavas are also characterised by unusually high MgO content. They and the ultrabasic lavas are known respectively as basaltic and peridotitic komatiites (Viljoen and Viljoen, 1969).

1.2 High-Grade Archaean Terrain

The high-grade Archaean appears to cover a smaller area than the granite-greenstone terrain; the metamorphism is generally upper amphibolite to granulite facies, with widespread development of gneissic banding. Linear shear belts commonly traverse the gneissic rocks. In some areas (e.g., Greenland) most of the rocks prior to metamorphism were probably granites and greenstones, but in others, including the Limpopo Belt, Southern Africa (Mason, 1973), and Southern India (Naidu, 1963) shelf facies rocks such as limestones and well-sorted clastic sediments play a major role.

The relationship between high-grade Archaean and granite-greenstone terrain is controversial. Windley and Bridgewater (1971) thought that high-grade terrain normally represents a basement to neighbouring greenstone belts. Glikson and Lambert (1973), however, considered the high-grade rocks to be the deeply eroded roots of the granite-greenstone areas. Shackleton (1976), takes a comparable view, arguing for metamorphic and structural continuity between adjacent high- and low-grade areas in India and Southern Africa, though he considers the shelf sediments of the high-grade regions to be possibly older than the neighbouring greenstone belts. Else-

where, for example in West Greenland, major high-grade metamorphic episodes post-date at least two greenstone sequences. It seems fairly certain that these three kinds of relationship all occur in different areas, but special interest attaches to those areas, such as the Limpopo Belt, where structural and metamorphic continuity can be demonstrated.

2. Methods of Archaean Geochronology

The Rb-Sr whole-rock isochron method plays a major part in dating granitoid rocks of Archaean age. Its application to both high-grade and low-grade metamorphic rock is, however, subject to many uncertainties, which are compounded by the complex history of Archaean samples. For example, from acid volcanic rocks it is frequently possible to obtain good Rb-Sr isochrons which can be shown to reflect some event which long post-dates their eruption; in some instances the event may be obviously metamorphic, but in others it may not correspond to visible metamorphic effects. Similarly, fine-grained pelitic metasediments commonly yield good Rb-Sr isochrons which have sometimes been regarded as dates of sedimentation; it has been shown, however, that even the lowest grade of metamorphism can produce a metamorphic isochron on such materials (Gebauer and Grünenfelder, 1974).

Rb-Sr dating of the basaltic rocks was for a long time ruled out by their low Rb/Sr ratios. However, recent improvements in mass spectrometric precision made possible systematic investigations of Rhodesian greenstone belts by Hawkesworth et al. (1975) and Jahn and Condie (1976). Interpretations of the data differ markedly, and in view of the demonstrated ease of metamorphic updating of fine-grained acid rocks, it would seem that caution is called for in the interpretation of basalt isochrons.

Clearly other methods than Rb-Sr must be considered for dating greenstone belts. U-Pb dating of zircons from acid volcanic rocks or associated high-level intrusions is potentially very precise (Krogh and Davis, 1971; Pidgeon, 1978). It appears that quartz porphyries normally contain usable quantities of zircon of fairly low U-content, giving results reasonably close to concordia. The scarcity of suitable samples limits the usefulness of that approach, and an alternative which can perhaps be applied to a much wider range of samples is the Samarium-Neodymium method. Sm-147 undergoes alpha decay to Nd-143 with a half-life of about 10^{11} years, and the Sm/Nd ratios in suites of basic volcanic rocks appear to vary enough to make possible the construction of Sm-Nd isochrons. Since rare earths partition preferentially into pyroxenes, both Sm and Nd are likely to be less mobile than are Rb and Sr in such rocks. The first Archaean application of this method gave 2640 ± 140 m.y. for a suite of variably metamorphosed samples from Rhodesian greenstone belts (Hamilton et al., 1977).

The obvious alternative to direct dating of greenstone belts is to bracket them between more easily dated events. Normally there is little problem in setting a younger age limit, either by means of an intrusive granite or a metamorphic isochron, but an older limit depends on an understanding of geological relationships which are often obscured, or even totally obliterated, by later tectonism. It is therefore strongly dependent on good field mapping. Bracketing of this nature has proved possible in East Africa (Dodson et al., 1975) and Rhodesia (Wilson et al., 1978) inter alia.

High-grade Archaean gneisses pose comparable problems of interpretation. Normally an Rb-Sr isochron age on such rocks reflects a metamorphic event, rather than crystallisation of an igneous predecessor, and it is necessary to use $^{87}Sr/^{86}Sr$ initial ratios to set some limits on the duration of the premetamorphic history (Moorbath, 1976). High-grade metamorphic events have also been successfully dated by the lead isochron method, using the slope of linear arrays on a $^{207}Pb/^{204}Rb$ vs. $^{206}Pb/^{204}Pb$ diagram; it appears that such metamorphism commonly results in substantial losses of uranium relative to lead (Moorbath et al., 1969).

3. The Oldest Rocks[1]

In the Godthaab area of western Greenland the high-grade Amitsoq gneisses and low-grade Isua supracrustals give well-established ages in the range 3600 to 3700 m.y. To the southwest in Labrador are found comparable ages on the Uivak and Hebron gneisses (Hurst et al., 1975; Barton, 1975).

The Amitsoq gneisses give an Rb-Sr isochron age of 3670 m.y. (Moorbath et al., 1972) and a lead isotope age of 3740 ± 100 m.y. (Moorbath et al., 1975). They consist of high-grade orthogneisses and amphibolites, and their measured age almost certainly reflects a major metamorphic event. From their initial $^{87}Sr/^{86}Sr$ ratios it appears that they could not have differentiated from the mantle much earlier than their measured age (Moorbath, 1976). However, no limit of this kind can be placed on the age of the abundant large xenoliths of supracrustal rocks which they contain, apparently the remnants of a former greenstone belt.

In the Isua area to the northeast of Godthaab are found banded ironstones and other supracrustals evidently belonging to a greenstone belt sequence which is partly hidden by the ice cap, partly destroyed by plutonism. The ironstones yield a lead-isochron age of 3700 ± 70 m.y., almost certainly a date of metamorphism (Moorbath et al., 1973). A suite of boulders, probably of an acid tuff, from the Isua series gave essentially the same Rb-Sr age as the Amitsoq gneisses (Moorbath et al., 1975).

High-grade rocks of very similar age are found near Messina in the centre of the Limpopo Belt, southern Africa. Basic dykes gave two isochron ages of 3570 ± 100 and 3060 ± 80 m.y. and their host gneisses, the Sand River formation, are said to yield a 3780 ± 110 m.y. Rb-Sr isochron (Barton et al., 1977).

The only other comparable result is a 3700 m.y. isochron of uncertain significance obtained for the Montevideo gneisses of southwestern Minnesota by Goldich and Hedge (1975).

Slightly younger ages ($\sim$ 3400 m.y.) have been obtained from high-grade terrain in these and several other areas. In Rhodesia the Mushandike granite gave a 3430 ± 250 m.y. Rb-Sr isochron, and the Mashaba gneisses which it intrudes yield essentially the same result (Hickman, 1974; Hawkesworth et al., 1975). The Vikan gneisses in Northern Norway give a lead-lead isochron age of 3400 ± 70 m.y. (Taylor, 1975), in contrast to

[1] All ages have been recalculated where necessary with the internationally recommended decay constants (Steiger and Jäger, 1977).

their 2250 m.y. Rb-Sr age. In Minnesota, discordant zircons from the Montevideo and Morton gneisses indicate a 3500 m.y. event (Goldich et al., 1970).

4. Ancient Greenstone Belts

Slightly younger than the Isua supracrustals, but more accessible, and studied in much greater detail, is the greenstone belt which makes up the Barberton Mountain Land on the border between Swaziland and the Transvaal. The rocks of that belt are known as the Swaziland sequence, and have been described in detail by Viljoen and Viljoen (1969). They are subdivided as follows:

Moodies Group		Banded ironstones, sandstones, quartzites, conglomerates
Fig Tree Group		Greywackés, tuffs, ferruginous cherts
Onverwacht Group	Upper	Tholeiites, felsic lavas and tuffs, Cherts, minor shales
	Middle Marker Horizon	Chert, limestone and shale
	Lower	Ultramafic and basaltic komatiites
? Ancient Gneisses		Tonalitic gneisses with basic dykes

Because of its age and excellent state of preservation, this belt has some claim to be the type against which others may be compared. Anhaeusser's (1973) views on the significance of greenstone belts in crustal evolution are based upon it. Amonst extensive geochronological investigations [reviewed by Davies and Allsopp (1976) and Jahn and Shih (1974)] the following data stand out:

1. the "Middle Marker Horizon" separating lower and upper Onverwacht, is at least 3305 ± 20 m.y. old, from an Rb/Sr whole-rock isochron (Hurley et al., 1972)

2. the Kaap Valley granite, intruding the Moodies Group, is 3310 ± 40 m.y. old from U-Pb measurements, giving a younger limit for the whole of the Swaziland sequence

3. a mineral isochron from a basaltic komatiite in the Lower Onverwacht yields 3430 ± 200 m.y., which may reflect the approximate date of eruption

4. the Ancient Gneisses, possibly basement to the Barberton system, yielded a Rb-Sr isochron of 3300 ± 300 m.y.

These results illustrate some of the difficulties in dating greenstone belts. The Middle Marker isochron age is almost certainly a date of metamorphism. The mineral isochron on the komatiite could be close to a primary age, as could the isochron on the Ancient Gneisses, but both these results are imprecise because of the small dispersion

of Rb/Sr ratios of the samples, a rather common problem in other Archaean tonalites and monzonites. Thus, while we have a secure younger limit to the age of the Swaziland sequence, there exists neither a precise primary age nor a convincing older limit. The best guess is that it is about 3400 m.y. old, and it is to be hoped that Sm-Nd work will help to place it more precisely.

Besides the Isua (Greenland) and Barberton supracrustals, the existence of very old greenstone belts has been demonstrated in Rhodesia (Zimbabwe) and Western Australia. In Rhodesia the Selukwe belt is cut by the 3350 ± 60 m.y. (Rb-Sr) Mont d'Or granite (Moorbath et al., 1976), while a dacite from the Pilbara block of Western Australia yielded a U-Pb zircon age of 3450 ± 15 m.y. (Pidgeon, 1978). No doubt other greenstone belts will eventually be shown to have ages approaching 3500 m.y., and it must not be forgotten that very old high-grade rocks commonly contain remnants of preexisting greenstone belts. However, well-preserved supracrustal rocks of that age are in a minority; the large majority of greenstone belts is probably younger than about 3000 m.y.

5. The Archaean Since ca. 3000 m.y.a.

The presence of two or three ages of greenstone belts in the same craton lends a special interest to the Archaean of Rhodesia (Zimbabwe). The very old supracrustal rocks of Selukwe, mentioned above, and possibly equally old rocks in the Fort Victoria area, can be clearly distinguished from the Upper Greenstones of Belingwe which are bracketed by 2700 and 2900 m.y. granitoid rocks (Wilson et al., 1978). The Upper Greenstones at Belingwe unconformably overlie a Lower Greenstone succession, but it is not certain whether the Lower Greenstones also have a 2900 m.y. older limit. If they do, there is clearly a rather short time for formation of two supracrustal sequences together with the intervening erosional phase. Rb-Sr data from the Rhodesian greenstone belts does not at present help to resolve this question, because of its limited precision and its disputed interpretation (Jahn and Shih, 1974; Wilson et al., 1978), but it seems likely that many of the Rhodesian belts are younger than 3000 m.y.

In North America, except for the Labrador coast and perhaps also the Minnesota River Valley, intensive study of the Archaean has shown a great preponderance of events in the late Archaean, and has failed to reveal much significant isotopic history prior to 3000 m.y.a. (e.g., Green and Baadsgaard, 1971; Hanson et al., 1971). Similarly in India (Crawford, 1969), Equatorial Africa (Cahen et al., 1976) and southwestern Australia (Arriens, 1971) late Archaean history overwhelmingly dominates the isotopic record. Furthermore, even very old Archaean terrain has usually been affected by or coexists with important events in the 2500-3000 m.y. interval – for example, extensive granulite facies metamorphism in the Limpopo Belt and West Greenland, younger granites in the Barberton Mountain Land, and younger granites and greenstone belts in Rhodesia. Understandably, in the excitement of the search for very old rocks, there has been a tendency to neglect detailed study of later Archaean history; in view of the world-wide distribution of events in that time range it should be very rewarding to try to resolve in more detail the chronology of individual cratons, to look for world-wide

correlations, and to use precise geochronological data to throw light on the relationship between adjacent high-grade and low-grade terrains. However, success in such work will demand the closest possible coordination between field geology and geochronology.

References

Anhaeusser, C.R.: The Evolution of the Early Precambrian Crust of Southern Africa. Sutton and Windley, 1973, pp. 359-388

Anhaeusser, C.R., Mason, R., Viljoen, M.J., Viljoen, R.P.: A reappraisal of some aspects of Precambrian Shield Geology. Bull. Geol. Soc. Am. *80*, 2175-2200 (1968)

Arriens, P.A.: The Archaean Geochronology of Australia. Glover, 1971, pp. 11-23

Barton, J.M.: Rb-Sr isotopic systematics and chemistry of the 3.6 b.y. Hebron Gneiss, Labrador. Earth Planet. Sci. Lett. *27*, 427-435 (1975)

Barton, J.M., Fripp, R.E.P., Ryan, B.: Rb/Sr ages and geological setting of ancient dykes in the Sand River area, Limpopo Mobile Belt, South Africa. Nature (London) *267*, 487-490 (1977)

Bickle, M.J., Martin, A., Nisbet, E.G.: Basaltic and peridotitic komatiites and stromatolites above a basal unconformity in the Belingwe greenstone belt, Rhodesia. Earth Planet. Sci. Lett. *27*, 155-162 (1975)

Cahen, L., Delhal, J., Lavreau, J.: The Archaean of Equatorial Africa: A Review. Windley, 1976, pp. 489-510

Crawford, A.R.: Reconnaissance Rb-Sr dating of the Precambrian rocks of Southern Peninsular India. J. Geol. Soc. India *10*, 117-166 (1969)

Davies, R.D., Allsopp, H.L.: Strontium isotopic evidence relating to the Lower Precambrian granitic crust in Swaziland. Geology *4*, 553-556 (1976)

Dodson, M.H., Gledhill, A.R., Shackleton, R.M., Bell, K.: Age differences between Archaean cratons of Eastern and Southern Africa. Nature (London) *254*, 315-318 (1975)

Gebauer, D., Grünenfelder, M.: Rb-Sr whole-rock dating of late diagenetic to anchimetamorphic Palaeozoic sediments in southern France (Montagne Noire). Contrib. Mineral. Petrol. *47*, 113-130 (1974)

Geol. Soc. S. Afr., 1969. Spec. Pub. No. 2, Upper Mantle Project

Glikson, A.Y., Lambert, I.B.: Relations in space and time between major Precambrian Shield units: an interpretation of Western Australia data. Earth Planet. Sci. Lett. *20*, 395-403 (1973)

Glover, J.E. (ed.): Symposium on Archaean Rocks. Geol. Soc. Austr. Spec. Pub. No. 3 (1971)

Goldich, S.S., Hedge, C.E.: 3800 m.yr. granite gneisses in southwestern Minnesota. Nature (London) *252*, 467-468 (1975)

Goldich, S.S., Hedge, C.E., Stern, T.W.: Age of the Morton and Montevideo gneisses and related rocks, southwestern Minnesota. Bull. Geol. Soc. Am. *81*, 3671-3696 (1970)

Green, D.C., Baadsgaard, H.: Temporal evolution and petrogenesis of an Archaean crustal segment at Yellowknife, N.W.T., Canada. J. Petrol. *12*, 177-217 (1971)

Hamilton, P.J., O'Nions, R.K., Evensen, N.M.: Sm-Nd dating of Archaean basic and ultrabasic volcanics. Earth Planet. Sci. Lett. *36*, 263-268 (1977)

Hanson, G.N., Goldich, S.S., Arth, J.G., Yardley, D.H.: Age of the Early Precambrian Rocks of the Saganage Lake – Northern Light Lake Area, Ontario–Minnesota. Can. J. Earth Sec. *8*, 1110-1124 (1971)

Hawkesworth, C.J., Moorbath, S., O'Nions, R.K., Wilson, J.F.: Age relationships between greenstone belts and granites in the Rhodesian Archaean craton. Earth Planet. Sci. Lett. *25*, 251-262 (1975)

Hickman, M.H.: 3500 m.y. old granite in southern Africa. Nature (London) *257*, 295-296 (1974)
Hurley, P.M., Pinson, J.W.H., Nagy, B., Teska, T.U.: Ancient age of the Middle Marker horison, Onverwacht Group, Swaziland sequence, South Africa. Earth Planet. Sci. Lett. *14*, 360-366 (1972)
Hurst, R.W., Bridgewater, D., Collerson, K.D., Wetherill, G.W.: 3600 m.y. Rb-Sr ages from the very early Archaean gneisses from Saglek Bay, Labrador. Earth Planet Sci. Lett. *27*, 393-403 (1975)
Jahn, B.M., Condie, K.C.: On the age of the Rhodesian greenstone belts. Contrib. Mineral. Petrol. *57*, 317-330 (1976)
Jahn, B.M., Shih, C.Y.: On the age of the Onverwacht Group, Swaziland Sequence, South Africa. Geochim. Cosmochim. Acta *38*, 837-885 (1974)
Krogh, T.E., Davis, G.L.: Zircon U-Pb ages of Archaean metavolcanic rocks in the Canadian Shield. Carnegie Inst. Washington Yearb. *70*, 241-242 (1971)
Mason, R.G.: The Limpopo Belt, Southern Africa. Sutton and Windley, 1973, pp. 463-486
Moorbath, S.: Age and Isotope Constraints for the Evolution of Archaean Crust. Windley, 1976, pp. 351-360
Moorbath, S., O'Nions, R.K., Pankhurst, R.J.: Early Archaean age for the Isua Iron Formation, West Greenland. Nature (London) *245*, 138-139 (1973)
Moorbath, S., O'Nions, R.K., Pankhurst, R.J.: The evolution of early Precambrian crustal rocks at Isua, West Greenland – geochemical and isotopic evidence. Earth Planet. Sci. Lett. *27*, 229-239 (1975)
Moorbath, S., O'Nions, R.K., Pankhurst, R.J., Gale, N.H., McGregor, V.R.: Further rubidium-strontium age determinations of the very early Pre-Cambrian rocks of the Godthab district, West Greenland. Nature Phys. Sci. *240*, 78-82 (1972)
Moorbath, S., Welke, H., Gale, N.H.: The significance of lead isotope studies in ancient, high-grade metamorphic basement complexes as exemplified by the Lewisian rock of northwest Scotland. Earth Planet. Sci. Lett. *6*, 245-256 (1969)
Moorbath, S., Wilson, A.F., Cotterill, P.: Early Archaean age for the Sebakwian group at Selukwe, Rhodesia. Nature (London) *264*, 536-538 (1976)
Naidu, P.R.J.: A layered complex in Sittampundi, Madras State, India. Min. Soc. Am. Spec. Pap. *1*, 116-123 (1962)
Pidgeon, R.T.: 3450 m.y. old volcanics in the Archaean layered greenstone succession of the Pilbara Block, Western Australia. Earth Planet. Sci. Lett. *37*, 421-428 (1978)
Shackleton, R.M.: Shallow and Deep-Level Exposures of the Archaean Crust in India and Africa. Windley, 1976, pp. 317-322
Steiger, R.H., Jäger, E.: Earth Planet. Sci. Lett. *36*, 359-362 (1977)
Sutton, J., Windley, B.F. (eds.): Evolution of Precambrian rocks. Philos. Trans. R. Soc. *A273*, 315-581 (1973)
Taylor, P.N.: An early Precambrian age for migmatitic gneisses from Vikan i Bø, Vesterålen, North Norway. Earth Planet. Sci. Lett. *27*, 35-42 (1975)
Viljoen, M.J., Viljoen, R.D.: A collection of nine papers on the Barberton granite-greenstone belt. Geol. Soc. S. Afr. Spec. Publ. No. 2 (1969)
Wilson, J.F., Bickle, M.J., Hawkesworth, C.J., Martin, A., Nesbit, E.G., Orpen, J.L.: Granite-greenstone terrains of the Rhodesian Archaean craton. Nature (London) *271*, 23-27 (1978)
Windley, B.F. (ed.): The Early History of the Earth. London: Wiley, 1976
Windley, B.F.: The Evolving Continents. London: Wiley, 1977
Windley, B.F., Bridgewater, D.: The evolution of Archaean low and high-grade terrains. Glover, 1971, pp. 33-46

Geochronology of the Crystalline Rocks of the Schwarzwald

A. W. HOFMANN

The Schwarzwald is one of the Hercynian crystalline massifs of central Europe. Intrusive granites are known to postdate Devonian schists and to predate Permian and Triassic redbeds. Consequently the ages of most of the intrusives are well bracketed by stratigraphic evidence and the geologic time scale. However, no stratigraphic age could be assigned to the large core of preintrusive migmatitic gneisses and the different phases of their development, except that they predate some or all of the intrusive granites. Geochronological research has therefore concentrated on two main problems: (1) The measurement of precise absolute ages of the Hercynian granites in order to work out a detailed sequence of Hercynian events; (2) the determination of the absolute chronology and origin of the older gneisses. For a review of the geology of the region the reader is referred to Metz and Rein (1958).

One of the earliest efforts in K-Ar geochronology attempted to solve both problems (Gentner and Kley, 1958).Most of these measurements were made on whole-rock samples or granites and gneisses and yielded widely scattered results, which were interpreted by Mehnert (1958) as indicating an early Hercynian age (300 m.y.) for the last, most pervasive, anatectic event affecting the gneisses, and a Carboniferous age of 260 to 300 m.y. for the granites. It is now known that the age of the Carboniferous is greater than was believed at the time of Mehnert's publication, and that all the ages obtained in these measurements are too young.

More recent age measurements by Faul and Jäger (1963) and by the geochronology laboratories at Hannover and Heidelberg have yielded ages between 260 and 360 m.y. for the Hercynian granites and about 470 m.y. for the Pre-Hercynian gneisses. These results are based primarily on whole-rock Rb-Sr data and some additional mineral ages (K-Ar and Rb-Sr on micas, U-Pb on zircons).

A good survey of the earlier age determinations has been given by Brewer and Lippolt (1972), but most of the more detailed work has been published subsequently (e.g., Hofmann and Köhler, 1973; Brewer and Lippolt, 1974b; v. Drach and Lippolt, 1974; v. Drach et al., 1974; Bierwirth and Ackermann, 1974; Fehn and Hahn-Weinheimer, 1974; Leutwein and Sonet, 1974; Wendt et al., 1974; Müller-Sohnius et al., 1976; Todt, 1976).

The evidence for a Caledonian age of the pre-Hercynian gneisses rests in part on two whole-rock Rb-Sr isochrons (Hofmann and Köhler, 1973), one for highly anatectic diatexites, and one for preanatectic orthogneisses. The two ages are identical (within analytical error) at about 460 to 470 m.y., and Hofmann and Köhler concluded tentatively that the entire pre-Hercynian sequence of events, intrusion of orthogneisses, first anatexis, deformation, second anatexis, which has been worked out by Hoenes,

Mehnert and others and reviewed by Metz and Rein (1958), must have taken place within less than 40 m.y. Zircon U-Pb measurements on a diatexite sample by Steiger et al. (1972) yielded a concordia intercept of 480 ± 20 m.y., and thus confirmed the Caledonian age, but showed the presence of a much older, probably detrital zircon fraction. The conclusions of Hofmann and Köhler rest critically on the assumption that the orthogneiss isochron dates the event of the original igneous intrusion. The evidence for this is circumstantial, and should be tested with additional measurements, especially U-Pb ages of zircons. Some additional age measurements were made by Leutwein and Sonnet (1974) who give a whole rock isochron age of 441 m.y. for six gneiss samples from widely scattered locations, but state that "there can be no doubt that they are Precambrian in age." Unfortunately, these authors give no evidence in support of this conclusion, and until such evidence is presented, the Precambrian age of the gneisses should probably be considered to be an item of geologic folklore that may or may not have some kernel of truth.

At present, the best available evidence indicates that all the gneisses were formed during a Caledonian event or series of events and that, except for the presence of some Precambrian detrital material (see zircon data of Steiger et al., 1972), these rocks had a relatively short crustal history prior to Caledonian time in this region.

During Hercynian time, large volumes of granitic magma were formed. Some of the granite bodies appear transitional in character between the older anatectic gneisses and later intrusive plutons. However, the bulk of the granitic material shows clearly intrusive relations. Emmermann (1977) reviewed the field relations, petrography, and trace element geochemistry of these granites. He showed that there was an early evolution from small plutons (now deformed) of two-mica granite to large bodies of biotite granite, and that this evolution is best explained by a process of progressive anatexis. The main phase of biotite granite production was followed by a late phase of highly differentiated two-mica granites. The late phase is distinguished from the main phase by a marked break in trace-element abundance trends, and the two phases are therefore not comagmatic (Emmermann, 1977).

Brewer and Lippolt (1974a) have proposed a somewhat different petrogenetic model for the region, based on the Rb-Sr systematics of the granites and gneisses. In this model, the Hercynian granite magmas are formed by crustal anatexis of the Caledonian crust, as was also discussed by Hofmann and Köhler (1973). In addition, however, Brewer and Lippolt concluded that "segregation of the partial melts from their solid residue as well as concomitant differentiation of the melts was a direct result of tectonism which occurred 330 m.y. ago. Further, the large magma chambers remained stable for tens of millions of years, until about 260 m.y. ago." These conclusions are based on two predominant trend lines on a Sr isotope evolution diagram (initial $^{87}Sr/^{86}Sr$ ratio versus age), one corresponding to a low Rb/Sr ratio (older gneisses and oldest Hercynain granites) and one corresponding to a much higher Rb/Sr ratio (post-tectonic Hercynian granites). The existence of these trend lines depends on the ages and initial Sr isotope ratios of the various plutons. The change of slope (low Rb/Sr ratio to high Rb/Sr ratio) is thought to be caused by fractional crystallization in the proposed large magma chambers, which in turn retain magma for as long as 70 m.y. These conclusions are of considerable geological and geophysical interest, especially

with regard to the postulated long lifetime of large magma chambers containing granitic magma. In view of the fact that such large magma chambers are mechanically unstable (because of their relatively low density) and must therefore have a limited lifetime, it seems reasonable to ask if the isotopic ages indeed require such a long duration of Hercynian magmatic activity. For this purpose, some of the age determinations, especially those of the oldest and the youngest Hercynian granites will be examined in more detail.

1. Pretectonic and Syntectonic Granites

These include the Klemmbach-Schlächtenhaus, Rand, and Hauenstein Granites. Brewer and Lippolt (1974a) assigned 363 ± 19, 363, and 329 ± 10 m.y. to these three plutons, respectively. Thus, at least the first two of these appear to be significantly older than the main phase of Hercynian magmatism which began about 330 m.y. ago (see below). However, examination of the actual data given by Brewer and Lippolt (1974b) shows that the data for the Klemmbach-Schlächtenhaus do not form an unambiguous isochron (because of considerable data scatter) so that age values had to be assigned by arbitrarily selecting apparently colinear points and omitting others. In such a case, the age interpretation is somewhat uncertain, and the assigned error of the age is meaningless. Because the age of the Rand Granite (363 m.y.) is derived from a "reference isochron based on the age of the Klemmbach-Schlächtenhaus Granite" (Brewer and Lippolt, 1974a), this age is even more uncertain. Therefore, the evidence that "the minimum age of formation of the magmas" (Brewer and Lippolt, 1974a) is 360 m.y., is not persuasive.

2. Posttectonic Granites

These include Malsburg, Bärhalde-Schluchsee, Forbach and Seebach granites, which according to Brewer and Lippolt (1974a) define the second, steeper trend line, with ages ranging from 313 ± 5 to 270 ± 19 m.y. The ages assigned to several of these granites are also open to question. The best example is the Bärhalde Granite and the closely related Schluchsee Granite, the age of which has been the subject of numerous publications (Hahn-Weinheimer et al., 1963; Brooks et al., 1968; Hahn-Weinheimer and Raschka, 1969; Wendt et al., 1970; Leutwein and Sonet, 1974; Fehn and Hahn-Weinheimer, 1974; Wendt et al., 1974; Bierwirth and Ackermann, 1974; Müller-Sohnius et al., 1976). The ages assigned on the basis of these investigations range from 218 to 325 m.y. Most of the more recent determinations indicate intrusion ages greater than 280 m.y., but the disagreement is still substantially greater than the assigned analytical errors. For example, Brooks et al. (1968) found apparently well-fitted whole rock isochrons of 284 ± 6 and 315 ± 10 m.y. for Bärhalde and Schluchsee granites, respectively. More recently, and using substantially improved analytical precision, Müller-Sohnius et al. (1976) found that both granites fit a single whole-rock isochron

of 305 ± 4 m.y. Yet this apparently excellent isochron age is still lower than K-Ar and Rb-Sr ages of micas, determined by Wendt et al. (1970) (e.g., four Bärhalde muscovites of 322 ± 2 m.y. and two Schluchsee biotites of 325 ± 5 m.y.) and Bierwirth and Ackermann (1974; Bärhalde biotite and muscovite of 313 m.y., no error assigned). Until these comparatively old mica ages can somehow be shown to be incorrect, the case for the Bärhalde Granite to be significantly younger than 320 m.y. remains unconvincing. Also, because of the relatively large number of laboratories involved in these age measurements, it is at present not clear how much of these discrepancies are the result of some sort of laboratory bias, and how much is contained in the samples themselves. Sample-related causes might be found in alteration due to late hydrothermal activity or even later weathering. Another possibility is that the whole-rock isochrons are systematically biased by preferential wall rock contamination of the samples with relatively high Rb/Sr ratios (and correspondingly low Sr concentrations). The body is strongly zoned, and the highest Rb/Sr ratios are found exclusively near the SW margin of the pluton (see for example Müller-Sohnius et al., 1976, for a sketch map and additional references). Sr contamination near the margin of an intrusive body (although on a much smaller scale) was demonstrated by Cliff (1971). Depending on the isotopic composition of the contaminating Sr, the resulting apparent isochron could be either too old or too young.

Another relatively young granite used in the petrogenetic model of Brewer and Lippolt is the Seebach Granite with an age of 270 ± 19 m.y. Yet, only one of the four samples analyzed by v. Drach et al. (1974) does not coincide with the isochron of 293 m.y. for the Forbach Granite, and v. Drach et al. concluded that the ages of the two granites are not significantly different at the two-sigma level. Even the age of the Forbach Granite itself (293 ± 1 m.y.) is not completely unambiguous, because one point (of a total of seven) does not lie on the isochron, although this discrepancy may be ascribed to fact that this sample was taken from the marginal zone of the granite and may have been contaminated by Sr derived from the country rock.

The Malsburg Granite was assigned an age of 310 ± 5 m.y. on the basis of a four-point Rb/Sr isochron (with a fifth point quite far off the line, see Wendt et al., 1970). More recently, Todt (1976) determined a U-Pb age of 328 ± 6 m.y. on the basis of the concordia intercept of slightly discordant zircons. This discrepancy may be in part the result of the uncertainty in the Rb decay constant ($\lambda = 1.47 \times 10^{-11} yr^{-1}$ used throughout this paper for ease of comparison with published data). Still, it would appear that the rather poorly defined Rb-Sr isochron gives an age that is slightly too young.

On the basis of the above discussion it could be argued that all the granites comprising Brewer and Lippolt's posttectonic trend line have indistinguishable intrusion ages, if the various imperfections in the individual isochrons and the other discrepancies are taken into account. If that is indeed the case, the trend line itself no longer exists, and the necessity for long-lived, large magma chambers disappears. It should be remembered, however, that this is a burden-of-proof argument and the ages and trend lines used by Brewer and Lippolt may yet be verified by additional measurements. Other results include a K-Ar of 332 m.y. for a biotite-quartz "isochron" (Bierwirth and Ackermann, 1974) and a Rb-Sr age of 313 ± 6 m.y. for biotite (Venzlaff, 1971) for the Albtal Granite and eight mica ages (K-Ar and Rb-Sr) between 300

and 320 m.y. from the granites of Triberg, Halbmeil, Mambach, and Sasbach-Walden (Faul and Jäger, 1963). In addition, Leutwein and Sonet (1974) have published a large number of Rb-Sr ages for the crystalline rocks of the Schwarzwald, the most remarkable of which is a whole-rock isochron of 427 ± 10 m.y. for the Hercynian Lenzkirch Granite. If correct, this age would extend the time span of Hercynian granite formation proposed by Brewer and Lippolt by another 60 m.y. Leutwein and Sonet do not explain their analytical techniques. For example, it is not clear whether they determined the Rb and Sr concentrations by isotope dilution or by some other technique, and neither their tables nor their isochron diagrams give any indication of the error in the Rb/Sr ratios. Other aspects of their presentation are also very difficult to assess: their Figure 5 shows a 400 m.y. isochron through more than ten whole rock points. The figure legend describes these as gneissic granites of the Klemmbach type, but several of the sample numbers do not correspond to the numbers given in their Table 3, and the age of 400 m.y. is never mentioned in the text. In view of these problems it is very difficult to assess the results given by these authors.

To summarize the current state of knowledge about the intrusion history of the Hercynian granites, it can be said with confidence that many of them intruded during the time interval of 330 to about 300 m.y. ago. A few of the granites, especially the Forbach and Seebach Granites, may be younger, while a few others may be older than this time interval, but the discordances between different methods of age determination and between different laboratories are such that we cannot be completely sure that any part of the intrusion sequence has been resolved by isotopic age determinations. There is at present no assurance that the vexing problems of interpretation presented by the large amount of age data on the Bärhalde Granite will not also appear with respect to other intrusives, once a sufficiently large body of data is available.

The above conclusion is intended as advice for caution in interpreting isotopic age measurements: it appears that it is relatively easy to determine approximate intrusion ages, but very difficult to obtain precise ages. The example of the Bärhalde Granite illustrates the fact (which is often recognized by the geochronologist, but not always acknowledged in the geological application of the results) that the actual ("geological") and laboratory related) errors in age determinations can be much greater than the apparent analytical errors (and the formal statistical errors of isochrons), even in the simplest of all geological settings, that of a posttectonic intrusive granite.

At present, the best method to gain more confidence in precise age determinations would be to demonstrate concordant results obtained by different methods on the same samples and the same methods on different samples. Otherwise, the data base of such interesting and important petrogenetic models as that of Brewer and Lippolt must remain in doubt.

3. Summary of the Geological History of the Crystalline Massif

Limited whole-rock Rb-Sr data and U-Pb data on zircons indicate that the pre-Hercynian were formed some time between 500 and 450 m.y. ago. No age resolution has been obtained for the complex series of two anatectic events and intervening deforma-

tion, as worked out by geological studies. Extensive Rb-Sr, and more limited K-Ar and U-Pb studies indicate voluminous Hercynian magmatism some time between 330 and 300 m.y. ago in the southern Schwarzwald and about 290 m.y. ago in the northern Schwarzwald, with possible earlier intrusions at 360 m.y. and later intrusions to about 260 m.y. A sufficient amount of conflicting evidence leads to the conclusion that the detailed chronology of all these granites remains unresolved. However, nearly all of the plutons have initial $^{87}Sr/^{86}Sr$ ratios typical of crustal-derived rocks ($\geqslant 0.708$), and they could therefore have been derived by anatexis from the Caledonian-age gneisses.

References

Bierwirth, G., Ackermann, W.: Initial argon diagrams of some granites of Eastern Bavaria and the Black Forest using the mineral quartz. Neues Jahrb. Mineral. Monatsh. 1974, *4*, 49-62 (1974)

Brewer, M.S., Lippolt, H.J.: Isotopische Altersbestimmungen an Schwarzwaldgesteinen, eine Übersicht. Fortschr. Mineral. *50*, Beih. 2, 42-50 (1972)

Brewer, M.S., Lippolt, H.J.: Petrogenesis of basement rocks of the Upper Rhine region elucidated by Rb-Sr systematics. Contrib. Mineral. Petrol. *45*, 123-141 (1974a)

Brewer, M.S., Lippolt, H.J.: Rb-Sr age determinations of pre-tectonic granites from the southern Schwarzwald, SW Germany. Neues Jahrb. Mineral. Monatsh. 1974, 28-41 (1974b)

Brooks, C., Wendt, I., Harre, W.: A two error regression treatment and its application to Rb-Sr and initial $^{87}Sr/^{86}Sr$ ratios of younger Variscan granitic rocks from the Schwarzwald massif, southwest Germany. J. Geophys. Res. *73*, 6071-6084 (1968)

Cliff, R.A.: Strontium isotope distribution in a regionally metamorphosed granite from the Zentralgneiss, South East Tauernfenster, Austria. Contrib. Mineral. Petrol. *32*, 274-288 (1971)

Emmermann, R.: A petrogenetic model for the origin and evolution of the Hercynian granite series of the Schwarzwald. Neues Jahrb. Mineral. Abh. *128*, 219-253 (1977)

Faul, H., Jäger, E.: Ages of some granitic rocks in the Vosges, the Schwarzwald, and the Massif Central. J. Geophys. Res. *68*, 3293-3300 (1963)

Fehn, U., Hahn-Weinheimer, P.: Rb-Sr ages of two epizonal granites of the southern Schwarzwald, Germany. J. Geol. *82*, 514-519 (1974)

Gentner, W., Kley, W.: Argonbestimmungen an Kaliummineralien V. Geochim. Cosmochim. Acta *14*, 98-104 (1958)

Hahn-Weinheimer, P., Johanning, H., Schütze, W.: Altersbestimmungen am Bärhalde-Granit nach der Rb-Sr Methode. Neues Jahrb. Mineral. Monatsh. *7*, 157-166 (1963)

Hahn-Weinheimer, P., Raschka, H.: Verteilung von Strontiumisotopen, Kalium und Rubidium in Graniten und deren Mineralphasen aus Südschwarzwald und Vogesen. Vortragsref. Tagung der Deutschen Geol. Ges., Hannover, 1969, pp. 11-16

Hofmann, A., Köhler, H.: Whole rock Rb-Sr ages of anatectic gneisses from the Schwarzwald, SW Germany. Neues Jahrb. Mineral. Abh. *119*, 163-187 (1973)

Leutwein, F., Sonet, J.: Geochronological studies in the southern Black Forest. Neues Jahrb. Mineral. Abh. *121*, 254-271 (1974)

Mehnert, K.R.: Argonbestimmungen an Kaliummineralien VI. Geochim. Cosmochim. Acta *14*, 105-113 (1958)

Metz, R., Rein, G.: Erläuterungen zur geologisch-petrographischen Übersichtskarte des Südschwarzwaldes 1 : 50,000. Lahr/Schwarzwald: Moritz Schauenburg 1958

Müller-Sohnius, D., Propach, G., Köhler, H.: Contemporaneous intrusion of the Bärhalde and Schluchsee granite. Neues Jahrb. Mineral. Abh. *127*, 174-186 (1976)
Steiger, R.H., Bär, M.T., Büsch, W.: The zircon age of an anatectic rock in the central Schwarzwald. Fortschr. Mineral. *50*, 131-132 (1972)
Todt, W.: Zircon-U/Pb age of the Malsburg granite from the Black Forest, Germany. Neues Jahrb. Mineral. Monatsh. 1976, 532-544 (1976)
Venzlaff, V.: Altersbestimmungen nach der Rb/Sr-Methode an Biotiten aus Gesteinen des Schwarzwaldes. Z. Naturforsch. *26a*, 1372-1373 (1971)
Von Drach, V., Lippolt, H.J.: Herkunft eines dioritischen Gesteins des Nordschwarzwalds, gedeutet aufgrund seiner K-Rb-Sr-Eigenschaften. Neues Jahrb. Mineral. Abh. *122*, 229-245 (1974)
Von Drach, V., Lippolt, H.J., Brewer, M.S.: Rb-Sr age determinations of granites from the Northern Schwarzwald, Germany. Neues Jahrb. Mineral. Abh. *123*, 38-62 (1974)
Wendt, I., Lenz, H., Harre, W., Schoell, M.: Total rock and mineral ages of granites from the southern Schwarzwald, Germany. Eclogae Geol. Helv. *63*, 365-370 (1970)
Wendt, I., Lenz, H., Höhndorf, A.: Das Alter des Bärhalde-Granites (Schwarzwald) und der Uranlagerstätte Menzenschwand. Geol. Jahrb. *E2*, 131-143 (1974)

Evolution of the European Continent

E. JÄGER

The continent of Europe has been intensively studied geochronologically. Many age determinations have been concentrated in a rather small area. The late Paleozoic history of the continental crust is well determined in many regions; however, early crustal formation is still a matter of dispute.

The evolutional history of the Schwarzwald, as described in the chapter by Hofmann, is typical of the development of the whole continent. The oldest ages found so far are U-Pb ages on paragneiss zircons, most probably detrital. Actually, when dating paragneiss zircons of central and western Europe, Precambrian ages up to 2700 m.y. are found. The question now arises whether these ages date the primary zircon formation in place, or whether the zircons originate from a nearby Precambrian terrain. The latter would indicate transportation of these zircons into the sedimentary basin and Rb-Sr total rock dating on paragneisses rather favors the second case.

In several regions attempts have been made to date the sedimentation by the Rb-Sr method (see description in the chapter *The Rb-Sr Method*). Interpretation of such data is not quite certain, and a small number of sedimentation ages would yield little information. But in many regions of Europe, e.g., the Moldanubian, the Schwarzwald, the Massif Central and the Alps, such age determinations have been made; without exception, the same result has been found, i.e., a maximum age of 900 m.y., or even less. Although this seems to contradict the older Precambrian zircon data, it in fact does not: zircons date the primary magma formation, not sedimentation, as analyzed with the Rb-Sr method. The following evolutional model would fit the U-Pb and the Rb-Sr data. In addition it does not contradict geologic facts.

In the late Proterozoic era, the paragneisses of the European continent were deposited as ocean sediments. This ocean basin is the source of the sedimentary rocks of much of the European continent: southern and south western Europe, including Italy, the Iberian Peninsula, and France, with the exception of the Precambrian terrain in northern Brittany and Normandy (see Cogné, 1972). Central Europe, including Germany and the Alps also originated from the "European ocean." Moldanubian crystalline rocks belong to the area of the European ocean, whereas the Moravian zone seems to represent the Precambrian crust (see Dudek and Melkova, 1975). Intensive movement during Grenville time, around 1000 m.y. ago, could have opened the European ocean basin.

This evolutional model seems to contradict geology. Especially in the Moldanubian basement and the French Massif Central, Precambrian rock formation with granulite metamorphism has been postulated. By Rb-Sr dating, Arnold and Scharbert (1973), showed that the Moldanubian granulite formation is not Precambrian in age, but is definitely younger, in the range of 400-500 m.y. The high-grade metamorphic rocks

must be considered as metamorphosed upper Proterozoic to Paleozoic sediments and magmatic rocks. To date, there is no single age result and no geologic fact that can disprove the proposed evolutional model. Nowhere in central and western Europe is the crystalline basement overlain by the late Precambrian sediments in undisturbed transgression. Sediments and crystalline rocks in every case are separated by tectonic lines. In the past few years, since this model was proposed [see Jäger (1977) and Vidal (1977)], many age results and new geologic evidence seem to support this idea.

Originally the sedimentary sequence could have had a thickness of around 6 km, approximately the thickness of the Barrandian sediments. Assuming a sedimentation time of 300 m.y., this would give a sedimentation rate of about 20 mm/1000 y. This is the actual sedimentation rate found in the eastern Mediterranean basin.

Consolidation of sediment began around 700 m.y. ago with magmatic rock formation in several places in Europe. Since then there has always been some geologic activity in Europe, although we differentiate between more active and quiet periods. The first climax of magmatic activity was reached in Caledonian time, 500-400 m.y. ago. Once more, the intensive Hercynian granite formation (360-270 m.y. ago), and in some areas intensive metamorphism, consolidated the continental crust. By addition of magmatic material and especially by tectonic overthrusting in Hercynian time, the continental crust reached its present normal thickness.

The kinetic model of continent formation seems rather complex. Small continental blocks seem to have their own distinct tectonic history. The origin of crustal material, especially in high grade metamorphic rocks, remains to be explained. Geochronology can add much to the understanding of the material evolution. In the Schwarzwald an

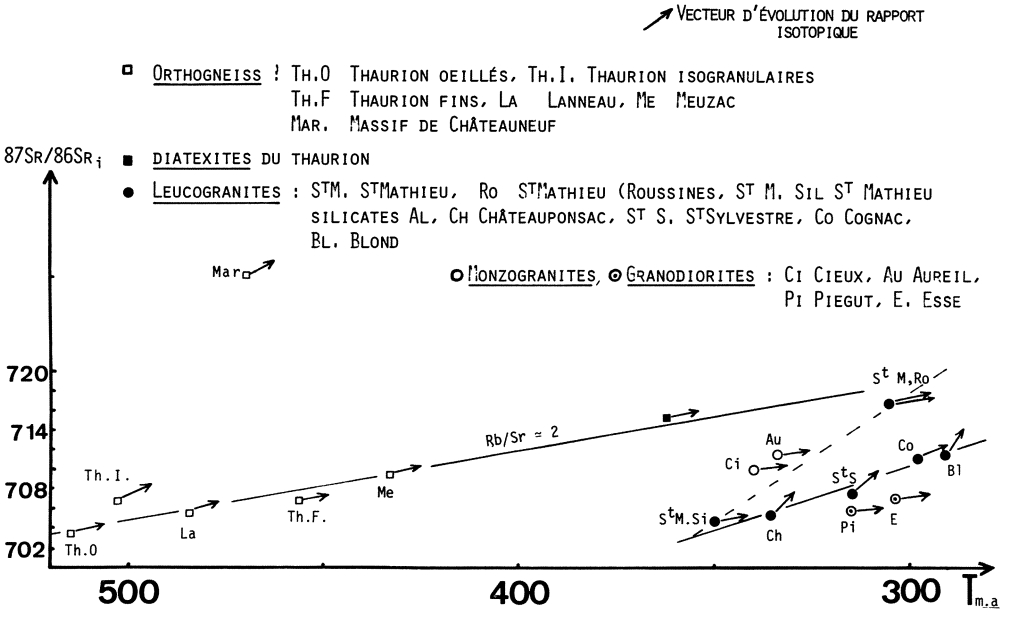

Fig. 1. Evolution of the initial strontium $^{87}Sr/^{86}Sr_i$ for orthogneisses and granites from the Nord Limousin, French Massif Central. [From Duthou (1977)]

important attempt has been made by Brewer and Lippolt (1974) and Emmermann et al. (1975), to explain the Hercynian granite formation (see the discussion by Hofmann). In the Limousin, the northwestern part of the French Massif Central, Duthou (1977) made a similar study on orthogneisses and granites. Figure 1 summarizes the Rb-Sr results of Duthou. Each point in the Sr-evolution diagram represents a Rb-Sr whole rock isochron, the age plotted against the initial $^{87}Sr/^{86}Sr$ ratio. Arrows indicate the growth of this ratio with time, according to the Rb-Sr ratio of the rock. It is very interesting that with repeated magma formation of the orthogneisses, the Rb/Sr ratio has remained constant, very similar to the host material, as indicated by the line Rb/Sr = 2. All these orthogneisses excluding the Hercynian granites seem to be related in their origin. The Hercynian granites represent a new rock association, the low initial $^{87}Sr/^{86}Sr$ ratios indicating the addition of material from a more basic source, probably mantle material. The geologic explanation of the orthogneiss data would be repeated crustal melting, without strong fractionation, but rather complete melting. Could such repeated crustal melting be caused by "moving hot spots? "

The contributions of Brewer and Lippolt (1974) and Duthou (1977) demonstrate that even the magmatic orthogneiss and granite formation require detailed study. They also show how much geology benefits from such study.

References

Arnold, A., Scharbert, H.G.: Rb-Sr-Altersbestimmungen an Granuliten der südlichen Böhmischen Masse in Österreich. Schweiz. Min. Petr. Mitt. *53*, 61-78 (1973)

Brewer, M.S., Lippolt, H.J.: Petrogenesis of basement rocks of the Upper Rhine region elucidated by rubidium-strontium systematics. Contrib. Mineral. Petrol. *45*, 123-141 (1974)

Cogné, J.: Le Briovérien et le cycle orogénique cadomien dans le cadre des orogènes fini-précambriens. Coll. Int. CNRS (Paris) *192*, 193-218 (1972)

Dudek, A., Melkova, J.: Radiometric age determination in the crystalline basement of the Carpathian Foredeep and of the Moravian Flysch. Bull. Geol. Survey Prague *50*, 257-264 (1975)

Duthou, J.L.: Chronologie Rb-Sr et géochimie des granitoides d'un segment de la chaine Varisque, relations avec le metamorphisme: Le Nord Limousin, Massif Central Français. Ann. Scient. Univers. de Clermont *63*, Geol. Min. 30. Fasc. (1977)

Emmermann, R., Daieva, L., Schneider, J.: Petrologic significance of rare earths distribution in granites. Contrib. Mineral. Petrol. *52*, 267-283 (1975)

Jäger, E.: The evolution of the Central and West European continent. La chaine varisque d'europe moyenne et occidentale. Paris: éd. CNRS, 1977

Vidal, Ph.: Limitations isotopiques à l'âge et à l'évolution de la croûte continentale en Europe moyenne et occidentale. Ca chaîne varisque d'europe moyenne et occidentale. Paris: éd. CNRS, 1977

Thermal Models of the Central Alps

S. P. CLARK, JR.

The pioneer work of Birch (1950) on the interpretation of heat-flow measurements in mountain ranges that are still geologically active first revealed the close relationship between the value of heat flow observed at the surface and recent uplift and denudation. The connection between these seemingly unrelated quantities can be visualized if one realizes that rock moving towards the surface (as it does when undergoing uplift and denudation) carries the isothermal surfaces upwards. Since the surface of the ground is essentially at a constant temperature, denudation tends to steepen the near-surface geothermal gradient.

The usual objective of heat-flow studies is to determine the long-term, equilibrium heat flow from deep in the earth. Uplift and denudation disturb this quantity. Traditionally this disturbance was removed by a correction analogous to the correction for another disturbance caused by nearby topographic irregularities. The possibility of reversing the argument and using heat-flow observations to give information about uplift and denudation was precluded by the fact that the undisturbed heat flow is not a priori known.

Since about the mid-1960's our knowledge of alpine tectonics has been expanded greatly by the extensive program of measurements of mineral ages carried out principally at Bern in Professor Jäger's laboratory (Jäger et al., 1967). These data show that, in the Central Alps, the ages of the micas, and especially the biotites, produced by alpine metamorphism show strong regional correlations. The interpretation of these results is that the ages do not date the climax of the alpine metamorphism, but rather they record the time at which the micas had cooled sufficiently to permit retention of radiogenic daughter products. That is, they represent cooling ages. The simplest method of cooling a metamorphic terrane is to transport the rocks to shallow depths by uplift and denudation.

This interpretation of the geochronological data does not by itself contain enough information to yield estimates of the rates of uplift and denudation. Although it is a direct measurement of the time at which loss of radiogenic daughters ceased, it does not reveal the depth at which the closure temperature was reached. The information supplied by the age determinations is incomplete, as is the information supplied by heat flow. But by combining the two sets of data through a thermal model of a mountain chain, it proves possible to set limits to the rates of uplift and denudation.

The model is constructed in the following way. Rates of uplift and denudation are taken to be the same and independent of position and time. The "initial" temperature at the beginning of uplift is assumed to be a simple function of depth, having a functional form chosen for mathematical convenience. The thermal properties of the crust are

taken to be those deduced from laboratory measurements on common crustal rocks. The loss of radiogenic daughters is assumed to be an "on-off" process. That is, loss is complete at temperatures above a critical closure temperature, and zero at lower temperatures. For further discussion of the model and evaluation of the parameters involved, see Clark and Jäger (1969) and the Appendix.

The computational procedure consists of assuming an initial temperature distribution and then finding, by trial and error, that rate of uplift (= rate of denudation) that locates the closure isotherm at just the depth given by the rate of uplift multiplied by the cooling age of the mineral. The heat flow observed at the surface at the present time does not enter explicitly. Rather it emerges as a consequence of the model. Only those ranges of values of the various parameters, and the resulting rates of uplift that lead to the correct values of heat flow can be accepted.

The model presented by Clark and Jäger (1969) contains some obvious oversimplifications. The first is the assumption that the rate of uplift is uniform with respect to position and time. In fact, it is the observation that the rate differs in different places that led to the construction of the thermal model. Further work on cooling ages of muscovite (closure temperature $\sim$ 500°C for Rb-Sr, 350°C for K-Ar) and apatite ($\sim$ 120°C for fission tracks), as well as biotite ($\sim$ 300°C for both Rb-Sr and K-Ar), has shown that the rate varies with time as well (Wagner et al., 1977). Unfortunately complicating the model by introducing nonuniform rates of uplift means that all hope of treating it analytically must be abandoned. It seems unwise to undertake an elaborate numerical analysis of the problem until we can be assured that the geochronological program is virtually complete.

A second simplifying assumption is easier to improve. Clark and Jäger (1969) assumed that radioactive heat generation (which is an integral part of the model) was uniformly distributed within the earth. It has been known since the beginning of this century that a shell of rock about 25 km in thickness, with radioactive heat generation characteristic of typical surficial rocks, could supply all of the heat flow observed at the surface. This observation implies that radioactivity must decrease markedly with depth, a conclusion that is entirely consistent with what is now known of the petrology of the lower crust and the mantle. Ingersoll and Zobel (1913) were apparently the first to suggest that the indicated decrease in heat generation with depth could conveniently be represented mathematically by a decaying exponential function. They developed solutions to some simple problems employing the exponential distribution. Slichter (1941) criticized the exponential law on the grounds that other distributions with qualitatively similar shapes but different mathematical formulations were more convenient to manipulate. On the other hand Jeffreys (1952, p. 292; 1976, p. 413) endorsed the exponential distribution.

Originally there was no particular geophysical reason to prefer the exponential distribution to any other with the same qualitative characteristics. All distributions that decreased rather sharply with increasing depth were equally satisfactory. An argument that distinctly favors the exponential distribution was given by Lachenbruch (1968). It is based on the observation, first noted by Birch et al. (1968), that heat flow is commonly a linear function of local heat generation at the surface. Lachenbruch showed that for this linear relation to survive differential erosion, the exponential distribution must hold.

Adopting the exponential distribution of radioactive heat generation introduces a new parameter into the problem. It is the scale height of the radioactive distribution, that is, the vertical distance through which the heat generation decreases by a factor 1/e. Lachenbruch (1968) and Birch et al. (1968) estimated it to be 10 and 6 km respectively, based on heat-flow observations in the U.S. Rybach and Labhart (1973) give about 4 km for the scale height in the Rotondo granite (Gotthard Massif) and the Mont Blanc granite. This number is based on measurements of radioactivity at various horizontal distances from the contact. The authors, however, present an argument suggesting that the horizontal and vertical variations are essentially the same. The general magnitude of these values is confirmed by a combination of measurements of radioactivity and detailed structural studies in the Eastern Alps (Hawkesworth, 1974). Thus we may take the scale height of the radioactivity to be in the range of 5 to 10 km.

The new solution, incorporating the exponential decrease in heat generation with depth, is given in the Appendix. Some results of its application to the geochronological and heat-flow data from the Gotthard, Simplon, and Tauern tunnels are compared with the earlier study by Clark and Jäger (1969) in Table 1. The new data are in essential agreement with the older ones, but they have a narrower range. This latter feature may simply result from the fact that a smaller number of models was examined in the present study, although the experience gained in the earlier work was used to produce as wide a range of rates of uplift as possible.

Table 1. Range of results for uplift, mm/yr

	Gotthard	Simplon	Tauern
Clark and Jäger	0.3 -0.8	0.3-1.1	0.3-0.8
Present	0.4-0.7	0.4- [a]	0.6-0.8

[a] None of the models giving rapid uplift in the Simplon yielded the correct heat flow.

A second feature of the models is that the radioactive heat generation at the initial surface, prior to the onset of denudation, is required to be very high in some cases. It ranges up to about 35×10^{-13} cal/cm^3 s, corresponding nominally to a uranium content of 26 ppm in the surficial rocks. This value is too high to be geochemically reasonable. It is, however, a purely formal consequence of the model that should not acutally be expected to occur. The exponential distribution of radioactivity in the crust is presumably due to high-temperature processes (igneous, metamorphic, hydrothermal, or some combination thereof) (Lachenbruch, 1968; Turcotte and Oxburgh, 1972), and there is no reason to suppose that it exists in rocks that have never been deeply buried and subjected to high temperatures. Besides, these highly radioactive rocks are the first to be removed by erosion. They have virtually no influence either on the thermal histories of the rocks surviving today or on the present heat flow. By the time the closure temperature of the micas was attained, the surficial radioactivity had fallen to much lower values corresponding to geochemically acceptable uranium concentrations of a few ppm.

In the present study no satisfactory upper limit for the rate of denudation in the Simplon tunnel could be found. This may be due to the fact that the actual denudation rate is strongly time-dependent, increasing markedly in the last 2.6 m.y. (Wagner et al., 1977). Such a pattern vitiates the assumption of the model that uplift was uniform in time. Finally, Cliff et al. (1971) have criticized the application of the model to the Tauern tunnel on the grounds that the initial temperatures were more complicated than assumed, and mechanisms of heat transfer other than conduction were important. If these objections are valid, the model should not be applied to the Eastern Alps without modification.

Acknowledgement. This work was supported by the National Science Foundation under Grant GA-40495.

References

Abramowitz, M., Stegun, I.A.: Handbook of mathematical functions. Nat. Bur. Stand., Appl. Math. Series *55*, 1046 pp. (1964)

Birch, F.: Flow of heat in the Front Range, Colorado. Bull. Geol. Soc. Am. *34*, 567-630 (1950)

Birch, F., Roy, R.F., Decker, E.R.: Heat flow and thermal history in New England and New York. In: Studies of Appalachian Geology. Zen, E-an, White, W.S., Hadley, J.B., Thompson, J.B. (eds.). New York: Interscience, 1968, pp. 475

Clark, S.P., Jäger, E.: Denudation rate in the Alps from geochronologic and heat flow data. Am. J. Sci. *267*, 1143-1160 (1969)

Cliff, R.A., Norris, R.J., Oxburgh, E.R., Wright, R.C.: Structural, metamorphic, and geochronological studies in the Reisseck and southern Ankogel groups, the Eastern Alps. Jahrb. Geol. Bundesanst. *114*, 121-272 (1971)

Hawkesworth, C.J.: Vertical distribution of heat production in the basement of the Eastern Alps. Nature (London) *249*, 435-436 (1974)

Ingersoll, L.R., Zobel, O.J.: Mathematical Theory of Heat Conduction. Boston: Ginn and Co., 1913, pp. 171

Jäger, E., Niggli, E., Wenk, E.: Rb-Sr Alterbestimmungen an Glimmern der Zentralalpen. Beitr. Geol. Karte Schweiz, 67 pp. (1967)

Jeffreys, H.: The Earth, 3rd ed. Cambridge University Press, 1952, pp. 392

Jeffreys, H.: The Earth, 6th ed. Cambridge University Press, 1976, pp. 574

Lachenbruch, A.H.: Preliminary geothermal model of the Sierra Nevada. J. Geophys. Res. *73*, 6977-6989 (1968)

Rybach, L., Labhart, T.P.: Regelmäßigkeiten der Radioaktivitätsverteilung in granitischen Gesteinskörpern (Beispiele aus den Schweizer Alpen). Schweiz. Mineral. Petrogr. Mitt. *53*, 379-384 (1973)

Slichter, L.B.: Cooling of the Earth. Bull. Geol. Soc. Am. *52*, 561-600 (1941)

Turcotte, D.L., Oxburgh, E.R.: Statistical thermodynamic model for the distribution of crustal heat sources. Science *176*, 1021-1022 (1972)

Wagner, G.A., Reimer, G.M., Jäger, E.: Cooling ages derived by apatite fission-track, mica Rb-Sr and K-Ar dating: the uplift and cooling history of the Central Alps. Mem. Inst. Geol. Mineral. Univ. Padova *XXX*, 28 (1977)

Appendix

As before (Clark and Jäger, 1969), we consider the region $x > 0$ moving with velocity U. The sign of U is chosen so that it is positive for uplift, i.e., positive U implies motion in the negative x-direction. Erosion removes the material as it crosses the plane $x = 0$, so the surface of the ground remains at $x = 0$. Formerly the heat generation was assumed to be the same everywhere in $x > 0$; now we wish to consider it exponentially distributed with depth. Since the radioactivity moves with the moving material, the heat generation is equal to $A_0 \exp - c\,(x + Ut)$. In this expression A_0 is the heat generation at $x = 0$ when $t = 0$, and $1/c$ is the scale height.

This problem can be solved by the methods outlined by Clark and Jäger. The notation used is collected below.

x	depth
t	time
α	thermal diffusivity
K	thermal conductivity
U	rate of uplift
Q	present surface heat flow
T (x, t)	temperature
T_c	critical temperature above which daughter products are lost
t'	time, since the close of the metamorphic cycle, at which the loss of daughter products ceased
t_p	present time reckoned from the close of the metamorphic cycle
a, T_0, b	parameters giving the initial temperature distribution, $T(x,0) = a\,x + T_0\,(1-e^{-bx})$
A_0, c	parameters giving the distribution of radioactivity, $= A_0\,e^{-c(x + U\,t)}$
p	the parameter of the Laplace transform
erfc u	the complementary error function, $= \frac{2}{\sqrt{\pi}} \int_0^\infty e^{-y^2}\,dy$

The solution to this modified problem is:

$$T = a(x + Ut) - (A_0/Kc^2)e^{-c(x + Ut)} + a/2\,F(x,t) + T_0\,G(x, t) + T_0/2\,H(x, t; b) - (A_0/2Kc^2)\,H(x, t; c) + (A_0/2Kc^2)\,I(x, t)$$

where

$$F(x, t) = (x - Ut)e^{-Ux/\alpha}\,\mathrm{erfc}\,\frac{x - Ut}{\sqrt{4\alpha t}} - (x + Ut)\mathrm{erfc}\,\frac{x + Ut}{\sqrt{4\alpha t}}$$

$$G(x, t) = 1 - 1/2\left[e^{-Ux/\alpha}\,\mathrm{erfc}\,\frac{x - Ut}{\sqrt{4\alpha t}} + \mathrm{erfc}\,\frac{x + Ut}{\sqrt{4\alpha t}}\right]$$

$$H(x, t; b) = e^{(\alpha b - U)bt}\left[e^{(b - U/\alpha)x}\,\mathrm{erfc}\,\frac{2\alpha bt + x - Ut}{\sqrt{4\alpha t}} - e^{-bx}\,\mathrm{erfc}\,\frac{2\alpha bt - x - Ut}{\sqrt{4\alpha t}}\right]$$

$$I(x, t) = e^{-U(ct + x/2\alpha)}\left[e^{-i\sqrt{Uc/\alpha - U^2/4\alpha^2}\,x}\,\mathrm{erfc}\,\frac{x - i\sqrt{4\alpha Uc - U^2}\,t}{\sqrt{4\alpha t}} + e^{i\sqrt{Uc/\alpha - U^2/4\alpha^2}\,x}\,\mathrm{erfc}\,\frac{x + i\sqrt{4\alpha Uc - U^2}\,t}{\sqrt{4\alpha t}}\right]$$

H(x, t; c) is equal to H(x, t; b), but with b replaced by c throughout the expression. I(x, t) contains two terms which are complex conjugates of each other. Their sum is therefore real. The only really new feature of the improved model is the appearance of error functions with complex arguments. These have been studied extensively in recent years (see for example Abramowitz and Stegun, 1964).

Geochronology of the Ophiolites

M. DELALOYE

1. Definitions

It would be useful to define precisely at the outset the term ophiolite, for it has had various meanings over the course of time. Although, used by Brongniart, Fouquet, Michel-Levy and Dana, one should start with the concept introduced by Steinmann in 1927 to cover the association of peridotites, gabbroes, diabases and spillites, the existence of a link between these different rock types has led to the word ophiolite being used more as a descriptive than a genetic term. The Penrose Conference of 1972 proposed a more restrictive definition, which, unfortunately, has not been generally accepted.

An opholite, as defined by the Penrose participants, is a distinct assemblage of mafic and ultramafic rocks; it is neither the name of a rock nor of a single lithology. In a complete ophiolite the following rock types are present: an ultramafic complex at the base, composed of harzburgite, lherzolite or dunite, usually showing a metamorphic tectonic fabric (sometimes serpentinized); a gabbroic complex above, with peridotites and pyroxenites having cumulate textures, overlain by a mafic-sheeted dyke complex, which is followed by a mafic volcanic complex, commonly pillowed. The concept that ophiolites represent oceanic crust is widely accepted.

2. The Interest of Ophiolites

With the prodigious development of the concept of plate tectonics and the crucial role in it played by the ocean floor, it is evident that the ophiolites can provide important information for palinspastic reconstructions. Of particular interest are the ophiolites of the Mediterranean region, where they appear in large massifs, such as at Troods, Vourinos, Kizil Dagh, Oman, and at many other locations; and those of the Alpine region, where they are found, more or less transformed, as for example at Mont Genèvre, in the Col des Gets, in the Zermatt region and at Versoyen.

There are many problems connected with the ophiolites; in addition to the question associated with their spatial relationships, their mode of emplacement and their connection with ocean crust, the problem of their age is of great importance.

In the Alps, for example, the ophiolites can be divided into two main groups. The ophiolites of type I have not undergone any apparent deformation or metamorphism, and their eruptive origin is evident. They form relatively modest masses in certain

Alpine areas: the Prealps, the upper Pennenic of the Grisons, Corsica, and also in the northern Appenines. Most workers, however, recognize that the type-I ophiolites have been metamorphosed to pumpellyite-prehnite or pumpellyite-actinolite grade. The other ophiolitic massifs of large size are situated in the Pennenic zone proper. During the Alpine regional metamorphism, these rocks were deformed and recrystallized to such an extent, that in most cases it is no longer possible to recognize the original rocks. These ophiolites, of type II, are encountered in the Valais, the Aosta valley, in Tessin, in the Grisons, and in Ubaye.

3. The Age of the Ophiolites

For several reasons which are explained below, ages of ophiolites in the Alps and elsewhere are not well known. Dating, whether stratigraphic or radiometric, runs into great difficulties, and has not aroused the enthusiasm of researchers. Stratigraphically speaking, the difficulties arise partly from the barren nature of the intercalated sediments, and partly from the generally irregular character of the contacts which are either tectonic or of olistostromic type. Geochronologically, the chemistry of the basic and ultrabasic rocks is such that only the potassium-argon method, or its variant the $^{40}Ar/^{36}Ar$ method, can be used. However, there are difficulties in using these two methods, arising from the low potassium content of the rocks, the probability of obtaining low ages because of the effects of metamorphism, and the danger of high ages because of the possible presence of inherited argon.

At this point, the question as to whether the ophiolites can be successfully dated, radiometrically, should be considered. The geochemical and petrographic character of the ophiolite rocks introduces some important limitations. Essentially, these are the low amount of potassium present and the problem of grain size.

3.1 The Problem of Potassium

In the K-Ar method ^{40}K decays to ^{40}Ar, the proportion of ^{40}K in natural K being about 0.001%. This requires that the method should be applied mainly to rocks or minerals relatively rich in potassium, which is not the case with the ophiolites. The potassium content of acidic rocks is high, but it becomes more and more impoverished in basic and ultrabasic rocks. Minerals rich in potassium (e.g., biotite and muscovite) hardly ever occur in ophiolites in amounts large enough to be separated; the biotite peridotite of Finero is one exception. Those mafic minerals in ophiolites containing potassium (amphiboles and pyroxenes) only rarely have amounts of more than 1%. The feldspars which are richer in potassium are not suitable for K-Ar dating for a number of reasons which are not developed here.

It will be apparent that severe precautions are needed for the potassium analysis. If samples contain more than 0.2% K, a standard deviation of about 3% is possible with conventional techniques; below that, however, potassium must be analyzed by isotope dilution mass spectrometric methods.

Ages of low-K minerals are susceptible to large errors. Analytical errors can be increased by contamination; even minor contamination can have a considerable effect on the age. The largest errors are those associated with the determination of radiogenic ^{40}Ar ($^{40}Ar^*$).

To a first approximation

$$^{40}Ar^* = {}^{40}Ar\ TOTAL - a_{36}^{40}\ {}^{36}Ar\ TOTAL$$

where a_{36}^{40} is the atmospheric $^{40}Ar/^{36}Ar$ ratio.

The errors on ^{40}Ar TOTAL and ^{36}Ar TOTAL are generally constant, as is the absolute error on $^{40}Ar^*$. However, the relative error increases as $^{40}Ar^*$ decreases. Thus ages measured on low-K samples are not very precise. Better precision can be obtained only by achieving the most rigorous analytical conditions (in particular, by using a digital voltmeter and computer data processing) and by increasing the number of measurements.

Another important source of error comes from the assumption that a_{36}^{40} (= 295.5) is a constant, for during their geologic history the samples could have absorbed argon having a $^{40}Ar/^{36}Ar$ ratio different from that of atmospheric argon. To obtain the correct age it would be necessary to distinguish between the atmospheric argon and the absorbed argon, but naturally this is impossible, since the $^{40}Ar/^{36}Ar$ ratio of the latter is not known. As a result $^{40}Ar^*$ and the age cannot be calculated precisely.

Graphical methods, however, can be used to estimate this $^{40}Ar/^{36}Ar$ ratio and to obtain the age. In the isotope ratio diagram $^{40}Ar/^{36}Ar$ is plotted against $^{40}K/^{36}Ar$; data from co-eval samples should define a straight line or isochron. Samples which have absorbed argon with the same $^{40}Ar/^{36}Ar$ ratio would have different conventionally calculated ages, but their isochron age, which is a function of the slope, would correspond to their true age and the intercept on the $^{40}Ar/^{36}Ar$ axis would give the $^{40}Ar/^{36}Ar$ ratio of the absorbed argon. This method used with whole rock age determinations is valid only with a suitable amount of data.

3.2 The Problem of Grain Size

Many ophiolitic rocks (particularly dolerites and pillow lavas) have aphanitic textures and the concentration or separation of K-rich minerals with good argon retention properties is difficult or impossible. Consequently, only whole rock samples can be used for dating. No such problems occur with the gabbroes, and it is easy to separate pyroxenes and amphiboles from them.

4. The Influence of Metamorphism on the Age

It is essential that the metamorphism in an ophiolite which has taken place on the ocean floor should be differentiated from that acquired during or after its emplacement in an orogenic zone. It is probable that ocean floor metamorphism occurs shortly after

the initial emplacement and consolidation of the rock, whereas the second metamorphism can take place at any time after emplacement. The latter can result in a resetting of the age if the initial $^{40}Ar/^{36}Ar$ ratio, calculated from an isotope ratio plot, is near 300. If it is above 300, other interpretations of the apparent ages must be evoked.

Ophiolitic rocks are frequently spilitized and there are several hypotheses explaining this process; in particular the timing of spilitization is controversial. Alkali exchange during spilitization would invalidate the closed system assumption, which is fundamental in geochronology. If it occurred at the time of emplacement in the ocean floor, there would be little effect on the age; subsequent alterations would be more serious. It is evident that the time of system closure in ophiolites is difficult to define.

5. Conclusion

It is correct to say that the geochronology of the ophiolites remains an intractable problem, to which uncertainties in the analytical methods and in the interpretation of the results contribute equally. In the absence of a large number of individual ages on the same ophiolitic massif or from the same region, the conclusions that can be drawn remain subject to caution.

Stable Isotope Geochemistry of Rocks and Minerals

J. R. O'NEIL

1. Introduction

Modern stable isotope geochemistry began with the classic paper of Harold Urey, published in 1947 and entitled *Thermodynamic Properties of Isotopic Substances.* For several light elements, Prof. Urey calculated isotopic fractionation factors between species of geochemical interest and, based on a suggestion by Prof. P. Niggli in Zürich, proposed that paleotemperatures of the ancient oceans might be determined by analysis of the oxygen isotope compositions of carbonate shell materials. Within a few years, the research group that Prof. Urey had assembled at the University of Chicago was successful both in increasing the precision of the Nier isotope ratio mass spectrometer by the necessary factor of 10, and in establishing an oxygen isotope paleotemperature scale. The Chicago group made studies of oxygen isotope variations in rocks and minerals and in natural waters, the carbon isotope variations in nature, and the hydrogen isotope variations in natural waters and in rocks and minerals. Early studies of sulfur isotope variations in nature were made by Profs. H. Thode in Canada and M. Trofimov in the Soviet Union. Toward the end of the 1950's, Prof. S. Epstein's group at Caltech showed that oxygen isotope fractionations between coexisting minerals in higher temperature rocks were indeed large enough to be useful in geothermometry and opened up a powerful field of geochemical research.

Today there are over 100 laboratories in the world where stable isotope analyses are being made of rocks, minerals and geologic fluids. Modern technology has developed to the point where stable isotope analyses of essentially any substance can be made for the elements H, C, N, O, Si and S. These data have two main applications in earth science: (1) geothermometry, and (2) tracer studies. The use of stable isotope abundances as tracers of source materials has become increasingly important in the last few years.

2. Terminology

2.1 The δ-Value

For most geochemical purposes, knowledge of only the *difference* in absolute isotopic ratios between two substances is sufficient. In addition, differences can be measured far more precisely than absolute ratios. Consequently, a relative difference function,

or δ-value, is used for reporting stable isotope abundances. If the absolute ratios of the standards are known, then the absolute ratio of any sample is readily calculated from its δ-value.

The δ-value is defined as follows:

$$\delta_X = \left(\frac{R_X - R_{std}}{R_{std}} \right) 10^3$$

where $R_X = (D/H)_X$, $(C^{13}/C^{12})_X$, $(O^{18}/O^{16})_X$, $(S^{34}/S^{32})_X$, etc. Note that R is always written as the ratio of the heavy (rare) isotope to the light (common) isotope. The δ-value, then, is the relative difference in isotope ratio between a sample and a standard expressed in parts per thousand, or permill (‰). A sample with a δO^{18}-value of + 10.0 is enriched in O^{18} (or is greater in O^{18}/O^{16} ratio) by 10‰, or 1%, relative to the standard. Negative δ-values indicate that the sample is depleted by that amount relative to the standard. The δ-value is the quantity actually measured on isotope ratio mass spectrometers. With modern spectrometers it is possible to measure δ-values with precisions of better than ± 0.5‰ for hydrogen and ± 0.05‰ for the other light elements.

2.2 The Fractionation Factor α

The isotope fractionation factor between two substances, A and B, is defined as

$$\alpha_{A\text{-}B} = \frac{R_A}{R_B}$$

In terms of δ-values this expression becomes

$$\alpha_{A\text{-}B} = \frac{1 + \delta_A/1000}{1 + \delta_B/1000} = \frac{1000 + \delta_A}{1000 + \delta_B}$$

If the isotopes are randomly distributed over all possible sites or positions in the species A and B, the fractionation factor is related to the equilibrium constant, K, for isotope exchange reactions in the following way:

$$\alpha = K^{1/n}$$

where n is the number of atoms exchanged. For simplicity, isotope exchange reactions are usually written such that only one atom is exchanged. For example, the oxygen isotope exchange reaction between CO_2 and H_2O can be written

$$1/2\, CO_2^{16} + H_2O^{18} \rightleftharpoons 1/2\, CO_2^{18} + H_2O^{16}$$

The equilibrium constant for this reaction is

$$K = \frac{(CO_2^{18})^{1/2}(H_2O^{16})}{(CO_2^{16})^{1/2}(H_2O^{18})}$$

and as a true equilibrium constant is a function of temperature. This is the basis of the use of stable isotope fractionation in geologic thermometry.

The equilibrium constant for the above reaction is to all intents and purposes equivalent to the fractionation factor between CO_2 and H_2O:

$$K = \alpha = \frac{(O^{18}/O^{16})_{CO_2}}{(O^{18}/O^{16})_{H_2O}}$$

Values of α are normally very close to unity, typically 1.00X. Commonly, isotopic fractionations are discussed in terms of the value of X, in permill. For example, the sulfur isotope fractionation factor between ZnS and PbS is 1.0036 at 200°C. One may say that at 200°C, (1) the sphalerite-galena fractionation is 3.6 (or 3.6 permill), or (2) sphalerite is enriched in S^{34} by 3.6 permill relative to galena.

2.3 $10^3 \ln\alpha$ and the Δ-Value

It is a useful mathematical fact that $10^3 \ln(1.00X) \cong X$. For the example mentioned above where $\alpha = 1.0036$, $10^3 \ln\alpha = 3.6$. That is, $10^3 \ln\alpha$ is the permill fractionation. This logarithmic function has added theoretical and experimental significance. For perfect gases, $\ln\alpha$ varies as $1/T^2$ and $1/T$ in the high and low temperature limits, respectively. In addition, smooth and often linear curves have been found to obtain when $10^3 \ln\alpha$ is plotted against $1/T^2$ for experimentally determined fractionation factors between mineral pairs or between mineral-water pairs.

The permill fractionation, $10^3 \ln\alpha$, is then of prime importance in stable isotope geochemistry. This quantity is very well approximated by the Δ-value:

$$\Delta_{A\text{-}B} = \delta_A - \delta_B \cong 10^3 \ln\alpha_{A\text{-}B}$$

That is, merely subtracting δ-values will be an excellent approximation to the permill fractionation and identical to it within the limits of analytical error for values of both Δ and δ which are less than about 10.

3. Standards

3.1 Oxygen

There are two internationally accepted reference standards used to report variations in oxygen isotope ratios: PDB and SMOW. The PDB standard is normally used only in ocean paleotemperature studies wherein $CaCO_3$ from fossil shells is analyzed. It is a sample of belemnite guard from the Peedee Formation in North Carolina, and was the laboratory working standard used at the University of Chicago during the time that the oxygen isotope paleotemperature scale was developed. The original supply of this standard has long been exhausted. However, numerous secondary standards have been developed and exchanged among workers in the field.

The SMOW (Standard Mean Ocean Water) standard was originally a hypothetical water sample with oxygen and hydrogen isotope ratios similar to those of an average sample of ocean water. It was defined by H. Craig in terms of a National Bureau of Standards reference water, NBS-1 as follows:

$$(O^{18}/O^{16})_{SMOW} \equiv 1.008\,(O^{18}/O^{16})_{NBS\text{-}1}$$

Subsequent to this definition, large quantities of two water standards called V-SMOW (Vienna SMOW) and SLAP (Standard Light Antarctic Precipitation) have been prepared and are distributed by the International Atomic Energy Agency in Vienna. A group of stable isotope geochemists met at the I.A.E.A. during Sptember, 1976 and established a δO^{18} scale fixed by δO^{18} values of 0.00 and −55.50 for V-SMOW and SLAP, respectively. Solid standards with recommended δO^{18} values on this new scale are being prepared at present.

To relate δO^{18} values of *calcite* on the PDB and SMOW scales, the following expressions are used:

$$\delta O^{18}(SMOW) = 1.03086\,\delta O^{18}(PDB) + 30.86$$
$$\delta O^{18}(PDB) = 0.97006\,\delta O^{18}(SMOW) - 29.94$$

3.2 Hydrogen

The SMOW standard is also used for reporting hydrogen isotope compositions and was originally defined in terms of NBS-1:

$$(D/H)_{SMOW} = 1.050\,(D/H)_{NBS\text{-}1}$$

As in the case of oxygen isotopes, a new scale has been established wherein δD-values for V-SMOW and SLAP are 0.00 and −428.0, respectively. Solid standards with recommended δD-values on this scale are being prepared at present. The Lake Michigan water standard used in the early literature from the U.S.A. is −42.4 on the SMOW scale.

Much of the deuterium data in the earlier literature was reported in percent, but this practice has virtually disappeared in favor of reporting permill variations.

3.3 Carbon

The PDB carbonate is the standard normally used to report carbon isotope compositions. NBS-20 (Solenhofen limestone) and NBS-21 (spectrographic carbon) are used occasionally and on the PDB scale have δC^{13}-values of -1.06 and -28.10, respectively. δC^{13}-values reported from laboratories in the U.S.S.R. are usually expressed in percent, although some authors have recently begun reporting permill variations.

3.4 Sulfur

Troilite from the Canyon Diablo meteorite is the internationally accepted standard used to report δS^{34} variations.

4. Analytical Methods

The development of reproducible chemical extraction techniques has been a critical aspect of stable isotope geochemistry. Methods by which essentially complete yields can be obtained are usually necessary because isotopic fractionations attendant on incomplete reactions can lead to serious errors in the analyses. Only about 5-15 mg of material are required for these analyses, except for deuterium analyses of hydrous minerals, which normally requires 50-100 mg. The elements are put into the following gaseous forms for mass spectrometric analysis:

hydrogen	H_2
carbon	CO_2
oxygen	CO_2, O_2
silicon	SiF_4
sulfur	SO_2, SF_6

Only a brief description of the most widely used extraction techniques will be presented here.

4.1 Hydrogen

Hydrous Minerals. The mineral (or whole rock) is degassed for several hours at 150°C under vacuum to remove extraneous waters. It is then decomposed at high temperatures to produce H_2 and H_2O. Normally, the H_2 is oxidized with CuO at 500°C and all the H_2O is then reacted with uranium metal at 800°C to produce H_2.

4.2 Carbon

Graphite or Diamond. The carbon is oxidized directly to CO_2 with either CuO or O_2 at 1000°C.

$$C \xrightarrow[1000^\circ]{[0]} CO_2$$

Simple combustion methods are also used for organic matter.

Carbonates. Thermal decomposition normally produces CO_2 in excellent yield with good isotopic reproducibility if CO formation can be avoided:

$$XCO_3 \xrightarrow[\Delta]{} XO + CO_2$$

More commonly carbonates are reacted with anhydrous H_3PO_4 at 25°C. Rhodocrosite, siderite, dolomite, and magnesite react sluggishly or not at all at 25°C, and temperatures of 50°C or higher are normally used for them.

$$3MCO_3 + 2H_3PO_4 \xrightarrow[T]{} M_3(PO_4)_2 + 3H_2O + 3CO_2$$

4.3 Oxygen

Carbonates. The reaction above with 100% H_3PO_4 is employed under extremely systematic conditions because only 2/3 of the oxygen is liberated as CO_2. The reaction is normally carried out at 25°C, but 50°C or higher is often used for the less reactive carbonates.

Silicates and Oxides. Reactions with various fluorinating reagents (F_2, BrF_5, BrF_3, XeF_2, CoF_3) in Ni vessels are normally used to liberate O_2 from silicates and oxides.

$$SiO_2 + 2F_2 \xrightarrow[500^\circ]{12\ h} SiF_4 + O_2$$

The liberated O_2 is generally converted to CO_2 for mass spectrometric analysis, although measurements are made of O_2 in a few laboratories. Carbon reduction is also used to extract the oxygen but spurious results are sometimes encountered when minerals rich in alkalis are reduced.

$$SiO_2 + 3C \xrightarrow[1800^\circ]{30\ min} SiC + 3CO$$

The CO is converted to CO_2 over activated Ni or by a glow discharge method.

Water. When milliliter quantities of water are available, analyses are usually made on CO_2 which has been equilibrated with the water at 25°C. Fluorination or carbon reduction is necessary for microliter quantities.

Sulfates. The sulfate is put into the $BaSO_4$ form and reduced with graphite at 1000°C to form a mixture of CO_2 and CO in the ratio $\sim 4:1$ or more. The CO is then converted to CO_2 and the gases added together.

4.4 Sulfur

Sulfides and Sulfur. These substances are ground intimately with Cu_2O and heated at 1000°C for 10 min to produce SO_2 in excellent yield. Whole-rock samples can also be analyzed by this simple technique. When SO_2 is used to measure S^{34}/S^{32} ratios, corrections must be made for variations in the O^{18}/O^{16} ratio of the gas. This problem is avoided if the sulfur-containing substance is converted to SF_6 by reaction with a fluorinating reagent. Excellent results are obtained if one initially converts the sulfur to Ag_2S and then extracts the sulfur by one of the above techniques.

5. Paleotemperature Studies

The establishment of the oxygen isotope paleotemperature scale remains as one of the truly outstanding developments in modern earth science. The scale of Epstein et al., developed in 1953, is as follows:

$$t(°C) = 16.5 - 4.3(\delta_c - \delta_w) + 0.14(\delta_c - \delta_w)^2$$

where δ_c is the δO^{18} value of CO_2 released from $CaCO_3$ by reaction with H_3PO_4 at 25°C, and δ_w is the δO^{18} value of CO_2 in equilibrium with the water at 25°C. The expression is independent of the standard used, although if δO^{18} of the water is assumed to be zero, the expression is valid if δ_c is given relative to the PDB standard. The temperature coefficient of the $CaCO_3$-H_2O fractionation over the temperature range of interest is approximately 0.2 permill/degree, which means that paleotemperatures of the ancient oceans could theoretically be determined to better than ± 0.5°C.

There are four major questions which must be considered in O^{18} paleotemperature work:

1. Was the $CaCO_3$ deposited in oxygen isotope equilibrium with the ocean?
2. What was the oxygen isotopic composition of the ocean at the time?
3. Has the original oxygen isotope record been preserved?
4. What is the relationship between isotopic temperatures and climate?

Many organisms deposit $CaCO_3$ in isotopic equilibrium with ocean water, but the isotopic composition of the shells of some organisms is controlled by kinetic factors related to some metabolic process. By careful study of modern species of known habitat and by the systematics observed among ancient species, this problem is fairly well

understood. Molluscs and foraminifera are frequently used in Cenozoic paleotemperature studies. Knowledge of the isotopic composition of the water from which the shell material was deposited remains a critical problem. A value for the water must always be assumed. A difference of 1 permill in salinity of ocean water can be accompanied by an error of 1°C, and the estimated changes in the isotopic composition of the ocean during glacial periods (between 0.8 and 1.3 permill) are in dispute among workers in this field. The water problem could be eliminated if it were certain that other phases coexistent with $CaCO_3$ were formed in isotopic equilibrium with the ocean. The temperature could then be calculated from the oxygen isotope fractionation between the carbonate and some other phase. Silica and phosphate occur only rarely and the initial work on these minerals indicates that the problem will not be resolved in this way. With respect to preservation of original isotopic ratios, it has been observed that the O^{18} contents of marine limestones decrease with increasing age (Fig. 1), and this has

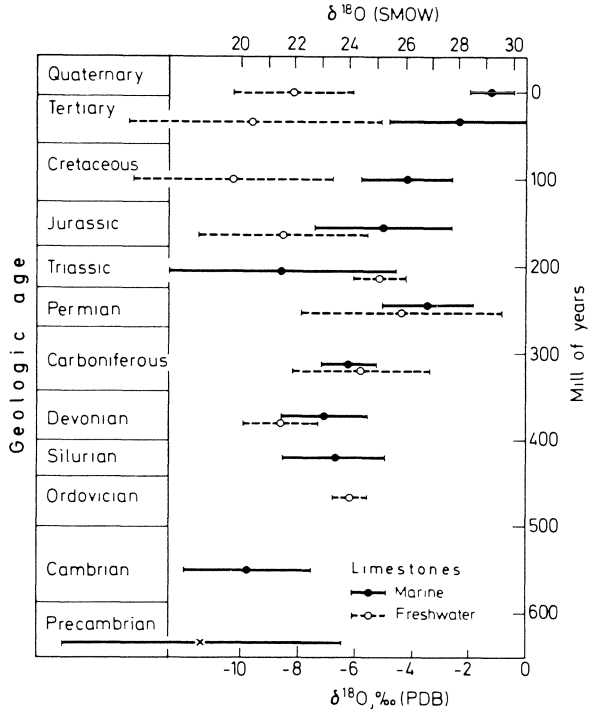

Fig. 1. Variations of δO^{18}-values of marine and fresh water limestones with time. (From Hoefs, 1973)

normally been attributed to isotopic exchange between the limestone and ground water. However, studies of natural and laboratory systems indicate that exchange rates between $CaCO_3$ and water are extremely low at low temperatures, particularly if the carbonate is coarse-grained. Also, several arguments indicate that the ancient oceans were indeed isotopically lighter than modern oceans. It is generally accepted that if the carbonate sample is aragonite, it has probably retained its original record. Conversion of aragonite to calcite could proceed by a solution-redeposition mechanism which certainly would be accompanied by isotopic exchange with the local

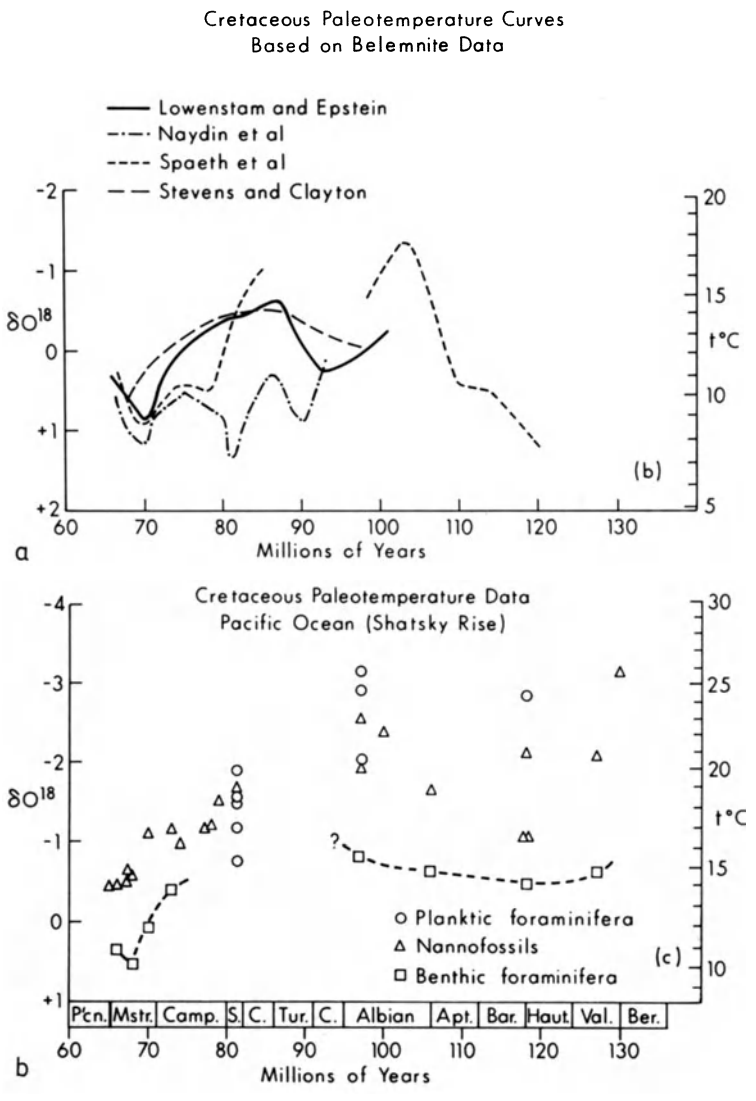

Fig. 2a. Cretaceous paleotemperature curves drawn by S. Savin from published isotopic anaylses of belemnites. Each curve was drawn through the most O^{18}-rich values for that data set. Relationship between δO^{18} scale and temperature scale was calculated assuming δO^{18} of water was 1.00 per mil relative to SMOW. **b** Paleotemperature data of Cretaceous nannofossils, planktic foraminifera, and benthic foraminifera from the Shatsky Rise (Douglas and Savin, 1975). The upward trend in temperature in Cenomanian times is suggested by a single analysis of benthic foraminifera from the Hess Rise (not shown). Relationship between δO^{18} scale and temperature scale was calculated assuming δO^{18} of water was 1.00 per mill relative to SMOW. (From Savin, 1977)

water. Seasonal variations are often detected in shell materials when they are analyzed at various positions across the growth direction. Preservation of these patterns is an excellent criterion for believing that the original isotopic composition material has not been disturbed.

Knowledge of climatic changes that have occurred during late Mesozoic and Cenozoic times has increased enormously in the last 15 years because (1) excellent materials have become available through sophisticated deep-sea sampling programs (2) modern refinements in biostratigraphy have resulted in good correlations between climatic changes in different parts of the world, and (3) the number of laboratories equipped to make oxygen isotope paleotemperature measurements has increased significantly.

Shown on Figure 2 is a comparison of Cretaceous paleotemperature curves from belemnites collected on land from various countries and from materials collected from the central Pacific Ocean. Prof. S. Savin has drawn the curves through the most O^{18}-rich analyses of a sample suite, because any alteration is likely to lower the δ-value. Temperatures appear to have been especially warm during Albian time in Northern Europe and in the tropical Pacific Ocean, but there is only a hint of that warm peak in the deep ocean water. Deep sea bottom temperatures must reflect surface conditions in some high latitude region. At some time during Albian or Cenomanian time, temperatures dropped. A temperature rise and a warm period followed in Turonian and/or Coniacian time. There was then a general lowering of temperatures until a minimum was reached in early Maestrichtian time. While the details of Late Cretaceous climatic history in different areas are uncertain, it is clear that at least most of the world experienced a significant net cooling of 8°-10°C between Albian time and the end of the Cretaceous period.

Oxygen isotope paleotemperature curves for the Tertiary are shown in Figures 3a and 4. The best data have been obtained from the Pacific Basin. The isotopic compositons of Tertiary benthic foraminifera from the North and South Pacific all lie close to a single smooth curve which reflects the temperature history of high latitude oceans during Tertiary time. In general, there has been a net lowering of isotopic temperatures at intermediate and high latitudes since the beginning of the Tertiary.

Information on paleoclimatic history can also be obtained from stable isotope analysis of speleothems, paleosols, ground water carbonates, tree rings, and fluid

---

Fig. 3a. Tertiary New Zealand paleotemperature data of Devereux (1967) replotted on the time scale of Berggren and van Couvering (1974). The curve is drawn essentially through the coldest isotopic temperatures. **b** Isotopic paleotemperature data for Tertiary planktic foraminifera (open symbols) and benthic foraminifera (closed symbols) primarily from the North Pacific. The curve through the benthic data was drawn to best fit the points from all the sites. The "Modern" and "Tertiary" benthic temperature scales were calculated assuming water δO^{18} values of -0.08 per mil and -1.00 per mil respectively. To estimate isotopic temperatures of planktic foraminifera add approximately 2.5°C to appropriate benthic temperature scale. (From Savin, 1977)

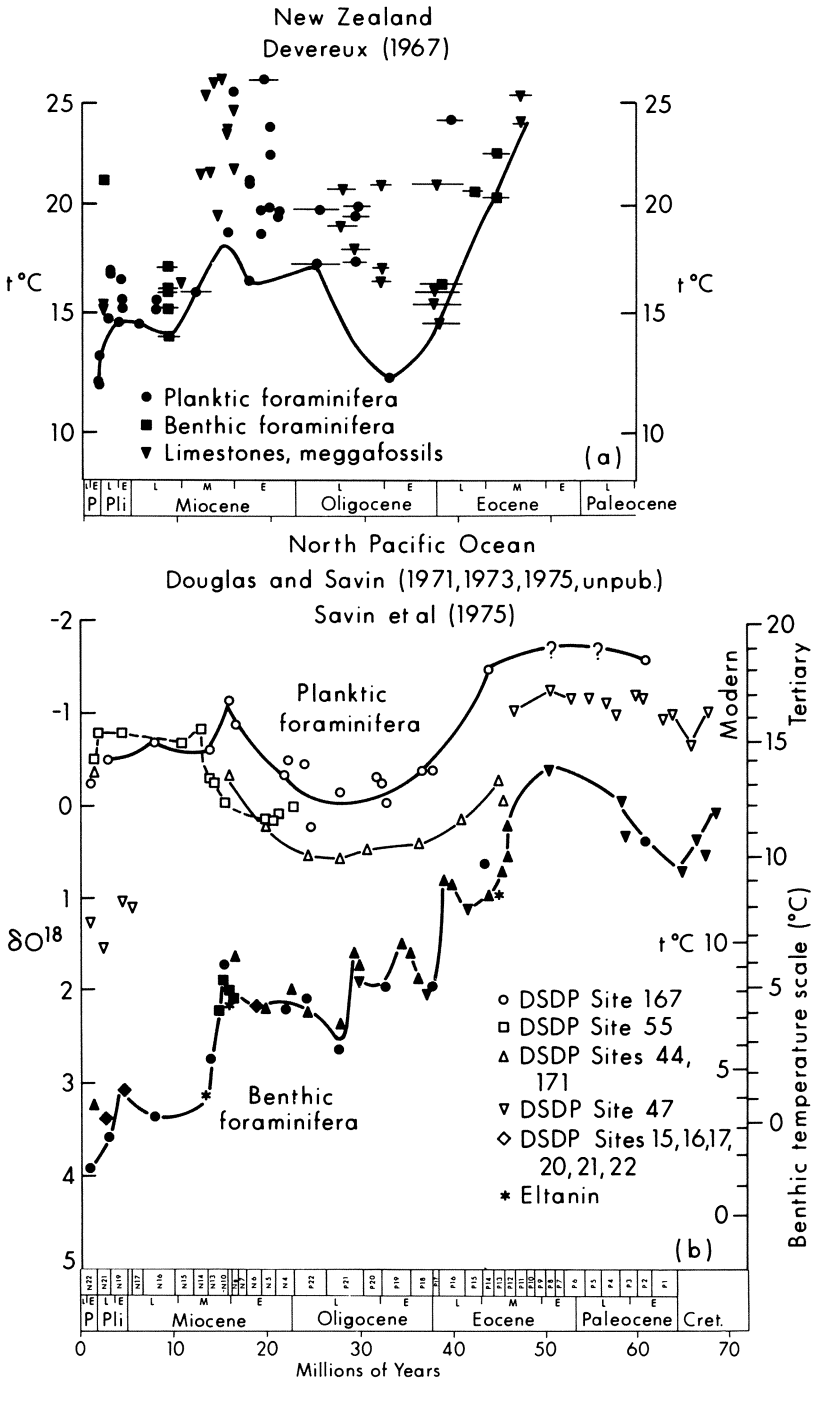

Fig. 3 a and b. (Legend see p. 244)

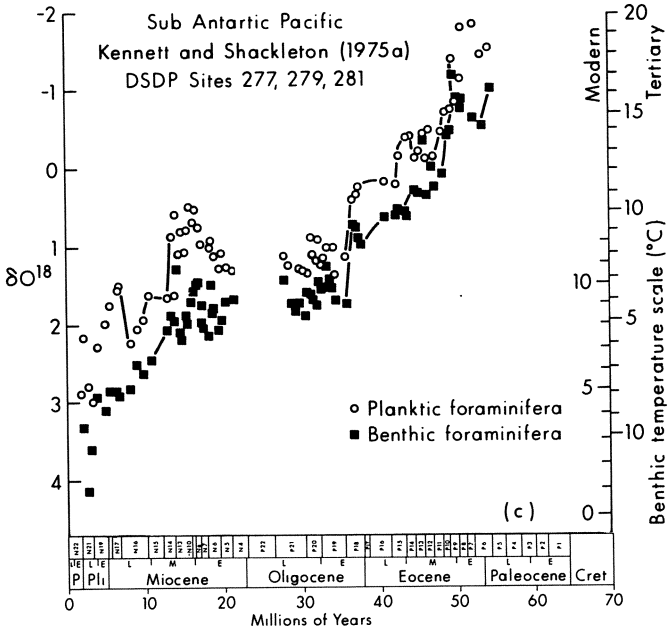

Fig. 4. Paleotemperature curve for foraminifera from the Sub Antarctic Pacific. Modern and tertiary scales calculated assuming δO^{18} values of water to be −0.08 and −1.00, respectively. (From Savin, 1977)

inclusions from epithermal ore deposits. Such studies are now being actively pursued in several laboratories.

6. Igneous Rocks

Hydrogen, carbon and sulfur isotope measurements have proved useful in the study of certain rocks, but oxygen isotope data is germane to most of the classical problems of igneous petrology. The attainment and retention of a high degree of oxygen isotope equilibrium among coexisting minerals in igneous rocks in commonly evidenced by the following: (1) there is a regularity in relative O^{18}-enrichment among igneous minerals, (2) Δ-values in plutonic rocks are about twice the values found in extrusive rocks, and (3) O^{18}-temperatures are usually in agreement with temperatures estimated from other petrologic evidence.

Compilations of δO^{18}-values and δD-values of igneous rocks and minerals from a variety of locations and geologic settings made by Prof. H. Taylor are shown in Figures 5 and 6. Deep-seated terrestrial rocks, lunar rocks, and ordinary chondrites all have δO^{18}-values in the narrow range of approximately 5 to 6, implying a common pre-planetary source material. In addition, this range of values serves as a reference point for interpreting the changes in oxygen isotope composition that accompany various

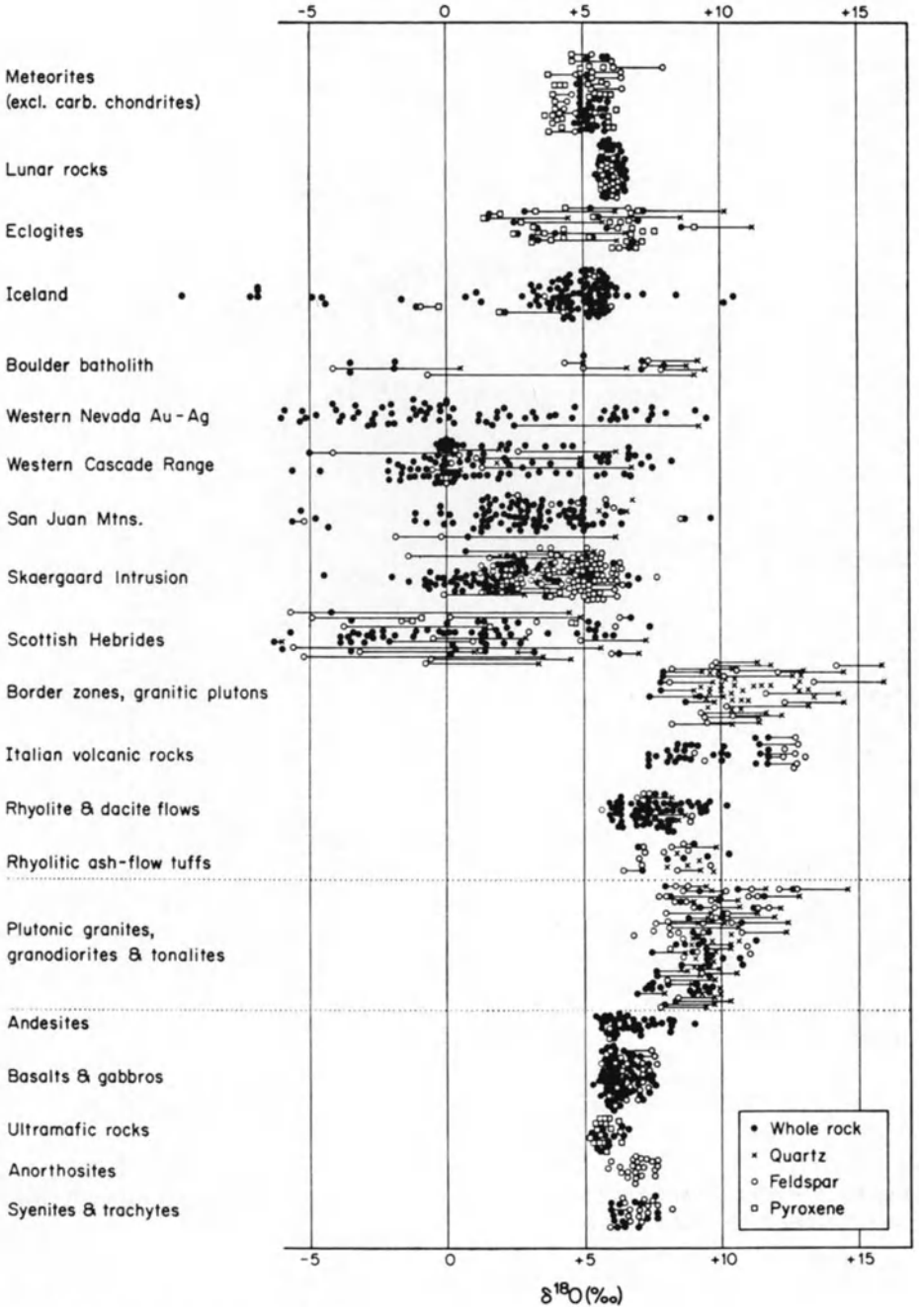

Fig. 5. δO^{18}-values of igneous rocks and minerals from a variety of localities. (From Taylor, 1974)

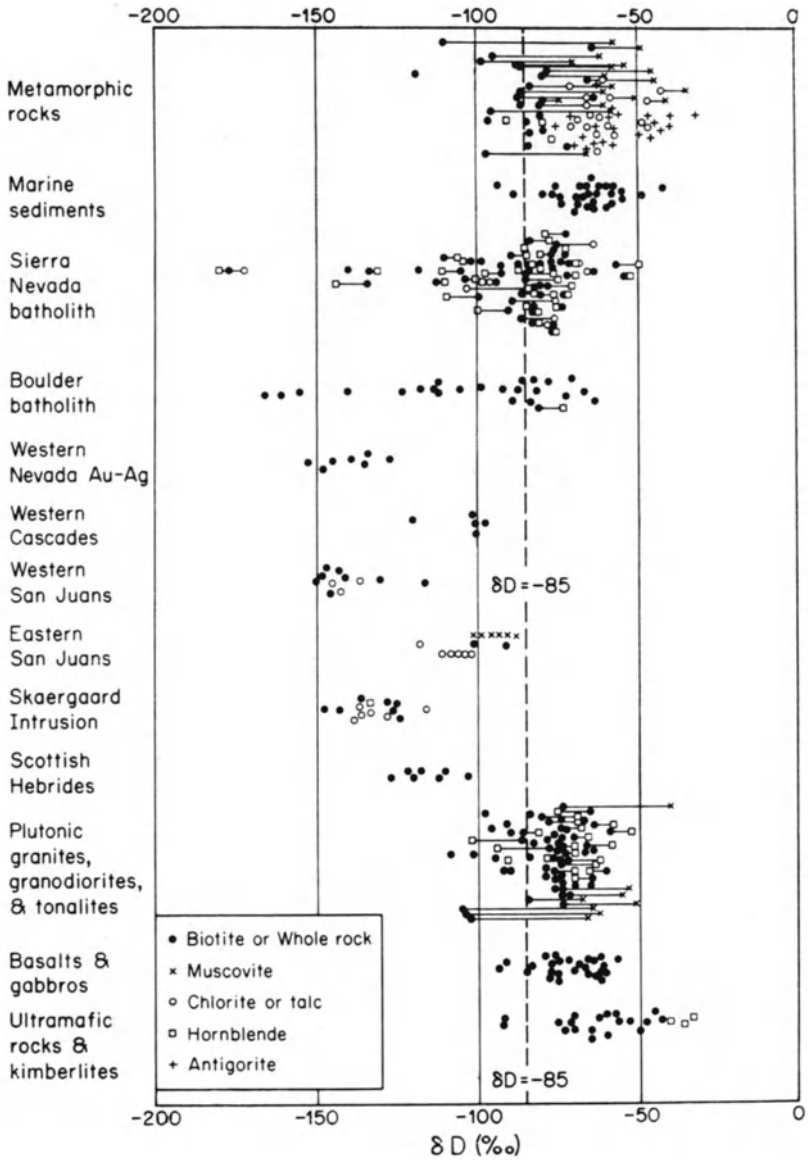

Fig. 6. δD-values of minerals from igneous metamorphic and hydrothermally altered rocks from a variety of localities. (From Taylor, 1974)

geologic processes. For example, low-temperature alteration of submarine basalts as low as 1%-2% can be detected by an increase in δO^{18} of $\sim$ 0.5‰ above the normal value.

6.1 General Conclusions from O^{18} Data

1. Most rhyolite obsidians, particularly from oceanic areas, have δO^{18}-values that are similar to basalts, gabbros, syenites, and andesites, indicating that they are differentiates of basaltic or andesitic magmas at high temperature ($\sim$ 1000°C) and that they cannot be melted sialic crust. Some obsidians from continental interiors have higher δO^{18}-values compatible with their having assimilated O^{18}-rich crustal materials.

2. Plutonic granites have higher O^{18}-contents than their volcanic equivalents mainly because their source materials contained O^{18}-rich sedimentary components, and partly because they may have differentiated at a lower temperature.

3. A correlation generally exists between the O^{18}-contents of SiO_2-rich differentiates and the chemical trends in volcanic complexes. High O^{18}-contents accompany those trends having lower Fe/Mg ratios, while ferrogabbro trends are associated with depletion in O^{18}. Variations in oxygen fugacity may be responsible for these effects, because abundant early precipitation of magnetite should lead to both O^{18}-enrichment and Fe-depletion in later differentiates.

4. Significant depletions in O^{18} (and D) have been observed in many igneous rocks, proving that these rocks exchanged with large quantities of isotopically light meteoric water during crystallization and partly during cooling of the plutons.

6.2 Water-Rock Interactions

The investigation of the interaction between igneous rocks and meteoric waters has been carried out principally by Prof. H. Taylor and his co-workers. The recognition and understanding of these large-scale interactions has profound implications in several areas, including processes of ore deposition and geochronology.

Hydrogen and oxygen isotope data have been obtained on a wide variety of granitic batholiths of various ages. The primary δD-values of the biotites and hornblendes are remarkably constant at about -50 to -85 (Fig. 6), identical to the values in regional metamorphic rocks, marine sediments, greenstones, and most weathering products in temperate climates. Therefore the primary water in these "normal" igneous rocks is probably not juvenile, but rather ultimately derived by dehydration and/or partial melting of the lower crust of subducted lithosphere.

Gigantic meteoric-hydrothermal convective circulation systems were apparently established in the epizonal portion of *all* batholiths, locally producing very low δO^{18}-values (particularly in feldspars) during subsolidus exchange. Some granitic plutons in such environments also were emplaced as low-O^{18} magmas probably formed by melting or assimilation of hydrothermally altered roof rocks. However, the water/rock ratios were typically low enough that over wide areas the only evidence for meteoric water exchange in the batholiths is given by δD-values (as low as -180). The lowering of δD-values commonly correlates with re-setting of K-Ar ages, implying that Ar loss can be caused by these meteoric-hydrothermal circulation systems. Figure 7 illustrates the changes in δD (biotite) and δO^{18} (feldspar) that would accompany exchange between a typical granodiorite and high-latitude meteoric water as a function of water/rock ratio. Such L-shaped patterns have been observed in natural systems.

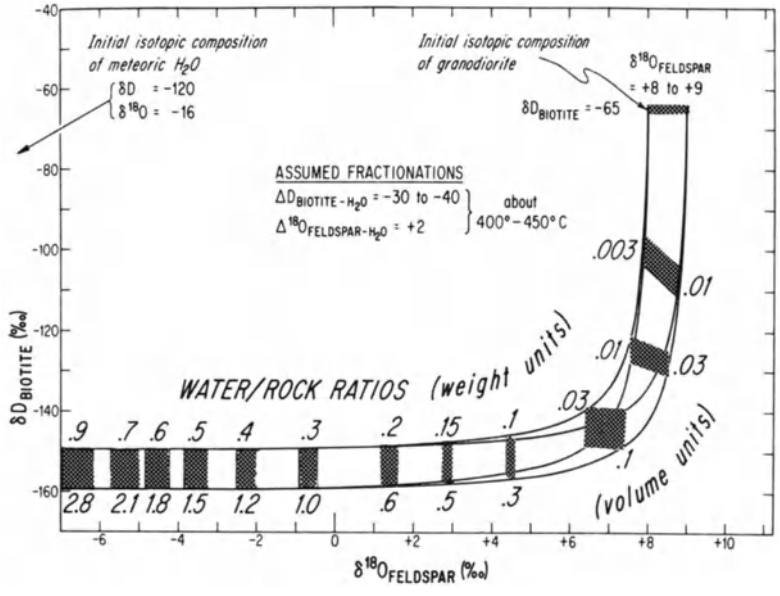

Fig. 7. Plot of calculated values of δD (biotite) and δO^{18} (feldspar) that would be obtained during the hypothetical meteoric-hydrothermal alteration of a typical granodiorite at varying water/rock ratios, assuming initial conditions shown on the diagram. (From Taylor, 1977)

Other studies of igneous rocks that have been made with the aid of stable isotope analyses include:

1. Discovery of an extremely primitive O^{16}-rich component in the silicate inclusions of some carbonaceous chondrites. This material was not generated in our solar system.
2. Classification of stony meteorites by δO^{18} -values of pyroxene.
3. Identification of S- and I-type granitoid rocks in southeastern Australia (i.e., recognition of anatexis of sedimentary source material).
4. Characterization of carbonatites as truly igneous.
5. Lunar rocks: thermometry; solar-wind origin of hydrogen; similarity of O^{18} contents to those of terrestrial ultramafic rocks.
6. Isotopic ratios of primitive rocks and mass balance considerations.
7. The origin of carbon in igneous rocks.
8. Sea-water basalt interactions.
9. Use of variations in isotopic ratios of igneous rocks along active faults in California to reconstruct extents of movement.
10. Oxygen isotope disequilibrium in ultramafic nodules.

7. Metamorphic Rocks

Stable isotope analyses of metamorphic rocks and minerals can provide information on (1) source materials, (2) temperatures of formation, (3) equilibrium or disequilibrium nature of mineral assemblages, (4) source and direction of flow of fluids, (5) mechanisms of mineralogic reactions, and (6) CO_2/H_2O ratios in certain metamorphic fluids.

7.1 General Features

Higher-rank metamorphic rocks have generally lower O^{18} contents and smaller Δ-values than lower-rank rocks. For example, gneissic rocks have δO^{18}-values which are almost indistinguishable from associated granitic rocks (7‰-10‰) and low grade pelitic rocks commonly have δO^{18}-values like thos of shales (15‰-18‰). Values of ΔO^{18}(Q-Mu) are typically around 3.0 in high-grade rocks whereas in blueschists they are as high as 5 or 6. There is evidence that oxygen isotope equilibrium is often closely attained at the highest temperature of metamorphism, and that these isotopic ratios are preserved during retrograde cooling. These conditions must be met in order for oxygen isotope temperatures to be meaningful. Stable isotope disequilibrium also occurs and recognition of this can often explain an apparent geochronological or geochemical anomaly. Isotopic disequilibrium can be recognized by either (1) discordancy in isotopic temperatures, or (2) isotopic reversals. With respect to the reversals, there is an order of relative O^{18} enrichment among the common rock-forming minerals which has been established on the basis of natural data, results of laboratory experiments, and theoretical considerations. A list of the minerals in decreasing tendency to concentrate O^{18} is as follows:

Quartz, dolomite, anhydrite
Alkali feldspar, calcite, aragonite
Leucite
Muscovite, nepheline, kyanite
Anorthite
Glaucophane, staurolite
Lawsonite
Garnet, common pyroxenes and amphiboles
Biotite
Olivine, sphene
Chlorite
Ilmenite, rutile
Magnetite, hematite
Pyrochlore

A discussion of the factors which influence the isotopic properties of minerals is given in an article by O'Neil entitled *Stable Isotopes in Mineralogy*, which appeared in Phys. Chem. Minerals *2*, 105-121 (1977).

7.2 Regional Metamorphism

The oxygen isotope compositions of coexisting minerals of suites of rocks from two areas are shown in Figure 8. The Esplanade Range (A) is a region of classical Barrovian

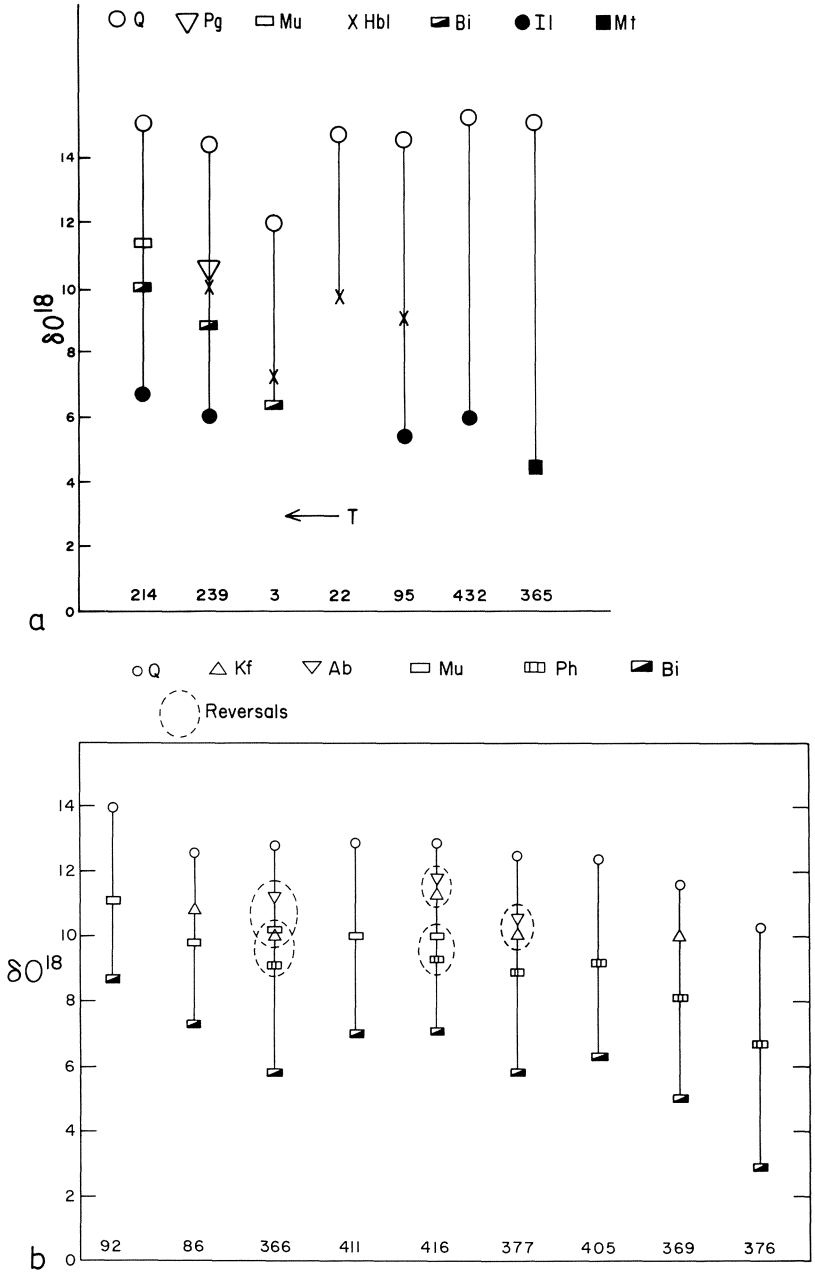

Fig. 8. Oxygen isotope relations among minerals in regionally metamorphosed rocks from (**a**) the Esplanade Range, British Columbia (from O'Neil and Ghent, 1975), and (**b**) the Monte Rosa Granite, Western Alps (from Frey et al., 1976)

metamorphism which is chemically and isotopically "well-behaved." There are no isotopic reversals; the oxygen isotope temperatures decrease with decreasing grade, and are in agreement with temperatures estimated by other criteria. With the exception of sample 3, the total range of δO^{18}-values of quartz is only $\sim$ 0.8 permill. The samples analyzed are from localities as much as 14.5 km apart, represent widely different protoliths, and have a broad range of modal proportions of quartz. These data suggest that there was good oxygen isotope communication over the entire area by means of a fluid of relatively fixed O^{18}/O^{16} ratio. Such oxygen isotope exchange between a pervasive widespread fluid and the rocks during regional metamorphism has been postulated for several areas. The δD-values of the individual hydrous minerals in this area have this uniformity as well.

The Monte Rosa region (b) is a complex polymetamorphic area and this is reflected in isotopic reversals, evidence of ground water interactions, and other isotopic effects. Optical methods, age measurements, and stable isotope analyses distinguish two distinct mineral assemblages in these rocks (Permian and Alpine). For the tectonically least affected rocks, excellent concordance between Q-Mu and Q-Bi formation temperatures of $\sim$ 530°C implies oxygen isotope equilibrium in Permian time which was undisturbed during Alpine metamorphism. Except for samples 366 and 376, which have obviously interacted with meteoric water (Fig. 9), the isotopic evidence suggests that the Monte

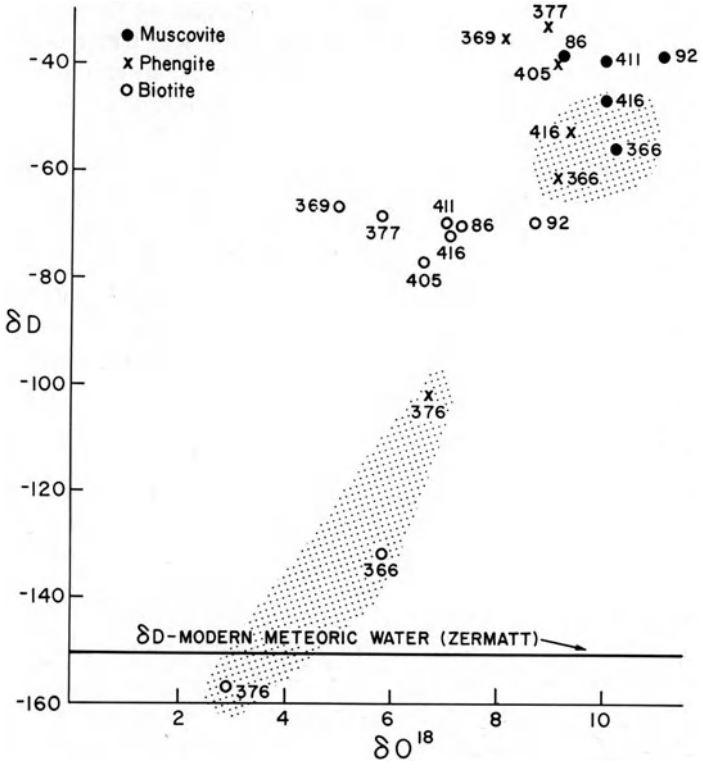

Fig. 9. D-O^{18} relationships for the hydrous minerals at Monte Rosa. *Dotted areas* indicate rocks with isotopic reversals (366 and 416) or evidence of ground water interaction (366 and 376). (From Frey et al., 1976)

Rosa granite "stewed in its own juices." The δD-values of ∿ –35 for white mica (Fig. 9) are relatively high and suggest that connate waters may originally have contributed hydrogen to this system.

7.3 Contact Metamorphism

The large differences in average δO^{18}-values between granitic rocks (7 to 9) and limestones (20 to 28) offer the possibility of studying the (isotopic) interaction of these rocks during intrusion, metamorphism and the formation of metamorphic skarns. The sources, temperature, CO_2/H_2O ratios, and direction of flow of metasomatic fluids were inferred from a thorough stable isotope study of the metasomatic Ca-Fe-Al-Si skarns in the Osgood Mountains, Nevada. Marked O^{18} enrichment in the margins of the granodiorite resulted from isotopic exchange with calcareous wall rocks, but the interior was found to be isotopically normal and homogeneous. During the first stage of development of the skarn, magmatic water ($\delta O^{18} = 9.4$; $\delta D = -45$) moved *out* from the pluton; at a later stage, meteoric water constituted between 20% and 50% of the metasomatic fluid; in the final stage the meteoric water comprised as much as 100% of the fluid. CO_2/H_2O ratios were estimated from the temperature, isotopic composition of initial reactants and the experimentally determined values of $\Delta(CO_2\text{-}H_2O)$.

The δD and δO^{18}-values of amphibole from granodiorite and skarn are shown in Figure 10a. Note the narrow range in δO^{18} of skarn amphiboles (because temperature is constant) and the large range in δD (because the amount of meteoric water in the fluid varied). The C^{13} and O^{18} relations for the various calcites are shown in Figure 10b. Although C^{13} is removed to a small extent by loss of CO_2, material balance calculations indicate a magmatic source of carbon for the skarn calcite. δS^{34}-values of near zero for the late stage sulfides indicate a magmatic source for sulfur as well. In a similar skarn deposit in Elkhorn, Montana, the metasomatic fluid was apparently entirely magmatic in origin, the only evidence of meteoric water involvement being in some late-stage serpentines. Epidote has proved to be a very useful mineral in these studies and others because $\Delta D(Ep\text{-}H_2O)$ seems to be about zero over a large range of temperature, and therefore δD-values of epidote are good estimates of the δD-values of the water.

7.4 Low-Temperature Metamorphism

High-grade diagenesis and low-grade metamorphism can be investigated by O^{18} analyses. Massive oxygen isotope exchange can occur at relatively low temperatures (200°-300°C) in rocks that appear lithologically to be ordinary shale and carbonate. The O^{18}/O^{16} ratios of coexisting quartz and illite from such rocks may be used to determine temperatures of burial metamorphism.

Serpentinization processes have been extensively investigated by stable isotope methods. The D-contents of Alpine chrysotile and lizardite correlate well with latitude, implying formation by the action of ground water. Large values of ΔO^{18}(serp.-mag.) and δO^{18}-values of present-day serpentinizing fluids suggest very low temperatures

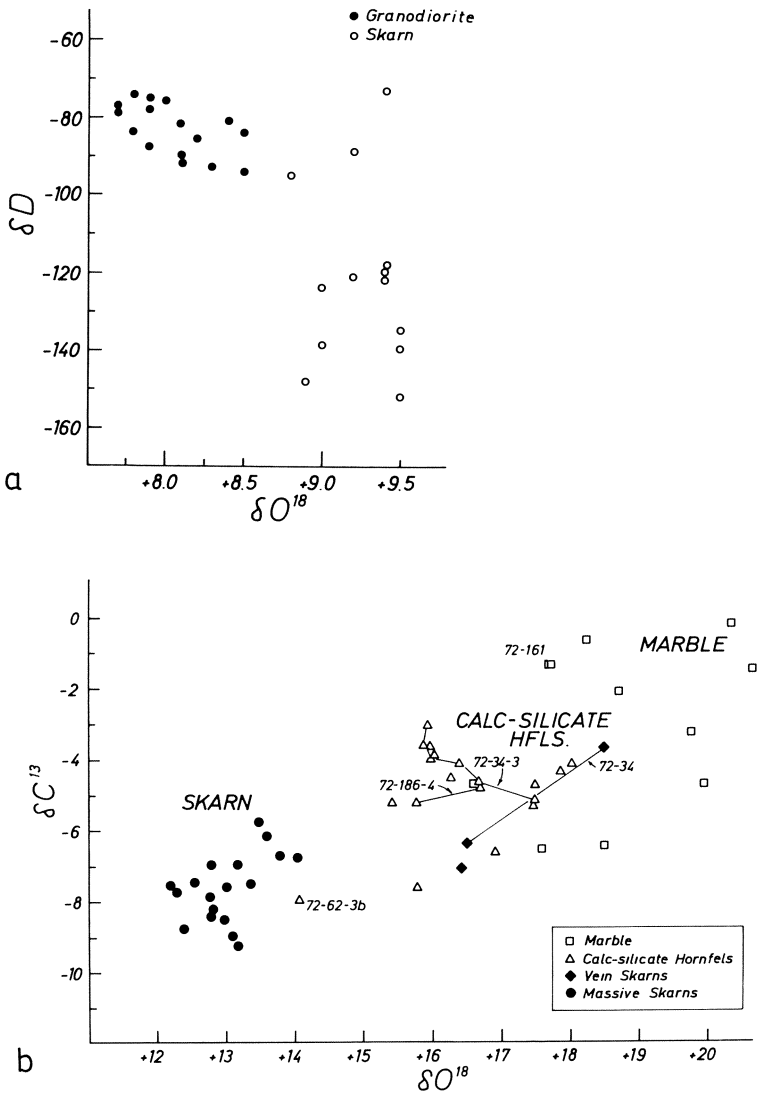

Fig. 10. Stable isotope variations in skarn from Osgood Mountains, Nevada. (From Taylor and O'Neil, 1977). **a** δD versus δO^{18} for amphibole from granodiorite and skarn. **b** δO^{18} versus δO^{13} for calcite in marble, hornfels and skarn

(down to surface temperatures). Isotopic temperatures for antigorite serpentinization are always higher (200°-400°C). The D-O^{18} signatures of oceanic serpentines are different from those of ophiolotic serpentines implying that different kinds of water were involved in their formation.

Oxygen isotope analyses of glaucophane-bearing rocks indicate that they form over a large range of temperature (200°-550°C). Blueschist rocks can be subdivided into a low-temperature lawsonite-aragonite facies and a higher-temperature epidote-rutile facies.

8. Sedimentary Rocks

Authigenic minerals and products of chemical weathering which form at low temperatures in the presence of large quantities of water are relatively O^{18}-rich because values of ΔO^{18} (mineral-H_2O) are very large (20-40‰) at low temperatures. Unaltered detrital minerals, on the other hand, may be relatively low in O^{18} if they originate in igneous rocks. Thus, the δO^{18}-values of sedimentary rocks span a large range from about 10 (certain sandstones) to about 35 (cherts). Ocean sediments are richer in O^{18} than continental weathering products because ocean water is richer in O^{18} than ground water, and also the formation temperatures in the ocean are often lower. Temperature is by far the dominant factor responsible for the generally high O^{18} contents of sedimentary rocks. It is clear from the above that oxygen isotope analyses provide an excellent discriminant for sediments of detrital and authigenic origin. Also, as we have seen earlier, sedimentary components to granitic melts are easily recognized by high δO^{18}-values.

The dolomitization process has been studied extensively by stable isotope techniques. From the fact that values of ΔO^{18}(dol.-cal.) of 2-4 are measured in hydrothermal deposits and in laboratory experiments at T = 250°-500°C, one concludes that this fractionation should have a value of 6-7 at sedimentary temperatures. Such a large fractionation is inferred from measurements of water and ordered dolomite which is forming at present in a lake in California. However, oxygen isotope analyses of coexisting dolomite and calcite in sedimentary rocks reveal ΔO^{18}-values very close to zero. One controversial interpretation of these data is that dolomite forms from precursor $CaCO_3$ by replacement of Ca^{2+} by Mg^{2+} in the solid state without breaking C-O bonds.

The sodium silicates magadiite and kenyaite are chemically precipitated precursor minerals to certain cherts. The chemistry of such conversions is illustrated for magadiite in the following reaction:

$$NaSi_7O_{13}(OH)_3 \cdot 3H_2O + H^+ \longrightarrow 7SiO_{2(S)} + Na^+ + 5H_2O$$

Oxygen isotope analyses were used to distinguish between the following possible mechanisms for these reactions: (1) percolating ground waters leach sodium from the precursor and form amorphus silica which is altered to quartz with time, and (2) the precursor is converted directly to quartz in a moderately or highly saline solution of low a_{SiO_2} and high pH. The saline brines which would be present in the second process are significantly enriched in O^{18} relative to normal ground waters. Such cherts, sampled in East Africa, range widely in δO^{18} (Fig. 11), but are relatively O^{18}-rich. δO^{18} correlates well with lake salinities that were inferred from geologic evidence. The data suggest that the precursors were transformed to chert in fluids of widely varying salinity and a_{Na^+}/a_{H^+} ratio, and indicate that most of this chert was formed from precursors in lake water trapped at the time of deposition.

On a δD versus δO^{18} diagram, sedimentary clay minerals plot on lines which are parallel to the meteoric water line. The data for kaolinites from a wide variety of geographical locations show little scatter, implying that kaolinite forms in equilibrium

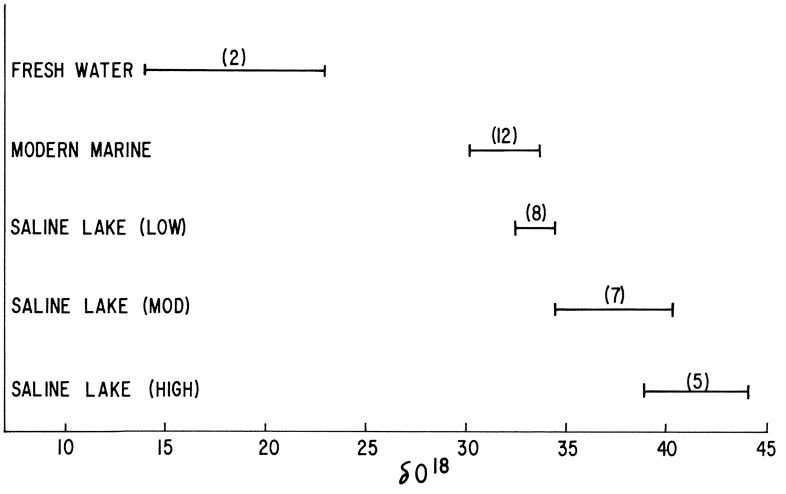

Fig. 11. Comparison of δO^{18}-values of cherts from various sources showing the pronounced enrichment of O^{18} in those from the saline lakes of East Africa and the O^{18}-salinity correlation. (From O'Neil and Hay, 1973)

with local ground water over a rather narrow range in temperature. Montmorillonite data are more scattered and this may be a result of a greater variation in formation temperatures. Most evidence suggests that clay minerals retain their original isotope ratios after formation and this opens up the possibility of using the isotopic compositions of paleosols as climatic indicators. In Figure 12 the meteoric water line and the

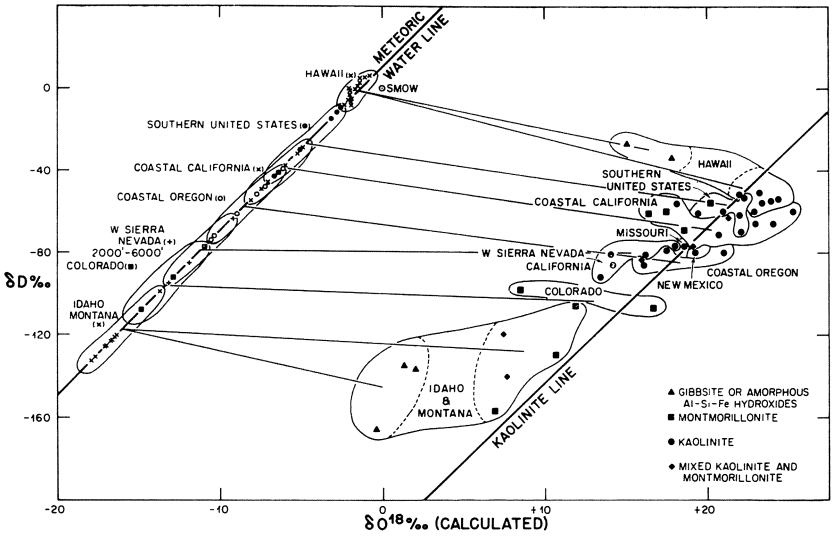

Fig. 12. δD-δO^{18} diagram of clay minerals and hydroxides from Quaternary soil zones of the U.S.A. (From Lawrence and Taylor, 1971)

kaolinite and montmorillonite lines are shown along with data for clay minerals and hydroxides from Quaternary soils of the U.S.A. The correlation between the isotope data for these minerals and corresponding present-day waters is excellent.

Oxygen isotope analyses have provided evidence of a dramatic climatic change in East Africa during the Pleistocene. There was a major increase in the δO^{18}-values of pedogenic and groundwater carbonates in the region around Lake Turkana 1.8 to 2.0 m.y. ago (Fig. 13). It is inferred that the climate prior to this time was much more

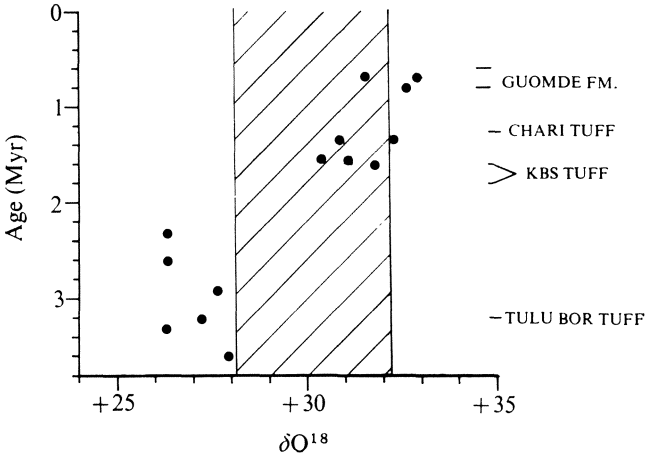

Fig. 13. A plot of δO^{18}-values of carbonate versus age at Lake Turkana. The *hachured area* represents the isotopic compositions of theoretical carbonates in isotopic equilibrium with waters that have the range of δO^{18} -values for modern rain in the area. (From Cerling et al., 1977)

humid, and that the meteoric water was 2‰-4‰ lower in O^{18} than that of average rain today. The rainfall since the time indicated has since decreased dramatically. In selected areas, the isotopic compositions of ground water carbonates can be very useful in reconstructing paleoclimatic conditions and have heretofore been only moderately exploited.

9. Ore Deposits

In the last few years, stable isotope techniques have been vigorously applied to problems of economic geology. The results of these studies have placed severe constraints upon models of ore deposition, and require that modification be made of many old concepts. Of particular importance has been the ability to identify sources of water in hydrothermal fluids by their hydrogen and oxygen isotope ratios. The relative roles of meteoric, connate, and magmatic water in ore-forming processes has been a controversial subject for many decades. Now the identification of water origins can often be

made unambiguously. The determination of sulfur and carbon isotope ratios in ore minerals can provide important information on the geochemical environment of ore deposition, as well as the origin of the sulfur and the carbon.

With respect to water origins, an interesting end-member case is provided by the epithermal Au-Ag vein deposits of the Great Basin, Nevada. The majority of vein minerals from these deposits has very low δO^{18}-values, indicating a significant component of meteoric water to the ore fluids. However, the δD-values of fluid inclusions are *uniformly* low with a range (−90 to −140) identical to that of the modern spring waters in the area. The deuterium measurements unambiguously demonstrate the dominance and probable exclusivity of meteoric water in the hydrothermal fluids of such deposits. The δD and calculated δO^{18}-values of inclusion fluids in these minerals are shown in Figure 14. Several samples lie directly on the meteoric water line. In keeping

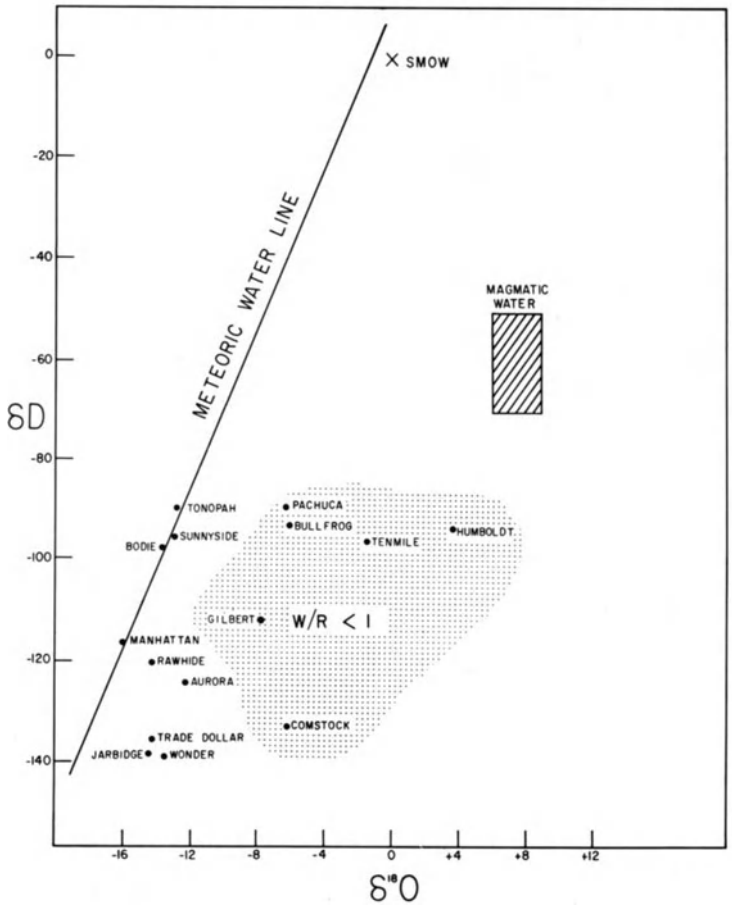

Fig. 14. Isotopic compositions of the inclusion fluids in epithermal Au-Ag deposits in relation to the modern meteoric water line. δO^{18} values of the fluids are calculated from δO^{18}-values of hydrothermal minerals at 250°C or using measured filling temperatures when available. W/R = integrated water/rock ratio. (From O'Neil and Silberman, 1974)

with this is the very low salt content (0-3 wt%) in the inclusions. Most waters have experienced an oxygen isotope shift to heavier values as a result of exchange between water and rock. From the O^{18} shift one can calculate roughly the water/rock ratios in these hydrothermal systems. Because meteoric water dominates *every* fluid examined, it is inferred that such water may be *necessary* for the formation of epithermal Au-Ag deposits.

Isotopic compositions of ore fluids may also be determined indirectly by isotopic analysis of hydrous minerals if you know the equilibrium D and O^{18} relationships between the mineral and water as a function of temperature (from laboratory experiments) and have an estimate of the temperature of formation. Such analyses from a variety of deposits are shown in Figure 15. From the general correlation between δD with latitude, it is clear that meteoric water was involved at some stage (particularly a late stage) in the development of the majority of ore deposits.

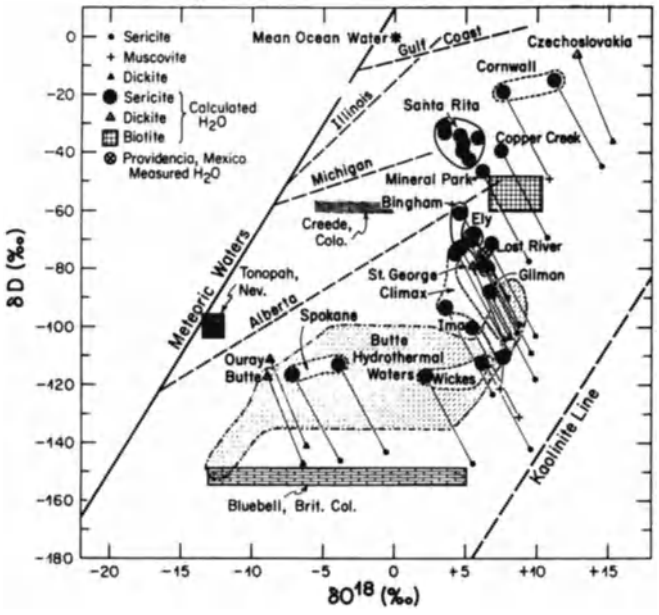

Fig. 15. δD-δO^{18} diagram for calculated hydrothermal waters from a variety of ore deposits. The biotite "box" shown represent the waters that would have coexisted in equilibrium with the hydrothermal biotites from Ely, Bingham, and Santa Rita at 650°C. Also shown are the trend lines for oil-field formation waters from various sedimentary basins in the mid-continent of North America. (From Taylor, 1974)

In Figure 16 are shown ranges of δS^{34}-values for sulfides and sulfates from a number of ore deposits covering wide ranges in age, formation temperature, mineralogy, and mode of occurrence. Some deposits exhibit a narrow range of values around zero, others a narrow range of positive values, and still others show a very wide range including both positive and negative values. Sulfates are always more S^{34}-rich than

coexisting sulfides. Traditionally, deposits with narrow ranges of δS^{34}-values around zero were interpreted to be of magmatic origin, and those with large ranges of values were considered to be of bacteriogenic origin, and this remains generally true. However, one must take into consideration that the δS^{34} (δC^{13}) values of hydrothermal minerals depend on the physicochemical conditions of the fluids (T, pH, f_{O_2}) as well as the isotopic composition of total sulfur (and carbon). The important sources of sulfur are the mantle, local country rocks, and sea water or evaporites. These distinctions are best made by determining δS^{34}-values of *total* sulfur in the hydrothermal fluid because this value may differ considerably from δS^{34}-values of individual minerals. Variation in δS^{34}-values of coexisting sulfur species that can occur on changing

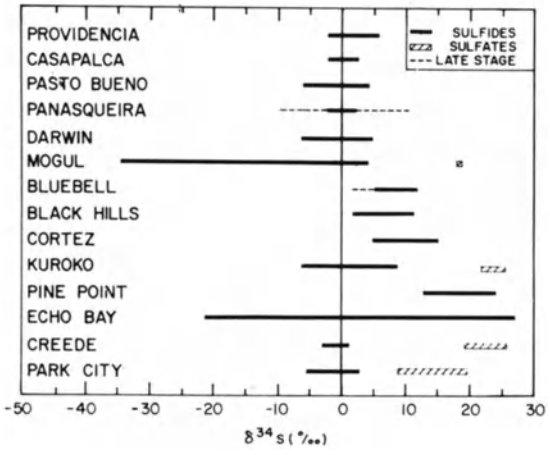

Fig. 16. Range of δS^{34}-values of sulfides and sulfates from various hydrothermal ore deposits. (From Hoefs, 1973)

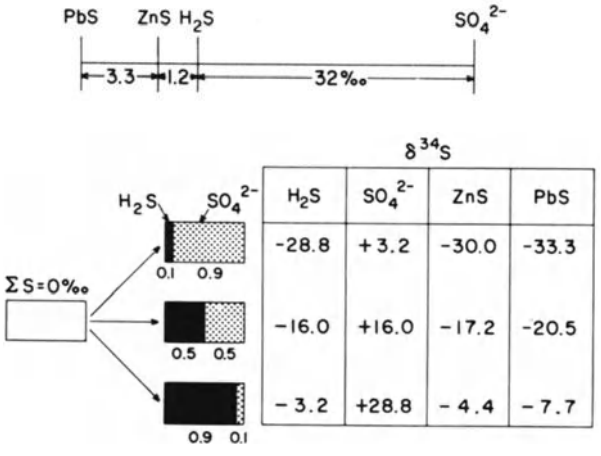

Fig. 17. Variation of δS^{34} of sulfate (ion or mineral), H_2S, and sulfide minerals with variation in H_2S/SO_4^{-2} of the hydrothermal solution at T = 200°C, $\delta^{34}S_{\Sigma S} = 0$ permill. (From Rye and Ohmoto, 1974)

the f_{O_2} in the fluid are shown in Figure 17. Unfortunately, sufficient knowledge of the physicochemical conditions of the hydrothermal fluids to make these material balance calculations is normally lacking.

Although the primary emphasis in stable isotope studies of ore deposits has been on the recognition of the sources for water, sulfur, and carbon, temperatures of formation can also be determined from O^{18} and S^{34} fractionations between cogenetic minerals. The O^{18} temperatures are normally made on gangue minerals of a complicated relationship to the ore minerals and are consequently difficult to interpret. S^{34} temperatures, however, are often in agreement with fluid inclusion and other temperature estimates and seem promising as a petrologic tool, particularly inasmuch as the temperatures are being determined from the actual sulfide ore minerals.

Extremely important contributions are made to economic geology when stable isotope analyses are made of ore minerals of known paragenesis. Each ore deposit is distinctive and a very thorough investigation of geologic, chemical, and isotopic characteristics of the individual deposit is obviously the best approach. However, good geologic control is not always available (for example in closed mines) and depending on the questions asked, much can be learned from the isotopic analyses of less well-documented samples.

References

General reference works:

Faure, G.: Principles of Isotope Geology. New York: John Wiley, 1977, pp. 464

Friedman, I., O'Neil, J.R.: Compilation of stable isotope fractionation factors of geochemical interest. U.S. Geol. Survey Prof. Paper 440-KK. In: Data of Geochemistry, 6th ed. Fleischer, M. (ed.). 1977

Friedman, I., O'Neil, J.R.: Hydrogen. In: Handbook of Geochemistry, 1-B. Wedepohl, K.H. (ed.). Berlin, Heidelberg, New York: Springer, 1978

Garlick, G.D.: The stable isotopes of oxygen. In: Handbook of Geochemistry, 8-B. Wedepohl, K.H. (ed.). Berlin, Heidelberg, New York: Springer, 1969

Hoefs, J.: Stable Isotope Geochemistry. Berlin, Heidelberg, New York: Springer, 1973, pp. 140

O'Neil, J.R.: Stable isotopes in mineralogy. Phys. Chem. Mineral. *2*, 105-123 (1977)

Savin, S.M.: The history of the earth's surface temperature during the past 100 m.y. Ann. Rev. Earth. Planet. Sci. *5*, 319-355 (1977)

Schwarcz, H.P.: The stable isotopes of carbon. In: Handbook of Geochemistry, 6-B-I. Wedepohl, K.H. (ed.). Berlin, Heidelberg, New York: Springer 1969

Stable Isotopes as Applied to Problems of Ore Deposits. Econ. Geol. *69*, no. 6 (1974)

Taylor, H.P., Jr.: The oxygen isotope geochemistry of igneous rocks. Contrib. Mineral. Petrol. *19*, 1-71 (1969)

References cited in text:

Cerling, T.E., Hay, R.L., O'Neil, J.R.: Isotopic evidence for dramatic climatic changes in East Africa during the Pleistocene. Nature (London) *267*, 137-138 (1977)

Frey, M., Hunziker, J.C., O'Neil, J.R., Schwander, H.W.: Equilibrium-disequilibrium relations in the Monte Rosa granite, Western Alps: Petrological, Rb-Sr and stable isotope data. Contrib. Mineral. Petrol. *55*, 147-179 (1976)

Hoefs, J.: Stable Isotope Geochemistry. New York, Heidelberg, Berlin: Springer, 1973

Lawrence, J.R., Taylor, H.J., Jr.: Deuterium and oxygen-18 correlation: Clay minerals and hydroxides in Quaternary soils compared to meteoric waters. Geochim. Cosmochim. Acta *35*, 993-1003 (1971)

O'Neil, J.R., Ghent, E.D.: Stable isotope study of coexisting metamorphic minerals from the Explanade Range, British Columbia. Geol. Soc. Am. Bull. *86*, 1708-1712 (1975)

O'Neil, J.R., Hay, R.L.: $^{18}O/^{16}O$ ratios in cherts associated with the saline lake deposits of East Africa. Earth Planet. Sci. Letters *19*, 257-266 (1973)

O'Neil, J.R., Silberman, M.L.: Stable isotope relations in epithermal Au-Ag deposits. Econ. Geol. *69*, 902-909 (1974)

Rye, R.O., Ohmoto, H.: Sulfur and carbon isotopes and ore genesis. A review. Econ. Geol. *69*, 826-842 (1974)

Savin, S.M.: The history of the Earth's surface temperature during the past 100 m.y. Ann. Rev. Earth Planet. Sci. *5*, 319-355 (1977)

Taylor, H.P., Jr.: The application of oxygen and hydrogen isotope studies to problems of hydrothermal alteration and ore deposition. Econ. Geol. *69*, 843-883 (1974)

Taylor, H.P., Jr.: Water/rock interactions and the origin of H_2O in granitic batholiths. J. Geol. Soc. Lond. *133*, 5o9-558 (1977)

Taylor, B.E., O'Neil, J.R.: Stable isotope studies of metasomatic Ca-Fe-Al-Si skarns and associated metamorphic and igneous rocks. Osgood Mountains, Nevada. Contrib. Mineral. Petrol. *63*, 1-49 (1977)

Stable Hydrogen and Oxygen Isotopes in the Water Cycle

U. SIEGENTHALER

1. Precipitation

The isotope ratios D/H and $^{18}O/^{16}O$ exhibit relatively large variations in natural waters. In precipitation one observes

1) a gradual decrease of the heavy isotope concentration when going from lower to higher latitudes, i.e., with decreasing temperature ("temperature effect"; see Fig. 1);

2) a decrease of $\delta^{18}O$ and δD when going from the coast of a continent inland ("continental effect");

3) seasonal variations which are approximately parallel to those of temperature (Fig. 2);

4) a lowering of the ^{18}O and D concentrations with increasing altitude ("altitude effect").

The primary reason for these phenomena is isotope fractionation during evaporation and condensation of water because $HD^{16}O$ and $H_2{}^{18}O$ have lower vapor pressures than $H_2{}^{16}O$, by a factor (fractionation factor) of 1.085 and 1.010, respectively, at 20°C. Water vapor is, therefore, lower by about 80‰ in D, and 10‰ in ^{18}O, than liquid water with which it is in equilibrium. During the outraining of a moist air mass, the vapor is continuously depleted in the heavy isotopes, since the precipitation leaving the system is enriched in ^{18}O and D. Figure 3 illustrates this process: water vapor which is evaporated from the oceans has a $\delta^{18}O$ of about −13‰ [1], (i.e., it is not in isotopic equilibrium with the ocean water, see below); the first condensate will have about −3‰, being in equilibrium with the vapor.

Due to the preferential removal of the heavy isotope, the remaining vapor becomes depleted in ^{18}O, and consequently the next condensate is also lower in ^{18}O, and so on. Since formation of precipitation is essentially a consequence of cooling, later condensation stages occur always at lower temperature, and this leads indirectly to a relation between temperature and $\delta^{18}O$ in precipitation. Condensation with continuous removal of the condensate can mathematically be described as a Rayleigh process, and Dansgaard (1964) and Friedman et al. (1964) showed that the observed global relationship between mean values of $\delta^{18}O$ and temperature can actually be described reasonably well by a Rayleigh-type formula. This may, however, be somewhat fortuitous, since the processes determining the isotope content of precipitation are very complex: besides condensation we have to consider evaporation from the oceans, different source regions – oceanic and continental – of the vapor, horizontal and vertical mixing of dif-

[1] The values are expressed in the SMOW scale, cf. O'Neil, this volume.

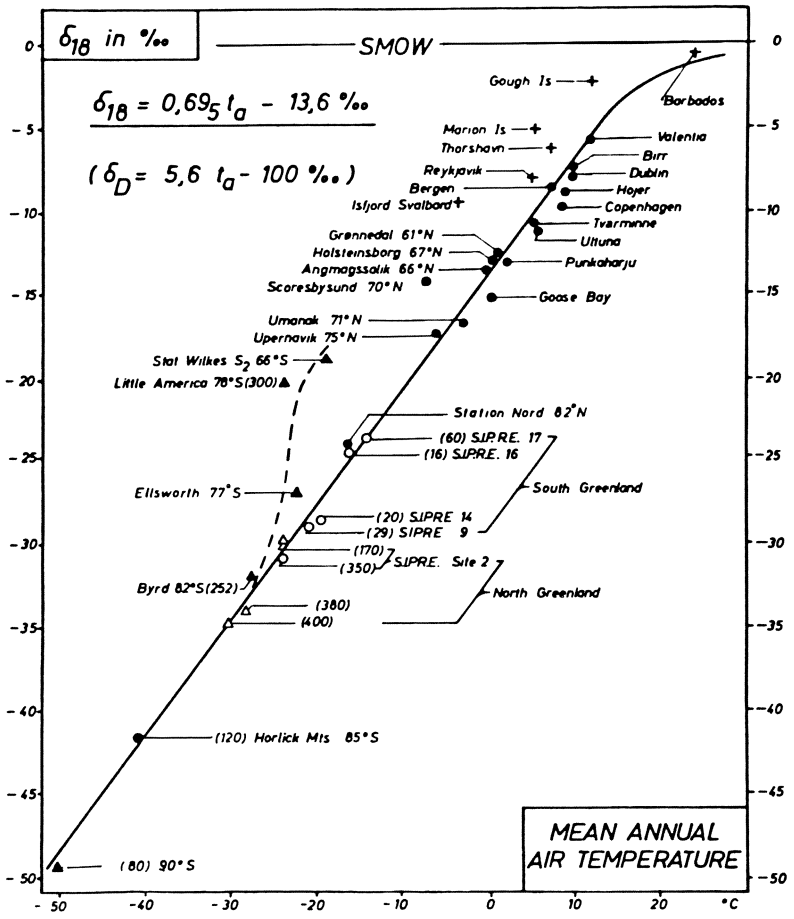

Fig. 1. Annual mean values of $\delta^{18}O$ and of air temperature for coastal and polar stations. (From Dansgaard, 1964)

ferent vapor masses, evaporation and isotope exchange of the falling raindrops or snowflakes with the ambient vapor. A complete description of all these phenomena has not been achieved up to now and will perhaps never be possible.

Figure 2 shows, besides the pronounced seasonal variations, a systematic decrease of $\delta^{18}O$ in precipitation with altitude. One reason for this altitude effect is the progressive rainout of the heavy isotopes during an orographic ascent of most air masses, which occurs on the windward side of a mountain range but not on its lee side. A beautiful example of this orographic effect was observed in the D/H ratio of snow at the Sierra Nevada (Friedman and Smith, 1970). Furthermore, due to evaporation and exchange with ambient vapor, raindrops are enriched in ^{18}O and D during their fall, which leads to an additional altitude effect for rain but not (or little) for snow.

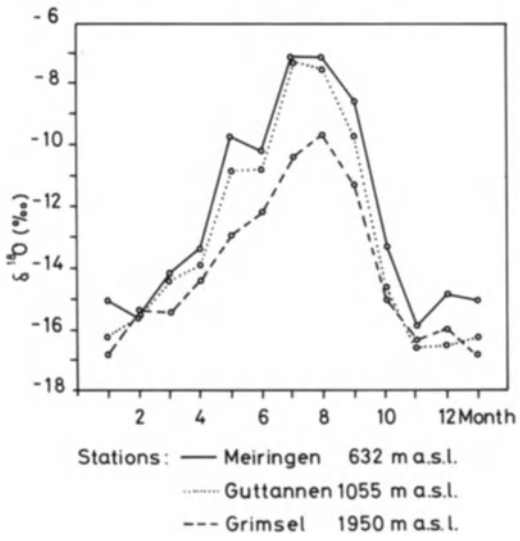

ig. 2. $\delta^{18}O$ in monthly precipitaon samples from three neighbour ations at different altitudes in the wiss Alps, averages for the period 970 to 1976

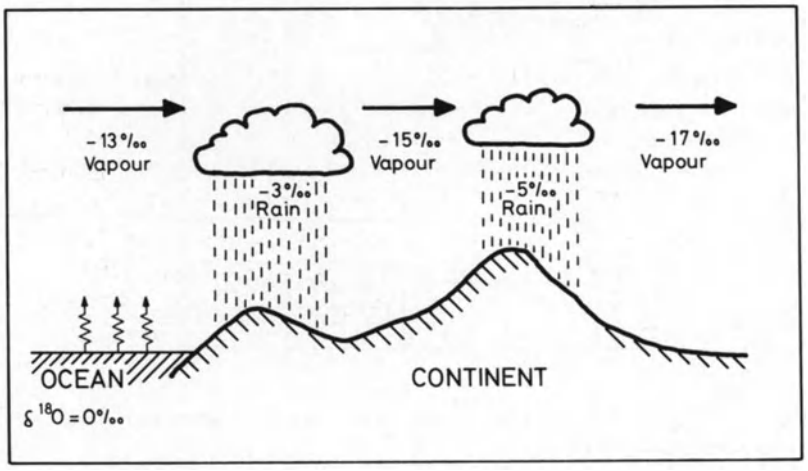

Fig. 3. Schematic ^{18}O fractionation in the atmospheric water cycle

Figure 4 shows mean $\delta^{18}O$ values against altitude for the Bernese Oberland, Switzerland. The average $\delta^{18}O$ gradient is about –0.2‰ per 100 m. Gradients found elsewhere in temperate regions are partly similar, e.g., in investigations in Czechoslovakia (Dinçer et al., 1970) and Greece (Stahl et al., 1974), but a deuterium altitude effect of –3 to –3.5 permill per 100 m was observed in Germany (Moser and Stichler, 1971), corresponding to an oxygen-18 gradient of about –0.4‰ per 100 m. In polar regions the effect is more pronounced, –0.6‰ per 100 m in Greenland (Dansgaard et al., 1969).

The variations observed in precipitation can be summarized qualitatively as a correspondence between temperature and $\delta^{18}O$. There is, however, no unique, globally valid relationship between temperature and $\delta^{18}O$. On a large scale we have, from Figure 1, for mean annual values at different coastal and polar stations 0.7‰/°C.

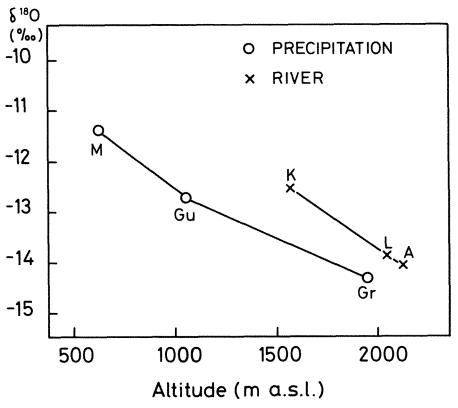

Fig. 4. Mean $\delta^{18}O$ against altitude in the Bernese Oberland, Switzerland, for precipitation (*M*, Meiringen; *Gu*, Guttannen, *Gr*, Grimsel) and for rivers (*K*, Kander; *L*, Lütschine; *A*, Aare). For the rivers the mean altitude of the catchment basin is given, neglecting the altitudinal variation in amount of precipitation

When comparing mean *monthly* values of $\delta^{18}O$ and of temperature at a fixed station, we find a ratio between seasonal variations of $\delta^{18}O$ and of temperature of about 0.5 ‰/°C for the stations shown in Figure 2. And when comparing annual means of $\delta^{18}O$ and temperature at Meiringen and Grimsel, we obtain only 0.35‰/°C.

The temperature dependence of the isotope concentration in precipitation has been used for obtaining valuable paleoclimatic information in studies on polar ice (Johnson et al., 1972) and in lake sediments (Stuiver, 1970; Eicher and Siegenthaler, 1976). Studies on groundwater in regions arid today have shown that old waters ("paleowaters") often have lower $\delta^{18}O$ and δD than recent groundwaters. This es especially well documented for the Middle East and North Africa (e.g., Gat, 1971; Job et al., 1975). The age of these waters, as determined by ^{14}C dating, is typically older than 15,000 years. From the relatively low deuterium and oxygen-18 values it is concluded that the climate in those regions must then have been colder and wetter than today.

2. General Hydrological Applications

The variation of $\delta^{18}O$ and δD with altitude can be used for estimating the altitude of unknown recharge areas of springs (Stahl et al., 1974; Siegenthaler and Schotterer, 1977).

The mixing of waters of differing isotopic composition can be studied by isotope analyses. In the region between Thun and Bern (Switzerland) water from the river Aare infiltrates into the groundwater aquifer and by measuring $\delta^{18}O$ the fraction of river water in the groundwater could be determined as a function of the distance from the channel (Siegenthaler and Schotterer, 1977), cf. Figure 5. The Aare with its catchment basin in the Alps at relatively high altitudes has a lower $\delta^{18}O$ value (about −12.9‰) than groundwater formed locally (−9.8‰).

Natural isotopes have been used for investigating the relationship between rainfall and runoff (Fritz et al., 1976; Mook et al., 1974). When the discharge of a river increases after a storm, it is obvious that the rain is the reason for the flood, but the question re-

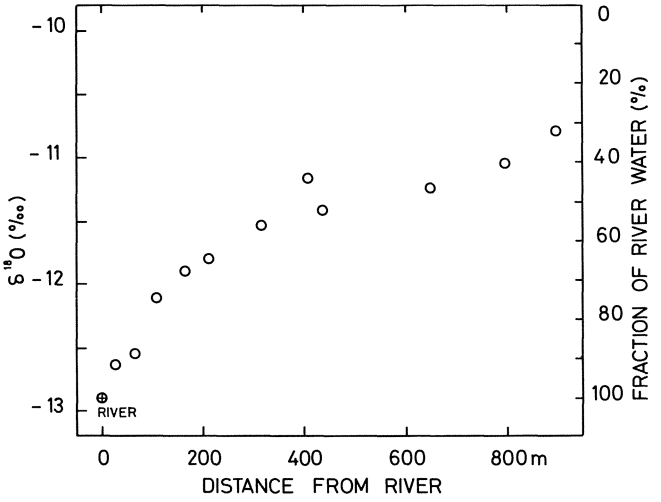

Fig. 5. $\delta^{18}O$ of the Aare river and of groundwater in the Aare valley between Thun and Bern, as a function of distance from the river. Since the local groundwater is known to have $\delta^{18}O \approx -9.8‰$, the relative amount of river water in the groundwater can directly be given *(right-hand scale)*

mains what fraction of the discharge is actually rainwater. In a conventional hydrograph analysis this problem is solved by graphical separation of the hydrograph (= curve of the discharge rate as a function of time) into base flow (older groundwater) and direct runoff (De Wiest, 1965). In contrast to this indirect method, it is possible to determine directly the relative contributions of the different components to the discharge by measuring the isotopic composition of the rainwater and the river water as a function of time. Fritz et al. (1976) measured $\delta^{18}O$ in a creek after a heavy rain; Figure 6 shows the variation of $\delta^{18}O$ and the corresponding separation of the hydrograph into direct runoff ("rainwater") and baseflow ("prestorm water"), assuming that the creek water is a mixture consisting of the two components, baseflow with either −14.0 or −14.5‰, and rainwater with −19.0‰. Even at its peak the discharge consists mainly of older groundwater, and Fritz et al. found that the amount of direct runoff could be accounted for simply by rain that fell directly on the stream channel. All the rest of the rainwater must, therefore, have infiltrated into the ground, and older groundwater came to discharge due to the enhanced hydrostatic pressure. Besides isotopes Fritz et al. also measured ionic concentrations which allowed to distinguish between groundwater components from different segments of the watershed.

Similar studies were performed using the radioactive hydrogen isotope tritium (Dinçer et al., 1970; Martinec et al., 1974). In these studies, too, it was found that a surprisingly large fraction of the discharge consisted of older groundwater. It seems, therefore, that the purely graphical method of hydrograph separation may lead to considerable overestimates of the direct runoff. However, this result cannot be generalized, since regional aquifer characteristics and other features may play an important role.

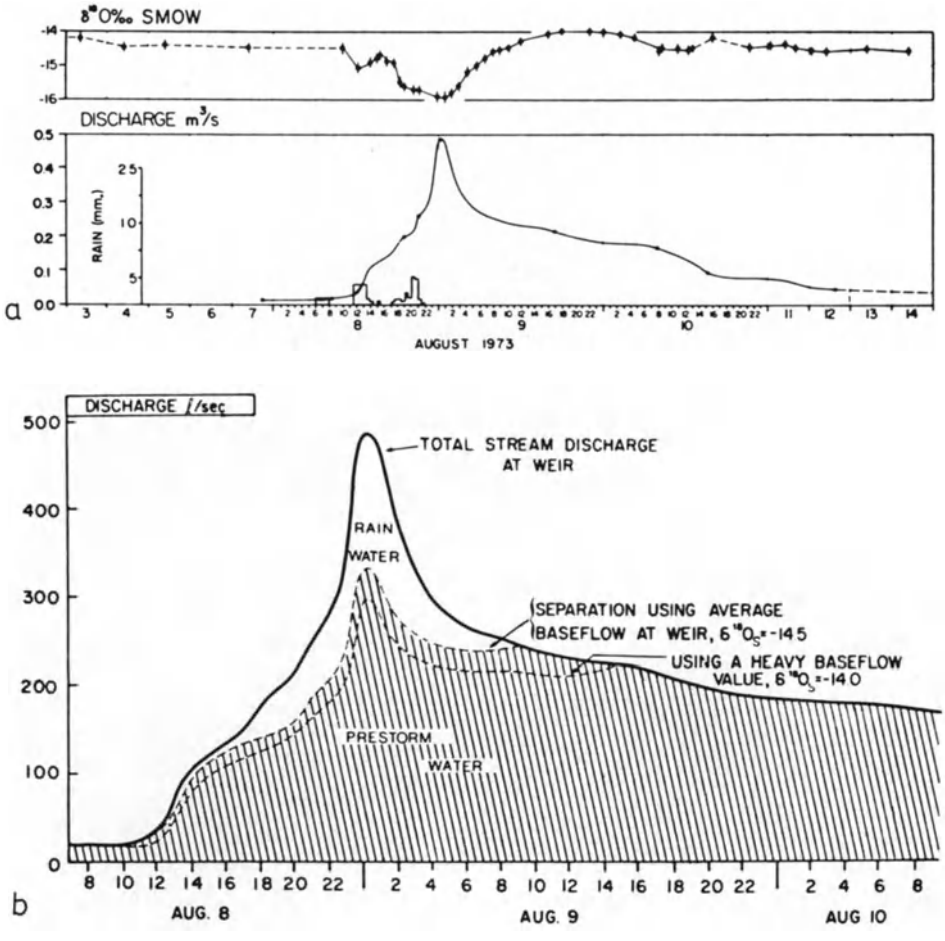

Fig. 6a. Discharge and $\delta^{18}O$ of creek water in Wilson Creek Experimental Watershed, Canada, during a storm event. **b** Separation of the hydrograph according to ^{18}O results, using values of −19.0‰ for the rain and −14.0 or −14.5‰ for baseflow (= prestorm water). (Taken from Fritz et al., 1976)

Indeed, in a case observed by Mook et al. (1974), $\delta^{18}O$ seems to vary, as would be expected from a graphical hydrograph separation.

3. Relationship Between Deuterium and Oxygen-18

In the hydrologic studies mentioned so far the conservative behavior of the environmental isotopes proved useful, that is the fact that their concentration does not change

in the ground, even over tens of thousands of years. However, in lakes and basins where evaporation plays an important role, the heavy isotopes ^{18}O and D are enriched. This is particularly well seen when plotting δD against $\delta^{18}O$. In temperature and cool climates the concentration of both isotopes in precipitation and groundwater is related by the "meteoric water-line" (Craig, 1961; Dansgaard, 1964)

$$\delta_D \cong 8 \cdot \delta_{18} + 10‰.$$

Figure 7 shows δD and $\delta^{18}O$ of monthly precipitation samples of Meiringen, Guttannen and Grimsel (cf. Fig. 2), and we see that the above relationship holds well[2]. The linear relation can be explained by the fact that at equilibrium the concentration difference between water and its vapor is about 8 times larger for δD than for $\delta^{18}O$.

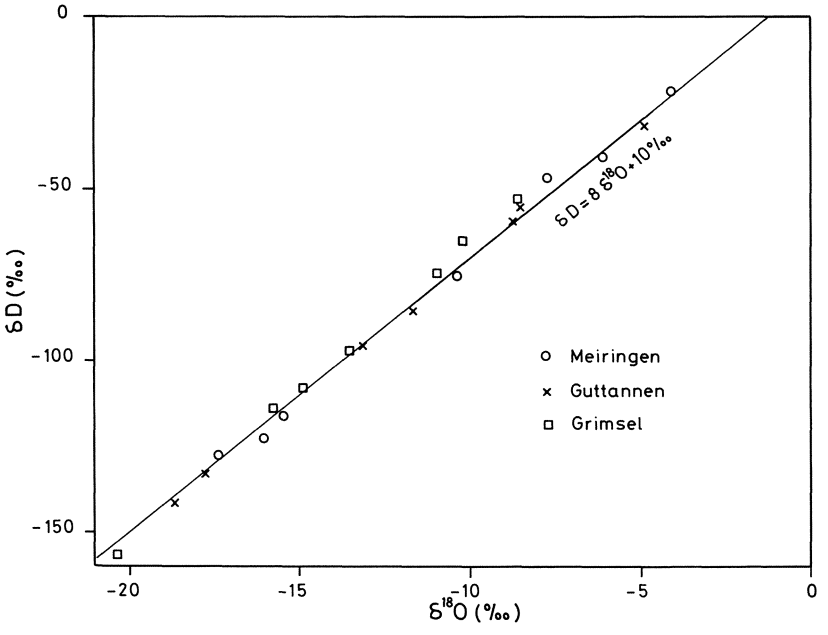

Fig. 7. δD-$\delta^{18}O$ plot for individual monthly precipitation samples. The line ("meteoric water-line") indicates the relationship found globally for most nonevaporated freshwaters (Craig, 1961)

Deviations from the equilibrium line are observed for lakes and other water bodies subject to intense evaporation (Fig. 8). During evaporation the lake water becomes enriched in ^{18}O and D. In contrast to condensation, evaporation in nature mostly takes place under nonequilibrium conditions (i.e., relative humidity significantly

[2] Deuterium was measured on these samples by W. Stichler, Institut für Radiohydrometrie, Gesellschaft für Strahlen- und Umweltforschung, München/Germany; the analyses are gratefully acknowledged.

smaller than 100%), and in addition to equilibrium fractionation there is a diffusional (or "kinetic") isotope fractionation which is stronger for $^{18}O/^{16}O$ than for D/H. This explains why the isotope concentrations in evaporating water, when represented in a δD-$\delta^{18}O$ plot, change according to a line with slope < 8 (Fig. 8). The kinetic fractionation effects are the more important the lower the relative humidity is; in detail, they depend in a relatively complex way amongst other things on the aerodynamic conditions above the air-water interface (Craig and Gordon, 1965; Merlivat and Coantic, 1975). There have been attempts to establish water balances for lakes by means of stable isotopes, but it turns out that even for achieving a modest accuracy, long series of detailed measurements of temperatures, humidity, isotopic composition of the water and of atmospheric water vapor are necessary (Zimmermann and Ehhalt, 1970).

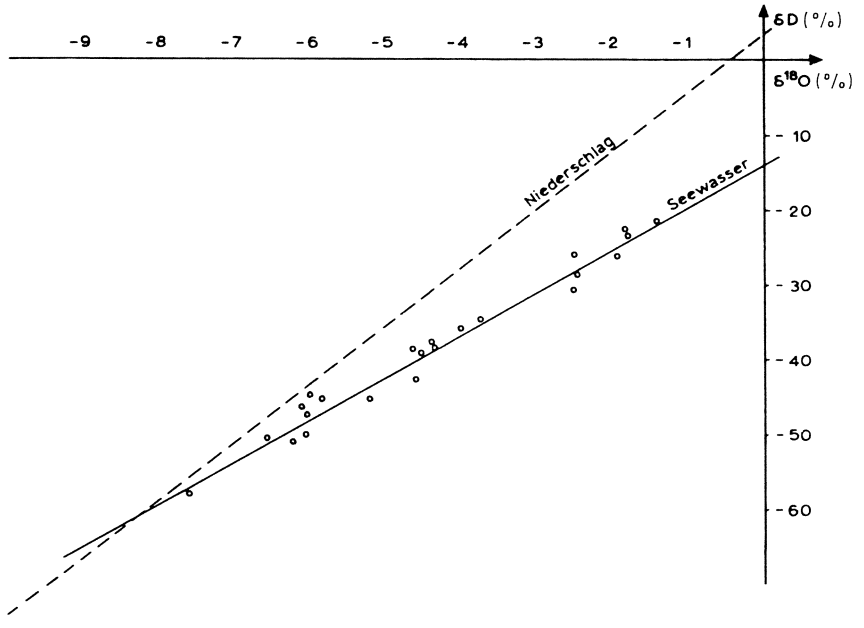

Fig. 8. δD-$\delta^{18}O$ relationship for Lake Neusiedl, Austria. *Circles* and *solid line:* lake water; *dashed line:* precipitation. (After Zimmermann, 1969)

Kinetic fractionation during evaporation from the ocean is responsible for the fact that the meteoric water-line, shown in Figure 7, does not pass through the point $\delta D = 0$, $\delta^{18}O = 0$, indicating the average seawater composition. Water vapor over the ocean has an initial composition of about $\delta D = -94‰$, $\delta^{18}O = -13‰$ (whereas equilibrium vapor would have $\delta D = -80‰$, $\delta^{18}O = -10‰$ at 20°C). Condensation proceeds in equilibrium since the relative humidity is always close to 100%, so the first condensate will have about $\delta D = -14‰$, $\delta^{18}O = -3‰$.

While the isotopic composition of groundwater remains constant with time under normal conditions, this need no longer be so at elevated temperatures, when oxygen

exchange with the surrounding rocks may become important. Thus in many thermal waters or steams $\delta^{18}O$ is shifted towards positive values compared to local meteoric water from which the springs are derived, as shown in Figure 9, taken from Craig (1963) who has studied many geothermal systems. The shift is towards $\delta^{18}O$ of the rocks because at the elevated temperatures at which the oxygen exchange takes place the isotopic fractionation vanishes. There is essentially no shift for deuterium which simply reflects the fact that the rocks contain hardly any hydrogen which could exchange with the water.

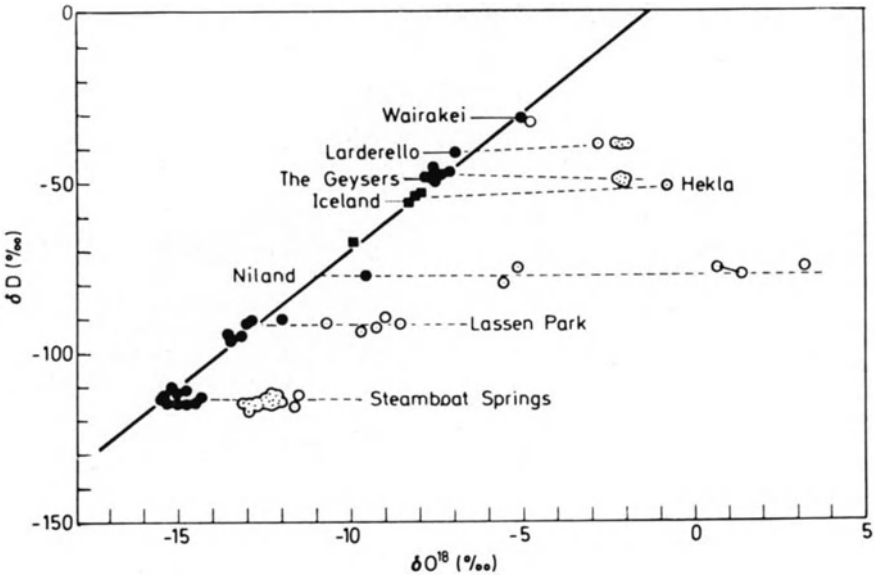

Fig. 9. δD-$\delta^{18}O$ plot for geothermal waters and steams (○) and local meteoric waters (●); after Craig (1963). Niland = Salton Sea geothermal area (California)

By means of these isotope results it was found that the water in most geothermal areas must be of meteoric origin and contains only small amounts, if any, of juvenile water ("juvenile" in the sense that this water has never taken part in the meteoric water cycle, i.e., excluding magmatic water which may be recycled surface water). As shown in Figure 9 the deuterium content of the thermal waters and steams coincides with that of local meteoric water. If the oxygen shifts were due to admixtures of juvenile water, there would also be a corresponding deuterium shift, and the lines in Figure 9 would converge towards a common origin indicating the isotopic composition of juvenile water.

References

Craig, H.: Science *133*, 1702-1703 (1961)
Craig, H.: The isotopic geochemistry of water and carbon in geothermal areas. In: Nuclear Geology on Geothermal Areas, Spoleto, 1963
Craig, H., Gordon, L.I.: In: Conf. Stable Isotopes in Oceanographic Studies and Paleotemperatures, Spoleto, Italy, 9-130, 1965
Dansgaard, W.: Tellus *16*, 436-468 (1964)
Dansgaard, W., Merlivat, L., Roth, E.: Meddelelser om Grønland *177*, 62-75 (1969)
Dinçer, T., Martinec, J., Payne, B.R., Yen, C.K.: In: Isotope Hydrology 1970 (Int. At. Energy Agency, Vienna), 23-42 (1970)
Dinçer, T., Payne, B.R., Florkowski, T., Martinec, J., Tongiorgi, E.: Water Resour. Res. *6*, 110 (1970)
Eicher, U., Siegenthaler, U.: Boreas *5*, 109-117 (1976)
Friedman, I., Redfield, A.C., Schoen, B., Harris, J.: Rev. Geophys. *2*, 1977 (1964)
Friedman, I., Smith, G.I.: Science *169*, 467-470 (1970)
Fritz, P., Cherry, J.A., Weyer, K.U., Sklash, M.: In: Interpretation of Environmental Isotope and Hydrochemical Data in Groundwater Hydrology (Int. At. Energy Agency, Vienna), 111-130 (1976)
Gat, J.R.: Water Resour. Res. *7*, 980-993 (1971)
Job, C., Moser, H., Rauert, W., Stichler, W., Zötl, J.: Naturwissenschaften *62*, 136-137 (1975)
Johnson, S.J., Dansgaard, W., Clausen, H.B., Langway, C.C.: Nature (London) *235*, 429-424 (1972)
Martinec, J., Siegenthaler, U., Oeschger, H., Tongiorgi, E.: In: Isotope Techniques in Groundwater Hydrology 1974 (Int. At. Energy Agency, Vienna). Vol. I, 139-143 (1974)
Merlivat, L., Coantic, M.: J. Geophys. Res. *80*, 3455-3464 (1975)
Mook, W.G., Groeneveld, D.J., Brouwn, A.E., van Ganswijk, A.J.: In: Isotope Techniques in Groundwater Hydrology 1974 (Int. At. Energy Agency, Vienna), Vol. I, 145-155 (1974)
Moser, H., Stichler, W.: Geol. Bavar. *64*, 7-35 (1971)
Siegenthaler, U., Schotterer, U.: Gas, Wasser, Abwasser *57*, 501-506 (1977)
Stahl, W., Aust, H., Dounas, A.: In: Isotope Techniques in Groundwater Hydrology 1974 (Int. At. Energy Agency, Vianna), Vol. I, 317-339 (1974)
Stuiver, M.: J. Geophys. Res. *75*, 5247-5257 (1970)
Wiest, R.J.M. De: Geohydrology. New York, London: Wiley, 1965
Zimmermann, U.: Ph.D. thesis, Heidelberg, 1969
Zimmermann, U., Ehhalt, D.H.: In: Isotope Hydrology 1970 (Int. At. Energy Agency, Vienna), 129-138 (1970)

Carbon Isotopes in Petroleum Geochemistry

W. J. STAHL

1. Variation of Carbon Isotopes in Kerogen and Petroleum

Carbon consists of two stable isotopes, carbon 12 and carbon 13, which differ by the mass of only one neutron in the nucleus. The ratio $^{13}C/^{12}C$ in organic and inorganic matter is approximately 0.01 and varies up to 10% in nature.

Carbon isotope ratios are determined by gas mass spectrometry and reported as δ-values. A δ-value is the difference between the isotope ratios of a sample and a standard, related to the isotope ratio of the standard used.

$$\delta = \frac{(^{13}C/^{12}C)^{\text{sample}} - (^{13}C/^{12}C)^{\text{standard}}}{(^{13}C/^{12}C)^{\text{standard}}} \cdot 1000\ (‰)$$

All data presented in this paper are compared with the PDB-standard. PDB is a standard formed by the extraction of CO_2 from the carbonate shell of the Belemnite rostrum taken from the Peedee Formation in the United States. It represents the $^{13}C/^{12}C$ composition of a marine carbonate.

Natural variations in carbon isotopes are caused by equilibrium exchange and kinetic fractionation processes (cf. Hoefs, 1973) in the different carbon cycles. In this way, carbon isotopes give information on the generation, maturation and genetic correlation of hydrocarbons and their precursors which can be used in oil and gas exploration. Figure 1 shows the carbon isotope variations of the methane in natural gases, crude oils, coals and their precursors.

Atmospheric carbon dioxide is the ultimate source of all natural carbon. It is in isotopic equilibrium with marine bicarbonate which is enriched in ^{13}C and which, in part, is used to build marine organisms. The photosynthetic fixation of carbon from atmospheric carbon dioxide is accompanied by a kinetic isotope fractionation in which carbon 13 becomes depleted in terrestrial plants. Terrigenous carbon is ^{13}C-depleted in comparison with marine organic carbon due to different fractionation processes during the fixation of carbon.

Plankton, plants, and marine organisms deposited in sedimentary basins are attacked in the unconsolidated sediment by bacteria and transformed into humic acid complexes. These complexes are diagenetically converted into kerogen, which is defined as the insoluble organic carbon in sediment, and is believed to be the source material of petroleum. The carbon isotope variation of kerogen is mainly characterized by δ-values from -33 to -17‰, but isotopically heavier carbon has to be expected if the photo-

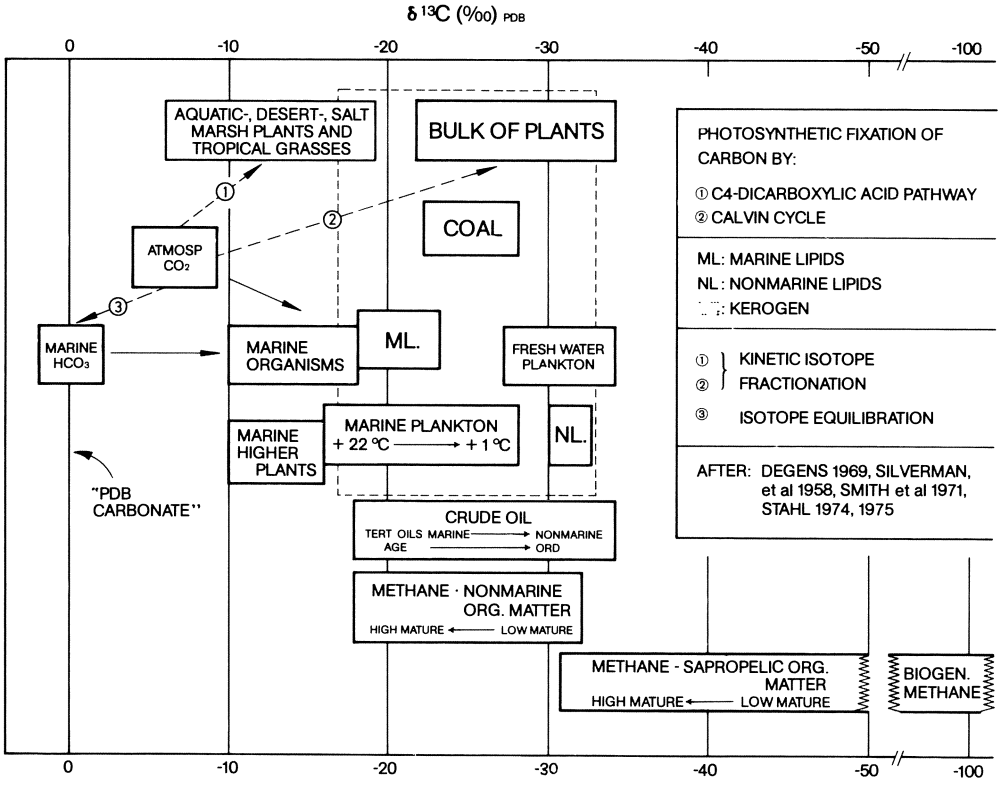

Fig. 1. Carbon isotope ratios of natural gases, crude oils and their source materials

synthetic fixation of carbon follows the C4-dicarboxylic acid pathway (Smith and Epstein, 1971).

Cruide oils are (about 2‰ or less) depleted in ^{13}C in comparison to the kerogen from which they were generated (Scalan, 1972). Most crude oils are characterized by δ-values between −34 and −18‰. The differentiation of marine and nonmarine crude oils by carbon isotopes should therefore be possible due to the isotope relationship between crude oil and kerogen. However, the isotopic differentiation works well only with Tertiary petroleums (Silverman and Epstein, 1958) due to masking by other isotope fractionation phenomena, for example, the slight age trend in favor of the ^{12}C isotope with increasing geologic age (Degens, 1969; Stahl, 1976). Methanes from nonmarine natural gas deposits have a spread in δ-values similar to coal, about −30‰ to −20‰, and show a relationship between the maturity of their organic source material and the carbon isotope composition (Stahl and Koch, 1974). The carbon isotope composition of methanes from predominantly marine source rocks is characterized by a similar maturity relationship. Methane from a marine environment is, however, ^{12}C enriched in comparison with "terrestrial" methane. Thermocatalytic gases from a marine environment have methane δ-values from about −50% (low mature) to −30%

(overcooked source rock). High ^{13}C depletions in methane gases are assumed to be characteristic of a bacterial gas formation ($\delta C_1 = -55‰$ to $-100‰$).

2. Carbon Isotope Fractionation During the Generation and Maturation of Hydrocarbons

Most commercial hydrocarbon accumulations have been generated by thermal transformation of kerogen during the burial of their source rocks. This maturation process is accompanied by systematic changes in the chemical (Tissot et al., 1974) and optical properties of organic matter, i.e., spore coloration (Gutjahr, 1966) and vitrinite reflectance (Stach et al., 1975). Vitrinite is mainly derived from the lignin-cellulose complex of plants. It is frequently found dispersed in marine sediments where it was carried in by continental runoff, winds, or rivers. The vitrinite reflectance, R_0, can be precisely measured on tiny particles using a sensitive microscope photometer. It changes from about $R_0 = 0.3\%$ in immature organic matter to $R_0 \geqslant 3\%$, which is characteristic of overcooked kerogen. Moreover, isotope fractionation in favor of the heavier isotope takes place during maturation which is caused by the difference in binding energies between ^{12}C-^{12}C- and ^{13}C-^{12}C-bonds. Methane produced from the organic carbon complexes under thermal stress is enriched in ^{12}C in comparison to its source material because less energy is needed to break ^{12}C-^{12}C-bonds. The organic matter and the emerging gaseous hydrocarbon components become isotopically heavier during maturation. These isotopic changes due to maturation are frequently masked in kerogen and crude oil, but are evident in the methane natural gas accumulations.

Figure 2 shows the δ-values of methane from natural gas deposits located in different sedimentary basins in relation to the maturity of the predominantly marine organic matter which is assumed to be the source of the gas.

The carbon isotope ratios of methane vary over a range of more than 80‰ (Fig. 1) and are determined by:

1. The mechanism of origin (biogenic or thermal generation)
2. the general type of the organic source material undergoing thermal alteration, and
3. the level of maturation of the organic source material.

Biogenic methanes are ^{13}C depleted and generally characterized by δC_1 values less than $-55‰$, with possible minimum values of less than $-100‰$. Methane produced from the thermal alteration of dominantly marine organic matter is characterized by carbon isotope ratios from about $\delta C_1 = -50‰$ ($R_0 \approx 0.5\%$) at the beginning of the oil window to $\delta C_1 = -32\%$ ($R_0 \approx 3\%$) at a depth where only methane can exist. The "oil window", i.e., the depth range in a sedimentary basin where the time-temperature conditions favor the generation of crude oil, is marked by $\delta C_1 \approx -50‰$ ($R_0 \approx 0.5\%$) to $\delta C_1 \approx -40‰$ ($R_0 \approx 1.2‰$). The carbon isotope ratios of methane derived by thermal alteration of predominantly nonmarine organic matter show a similar maturation trend, but the methane is generally enriched in ^{13}C by approximately 14‰ in comparison to methane coming from a marine source of the same maturity (Stahl and Koch, 1974).

$^{13}C/^{12}C$ analyses on methane from natural gas deposits allow the determination of the type and maturity of the organic matter which has generated the gases and the distinction between thermal and bacterial gases.

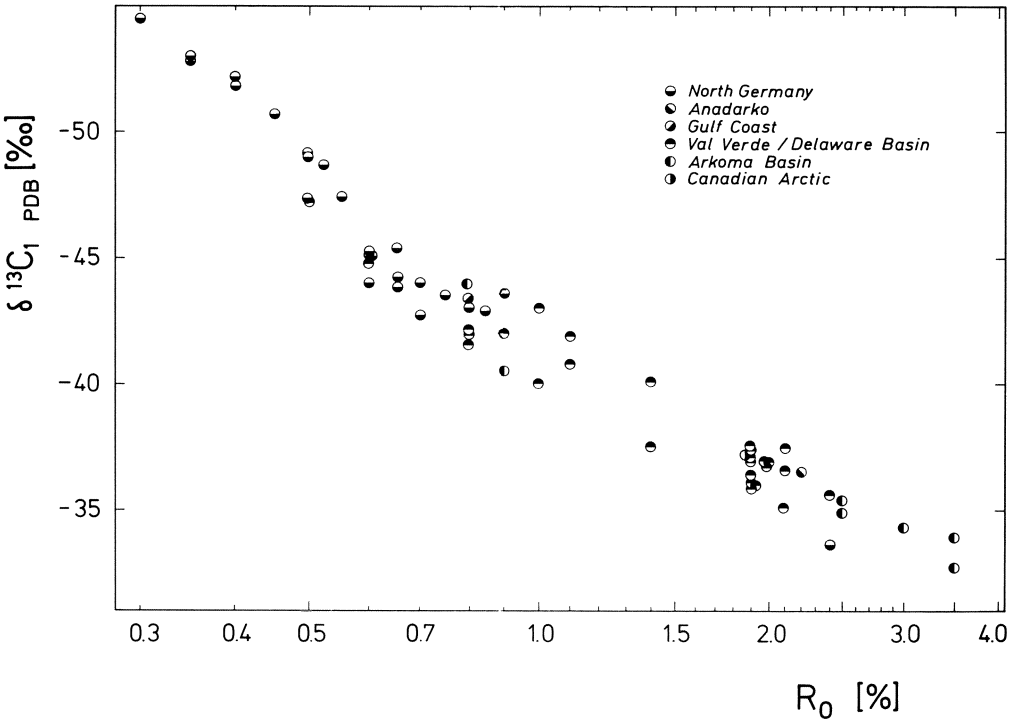

Fig. 2. δC_1 data of natural gases from different basins in relation to the maturity of their source material. (Anadarko-, Arkoma-, Val Verde-, Delaware Basin, Gulf Coast, Canadian Arktic and North Germany)

3. Carbon Isotopes in the Methane of Adsorbed Gas from Cuttings

Analyses of the $^{13}C/^{12}C$ ratios of gases adsorbed in cuttings which have been collected and canned from different depths during drilling is a technique that was recently introduced as a tool for obtaining data on the generation and maturation of hydrocarbons (Menendez, 1973; Stahl et al., 1977). Hydrocarbon composition and the carbon isotope ratios of these gases, however, can be considerably changed by secondary desorption fractionation due to the pressure decrease which takes place while the cuttings are being brought to the surface. Desorption fractionation is most pronounced in cutting gases taken from sandy sections, and less so, at least for the isotope data, in cuttings from shales.

Desorption effects can be recognized in depth plots by:

1. High methane readings in the gas log, but a low methane content in the headspace of the corresponding can, and

2. an anomalously high content of higher hydrocarbons and ^{13}C enriched methane in the desorbed gas from the cuttings.

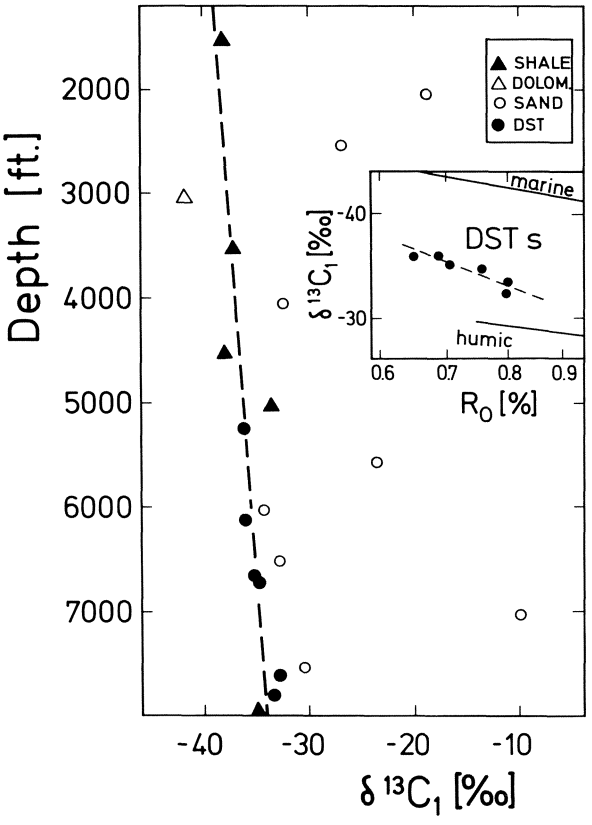

Fig. 3. Carbon isotopes of methane in relation to depth and maturity: δC_1 data of gases, desorbed from cuttings in comparison with the carbon isotope composition of the methane from drill stem tests (DST's)

Figure 3 shows an isotope-depth profile from an offshore well near Thailand, where δC_1-values, desorbed from shales and sands, are compared with the carbon isotope composition of methanes from drill stem tests. The isotope ratios of gases desorbed from shale cuttings are in contrast to the gases desorbed from sands fully in line with the isotope determinations on the methane from the gas tests. The comparison of δC_1 with the maturity data indicates that the gases have been formed by a mixed, predominently humic, source rock (Faber et al., 1977).

Isotope analyses of the methane desorbed from cuttings and corrected for secondary fractionation, will indicate in a depth plot:

1. The level of maturation and its increase with depth,
2. the general type of organic source material from which the hydrocarbons adsorbed in the cuttings had been generated, and
3. the presence of migrated gases and the approximate maturity of their source rocks.

4. The Use of Carbon Isotopes in Correlation Studies

Carbon isotopes have been used in correlation studies for many years. The $^{13}C/^{12}C$ ratios of kerogen, extract, and oil are equal or only slightly divergent if the kerogen, extract, and oil are genetically related. Oil-oil correlations, based on carbon isotopes, have been established by the separation of crude oils into small distillation fractions, i.e., into fractions based on the size of hydrocarbon molecules (Silverman, 1971). Another correlation method, the isotopic type-curve technique, is based on the separation of crude oils or extracts into fractions of different molecular types, i.e., into saturated hydrocarbons, aromatics, heterocompounds and asphaltenes (Stahl, 1978). The crude oil or extract fractions show a systematic ^{13}C enrichment with increasing polarity or polarizibility, i.e., the isotopic composition of the saturated hydrocarbon fractions is isotopically lightest, and that of the asphaltene fractions is the most enriched in ^{13}C. The $^{13}C/^{12}C$ ratios of asphaltenes and kerogen are very similar if the asphaltene fraction and the kerogen are genetically related. An empirical estimate of the $\delta^{13}C$ kerogen value from which a crude oil or an extract has been derived can be carried through by extrapolation of the systematically increasing $^{13}C/^{12}C$ ratios of the crude oil or extract fractions. The extract-kerogen correlation (Fig. 4) indicates that the extract fractions have been formed in situ and are genetically related to the kerogen under discussion.

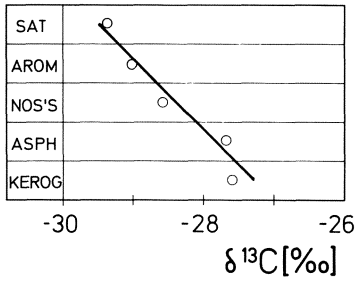

Fig. 4. Extract-kerogen correlation, North Sea, Jurassic

Moreover, the relationship between the carbon-isotope ratios of methane, maturity and type of organic matter from which the natural gas has been formed, can be used to correlate gases and with source rocks (cf. Fig. 5).

5. Application of Carbon Isotopes in Petroleum Exploration

The application of carbon isotopes in petroleum exploration is based on correlation methods; they have been used for correlations of gases with source rocks in wildcat wells drilled in the Arctic and offshore from Egypt, where gases from immature,

mature, and overcooked rocks have been recognized. Figure 5 gives an example (Stahl et al., 1977).

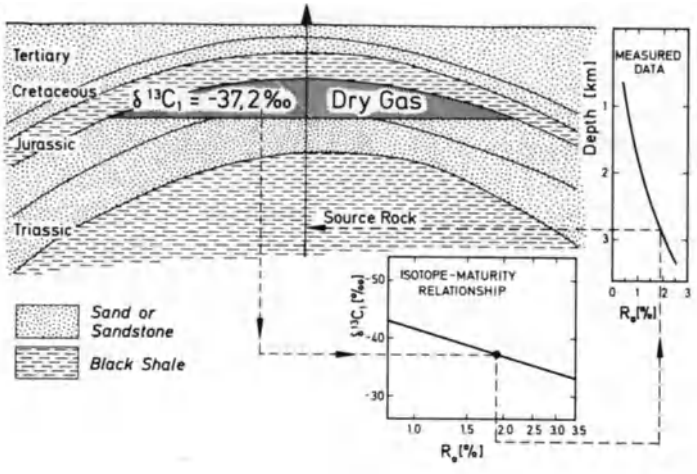

Fig. 5. Isotopic gas source rock correlation – Canadian Arctic

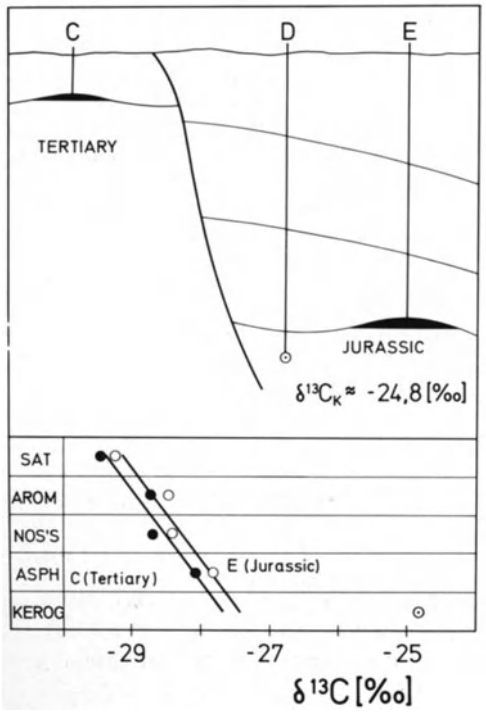

Fig. 6. Oil-oil and source rock-oil correlation, North Sea

A gas was discovered in a Jurassic sand on a large anticline in the Arctic. The dry gas could have originated in the relatively immature deltaic facies of the Lower Cretaceous-Jurassic section (R_0 of 0.50% to 0.65%) or from a thermally overcooked Triassic black shale (R_0 of 1.03% to 2.00%). The isotope analysis yielded $\delta^{13}C_1 = -37.2‰$, and an "isotopic" vitrinite reflectance of $R_0 = 1.9\%$). The gas thus could only have originated in the Triassic black shales at a considerable depth below the horizon. It was apparent to the exploration geologists that any search for similar type deposits of gas was dependent on the existence of the Triassic black shale beneath the reservoir objective, and should be independent of the organic facies of the Lower Cretaceous-Jurassic section.

An example of a positive crude oil-crude oil and a negative crude oil-source rock correlation is presented in Figure 6 (Stahl et al., 1977).

Both the Tertiary and the Jurassic crude oil are isotopically more or less identical. This strongly points to a common organic source material. The $^{13}C/^{12}C$ ratio of the kerogen, however, is not in line with the type-line, thus indicating a migration from elsewhere into both reservoirs.

The use of carbon isotopes in the search for petroleum (Fuex, 1977; Stahl, 1977) is more and more accepted as a valuable tool which can efficiently support hydrocarbon exploration.

References

Degens, E.T.: Biochemistry of stable carbon isotopes. In: Organic Geochemistry. Eglington, Murphy, M.T.J. (eds.). Berlin, Heidelberg, New York: Springer, 1969

Faber, E., Stahl, W., Carey, B.D.: Anwendung von Isotopenmethoden bei der Exploration auf Kohlenwasserstoffe. Erdöl Kohle, Compendium 77/78, 380-391. Leinfelden-Echterdingen: v. Hernhaussen 1977

Fuex, A.N.: The use of stable isotopes in hydrocarbon exploration. J. Geochem. Explor. *7*, No. 2, 155-188 (1977)

Gutjahr, C.C.M.: Carbonisation measurements of pollen grains and spores and their application. Leidse Geol. Meded. *38*, Leiden (1966)

Hoefs, J.: Stable Isotope Geochemistry. Berlin, Heidelberg, New York: Springer, 1973

Menendez, R.: Composition isotopique du carbone dans les gaz provenant de sondages d'Aquitaine. Bull. Cent. Rech. Pau – SNAP *7*, 1, 69-81 (1973)

Scalan, R.S.: Reservoir analysis, US Patent 3.649.201 – 14.3.1972

Silverman, S.R.: Influence of petroleum origin and transformation on its distribution and redistribution in sedimentary rocks. Proc. 8th World Petrol. Cong. *2*, 47-54 (1971)

Silverman, S.R., Epstein, S.: Carbon isotopic compositions of petroleums and other sedimentary organic materials. AAPG Bull. *42*, No. 5, 998-1012 (1958)

Smith, B.N., Epstein, S.: Two categories of $^{13}C/^{12}C$ ratios for higher plants. Plant Physiol. *47*, 380-384 (1971)

Stach, E., Mackowsky, M.-Th., Teichmüller, M., Taylor, G.H., Chandra, D., Teichmüller, R.: Coal Petrology. Berlin, Stuttgart: Gebrüder Bornträger, 1975

Stahl, W.: Kohlenstoff-Isotopenverhältnisse von Erdgasen – Reifekennzeichen ihrer Muttersubstanzen. Erdöl Kohle *28*, 188-191 (1975)

Stahl, W.: Economically important applications of carbon isotope data of natural gases and crude oil. In: Nuclear Techniques in Geochemistry and Geophysics. Wien: Int. Atomic Energy Agency, 1976

Stahl, W.: Carbon and Nitrogen Isotopes in Hydrocarbon Research and Exploration. Chem. Geol. *20*, 121-149 (1977)
Stahl, W.: Source rock – crude oil correlation by isotopic type-curves. Geochim. Cosmochim. Acta *42*, 1573-1577 (1978)
Stahl, W., Faber, E., Schmitt, M.: Carbon isotopes in oil and gas exploration. In: Nuclear Techniques and Mineral Resources 1977. Wien: Int. Atomic Energy Agency, 1977
Stahl, W., Koch, J.: $^{13}C/^{12}C$-Verhältnis norddeutscher Erdgase – Reifemerkmal ihrer Muttersubstanzen. Erdöl Kohle *27*, 623 (1974)
Tissot, B., Durand, B., Espitalie, J., Combaz, A.: Influence of nature and diagenesis of organic matter information of petroleum. AAPG Bull. *58*, No. 3, 499-506 (1974)

Sulfur Isotopes

H. NIELSEN

1. Introduction

Sulfur, the element number 16, is characterized chemically by its position between oxygen and selenium in the sixth group of the periodic table. It comprises four stable isotopes with the following relative abundances in terrestrial materials:

$^{32}S \approx 95\%$
$^{33}S \approx 0.77\%$
$^{34}S \approx 4.2\%$
$^{36}S \approx 0.017\%$

Because abundance variations from isotope fractionation depend on the relative mass differences, each geologic sample of homogeneous isotopic composition is characterized unequivocally by a single ratio value. It is convenient to measure the ratio between the two most abundant isotopes, i.e., $R = {}^{34}S/{}^{32}S$. The two other ratios $^{33}S/^{32}S$ and $^{36}S/^{32}S$ are of interest only for extraterrestrial materials, where excessive amounts of these rarest isotopes can be produced by nuclear reaction with high energy radiation.

Sulfur isotope data are published normally in the δ-notation:

$$\delta^{34}S\,(‰) = \frac{R_{sample} - R_{standard}}{R_{standard}} \times 1000$$

Primary standard is troilite sulfur from the Canon Diablo meteorite. Its $^{34}S/^{32}S$ is taken as 0.0450045 (or $^{32}S/^{34}S = 22.220$) by convention (Ault and Jensen, 1962).

Care must, however, be taken with the data of some early papers applying different δ equations or zero point adjustments. Furthermore, some Russian authors were still recently applying a % instead of the ‰ scale, and in some translated papers these different symbols have been confused.

Figure 1 gives a synopsis of the S isotope distribution in a variety of typical natural sulfur compounds. Because troilite sulfur agrees isotopically with the overall mean of terrestrial sulfur, the δ values of individual samples can be interpreted directly in terms of the net fractionation of the materials against the terrestrial mean.

The whole δ range of natural samples reported until late 1977 extends from $\sim -65‰$ to $\sim +95‰$, but 98% of all samples investigated at the Göttingen lab are within $-40‰$ and $+40‰$. This "typical δ range" of about 80‰ can be compared with the date re-

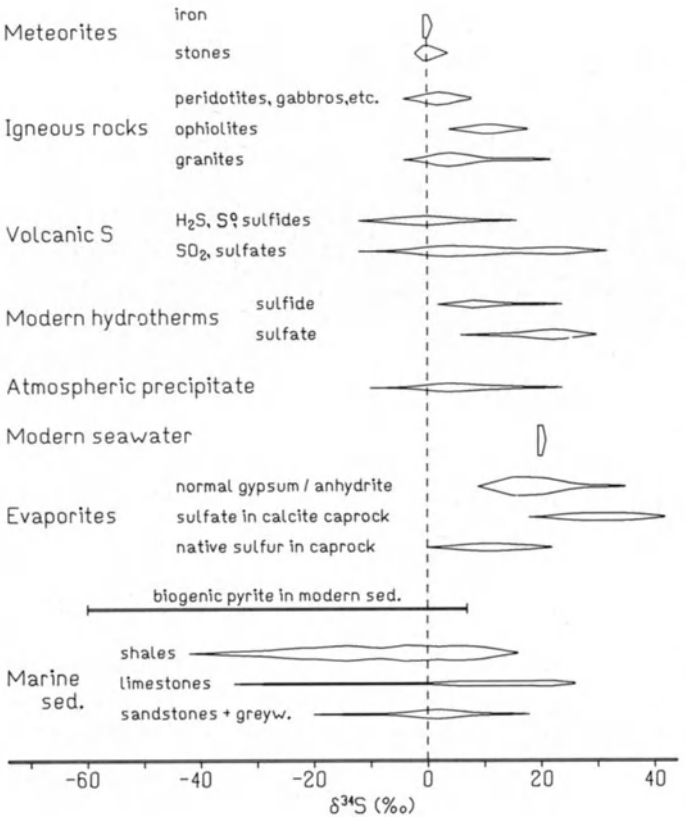

Fig. 1. Synopsis of $\delta^{34}S$ distribution patterns of some natural material of geochemical relevance

ported for other light elements only, when the relative mass differences between the isotopic species are taken into account. Then it comes out that sulfur is the element with the most effective stable isotope fractionation processes in nature. This is due to some peculiarities in its chemical behavior under the conditions prevailing at the uppermost levels of the Earth's crust:

1. Under varying redox conditions the valence of the sulfur atom can change from S^{2-} via S^0 to S^{4+} and S^{6+}. Metastable complexes with intermediate valences such as S_2^{2-}, S_3^{2-}, S_4^{2-}, S_5^{2-}, S_6^{2-}, $S_2O_3^{2-}$, can appear during the gentle oxidation of dissolved H_2S. The S_2^{2-} (or S^{1-}) group, however, forms the stable mineral pyrite (FeS_2) and this is by far the most abundant sulfide mineral in sedimentary rocks.

2. Inorganic reduction of sulfate needs such a high activation energy that the reaction with naturally available reductants is confined to temperatures probably above 250°C, i.e., to environments deep in the crust. Enzymatic complexing of the sulfate ion lowers this threshold and enables the reduction by living cells. This is the entry step into the "biological sulfur cycle" and the mechanism responsible for most of the global variation in S isotopic composition.

3. In cold water metal sulfides are practically insoluble, while the solubility of sulfates (even that of $BaSO_4$) is high enough to make sulfate the mobile sulfur phase on

Earth's surface. When a rock unit contains sulfide and sulfate under equilibrium conditions, any circulation of groundwater will extract dissolved sulfate from the system. Generally this involves also a spatial separation between isotopically "light" and "heavy" sulfur.

4. This geochemical behavior favors the formation of local accumulations of sulfur minerals, either sulfides or sulfates, in an environment with consistently lower background concentration of sulfur. Once consolidated, such local "pools" withstand the attack of geologic processes for geologic times, and they will also preserve their natural S isotope record. Most of the data collected in Figure 1 have been obtained from such accumulations of the different sulfur species.

2. Mechanisms of S Isotope Fractionation

Sulfur isotopes can be fractionated in equilibrium systems and during kinetic reactions. Typical systems with **isotope exchange** under (approached) **equilibrium fractionation** are:

1. Sulfide and sulfate in the magmatic environment and in hydrothermal fluids at temperatures above 250°C (?)
2. H_2S and SO_2 in volcanic vents
3. dissolved sulfide and precipitating sulfide minerals in hydrothermal fluids.

In the most interesting temperature range the fractionation factor

$$\alpha_{1,2} = \frac{R_1}{R_2}$$

between the exchanging sulfur species 1,2 is proportional to $1/T^2$ (K). As is explained in some detail in the chapter by O'Neil, the measured δ difference Δ between the individual samples is related with α by the approximation

$$\Delta_{1,2}\ (‰) \equiv \delta_1 - \delta_2 \approx 1000 \ln \alpha.$$

The curves in Figure 2 show the variation with temperature of 1000 ln α for some major sulfur compounds. These curves enable the construction of geologic thermometers, but care must be taken with the interpretation of the thermometer readings.

For example, in most hydrothermal ore deposits the sulfate-sulfide thermometer gives too high "temperatures". In some cases this may be interpreted with a quenched isotope equilibrium distribution from greater depth, but in other cases the δ distribution patterns demonstrate clearly that equilibrium has never been attained.

A specific S isotope thermometer is established for pairs of base metal sulfides that have been deposited simultaneously from a common hydrothermal ore fluid (Fig. 3). This thermometer has found some application in the classification of ore deposits. The best results are obtained from the pair sphalerite-galena, while pairs with pyrite frequently exhibit irregular Δ values. Apparently some of the pyrite in hydrothermal ore deposits originates from other sources of sulfur.

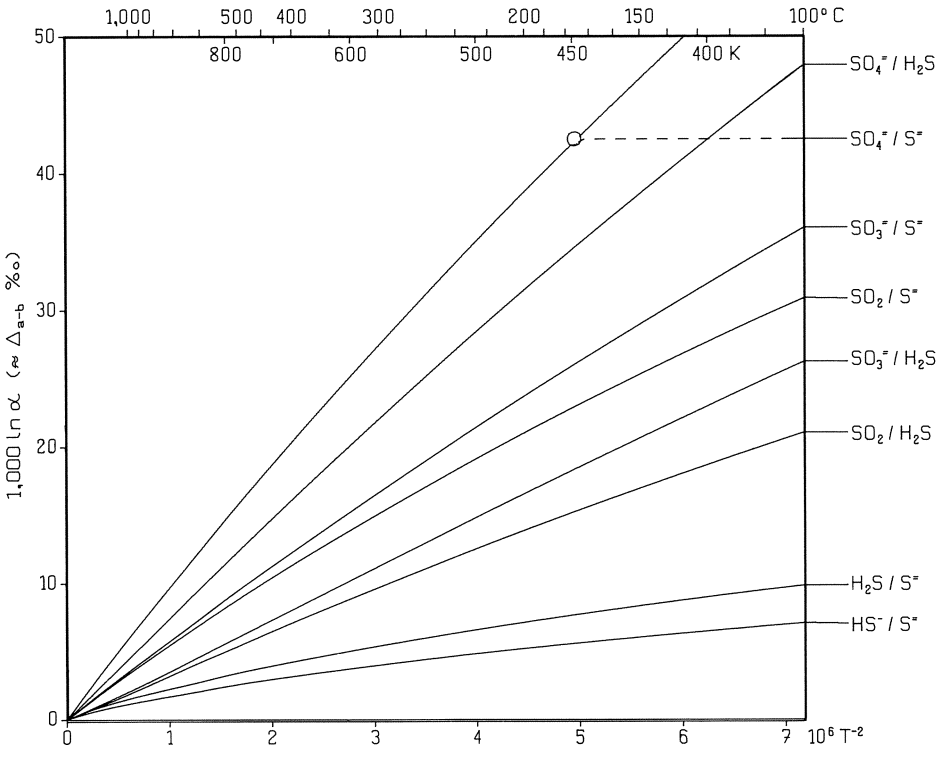

Fig. 2. Calculated temperature curves of the "reduced fractionation factors" 1000 ln α for some major pairs of sulfur compounds under isotope exchange equilibrium. Data calculated by H. Sakai in 1977

When mineral assemblages have been deposited under (approached) isotopic equilibrium, the δ values also give indications of changes in pH and oxygen activity. With respect to the importance of such information for the understanding of ore-forming processes the theoretical background will be treated briefly in this chapter. For more details the reader is referenced to Sakai (1968), Ohmoto (1972), or Rye and Ohmoto (1974).

The pH-logf_{O_2}-T diagram of Figure 4 comprises three major arrays with either molecular H_2S, the S^{2-}ion, and sulfate as the predominant dissolved sulfur species. The transitional zones, combined to a Y-shaped body with stippled signature, are drawn in such a manner that in their interior the partitioning of the individual species varies between 1 : 10 and 10 : 1. Furthermore the stability fields of pyrite, pyrrhotite, and barite are inserted at the 250°C plane. The boundaries are calculated for a total S content of 0.1 mol/kg H_2O. Higher S concentrations would draw the boundaries, especially of the pyrite field, to higher pH and lower f_{O_2} values.

Let us assume a model ore fluid with a bulk isotopic composition of its sulfur load $\delta_{\Sigma S} \equiv 0$. At 250°C, pH = 5, and logf_{O_2} = –38 about 95% of this sulfur would

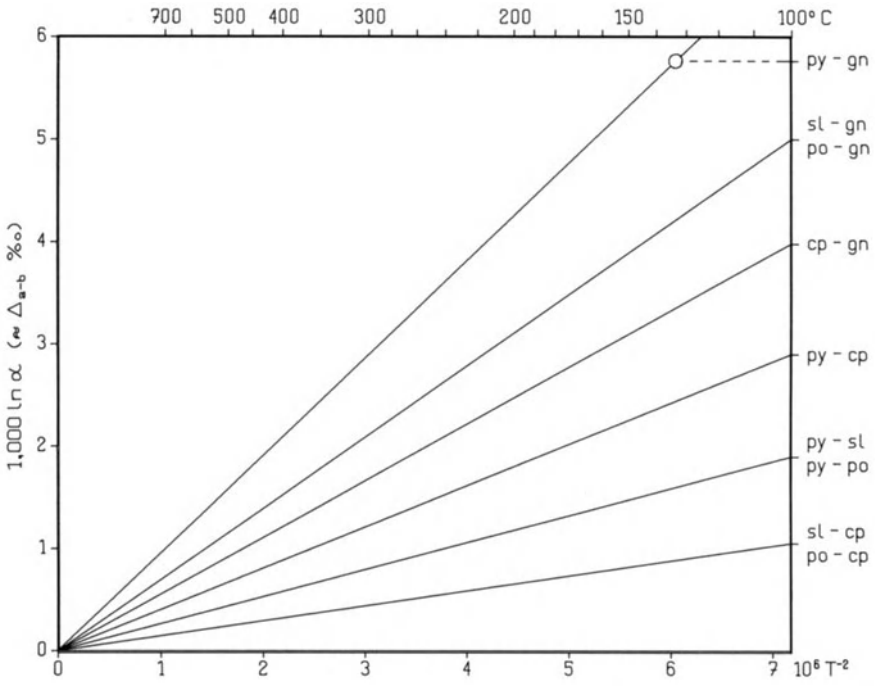

Fig. 3. Calibration curves for the "sulfide pair thermometers". The sulfides are each assumed to be in isotopic exchange equilibrium with the dissolved sulfide in a common fluid. Data from calculations and laboratory experiments

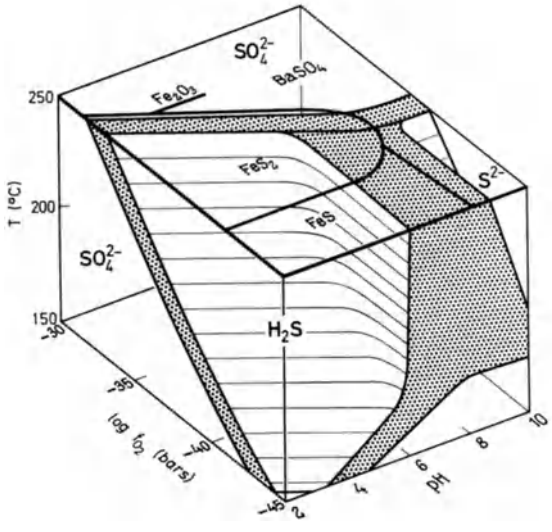

Fig. 4. Sulfur species in a hydrothermal system under the regime of pH, oxygen partial pressure, and temperature. Data for construction of pH-logf_{O_2}-T diagram from Helgeson and other sources, for references, see Ohmoto (1972). Assumed fluid composition: ΣS = 0.1 mol/kg H_2O and $Ba^{2+} = 10^{-5}$ mol/kgH_2O. Further details in text

be present as undissociated H_2S, and hence δ_{H_2S} would be ≈ 0. The corresponding δ values of the other components can be deduced from Figure 2; the result is shown in Figure 5a. The diagram contains also the δ values of some major ore sulfides.

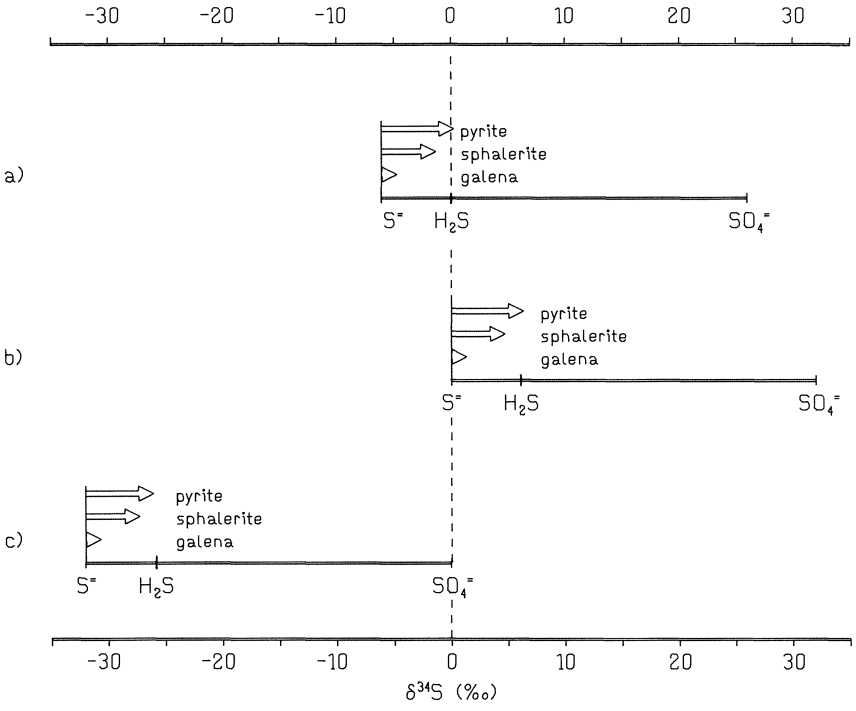

Fig. 5. $\delta^{34}S$ values of sulfur species in a fluid under isotope exchange equilibrium at 250°C with $\delta_{\Sigma S} \equiv 0$. **a**, pH < 5 and $\log f_{O_2} < -36$. **b**, pH > 9.5 and $\log f_{O_2} < -38.5$. **c**, $\log f_{O_2} > -37$ at high pH and increasing to < -32 in strongly acid fluid

An increase in pH, caused by the interaction of the acidic fluid with carbonatic host rocks, shifts the position of the model fluid towards the field of dissociated sulfide. Then the S^{2-} ion becomes the dominating dissolved sulfur species, and its δ value must approach zero. As far as the temperature remains constant, the internal Δ values will remain the same, and the whole δ pattern is shifted to the position shown in Figure 5b. A still more drastic δ shift occurs, when the oxygen partial pressure is augmented. As soon as the fluid enters the field of SO_4^{2-} (i.e., when most of the sulfur is oxidized to sulfate) the δ value of the latter becomes zero, and the whole δ pattern is shifted to the position shown in Figure 5c. It is clear that this shift happens mostly within the stippled zone in Figure 4, when the partitioning of H_2S goes down by an order of magnitude.

Figure 4 shows that the fluid reaches the sulfate field not only by an increase of the oxygen partial pressure, but also by cooling. Theoretically the resulting δ pattern

then should be a stretched version of Figure 5c, i.e., the sulfide δs should be still more negative, due to the $1/T^2$ dependence of the fractionation factors. In reality, however, most $\Delta_{\text{sulfate-sulfide}}$ values of hydrothermal mineral assemblages remain below the equilibrium value. In spite of this handicap the above model has gained a broad application in the interpretation of S isotope data from hydrothermal ore deposits.

Kinetic fractionation of sulfur isotopes occurs in all cases where a unidirectional reaction directly affects the sulfur bond. As a general rule, the reaction goes faster with the light isotope. The most interesting kinetic mechanism producing S isotope fractionation is involved in bacterial sulfate reduction.

Sulfate is reduced by living cells for two different aims: Firstly, all autotrophic organisms need sulfur for the synthesis of specific organic molecules, for example proteins. The reduction of sulfate involved in this biosynthesis is called **"assimilatory sulfate reduction."** The rate-controlling step is the uptake of sulfate and its complexing by specific enzymes. Because the energetic level of the S atom in the complex is roughly the same as in the dissolved sulfate ion, no spectacular fractionation can be expected. For example, the organic sulfur of living marine organisms is depleted in ^{34}S by 0‰ to 5‰ with respect to the surrounding oceanic sulfate.

When speaking of bacterial sulfate reduction, however, normally the **"dissimilatory"** or "respiratory" application of dissolved sulfate by specific bacteria (*Desulfovibrio*, etc.) is meant. They live in a strictly anaerobic environment and apply the sulfate ion as an electron acceptor (=oxygen source) for their metabolism. Because of their heterotrophic nature, they cannot utilize the produced H_2S for biosynthesis, and release it to the environment. The reaction chain can be characterized by the following scheme:

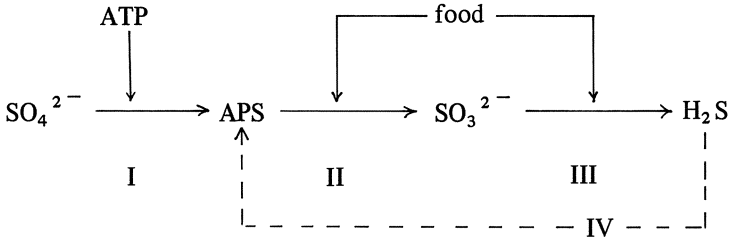

(ATP = Adenosine triphosphate, APS = Adenosine-5'-phosphosulfate).

For more details, the reader is referenced to Goldhaber and Kaplan (1974).

The S isotope fractionation in this process depends on the difference between the two reaction rates

$$^{34}SO_4^{2-} \xrightarrow{k_1} H_2{}^{34}S$$

$$^{32}SO_4^{2-} \xrightarrow{k_2} H_2{}^{32}S$$

The individual rates k_1 and k_2 of the whole chain are determined by the slowest step, and therefore also the ratio k_1/k_2 depends on the change in energetic levels of the sulfur bond achieved through this rate-controlling step. Under normal conditions this is Step II, i.e., the breaking of the first S–O bond. Theoretical calculation then

gives a $k_1/k_2 \approx 0.975$. With reference to the terminology in equilibrium fractionation, k_1/k_2 is called the "instantaneous fractionation factor" α^*. With the above value, the Δ value between sulfide and sulfate should be

$$\Delta_{H_2S-SO_4^{2-}} \approx 1000 \ln \alpha^* \approx -25 \text{ (‰)}.$$

Values of this magnitude are observed in laboratory cultures, but the environmental parameters may strongly influence the hierarchy of the reaction rates. Extremely low sulfate concentration or abnormally high supply of food, for example, makes Step I rate-controlling and brings the net fractionation to zero. Fore more details, see Kemp and Thode (1968) and McCready et al. (1974).

Bacterial activity in natural environments is distinguished from the conditions in laboratory cultures especially by much slower growth rates and hence a much slower turnover of sulfur through the cell. Then Step IV, the back-reaction between the enzymatically bound sulfur species (Trudinger and Chambers, 1973), may become important and introduce some equilibrium exchange reaction between the complexing species. Thus the $\Delta_{H_2S-SO_4^{2-}}$ values in natural samples frequently exceed the −25‰ mark and may reach −65‰.

For the sake of completeness it must be mentioned that kinetic processes do not in each case produce light sulfide and heavy sulfate. When an oxidation step is rate-controlling, the reaction will, in contrast, produce light sulfate and heavy sulfide. Such δ patterns are observed in stony meteorites (see the following paragraph). A possible reaction leading to such δ distribution is the oxidation of elemental sulfur by H_2O (Lewis and Krouse, 1969):

$$S^0 + 4H_2O \longrightarrow H_2SO_4 + 3H_2$$

The hydrogen then reacts with other sulfur atoms:

$$3S^0 + 3H_2 \longrightarrow 3H_2S.$$

3. Sulfur Isotopic Distribution in Meteorites and Magmatic Rocks

Meteorites and lunar samples are the only materials available for S isotope studies, for which effects of biologic fractionation can be excluded absolutely.

All the $\delta^{34}S$ values published from troilite samples of iron meteorites are within −0.5‰ and +1.3‰ on our δ scale. Even δ values from the Cañon Diablo meteorite vary by some tenths of a per mil and this scatter can be ascribed only partly to measurement uncertainties. Nevertheless, the Cañon Diablo standard is an excellent representative for the mean S isotopic composition within the part of the universe where all our samples come from.

The δ values in stony meteorites are clustered around zero as well, but the total spread is significantly larger (Fig. 1). Sulfate is typically light with an extreme value

close to –6‰ and sulfide is heavy with a maximum above +3‰. The explanation for this "irregular" behavior is mentioned above.

Terrestrial mafic igneous rocks of assumed mantle provenance have δ values close to zero, with a most probable mean at +1‰ (Fig. 1), while felsic igneous rocks exhibit a broader δ range. The mean is about +2‰, but some granites even contain sulfides with up to +30‰. Such extreme values reflect the uptake of sedimentary sulfur.

Ophiolitic rocks, formed in connection with ocean floor spreading, also appear to be affected in their contents and S isotopic composition by sulfur from their (marine) environment (Fig. 1).

4. The Sedimentary Sulfur Cycle

The importance of S isotope variation in the sedimentary shell depends on the large amount of sulfur concentrated in the sediments and on the very large δ spread in most sediments. For a rough estimation we can assume that the mean S contents in sediments is higher by almost an order of magnitude than in magmatic/metamorphic rocks. On the other hand, the total mass of sediments makes up only about 10% of the crust; thus the sedimentary shell harbors roughly half of all crustal sulfur.

In a geologic time scale this sulfur is circulated very effectively through the different units of the outer crust: Sulfides on the Earth's surface will be weathered rapidly to sulfate, and the latter is transferred to the ocean by river waters. After a residence time of about 10^7 years it is introduced into sediments – either directly as sulfate or after bacterial reduction as sulfide. When sedimentary strata are uplifted after a mean time of burial of the order of some 10^8 years, the cycle begins once more.

The strong S isotope fractionation involved in bacterial sulfate reduction on the sea floor splits up the dissolved marine sulfate into a reduced light fraction entering the sediment as pyrite, and a heavy fraction remaining unreduced sulfate. In salinar basins also large masses of sulfate are laid down and play an episodic role as gypsum or anhydrite in the continent.

On the next pages some aspects of this sulfur cycle are discussed in detail. We must, however, always keep in mind that S isotope fractionation effects on the Earth's surface have strong implications on rocks of the deeper crust that come into contact with surface materials either by deep burial or subduction of sediments, or by the circulation of deep brines.

5. Ocean Water and Evaporites

Modern ocean water sulfate has a rather uniform δ of $\approx$ 20‰. Evaporite sulfates are deposited with only negligible S isotope fractionation, and thus preserve the $\delta_{SO_4^{2-}}$ of the seawater flowing into the salinar basin. Systematic variations in S isotopic composition within the oceanic reservoirs during Earth history have been deduced from the δ record of marine evaporites of different geologic ages (Fig. 6).

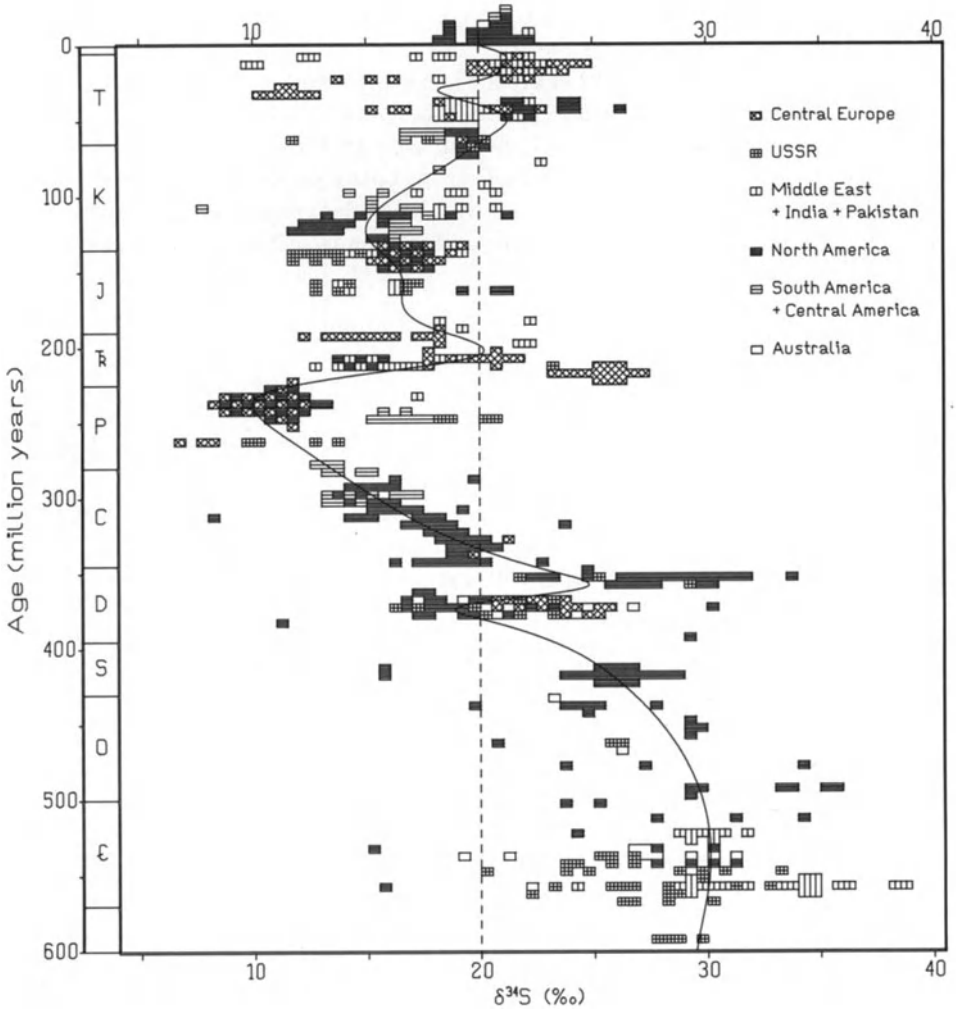

Fig. 6. $\delta^{34}S$ values of evaporite sulfates (gypsum = anhydrite) of different geological ages and assumed "age curve" of $\delta^{34}S$ variation in the world ocean. The diagram is constructed from more than 1000 raw data, measured by different laboratories. For the Permian each rectangle represents more than ten samples from different locations

It is suggested that these variations are caused by major changes in the budget between the individual reservoirs: periods of high biologic activity increase the marine δ; extended weathering introduces additional light continental sulfur to the ocean. High activity of sulfate-reducing bacteria needs a favorable paleographic situation (for example marginal basins in the humid zone) and a high primary organic production. Periods with high marine δ values (Cambrian, Devonian, etc.) are characterized by extended beds of carbon-rich sediments and economically important accumulations of petroleum or bitumens. Extended weathering is possible only during periods of

increased orogenic activity. The pronounced δ decrease from the Devonian to the Permian falls into the Variscan Orogeny.

Assuming a starting δ in the ocean of +20‰ and an inflow of oxidized sulfide sulfur with −20‰, roughly one third of the total original sulfur load of the ocean must have been added to bring down the oceanic sulfate to the Permian value of +10‰. The necessary supply of molecular oxygen is of the same order of magnitude as the oxygen content of the present atmosphere. Hence any such major change in the sulfur cycle must have strong implications on the atmospheric oxygen budget and vice versa.

6. Sedimentary Rocks

Typical source materials and processes responsible for the sulfur content and S isotopic distribution in sedimentary rocks are:

1. sulfide of detrital matter
2. precipitation of gypsum (anhydrite) from evaporating seawater
3. trapping of dissolved sulfate in the pore space of the fresh sediment
4. bacterial sulfate reduction in the (partly) "open system" of the uppermost sediment layer
5. bacterial reduction of pore water sulfate under "closed-system" conditions at deeper levels below the sediment surface
6. bacterial reduction of sulfate from groundwater flowing through levels rich in organic matter
7. deposition of sulfur-containing organic matter
8. dissolution and removal of sulfate by rainwater or groundwater
9. oxidation of sulfide by rainwater or aerated groundwater and its re-precipitation as gypsum, alunite, etc.

(2) to (5) are responsible for most of the sedimentary sulfur. Mechanism (4) and its gradual transition to (5) with deeper burial are essential for the understanding of the $\delta^{34}S$ distribution in argillaceous sediments. The accumulation of substantial amounts of biogenic sulfide needs not only a sufficient supply of dissolved sulfate and of food, but also a "trap" for H_2S to keep down its concentration below the poisonous level. At the interface between oxidizing and reducing environment, H_2S metabolizing bacteria (*Beggiatoa* etc.) may play this role, but deeper in the reducing zone of the sediments the H_2S can only be bound to reactive iron (or other heavy metals). Argillaceous sediments, the clay/mica minerals of which carry iron oxide coatings from the continental runoff, are thus the most promising hosts for high sulfide accumulation.

The permeability of the uppermost sediment layer enables an effective exchange of dissolved sulfate with the overlying water column. Therefore, the sulfate which has already lost a part of its light isotopes to the sediment can be replaced by "fresh" sulfate with the original S isotopic composition. Thus a high amount of light biogenic sulfide can be accumulated in the sediment during the "open-system" stage. When the bottom water is stagnant and has already lost most of its dissolved molecular oxygen to the metabolism of aerobic organisms, the sediment will become reducing almost to the uppermost millimeters, and the bacteria will be able to accumulate up to 10,000 ppm

of sulfide sulfur with δ values 50‰ to 60‰ below those of the marine sulfate (Vinogradov et al., 1962; Hartmann and Nielsen, 1969). This (partly) open zone, however, ends at a depth of about 6 cm. Below this level the sediment becomes a "closed system" for sulfate, i.e., only the interstitial sulfate remains disposable to the sulfate reducers.

The different behaviors of sulfur in the open and closed system zones are demonstrated in the profiles of Figure 7. The S concentration (right) increases and the δ value of total sulfur (left) becomes more and more dominated by the light biogenic sulfide through the uppermost 6 cm. At greater depth, both values remain fairly constant, but the bacterial consumption of sulfate continues and the isotope ratio $R_t = {}^{34}S/{}^{32}S$ of the unreduced sulfate follows the Rayleigh equation:

$$R_t = R_0 f^{(\alpha^* - 1)}$$

with R_0 being the starting value and f the fraction of sulfate remaining in solution.

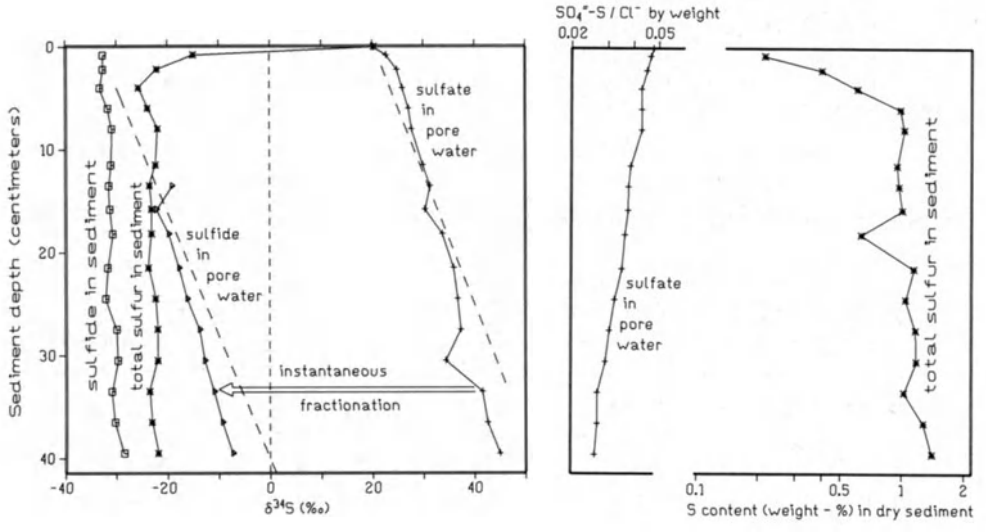

Fig. 7. $\delta^{34}S$ variation *(left)* and increase in S concentration *(right)* with depth in a moderne marine sediment from the Baltic Sea off Kiel (Hartmann and Nielsen, 1969)

(7) is of minor importance. The typical S/C ratio in living cells is ∿ 1 : 100, and therefore the contribution of organic sulfur should not exceed 1% of the C_{org} in the sediment. In most sulfur-rich sediments, however, the S/C_{org} ratio is in the range 1 : 10 and may even reach 1 : 1, thus indicating a contribution of organic sulfur to the total sulfur of only 1% to 10%.

(6) frequently produces sulfide concretions with highly variable (mostly negative) δ values or with δ zonation. Formation waters in environments with bacterial activity are characterized by variable (mostly positive) δ values; concretionary barites frequently show strong δ zonation.

7. Atmospheric Sulfur

Sulfur has a relatively short residence time in the atmosphere. H_2S and SO_2 are oxidized to sulfate which is bound to aerosol particles and is washed out by wet precipitates. The atmospheric sulfur cycle is fed by sea spray aerosols ($\delta \approx +20$) and by biologically produced H_2S, mercaptane, dimethyl sulfide etc. (variable δ's, either around zero or mostly negative). Volcanic exhalations (also with a global mean δ around zero) are considered the "primary" source of most of the sulfur of the upper crust, but their contribution to the actual atmospheric sulfur cycle is only a few percent. In highly industrialized areas the man-made pollution by combustion of fossil fuels and locally by the chemical industry (especially by sulfide roasting) dwarfs all these natural contributions, and even on a global scale the level of anthropogenic sulfur has exceeded the amounts from natural sources. Because the δ ranges of the possible sources of atmospheric sulfur are known it appears reasonable to apply the isotopic composition in atmospheric precipitates or aerosols as a "fingerprint" to identify industrial pollutants. Some successful results of this technique have been published, among others, by Grey and Jensen (1972). In highly industrialized areas, however, such local effects will be camouflaged mostly by the background pollution from a diversity of sources with variable δ patterns, depending for example on the varying provenance of the consumed fuels.

8. Surface Water on the Continent

Sulfate in lake and river waters may originate from weathering of sulfide and sulfate in the catchment area. In humid climates with extensive rock weathering, this source will strongly exceed the inflow of sulfate from atmospheric precipitates, but in arid climates or in coastal areas the latter may dominate.

The sulfate δ in freshwater basins is mostly close to zero, while many inner-continental saline basins (Dead Sea, Caspian, Great Salt Lake/Utah, etc.) exhibit δ values in the 10‰ to 15‰ range. As far as the sulfate concentration is low, however, bacterial reduction in the bottom muds or at deeper levels of stratified water bodies may alter the δ pattern in a drastic manner.

9. Groundwater

The sulfate content in groundwater ranges from nil to saturated solutions. Drinking water ought to carry sulfate only in the 0-10 mg/l range, but this is quite an exception, and in many regions values even beyond the 100 mg/l mark must be tolerated. Therefore, the mechanisms responsible for such high sulfate concentrations are of primary interest to people engaged in groundwater prospection.

Because the sulfate concentrations of most groundwaters are much too high to be explained with the atmospheric inflow, this sulfate must originate directly from the

aquifer system, i.e., from the dissolution of rock sulfate (evaporitic gypsum/anhydrite) or from oxidative weathering of sulfides. Only in coastal areas or in arid climates, where most of the rainwater re-evaporates before reaching the groundwater table, may the atmospheric inflow dominate. All these different mechanisms of sulfur uptake can be distinguished by the S isotope record in the dissolved sulfate, and in the case of evaporite leaching, the $\delta^{34}S$ value even enables us to discriminate between evaporites of different geologic ages. Figure 8 compiles some results of this work.

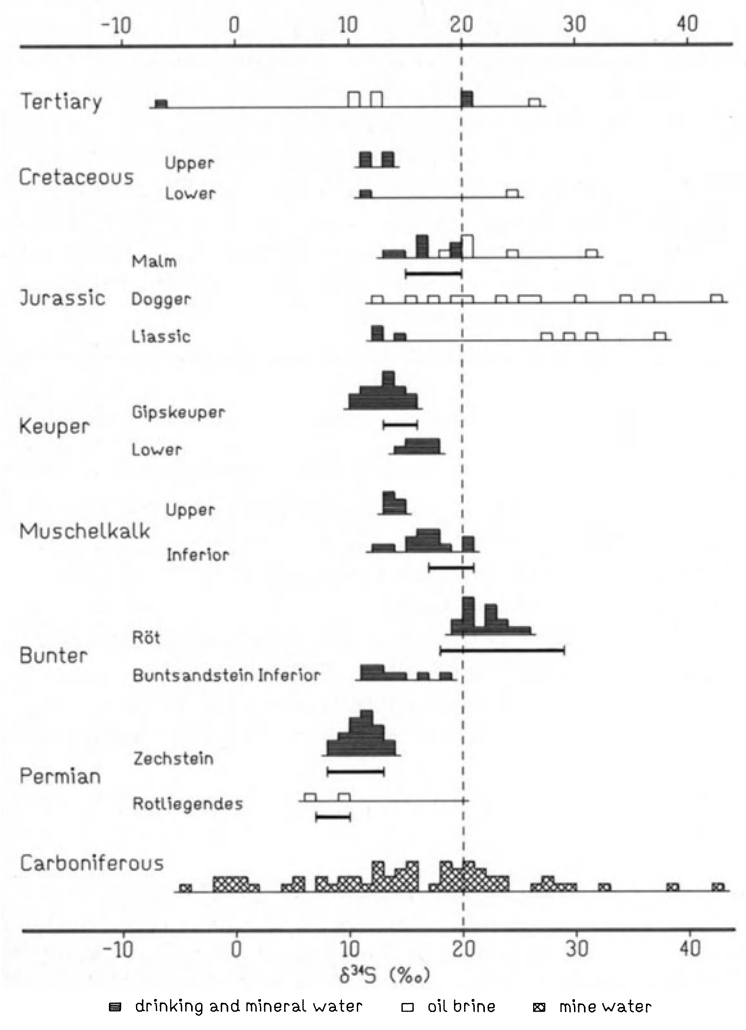

Fig. 8. $\delta^{34}S$ histograms of dissolved sulfate in groundwaters from aquifers of different geologic ages in FRG. *Black bars* below the histograms give the δ ranges of evaporite sulfates occurring at the same stratigraphic levels

When sulfate-bearing groundwaters penetrate strata rich in organic matter, H_2S will be produced by sulfate-reducing bacteria. As far as this H_2S is trapped effectively by heavy metals, the bacterial activity at depth can be traced only from the lowered sulfate concentration and the increased $\delta^{34}S$ value. If the groundwater body can be regarded as a "closed system", the mechanism follows the Rayleigh equation (explained above). For quantitative calculations two of the three parameters – namely the starting δ value (or R_0), the fraction f of unreacted sulfate or the instantaneous fractionation factor α^* must be known. In the example of Figure 9 this presumption is fulfilled

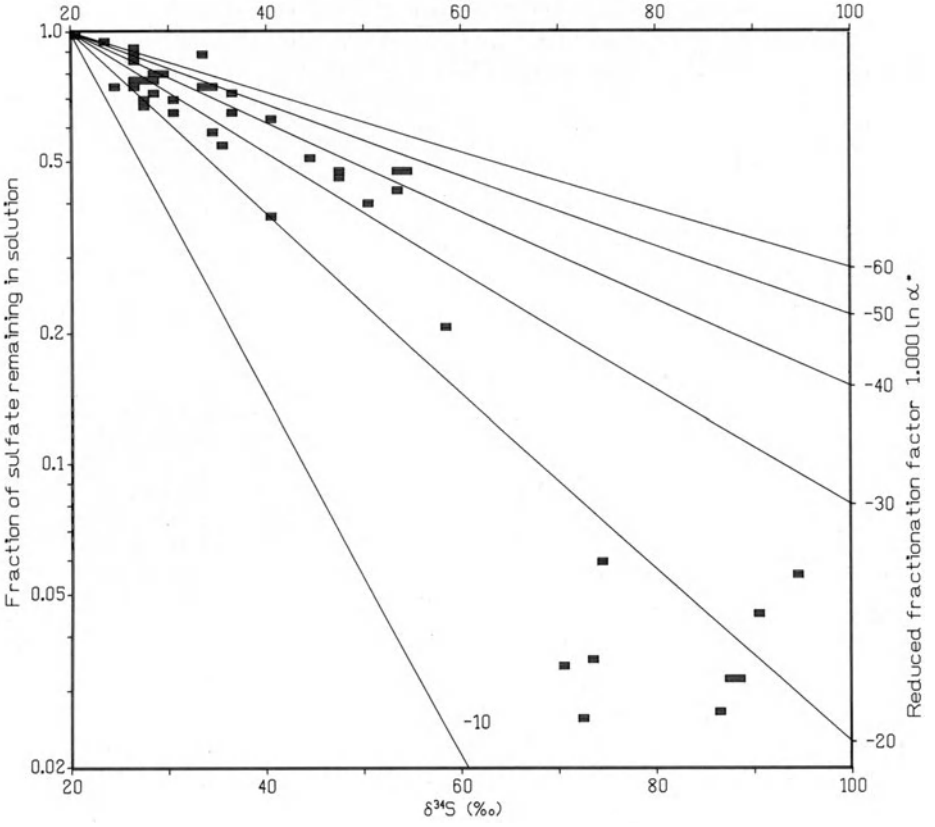

Fig. 9. Rayleigh fractionation, due to bacterial (dissimilatory) sulfate reduction in a "closed system." Curves are calculated with the equation on page 294. Because the δ scale is approximately logarithmic the curves are almost straight lines. The inserted $\delta^{34}S$ values of groundwater sulfate samples originate from Wittmund, a site at the German North Sea coast close to Wilhelmshaven

for R_0 and f. The groundwater originates from "modern" North Sea water that had intruded into Tertiary sediments close to the German NW coast during a catastrophic Medieval tidal wave. The sediment comprises peat seams forming a large number of

groundwater lenses, sealed against each other by clays. In spite of dilution with fresh water, f can be deduced for each of these "closed-system" lenses from the SO_4^{2-}/Cl^- ratio, and thus α^* can be calculated or be read directly from the diagram.

When heavy metals are lacking, the H_2S remains dissolved and the groundwater may come to the surface as a "sulfur spring". Figure 10 shows a specific type of S isotopic relation in such sulfur springs: the groundwater sulfate in this area originates largely from the oxidative weathering of the pyrite content of bituminous marine shales, deposited during the Lower Jurassic. With respect to the starting seawater δ value, this pyrite is depleted in ^{34}S by about 30‰. When the (modern) groundwater migrates to a reducing environment, sulfate reducers produce H_2S and fractionate the sulfur isotopes by another 30‰. At other locations this "batch type" fractionation mechanism has yielded in H_2S with δ values even in the −60‰ to −65‰ range, and these are the lowest $\delta^{34}S$ values reported for natural samples.

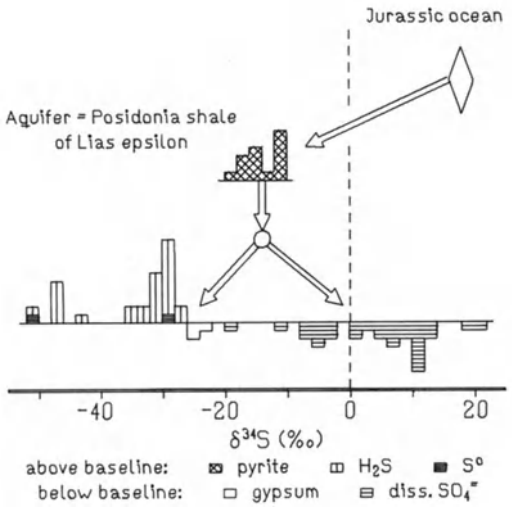

Fig. 10. Batch-type fractionation of sulfur isotopes in a hydrological system with extended weathering of sedimentary sulfides and modern H_2S production by bacterial activity in sulfur springs, applied for medical purpose at Sebastiansweiler Spa, West Germany

10. Native Sulfur

Native sulfur is commonly found at locations where H_2S enters the level of aerated surface water. The H_2S may be oxidized inorganically or by "sulfur bacteria" (*Thiobacillus,* Purple Bacteria) with negligible isotope fractionation. Biogenic H_2S is normally light, and the same is true for its oxidation product S^0. During migration the H_2S and the S^0 become largely homogenized in their isotopic composition.

Sulfate-reducing bacteria in the sulfatic caprock of a salt dome obtain their sulfate supply from the immediate vicinity and thus give rise to a strong δ increase in the adjacent grains of gypsum (Fig. 1). Their food is organic matter (oil constituents?), migrating upward on the flanks of the salt dome. The metabolic reactions follow the scheme where C–H stands for some unknown organic compounds:

$$Ca^{2+}_{sol} + SO_4{}^{2-}_{sol} + C{-}H \xrightarrow{\text{bact}} H_2S_{sol} + \text{calcite}$$
$$\downarrow$$
$$S^0$$

The oxidation mechanism is still debatable, but finally the gypsum caprock is transformed to a sulfur-bearing calcite caprock with its carbonate C originating from the organic matter. This is verified by low $\delta^{13}C$ values of the newly formed calcite. When H_2S is produced under "closed-system" conditions, the δ value of the total sulfide approaches the δ value of the starting sulfate, when sulfate consumption goes to completeness. Therefore, in a sulfur prospect, the δ difference between S^0 and unaffected sulfate is indicative of the efficiency of bacterial production, and hence of the reserves to be expected.

Volcanic fumaroles or solfataras contain appreciable amounts of sulfur. At depth, the proportion between H_2S and SO_2 is controlled by temperature and f_{O_2}. Further access of oxygen enables the formation of elemental sulfur and of thio-compounds, which interact with each other under strong S isotope fractionation.

11. Petroleum, Gas and Coal

Living organisms need sulfur as a key element in several cell constituents (proteins, enzymes etc.). The mean S content of most organisms is $\leqslant 1\%$. The uptake of this sulfur by "assimilatory sulfate reduction" involves minor S isotope fractionation. Immediately after burial, the S/C ratio in the dead organic matter begins to increase, and the S isotope composition begins to change towards that of the enclosing sediments (Nissenbaum and Kaplan, 1972). Several compounds of the decaying organic matter react easily with elemental sulfur:

$$R{-}H + S^0 \longrightarrow R{-}S{-}H \quad \text{(thiols)}$$
$$2R{-}H + 2S^0 \longrightarrow R{-}S{-}R{-} + H_2S \quad \text{(thiaalkanes)}$$
$$RC_4H_9 + 2S^0 \longrightarrow R\langle\overline{S}\rangle + H_2S \quad \text{(cyclothiaalkanes)}$$

Therefore, organic matter deposited in a marine sediment is the most probable source material of high-sulfur petroleums with a "typical" δ range 10‰ to 20‰ below that of the coeval seawater (Fig. 11a).

At elevated temperatures the sulfur-organic molecules are cracked together with the heavier carbohydrates, and the sulfur is released as H_2S. This explains the frequently observed high concentrations of H_2S in crude gas. On the other hand, organic materials also provide inorganic reduction of sulfate at sufficiently high temperatures ($\approx 250°C$?). Therefore, the effects overlap and cannot in all cases be interpreted.

Coals also have taken up the larger part of their sulfur during diagenesis or during later events. Coals of continental provenance are expected to contain less sulfur than those originating from coastal swamps, but this difference may be eliminated, when sulfate rich groundwaters pass through the unmaturated coal seams. In the Ruhr

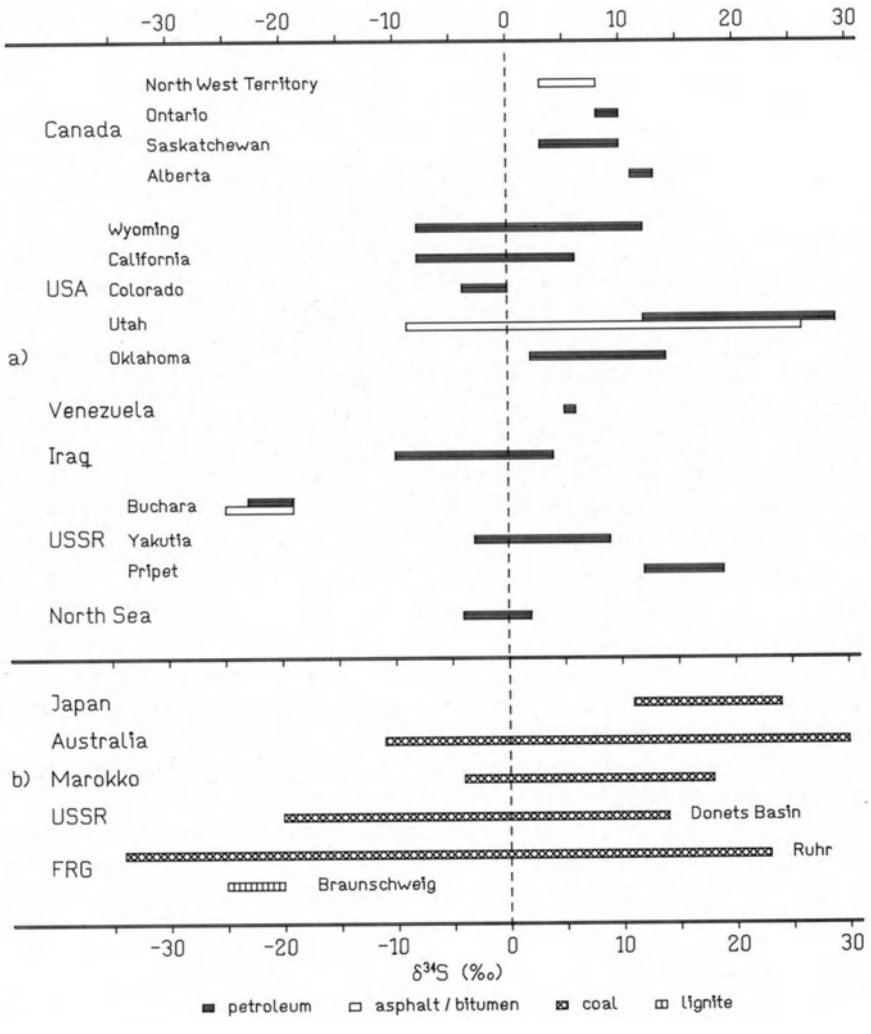

Fig. 11. $\delta^{34}S$ ranges in fossil fuels of different provenance. **a**, organically bound sulfur in hydrocarbons from some major oil fields. **b**, sulfur in coal seams (mostly occurring as pyrite)

district (FRG) for example, the S concentration in groundwaters and coal seems to be controlled much more by the extension of the overlying Zechstein (= Permian) evaporite basin than by the paleographic position during the productive period of the Carboniferous (Fig. 11b).

12. Introduction to Stable Isotopes in Ore Deposits

The most striking result of the earliest measurements in 1949/53 was the difference between the S isotope patterns of magmatic and biogenic sulfur. The simple scheme appeared to be: "narrow δ range around zero → magmatic, and large scatter with preferably light sulfide and heavy sulfate → biogenic." It was considered reasonable to apply this scheme also to the classification of ore deposits, and during the first two decades of S isotope work, a great deal of all measurements was concerned with ore samples. The increasing number of data collected during this period, however, made clear that the above scheme was too simple to explain the natural variation in S isotopic distribution. Thanks to Hitoshi Sakai, the theoretical background of the behavior of sulfur isotopes in a hydrothermal fluid was clarified, but the inauguration of the modern concept of stable isotope work on ore deposits is dated by Hiroshi Ohmoto's (1972) extension of Sakai's ideas to a combined treatment of sulfur and carbon isotopes in an ore fluid.

In spite of the great attention which the subjects of the foregoing chapters have attracted in the meantime, today still many S isotope papers are concerned with ore deposits. This work was partly "basic research" and has played an important role in the development of modern concepts of metal transportation and accumulation. A lot of work, however, was also done for prospection purposes. Until late 1977 the total number of published S isotope investigations on ore deposits had exceeded 400, and only a few titles have been inserted into the literature list of this article. The reader, however, will find many references in the book of Grinenko and Grinenko (1974), or in the review papers by Nielsen (1978), Rye and Ohmoto (1974), Sangster (1968), Schwarcz and Burnie (1973).

13. Magmatic and Hydrothermal Ores

It can be concluded from the curves in Figure 2 that S isotope fractionation must be small in the temperature range of magmatic processes. Thus we can expect δ values close to zero in ores that are ascribed to segregation of magmatic melts. This fits, for example, for the pentlandite assemblages of the Sudbury irruptive and other layered intrusions, where the "typical δ range" is about 0 to +5‰ (Fig. 12). The same δ range is found in the sulfide ores of the carbonatite stock at Palabora, Transvaal.

When magmatic material has intruded sedimentary strata, the concentration gradient of sulfur is frequently directed from the host rock toward the intrusion. This sulfur from the environment may be mobilized and react with the silicates of the magmatic melt. The intrusion at Norils'k, for example, is settled in Devonian host rocks with abundant anhydrite lenses. The δ values of the pyrite ore cover the range from +7‰ to +10‰ (Fig. 12).

Most ore accumulations are formed during the hydrothermal stage, i.e., the metals and the sulfur are transported by a fluid or liquid water phase and are deposited when the solubility product is exceeded by cooling or by other effects. Intrusions may be

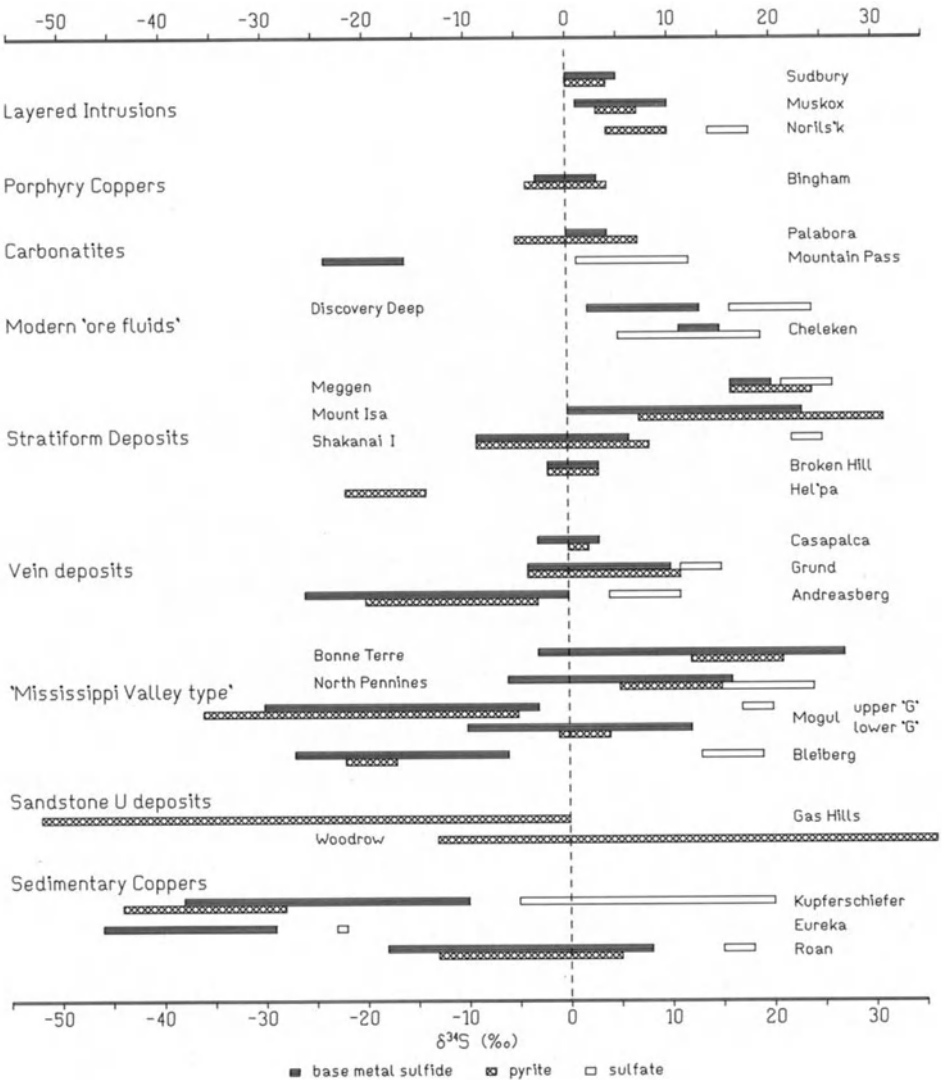

Fig. 12. $\delta^{34}S$ ranges in sulfide and sulfate of ore deposits of different genetic types. The locations of the individual mines are: Sudbury, Ontario, Canada; Muskox, North West Territory, Canada; Norils'k, NW of Siberian Platform, USSR; Bingham, Utah, USA; Palabora, South Africa; Mountain Pass, California, USA; Discovery Deep, median trench of Red Sea; Cheleken peninsula, Caspian, USSR; Meggen, FRG; Mount Isa; Queensland, Australia; Shakanai I (Kuroko type ore), Honshu, Japan; Broken Hill, New South Wales, Australia; Hel'pa, Yugoslavia; Casapalca, Peru; Grund and Andreasberg, Harz Mts., FRG; Bonne Terre, Missouri, USA; North Pennines, northern England; Mogul Mine, Silvermines Co., Ireland; Bleiberg, Carinthia, Austria; Gas Hills district, Wyoming, USA; Woodrow Mine, New Mexico, USA; Kupferschiefer, samples from diverse sites, mainly in northern FRG; Eureka Mine, New Mexico, USA; Roan, Zambia

the suppliers of ore constituents or merely act as a "heat engine" that promotes the convective circulation within the hydrothermal system and enables extraction of metals at depth.

Extensive information about the nature of hydrothermal fluids comes from fluid inclusion studies, but metal-bearing thermal waters do also ascend in modern times. The δ range observed for example in samples from the Atlantis II Deep in the median trench of the Red Sea and from oil wells at Cheleken peninsula, Caspian, USSR, is shown in Figure 12. These data show clearly that the fluids bear no "mantle sulfur". It is assumed that the hydrothermal convection system responsible for the hot brine pools at the bottom of the Red Sea has gathered its sulfate by leaching Tertiary evaporites in the environment. Partial inorganic reduction at depth enabled the deposition of sulfide. The $\Delta_{SO_4\text{-}S^{2-}}$ values range about 15‰, and in a supposed isotope equilibrium model this would imply reaction temperatures around 450°C (see Fig. 2). A more reasonable explanation ascribes the observed Δ values to the kinetic fractionation involved in the (inorganic) reduction step at depth.

Convective brine systems of the type now active in the rift system of the Red Sea graben are a possible supplier of ore constituents of the "stratiform" (or "strata-bound") ore deposits, which are not only the world's largest resources of base metals, but also the largest local accumulations of sulfide sulfur. Their S isotope distribution is manifold; the δ mean values of the individual ore lenses vary from ≈ -20‰ to +20‰, and in some cases the internal spread remains within a few per mil, in others covers 30‰ and more. "Families" of ore lenses ascribed to a common geologic event may have almost identical δ patterns, but the values may also differ so strongly from each other that no systematic correlation can be deduced.

The dense fluid entering a local depression at the sea floor is expected to be homogeneous in isotopic composition, and hence all the sulfide minerals formed at a given instant should agree in their δ values. When the chemistry of the ore fluid has changed with time, this is reflected not only in the succession of different ore types from bottom to top of the ore lens, but also in a systematic δ increase or decrease (Fig. 13). Then the laterally homogeneous values can be applied as a "stratigraphic marker."

In the example of Figure 13 all the base metal sulfide δ's follow this regular trend, while the majority of all pyrite δ's exhibits a broad scatter towards negative values. This argues clearly for two independent sulfur suppliers – namely the hydrothermal fluid and bacterial activity. Similar results have been found at some other places.

Many speculations are concerned with the provenance of the sulfur brought up by the hydrotherms. Sangster (1968) drew attention to the fact that, in many cases, the mean δ in the deposit is about 15‰ lower than in seawater sulfate of the same age. This leads to a model not very different from the one referred to above. Ohmoto (1976) showed in a laboratory experiment, that seawater reacts with basalt at 300° to 500°C to form sulfide with δ values similar to those found in many stratiform ore deposits. This demonstrates the validity of the above model to explain the formation of some stratiform ore deposits, especially of the Kuroko-type in Japan. Furthermore, the result may explain the δ patterns in ore deposits related to ophiolitic sequences.

Vein fillings are another type of hydrothermal ore deposit. Depending on the low solubility products of most base metal sulfides, a simple solution with metal and sulfide ions would need unreasonably large amounts of water to fill a normal vein with sulfide

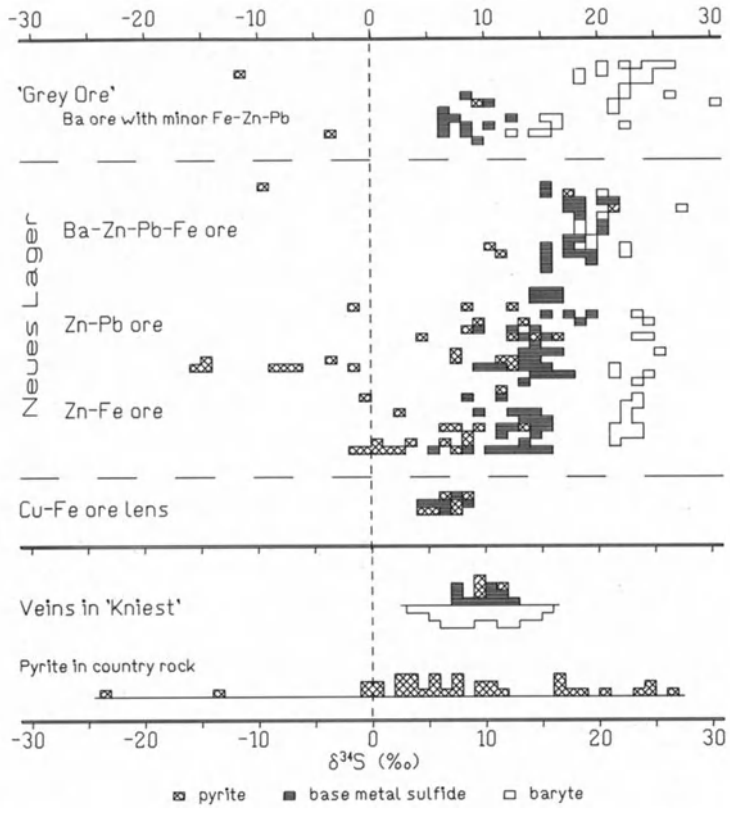

Fig. 13. Sulfur isotopic distribution in the Rammelsberg mine, West Germany. The sequence from bottom to top represents roughly the age relations between the individual mineralizations. "Kniest" is a brittle, strongly silicified rock underlying the ore lenses. The "Neues Lager" has a thickness of 20 to 50 m. The sulfate δ's in the "Neues Lager" agree roughly with the assumed value for oceanic sulfate of the Middle Devonian (Anger et al., 1966)

ores. This problem disappears when the metals are transported as dissolved complexes, for example with chloride. Deposition then would need the release of metal ions from the complex, and this happens when the temperature of the fluid decreases or when the activity of the complexing medium is lowered by dilution with freshwater.

Furthermore, the ascending ore fluid normally comes to environments with higher oxidation potential, and in many cases also the pH of the fluid will be increased. For the sake of simplicity both effects will be discussed separately under the assumption that the fluid enters the site of ore deposition with $\delta_{\Sigma S} \equiv 0$, pH = 5, $\log f_{O_2} = -38$ and T = 250°C (see Figs. 4 and 5).

Let us first consider the effect of pH increase, due to the reaction of an acidic fluid with carbonatic host rocks (i.e., the formation of calc-silicate hornfelses, etc.). At pH 5 practically all of the dissolved sulfur is undissociated H_2S, and hence the δ values of the individual species are those inserted in Figure 5a. At pH 9 the dissolved sulfide is almost

entirely dissociated, and the resulting δ values are given in Figure 5b. The (theoretical) maximum δ increase of the deposited pyrite then would be $\approx 6‰$.

When the pH of the fluid increases slowly from 5 to 9 during migration through the site of ore deposition, this δ increase can be traced by comparing "early" and "late" pyrites or ores close to and farther away from the feeder channels. At 250°C the $H_2S/HS^-/S^{2-}$ ratios at the intermediate pH values 6, 7, and 8 are approximately 80 : 20 : 0, 35 : 35 : 30, and 5 : 25 : 70. The corresponding δ increase is $\approx 1‰$, 3.5‰ and 5‰. With the assumed concentration S = 0.1 mol/kg H_2O, the stability field of pyrite is confined to pH $\leqslant 8$, and thus the δ increase will not exceed 5.5‰.

An increase in oxygen partial pressure increases the SO_4^{2-}/H_2S ratio. The strong S isotope fractionation between sulfate and sulfide has much stronger implications on the δ pattern than in the case of a pH change. Figure 5c shows the S isotopic distribution when the fluid has reached a position in the $\log f_{O_2}$-pH-T diagram, where the dissolved sulfur is almost completely oxidized. Barite is deposited from dissolved SO_4^{2-} with negligible fractionation (at 250°C $\Delta_{ba\text{-}SO_4^{2-}sol} \leqslant 0.3‰$), and therefore the values of SO_4^{2-} in Figure 5 can be applied to the δ_{ba} of the barite. With the parameters of our model the first barite can be expected when the position of the fluid touches the stippled zone in Figure 4, i.e., $SO_4^{2-}/H_2S = 1 : 10$. Then the theoretically expected δ values of pyrite and barite are $\delta_{py} \approx -3$ and $\delta_{ba} \approx +23‰$. In the center of the stippled zone ($SO_4^{2-}/H_2S = 1 : 1$) the values are: $\delta_{py} \approx -13$ and $\delta_{ba} \approx +13‰$. At the high-oxygen side of the stippled zone ($SO_4^{2-}/H_2S = 10 : 1$) $\delta_{py} \approx -23$ and $\delta_{ba} \approx +3‰$, and finally, at the high-oxygen boundary of the stability field of pyrite $\delta_{py} \approx -26$ and $\delta_{ba} \approx 0‰$.

The above model is based on the assumption of a permanently established S isotope equilibrium between dissolved sulfide and sulfate. Unfortunately, this premise is not fulfilled in many natural settings, and then $\Delta_{ba\text{-sulfide}}$ is lower than theoretically expected. Nevertheless, the trends in S isotope fractionation remain consistent and give us valuable information about the ranges of f_{O_2}, pH, and T during a specific event of ore deposition.

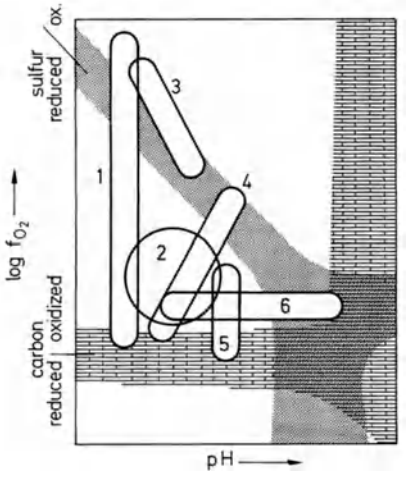

Fig. 14. Reconstruction of environmental pH and oxygen partial pressures for some types of hydrothermal ore deposits. *1*, Echo Bay, North West Territory, Canada; *2*, Casapalca, Peru (see Fig. 12); *3*, Shakanai I, Honshu, Japan (see Fig. 12); *4*, Mogul Mine, Silvermines District, Ireland; *5*, Pine Point, North West Territory, Canada; *6*, Darwin, California. The zone with *stippled signature* agrees with that in Figure 4 and, is characterized by strongly variable $\delta^{34}S$ values for sulfide and sulfate. The brick signature marks the zone where $\delta^{13}C$ is variable, due to change from reduced to oxidized or from undissociated to dissociated state. From Rye and Ohmoto (1974)

In Figure 14 the positions of some types of hydrothermal ore deposits are plotted in a schematic f_{O_2}-pH diagram. The controlling parameters have been concluded from mineral assemblages and from the $\delta^{34}S$ and $\delta^{13}C$ values. Among the deposits are vein mineralizations (nos 1 and 2), a stratiform "Kuroko" deposit (no 3) and replacement or impregnation ores (nos 4 to 6).

In example no 2, the parameters remained very constant throughout the whole period of ore accumulation. The sulfide δ's range about zero, and the theoretical considerations given above render it highly probable that this fits also for the $\delta^{34}S$ within the fluid. In deposit no 4, we find two populations of sulfide ores. The one represented by the lower section of the plot in Figure 14 was deposited adjacent to a major fault, which is regarded as the feeder channel. The δ's cluster around zero (see Fig. 12, Mogul Mine, lower "G" orebody). The other population covers a very broad range to negative δ values (upper "G" orebody). Close to the feeder the δ values lie between zero and −20‰, and with distance from the feeder, they become systematically lower and reach the −35‰ mark about 400 m away from the assumed feeder. In the hydrothermalist's concept, this decrease in δ reflects the increase in oxygen partial pressure and decrease in temperature with distance from the feeder. In the following chapter another explanation will be given.

The no 1 of Figure 14 refers to an example with increasing oxidation potential. The first Cu sulfides, occurring together with hematite, have δ values around −20‰. The base metal sulfides of the main stage mineralization range from −5‰ to +15‰, and the latest sulfosalts, occurring in assemblages with graphite, range from +20% to +30‰.

14. Biogenic Ore Deposits

The results referred to in the foregoing chapter demonstrate that the discrimination by means of S isotope data between bacterial and inorganic sulfur in ore deposits is not a trivial task. The net fractionation involved in bacterial sulfate reduction can reach a value almost twice as large as the maximum fractionation in inorganic settings, and for this reason we are justified in considering δ values far from zero as strongly indicative of biogenic sulfur. Unfortunately, the term "far from zero" cannot be defined precisely.

A certain limitation of the fractionation possible in inorganic reactions comes from the minimum temperature at which sulfate can be reduced inorganically with the naturally available reductants. This temperature determines also the maximum $\Delta_{SO_4^{2-}\text{-sulfide}}$ in a sulfate-sulfide equilibrium system. The published values for this temperature – and hence for Δ_{max} – are somewhat controversial, depending on different assumptions about the chemistry of the fluid. When we take a limiting temperature of $\sim 250°C$, a fluid with $\delta_{\Sigma S} = 0$ would give a total range of all sulfide and sulfate δ values between $\sim$ −32‰ and +32‰ (Fig. 5). Only a few hydrotherms, however, are assumed to bear "mantle sulfur" with $\delta \approx 0$.

When the fluid belongs to a convection system, it can have gathered much of its sulfur from leached sediments. Then the heritage from previous bacterial processes

may shift the whole S isotope pattern strongly to the positive (leached evaporites) or negative (sulfide-rich strata) side of the δ scale.

For this reason, the absolute δ values are an unreliable guide. Therefore, only the internal δ spread can be applied as a criterion for discriminating between biologic and inorganic processes. Remarkably large δ spreads are generally due to sulfate reduction within a limited reservoir. This fits for biologic processes as well as for inorganic reactions, and therefore the existence of larger δ differences themselves is not an unequivocal criterion for biogenic provenance. If, however, individual sulfide grains at a distance of only a few millimeters or centimeters exhibit strong and nonsystematic δ-differences, it will be almost certain that this sulfur originates from bacterial sulfate reduction. Such δ patterns have been found, for example at Górny Śląsk, where the apparently irregular δ variation within single hand specimens exceeds 50‰ (Gehlen and Nielsen, 1969).

These irregular δ variations are easily understood when we assume the existence of bacterial populations growing in reducing micro-environments around individual particles of organic matter, and consuming mainly the sulfate available in their immediate neighborhood. In contrast, inorganic sulfate reduction would need a considerable supply of thermal energy, which can be carried only by the ascending hot fluid. Mobility of dissolved sulfate and reduction in small-scale "closed system" cells, however, are contradictory to each other, and therefore bacterial sulfate reduction remains the only reliable explanation of the above δ pattern.

Unfortunately, this excellent test for biologic activity is confined to deposits that have not been affected too strongly by later thermal events. The nonequilibrium δ differences, of course, are thermodynamically unstable and are easily wiped out at higher temperatures, when a mobile sulfur (vapor) phase is present. The latter may originate, for example, from the thermal breakdown of pyrite ($FeS_2 \rightarrow FeS + S^0$).

Figure 12 contains the δ plots of some deposits where the biogenic nature was already known from conventional geologic investigations, and where the S isotope composition fits exactly into the expected scheme of a broad range of preferably negative δ values.

The first of these examples concerns the "**sandstone-type**" uranium mineralization in the Colorado Plateau and in adjacent areas. The reported values date from the pioneer period of S isotope work, and they contributed a great deal to the interest of ore geologists in the "sulfur isotope method". The genetical conclusions drawn from S isotope measurements on the so-called roll-type ores are discussed by Warren (1972).

Ore rolls are extended bodies of barren pyrite cementation with a front rich in uraninite. When metal-bearing groundwaters flow through the permeable sandstone, the metals may be trapped in zones of bacterial H_2S production by precipitation of pyrite + base metal sulfides and by reduction of U^{6+} to the insoluble U^{4+}. Favorable sites of ore accumulation are constrictions in the groundwater flow by channel-like structures of the former land surface. Re-oxidation at the upstream side of the sulfide zone and re-deposition downstream leads to a continuously increasing concentration of economically important metals. This change in redox potential also provided the "batch type" S isotope fractionation responsible for the extremely low δ values (for comparison see Fig. 10).

The second example of biogenic ores concerns the **Kupferschiefer** in Central Europe. This is the stratigraphic name of a thin bed of bituminous marls at the base of the Upper Permian (Zechstein). The bed itself extends from the UK through the Netherlands, FRG, GDR to Poland, but copper, zinc and lead concentrations of economic importance are confined to a marginal zone of the Kupferschiefer basin (for further details see Wedepohl, 1971). The total sulfide concentration is comparable to the values found in other bituminous sediments, and when the sulfate-δ of $\sim$ +10‰ in the Permian ocean (see Fig. 6) is taken into account, then also the δ values agree with those given in Figure 7. Therefore, there is no doubt whatsoever about the biogenic origin of the sulfide sulfur.

From a naive standpoint, one might speculate that this clear indication should easily be adopted to other ore deposits of similar appearance. This, however, is not the case. Two "sedimentary copper" deposits have been selected for comparison (Fig. 12): The δ range in the Eureka mine agrees roughly with that of the Kupferschiefer, but at Roan (one of the major Zambian Copperbelt mines, see Dechow and Jensen, 1965) all the δ values are systematically higher. This is also true for the other Copperbelt deposits and for several other sedimentary copper ores. The latter are mostly of Precambrian age, and if the seawater δ value was substantially higher during the time of ore deposition than during the Permian, the δ difference would not exclude a biogenic nature. The metamorphic overprint on all these ore minerals and on their internal S isotopic distribution, however, renders all further conclusions speculative.

It has already been mentioned that in a single ore deposit biogenic activity and hydrothermal fluid may compete as sulfur suppliers. In the example of the Rammelsberg (Fig. 13), the base metal sulfides are thought to have been deposited on the seafloor from outflowing hydrotherms, while the pyrite was formed diagenetically in this freshly formed ore mud by sulfate-reducing bacteria (Anger et al., 1966).

When an ore fluid deficient in sulfide sulfur mineralizes epigenetically a sediment bed rich in primary (= biogenic) pyrite, the latter will be partly consumed for the deposition of base metal sulfides and the δ trend of these "hydrothermal" sulfides will partly reflect the δ trend of the primary sulfide content. Both models (i.e., exhalative and epigenetic base metals) have been discussed for the McArthur prospect, Queensland, Australia (Croxford et al., 1975).

As has already been mentioned the systematic δ decrease in the upper "G" ore body of the Mogul Mine can also be explained in another manner than is done by the hydrothermalists: When we postulate, that the sediment layer now bearing the upper "G" ore-body already had a primary (= biogenic) pyrite content with uniformly low δ values, it is quite evident that the later addition of hydrothermal sulfides with $\delta \approx 0$ must have changed the whole δ pattern in the observed manner: close to the feeder the δ values were shifted strongly towards zero, and with greater distance to the feeder the influence of the hydrothermal component became smaller and smaller (Coomer and Robinson, 1976).

15. Summary and Outlook

The present report can give only a condensed review on the principles and possible applications of sulfur isotope geochemistry. The available space does not allow reference to all the different topics of investigation now under way. The reader interested in more details should consult the diverse review papers cited in the text. There he will also find more comprehensive reference lists.

Sulfur isotope geochemistry was "invented" during the late forties independently at two different places: at the Chemistry Department of McMaster University, Hamilton, Ontario, H.G. Thode and co-workers published in 1949 the results of the first 62 measurements on S isotopic variation between natural samples, and in the same year, A. Trofimov, Institue of Geochemistry and Analytical Chemistry, V.I. Vernadski, Moscow, came out with another eight preliminary data. Then followed a period of 6 years during which S isotope geochemistry appeared as a "private" domane of the McMaster people. The five papers appearing between 1950 and 1954 brought only about twice the number of data of the first year, but these few results demonstrated so clearly the importance of this new field of research that, during the short interval from 1956 to 1964, a dozen new S isotope laboratories were founded. These additional activities substantially increased the output of information. Until the beginning of 1978 the number of laboratores (including commercial facilities) that are more or less continuously working on sulfur isotope problems has grown to about 35. Their common output of scientific results amounts to about 40 to 50 original papers per annum and to perhaps some 20 to 30 abstracts of conference lectures with a total number of about 3000 S isotope data.

The "accoucheurs" of S isotope geochemistry were physicists or physico-chemists, whose main interest was to demonstrate the possibility of S isotopic fractionation during natural processes and to verify the capability of their mass spectrometers to resolve these small isotopic differences. Therefore, the scientists did not bother much about the geochemical background of these samples, but simply took what they were able to gather from museum collections. Fortunately, however, these initial measurements already gave such a good insight into the major trends of S isotope fractionation that specific research programs could be set up at a very early stage. It is easily understood that objects of major economic interest, such as sulfide ores or deposits of elemental sulfur and petroleum already played an important role among these early topics of investigation. Prospection on economic deposits was also a major argument for stimulating and funding the further work. Nevertheless, we can state that S isotope measurements have never been integrated so completely into mere routine prospection as is the case, for example, with the determination of $\delta^{13}C$ and δD for the oil and gas prospection.

It is not easy to predict future trends in S isotope geochemistry. Much will depend on recent and future improvements in the measurement techniques. During the pioneer period – before doing any S isotope measurements – the researchers had first of all to construct their machinery. The timing of the "boom" in laboratory foundations in the late fifties was not only a matter of the growing interest in this new branch of research, but also a consequence of the availability of commercial mass spectrometers at that time. Nevertheless, first of all, a great deal of basic engineering knowledge had to be

invested by those people installing these laboratories before any satisfactory results could be expected. Now, at the end of the seventies, commercial gas mass spectrometers for stable isotope work have reached such a high standard that no extraordinary developments will be expected in the near future. For this reason, the progress in S isotope geochemistry will probably depend on other lines of technical evolution.

One of the most outstanding demands concerns the consumption of sample material for measurement. This restricts the resolution for narrow-space fractionation processes to sample volumes of about 0.1 mm^3 for a single measurement in the case of pure sulfide or elemental sulfur, and of course to much larger volumes in samples of lower S content. With the machines available in the late seventies, the sample amount can be reduced by an order of magnitude, but even that remains still too much for a proper "micro-scale S isotope geochemistry."

The conventional stable isotope measurement applies gaseous samples for the sake of constant ion beam intensity and rapid switching between sample and "standard". The conversion of the source material into a gas sample implies complicated chemical procedures which are easily affected by isotope fractionation due to incomplete yields. The problem exists already with the aliquots applied hitherto – the preparational error in S isotope geochemistry is estimated in most cases to range from about 0.1‰ to 0.2‰, but recovery problems during the extraction of S from very poor samples may even increase this error by an order of magnitude. This source of error can only be eliminated when the conventional sample chemistry is abondoned, and this means, when the original sample compounds are loaded directly into the ion source of the mass spectrometer. In principle, this can be done by a Knudsen probe, i.e., a small furnace where a molecular beam of sulfur vapor is generated directly from a thermally decomposed sulfide grain.

The ion probe mass spectrometer appears to be an even more promising facility where ions are produced from the surface of a macroscopic sample by bombardment with a beam of fast ions. Similar to the mode of operation of an electron microprobe, the primary ion beam is scanned across the surface of the sample, and thus a two-dimensional isotopic profile can be obtained directly from the object of investigation. The handicap, however, of all direct loading techniques is the inconstant intensity of the ion beams. It can be eliminated by ion counting (instead of the conventional integrated current measurement) but the present engineering will have to be improved substantially before the first ion probe or secondary (sputtering) ion mass spectrometer (SIMS) will become a routine instrument in stable isotope laboratories.

Finally, some short remarks about the problems involved in handling the outcoming data. The story is always the same: at an early stage of research the output of information is usually so clear that most investigators would reject the idea of making use of the computer facilities for these few data as being a mere pastime. However, the situation is changing imperceptibly, and once the flood of data has exceeded the storage capacity of the human brain, a tremendous effort will be necessary to become acquainted with the new techniques. In 1963 the author began to use computer facilities for the evaluation of his own results with a total number of about 2000 data. When the Göttingen data bank approached the 10,000 data mark (plus the necessary sample information) there was a sound basis to propose an interlaboratory exchange of data files. This

was in 1968 (Nielsen, 1968), but only 10 years later was the first response to this offer registered.

Now the reservation against a profitable application of computer facilities could be justified, if the only advantage were a greater comfort in the storage of one's own and foreign mass spectrometer data. In reality, however, data storage is the prerequisite for many sophisticated re-evaluations. Among these are, for example, the refinement of isotopic budgets for the entire crust or for specific geologic units. Another outstanding task is the search for correlations between isotope data and other geochemical parameters (trace element distribution, etc.) of the sample material. Of course this can also be done (and has already been performed) manually, if not too many input data are applied. On the other hand, it is just the large number of data available that gives us the chance to detect correlations previously hidden behind the sample statistics. Once the data file has been filled up with all the results obtained hitherto, it will need only little effort to exercise any desired evaluation by means of the library routines available at the computer center, and it will be easy to re-examine the conclusions each time when new data are being added to the file.

It is evident that this kind of data handling also has implications on the style of data presentation in original and review papers. It has been a matter of dispute for a long time, whether extended tables with numerical data are opportune in scientific journals. In most cases a diagram shows more clearly what the author wishes to demonstrate, and readers interested in further details can be supplied with specified computer output lists directly from the data file; but the computer can also produce the diagrams for publication. All the figures of this article comprising S isotope data have been plotted from the Göttingen data file. As far as data from other laboratories were needed (see Figs. 1 and 6), they were inserted manually into the data file.

References

Anger, G., Nielsen, H., Puchelt, H., Ricke, W.: Sulfur isotopes in the Rammelsberg ore deposit (Germany). Econ. Geol. *61*, 511-536 (1966)

Ault, W.U., Jensen, M.L.: Summary of sulfur isotope standards. In: Biogeochemistry of Sulfur Isotopes. Jensen, M.L. (ed.). New Haven, 1962

Ault, W.U., Kulp, J.L.: Isotopic geochemistry of sulphur. Geochim. Cosmochim. Acta *16*, 201-235 (1959)

Coomer, P.G., Robinson, B.W.: Sulphur and sulphate-oxygen isotopes and the origin of the Silvermines deposits, Ireland. Miner. Deposita *11*, 155-169 (1976)

Croxford, N.J.W., Gulson, B.L., Smith, J.W.: The McArthur deposit: A review of the current situation. Miner. Deposita *10*, 302-304 (1975)

Dechow, E., Jensen, M.L.: Sulfur isotopes of some Central African sulfide deposits. Econ. Geol. *60*, 894-941 (1965)

Gehlen, K. von, Nielsen, H.: Schwefelisotope aus Blei-Zink-Erzen von Oberschlesien. Miner. Deposita *4*, 308-310 (1969)

Goldhaber, M.B., Kaplan, I.R.: The sedimentary sulfur cycle. In: The Sea. *4*. Goldberg, E.D. (ed.). New York: Wiley, 1974

Grey, D.C., Jensen, M.L.: Bacteriogenic sulfur in air pollution. Science *177*, 1099-1100 (1972)

Grinenko, V.A., Grinenko, L.N.: Geokhimia Isotopov Sery. Moskow: Isdatelstvo Nauka, 1974

Hartmann, M., Nielsen, H.: δ^{34}S-Werte in rezenten Meeressedimenten und ihre Deutung am Beispiel einiger Sedimentprofile aus der westlichen Ostsee. Geol. Rundsch. *58*, 621-655 (1969)

Kemp, A.L.W., Thode, H.G.: The mechanism of the bacterial reduction of sulphate and of sulphite from isotope fractionation studies. Geochim. Cosmochim. Acta *32*, 71-91 (1968)

Lewis, J.S., Krouse, H.R.: Isotopic composition of sulfur and sulfate produced by oxidation of FeS. Earth Planet. Sci. Lett. *5*, 425-428 (1969)

McCready, R.G.L., Kaplan, I.R., DIN, G.A.: Fractionation of sulfur isotopes by the yeast *Saccharomyces cerevisiae*. Geochim. Cosmochim. Acta *38*, 1239-1253 (1974)

Nielsen, H.: Data handling in precise isotope ratio research. In: Advances in Mass Spectrometry *4*. Kendrick, E. (ed.). London: The Institute of Petroleum, 1968

Nielsen, H.: Sulfur isotopes in nature. In: Handbook of Geochemistry. Wedepohl, K.-H. (ed.). Berlin, Heidelberg, New York: Springer 1978

Nissenbaum, A., Presley, B.J., Kaplan, I.R.: Early diagenesis in a reducing fjord, Saanich Inlet, British Columbia I. Geochim. Cosmochim. Acta *36*, 1007-1027 (1972)

Ohmoto, H.: Systematics of sulfur and carbon isotopes in hydrothermal ore deposits. Econ. Geol. *67*, 551-578 (1972)

Ohmoto, H.: Application of experimental data on the fractionation of stable isotopes to problems of ore genesis. 25. Internation Geologic Congress, Abstracts *3*, 822-823 (1976)

Rye, R.O., Ohmoto, H.: Sulfur and carbon isotopes and ore genesis: A review. Econ. Geol. *69*, 826-842 (1974)

Sakai, H.: Isotopic properties of sulfur compounds in hydrothermal processes. Geochem. J. *2*, 29-49 (1968)

Sangster, D.F.: Relative sulphur isotope abundances of ancient seas and strata-bound sulphide deposits. Geol. Assoc. Can. Proc. *19*, 79-91 (1968)

Schwarcz, H.P., Burnie, S.W.: Influence of sedimentary environments on sulfur isotope ratios in clastic rocks: A review. Miner. Deposita *8*, 264-277 (1973)

Thode, H.G., McNamara, J., Collins, C.B.: Natural variations in the isotopic content of sulphur and their significance. Can. J. Res. *27*, 361-3373 (1949)

Trofimov, A.: Isotopny sostav sery meteoritakh i v'semykh objektakh. Doklady Akad. Nauk SSR *66*, 181-184 (1949)

Trudinger, P.A., Chambers, L.A.: Reversibility of bacterial sulfate reduction and its relevance to isotope fractionation. Geochim. Cosmochim. Acta *37*, 1775-1778 (1973)

Vinogradov, A.P., Grinenko, V.A., Ustinov, V.I.: Isotopic composition of sulfur compounds in the Black Sea. Geochemistry 973-997 (1962)

Warren, C.G.: Sulfur isotopes as a clue to the genetic geochemistry of a roll-type uranium deposit. Econ. Geol. *67*, 759-767 (1972)

Wedepohl, K.-H.: "Kupferschiefer" as a prototype of synsedimentary ore deposits. Soc. Mining Geol. Japan. Spec. Issue *3*, 268-273 (1971)

Subject Index

Contributions to Mineralogy and Petrology

In Cooperation with the International Mineralogical Association (I.M.A.)

The journal has been founded in 1947 as "Heidelberger Beiträge zur Mineralogie und Petrographie". It publishes contributions to the petrology and geochemistry of igneous, metamorphic and sedimentary rocks, including experimental petrology, mineralogy, isotope geochemistry, and geochronology. In addition to original investigations, high-quality review articles are included.

Springer-Verlag
Berlin
Heidelberg
New York

Fields of Interest: Mineralogy, Petrology, Geochemistry, Sedimentology, Geology, Mining Industry.

Languages used: Approximately 95% of the articles are in English; the others, in German and French, are preceded by an English abstract.

Subscription Information and sample copy upon request.

B.R. Doe

Lead Isotopes

1970. 24 figures. IX, 137 pages
(Minerals and Rocks, Volume 3)
ISBN 3-540-05205-4

"The monograph is basically a review of the status of lead isotopes till a few years ago. However, the quantity of data incorporated is so vast that it will be of great use to geologists for a long time... this is really an outstanding contribution to lead isotope research. The survey of Soviet literature is probably the most remarkable aspect of this book, and it has been long overdue. The extensive bibliography is probably one of the most useful aspects of this book and will be used extensively. This monograph will certainly become a "must" reading for geologists and researchers in this field and with the typical Doe style of writing, it makes it so much easier."

The American Mineralogist

"...The first section describes briefly the theoretical background of the uranium lead-dating methods, and the principles of dating discordant U/Pb-systems by means of the "Concordia" method are explained. The currently used chemical tecniques for the preparation of samples for isotope studies are described in detail. Results and experiences in dating of different minerals such as zircon, sphene etc. are discussed.
Section 2 summarises formulas and constants for the mathematical treatment of different lead containing systems in nature. A very comprehensive review of important lead isotope data including results of moon-samples is given in an appendix. This book represents a very valuable compilation of lead isotope data."

Geophysical Prospecting

Springer-Verlag
Berlin
Heidelberg
New York

G. Faure, J.L. Powell

Strontium Isotope Geology

1972. 51 figures. IX, 188 pages
(Minerals and Rocks, Volume 5)
ISBN 3-540-05784-6

"...Widespread and increasing use of strontium isotope measurements in the dating of rocks and in isotopic tracer studies of geologic processes makes this compact book extremely useful for geologists and other scientists. The authors... have made numerous and critical additions to the field of strontium isotope geology, and their book is a succinct but complete, very carefully written, description of the field... I found this book exceptionally well organized and conceived..."

Economic Geology

"...The book is well written and does achieve the objective of being an introduction to strontium isotope geochemistry. In bringing together the various aspects of the subject it will be of particular value to geologists wishing to acquire an understanding of strontium isotopic data and the type of problems to which this type of analysis is applicable..."

Geographical Magazine

J. Hoefs

Stable Isotope Geochemistry

1973. 37 figures. IX, 140 pages
(Minerals and Rocks, Volume 9)
ISBN 3-540-06176-2

"...which is essentially an up to date review of the most significant contributions to stable isotope geochemistry over the last ten years... is divided into three main sections. ...
Overall the text is easy to follow, largely as a result of the crisp style and of the economy of words, which allow the significant contributions in a comprehensive bibliography of about 500 references to be covered in a relatively short space... This book should provide invaluable reference work for many who teach and do research in geochemistry."

Nature